Temporal Aggregation Methods for Energy System Modeling

Zeitreihenaggregationsmethoden für die Energiesystemmodellierung

Von der Fakultät für Maschinenwesen
der Rheinisch-Westfälischen Technischen Hochschule Aachen
zur Erlangung des akademischen Grades eines
Doktors der Ingenieurwissenschaften
genehmigte Dissertation

vorgelegt von

Maximilian Alexander Camillo Hoffmann

Berichter:
Univ.-Prof. Dr.-Ing. Detlef Stolten
Univ.-Prof. Dr. rer. oec. Christoph Weber

Tag der mündlichen Prüfung: 01.12.2022

Diese Dissertation ist auf den Internetseiten
der Universitatsbibliothek online verfügbar.

Forschungszentrum Jülich GmbH
Institut für Energie- und Klimaforschung (IEK)
Techno-ökonomische Systemanalyse (IEK-3)

Temporal Aggregation Methods for Energy System Modeling

Maximilian Alexander Camillo Hoffmann

Schriften des Forschungszentrums Jülich
Reihe Energie & Umwelt / Energy & Environment Band / Volume 605

ISSN 1866-1793 ISBN 978-3-95806-683-0

Bibliografische Information der Deutschen Nationalbibliothek.
Die Deutsche Nationalbibliothek verzeichnet diese Publikation in der
Deutschen Nationalbibliografie; detaillierte Bibliografische Daten
sind im Internet über http://dnb.d-nb.de abrufbar.

Herausgeber und Vertrieb:	Forschungszentrum Jülich GmbH Zentralbibliothek, Verlag 52425 Jülich Tel.: +49 2461 61-5368 Fax: +49 2461 61-6103 zb-publikation@fz-juelich.de www.fz-juelich.de/zb
Umschlaggestaltung:	Grafische Medien, Forschungszentrum Jülich GmbH
Druck:	Grafische Medien, Forschungszentrum Jülich GmbH
Copyright:	Forschungszentrum Jülich 2023

Schriften des Forschungszentrums Jülich
Reihe Energie & Umwelt / Energy & Environment, Band / Volume 605

D 82 (Diss. RWTH Aachen University, 2022)

ISSN 1866-1793
ISBN 978-3-95806-683-0

Vollständig frei verfügbar über das Publikationsportal des Forschungszentrums Jülich (JuSER)
unter www.fz-juelich.de/zb/openaccess.



This is an Open Access publication distributed under the terms of the Creative Commons Attribution License 4.0,
which permits unrestricted use, distribution, and reproduction in any medium, provided the original work is properly cited.

Abstract

Renewable energy sources are a crucial cornerstone in the future energy sector to decelerate global warming and to reach the international reduction targets for CO_2 emissions. However, the rising share of renewable energy sources challenges the planning and operating of energy systems in multiple regards: On the one hand, these sources are often intermittent and in order to provide a safe energy supply, energy storage technologies gain importance. On the other hand, different energy sectors are progressively coupled because the supply security can profit from the option to exchange energy among different sectors.

In order to appropriately foresee these developments and derive realistic designs of cost-efficient future energy systems, spatiotemporally resolved energy system models have emerged as a powerful tool. Yet, just as the real energy systems, the models are becoming increasingly complex and the consideration of intermittent renewable energy sources require high temporal resolutions within these models. Accordingly, energy system models are either limited in the size of the regarded energy system, limited in the accuracy or computationally simply intractable. Therefore, methods were developed that strive to reduce the mathematical complexity of energy system models without sacrificing too much of the model's accuracy. One of these methods is temporal aggregation, i.e. the reduction of the number of time steps considered by an energy system model in order to capture transient changes of its operation schedule.

This thesis contributes to the research field of temporal aggregation techniques for energy system modeling by systematically comparing four fundamentally different energy system models to each other, using a two-fold temporal aggregation for efficiently decreasing the computational burden of the regarded energy system models. Furthermore, it introduces novel algorithms to increase the accuracy of temporally aggregated energy system models significantly. In contrast to prior works in the literature, this thesis does not only assess the developed methods analytically, but also stochastically with a wide variety of different temporal aggregation configurations in order to take the differences of the models into account. The results reveal that the optimal temporal aggregation depends on two factors: The existence of temporally coupling constraints in the model, e.g. as introduced by storage technologies, and the types of time series used as input to the models. Moreover, the methods found in literature are outperformed consistently and significantly by the methods proposed within this thesis.

All methods were generically implemented in the Framework for Integrated Energy System Assessment (**FINE**) and resulted in a fundamental restructuring and extension of the time series aggregation module (**tsam**). The latter module is a python-based out-of-the-box solution for temporal aggregation techniques and is currently used by multiple different energy system modeling frameworks.

Kurzfassung

Aufgrund der internationalen Klimaziele, den CO_2-Ausstoß zu verringern und dadurch das Fortschreiten des Klimawandels zu verlangsamen, übernehmen erneuerbare Energiequellen eine zentrale Rolle im künftigen Energiesektor. Demgegenüber stellt ein steigender Anteil erneuerbarer Energien große Herausforderungen an die Planung und den sicheren Betrieb von Energiesystemen: Einerseits unterliegen erneuerbare Energien oftmals einer schwankenden Verfügbarkeit, wodurch Technologien zur Energiespeicherung im gleichen Maße an Bedeutung gewinnen, um auch in Zukunft eine Versorgungssicherheit gewährleisten zu können. Andererseits werden verschiedene Energiesektoren zunehmend miteinander gekoppelt, da die Versorgungssicherheit auch von der Möglichkeit profitiert, Energie bei Bedarf zwischen verschiedenen Energiesektoren zu transferieren.

Um diese Entwicklungen angemessen voraussagen und realistische Auslegungen für kosteneffiziente künftige Energiesysteme ableiten zu können, etablierten sich räumlich und zeitlich aufgelöste Energiesystemmodelle als geeignete Werkzeuge. Allerdings steigt mit der Komplexität der Energiesysteme auch die ihrer Modelle und die Berücksichtigung erneuerbarer Energien mit schwankender Verfügbarkeit erfordert hohe zeitliche Auflösungen innerhalb jener Modelle. Dementsprechend sind die Modelle entweder hinsichtlich der Größe des modellierten Energiesystems begrenzt, in ihrer Genauigkeit eingeschränkt oder ihre mathematische Komplexität derart groß, dass sie für bestehende Computerressourcen schlicht unlösbar werden. Aus diesem Grund entwickelten sich in der Vergangenheit Methoden, um die mathematische Komplexität von Energiesystemmodellen mit kleinstmöglicher Beeinträchtigung der Modellgenauigkeit zu reduzieren. Eine dieser Methoden ist die sogenannte Zeitreihenaggregation, d.h. die Reduktion der Anzahl an durch das Energiesystemmodell berücksichtigten Zeitschritten, um zeitliche Veränderungen im Betrieb des Energiesystems abzubilden.

Die vorliegende Arbeit trägt zum Forschungsfeld der Zeitreihenaggregationsmethoden für die Energiesystemmodellierung bei, indem sie vier fundamental unterschiedliche Energiesysteme miteinander vergleicht und eine zweistufige Zeitreihenaggregation verwendet, um die Größe der betrachteten Energiesystemmodelle sowie ihre mathematische Komplexität effizient zu verringern. Darüber hinaus werden im Rahmen der Arbeit neue Algorithmen entwickelt, um die Genauigkeit der aggregierten Energiesystemmodelle deutlich zu erhöhen. Aufgrund der Verschiedenheit der betrachteten Modelle analysiert die vorliegende Arbeit im Gegensatz zu anderen Arbeiten in diesem Forschungsfeld die entwickelten Methoden nicht nur analytisch, sondern auch stochastisch mittels einer großen Zahl von verschiedenen Aggregationskonfigurationen. Die Ergebnisse zeigen, dass die optimale Zeitreihenaggregation in erster Linie von zwei Faktoren abhängt: Der Existenz von zeitschrittkoppelnden Nebenbedingungen, wie sie beispielsweise durch die Berücksichtigung von Speichertechnologien im Modell Anwendung finden, sowie der Art der für das Energiesystemmodell berücksichtigten Zeitreihen. Zudem offenbaren die Ergebnisse die konsequente Überlegenheit der in dieser Arbeit entwickelten Aggregationsmethoden gegenüber jenen, die in der Literatur breite Anwendung finden.

Abschließend wurden alle im Rahmen dieser Arbeit entwickelte Methoden generisch im Framework for Integrated Energy System Assessment (**FINE**) implementiert und bedingten eine fundamentale Neugestaltung und Erweiterung des time series aggregation modules (**tsam**). Letzteres stellt eine python-basierte Out-of-the-Box Lösung für Zeitreihenaggregationsmethoden dar und wird bereits von verschiedenen Energiesystemmodellierungsframeworks verwendet.

Introductory Remark

This work is partly based on journal articles published by the author of this thesis during his time as a PhD student at the Jülich Research Centre.

Passages from publications, for which the author of this thesis took over the lead authorship, have been verbatim quoted in parts of Chapter 1, 2 as well as Section 4.3 and Appendix A to F, I and J. Adapted content and reused figures appear in Section 3.1, 3.2, 3.3, 4.1 and 4.2. The corresponding publications, to which is explicitly referred at the respective passages, are the following:

- Hoffmann, M., L. Kotzur, D. Stolten, and M. Robinius, A Review on Time Series Aggregation Methods for Energy System Models. Energies, 2020. 13(3), DOI: https://doi.org/10.3390/en13030641. (Open access) [1]
- Hoffmann, M., J. Priesmann, L. Nolting, A. Praktiknjo, L. Kotzur, and D. Stolten, Typical periods or typical time steps? A multi-model analysis to determine the optimal temporal aggregation for energy system models. Applied Energy, 2021. 304: p. 117825, DOI: https://doi.org/10.1016/j.apenergy.2021.117825. © 2021 Elsevier. Reprinted with permission. [2]
- Hoffmann, M., L. Kotzur, and D. Stolten, The Pareto-optimal temporal aggregation of energy system models. Applied Energy, 2022. 315: p. 119029, DOI: https://doi.org/10.1016/j.apenergy.2022.119029. © 2022 Elsevier. Reprinted with permission. [3]

Content of publications, to which the author of this thesis has contributed to as a co-author, has **not** been reused. These publications is referred to with plain citations and they are listed in the following:

- Kannengießer, T., M. Hoffmann, L. Kotzur, P. Stenzel, F. Schuetz, K. Peters, S. Nykamp, D. Stolten, and M. Robinius, Reducing Computational Load for Mixed Integer Linear Programming: An Example for a District and an Island Energy System. Energies, 2019. 12(14): p. 2825, DOI: https://doi.org/10.3390/en12142825. [4]
- Kotzur, L., L. Nolting, M. Hoffmann, T. Groß, A. Smolenko, J. Priesmann, H. Büsing, R. Beer, F. Kullmann, B. Singh, A. Praktiknjo, D. Stolten, and M. Robinius, A modeler's guide to handle complexity in energy systems optimization. Advances in Applied Energy, 2021. 4: p. 100063, DOI: https://doi.org/10.1016/j.adapen.2021.100063. [5]
- Singh, B., O. Rehberg, T. Groß, M. Hoffmann, L. Kotzur, and D. Stolten, Budget-Cut: Introduction to a budget based cutting-plane algorithm for capacity expansion models. Optimization Letters, 2021, DOI: https://doi.org/10.1007/s11590-021-01826-w. [6]

Table of Contents

Abstract VI
Kurzfassung VII
Introductory Remark VIII
Table of Contents IX
List of Figures XIII
List of Tables XXVI
List of Symbols XXVIII
List of Abbreviations XXX
1. Motivation 2
1.1. Drivers of Model Complexity 2
1.2. Motivation and Scope of the Thesis 4
1.3. Structure of the Thesis 6
2. State of the Art 8
2.1. Methodology and Structure of Chapter 2 8
2.1.1. Methodology of the Literature Research 8
2.1.2. Structure of the Review 9
2.2. Time Series Aggregation 11
2.2.1. Resolution Variation 15
2.2.2. Typical Periods 19
2.2.3. Random Sampling 35
2.2.4. Miscellaneous Methods 37
2.2.5. Trends in Time Series Aggregation 39
2.3. Preserving Additional Information 42
2.3.1. A Priori Methods 42
2.3.2. A Posteriori Methods 50
2.3.3. Trends in the Integration of Additional Information 55
2.4. Review Summary 57
3. Methodology 59
3.1. The Process of Time Series Aggregation 60
3.1.1. Period Clustering 60

3.1.2. Segmentation 61
3.1.3. Combination of Period Clustering and Segmentation 64
3.2. Representation Methods 65
3.2.1. Centroids 66
3.2.2. Medoids 67
3.2.3. Maxoids 69
3.2.4. Maximum- and Minimum Representation 72
3.2.5. Distribution Preserving Representation 74
3.2.6. Summary of Representation Methods 80
3.3. Error and Complexity Indicators 82
3.3.1. A Priori Indicators 84
3.3.2. A Posteriori Indicators 88
3.3.3. Quantifying the Quality of A Priori Indicators 89
3.3.4. Optimal Aggregation Based on A Priori Indicators 91
3.4. Methods for Systematic Over- and Underestimations 98
3.4.1. Upper and Lower Bounds for LPs and MILPs 99
3.4.2. Upper and Lower Bounds for MILPs 101
4. Validation and Results 104
4.1. Model Overview and Data Resources 107
4.1.1. The Island System 107
4.1.2. The Self-Sufficient Building Model 108
4.1.3. The European Model 110
4.1.4. The Electricity Dispatch Model 113
4.1.5. Model Summary 116
4.2. The Optimal Aggregation: A Sensitivity Analysis 118
4.2.1. Analyses of the Island System Model 119
4.2.2. Analyses of the Self-Sufficient Building 135
4.2.3. Analyses of the European Model 142
4.2.4. Adaption of the Distribution-Preserving Algorithm 166
4.2.5. Summary 175

4.3. Typical Days or Typical Time Steps 177
4.3.1. Input-Data Driven Analysis 179
4.3.2. Output-Data Driven Analysis 181
4.3.3. In-depth Analysis of Computational Resources 186
4.3.4. Summary 190
4.4. Error Bounding Methods 193
4.4.1. Bounds Based on Over- and Underestimation 193
4.4.2. Model-Specific Bounds for MILPs without Cost Time Series 198
4.4.3. Summary 201
4.5. Discussion 202
4.5.1. Discussion of the Main Results 202
4.5.2. Temporal Aggregation in the Context of Other Simplifications 206
5. Summary 213
5.1. Scope and Objective 213
5.2. General Approach and State of the Art 214
5.3. Methodology 215
5.4. Results and Main Conclusions 217
Appendix 220
A. Glossary Used For Literature Research 220
B. Table of Methods 222
C. Customer and Unit Partitioning 239
D. An Example for Time Series Normalization 241
E. Clustering Algorithms Applied in the Literature 242
F. Modified Feature-Based Merging 247
G. Proofs and Lemmata for Section 3.2 249
H. Classification of Optimization Problems 256
H.1. Linear Programs (LPs) 256
H.2. Mixed-Integer Linear Programs (MILPs) 260
H.3. Quadratic Programs (QPs) 264

H.4. Summary 269
I. Matrix Aggregation and Error Bounding 270
I.1. Matrix Aggregation 270
I.2. Error Bounding 280
I.2.1. A General Workflow to Determine Bounds 281
I.2.2. Upper bounds 291
I.2.3. Lower Bounds 299
J. Techno-Economic Model Assumptions 315
J.1. Model Assumptions for the Island System Model 315
J.2. Model Assumptions for the Self-Sufficient Building Model 317
J.3. Model Assumptions for the Electricity Dispatch Model 318
Bibliography 320

List of Figures

Figure 1.1. Classification of energy system models, the sub-dimensions of bottom-up models and the scope of the thesis (taken from Hoffmann et al. [1]) 4
Figure 1.2. Time series aggregation defined as the reduction of the number of time steps considered in bottom-up energy system models 5
Figure 1.3. Structure of the thesis 7
Figure 2.1. Mind map of the methods presented in the review, their methodological connection (marked by same colors) and decisions to be made or steps to be taken when applying time series aggregation (taken from Hoffmann et al. [1]) 10
Figure 2.2. One year of hourly resolved photovoltaic capacity factors simulated with PV-Lib [65] (RMSE=0) (taken from Hoffmann et al. [1]) 10
Figure 2.3. Set of time series entering the energy system boundaries and defining constraints that the energy system model must satisfy 11
Figure 2.4. Exemplary set of time series (adapted from Hoffmann et al. [1]) 11
Figure 2.5. Reduction of the number of time series using customer and unit partitioning (adapted from Hoffmann et al. [1]) 12
Figure 2.6. Reduction of the number of time steps using resolution variation (adapted from Hoffmann et al. [1]) 13
Figure 2.7. Reduction of the number of time steps using typical periods (adapted from Hoffmann et al. [1]) 14
Figure 2.8. The time series of photovoltaic capacity factors downsampled to 1460 6h time steps (RMSE=0.1295) (taken from Hoffmann et al. [1]) 16
Figure 2.9. The time series of photovoltaic capacity factors segmented to 1460 time intervals using hierarchical merging of adjacent time steps based on centroids as proposed by Pineda et al.

[77] (RMSE=0.0388) (taken from Hoffmann et al. [1]) 18
Figure 2.10. The time series of photovoltaic capacity factors represented by twelve monthly averaged periods as used in other studies [60, 104, 105] and reproduced by Kotzur et al. [48] using the python package **tsam** [48] (i.e., 288 different time steps) (RMSE=0.1126) (taken from Hoffmann et al. [1]) 21
Figure 2.11. The time series of photovoltaic capacity factors represented by twelve time slices (average Wednesday, Saturday and Sunday for each season) as used by Nicolosi et al. and Haydt et al. [109, 110] (i.e., 288 different time steps) (RMSE=0.1509) (taken from Hoffmann et al. [1]) 23
Figure 2.12. Steps for clustering time series for energy system models (adapted from Hoffmann et al. [1]) 25
Figure 2.13. The time series of photovoltaic capacity factors represented by twelve typical days (typical days) using k-means clustering and the python package **tsam** [48] (i.e., 288 different time steps) (RMSE=0.0552) (taken from Hoffmann et al. [1]) 26
Figure 2.14. Storage formulation based on regular order of time slices according to Welsch et al. [111] and the seasonal checkpoint for two day types and three time slices each according to Timmerman et al. [112] 32
Figure 2.15. The cluster-based superposition approach to modeling seasonal storages proposed by Kotzur et al. [20] 34
Figure 2.16. The difference between random sampling and clustering 36
Figure 2.17. Trends in basic temporal aggregation methods for energy system models based on the major approaches presented in Section 2.2 (taken from Hoffmann et al. [1]) 39

Figure 2.18. A drawback of time series aggregation: Outliers of the dataset being potentially design relevant are neglected 43
Figure 2.19. Impact of adding “shoulder values” as proposed by Frew et al. [167] as extreme values for a rising number of attributes (taken from Hoffmann et al. [1]) 46
Figure 2.20. Mutual dependencies in aggregated energy system optimizations that necessitate feedback loops (taken from Hoffmann et al. [1]) 51
Figure 2.21. Trends in methods to preserve additional information in temporal aggregation methods for energy system models based on the major approaches presented in Section 2.3 (taken from Hoffmann et al. [1]) 56
Figure 3.1. Clustering and representation as separate steps of clustering (taken from Hoffmann et al. [3]) 59
Figure 3.2. The procedure of period clustering using an arbitrary clustering algorithm (adapted from Hoffmann et al. [3]) 61
Figure 3.3. The procedure of segmentation using constrained hierarchical clustering (adapted from Hoffmann et al. [3]) 63
Figure 3.4. Time step reduction based on a combination of period clustering and segmentation (taken from Hoffmann et al. [3]) 64
Figure 3.5. An exemplary data cloud used for visualizing the clustering process 65
Figure 3.6. The yearly duration curve of an exemplary electricity profile and its profile during a week in February 66
Figure 3.7. A clustered data cloud including the cluster’s centroids 66
Figure 3.8. The yearly duration curve of an exemplary electricity profile, its profile during a week in February and the corresponding aggregated time series as predicted by eight typical days using hierarchical clustering and centroids as representatives (taken from Hoffmann et al. [3]) ... 67

Figure 3.9. A clustered data cloud including the cluster's medoids 68
Figure 3.10. The yearly duration curve of an exemplary electricity profile, its profile during a week in February and the corresponding aggregated time series as predicted by eight typical days using hierarchical clustering and medoids as representatives 68
Figure 3.11. A clustered data cloud including the cluster's maxoids 70
Figure 3.12. The yearly duration curve of an exemplary electricity profile, its profile during a week in February and the corresponding aggregated time series as predicted by eight typical days using hierarchical clustering and maxoids as representatives 71
Figure 3.13. A clustered data cloud including the cluster's minimum values for one attribute and maximum values for the other attribute as time representatives 72
Figure 3.14. The yearly duration curve of an exemplary electricity profile, its profile during a week in February and the corresponding aggregated time series as predicted by eight typical days using hierarchical clustering and the minimum values per time step and cluster 73
Figure 3.15. The yearly duration curve of an exemplary electricity profile, its profile during a week in February and the corresponding aggregated time series as predicted by eight typical days using hierarchical clustering and the maximum values per time step and cluster 73
Figure 3.16. The flow chart for the distribution preserving representation method 77
Figure 3.17. The graphical interpretation of the operations in Figure 3.16 (taken from Hoffmann et al. [3]) 78
Figure 3.18. A clustered data cloud including the cluster's approximately distribution preserving representatives 79

Figure 3.19. The yearly duration curve of an exemplary electricity profile, its profile during a week in February and the corresponding aggregated time series as predicted by eight typical days using hierarchical clustering and the approximately distribution preserving representation method (taken from Hoffmann et al. [3]) 79
Figure 3.20. The different definitions of a priori indicators comparing evaluating aggregated **input** data to the model and a posteriori indicators accessing **output** data of the model (taken from Hoffmann et al. [2]) 83
Figure 3.21. Scheme of two aggregation methods in which the second one strictly dominates the first one 83
Figure 3.22. Illustration of squared summands used for calculating the root-mean-square error (taken from Hoffmann et al. [2]) 85
Figure 3.23. Illustration of squared summands between duration curves used for calculating the root-mean-square error of the duration curve (taken from Hoffmann et al. [2]) 86
Figure 3.24. Illustration of absolute summands between duration curves used for calculating the MAE 87
Figure 3.25. Three subsequent steps of the proposed algorithm to find the optimum number of segment and typical days (taken from Hoffmann et al. [3]) 94
Figure 3.26. The optimal pathway algorithm from minimum to maximum resolution (taken from Hoffmann et al. [3]) 95
Figure 3.27. The proposed algorithm for the root-mean-square error (RMSE) of an exemplary global horizontal irradiance and a wind speed profile (taken from Hoffmann et al. [3]) 96
Figure 3.28. The concept of upper and lower bounds to the estimate the maximum deviation from the optimal objective function value of the fully resolved reference case 98

Figure 3.29. A multi-level approach to determine upper and lower bounds of the original mathematically complex mixed-integer linear program (MILP) using aggregated time series, tightening and relaxation 102
Figure 4.1. Structure of Chapter 4 104
Figure 4.2. Technology portfolio of the island system 108
Figure 4.3. A simplified scheme of the self-sufficient building model taken from Hoffmann et al. [2]) ... 108
Figure 4.4. The layout of the European model (taken from Hoffmann et al. [3]) 112
Figure 4.5. The layout of the dispatch model (taken from Hoffmann et al. [2]) 114
Figure 4.6. Input data of the dispatch model: Aggregated transmission lines, installed capacities, and yearly energy demand (taken from Hoffmann et al. [2]) 115
Figure 4.7. Common model features covered by the case studies 116
Figure 4.8. Number of total time steps depending on typical day and segment configurations that were considered in the sensitivity analysis for four different representation methods (taken from Hoffmann et al. [3]) 118
Figure 4.9. The island system and the corresponding normed optimal objectives over computation times for all considered configurations 119
Figure 4.10. The deviation from the optimal objective of the fully resolved case depending on the configuration of the number of typical days and segments as well as the representation method . 121
Figure 4.11. The total annualized costs of the photovoltaic panels and the wind turbines normed by their total annualized costs in the fully resolved case . 125
Figure 4.12. The correlation between a priori and a posteriori indicators for the representation by centroids 126
Figure 4.13. The root-mean-square error (RMSE) depending on the number of typical days and segments in the case of a representation by centroids 128

Figure 4.14. The correlation between a priori and a posteriori indicators for the representation by medoids 130
Figure 4.15. The pathway found by the proposed algorithm for an optimal ratio between the number of typical days and segments depending on the representation method 131
Figure 4.16. Convergence behavior of the different representation methods if an optimal ratio between the number of typical days and the number of segments is chosen based on the root-mean-square error compared to the convergence behavior of different typical day numbers at an hourly resolution..... 134
Figure 4.17. The identified optimal aggregation method among all tested aggregation approaches (left) and a direct comparison to state-of-the-art aggregation methods as used in **FINE** (right) 135
Figure 4.18. The self-sufficient building model and the corresponding normed optimal objectives over computation times for all considered configurations (adapted from Hoffmann et al. [3]) 135
Figure 4.19. The deviation from the optimal objective of the fully resolved case depending on the configuration of the number of typical days and segments as well as the representation method (adapted from Hoffmann et al. [3]) 137
Figure 4.20. The correlation between a priori and a posteriori indicators for the representation by centroids (top) and by medoids (bottom)..... 138
Figure 4.21. The pathway found by the proposed algorithm for an optimal ratio between the number of typical days and segments depending on the representation method (adapted from Hoffmann et al. [3])..... 139
Figure 4.22. Convergence behavior of the different representation methods if an optimal ratio between the number of typical days and the number of segments is chosen based on the root-mean-square error compared to the

convergence behavior of different typical day numbers at an hourly resolution (adapted from Hoffmann et al. [3]) 141
Figure 4.23. The identified optimal aggregation method among all tested aggregation approaches (left) and a direct comparison to state-of-the-art aggregation methods as used in **FINE** (right) (adapted from Hoffmann et al. [3]) 142
Figure 4.24. The European model and the corresponding normed optimal objectives over computation times for all considered configurations (adapted from Hoffmann et al. [3]) 144
Figure 4.25. The deviation from the optimal objective of the fully resolved case depending on the configuration of the number of typical days and segments as well as the representation method (adapted from Hoffmann et al. [3]) 145
Figure 4.26. The total annualized costs of the photovoltaic technologies and the wind plants normed by their total annualized costs in the fully resolved case 148
Figure 4.27. Energy supply and storage capacities depending on a varying number of typical days and segments using a representation by centroids (taken from Hoffmann et al. [3]) 153
Figure 4.28. The correlation between a priori and a posteriori indicators for the representation by centroids (top) and by medoids (bottom)..... 155
Figure 4.29. The correlation between the logarithm of runtime and the logarithm of the total number of time steps..... 156
Figure 4.30. The pathway found by the proposed algorithm for an optimal ratio between the number of typical days and segments depending on the representation method (adapted from Hoffmann et al. [3])..... 157
Figure 4.31. Convergence behavior of the different representation methods if an optimal ratio between the number of typical days and the number of segments is chosen based on the

root-mean-square error compared to the convergence behavior of different typical day numbers at an hour (adapted from Hoffmann et al. [3]) 159
Figure 4.32. The identified optimal aggregation method among all tested aggregation approaches (left) and a direct comparison to state-of-the-art aggregation methods as used in **FINE** (right) 160
Figure 4.33. Impact of the centroid (C) and distribution-preserving (DP) representation on both, the inner-daily and inter-daily variance 161
Figure 4.34. Variance of daily means of onshore capacity factors for varying numbers of typical days depending on the representation method 163
Figure 4.35. The convergence behavior of the three different aggregated energy systems' optimal objective value to the reference value, if centroid-based typical days with an hourly resolution (no segmentation) are used (adapted from Hoffmann et al. [3]) 166
Figure 4.36. The graphical interpretation of the adapted distribution-preserving algorithm 167
Figure 4.37. Variance of daily means of onshore capacity factors for varying numbers of typical days depending on the representation method 168
Figure 4.38. The pathway found by the proposed algorithm for an optimal ratio between the number of typical days and segments depending on the representation method (adapted from Hoffmann et al. [3]) 169
Figure 4.39. The normed optimal objective for all considered representation methods over the corresponding runtime (left) and the normed objectives along the optimal pathway for the distribution preserving algorithm, the medoid representation and the modified distribution preserving algorithm (right) (adapted from Hoffmann et al. [3]) 170
Figure 4.40. The deviation from the optimal objective value of the reference case and the total cost shares

of photovoltaic and wind capacities for the medoid and adapted distribution-preserving representation 171
Figure 4.41. The total cost shares of battery and salt cavern capacities for the medoid and adapted distribution-preserving representation 172
Figure 4.42. Energy supply capacities depending on a varying number of typical days and segments using the medoid and the adapted distribution-preserving representation 174
Figure 4.43. The energy supply capacities for 365 typical days, 24 segments and the adapted distribution-preserving representation 175
Figure 4.44. Method applied to compare typical periods and typical time steps for different types of energy system models (adapted from Hoffmann et al. [2]) 177
Figure 4.45. Error indicators for the self-sufficient building (top) and the dispatch model (bottom) for both, typical days and typical time steps (adapted from Hoffmann et al. [2]) 180
Figure 4.46. Absolute deviation from the optimized objective function value of the fully resolved case over calculation time for the self-sufficient building (top) and the dispatch-model (down) (adapted from Hoffmann et al. [2]) 182
Figure 4.47. The individual cost contributions for the self-sufficient model (top) and the dispatch model (bottom) for all aggregation configurations (adapted from Hoffmann et al. [2]) 184
Figure 4.48. Calculation times of the self-sufficient building (top) and the dispatch-model (bottom) depending on the aggregation configuration (adapted from Hoffmann et al. [2]) 187
Figure 4.49. Memory consumption of the self-sufficient building (top) and the dispatch-model (bottom) depending on the aggregation configuration (adapted from Hoffmann et al. [2]) 189
Figure 4.50. Summary of the findings of Section 4.3 (adapted from Hoffmann et al. [2]) 192

Figure 4.51. Upper and lower bounds of the island system model depending on the aggregation configuration 194
Figure 4.52. Upper and lower bounds of the island system model depending on the runtime 195
Figure 4.53. Upper and lower bounds of the self-sufficient building model depending on the aggregation configuration: 196
Figure 4.54. Upper and lower bounds of the self-sufficient building model depending on the runtime 197
Figure 4.55. Increasing distance from over- or underestimating representative values for a rising dimensionality of the considered data 198
Figure 4.56. Left: Lower bounds obtained from temporal aggregation using centroid representation (yellow) and relaxation of the mixed-integer linear program (red) and an upper bound using a linear program with fixed binary variables based on the optimal solution of a preceding aggregated model run (green). Right: Gap depending on runtime for the respective Pareto-optimal combination of bounds 199
Figure 4.57. Decision tree illustrating how to find an optimal temporal aggregation based on the model type and the findings of Section 4.2 and 4.3 203
Figure 4.58. Root-mean-square error (RMSE) of the cost shares and deviation of the total annualized costs from the fully resolved reference case depending on the runtime. The color of the sample points represents the number of total time steps of the respective model run and those with a red edge are Pareto-optimal. The points connected by red and orange arrows are configurations that differ by only one model attribute. 209
Figure H.1. A hypothetical simple energy system 257
Figure H.2. The picture at the top shows the solution space and the optimal value for the optimization problem above. The picture on the bottom left shows the standard simplex algorithm for a

linear program. The picture on the bottom right shows the interior point algorithm for a linear program 258
Figure H.3. The solution space of the mixed-integer linear program is depicted on the left and the single Branch-and-Bound step to determine the solution with linear programs is shown on the right 262
Figure H.4. The graph at the top illustrates the quadratic program at hand, the bottom left and the bottom right picture highlight the impact definiteness on the existence of a single minimum of a quadratic program 266
Figure H.5. A summary of general energy system features whose consideration transforms the program type into another one 269
Figure I.1. Modified sample energy system with an additional battery storage 271
Figure I.2. The general structure of energy system models with variables sorted by time steps 273
Figure I.3. The general structure of energy system models with variables sorted by time steps without complicating constraints 274
Figure I.4. The general structure of aggregated energy system models with variables sorted by clustered time steps 275
Figure I.5. The general structure of aggregated energy system models with variables sorted by clustered time steps without complicating constraints 276
Figure I.6. The general structure of energy system models with variables sorted by periods 277
Figure I.7. The general structure of energy system models with variables sorted by periods 278
Figure I.8. A generally applicable workflow for determining aggregation-induced upper and lower bounds for energy system models 284
Figure I.9. The original optimization problem (top), the upper bound due to equalizing variables and removing redundant constraints (bottom left),

and the lower bound due to removal of the asymmetric constraint and equalizing variables due to symmetry (bottom right) 289
Figure I.10. The adapted energy system comprising two different renewable energy sources 295
Figure I.11. The optimal solution for three time steps (top) and the optimal solution for the aggregated overestimation (bottom left) as well as the optimal solution for the aggregated overestimation with a manipulated fourth equation (bottom right) 296
Figure I.12. The feasible space F and the feasible space based on averaged constraints F 306
Figure I.13. The problem introduced before with lower bounds based on the proposed minimization approach and based on averaging 309
Figure J.1. Trade-Off between fixed and capacity-specific expenditures 315

List of Tables

Table 2.1. Overview over frequently used methods and their possible combinations (taken from Hoffmann et al. [1]) 14
Table 2.2. Configurations of time slices used in the literature 22
Table 2.3. Clustering algorithms applied in the literature 28
Table 2.4. Root-mean-square error of the introduced methods applied the to exemplary solar profile introduced in Figure 2.2 depending on the number of remaining time steps 41
Table 2.5. Pros and cons of the presented major aggregation methods (taken from Hoffmann et al. [1]) 41
Table 3.1. Overview of the discussed indicators and indicator types 89
Table 3.2. Time series to be over- or underestimated in order to receive an upper bound of the fully resolved reference system 100
Table 3.3. Time series to be over- or underestimated in order to receive a lower bound of the fully resolved reference system 100
Table 4.1. Computational resources used for Chapter 4 105
Table 4.2. Techno-economic key features of the considered models 117
Table 4.3. Numerical outliers of the European model 145
Table 4.4. Differences of the self-sufficient building model and the dispatch model with a mathematical relevance 177
Table 4.5. The model run configuration with respect to the total number of time steps considered (adapted from Hoffmann et al. [2]) 178
Table 4.6. Estimations of time series to obtain upper or lower bounds of the island system model 193
Table 4.7. Estimations of time series to obtain upper or lower bounds of the self-sufficient building model 196
Table 4.8. The model runs connected by red and orange arrows: Each configuration differs from the

respective base case by only one attribute, which is further simplified 210
Table A.1. Glossary used for literature research (taken from Hoffmann et al. [1]) 220
Table B.1. Table of methods (taken from Hoffmann et al. [1]) 222
Table I.1. Time series to be over- or underestimated in order to receive an upper bound of the fully resolved reference system 293
Table I.2. Time series to be over- or underestimated in order to receive a lower bound of the fully resolved reference system 301
Table J.1. Unit parameters of the island system derived from Kotzur et al. [20]..... 315
Table J.2. Cost parameters of the self-sufficient building (taken from Hoffmann et al. [2]) 317
Table J.3. Cost parameters of the dispatch model (taken from Hoffmann et al. [2]) 319

List of Symbols

Variables and Parameters

Binary Variable	$b \in \{0,1\}$
Discrete Value of Time Series	x'
Normed Discrete Value of Time Series	x
A-Priori and A-Posteriori Indicator	I_{pre}, I_{post}
Number of Items in a Set	N
Cluster Representative (as Defined)	r
Matrix Path for Dynamic Time Warping	w
Binary Assignment of Candidate i to Cluster j	$z_{i,j} \in \{0,1\}$

Greek Symbols

Minkowski Exponent	γ
Incremental of the Total Number of Time Steps	δ
Mean	μ
Pearson and Spearman Correlation Coefficient	ρ_P, ρ_S
Standard Deviation	σ

Sets and Indices

Set of Cluster Candidates	$d \in D$
Set of Attributes	$a \in A$
Set of Total Time Steps	$s \in S$
Set of Periods	$p \in P$
Set of Inner-Period Time Steps	$t \in T$
Set of Clusters	$k \in C$

Sets of the Distribution-Preserving Algorithm

Cluster's Mean Values	$M_{a,k}$
Sorted Cluster's Mean Values	$\widetilde{M}_{a,k}$
Values of Periods Assigned to Cluster	$X_{a,k}$
Cluster's Sorted Value Distribution	$\widetilde{X}_{a,k}$
Optimally Assigned Profile	$Y_{a,k}$
Stepwise Mean Values of the Distribution	$\widetilde{Y}_{a,k}$

Energy System Model (Vectors and Matrices)

General Design or Operation Variable Vector	x
Cost Vector	c
Equation Constraint Matrix (General)	A
Equation Constraint Matrix (TI Variables, TD)	$\mathrm{A_t}$
Equation Constraint Matrix (TD Variables, TD)	$\mathrm{B_t}$
Equation Constraint Matrix (Time-Linked, TD)	$\mathrm{BL_t}$
Equation Constraint Vector	b
Inequality Constraint Matrix (General)	C
Inequality Constraint Matrix (TI Variables, TD)	$\mathrm{C_t}$
Inequality Constraint Matrix (TD Variables, TD)	$\mathrm{D_t}$
Inequality Constraint Matrix (Time-Linking, TD)	$\mathrm{DL_t}$
Inequality Constraint Vector (General)	d
Lower Inequality Constraint Vector	dl
Lower Time-Linked Inequality Constraint Vector	dll
Upper Inequality Constraint Vector	du
Upper Time-Linked Inequality Constraint Vector	dlu
Quadratic Cost Matrix	Q
Weight Factor for Aggregated Time Step	w

Miscellaneous

Distance	dist
Optimality Gap	gap
Rank of an Ordered Set	rg
Mean Average Error	MAE
Root-Mean-Square Error	RMSE
Root-Mean-Square Error of the Duration Curve	$\mathrm{RMSE_{DC}}$
Sum of Squared Errors	SSE

List of Abbreviations

CHP	Combined Heat and Power
FINE	Framework for Integrated Energy System Assessment
LP	Linear Program
MILP	Mixed-Integer Linear Program
QP	Quadratic Program
TAC	Total Annual Cost
tsam	Time Series Aggregation Module

1. Motivation

1.1. Drivers of Model Complexity

“Due to the climate change caused by anthropogenic CO_2 emissions resulting from the burning of fossil fuels, a major turnaround in the fields of energy supply and consumption is an increasing necessity. Key aspects of addressing this challenge are the integration of renewable energy sources into existing energy systems, and a closer coupling of energy forms and sectors [7].

The evolution of the energy sector has been accompanied by a consistent effort to model, predict, and plan its development. Early attempts to forecast future energy demands can be traced back to the 1950s and constituted simple, assumption-based scenarios [8]. Another theoretical foundation for modern energy system models is the principle of peak-load-pricing first described by Boiteux in 1949 [9] (English translation in 1960 [10]) and Steiner in 1957 [11]. This approach distinguishes between capacity and operation costs of facilities producing non-storable goods. Thus, it applies to many simple energy systems with a single good (commodity), e.g., electricity, which has led to the development of approaches to solve simple capacity expansion planning problems with the annual load duration curve as shown by Sherali et al. [12]. Three factors are of particular significance as key drivers for the early progress of energy system modelling:

- The need for security of supply to be provided for the growing demand by governmental quasi-monopolistic institutions through the 1970s, as well as the building of a reliable connection between a more competitive energy sector and later public interest [13, 14].
- The progress of computational resources that enabled more complex models [15].
- The integration of non-dispatchable technologies, such as most of the renewable energy sources and their impact on energy pricing; an effect that has constantly gained importance and which was first described in 1982 [16].

Ever since the first energy system models were developed during the 1970s and 1980s [15, 17], which were based on optimizations rather than just simulations, two major options arose for their developers, namely whether to focus on economic mechanisms,

sometimes described as a top-down approach, or on the technical dimension, usually known as a bottom-up one [18, 19]. Amongst the bottom-up frameworks this thesis focuses on, a vast number of approaches exist for modeling the different dimensions of energy systems, including methodologies such as optimizations and simulations [15, 18, 19]. With respect to the scope of energy system models, two fundamental dimensions can be delineated: A spatiotemporal and a techno-economic one. The spatiotemporal dimension comprises the setting of input data that a model is intended to incorporate. The spatial sub-dimension is focused on the number of regions and their connections to each other, as energy systems on a national or even larger scale usually face the challenge of taking energy transmission between different regions into account. The temporal sub-dimension is divided into two aspects, namely temporal resolution, often referred to as time steps, and the overall time horizon [15], which also concerns questions of storage modeling [20-26] as well as the linking of dynamic processes [27-29] and investment dynamics [30, 31]. In contrast, the techno-economic dimension deals with the question as to how the components are represented in the model and whether their design and/or operation are optimized or if their operational behavior is simply simulated, how they are mathematically represented and if the impact of supply and demand on energy prices is dynamically modeled or not [19]. Each of the dimensions listed above drives the overall complexity of energy system models, while the spatiotemporal resolution also affects the techno-economical one directly, e.g., the temporal resolution also limits the (technical) operational exactness of components in the energy system.

Figure 1.1 illustrates the classification into top-down and bottom-up models [19, 27, 32-34], top-down model types [35, 36] and bottom-up model dimensions [19].

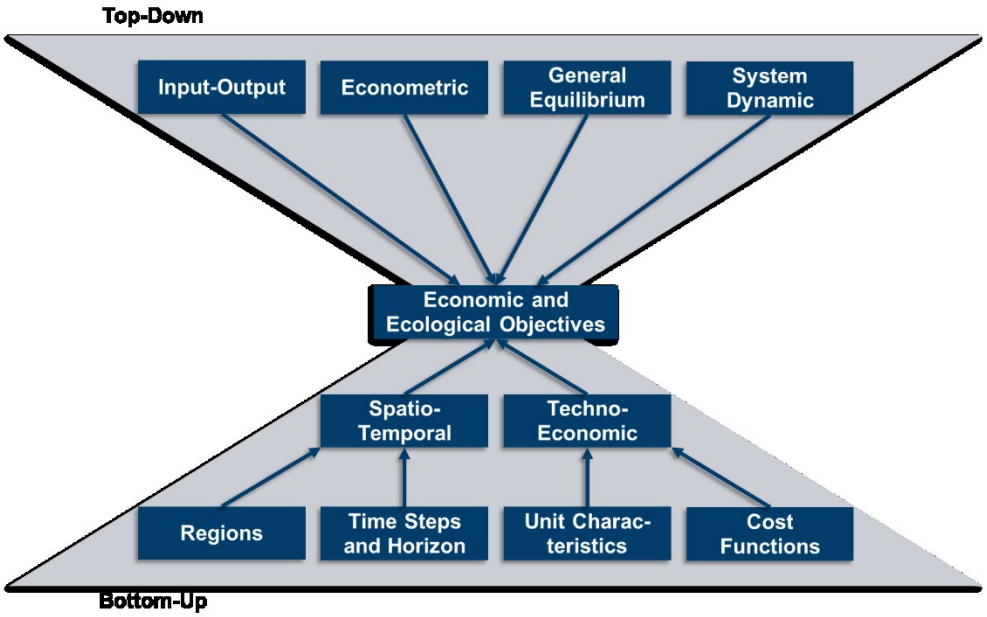

Figure 1.1. Classification of energy system models, the sub-dimensions of bottom-up models and the scope of the thesis (taken from Hoffmann et al. [1])

1.2. Motivation and Scope of the Thesis

Although Moore's law held true for approximately 40 years [37, 38] and there have been significant speed-ups of the branch-and-bound algorithms used for solving big mixed integer linear programs (MILPs) such as those used in energy system optimization models [39], a decelerating increase of transistor density could be observed in recent years [40]. On the other hand, liberalization, decentralization and an increasing volatility in energy generation [41] are leading to more complex applications for energy system models. Therefore, the recent number of publications dealing with aggregation methods in energy system models illustrates the fact that many application cases are too complex to be overcome solely by computational power and mathematically equivalent transformations.

The temporal sub-dimension in energy system models is crucial for the implementation of storages and the description of system dynamics, which is especially important for energy system models considering a high share of intermittent renewable energy sources [42-47]. This applies for both single-node and multi-node energy system models, and the group of aggregation methods employed to tackle this issue is broad and diverse. Hence, this work addresses the issue of systematically categorizing the methods and

their assumptions, as well as recent trends and the general shortcomings in the development of temporal aggregation methods. Based on this overview, this new computationally efficient temporal aggregation approaches are developed by combining, modifying and extending existing methods to tackle the presented shortcomings. […]

As the input time series for constrained bottom-up energy system models are often not only auto-correlated, i.e. to some extent periodic, but also cross-correlated, an aggregation based on time series can be applied in multiple ways. This work is exclusively focusing on the aggregation of time series based on their auto-correlation, i.e. the reduction of the number of time steps, e.g., by representing a whole year of data by a small number of typical days." (Hoffmann et al. [1]) This is represented by the gray arrow in Figure 1.2 and will be defined as time series aggregation in the narrow sense. As shown, bottom-up energy system models can be interpreted as network graphs with a time-discrete operation schedule. Accordingly, each time step can be interpreted as a layer of the respective graph. Therefore, a reduction of the number of time steps reduces the number of graph layers and ultimately the number of constraints and variables considered in these graphs.

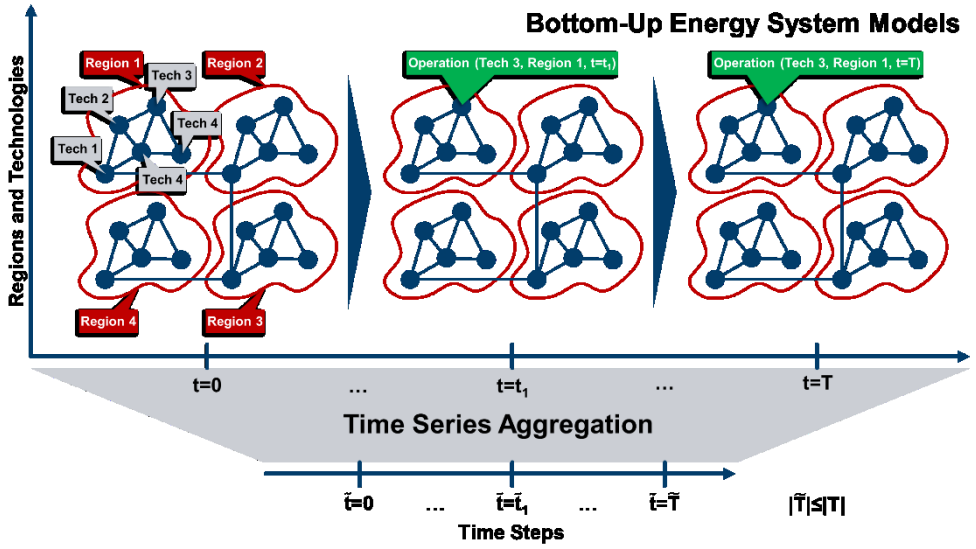

Figure 1.2. Time series aggregation defined as the reduction of the number of time steps considered in bottom-up energy system models

1.3. Structure of the Thesis

In order to systematically assess the potential of temporal aggregation methods and contribute to their accuracy and reliability, this work aims at developing new aggregation techniques and comparing them to existing ones by applying them on substantially different energy system models.

The remainder of this work is structured as depicted in Figure 1.3. In Chapter 2, the current state of temporal aggregation methods for energy system modeling is reviewed and promising trends are identified.

In Chapter 3, the most promising temporal aggregation techniques are isolated and systematically extended based on well-known shortcomings of the existing methods. Further, the methods were implemented in a freely combinable way, which theoretically allows for creating several dozens of user-specified methods.

Chapter 4 consists of four main subchapters. Section 4.1 introduces the models used for validating the superiority of the methods developed in Chapter 3. In order to minimize the impact of specific model structures on the evaluation of the applied aggregation techniques, the models are intentionally very different with respect to modeling scope and application case.

In Section 4.2, the methods developed in Chapter 3 are cross-combined and applied to the models introduced in Section 4.1 resulting in a total number of 1836 different model runs.

Section 4.3 and Section 4.4 focus on additional research questions and options offered by temporal aggregation techniques that are not completely covered by the sensitivity analysis in Section 4.2. Therefore, Section 4.3 addresses the question of the impact of the period length chosen for aggregation depending on certain model features. Additionally, Section 4.4 assesses the potential of temporal aggregation techniques for determining upper and lower bounds to the fully resolved energy system model in order to quantify the error made by temporal aggregation if the reference model is not solvable due to its size.

The results of Chapter 4 are critically discussed in Section 4.5 and the work as well as its main conclusions are summarized in Chapter 5.

All developments are moreover implemented in the python-based time series aggregation module (**tsam**) [48] and can be directly applied in the Framework for Integrated Energy System Assessment (**FINE**).

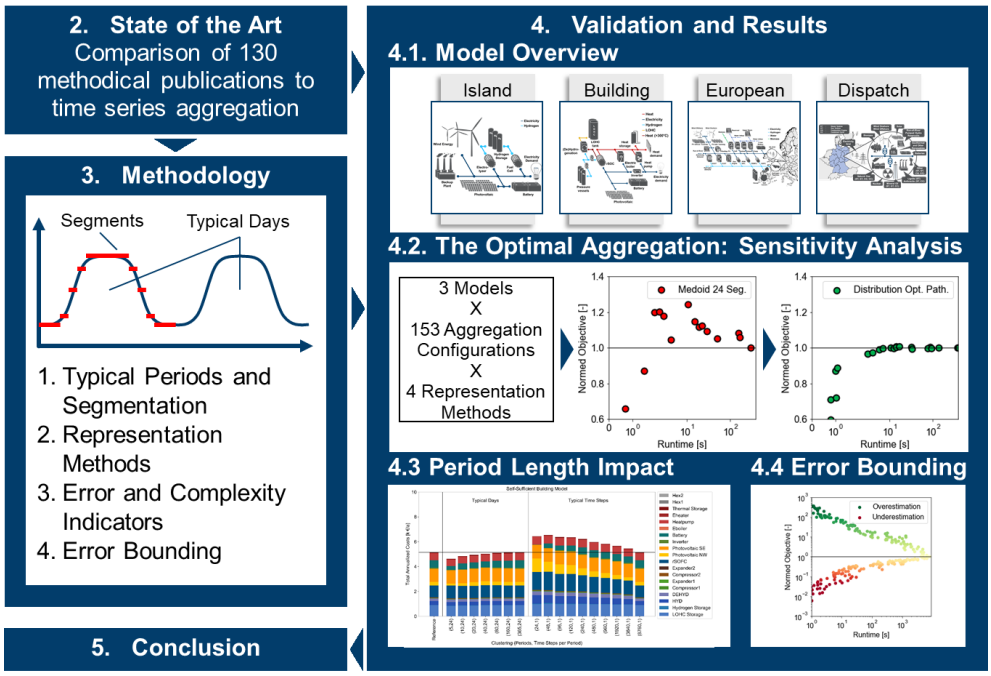

Figure 1.3. Structure of the thesis

2. State of the Art

2.1. Methodology and Structure of Chapter 2

The following chapter focuses on the review of “temporal aggregation methods in bottom-up energy system optimization models that include capacity expansion planning, as well as unit commitment and have constantly emerged and evolved since the late 1970s and 1980s [15, 17]. Among the early energy system models, one group focuses on long-term system planning and has usually only one time step per year such as LEAP [49], EFOM [50] and BESOM [51], which are not subject to aggregation techniques and thus neglected in the following. The temporal dimension of the other major group of early bottom-up energy system models such as TIMES [52-55], its predecessor MARKAL [56] MESSAGE [18, 57], IKARUS [15] and PERSEUS [58] is based on time slice formulations (in the case of PERSEUS called “time slots”), which are explained in more detail in Section 2.2.2.1. Although the long-term planning models with only one time step per year were consecutively combined with models with a higher temporal resolution as it is the case for TIMES [52-55] as a combination of MARKAL [56] and EFOM [50], the time slice approach, which is based on the modeler’s experience only, remained unchanged for decades. With the first approaches to classify and group demand curves using unsupervised learning techniques which could be traced back to 1999 [59], new techniques for defining the temporal dimension of energy system models arose. To the best of the author’s knowledge, this was first done manually in 2008 [60] and by using a standard clustering algorithm in 2011 [61]. In order to investigate the rapid and manifold development of complex temporal aggregation methods based on feature-based grouping in detail, the start year for the literature review was set to 1999 and the literature research was stopped in July 2019. To avoid a bias towards the new methods based on unsupervised learning techniques, publications within the relevant time interval, which are based on long-existing and constantly evolving frameworks such as TIMES, are also considered.

2.1.1. Methodology of the Literature Research

With respect to a systematic and keyword-based search for temporal aggregation methods, the major challenge was the inconsistent naming of the applied methods. Furthermore, the majority

of publications did not explicitly address the comparison of the different aggregation methods. Instead, the temporal aggregation methods were often simply applied. Therefore, terms such as time series aggregation, typical days, complexity reduction or clustering, which are crucial for identifying temporal aggregation methods, only appear in a minority of publications as keywords. Moreover, a number of terms was found to be inconsistently or redundantly used by different research communities. Examples for this are the terms “representative days” and “typical days”. Therefore, a heuristic approach was used as starting point that focused on a search for methods based on citations of earlier works.

Simultaneously, terms that appeared in multiple publications were considered to be keywords and, to overcome the problem of co-citation clusters [62] with own terms, these newly defined keywords were used for an additional search on the internet. The keywords used for the literature research that arose from this analysis are listed in Appendix A along with their definitions and terms that are synonymously used in the literature.

Building upon the analyzed literature and the basic features of a time series aggregation process introduced by Nahmmacher et al. [63],Kotzur et al. [48] and Schütz et al. [64], the table of methods in Appendix B was derived for categorizing and comparing the different methods. Moreover, the methods were also investigated based on their capacity to link all time steps across the original time horizon, which enables seasonal storage, and their premise to approximate the duration curve or the unsorted time series. This ultimately leads to the structure of the following chapters.

2.1.2. Structure of the Review

From the categorization in Figure 2.1, the methods presented in Section 2.2 are derived as the basic aggregation methods, as well as Miscellaneous Methods that cannot be clearly categorized. As aggregation methods commonly suffer from certain drawbacks, a number of methods exist to preserve additional information of the original input time series, which are presented in Section 2.3. Along with both, Section 2.2 and 2.3, the individual trends and possible reasons for them are discussed in the Sections 2.2.5 and 2.3.3. The major results of the review are concluded in Section 2.4.

Figure 2.1 illustrates the structure of the following sections by highlighting comparable ideas with the same colors and steps to be taken or decisions to be made for applying an aggregation method with blue arrows. The grey backgrounds distinguish the basic aggregation process presented in Section 2.2 from the preservation of additional information of the original time series presented in Section 2.3.

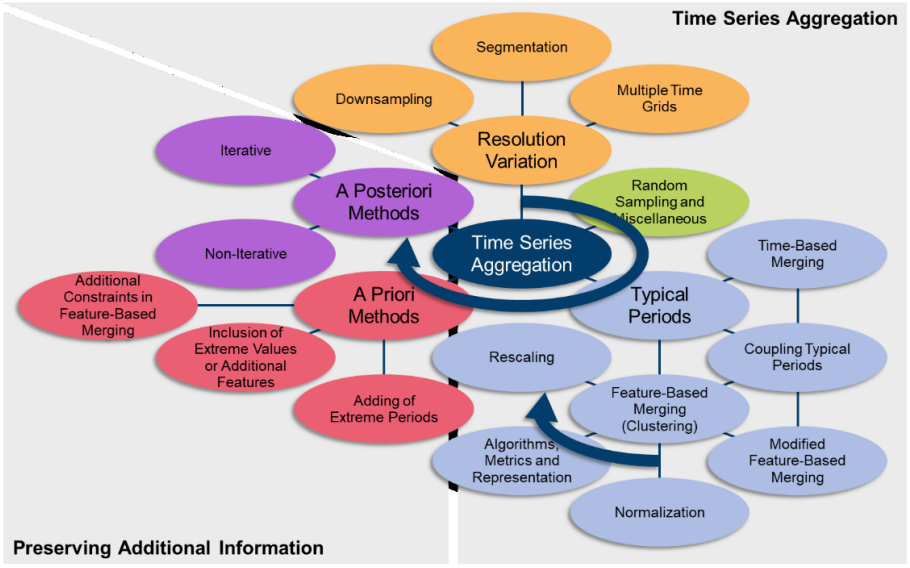

Figure 2.1. Mind map of the methods presented in the review, their methodological connection (marked by same colors) and decisions to be made or steps to be taken when applying time series aggregation (taken from Hoffmann et al. [1])

Along with the introduction of a new aggregation method, the impact of this method on potential input data is visualized. For this, a time series for photovoltaic capacity factors is used, which consists of 8760 hourly time steps for one year, and is illustrated in Figure 2.2." (Hoffmann et al. [1]) Furthermore, the aggregation-induced deviation from the original time series is quantified using the root-mean-square error (RMSE), which is explained in detail in Section 3.3.1.

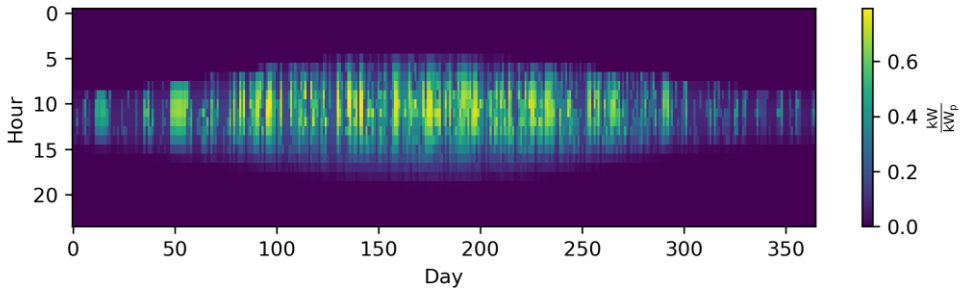

Figure 2.2. One year of hourly resolved photovoltaic capacity factors simulated with PV-Lib [65] (RMSE=0) (taken from Hoffmann et al. [1])

2.2. Time Series Aggregation

“The following section deals with the general concept of time series aggregation. For the mathematical examinations of the following section, the nomenclature as defined in the List of Symbols is used.

The input data D usually consists of one time series for each attribute, i.e., $\mathrm{D} = \mathrm{A} \times \mathrm{S}$. The set of attributes A describes all types of parameters that are known beforehand for the energy system, such as the capacity factors of certain technologies at certain locations or demands for heat and electricity to be satisfied, which is exemplary depicted in Figure 2.3.

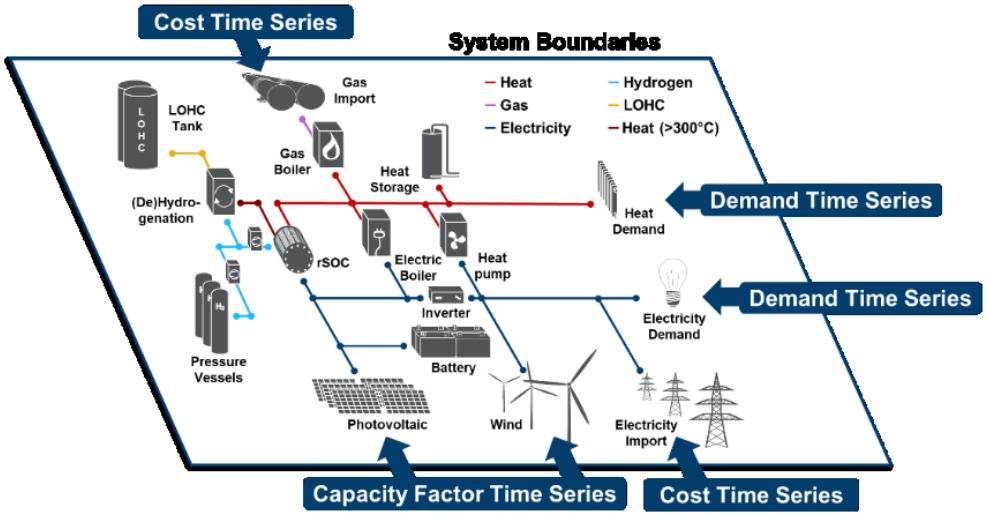

Figure 2.3. Set of time series entering the energy system boundaries and defining constraints that the energy system model must satisfy

The set of time steps describes the shape of the time series itself, i.e., sets of discrete values that represent finite time intervals, e.g., 8760 time steps of hourly data to describe a year. For all methods presented in the following, it is crucial that the time series of all attributes have identical lengths and temporal resolution. The possible shape of this highly resolved input data is shown Figure 2.4.

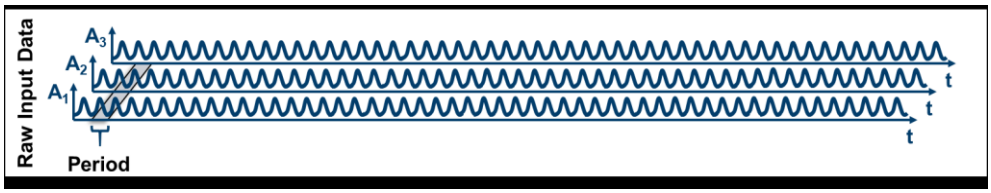

Figure 2.4. Exemplary set of time series (adapted from Hoffmann et al. [1])

One approach for aggregating the input time series is to merge multiple time series of attributes with a similar pattern. However, this can only be performed for attributes describing similar units (e.g., the capacity factors of similar wind turbines) or similar customer profiles (i.e., the electricity demand profiles of residential buildings). As this approach is often chosen to merge spatially distributed but similar technologies, it is not considered as time series aggregation in the narrow sense, but as spatial or technological aggregation, as the number of time steps is not reduced in these cases. This is illustrated in the right field in Figure 2.5 and some examples from the literature are given in Appendix C.

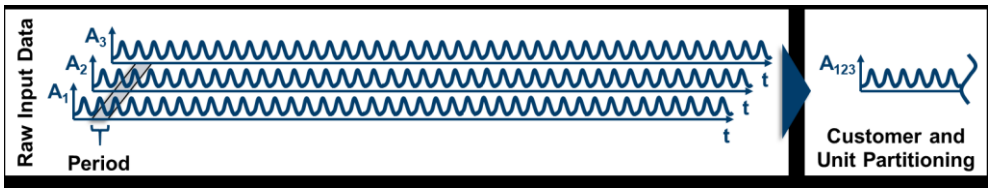

Figure 2.5. Reduction of the number of time series using customer and unit partitioning (adapted from Hoffmann et al. [1])

Time series aggregation, as it is understood in this work, is the aggregation of redundant information within each time series, i.e., in the case of discrete time steps, the reduction of the overall number of time steps. This can be done in several ways. One way of reducing the number of time steps, as is shown in the lower field of Figure 2.6, is the merging of adjacent time steps. This can either be done in a regular manner, e.g., every two time steps are represented by one larger time step (downsampling) or in an irregular manner according to, e.g., the gradients of the time series (segmentation). A third possible approach is to individually variate the temporal resolution for each attribute, i.e., using multiple time grids, which could also be done in an irregular manner, as pointed out by Renaldi et al. [66]. These three methods directly decrease the temporal resolution and they will be presented in Section 2.2.1.

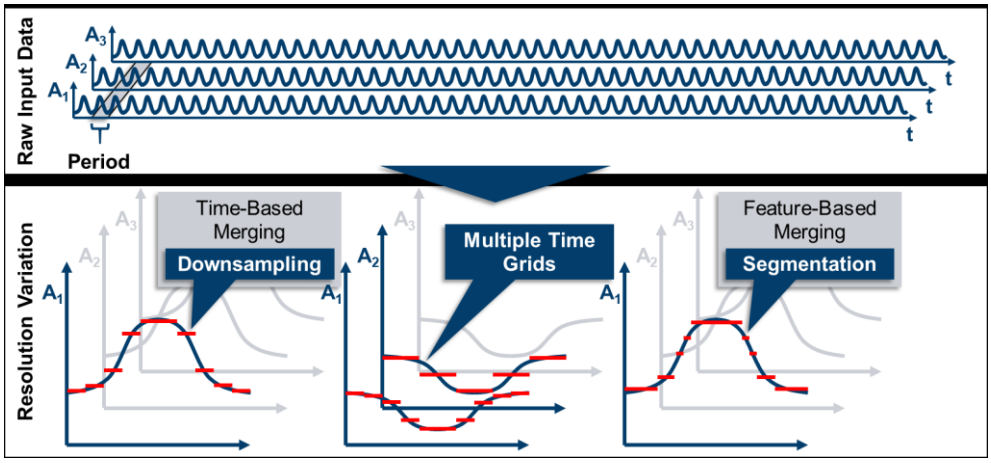

Figure 2.6. Reduction of the number of time steps using resolution variation (adapted from Hoffmann et al. [1])

Another approach for time series aggregation is based on the finding that many time series exhibit a periodic pattern, i.e., time series for solar irradiance have a strong daily pattern. In the case of perfect periodicity, a time series could thus be represented by one period and its cardinality without the loss of any information. Based on this idea, time series are often divided into periods as shown in the middle of Figure 2.7. As the periods are usually not constant throughout a year (e.g., the solar irradiance is higher in the summer than in the winter), the periods can either be merged based on their position in the calendar (time slices and averaging) or based on their similarity (clustering), as shown at the bottom of Figure 2.7. These methods will be described in Section 2.2.2. Moreover, information about the order in which the periods appear in the original time series must be preserved to be able to model temporal linkages such as the states of charge of storage technologies, which will be referred to as “intertemporal constraints” in the following. This is discussed in Section 2.2.2.3.

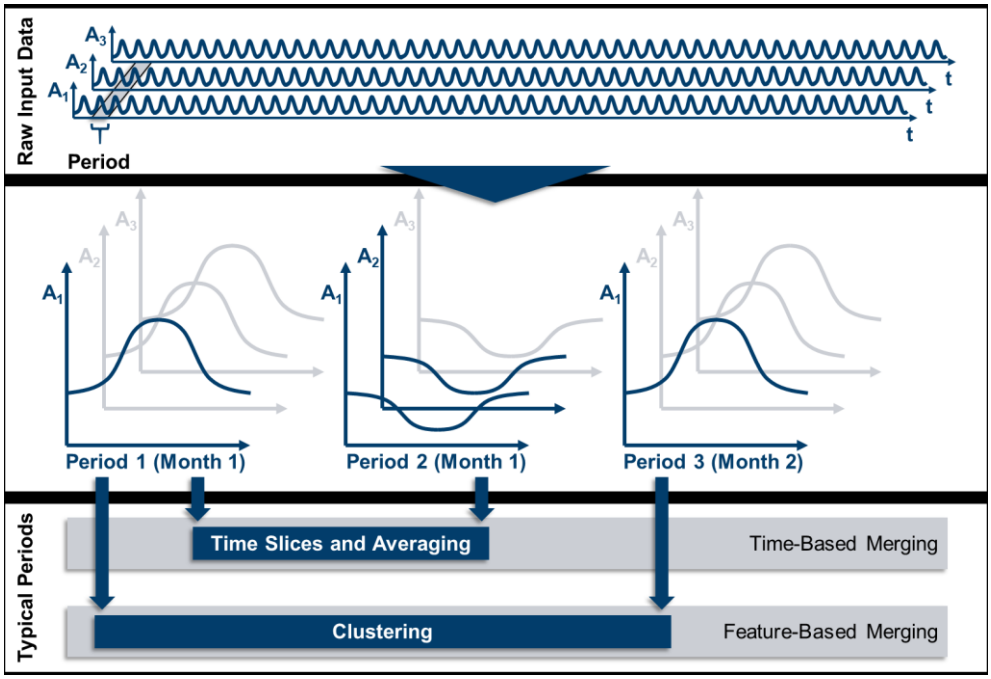

Figure 2.7. Reduction of the number of time steps using typical periods (adapted from Hoffmann et al. [1])

The temporal resolution can also be reduced within the periods. This leads to Table 2.1, which illustrates the possible combinations of the methods presented above. Here, each method from column one could be combined with each method from column two. The methods in the table dealing with Resolution Variation are described in Sections 2.2.1.1 and 2.2.1.2. The method of using Multiple Time Grids explained in Section 2.2.1.3 is neglected in the table due to its seldom usage in energy system models. The methods concerning Typical Periods are described in the Sections 2.2.2.1 and 2.2.2.2. Moreover, a small number of methods based on Random Sampling and Miscellaneous Methods exist, which cannot be properly categorized in Table 2.1. However, they will be described in Sections 2.2.3 and 2.2.4. In this way, Table 2.1 mirrors the structure of the Section 2.2.

Table 2.1. Overview over frequently used methods and their possible combinations (taken from Hoffmann et al. [1])

	Resolution Variation	Typical Periods
Time-Based	Downsampling	Time Slices and Averaging
Feature-Based	Segmentation	Clustering

In the following, methods that merge time steps or periods in a regular manner, i.e., based on their position in the time series only, will be referred to as time-based methods; whereas aggregation based on the time steps' and periods' values will be called feature-based. In this context, features refer not only to statistical features as defined by Nanopoulos et al. [67], but in a broader sense to information inherent to the time series, regardless of whether the values or the extreme values of the time series themselves or their statistical moments are used [68].

2.2.1. Resolution Variation

The simplest and most intuitive method for reducing the data volume of time series for energy system models is the variation of the temporal resolution. Here, three different procedures can be distinguished.

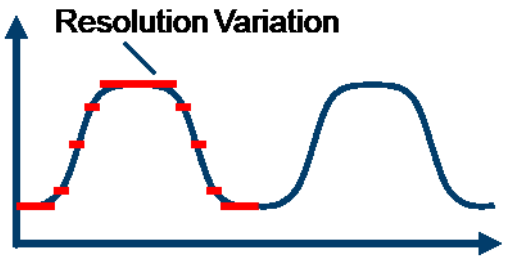

2.2.1.1. Downsampling

Downsampling is a straightforward method for reducing the temporal resolution by representing a number of consecutive discrete time steps by only one (longer) time step, e.g., a time series for one year of hourly data is sampled down to a time series consisting of 6 h time steps. Thus, the number of time steps that must be considered in the optimization is reduced to one sixth, as demonstrated by Pfenninger et al. [43]. As the averaging of consecutive time steps leads to an underestimation time series' variance, capacities for renewable energy sources tend to be underestimated because their intermittency is especially weakly represented [43]. Figure 2.8 shows the impact of downsampling the PV profile from hourly resolution to 6 h time steps, resulting in one sixth of the number of time steps. In comparison to the original time series, the underestimation of extreme values is remarkable. This phenomenon also holds true for sub-hourly time steps [44, 69, 70] and, for instance, in the case of an energy system model containing a PV cell and a battery for a residential building, this not only has an impact on the built capacities, but also on the self-consumption rate [44, 70]. For wind time series, the impact is comparable [69]. As highlighted by Table 2.1, downsampling can also be applied to

typical periods. To the best of the author's knowledge, this was initially evaluated by Yokoyama et al. [71] with the result that it could be a crucial step to resolve highly complex problems at least close to optimality. The general tendency of downsampling to underestimate the objective function was shown in a subsequent work by Yokoyama et al. [72] and the fact that this is not necessarily the case when combined with other methods in a third publication [73]. Other works that deal with combined approaches will be discussed in Section 2.2.2.1.3.

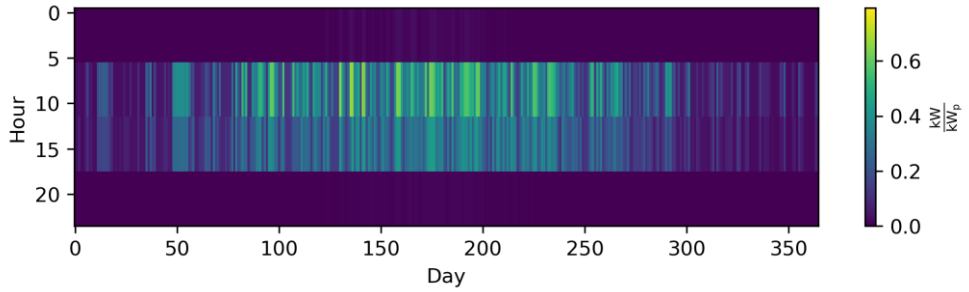

Figure 2.8. The time series of photovoltaic capacity factors downsampled to 1460 6h time steps (RMSE=0.1295) (taken from Hoffmann et al. [1])

2.2.1.2. Segmentation

In contrast to downsampling, segmentation is a feature-based method of decreasing the temporal resolution of time series with arbitrary time step lengths. To the best of our knowledge, Mavrotas et al. [60] were the first to present an algorithm for segmenting time series to coarser time steps based on ordering the gradients between time steps and merging the smallest ones. Fazlollahi et al. [74] then introduced a segmentation algorithm based on k-means clustering in which extreme time steps were added in a second step. In both works, the segmentation methods were applied to typical periods, which will be explained in the following sections. Bungener et al. [75] used evolutionary algorithms to iteratively merge the heat profiles of different units in an industrial cluster and evaluated the different solutions obtained by the algorithm with the preserved variance of the time series and the sum of zero-flow rate time steps, which indicated that a unit was not active. Deml et al. [76] used a similar, but not feature-based approach as Mavrotas et al. and Fazlollahi et al. [60, 74] for the optimization of a dispatch model. In this approach, the temporal resolution of the economic dispatch model was more reduced the further time steps lay in the future, following a discretized exponential function. Moreover, they

compared the results of this approach to those of a perfect foresight approach for the fully resolved time horizon and a model-predictive control and proved the superiority of the approach, as it preserved the chronology of time steps. This was also pointed out in comparison to a typical periods approach by Pineda et al. [77], who used the centroid-based hierarchical Ward's algorithm [78] with the side constraint to only merge adjacent time steps. Bahl et al. [79], meanwhile, introduced a similar algorithm as Fazlollahi et al. [74] inspired by Lloyd's algorithm and the partitioning around medoids algorithm [80, 81] with multiple initializations. This approach was also utilized in succeeding publications [82, 83]. In contrast to the approach of Bahl et al. [79], Stein et al. [84] did not use a hierarchical approach, but formulated a mixed-integer linear program, in which not only extreme periods could be excluded beforehand, but also the grouping of too many adjacent time steps with a relatively small but monotone gradient could be avoided. The objective function relied on the minimization of the gradient error, similar to the method of Mavrotas et al. [60]. Recently, Savvidis et al. [85] investigated the effect of increasing the temporal resolution at times of the zero-crossing effect, i.e., at times when the energy system switches from the filling of storage components to withdrawing and vice versa. This was compared to the opposite approach, which increased resolution at times without zero crossing. They also arrived at the conclusion that the use of irregular time steps is effective for decreasing the computational load without losing substantial information. Figure 2.9 shows advantages of the hierarchical method proposed by Pineda et al. [77] compared to the simple downsampling in Figure 2.8. The inter-daily variations of the PV profile are much more accurately preserved choosing 1460 irregular time steps compared to simple downsampling with the same number of time steps shown in Figure 2.8, which is also mirrored by the smaller root-mean-square error.

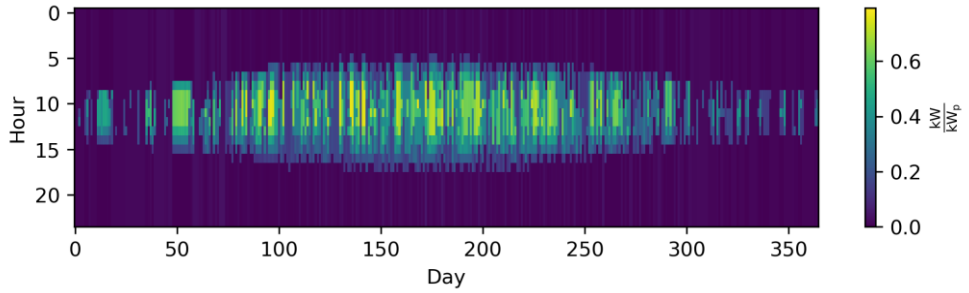

Figure 2.9. The time series of photovoltaic capacity factors segmented to 1460 time intervals using hierarchical merging of adjacent time steps based on centroids as proposed by Pineda et al. [77] (RMSE=0.0388) (taken from Hoffmann et al. [1])

2.2.1.3. Multiple Time Grids

The idea of using multiple time grids takes into account that different components that link different time steps to each other, such as storage systems, have different time scales on which they operate [20, 21, 86]. For instance, batteries often exhibit daily storage behavior, whereas hydrogen technologies [20, 21] or some thermal storage units [86, 87] have seasonal behavior, unless electrolyzers are used to take up or shed loads. In this case, the underlying storage cycle will remain seasonal, whereas the electrolyzer behaviour may be extremely dynamic. Still, seasonal storage is expected to be accurately modeled with a smaller number of coarser time steps. Renaldi et al. [66] applied this principle to a solar district heating model consisting of a solar thermal collector, a backup heat boiler and a long- and a short-term thermal storage system. They achieved the optimal tradeoff between the computational load and accuracy for modeling the long-term thermal storage with 6 h time steps and the remaining components with hourly time steps. It is important to highlight that the linking of the different time grids was achieved by applying the operational state of the long-term storage to each time step of the other components if they lay within the larger time steps of the long-term storage. However, increasing the step size even further led to an increase in calculation time, as the operational flexibility of the long-term storage became too stiff and the benefit from reducing the number of variables of the long-term storage decreased. Thus, this method requires knowledge about the characteristics of each technology beforehand.

2.2.2. Typical Periods

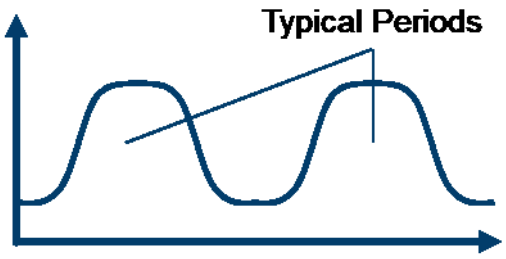

The aggregation of time series to typical periods is based on the idea that energy systems behave similarly under similar external conditions, e.g., similar energy demands and capacity factors of renewable energy sources [88]. Typical periods can consist of single time steps, which are called “system states” [25, 88-91] “snapshots” [68, 92] or “external operation conditions” [93] in the literature or periods containing more than one time step, e.g., “typical days” or “representative days” that were used by the majority of authors. In the context of control engineering, the term “system states” is especially misleading, as the state of a system not only depends on external parameters such as capacity factors and demands to be fulfilled, but also on storage levels and other endogenous state variables. Therefore, the term “system state” in discrete energy system models is only equivalent to time steps if the system is not temporally coupled, i.e., neither state variables, nor intertemporal constraints linking them with each other exist. The following will refer to “typical time steps” if the typical period consists of only one time step. If not stated differently in the following, the authors used typical days. However, longer periods such as typical (also called representative) weeks ([48, 94-96] (“typical weeks”), [97-100] (“representative weeks”)) also exist. This work only makes further use of the word “representative” in the context of clustering, as the representative of each cluster [101] is then interpreted as the new typical period. Analogously to the previous section, a number of time-based and feature-based methods exist that will be explained in the following.

2.2.2.1. Time-Based Merging

Time-based approaches of selecting typical periods rely on the modeler’s knowledge of the model. This means that those characteristics are included that are expected to have an impact on the overall design and operation of the energy system model. As will be shown in the following, this was most frequently done for typical days, although similar approaches for typical weeks [94] or typical hours (i.e., typical time steps) [102] exist. As pointed out by Schütz

et al. [64], the time-based selection of typical periods can be divided into month-based and season-based methods, i.e., selecting a number of typical periods from either each month or from each season. However, we divide the time-based methods in consecutive typical periods (averaging) and non-consecutive typical periods with a regular pattern (time slices).

2.2.2.1.1. Averaging

The method that is referred to as averaging in the following, as per Kotzur et al. [48], focuses on aggregating consecutive periods into one period. To the best of our knowledge, this idea was first introduced by Marton et al. [103], who also introduced a clustering algorithm that indicated whether a period of consecutive typical periods of Ontario's electricity demand had ended or not. In this way, the method was capable of preserving information about the order of typical days. However, it was not applied to a specific energy system model. In contrast to that method, one typical day for each month at hourly resolution, was used by Mavrotas et al. [60], Lozano et al. [104], Schütz et al. [105] and Harb et al. [106] resulting in 288 time steps. Although thermal storage systems have been considered in the literature [104-106], they were constrained to the same state of charge at the beginning and end of each day. The same holds true in the work of Kotzur et al. [48]. Here, thermal storage, batteries and hydrogen storage were considered and the evaluation was repeated for different numbers of averaged days. Buoro et al. [94] used one typical week per month to simulate operation cycles on a longer time scale. Kools et al. [107], in turn, clustered eight consecutive weeks in each season to one typical day with 10 minute resolution, which was then further reduced to 1h time steps. The same was done by Harb et al. [106], who compared twelve typical days of hourly resolution to time series with 10 min. time steps and time series reduced to 1h time steps. This illustrates that both, downsampling and averaging, can be combined. Voll et al. [108] aggregated the energy profiles even further with only one time step per month. To account for the significant underestimation of peak loads, the winter and summer peak loads were included as additional time steps. Figure 2.10 illustrates the impact of representing the original series by twelve monthly averaged consecutive typical days, i.e. 288 time steps instead of 8760 and the corresponding root-mean-square error.

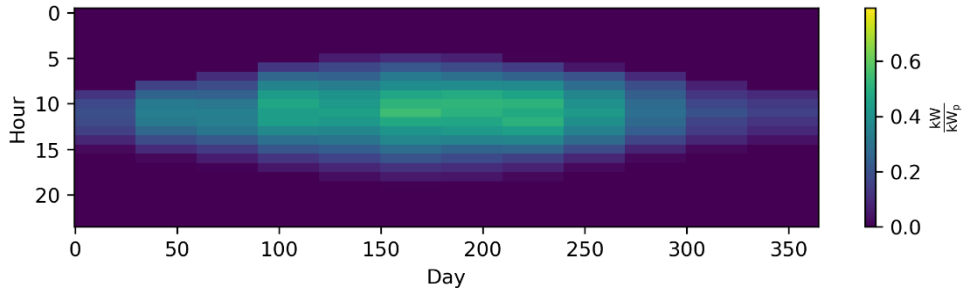

*Figure 2.10. The time series of photovoltaic capacity factors represented by twelve monthly averaged periods as used in other studies [60, 104, 105] and reproduced by Kotzur et al. [48] using the python package **tsam** [48] (i.e., 288 different time steps) (RMSE=0.1126) (taken from Hoffmann et al. [1])*

2.2.2.1.2. Time Slices

To the best of our knowledge, the idea of time slices was first introduced by the MESSAGE model [15, 57] and the expression was reused for other models, such as THEA [109], LEAP [110], OSeMOSYS [111], Syn-E-Sys [112] and TIMES [54, 55]. The basic idea is comparable to that of averaging, but not based on aggregating consecutive periods. Instead, time slices can be interpreted as the general case of time-based grouping of periods. Given the fact that electricity demand in particular not only depends on the season, but also on the weekday, numerous publications have used the time slice method for differentiating between seasons and amongst days. In the following, this approach is referred to as time slicing, although not all of the cited publications explicitly refer to the method thus. Instead, the method is sometimes simply called “representative day”, “typical days”, “typical daily profiles”, “typical segment”, “time slot” or “time band”. However, the term “time slice” is used by the majority of authors. The most frequent distinction is made between the four seasons or between summer, winter and mid-season, but also other distinctions such as monthly, bi-monthly, bi-weekly or others can be found. Within this macro distinction, a subordinate distinction between weekdays and weekend days, weekdays, Saturdays and Sundays or Wednesdays, Saturdays and Sundays can be found.” (Hoffmann et al. [1]) Table 2.2 depicts the configurations of time slices that can be found in the literature.

Table 2.2. Configurations of time slices used in the literature

Publication	Referred to as	Seasonal			Weekly			
		Four Seasons	Summer, Winter, Mid-Season	Monthly, Bi-Monthly, Weekly or Other	Weekdays and Weekend days	Weekdays, Saturdays and Sundays	Wednesdays, Saturdays and Sundays	None/ Other
[109]	Time slices	✖					✖	
[110]		✖					✖	
[113]		✖				✖		
[114]				✖				✖
[111]		✖			✖			
[115]		✖				✖		
[116]		✖						✖
[42]		✖						✖
[117]		✖						✖
[112]		✖			✖			
[45]		✖						✖
[57]			✖		✖			
[72]	Representative days		✖					✖
[118]			✖					✖
[119]			✖					✖
[118]			✖					✖
[120]			✖					✖
[71]			✖					✖
[121]				✖	✖			
[122]			✖					✖
[123]				✖	✖			
[60]	Typical days		✖					✖
[124]				✖				✖
[125]		✖				✖		
[126]				✖	✖			
[127]			✖					✖
[128]			✖					✖
[129]				✖				✖
[130]			✖					✖
[131]		✖			✖			
[22]	Typical daily profiles	✖			✖			
[23]		✖			✖			
[132]	Segments			✖	✖			
[58]	Time slots	✖						✖
[133]	Time bands		✖		✖			

“In contrast to the normal averaging, each time slice does not follow the previous one, but is repeated in a certain order a certain number of times (e.g., five spring workdays are followed 13 times by two weekend spring days before the summer periods follow). This is especially important when seasonal storages are modeled

[22, 23, 111], which will be explained in greater depth in Section 2.2.2.3. As a visual inspection of Figure 2.10 and Figure 2.11 shows, the time slice method relying on the distinction between weekdays and seasons is not always superior to a monthly distinction. The reason for this is that some input data such as the PV profile from the example have no weekly pattern and spacing the typical periods equidistantly is the better choice in this case if no other input time series (such as, e.g., electricity profiles) must be taken into account. Thus, the choice of the aggregation method should refer to the pattern of the time series considered especially important for the energy system model. For instance, the differences between week- and weekend days is likely more important to an electricity system based on fossil fuels and without storage technologies, whereas an energy system based on a high share of renewable energy sources is more affected by seasonality. Against this background, the widespread application of time slices in traditional modeling frameworks such as TIMES can be explained by the fact that they mainly focused on demand time series with a strong weekly pattern and a small share of renewable energy sources as well as the fact that the integration of time slices does not require additional data processing.

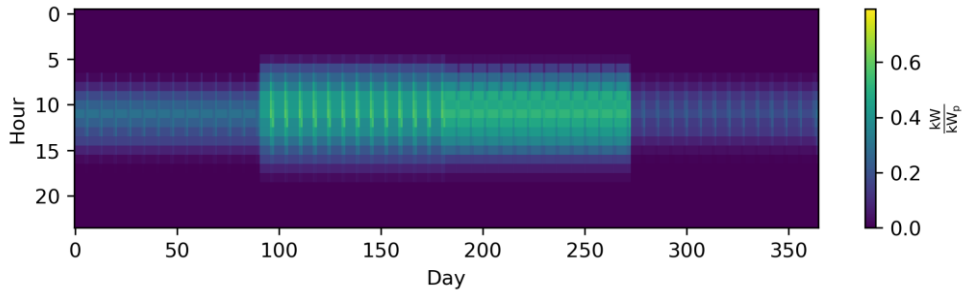

Figure 2.11. The time series of photovoltaic capacity factors represented by twelve time slices (average Wednesday, Saturday and Sunday for each season) as used by Nicolosi et al. and Haydt et al. [109, 110] (i.e., 288 different time steps) (RMSE=0.1509) (taken from Hoffmann et al. [1])

2.2.2.1.3. Combination of Period and Resolution Reduction

Like the simple averaging of consecutive time periods that can be further sampled down, e.g., as done by Harb et al. [106], the typical periods in the time slice method can also be further sampled down. This can be done, for instance, by downsampling to 2h time slices [126, 128, 132], 4h time slices [46] or a number of different time

step sizes to investigate the downsampling impact [71-73]. Moreover, day and night cycles (two diurnal time slices) [42, 109, 115-117], optionally including the peak hour of the day [42, 116, 117] or other time slices of irregular length [45, 60, 111, 112, 122, 133, 134], were also used. Mavrotas et al. [60] also implemented an algorithm for segmenting the chosen typical days to coarser time slices based on ordering of the gradients between time steps and merging the smallest ones.

The extreme case of both the downsampling method and averaging/time slice method is the representation of the total time series by its mean, which was performed by Merrick et al. [46]. As this approach is unable to consider any dynamic effects, it only served as a benchmark.

2.2.2.2. Feature-Based Merging

In contrast to representing time series with typical periods based on a time-based method, typical periods can also be chosen based on features. For instance, time steps or periods can be aggregated based on the mutual similarity of their values. In this section, the clustering procedure is explained both conceptually and mathematically.

To the best of the author's knowledge, one of the first and most frequently cited works by Domínguez-Muñoz et al. [61] used this approach to determine typical demand days for a CHP optimization, i.e., an energy system optimization model with discrete time steps, even though it was not applied to a concrete model in this work. For this purpose, all time series are first normalized to encounter the problem of diverse attribute scales. Then, all time series are split into periods P, which are compared to each other by transforming them for each value x of each attribute a at each time step t within the period to a hyper-dimensional data point. Those data points with low distances to each other are grouped into clusters and represented by a (synthesized or existing) point considered a "typical" "representative" period. Additionally, a number of clustering algorithms are not centroid-based, i.e., they do not preserve the average value of the time series [64] which could, e.g., lead to a wrong assumption of the overall energy amount provided by an energy system across a year. To overcome this problem,

time series are commonly rescaled in an additional step. The methods for this are presented in Section 2.2.2.2.3. This means that time series clustering includes five fundamental aspects:

- A normalization (and sometimes a dimensionality reduction)
- A distance metric
- A clustering algorithm
- A method to choose representatives [135]
- A rescaling step in the case of non-centroid based clustering algorithms and subsequent backscaling

As the clustered data is usually relatively sparse, while the number of dimensions increases with the number of attributes, the curse of dimensionality may lead to unintuitive results incorporating distance metrics [136], such as the Euclidean distance [135, 137-139]. Therefore, a dimensionality reduction might be used in advance [140-142], but is not further investigated in this work for the sake of brevity. In the following, each of the bullet points named above will be explained with respect to their application in time series aggregation for energy system models. Besides, the distance metric, clustering method and the choice of representatives will be shortly presented in Section 2.2.2.2.2, because the number of clustering methods used for energy system models is small. Figure 2.12 shows the mandatory steps for time series clustering used for energy system models, which are presented in the following. The grey boxes contain optional methods for maintaining additional information that is important for the system design and which are presented in Section 2.3. Figure 2.13 shows the time series of photovoltaic capacity factors represented by 12 typical days (typical days) using k-means clustering and the python package **tsam** [48].

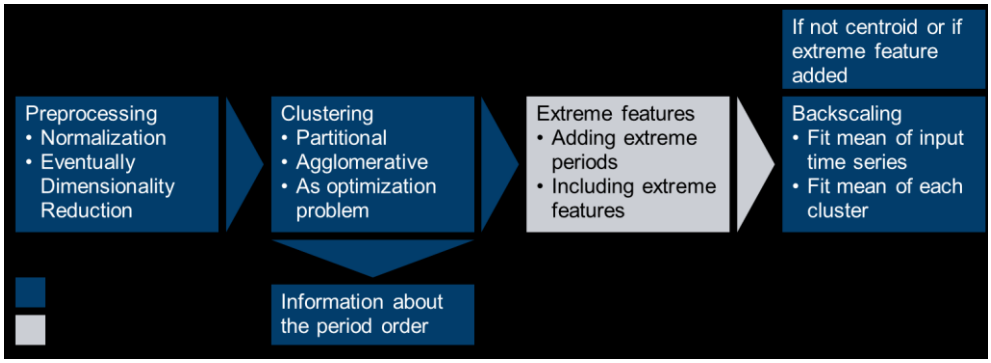

Figure 2.12. Steps for clustering time series for energy system models (adapted from Hoffmann et al. [1])

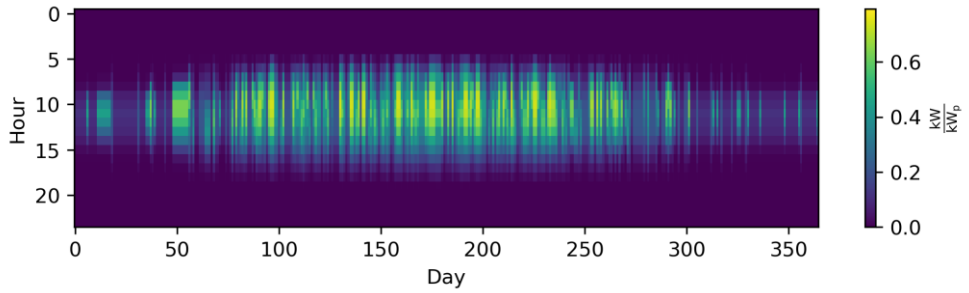

*Figure 2.13. The time series of photovoltaic capacity factors represented by twelve typical days (typical days) using k-means clustering and the python package **tsam** [48] (i.e., 288 different time steps) (RMSE=0.0552) (taken from Hoffmann et al. [1])*

2.2.2.2.1. Preprocessing and Normalization

Clustering normally starts with preprocessing the time series, which includes a normalization step, an optional dimensionality reduction and an alignment step. Because of the diversity of scales and units amongst different attributes, they must be normalized before applying clustering algorithms to them. Otherwise, distance measures used in the clustering algorithm would focus on large-scaled attributes and other attributes would not be properly represented by the cluster centers. For example, capacity factors are defined as having values of between zero and one, whereas electricity demands can easily reach multiple gigawatts. Although a vast number of clustering algorithms exist, the min-max normalization is used in the majority of publications [4, 20, 24, 45, 48, 64, 74, 97, 98, 140, 143-145]. For the time series of an attribute $a \in A = \{1, \dots, N_a\}$ consisting of $s \in S = \{1, \dots, N_s\}$ time steps, the normalization of a value of a at time step s is calculated as follows:

$$x_{a,s} = \frac{x'_{a,s} - \min(x'_a)}{\max(x'_a) - \min(x'_a)} \tag{2.1}$$

In cases in which the natural lower limit is zero, such as time series for electricity demands, this is sometimes [43, 63, 91, 93, 99, 146-148] reduced to:

$$x_{a,s} = \frac{x'_{a,s}}{\max(x'_a)} \tag{2.2}$$

Another normalization that can be found in literature [47, 102, 149-151] is the z-normalization that directly accounts for the standard deviation, rather than for the maximum and minimum outliers,

which implies a normal distribution with different spreads amongst different attributes:

$$x_{a,s} = \frac{x'_{a,s} - \bar{x}'_a}{\sigma(x'_a)} \tag{2.3}$$

In the Appendix D, normalization approaches are exemplarily illustrated for a hypothetical short time series.

A time series can further be divided into a set of periods P and a set of time steps within each period T, i.e., $S = P \times T$. The periods are clustered into non-overlapping subsets P_C, which are then represented by a representative period, respectively. A representative period consists of at least one discrete time step and, depending on the number and duration of time steps, it is often referred to as a typical hour, snapshot or system state, typical or representative day or typical week. The data $D = A \times P \times T$ can thus be rearranged so that each period is represented by a row vector in which all inter-period time steps of all attributes are concatenated, i.e.:

$$D_{arr} = \begin{pmatrix} x_{1,1,1} & \cdots & x_{1,1,N_t} & x_{1,2,1} & \cdots & x_{1,N_a,N_t} \\ \vdots & \ddots & \vdots & \vdots & \ddots & \vdots \\ x_{N_p,1,1} & \cdots & x_{N_p,1,N_t} & x_{N_p,2,1} & \cdots & x_{N_p,N_a,N_t} \end{pmatrix} \text{ with } \begin{matrix} a \in A = \{1, \dots, N_a\} \\ p \in P = \{1, \dots, N_p\} \\ t \in T = \{1, \dots, N_t\} \end{matrix} \tag{2.4}$$

The row vectors of D_{arr} are now grouped with respect to their similarity. Finally yet importantly, it must be highlighted that the inner-period time step values can also be sorted in descending order, which means that in this case the duration curves of the periods are clustered as done in other studies [4, 24, 152, 153]. This can reduce the averaging effect of clustering time series without periodic patterns such as wind time series.

2.2.2.2.2. Algorithms, Distance Metrics, Representation

Although a vast number of different clustering algorithms exist [101, 154] and have been used for time series clustering in general [135], only a relatively small number of regular clustering algorithms has been used for clustering input data for energy system optimization problems, which will be presented in the following. Apart from that, a number of modified clustering methods have been implemented in order to account for certain properties of the time series, which is presented in Appendix F. The goal of all clustering methods is to meaningfully group data based on their simi-

larity, which means minimizing the intra-cluster difference (homogeneity) or maximizing the inter-cluster difference (separability) or a combination of the two [155]. However, this depends on the question of how the differences are defined." (Hoffmann et al. [1]) The clustering algorithms used for temporal aggregation can be separated into partitional, deterministic hierarchical algorithms and time-shift tolerant clustering algorithms. The latter are sparsely applied and capable of comparing values of time series that are temporally shifted against each other. Table 2.3 lists the number of publications that have applied the respective algorithm. A detailed description of the algorithms is given in Appendix D.

Table 2.3. Clustering algorithms applied in the literature

Algorithm	Type	Number of Publications	
K-Means	Partitional	36	
K-Medoids		20	
K-Medians		2	
K-Centers		2	
Hierarchical	Agglomerative	14	2 Centroids
			12 Medoids
K-Shape	Time-Shift Tolerant	2	
Dynamic Time Warping		3	

2.2.2.2.3. Rescaling

"Due to the fact that not all of the methods rely on the representation of each cluster by its centroid (i.e., the mean in each dimension), these typical periods do not meet the overall average value when weighted by their number of appearances and must be rescaled. This also holds true for the consideration of extreme periods, which will be explained in the following sections. Accordingly, the following section will be referred to if rescaling is considered in the implementation of extreme periods. To the best of our knowledge, the first work that used clustering not based on centroids was that of Domínguez-Muñoz et al. [61], in which the exact k-medoids approach was chosen as per Vinod et al. [156]. Here, each attribute (time series) of each typical day was rescaled to the respective cluster's mean, i.e.:

$$c^{*}_{k,a,t} = c_{k,a,t} \frac{\sum_{p \in C_k} \sum_{t=1}^{N_t} x_{p,a,t}}{|C_k| \sum_{t=1}^{N_t} c_{k,a,t}} \quad \forall \quad k, a, t \tag{2.5}$$

Furthermore, Domínguez-Muñoz et al. [61] discarded the extreme values that were manually added from the rescaling procedure. A similar procedure, which was applied for each time series, but not for each typical day, was introduced by Nahmmacher et al. [63], who used hierarchical clustering based on Ward's algorithm [78] and chose medoids as representatives, which was later used in a number of other studies [4, 20, 24, 47, 48, 157]. Here, all representative days were rescaled to fit the overall yearly average when multiplied by their cardinality and summed up, but not the average of their respective clusters, i.e.:

$$c^{*}_{k,a,t} = c_{k,a,t} \frac{\sum_{p=1}^{N_p} \sum_{t=1}^{N_t} x_{p,a,t}}{\sum_{\tilde{k}=1}^{N_k} \left(|C_{\tilde{k}}| \sum_{t=1}^{N_t} c_{\tilde{k},a,t} \right)} \quad \forall \; k, a, t \tag{2.6}$$

Schütz et al. [64, 144], Bahl et al. [79] and Marquant et al. [152, 153] refer to the method of Domínguez-Muñoz et al. [61], but some used it time series-wise and not cluster- and time series-wise. Schütz et al. [64, 144] were the first to highlight that both approaches are possible. It also needs to be highlighted that these methods are not the only methods, as Zatti et al. [145], for instance, presented a method to choose medoids within the optimization problem without violating a predefined maximum deviation from the original data, but for the sake of simplicity, it focused on the most frequently used post-processing approaches. Additionally, other early publications, such as per Schiefelbein et al. [158], did not use rescaling at all. Finally, yet importantly, the rescaling combined with the min-max normalization could lead to values over one. Accordingly, these values were reset to one to not overestimate the maximum values and the rescaling process was re-run in several studies [4, 20, 24, 48, 63]. In contrast, Teichgräber et al. [47, 157] used the z-normalization with rescaling in accordance with Nahmmacher et al. [63], but did not assure that the original extreme values were not overestimated by rescaling." (Hoffmann et al. [1])

In a last step, the time series are scaled back to their original scales using the invers function of the respective normalization function presented in Section 2.2.2.2.1.

Apart from the methods presented in this section, a number of publications can be found in the literature, which focus on statistical

features or use grouping methods other than clustering. These methods are presented in detail in Appendix F and are skipped at this point for the sake of brevity.

2.2.2.3. Linking of Typical Periods

“As mentioned above, the modeling of some system dynamics, such as the state of charge of storage components, require the linking of consecutive time steps by means of intertemporal constraints. The representation of time series by a few typical days or weeks does not generally take their order across the entire time horizon into account. This means that the modeling of filling levels is normally only possible within these typical periods with a periodic boundary condition for the state of charge. In this case, the order of typical periods no longer plays a role. On the other hand, seasonal storage cannot be sufficiently modeled by this method. Yet, this is especially important for energy systems based on a high share of renewable energy sources. For a long period of time, the only approach to model seasonal storage was to drastically reduce the temporal resolution, as by Tveit et al. [159], making it impossible to model short-term storage. To overcome this issue, different methods have been developed that take the linking of typical days into account. Here, the approaches differ depending on the formation of typical periods, i.e. whether they are formed time-based in a certain pattern or feature-based using clustering.

2.2.2.3.1. Linking Periods with a Regular Pattern

To the best of the author’s knowledge, the TIMES framework was the first framework capable of linking time slices not only consecutively, but also between periods to model storages that work on a larger time scale ([52-55]). However, since the inter-period storages are meant to work between different years, e.g., as waste disposal sites [52], they are not linked to the intra-period storages, which only link consecutive time slices (segments) within one typical period, such as weekdays in spring.

Welsch et al. [111] and Samsatli et al. [22] independently developed a non-uniform hierarchical time discretization that is based on the selection of time slices. In two publications [22, 23], Samsatli et al. chose two typical days with hourly data for both the week and weekend which was done for each season consisting of 13 weeks. This resulted in 192 time steps. For the modeling of the

seasonal storage, the energy surplus across each time scale was determined and added up. As the chosen days appeared in a regular order within each season, the capacity constraints were not postulated for each time step. Instead, they were only defined for the first and last instance of each day type, the first and last week of each season and the first and last season of each year, if a multiple year approach was chosen.

Welsch et al. [111] chose a similar approach that consisted of three time slices for a workday and a weekend day in each season. However, the case study was only run with one typical day with an hourly resolution. Both approaches did not consider state changes depending on the states themselves, i.e., self-discharge rates. The approach of Welsch et al. [111] was later developed by Timmerman et al. [112] to handle self-discharge and re-used by van der Heijde et al. [100].” (Hoffmann et al. [1]) The approach and critical points at which the state of charge must be checked is depicted in Figure 2.14 for one typical weekday and weekend day per season consisting of three daily time slices each, as per Timmerman et al. [112]. The red and blue dots mark the critical time steps at which the state of charge must be checked in the first and final week of each season. “As each week consists of only two day types, of which the first is repeated five times and the second is repeated twice, the intermediate weekdays representing Tuesday, Wednesday and Thursday cannot include critical states of charge. This holds true for both, a rising state of charge across the weekdays (the critical day would be Friday) and for a decreasing one (the critical day would be Monday). The same applies to the intermediate weeks in each season. As they are repeated 13 times, either the first or last week of each season is critical with respect to the state of charge of seasonal storage and their capacity.

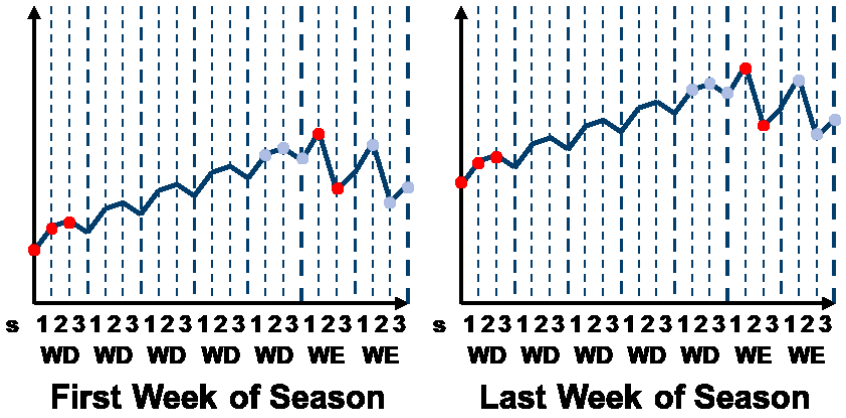

Figure 2.14. Storage formulation based on regular order of time slices according to Welsch et al. [111] and the seasonal checkpoint for two day types and three time slices each according to Timmerman et al. [112]

Similarly, but again independently, Spiecker et al. [126] developed a comparable approach that linked workdays and weekend days for every second month in an inter-daily manner for pumped storage plants and an inter-month manner for large-scale storage systems in the E2M2s model. Moreover, the typical days were based on a recombining decision tree of 2 h segments and were thus capable of modeling the storage size stochastically.

2.2.2.3.2. Linking Periods with an Irregular Pattern

Gabrielli et al. [21] developed a method to couple typical days using a function σ that assigns each day of the original time series to the typical day it is represented by. This function was used to couple the state of charge of consecutive (typical) days in an additional equation, which means that the operation of the components is modeled for a number of typical days, while the state of charge of the storages is modeled for the entire time horizon represented by a sequence of typical days. The approach was tested for a different number of typical days, as well as in a later publication [21, 160].

Wogrin et al. [90] earlier proposed the same approach as Gabrielli et al. [21] for typical time steps and took the information of the clustering indices, i.e., which original time step was represented by which typical time step, to link typical time steps in order to consider start-up and shut-down costs. This was later re-used by Tejada-Arango et al. [25] for the calculation of storage levels using typical periods (days and weeks). However, in contrast to Gabrielli et al. [21], the storage levels were not constrained for each time

step by Tejada-Arango et al. [25], but only at intervals of one week. Additionally, a similar method was applied to avoid unnecessary unit transitions at the border between two consecutive typical days.

Like the idea of Gabrielli et al. [21], Kotzur et al. [20] introduced a similar method of linking typical days in a chronologically correct order. Instead of directly linking each state of charge to the preceding one, the superposition principle was used to distinguish intra-period and inter-period states of charge. The sum of both values, i.e., the intraday state of charge for a given number of typical days, along with the inter-day state of charge, which was determined by a surplus of energy of each typical day in the corresponding sequence, was then used to determine the necessary storage levels. This approach was also used in later publications dealing with seasonal storage [4, 24]" (Hoffmann et al. [1]) and is depicted in Figure 2.15. The upper part of the figure shows an exemplary profile of an intra-day storage level for a hypothetical typical day. Although the relative changes of the state of charge within all days of the same typical day type are the same, the absolute storage levels differ, as the superposition principle, according to Kotzur et al. [20], allows a difference in the state of charge across each typical day expressed by $\Delta SOC_{c=1}$. To determine the state of charge at the beginning of each day, these inter-day differences are summed up over the entire time horizon according to the sequence of different typical days, as shown in the lower part of Figure 2.15. The state of charge at each time step is then given by the sum of the inter-day state of charge at the beginning of each day and the relative changes of the state of charge throughout the corresponding typical day given by the intra-day state of charge.

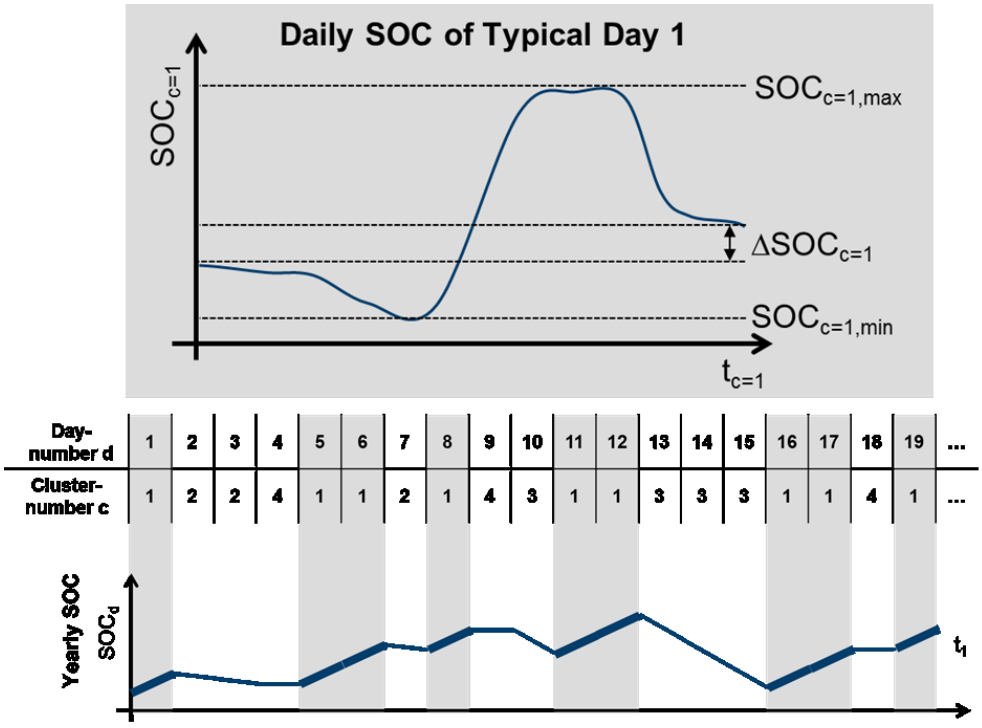

Figure 2.15. The cluster-based superposition approach to modeling seasonal storages proposed by Kotzur et al. [20]

“Another slight deviation of this method was applied by van der Heijde et al. [26], who also used the superposition principle discussed by Kotzur et al. [20] to couple typical days. However, they did not use clustering algorithms to group similar days and represented these by one typical day for each cluster, but instead searched for a linear combination of days that minimized the deviation from the yearly duration curve; a procedure introduced by Poncelet et al. [147]. In contrast to clustering algorithms, this procedure did not directly lead to an assignment of original days to groups represented by single typical days. This meant that this had to be performed in a separate step. For this, an mixed-integer quadratic program (MIQP) was formulated that sought to minimize the sum of squared errors of each day of the original time series to the typical days. The outcome of this was a sequence of typical days that represented the original time series, which was crucial for linking the typical days in accordance with the aforementioned approach of Kotzur et al. [20]. Recently, Baumgärtner et al. [82] included the storage formulation of Kotzur et al. [20] in their rigorous synthesis of energy systems using aggregation approaches to define upper and lower bounds for the objective function with full time resolution, which will be explained in detail in Section 2.3.2.

The fact that a number of methods for linking typical periods were independently developed [20-22, 90, 111]" (Hoffmann et al. [1]) emphasize the relevance of the topic but also the heterogeneity of the community, which is firstly brought together in this review.

2.2.3. Random Sampling

"Another minor group of publications uses time series aggregation based on random sampling. This means that the time steps or periods are randomly chosen from the original time series and considered representative for the entire time series instead of being determined based on clustering.

Most of the methods in the following deal with single time steps instead of periods, which is an acceptable simplification when the impact of storage capacity or other intertemporal constraints on the system design can be neglected [161]. In contrast to the methods presented above, the time steps or periods are thus neither time- nor feature-based grouped or merged. Methods that are only run once based on random or user-specified selection will be defined as "Unsupervised". However, the majority of random sampling methods presented in the literature are repeated several times in order to determine a set of random samples that best captures the original time series' features. In the following, these methods are termed "Supervised"." (Hoffmann et al. [1]) Here, the terms "Supervised" and "Unsupervised" are adopted from the corresponding concepts in the research field of machine learning [162, 163].

The difference between feature-based merging and random sampling is depicted in Figure 2.16. While clustering guarantees that the samples used as representatives of the full dataset are distributed over the whole dataset, this cannot be guaranteed by random sampling methods, which explains the development of supervised sampling methods as an alternative to clustering.

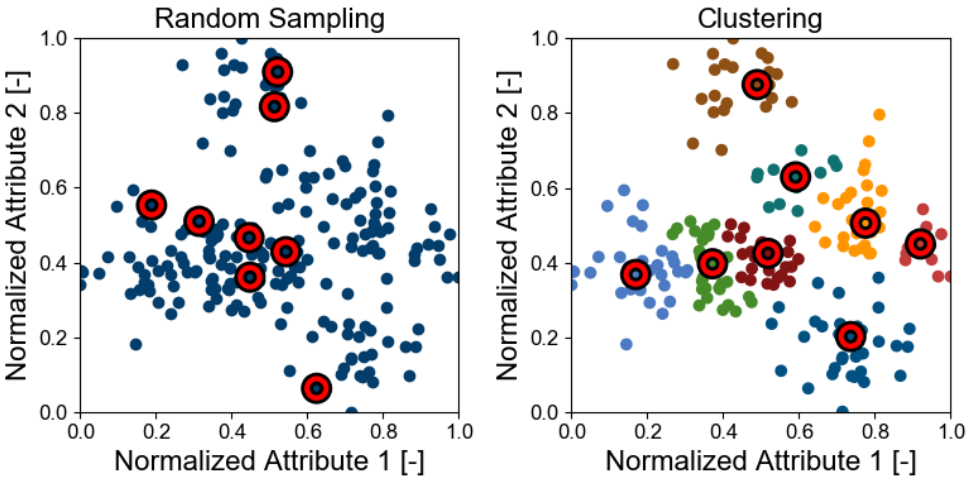

Figure 2.16. The difference between random sampling and clustering

2.2.3.1. Unsupervised

"As with supervised random sampling methods, unsupervised random sampling methods can be applied to typical periods or single time steps. However, they appeared earlier than the supervised methods (2011 and 2012).

Ortiga et al. [164] introduced a graphical method for which a number of days from the dataset had to be defined. In a second step, the algorithm minimized the deviation between the duration curve of the original dataset and a duration curve of the chosen periods multiplied by a set of variable factors for the number of appearances of each typical day.

With respect to the random sampling of time steps, Van der Weijde et al. [165] sampled 500 out of 8760 hours to capture major correlations of the input data for seven regions.

However, in the years since 2012, these methods were substituted by supervised random sampling methods.

2.2.3.2. Supervised

Munoz et al. [166] applied supervised random sampling for 1 up to 300 daily samples out of a dataset of seven years, which were then benchmarked against the k-means clustering of typical hours. A similar method was used by Frew et al. [167], who took two extreme days and eight random days from their dataset and weighted each day so that the sum of squared errors to the original wind, solar and load distribution was minimized. This procedure was then repeated for ten different sets of different days, with the average

of each optimization outcome calculated at the end. With respect to time steps, Härtel et al. [91] either systematically determined samples taking every n_{th} element from the time series or randomly chose 10,000 random samples from the original dataset and selected the one that minimized the deviation to the original dataset with respect to moments (e.g., correlation, mean and standard variation). Another algorithm for representing seasonal or monthly wind time series was proposed by Neniškis et al. [57] and tested in the MESSAGE model. This approach took into account both the output distribution (duration curve) for a typical day and the inter-daily variance, not to be exceeded by more than a predefined tolerance, while using a random sampling process. However, only the typical days for wind were calculated in this way, whereas the other time series (electricity and heat) were chosen using time slices. Recently, Hilbers et al. [161] used the sampling method twice with different numbers of random initial samples drawn from 36 years. From a first run, the 60 most expensive random samples were taken and included in a second run with the same number of samples.

These methods are comparable to the method of clustering typical time steps. However, the initial selection of samples is based on random choice.

2.2.4. Miscellaneous Methods

Apart from the random sampling methods that cannot be systematically categorized with the scheme in Table 2.1, an even smaller number of publications cannot be categorized with respect to their temporal aggregation methods. For the sake of completeness, however, they are presented in the following.

Lee et al. [168] used an improved particle swarm optimization to optimize the unit commitment of a power system with respect to fuel and outage costs. This method was based on an evolutionary algorithm that iteratively determined the “fittest” solutions and thus was quite comparable to supervised random sampling methods. However, the use of an own class of optimization algorithm is a unique feature. A similar approach to solve the unit commitment problem of a grid-connected building with renewable energy sources and a battery was presented by Quang et al. [169]. In their work, a genetic algorithm and a particle swarm algorithm were

used for different charge and discharge rates of the battery based on half-hourly time steps. It is worth mentioning that apart from these publications, a number of other works exist which use, among other methods, genetic algorithms or particle swarm algorithms to optimize unit commitment models. A comprehensive review on the methods to address the unit commitment problem was given by Saravanan et al. [170]. However, these approaches are based on a survival of the fittest principle instead of a classic optimization problem to find feasible and cost-efficient operation schedules so that an aggregation can only be applied by downsampling the time steps used for simulation. Moreover, these approaches are not directly applicable to combined unit commitment and capacity expansion planning models. Therefore, these methods are not analyzed further within the scope of this thesis.

Xiao et al. [171] optimized the capacity of a battery and a diesel generator for an island system by searching for the optimal cut-off frequency at which running a diesel generator was more convenient without causing overly high fuel costs, whereas the battery capacity would be too large if it was run on a low frequency band. For this, an analysis based on Discrete Fourier Transform (DFT) was used highlighting the different specific cost-dependent time scales on which different technologies operate.

More recently, Pöstges et al. [172] introduced an analytical approach to aggregate the time steps of a demand duration curve for a simple energy system model without storage units and with only one energy type. Interestingly, this method led to a simplified problem formulation based on a minimum number of time steps without causing an error in the objective function. In this case, the supply technology costs are based on capacity- and operation-specific costs and the approach was inspired by an earlier work of Sherali et al. [12]. Sherali et al. proved in 1982 that the cost optimal operation of these simple systems can be interpreted as an optimization problem which is closely related to the peak load pricing theory introduced by Boiteux in 1949 [9] (English translation in 1960 [10]) and Steiner in 1957 [11].

To summarize, special methods that cannot be categorized in any way appear in an irregular manner, but can have special implications for the improvement of preexisting methods.

2.2.5. Trends in Time Series Aggregation

Because the methods from Table 2.1 can be combined with each other and are based either on the careful selection of the modeler or on feature-based algorithms, it is an open question whether a clear trend can be observed with respect to the application of the methods.

For this purpose, Figure 2.17 shows the number of investigated publications containing at least one of the basic aggregation methods presented above. The Random Sampling and the Miscellaneous Methods were disregarded due to the small number of publications with no statistical significance. Moreover, the modified feature-based period merging methods were considered to belong to the same group of feature-based merging as the normal clustering methods for typical periods. Moreover, it should be highlighted that the search for literature was ended in July 2019 and that the trends are methodology-driven and not keyword-driven for the reasons given in Section 2.1.1.

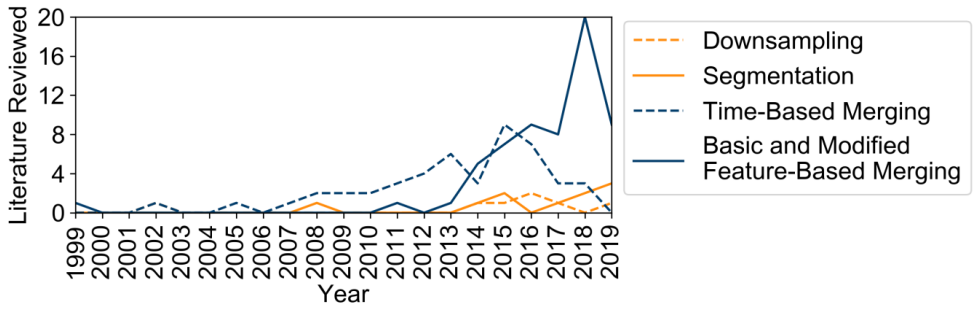

Figure 2.17. Trends in basic temporal aggregation methods for energy system models based on the major approaches presented in Section 2.2 (taken from Hoffmann et al. [1])

At first sight, a comparison between the straightforward downsampling and feature-based segmentation reveals no trend. However, publications dealing with downsampling mainly address the question what temporal resolution is sufficient for a given problem, rather than improving the calculation time of a problem with a given temporal resolution without deteriorating the results. Furthermore, downsampling sometimes serves as a benchmark [43] only, which is outperformed by the other existing methods. In contrast to that, the development of slightly variated segmentation methods is ongoing. Segmentation could even offer the option to increase the

temporal resolution iteratively at crucial time steps instead of coarsening only.

With regard to typical periods, the feature-based methods mainly represented by clustering have a rising trend, in contrast to the time-based definition of time slices and “averaging”. Interestingly, the number of publications based on time slices kept increasing for some time after the development of the clustering approach in 2011. The reasons for this are twofold: First, the approach was only proposed by Domínguez-Muñoz et al. [61], but its superiority was not proven in an energy system model. Secondly, models such as the TIMES framework [52-55] have constantly been used ([110, 113, 115, 116]) since their publication. Accordingly, the method expires no sooner than the framework by which it is used unless the framework itself is updated. This explains the inertia of new methods and the need for proper validation and benchmarking rather than the simple proposal of a method alone. Additionally, the share of renewable energy sources is slowly increasing in energy systems and, accordingly, the requirements for models and their temporal resolution are changing as well [42-47].

Finally, yet importantly, the small number of publications that deal with a decrease in the temporal resolution, in contrast to the high number of typical period approaches, is notable. This is due to the relatively low potential of decreasing the number of time steps in energy system optimizations if the periodicity of day and night cycles is not exploited. However, the impact of larger time steps can be increased by magnitudes if it is combined with a typical period approach.

Overall, Figure 2.17 shows that the future aggregation methods will most likely be feature-based, i.e., either consist of clustering only or rely on both clustering and segmentation.” (Hoffmann et al. [1]) This is also supported by Table 2.4, which lists the root-mean-square error of the introduced methods applied to the exemplary solar profile depending on the number of remaining time steps. Here, it can be observed that Segmentation and Clustering lead to the smallest root-mean-square error values among the respective concepts of resolution variation and typical periods for a given number of remaining time steps.

Table 2.4. Root-mean-square error of the introduced methods applied the to exemplary solar profile introduced in Figure 2.2 depending on the number of remaining time steps

Concept	Method	Time Steps	RMSE
	Reference	8760	0
Resolution Variation	Downsampling	1460	0.1295
	Segmentation	1460	0.0388
Typical Periods	Averaging	288	0.1126
	Time Slices	288	0.1509
	Clustering	288	0.0552

“Table 2.5 sums up the key aspects the observed trend towards feature-based merging.

Table 2.5. Pros and cons of the presented major aggregation methods (taken from Hoffmann et al. [1])

	Resolution Variation	Typical Periods
Time-based	• Downsampling • Does not exploit repeating time series patterns • Does not differentiate between more and less variant sections of the time series	• Time Slices and Averaging • Exploits repeating time series patterns • Based on the modeler’s experience • Does not merge similar adjacent time steps
Feature-based	• Segmentation • Does not exploit repeating time series patterns • Differentiates between more and less variant sections of the time series	• Clustering • Exploits repeating time series patterns • Automatic identification of similar patterns • Does not merge similar adjacent time steps

The combination of clustering and segmentation in order to compensate their remaining shortcomings named in Table 2.5 was first applied by Mavrotas et al. [60], later by Fazlollahi et al. [74] and a similar approach was recently used by Bahl et al. [79] and Baumgärtner et al. [82, 83]. However, a detailed examination if there is an optimal trade-off between intra-period resolution and the number of periods is a subject for current research and therefore addressed in Section 3.3.4.

2.3. Preserving Additional Information

As highlighted in Section 2.2, temporal aggregation methods are based on the representation of discrete time series by less time steps. These approaches are usually approximation methods, i.e. not analytically equivalent transformations, which often also include averaging procedures. From this, two major drawbacks arise:

- Values of the original time series, which could be especially important for the energy system model, are usually not preserved.
- A reliable estimation of the deviation of the optimization result based on aggregated time series from the one based on full time series can usually not be given.

In order to address the first problem, Section 2.3.1 presents approaches found in literature to keep additional information of the original time series considered important for the energy system model during the aggregation process. Section 2.3.2 introduces methods to re-evaluate the quality of the aggregation after solving the aggregated energy system model optimization to address the second issue.

2.3.1. A Priori Methods

Apart from the methods presented for time series aggregation, the integration of periods or time steps considered “extreme” is a common procedure not only used in heuristic time-based, but also in feature-based approaches such as segmentation and clustering. Most of the methods are based on the assumption that extreme values in the input data lead to a design that is robust for all remaining time steps so that integrating these extreme periods ensures a feasible system design, despite the time series aggregation.” (Hoffmann et al. [1]) Figure 2.18 visualizes how outliers of the dataset being potentially design relevant are neglected in aggregated data. On the left, a clustered sample dataset is represented by a subset of eight medoids represented by red rings. However, they do not cover the outliers of the dataset, which are given by the green rings in the right graph. These value tuples form a convex hull of the data set and represent time steps or periods that are potentially design relevant.

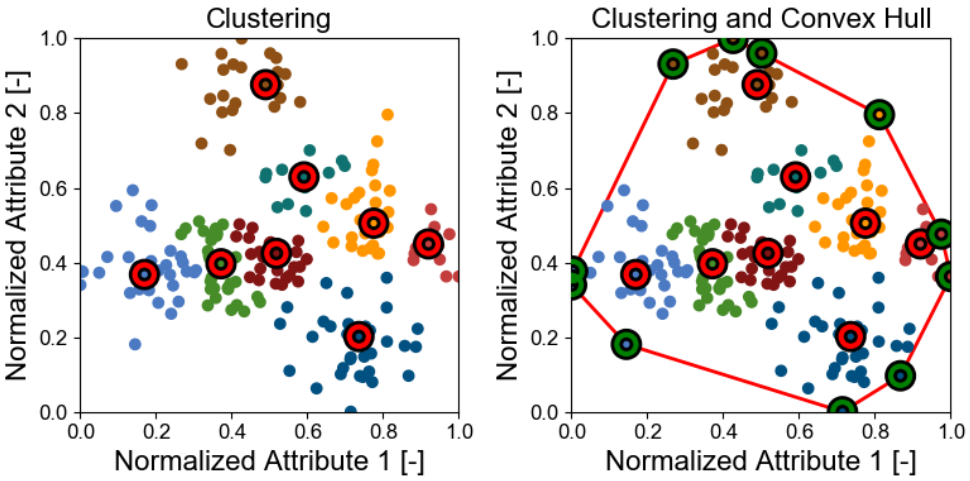

Figure 2.18. A drawback of time series aggregation: Outliers of the dataset being potentially design relevant are neglected

"In this section, approaches based on the input data only are presented, i.e., a priori methods. The integration of time series features considered extreme can happen in three different ways:

- By adding extreme periods to the set of typical periods
- By the inclusion of extreme periods or time steps into typical periods using replacement
- By directly modifying the corresponding feature-based merging algorithm used for time series aggregation in such a way that it automatically accounts for atypical periods

2.3.1.1. Adding Extreme Periods

A straightforward approach to consider extreme values is to add them to the aggregated time series directly. Of course, this depends on the way in which the time series are aggregated. In the case of typical time steps, i.e., single time steps that were derived from the original input data, extreme values can simply be taken from the original input data. For example, Munoz et al. [166] forced the top ten peak demand hours to be individual clusters for the IEEE Reliability Test System [173]. The same holds true for energy system models based on time slices. As Devogelaer et al. [114] pointed out, the TIMES framework generally uses three daily levels as time slices: day, night and a short peak slice (for electricity demand), which was also cited in other publications [42, 116, 117]. Additionally, Mallapragada et al. [45] used time slices without a peak time slice, but highlighted that the original set-up in the ReEDS model [174], by which the method was inspired, used an

additional time slice that captured all the peak loads throughout a year. Similarly, Voll et al. [108] added two more time steps for winter and summer peak loads to their monthly-averaged demand profiles." (Hoffmann et al. [1])

In the simple 2D example in Figure 2.18, it can already be observed that a significant number of samples are potential outliers to the dataset. However, not all outliers are necessarily design relevant. For example, if the system considered one demand and one supply time series, only those time steps with high demand and low supply might be considered extreme, i.e. only a subset of samples forming the convex hull in Figure 2.18.

Therefore, "extreme periods are usually defined as periods containing an extreme value of at least one attribute. For instance, Domínguez-Muñoz et al. [61] and Ortiga et al. [164] included the days containing the peak heating and peak cooling demands of their building models. The same was done for typical weeks by de Sisternes et al. [97, 98] by either adding the week or a separate day containing the peak net-load hour. It was also pointed out that the integration of an additional day affected the approximation of the duration curve less than forcing the algorithm in selecting an entire week. Stadler et al. [123] included one peak demand day per month in their DER-CAM model. Wakui et al. [118-120], in turn, included one peak day for winter and one for summer regarding the energy demand of a residential building. Marquant et al. [152, 153] included a peak heating and peak electricity demand day for a district energy supply system, while neglecting the extreme values of possible PV feed-in in the latter publication [153]. Frew et al. [167] not only included maximum days, but also minimum days for each attribute into their POWER model [175]. For this, an extreme day was defined as a day that included the peak or minimum value of one of the three attributes of wind, solar or e-demand averaged across all eligible regions. Merrick et al. [46] took one peak electricity demand day per month into account while neglecting the days with minimum capacity factors for wind and solar energy sources. Patteeuw et al. [99] added the coldest week, which coincided with the highest e-demand, into a system model for a residential building, but again neglected the possible impact of solar thermal units and the PV panel. Heuberger et al. [176] integrated the day containing the peak electricity demand, neglecting the

days of minimum potential wind and PV feed-in into a national hybrid capacity expansion planning and unit commitment model as well. Pfenninger et al. [43] tested various combinations of extreme days and weeks defined by the maximum or minimum wind and solar availability across the UK or the maximum or minimum difference between wind feed-in and electricity-demand.

For typical periods, Kotzur et al. [48] presented two different methods for adding extreme periods to aggregated time series following the clustering process based on time series aggregation to typical periods. The first method simply appends the extreme periods, i.e., a period with a maximum or minimum (average daily or single time step) value is excluded from the cluster it was first assigned to, and is separately integrated as a typical day appearing only once. The second approach is to reassign all the days within the cluster, which are closer to the extreme day than to the cluster center, i.e., the extreme period becomes the representative of a new cluster.

Furthermore, the clustering tool **tsam** introduced by Kotzur et al. [48] can include typical periods with a maximum or minimum **average** across the period for a chosen attribute, i.e. extreme values with respect to the first momentum. This approach was also employed by Pfenninger et al. [43] for wind and solar time series. Similarly, Poncelet et al. [147] included the days containing the highest and lowest value for electricity demand and those with the highest and lowest **average** of wind and solar capacity factors for a capacity expansion planning model to benchmark their own feature-based approach. However, a comprehensive study on whether time series for energy system optimizations can efficiently be clustered by means of their statistical momentums (average, standard variation, etc.) is still an open research question addressed in Section 3.2.5.

Recently, Pöstges et al. [172] showed that for extremely simple energy systems with supply units with capacity-specific and operation time-specific linear cost functions, as well as only one considered energy commodity, the optimal operation time and necessary capacities can be derived analytically using the segments in the demand duration curve, in which each technology is the most profitable one.

A major drawback from which all of the methods presented above suffer is the fact that the number of extreme constellations grows exponentially with the number of time series taken into account. Figure 2.19 illustrates this for a hypothetical demand (**D**), wind capacity factor (**W**) and solar capacity factor (**S**) time series.

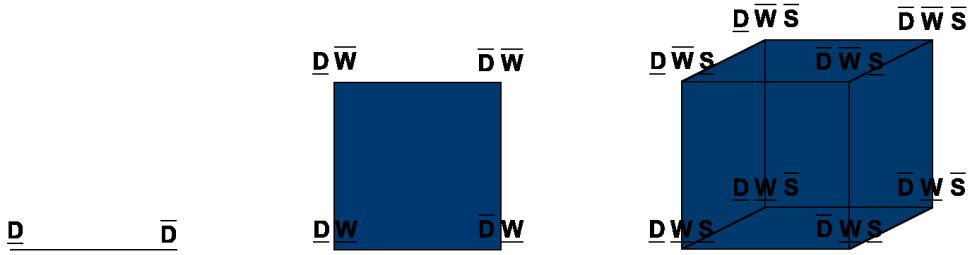

Figure 2.19. Impact of adding "shoulder values" as proposed by Frew et al. [167] as extreme values for a rising number of attributes (taken from Hoffmann et al. [1])

As illustrated, the consideration of the minimum and maximum electricity demand $\underline{\mathbf{D}}$ and $\overline{\mathbf{D}}$ leads to two additional typical periods. Taking the extreme periods of an additional attribute into account leads to four potential extreme constellations, while the integration of three attributes potentially leads to eight extreme constellations, as in the publication of Frew et al. [167]. It is obvious that for a certain number of locations and technologies, more extreme days (minimums and maximums) are needed than there exist days in a year (assuming that no period is extreme for more than one attribute). In the case of typical days including "shoulder values", i.e. the corners of the hypercube, this number is reached for only nine different attributes ($2^9 = 512 > 365$). If the extreme periods are considered for each attribute alone without deriving potential shoulder values, the number of extreme periods grows linearly with the number of time series, which refers to the number of corners for the 1D figure, the number of sides of the square and the number of surfaces for the cube. In the case of typical days, including the extreme period or value for just one attribute each, this number is reached for ($183 \cdot 2$ extreme values $= 366 > 365$) different attributes. This is the reason why some authors such as Pfenninger et al. [43] only considered the extreme values averaged across all regions. Other approaches aimed at automatically including certain extreme features in the once chosen typical periods [60, 177] or searching for atypical days within the dataset with some additional

constraints [145] which will be described in detail in the following two sub-sections.

2.3.1.2. Inclusion of Extreme Values or Additional Features

Given the fact that averaging across different periods or time steps, as is the case in many temporal aggregation approaches, leads to an underestimation of the inner-period variance, while manually adding periods considered to be extreme increases the computational load, different algorithms have been implemented on the basis of the inclusion of extreme values or additional features. Mavrotas et al. [60] synthesized seasonal 24h profiles of heat demand using monthly averages. Of all the monthly averaged samples used for determining the seasonal profile, the overall maximum value was included in it. The adjacent time steps around the maximum were calculated with weighted averages in order to smoothen the profile, i.e., the day including the maximum value was weighted with 100% at the peak time step, with 75% in the neighboring time steps and 50% in the second adjacent time steps. As the cumulative sum of that profile no longer fitted the average cumulative sums of the used monthly profiles, the remaining 19 time steps per day were rescaled.

Green et al. [177] presented an approach for including dominant or common ramps into the profiles obtained by k-means clustering. For the dominant ramp method, the gradients of the centroid profiles were determined and, according to these, the mean gradients of those cluster members with the same gradient direction as the centroid profile were used to construct the ramps of the representative profile. The common ramp approach was based on the same idea of using the mean of gradients of pointing in the same direction; however, the choice which subset of gradients is used was made by the median of all gradients in each time step and not according to the gradient of the mean profile. A drawback of this method was that it could lead to significant offsets between the first and last time step of each period.

Regarding the integration of extreme periods, Kotzur et al. [48] also proposed the method to use the extreme period within a cluster as the cluster's representative, which should usually lead to a fairly conservative assumption, as this approach overestimates the frequency of extreme periods appearing in the time series.

Apart from that, some publications have aimed at increasing the robustness of their energy system models by artificially adding bias to the (aggregated) input data or favored stochastic optimization.

Spiecker et al. [126] used the stochastic E2M2s model implemented in GAMS to minimize the total annual costs of an energy system by establishing a recombining tree structure to the model consisting of two possible hydro power plant states and three possible wind feed-in states that changed in 2h intervals. Furthermore, the storage levels across an entire year were also stochastically modeled. Wouters et al. [127] included variability of the season-based PV infeed into a neighborhood microgrid by splitting up the daily infeed into input-level histograms for each season. Then, the potential output profiles were determined by averaging all feed-in profiles within one season and the same cumulative feed-in level. Finally, the outputs of the PV panels for each season were determined using the seasonal average weighted by the days of occurrence at each feed-in level appearing in that season. Kools et al. [107] used synthesized PV profiles with minutely, quarter-hourly and hourly resolution and artificially added fluctuations using a normal distribution and gamma distribution with a stochastic decomposition algorithm for a distributed generation system. Furthermore, the designs obtained for different temporal granularities were cross-compared with respect to the energy losses when operating the systems on a finer time scale.

Brodrick et al. [102] isolated three critical hours within six representative days for an integrated solar combined cycle through excessive testing and used this strongly reduced model for a multi-objective optimization based on an iteratively tightened CO_2 constraint which resembled an exhaustive approach. Although this method is not necessarily computationally less expensive, it differs from all the others because the aggregated amount of input data was not increased by this method.

2.3.1.3. Additional Constraints in Feature-Based Merging

Apart from assuring that the representation retains certain characteristics, methods that are even more complex are capable of excluding extreme periods in the clustering process itself. For segmentation processes, Stein et al. [84] illustrated this, introducing a

mixed-integer program (MIP) that minimized the inter-time step differences for a given number of merging steps. Here, time steps not to be merged such as extreme values could be excluded with an additional side constraint. Moreover, it was assured that a maximum number of adjacent merges was not exceeded with an additional constraint. A similar approach was previously introduced in a publication by Fazlollahi et al. [74], in which the segmentation algorithm was based on iterative k-means clustering and maximum values were automatically excluded. Furthermore, the segmentation was applied to typical periods that were determined using a clustering process to which extreme periods could be manually added. It is important to highlight that only maximum values were expected to be extreme. With respect to supply data such as the capacity factors of renewable energy sources, it is trivial that periods with minimum values are likely critical as well.

With respect to an automatic inclusion of extreme days within a clustering algorithm, Zatti et al. [145] introduced the so-called k-MILP clustering, which is a modified version of the exact k-medoids algorithm and automatically excludes atypical periods. For this, the side constraint that each day from the original time series must be assigned to a representative day was relaxed so that the atypical days increasing the sum of distances the most could be excluded. However, the number of atypical days that were allowed to be excluded had to be set by an additional constraint. Moreover, additional constraints were added in order to assure that the sum over the repetition of representative days did not differ from that of the original data beyond a predefined share. Additionally, it was imposed that for some selected attributes, the extreme periods had to contain at least one day that was also close to the absolute extreme value of the respective attribute.

Apart from that, Gabrielli et al. [21] constrained the clustering procedure for typical days to maintain the maximum and minimum values of the heat and electricity demand profile used for a multi-energy district system, although this also included a solar input time series.

Concerning algorithms used for the integration of extreme events into typical time steps, i.e., typical periods lasting for only one time step, a method based on a moving average has been proposed by

Härtel et al. [91]. Here, the determined hourly typical time steps derived from clustering were compared to their moving average within a 6 h window of the full time series. If more than 95% of these values were above or below the values in the cluster, the highest or lowest candidate within the system state cluster was chosen as representative.

The presented methods illustrate that considerable efforts have been made to integrate extreme periods into the clustering processes. However, as pointed out by Scott et al. [178], the extreme periods cannot be known in advance for most synthesis problems because the built capacities of each technology are an endogenous outcome from the optimizations, e.g., the peak capacity factors of wind turbines are not relevant if wind turbines are not chosen to be built in a greenfield energy system optimization. This imposes the need to gain information about possible designs of the energy system with preliminary optimizations, which ultimately led to the development of multi-level approaches.

2.3.2. A Posteriori Methods

The implementation of extreme periods normally increases the robustness of the aggregated energy system optimizations, but does not necessarily lead to feasible solutions for the full time series, for instance, because the component, for which an extreme value is integrated, is not chosen in the optimization. Storage units that smooth out the impact of extreme periods can be another reason why extreme values in the input time series are not necessarily the critical time steps in the energy system. Therefore, a number of publications focus on multi-level approaches in order to increase the robustness or operational exactness of aggregated energy system optimizations. The presented approaches can be divided into non-iterative and iterative methods. Figure 2.20 illustrates the interdependences of temporally aggregated energy system optimizations that motivate the inclusion of multi-stage approaches.

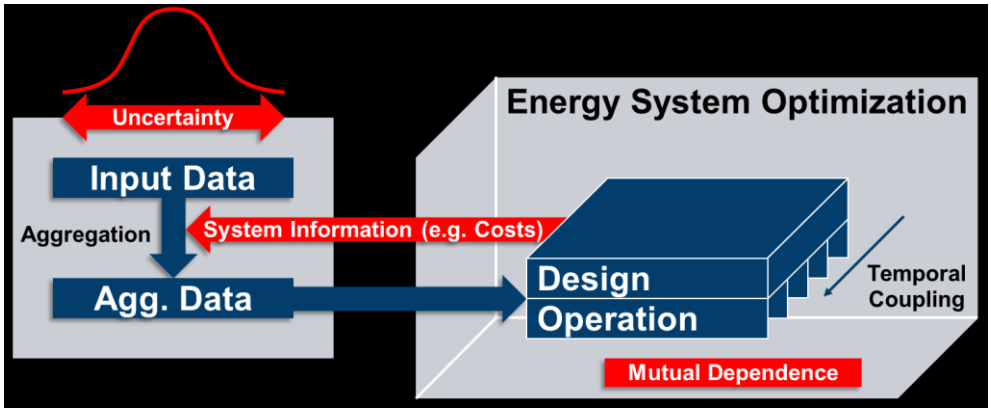

Figure 2.20. Mutual dependencies in aggregated energy system optimizations that necessitate feedback loops (taken from Hoffmann et al. [1])

The main driver in the use of multi-stage approaches is based on the problems related to the inclusion of extreme periods. As the absolute importance of a single component with a given time series is unknown in advance, the impact of outliers within this time series is unknown as well. Therefore, different approaches aim at isolating certain information about potential energy system designs with preliminary optimizations in order to improve the aggregation process of the input data without increasing the size of the optimization problem. A second driver for multi-stage approaches is binary variables for design and operation, which significantly increase the complexity of large-scale energy system models. However, the operational decisions depend on the design decisions and vice versa. Simply put, a component that is not chosen to be built is not operated. This can be exploited by deriving simpler aggregated design problems and separated optimization problems that can significantly reduce the complexity. Thirdly, not only aggregated energy system models but also the real energy systems face uncertain input data. Temporal aggregation methods can thus be used to simplify models, which are then re-calculated for slight variations in the input data. The resulting designs can then be compared to each other by checking the operational feasibility when being exposed to the time series of the other scenarios.

In the following, however, the approaches are divided into non-iterative approaches and iterative approaches, as iterative approaches focus on outperforming state-of-the-art solvers, while non-iterative approaches focus on the generation of fast and robust but suboptimal, or fast and optimal but only relatively robust, solutions.

2.3.2.1. Non-Iterative

Due to the fact that the main complexity of mixed-integer linear programs is caused by binary variables, Gabrielli et al. [21] introduced a method for reducing the number of binary operational variables, i.e., the on/off status of components. For this, the binary variables were modeled based on a typical day formulation obtained using k-means and linked to the fully resolved continuous variables by means of an assignment function. This approach did not necessarily lead to feasible solutions for less than six typical days, as the reconversion of hydrogen from the hydrogen storage involved was not able to match the thermal demand for a too limited number of operational modes.

A similar approach that focused on the reduction of binary variables was employed by Kannengießer et al. [4], who used the hierarchical clustering of sorted time series in a first step and determined the binary design variables of two energy system models. In a second step, the binary variables from the first step were taken as input parameters for a second iteration in which the capacities and (linearized) operation of the components were optimized for the full time series. This method was capable of identifying a feasible but not necessarily optimal system design with an overall computation time for the aggregated mixed-integer linear program and fully resolved linear program that was smaller than the fully resolved mixed-integer linear program.

Apart from that, two recent publications dealt with the improvement of existing aggregation approaches for the input data. Sun et al. [140] introduced a cost-oriented two-level approach for solving an electricity investment model. Here, the model was independently solved for each input day and the cost factors for each unit were determined. These were dimensionally reduced with Laplacian Eigenmaps and then clustered for determining the cost-related typical days by choosing the medoid of each cluster in the dimensionally reduced cost space, which was proven effective, compared to clustering solely based on input data.

Hilbers et al. [161] presented an approach based on random time steps. In a first run, a defined number of random samples was taken from 36 years of data and the energy system optimization (in the test case a power system model run with Calliope) was run

once. From this, the 60 time steps with the highest variable costs were taken and introduced into a second set of random time steps that added up to the same total number of time steps. In order to avoid an overly conservative system design, the 60 extreme time steps were expected to appear only once in 36 years, which was considered with a corresponding small weight.

2.3.2.2. Iterative

Lin et al. [179] presented a two-stage approach for solving a semi-coarse model of a fully resolved mixed-integer linear program for cogeneration in energy-efficient buildings. For this, typical days were determined using k-means and the real days were chosen that were closest to the calculated centroids. The semi-coarse model was defined as a mixed-integer linear program with aggregated variables but a full number of constraints, while the coarse model was defined as a mixed-integer linear program with aggregated variables and constraints. Thus, the semi-coarse model was solved by solving the coarse model and iteratively adding violated constraints from the full model. The resulting semi-coarse model was an upper bound of the original problem with guaranteed feasibility, which was not the case for the coarse model.

A similar approach was introduced by Bahl et al. [180], who chose k-means clustering for determining typical time steps for a distributed energy supply system without storage technologies. The system, optimized for the aggregated typical time steps, was then operationally optimized for the full time series. If the system design was not feasible, additional feasibility time steps were defined for the aggregated optimization problem. When an operationally feasible design was obtained for both the aggregated and full time series, the difference between them was calculated and, if it was below a pre-defined threshold, the iteration was terminated. Otherwise, the number of typical time steps was increased. It is noteworthy that a feasible operational optimization with the full time series for a system design based on an aggregated optimization is in general an upper bound for the original problem of a combined design and operational energy system optimization. Based on this initial approach, four consecutive publications [79, 82, 83, 181] introduced an advanced iterative approach for simultaneously over- and underestimating the objective function of the original mixed-integer linear program by using time series aggregation.

With respect to creating a robust system design, Gabrielli et al. [160] recently introduced an approach for creating artificial variance within given input data, deriving optimal energy systems from all the synthesized input scenarios and operationally testing these system designs for all other scenarios. The results revealed that energy systems designed for a minimum emission of CO_2 also tended to be the most robust ones with respect to satisfying heat demand with a connection to the electricity grid only.

In another line of publications [71-73] by Yokoyama et al., semi-heuristic decomposition methods for energy systems without storage units or other intertemporal constraints were introduced, but with binary variables for both, the design and operation of components. Here, the fact that operational binary variables generally depend on the design decision, i.e., if a unit is not built, the operational binary variables must be zero at any point in time, was exploited.

In the first publication [71], the original mixed-integer linear program was sub-optimally, but feasibly solved and simplex variables were derived from the result. Then, sub-problems, each containing only one binary variable, were created and depending on this variable's impact on the optimal solution of the subproblem, it either was set to zero, one or remained a variable. Then, the original mixed-integer linear program was solved again with partly fixed binary variables and, if a better solution was found, the process was repeated. Otherwise, it was terminated with a suboptimal solution. In the second publication [72], the operational binary variables in the design problem were relaxed and the design binary variables were investigated using the branch and bound method with a parallelization optimization of sub-problems on the operational level. This method was again not applicable to any system that included storage technologies. In the most recent publication [73], this method was used in combination with a downsampling approach and further improved by defining bounds at the upper design and lower operational optimization level. This should help to discard solutions that would not be able to improve the objective function without calculating all the possible master and sub-problems. Additionally, an ordering strategy was also applied to increase the chance of discarding sub-optimal solutions more rapidly.

In summary, multi-level approaches based on time series aggregation in energy system optimizations try to exploit five different features that are not given in simple aggregation approaches:

- Separating complicating binary variables from the vast majority of continuous variables
- Separating the design problem from the operational problem
- Obtaining feasible but suboptimal solutions instead of optimal but infeasible solutions for the fully resolved input data
- Deriving implications for a meaningful time series aggregation from the system itself instead of the input data only
- Determining a more robust energy system by exposing the once optimized energy systems to different input data scenarios

With respect to iterative approaches, however, it must be called into question as to whether these approaches are more efficient than well-known iterative decomposition approaches such as Benders- or Dantzig-Wolfe decomposition [182] (e.g., as used by Lara et al. [30] and Schwele et al. [183]).

2.3.3. Trends in the Integration of Additional Information

With respect to the methods to increase or even ensure the robustness of models optimized with aggregated time series, Figure 2.21 shows the number of publications that deal with at least one of the approaches presented above. Here, the Inclusion of Extreme Values or Additional Features and the Additional Constraints in Feature-Based Merging are summed up in one group, as both approaches do not increase the number of periods to be considered and thus do not suffer from the combinatorial problem presented in Section 2.3.1.1. Again, the trends are not keyword-driven, but methodology-driven for the reasons given in Section 2.1.1.

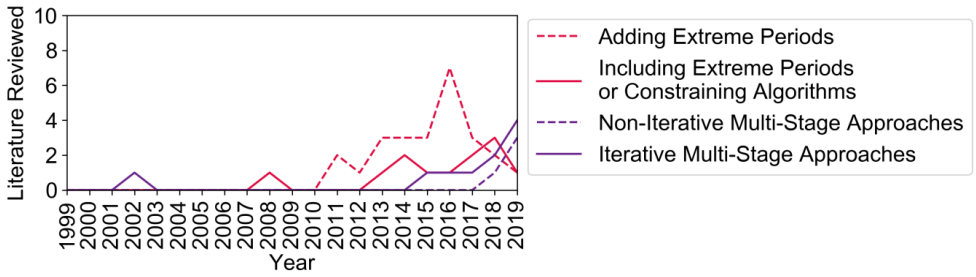

Figure 2.21. Trends in methods to preserve additional information in temporal aggregation methods for energy system models based on the major approaches presented in Section 2.3 (taken from Hoffmann et al. [1])

In contrast to the clear trends in aggregation methods, the development of methods in the area of robustness is rather vague. The manual adding of extreme periods had a growing trend until 2016, but then drastically decreased again. As mentioned above, an extreme event in the input time series of a single attribute does not necessarily mean that it is also an extreme situation in the energy system. This is even more the case if storage capacities are considered. Moreover, the number of extreme periods is growing with the number of input time series, which makes this approach intractable for a large number of regions if all cases of potentially extreme periods are considered. This might explain why this method is slowly becoming unfavorable in times of growing energy system models. In contrast, the inclusion of extreme values or algorithmic considerations of extreme features within a given number of typical periods or the definition of atypical days as extreme days are not subject to a combinatorial problem and therefore appear occasionally in the literature with a slightly rising trend. However, these methods neither guarantee robustness.

In contrast, the multi-stage approaches appear to have a clear upward trend, as they can be capable of guaranteeing robust but suboptimal solutions with respect to the non-aggregated time series. However, the convergence against the optimal solution can, to this end, only be guaranteed by increasing the number of typical periods and using a sophisticated iterative approach [82, 83], which results in a resemblance to well-established and commercially available solving algorithms. This leads to the question if convergence to the real optimum is the main target of aggregation methods, or if their focus will remain the creation of fast but satisfactorily accurate approximations that can be achieved by only two stages of design and operational optimization [4].

Overall, the question of robustness is highly dependent on the size of the model, the considered attributes and the temporal interconnectedness. A field of future research thus remains the derivation of mathematical theorems, as introduced by Lin et al. [179] and Teichgräber et al. [47]. For example, the conditions under which an extreme input event leads to an extreme system situation or clear statements of under- and overestimation of the identified results for temporally-strongly coupled systems are of great interest" (Hoffmann et al. [1]), to which this work contributes with theoretical considerations in Appendix H and I.

2.4. Review Summary

"This review of temporal aggregation methods for energy system models has revealed manifold key findings. Firstly, it is possible to categorize the methods based on their underlying idea, the addressed problem and their compatibility. Secondly, the advances in temporal aggregation methods are clearly driven by shortcomings in both computational tractability and existing methods in models with changing requirements. Thirdly, it was shown that there are rival methods, of which the feature-based ones are outperforming the time-based ones, as well as complementary methods. Moreover, compatible approaches can be applied stepwise and contain further sub-steps, such as clustering.

However, a systematic overview was lacking to this end, which Chapter 2 has tried to rectify. One reason for this is also a major limitation of this literature review: As many publications focus more on the solvability of energy system models than on the applied aggregation methods itself, a keyword- or title-driven meta-analysis is not leading to a meaningful overview of existing methods and possible trends. This issue was addressed by defining a clear interval of publication dates and giving an as holistic categorization of the methods found in literature as possible.

Apart from that, open research questions are derived which are also addressed in the following:

- The question of the most important statistical features of the time series to be kept addressed in Section 3.2.

- Developing an approach that is capable of identifying good combinations of aggregation techniques and temporal resolutions of the input time series in an empirical manner addressed in Section 3.3.
- A way to measure the accuracy of different aggregation methods a priori by defining bounds that are also valid for the computationally intractable problem addressed in Section 3.4.
- Expanding mathematical theorems regarding upper and lower bounds as introduced by Yokoyama et al. [72], Lin et al. [179] and Teichgräber et al. [47] to more general ones applicable to strongly temporally-interconnected energy system models addressed in Appendix H and I.

However, it should be highlighted that temporal aggregation methods are always based on the complexity reduction of not perfectly redundant input data. Therefore, they introduce deviations from fully resolved models. Accordingly, they should only be used for the sake of computational tractability. Apart from that, the clustering procedures can also be time-intensive, which can lead to trade-offs between the computational load of clustering and the saving of computational resources using the aggregated models.

Moreover, the trends in time series aggregation also imply that the frequently used k-means, k-medoids and hierarchical clustering approaches to determine typical days are still state-of-the-art," (Hoffmann et al. [1]) which is why hierarchical clustering is used in the remainder of this thesis due to its preferable deterministic behavior allowing for result reproducibility.

3. Methodology

In this chapter, the most promising aggregation techniques from Chapter 2 are systematically extended and explained in detail. A shortened version of the methodologies introduced in Sections 3.1, 3.2 and 3.3 can also be found in two preceding publications by the author [2, 3].

A novelty of this thesis is the separation of the clustering process from the representation of the once determined clusters as depicted in Figure 3.1. Accordingly, the representation methods, which also comprise procedures to consider additional features of the original time series without increasing the computational complexity, are analyzed separately in Section 3.1 and 3.2.

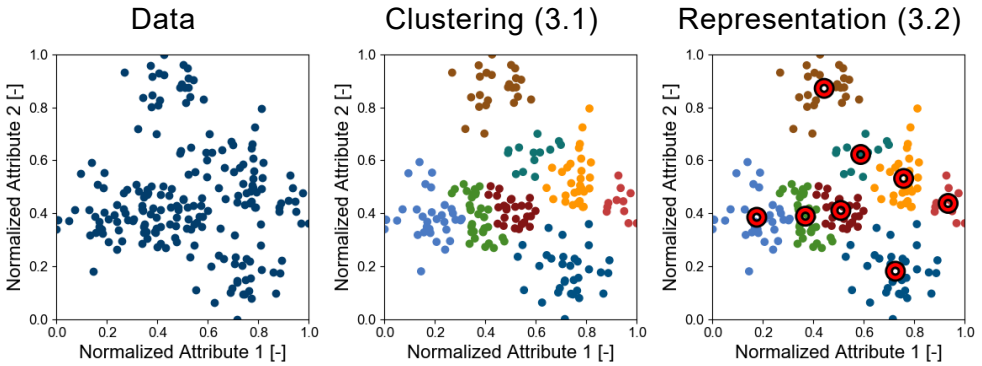

Figure 3.1. Clustering and representation as separate steps of clustering (taken from Hoffmann et al. [3])

Section 3.3 introduces error indicators for both, the aggregation and its impact on the energy system optimization. The chapter closes with an assessment of methods for bounding the aggregation-induced error in Section 3.4.

3.1. The Process of Time Series Aggregation

As described in the preceding chapter, temporal aggregation can be divided fundamentally into the merging of adjacent time steps (downsampling and segmentation) and the merging of periods (time slices and period clustering). As a clear trend towards the feature-based merging techniques, i.e. period clustering and segmentation can be observed in literature, which bears advantages with respect to aggregation-induced deviations from the original time series data, the following focuses exclusively on period clustering and segmentation.

3.1.1. Period Clustering

Figure 3.2 summarizes the process of period clustering for a set of (already normed) time series. First, the N_a time series are rearranged so that each candidate period comprises all time steps that fall within that period of all attributes as row vector. This leads to $N_a \times N_t$-dimensional samples, whose dimensionality rise with the number of time series N_a and the number of time steps per period N_t. As the product of the number of time steps N_t and the number of candidate periods N_p has to equal the total number of time steps N_s, the number of the N_p samples decreases with the length of each period, whereas the dimensionality of the samples rises. This means, while one year results in 365 candidate days, it only results in approximately 52 candidate weeks with a seven times higher dimensionality.

After the rearrangement shown in the center of Figure 3.2, each row vector representing a period can be interpreted as sample with a certain distance to other samples. As each candidate period can generally be assigned to a cluster with any other period freely, an arbitrary clustering algorithm, which assures that each period is assigned to a cluster, can be chosen.

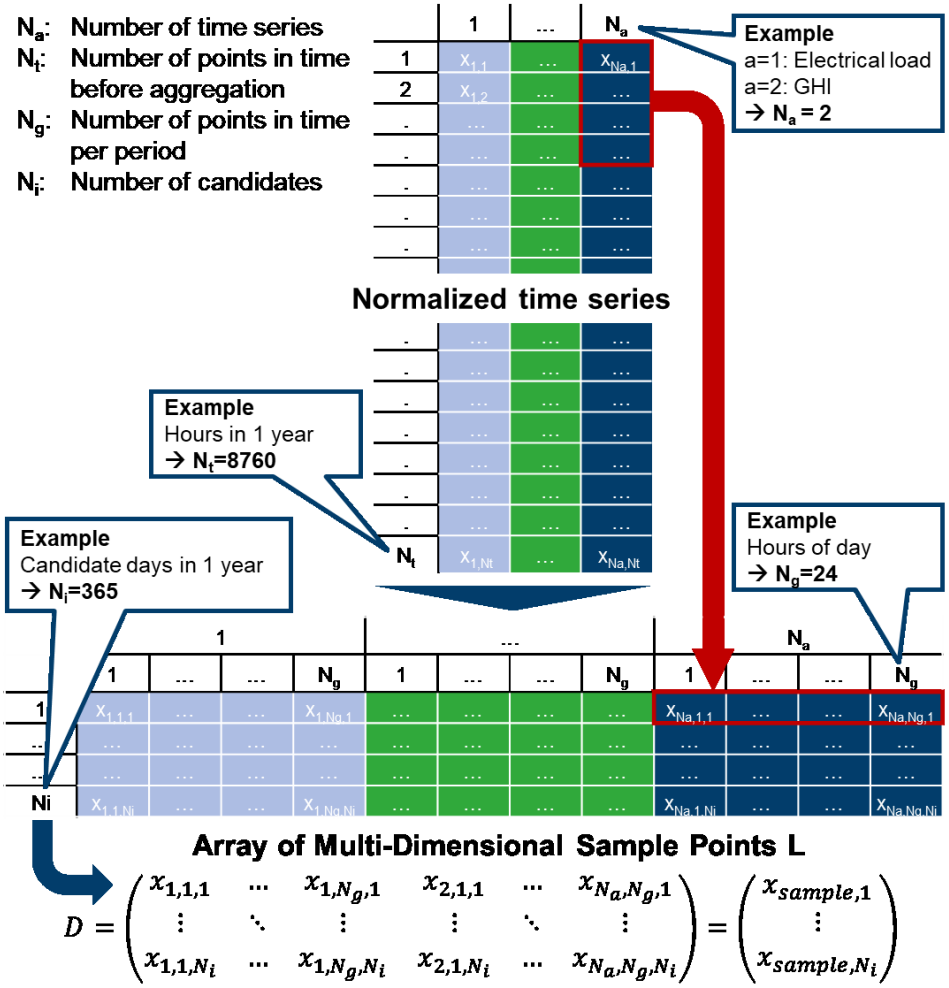

Figure 3.2. The procedure of period clustering using an arbitrary clustering algorithm (adapted from Hoffmann et al. [3])

3.1.2. Segmentation

In contrast to period clustering, segmentation focuses on the reduction of the temporal resolution by representing a number of adjacent time steps by a single one. As this process does not happen in a regular manner like in the case of downsampling, but based on the mutual similarity of adjacent time steps, this process leads to a coarser temporal resolution, but depending on the local variance of the original time series, irregular time step lengths.

As the decision, whether two adjacent time steps are grouped to a larger time step based on their similarity, the process can generally

by understood as a clustering problem. However, the premise that the time steps have to be adjacent, i.e. that the samples cannot be assigned to clusters freely, is a major difference to period clustering. Further, most clustering algorithms are not capable to group samples while complying with side constraints. One of the few exceptions is Ward's hierarchical algorithm, because the hierarchical structure allows for a stepwise consideration of only those samples that are considered as potential candidates for merging.

Figure 3.3 illustrates the process of segmentation based on Ward's hierarchical algorithm under the constraint of the adjacency of time steps. In contrast to the clustering of periods, each sample comprises only a single time step. Accordingly, the values of all time series N_a at the respective time step are transformed to an N_a-dimensional row vector, as shown in the upper part of Figure 3.3. Generally, segmentation can either directly be applied to the fully resolved original time series resulting in $N_p \times N_t$ samples. However, if the segmentation is applied to N_k typical periods in order to further temporally aggregate the energy system model, the process results in N_k independent segmentation problems with N_t samples each.

Ward's hierarchical algorithm starts by calculating the distances between each sample as shown in the lower left part of Figure 3.3. Then, those time steps are merged, which increase the inner-cluster variance the least. In this step, the algorithm can be constrained to consider only adjacent time steps, for which a connectivity matrix can be defined. The connectivity matrix in case of segmentation is shown in the lower right part of Figure 3.3 with entries of ones on the first upper and lower diagonal stating that $x_{sample,t}$ can only be merged with $x_{sample,t+1}$ and $x_{sample,t-1}$. Accordingly, the clustering algorithm chooses only a subset of samples for potential merging. Here, the distance between the newly created larger time step and the remaining other time steps can be calculated using a recursive formula and the distance matrix as well as the connectivity matrix can be shortened by one row and one column as two samples have been merged. Thus, Ward's hierarchical clustering algorithm is capable of respecting the adjacency constraint at every iteration until the desired number of time steps is achieved.

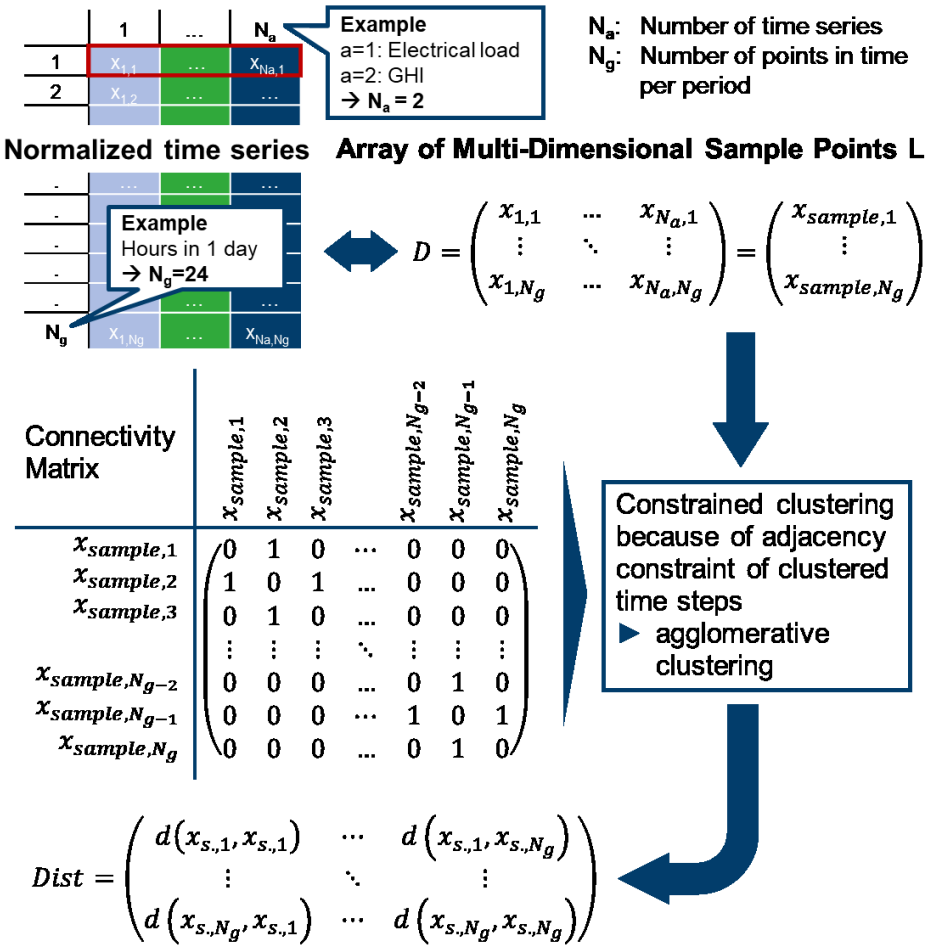

$$D = \begin{pmatrix} x_{1,1} & \cdots & x_{N_a,1} \\ \vdots & \ddots & \vdots \\ x_{1,N_g} & \cdots & x_{N_a,N_g} \end{pmatrix} = \begin{pmatrix} x_{sample,1} \\ \vdots \\ x_{sample,N_g} \end{pmatrix}$$

$$Dist = \begin{pmatrix} d(x_{s.,1}, x_{s.,1}) & \cdots & d(x_{s.,1}, x_{s.,N_g}) \\ \vdots & \ddots & \vdots \\ d(x_{s.,N_g}, x_{s.,1}) & \cdots & d(x_{s.,N_g}, x_{s.,N_g}) \end{pmatrix}$$

For the Euclidean distance, d between time step $x_{sample,i}$ and time step $x_{sample,j}$ is defined **by the summarized distance of all characteristics** between time steps:

$$d(i,j) = \sum_{a=1}^{N_a} \left(x_{a,g,i} - x_{a,g,j}\right)^2$$

Figure 3.3. The procedure of segmentation using constrained hierarchical clustering (adapted from Hoffmann et al. [3])

Although the presented clustering algorithms iterate over alternating assignment and representations steps and thus try to minimize a certain objective function, an arbitrary method can be chosen to represent the clusters, once the clustering algorithm has converged. This is an especially important option because a major outcome of the literature review is the abundance of methods to preserve additional information in the aggregation process, which is expected to be important for the energy system optimization, e.g. extreme values of the original time series. In addition to that, the adaption of a cluster's representative is more convenient than the

addition of extreme periods because of the number of potential extreme values that grows exponentially with the number of considered time series.

3.1.3. Combination of Period Clustering and Segmentation

As mentioned in Chapter 2, clustering and segmentation can be freely combined. The advantage of combining both methods is shown in Figure 3.4. Here, an exemplary hourly resolved electricity time series for one year was stepwise reduced to eight typical days containing eight segments each, which results in 64 instead of 8760 time steps. Despite the aggregation to less than 1% of the original number of time steps, the green curve in the lower right subgraph still resembles the original one in the upper left graph. Further, a combination of methods does not significantly increase the root-mean-square error compared to single aggregation approaches either focusing on typical periods or segmentation.

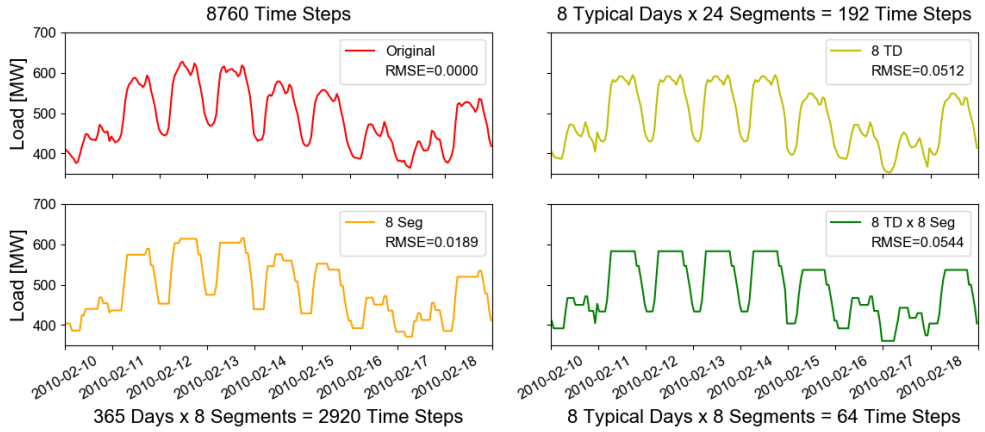

Figure 3.4. Time step reduction based on a combination of period clustering and segmentation (taken from Hoffmann et al. [3])

3.2. Representation Methods

Section 3.2 focuses on the representation step of the determined cluster groups. As mentioned before, certain clustering algorithms use specific representation methods. For example, in each iteration of the k-means algorithm, the determined clusters are represented by centroids. Analogously, an iterative medoid representation is applied by the k-medoids algorithm and k-maxoids uses maxoids for the representation steps. However, after an algorithm has converged and the final clusters are determined, they can be represented by an arbitrary point inside or even outside of the respective cluster.

The maximum and minimum representation techniques as well as the distribution preserving representation, which is a novelty within the scope of this thesis, can be interpreted as methods that focus on the consideration of additional information and are thus replacing the manual addition of extreme periods. Further, the maximum and minimum representation have a special function for error bounding methods that will be presented in Section 3.4.1.

In the following, each of the mentioned representation methods will be analyzed for two exemplary data sets. The first dataset represents two one-dimensional attributes normalized to values between 0 and 1 (minmax-normalization) resulting in a 2-dimensional data cloud, which is used to illustrate the respective method in a representable way. The dataset is depicted in Figure 3.5 and is based on randomized data. The second dataset is the hourly resolved ENTSO-e profile for Germany in 2010, which was used and normalized to 1 MW peak demand. The respective duration curve as well as the profile during a week in February are shown in Figure 3.6. In the following, this dataset comprising a single attribute is clustered to typical days, i.e. it is clustered in a 24-dimensional space as described in the preceding section. This dataset has a higher practical relevance because e.g. the impact of clustering on the duration curve can be

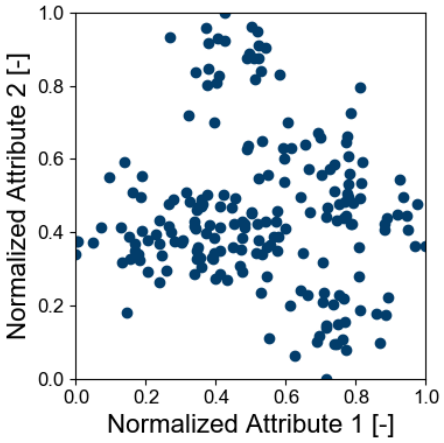

Figure 3.5. An exemplary data cloud used for visualizing the clustering process

examined. However, the illustration of the data space itself is not possible due to its high dimensionality. Furthermore, both datasets were grouped into eight clusters using Ward's (deterministic) hierarchical algorithm in order to guarantee an identical set of clusters throughout all sections, which facilitates the a comparison among the representation methods and isolates their impact.

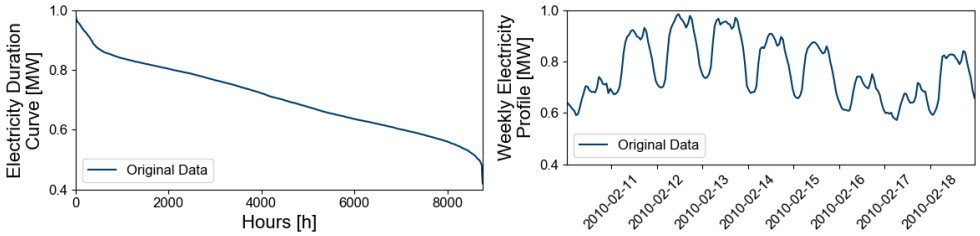

Figure 3.6. The yearly duration curve of an exemplary electricity profile and its profile during a week in February

3.2.1. Centroids

The simplest and most frequently used method to represent a cluster is to take its centroid as representative. The centroid of a cluster is given by the arithmetic mean position of all points belonging to the respective cluster in each dimension, i.e.:

$$r_{k,a,t} = \frac{1}{|C_k|} \sum_{p \in C_k} x_{p,a,t} \tag{3.1}$$

Generally, the arithmetic mean does not coincide with an existing candidate point, which is highlighted in Figure 3.7. Theses clusters were subsequently represented by their centroids depicted as colored rings. Moreover, none of the cluster centers is lying on the edges of the normalized solution space, which is defined by the minimum and maximum positions of the data cloud in each direction. The reason for this is that all of the representatives lie within the middle of their respective clusters. With respect to temporal aggregation based on clustering, this leads to an underestimation of the time series' maximum values and an overestimation of its minimum

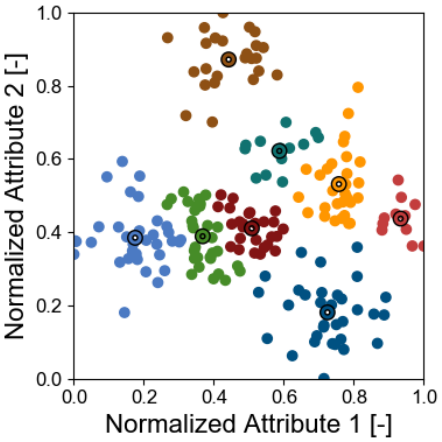

Figure 3.7. A clustered data cloud including the cluster's centroids

values as predicted by the aggregated time series, which is exemplary shown in the left and right graph of Figure 3.8. As extreme values in time series represent extreme situations an energy system needs to handle, a centroid-based representation is likely to lead to component designs that are not operationally feasible for the extreme events in the original time series.

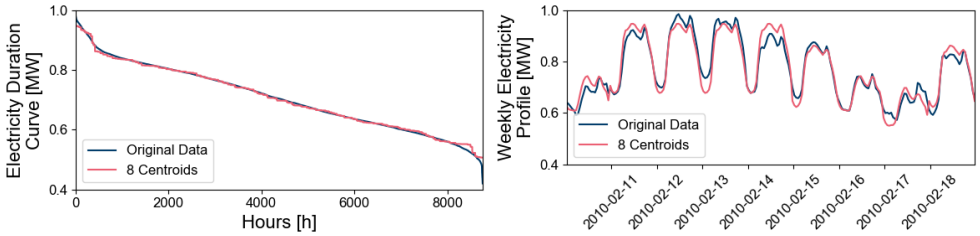

Figure 3.8. The yearly duration curve of an exemplary electricity profile, its profile during a week in February and the corresponding aggregated time series as predicted by eight typical days using hierarchical clustering and centroids as representatives (taken from Hoffmann et al. [3])

According to **Lemma 1** in Appendix G, the representation by centroids minimizes the sum of squared distances between predicted and aggregated time steps. Hence, this representation method also minimizes the root-mean-square error despite of the underestimation of extreme values. As the root-mean-square error is often used for evaluating the quality of an aggregation, but the extreme values of the original time series are likely important for the system design, this emphasizes that small input-based error metrics such as the root-mean-square error do not necessarily indicate that the design relevant characteristics of the time series are captured.

In summary, the representation by centroids is the method with the minimum root-mean-square error, but simultaneously the method, which suffers the most from a loss of design-relevant variance in the aggregated time series.

3.2.2. Medoids

Another method to represent clusters is the selection of medoids. A medoid is defined as the sample point within a cluster that minimizes the sum of distances to the remaining points in the cluster. In contrast to the centroid, a cluster's medoid thus stems from the original data set. The medoid is generally defined by that sample point within a cluster that minimizes the sum of squared Euclidean distances to all the other sample points assigned to that cluster [48, 156], i.e.:

$$r_{k,a,t} = \underset{l \in C_k}{\operatorname{argmin}} \sum_{p \in C_k} \operatorname{dist}(x_{p,a,t}, x_{l,a,t}) \tag{3.2}$$

With

$$\operatorname{dist}(x_{p,a,t}, x_{l,a,t}) := \sum_{a=1}^{N_a} \sum_{t=1}^{N_t} (x_{p,a,t} - x_{l,a,t})^2 \tag{3.3}$$

Mathematically, the medoid is the sample point within a cluster, which is closest to the centroid. This is proven by **Lemma 2** which is derived from Sifa et al. [184]. Therefore, many basic traits of medoids are comparable to those of centroids. This can also be observed in Figure 3.9, which depicts the same clusters as Figure 3.7, but with medoids as representatives that are illustrated as rings with the color of their cluster. They now always encircle a sample point, which emphasizes that they always coincide with a point stemming from the original data set. Analogously to centroids, they neither lie on the edges of the normalized clustering space, which leads to an underestimation of extreme values if the data set is represented by its medoids. This can also be observed for the duration curve and the weekly profile of the exemplary electricity demand time series shown in Figure 3.10.

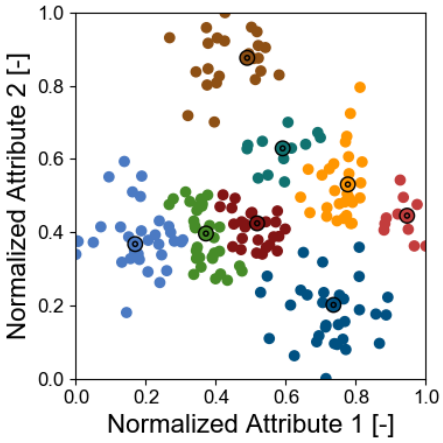

Figure 3.9. A clustered data cloud including the cluster's medoids

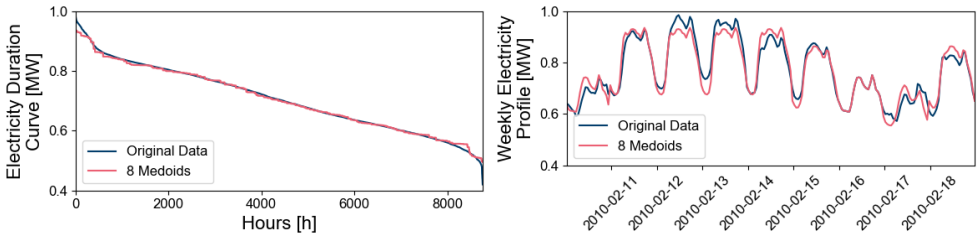

Figure 3.10. The yearly duration curve of an exemplary electricity profile, its profile during a week in February and the corresponding aggregated time series as predicted by eight typical days using hierarchical clustering and medoids as representatives

In comparison to the centroid-based duration curve, almost no deterioration of the match between the medoid-based duration curve and the duration curve of the original data can be observed. However, a small deterioration with respect to the root-mean-square error is always present due to the constraint that a medoid has to stem from the original data set. This is also highlighted by the weekly profile in the right graph of Figure 3.10, because the profile based on aggregated data on February 16, 2016 is completely matching the profile of the non-aggregated time series on that day, which means that this day was chosen as a medoid.

In conclusion, the representation by medoids differs only slightly from the representation by centroids, but the use of existing sample points or typical periods generally leads to a slightly higher inner-daily variance. This could (but not necessarily) lead to more robust system designs at a given temporal resolution at the cost of deviating mean values, e.g. the average energy supply of a whole year.

3.2.3. Maxoids

In contrast to the medoid, the maxoid is defined by Sifa et al. [184] as the point that maximizes the sum of squared Euclidean distances to all the other points within a dataset, i.e.:

$$x_{maxoid} = \underset{l \in P}{\operatorname{argmax}} \sum_{p=1}^{N_p} \sum_{a=1}^{N_a} \sum_{t=1}^{N_t} \left(x_{p,a,t} - x_{l,a,t}\right)^2 \tag{3.4}$$

With

$$\operatorname{dist}\left(x_{p,a,t}, x_{l,a,t}\right) := \sum_{a=1}^{N_a} \sum_{t=1}^{N_t} \left(x_{p,a,t} - x_{l,a,t}\right)^2 \tag{3.5}$$

Furthermore, Sifa et al. [184] have shown that the maxoid of a (general) dataset is thus the point which is furthest away from that specific dataset's centroid, which is also proven by **Lemma 2**. This is a convenient feature of maxoids because the underestimation of extreme values emerged as a potential drawback from the analysis of the aforementioned representation techniques. Because every cluster has to be represented by an own maxoid but it is preferable to represent the clusters of a data set by the points that are farthest away from all the other sample points of the **whole** data set, we define a cluster's maxoid as follows:

$$r_{k,a,t} = \underset{l \in C_k}{\operatorname{argmax}} \sum_{p=1}^{N_p} \operatorname{dist}(x_{p,a,t}, x_{l,a,t}) \tag{3.6}$$

This approach is a novelty in the field of energy system modelling because it provides an automatic detection of outliers in a straightforward manner without a user-specified addition of extreme periods. Figure 3.11 illustrates the impact of the proposed representation method on the exemplary clustered data set of the preceding sections. As it can be seen, the representatives of all clusters are constrained to be points of the original data set, which is analogous to the medoids representation. Moreover, all representatives strive to maximize their distance to the data set's centroid, which also means that the representatives of the outer clusters form an approximation of a convex hull of the data cloud. In combination with the k-maxoids algorithm, the inner clusters also tend to move to the outer regions of the data cloud. However, this cannot be observed here because the clusters were determined with Ward's hierarchical algorithm in order to guarantee comparability with the other representation methods. Moreover, it can be seen that the maxoid representation does not necessarily identify those cluster points containing a minimum or maximum attribute value, because it maximizes the circular (Euclidean) distance to the data set's centroid. However, it is noteworthy that the proposed representation method succeeds in finding three out of four data points containing an extreme value for one of the two attributes. Moreover, if we consider both attributes as additive energy demands, it is obvious that e.g. the determined representative of the yellow cluster might be a more critical operation point than those of the brown and the light red cluster in *Figure 3.11*.

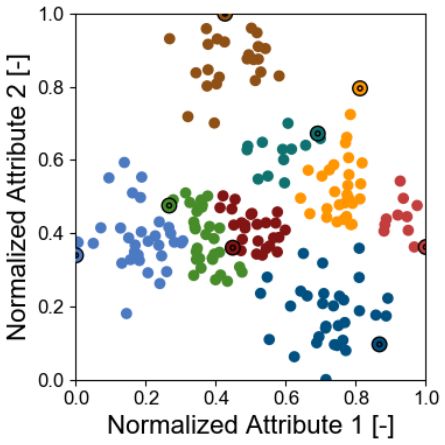

Figure 3.11. A clustered data cloud including the cluster's maxoids

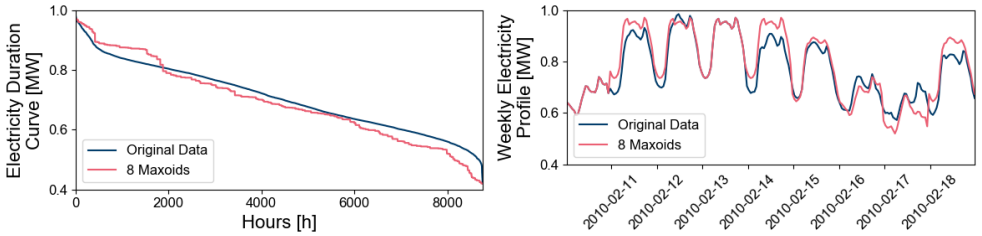

Figure 3.12. The yearly duration curve of an exemplary electricity profile, its profile during a week in February and the corresponding aggregated time series as predicted by eight typical days using hierarchical clustering and maxoids as representatives

With respect to the aggregation of the exemplary energy demand to eight typical days using maxoids as representation it can be seen that the duration curve of the aggregated time series deviates stronger from the duration curve of the original time series compared to the centroid and medoid representation. This, however, is intended because each maxoid is the point of a cluster with the maximum distance to all other points of the data cloud. On the other hand, the extreme values of the maxoid-based aggregated time series are significantly closer to the original time series' extreme values compared to the previously analyzed representation methods. Nevertheless, it can also be observed that the maxoids neither succeed to capture the overall maximum (and minimum) of the duration curve. The reason for this is the high dimensionality of typical periods in the clustering space: As a typical day for one attribute of hourly data already consists of 24 dimensions in the solution space, the outmost data point is unlikely to be an extreme point in each of its dimensions. This finding is supported by the previously investigated two-dimensional data cloud for which the three maxoids coincided with three out of four data points containing an extreme value of one of the attributes. Finally yet importantly, the weekly profile to be seen in the right part of Figure 3.12 reveals that the maxoids are analogously to medoids part of the original data set because the profile of the aggregated time series for February 10, 2010 matches with the original data on that day.

To sum up, the representation by maxoids is a promising aggregation approach if a time series' extreme values are of specific interest. This is e.g. given for capacity expansion models that need to lead to feasible system designs.

3.2.4. Maximum- and Minimum Representation

The fourth option to represent clusters implemented within the scope of this thesis is the representation by time step- and cluster-wise minimums or maximums of the respected attribute. This approach is an essential part of the systematic definition of upper and lower bounds of an aggregated energy system model's optimal objective presented in Section 3.4. For this purpose, a set M is defined, which contains those attributes, whose time steps should be represented by the minimum values within each cluster. The time steps of those attributes that are not contained in the dictionary are represented by their maximum within each cluster. Mathematically, this procedure can by described as follows with $\mathrm{b_{a,t}}$ a vector of binaries defining whether the time steps of an attribute should be represented by its cluster's minimum or maximum values.

$$\mathrm{r_{k,a,t}} = \min_{\mathrm{p \in C_k}} \mathrm{x_{p,a,t}} \cdot \mathrm{b_{a,t}} + \max_{\mathrm{p \in C_k}} \mathrm{x_{p,a,t}} \cdot \left(1 - \mathrm{b_{a,t}}\right) \quad \forall \quad \mathrm{a \in A, t \in T} \tag{3.7}$$

With

$$\mathrm{b_{a,t}} = \begin{cases} 1 \text{ if } \mathrm{a \in M_{minimize}} \\ 0 \text{ if } \mathrm{a \notin M_{minimize}} \end{cases} \forall \mathrm{t \in T} \tag{3.8}$$

The approach to represent time steps by their minimum values within the cluster was first proposed by Bahl et al. [181] for the time series of a heating and cooling demand. However, the attribute-specific option to under- or overestimate attributes is a novelty presented in this thesis. Figure 3.13 emphasizes the impact of the proposed method on the two-dimensional exemplary data set for two attributes. Here, the minimum value of each time step was chosen as representation of Attribute 1 and the maximum value for Attribute 2. Thus, the representatives lie in the upper left corner of an imaginary rectangle around the respective cluster. Moreover, it

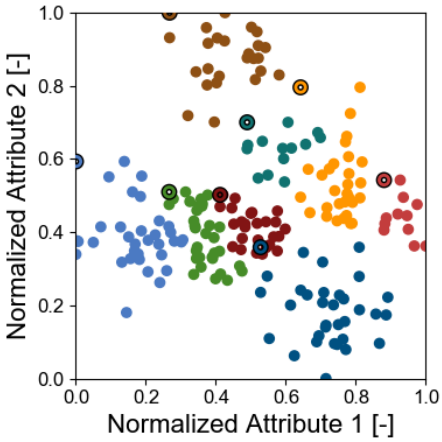

Figure 3.13. A clustered data cloud including the cluster's minimum values for one attribute and maximum values for the other attribute as time representatives

can be seen that the representatives are not samples from the original data set. Instead, each value of the representative's time step is taken from another sample within the cluster. It is noteworthy that the representation of each cluster by a predefined extreme value of the attribute leads to a systematic bias with respect to the aggregated time series' mean values.

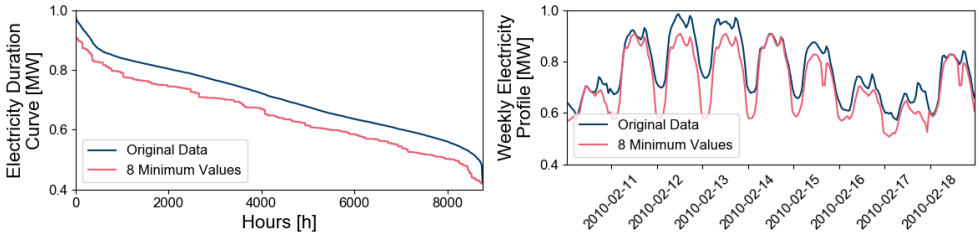

Figure 3.14. The yearly duration curve of an exemplary electricity profile, its profile during a week in February and the corresponding aggregated time series as predicted by eight typical days using hierarchical clustering and the minimum values per time step and cluster

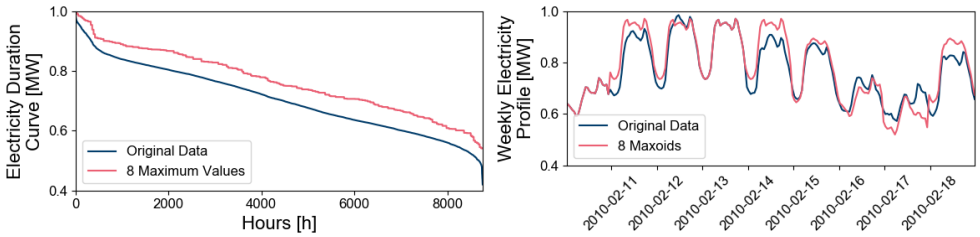

Figure 3.15. The yearly duration curve of an exemplary electricity profile, its profile during a week in February and the corresponding aggregated time series as predicted by eight typical days using hierarchical clustering and the maximum values per time step and cluster

Figure 3.14 and Figure 3.15 illustrate the two proposed representation options for the hourly resolved yearly electricity demand. As the left picture in Figure 3.14 illustrates, the representation of each time step within a typical period by the cluster's minimum value at that time step leads to a strict underestimation of the original time series' distribution of values. The same can be observed for the weekly profile in the right graph of Figure 3.14: As indicated by the weekly profile, the time series predicted by aggregated data using the minimum representation defines a lower bound for all time steps of the original time series.

The opposite can be observed for the representation by maximum values as shown in Figure 3.15. Here, the duration curve based on aggregated data strictly overestimates the original time series' one. Moreover, the same holds true for the unsorted profiles of the

original time series and the one based on aggregated data as shown in the right half of Figure 3.15. Thus, the representation by time step- and cluster-wise maximum values defines an upper bound of the original time series. Analogously to the representation by maxoids, these proposed aggregated methods obviously do not strive to maintain the mean value of a time series. However, the deviation between the predicted lower and upper bound is decreased by increasing the number of typical periods.

Finally yet importantly, it needs to be highlighted that the over- or underestimation depending on the attribute is the only method that requires additional knowledge of the modeler on the energy system model. E.g. for a robust system design, energy demand time series need to be overestimated, while the capacity factors of renewable energy sources need to be underestimated within the same model run.

3.2.5. Distribution Preserving Representation

The last representation approach and simultaneously the most complex one is a completely novel approach developed within the scope of this thesis that strives to preserve two important statistical features of the original time series: The mean and the sorted value distribution (and therefore also the variance) of an attribute's time series. In particular, this means that not only the original time series, but also their sorted value distributions, which is commonly referred to as duration curves in the energy sector, are approximated as close as possible. As mentioned in the introduction, aggregation techniques can be found in literature that focus on approximating a time series' duration curve instead of the time series itself [24, 98, 185], but to the best of the author's knowledge, no approach exists so far that focuses on approximating both simultaneously as close as possible.

Given a set of periods p for an attribute a with and inner-period time steps t being assigned to a cluster k, i.e. $X_{a,k} = \{x_{p,a,t}\}_{p \in C_k, t \in T}$ with the size $|T| \times |C_k|$, we can sort the values of the set $X_{a,k}$ in descending order, such that we yield the following sequence:

$$\widetilde{X}_{a,k} = \left(x_i \in X_{a,k} \middle| x_{i+t} \leq x_i\right)_{i \in N} \tag{3.9}$$

Accordingly, each cluster has an own sorted value distribution for each attribute consisting of $|T| \times |C_k|$ values. Note: The union of all

clusters' sorted value distributions thus yields the original sorted value distributions (duration curve) of the attribute, i.e.:

$$\widetilde{X}_a = \left(x_i \in \cup_k X_{a,k} \,\middle|\, x_{i+t} \leq x_i\right)_{i \in N} \tag{3.10}$$

Hence, the duration curve of the attribute's original time series is well approximated if the sorted value distributions of the respective clusters are properly represented. For that, we now average every $|C_k|$ values of the duration curve of each cluster so that it results in a sequence consisting of $|T|$ elements:

$$\widetilde{Y}_{a,k} = \left(y_i = \frac{1}{|C_k|} \sum_{j=i\times|C_k|}^{(i+1)\times|C_k|-1} \widetilde{X}_{a,k}(j) \,\middle|\, y_{i+t} \leq y_i\right)_{i \in N} \tag{3.11}$$

The sequence $\widetilde{Y}_{a,k}$ is containing the $|T|$ values that are meant to form the representative's values for the $|T|$ inner-period time steps of a specific attribute in a specific cluster. However, their order to represent the original periods assigned to the specific cluster optimally are still unknown. For this, we define a mixed-integer linear program that orders the values within the set $\widetilde{Y}_{a,k}$ in such way that the sum of squared distances to all $|C_k| = K$ values at a specific time step in $X_{a,k}$ are minimized. For $y_i \in \widetilde{Y}_{a,k}$ and $x_{j,p} \in X_{a,k}$ with $i, j \in T$ and $p \in C_k$, the optimization problem thus yields:

$$\begin{aligned} \min & \sum_{i=1}^{|T|} \sum_{j=1}^{|T|} \sum_{p \in C_k} \left\| y_i - x_{j,p} \right\|^2 \times z_{i,j} \\ \text{s.t.} & \sum_{i=1}^{|T|} z_{i,j} = 1 \;\forall\, j \\ & \sum_{j=1}^{|T|} z_{i,j} = 1 \;\forall\, i \\ & z_{i,j} \in \{0,1\} \;\forall\, i, j \end{aligned} \tag{3.12}$$

Here, the first equation is the objective, i.e. to minimize the sum of squared distances of the $|T|$ values y_i to the $|T| \times |C_k|$ values $x_{j,p}$. $z_{i,j}$ is a $|T| \times |T|$ matrix that defines which value y_i is mapped to which inner-period time step in $|T|$ so that the sum of squared distances to all $|C_k| = K$ values at that specific time step in $X_{a,k}$ are minimized. The side constraints define that only exactly one value y_i is assigned to one time step in $|T|$.

As **Lemma 3** shows, the optimal assignment of the y_i can also be obtained by solving the mixed-integer linear program

$$\begin{aligned} \min & \sum_{i=1}^{|T|} \sum_{j=1}^{|T|} \left\| y_i - \mu_j \right\|^2 \times z_{i,j} \\ \text{s.t.} & \sum_{i=1}^{|T|} z_{i,j} = 1 \; \forall \, j \\ & \sum_{j=1}^{|T|} z_{i,j} = 1 \; \forall \, i \\ & z_{i,j} \in \{0,1\} \end{aligned} \tag{3.13}$$

With

$$\mu_j = \frac{1}{|C_k|} \sum_{p \in C_k} x_{j,p} \tag{3.14}$$

As **Lemma 4** proves that the relaxation of this mixed-integer linear program is a linear program and hence convex. Therefore, each mathematical operation that improves the objective is an iteration towards the optimal solution. As **Lemma 5** illustrates, swapping two columns within $z_{i,j}$ does not violate the mixed-integer linear program's constraints. Furthermore, it is shown for a single swap that the optimal solution is obtained by assigning the i_{th} biggest $y_i \in \widetilde{Y}_{a,k}$ to the j_{th} biggest $\mu_j \in M_{a,k}$. Accordingly, the optimization problem can be avoided with a simple sorting algorithm.

To summarize the mathematical findings, Figure 3.16 and Figure 3.17 illustrate the steps that are needed to determine distribution and mean-preserving representatives as flowchart and the corresponding graphical interpretation.

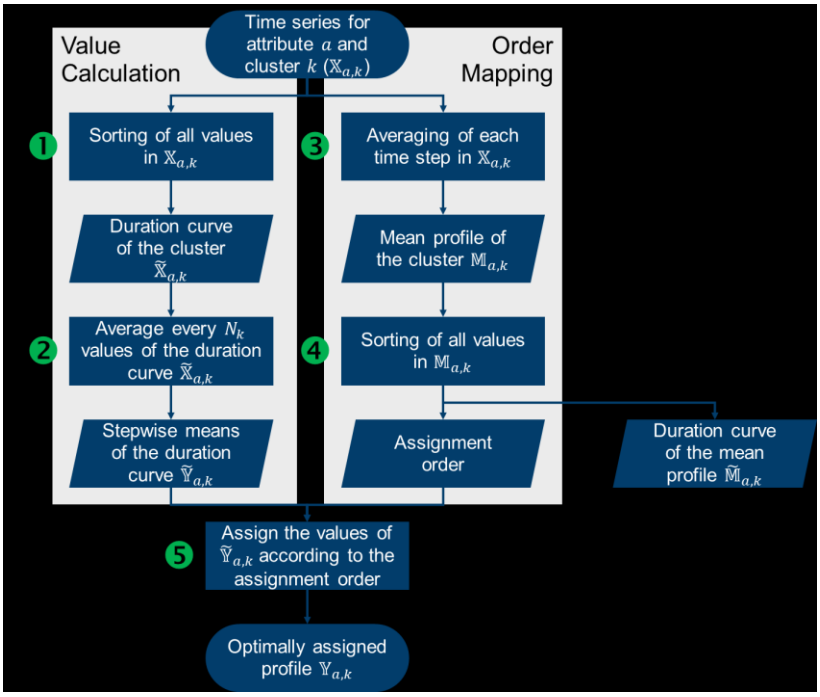

Figure 3.16. The flow chart for the distribution preserving representation method

1. "For a specific attribute a, sort all values of those periods that are assigned to a specific cluster k and yield the cluster's duration curve $\widetilde{X}_{a,k}$. This is illustrated by the green duration curve in Figure 3.17.
2. Average every $|C_k|$ values of the cluster's duration curve $\widetilde{X}_{a,k}$ in order to obtain the duration curve of the cluster's representative $\widetilde{Y}_{a,k}$, which is represented by the brown line in Figure 3.17.
3. Simultaneously, calculate the mean (i.e. centroid) profile $M_{a,k}$ for the specific attribute a using all periods assigned to cluster k for each time step represented by the dark blue line in Figure 3.17.
4. Determine the mean profile's duration curve $\widetilde{M}_{a,k}$ by sorting its values and extract the order of time steps t in which they appear in the sorted curve $\widetilde{M}_{a,k}$. The sorted mean profile is represented by the yellow line in Figure 3.17.
5. Assign the index order from $\widetilde{M}_{a,k}$ to the sorted values of $\widetilde{Y}_{a,k}$ and sort them such that the attached indices of $\widetilde{Y}_{a,k}$ are in ascending order. The result is the representative profile $Y_{a,k}$ and is depicted as red line in Figure 3.17." (Hoffmann et al. [3])

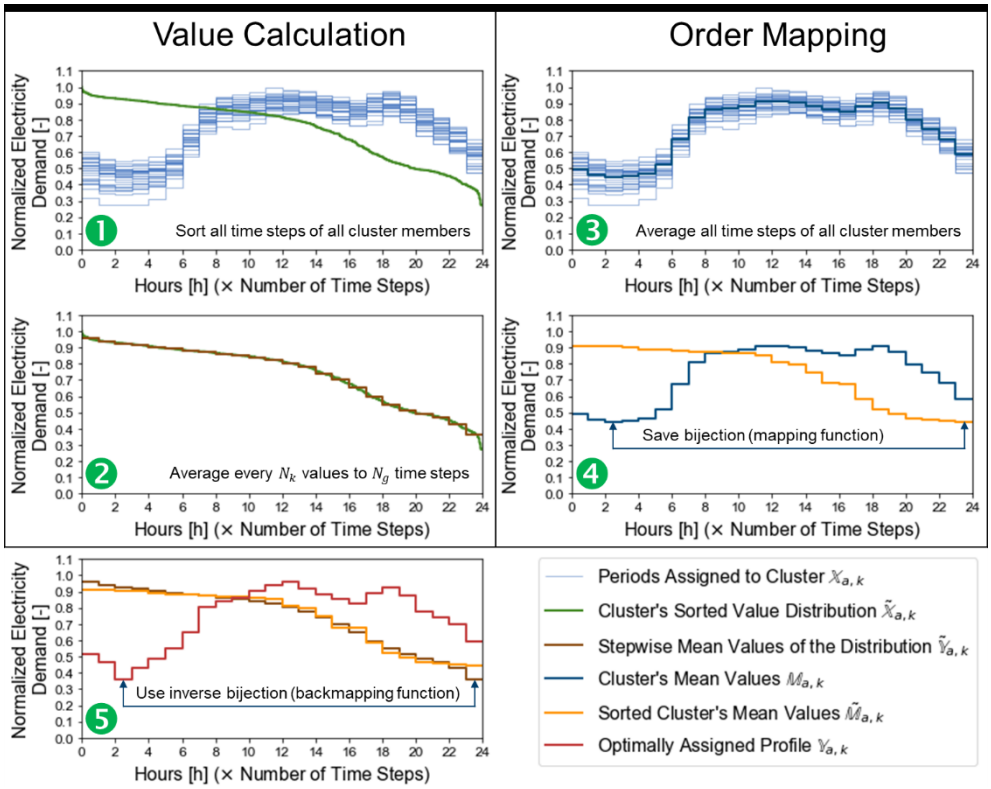

Figure 3.17. The graphical interpretation of the operations in Figure 3.16 (taken from Hoffmann et al. [3])

It is worth mentioning that the stepwise averaged duration curve $\widetilde{\mathrm{Y}}_{\mathrm{a,k}}$, which is represented by the brown line in Figure 3.17, is also slightly underestimating the variance of the cluster's original duration curve $\widetilde{\mathrm{X}}_{\mathrm{a,k}}$ given by the green line because of the averaging itself which, as shown by **Lemma 1**, is always minimizing the variance of the values being averaged. Therefore, the proposed method is only approximating the original time series' variance. Furthermore, this effect is increasing for a larger number of values, i.e. larger $|\mathrm{C_k}|$. This goes along with an underestimation of the maximum and overestimation of the minimum values. However, when comparing the stepwise averaged duration curve $\widetilde{\mathrm{Y}}_{\mathrm{a,k}}$ to the duration curve of the mean profile $\widetilde{\mathrm{M}}_{\mathrm{a,k}}$ given by the yellow line in Figure 3.17, it is obvious that the cluster's original variance is much closer approximated by $\widetilde{\mathrm{Y}}_{\mathrm{a,k}}$ than by $\widetilde{\mathrm{M}}_{\mathrm{a,k}}$.

The difference between $\widetilde{Y}_{a,k}$ and $\widetilde{M}_{a,k}$, however, decreases with a decreasing number of time steps $|T|$ per period. In case of typical time steps, i.e. typical periods with a length of only one time step, both single-valued duration curves $\widetilde{Y}_{a,k}$ and $\widetilde{M}_{a,k}$ coincide. This finding is supported by Figure 3.18, which shows the result of the proposed approach for the exemplary data set that was already used in the prior sections. As it can be seen, the clusters' representatives coincide with the clusters' centroids, because the attributes of this data set consist of a single time step only.

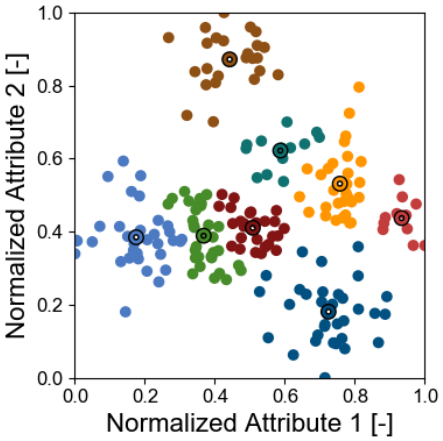

Figure 3.18. A clustered data cloud including the cluster's approximately distribution preserving representatives

In contrast to that, the hourly resolved electricity profile was aggregated to typical days, i.e. $|T| = 1$. Accordingly, the advantage of the proposed representation method with respect to the approximation of the original time series' duration curve is clearly shown in Figure 3.19.

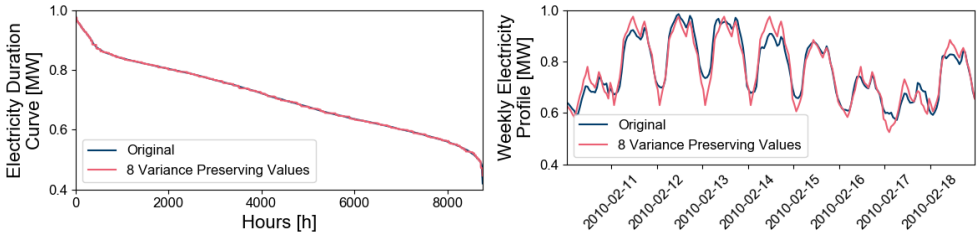

Figure 3.19. The yearly duration curve of an exemplary electricity profile, its profile during a week in February and the corresponding aggregated time series as predicted by eight typical days using hierarchical clustering and the approximately distribution preserving representation method (taken from Hoffmann et al. [3])

As the left graph of Figure 3.19 illustrates, the method proposed in this section clearly outperforms all previously introduced methods with respect to their capability of preserving the original time series' value distribution. However, the weekly electricity profile in the right half of Figure 3.19 reveals that the inner-daily variance is slightly overestimated because the proposed method is designed to preserve the variance of the clusters, not the one of candidate days individually. As different days might have a low inner-daily

variance, but differ from each other with respect to their 24h-mean, they might imply a strong common variance when they are assigned to the same cluster. Furthermore, it needs to be highlighted that the root-mean-square error between the unsorted original and predicted time series based on this representation method is bigger than that of the centroid-based representation due to **Lemma 2**. Finally yet importantly, the order for distributing the values in $\widetilde{Y}_{a,k}$ differs for each attribute. Therefore, a correlation between certain attributes might deviate from the one of the original time series to a certain degree.

In conclusion, the method succeeds in approximating the extreme values of the time series without creating a systematic bias to either side and neither increases the number of necessary typical periods, nor requires specific information on the attribute type. Moreover, it is an original contribution of this thesis and its effectiveness will excessively be validated for the test systems introduced in Section 4.1.

3.2.6. Summary of Representation Methods

In conclusion, the five introduced representation methods focus on different purposes with respect to time series aggregation for energy system models: The first two, i.e. the centroid- and medoid-based representations, are well-known methods that are adequately explored in literature and focus on the conservation of mean values only. However, the approach to separate the final representation step from those within the aggregation process a novelty of this thesis.

The maxoid representation is a diametrically opposed approach, which aims at approximating a convex hull of the clustered data cloud with a subset of representatives. Although the k-maxoids algorithm was introduced in 2015 by Sifa et al. [184], it has not been applied in the field of energy system models before.

To the best of the author's knowledge, the systematic underestimation of time series using aggregation and a representation by minimum values was first introduced by Bahl et al. [181]. Yet, the free option of attribute-wise under- or overestimation depending on the attribute's meaning for the energy system model and whether an upper or lower bound for the model is desired is an extension to the preexisting concepts.

Lastly, the approximately distribution-preserving representation method is a fundamental novelty, which will be benchmarked against the aforementioned methods in order to estimate its effectiveness.

Finally, none of the proposed methods needs additional extreme periods, which would increase the computational load. Accordingly, the combinatorial problem of adding extreme periods for a large number of time series as described in Chapter 2 is avoided.

3.3. Error and Complexity Indicators

As highlighted before, clustering is generally striving to minimize the deviation between an aggregated dataset and the original dataset. This feature makes it superior to other temporal aggregation techniques, but it also drove the development of error metrics, which strive to quantify the error that occurs when a data set is reduced. Moreover, an intrinsic motivation for time series aggregation in general is to derive approximate solutions of energy system models, which would be computationally intractable in the fully resolved case. As the fully resolved case is unknown, the deviation of the aggregated solution from the optimal solution of the fully resolved energy system is often unknown. This paradox further motivated the application of clustering indicators in place of a not quantifiable deviation between the optimal solution of the aggregated optimization problem and the fully resolved optimization problem. However, to this end, the validity of clustering indicators for quantifying the aggregation-induced deviation of the energy system's optimal solution from the reference case has never been assessed in the literature. The following section addresses this question by introducing an approach for assessing the suitability of a clustering indicator for implying a suitable temporal aggregation of the optimization problem if the fully resolved system is small enough to be solved.

As stated above, the actual error that is made due to using aggregated time series can only be determined after the energy system optimization has been executed for both, the aggregated and the fully resolved case. We therefore refer to these error metrics as a posteriori error indicator. In contrast to that, clustering indicators exclusively estimate the error between the aggregated time series and the fully resolved time series. Accordingly, these errors can be determined without an optimization of the energy system model. For that reason, we refer to them as a priori error indicators in the following.

Figure 3.20 illustrates the definitions of a priori indicators and a posteriori indicators. Further, it depicts the tools used for performing the aggregation **tsam** and the tool for performing the energy system optimization **FINE**.

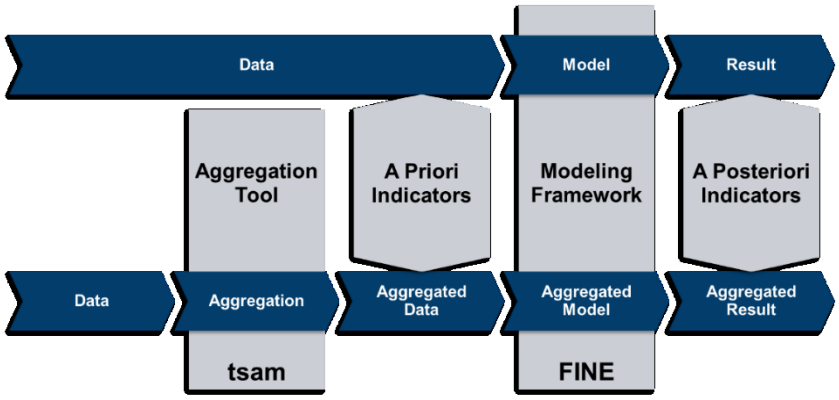

*Figure 3.20. The different definitions of a priori indicators comparing evaluating aggregated **input** data to the model and a posteriori indicators accessing **output** data of the model (taken from Hoffmann et al. [2])*

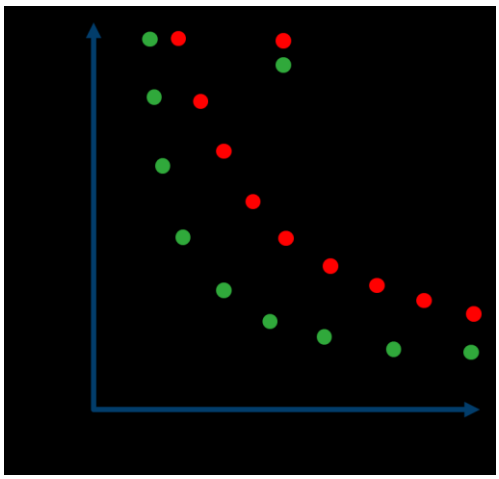

Figure 3.21. Scheme of two aggregation methods in which the second one strictly dominates the first one

As temporal aggregation is always a trade-off between accuracy and computational speed-up, the quality of an aggregation method can only be accessed by evaluating both, the aggregation-induced error and the remaining complexity of the input time series or the model itself. For that reason, error indicators are complemented by complexity indicators. In that way, aggregation techniques can be evaluated independently from the individual level of aggregation, e.g. by using the criterion of Pareto-optimality. This is exemplary illustrated by Figure 3.21, in which aggregation method 2 strictly dominates aggregation technique 1 with respect to its trade-off between complexity reduction and accuracy preservation. This means that an aggregation technique that consistently leads to smaller deviations from the fully resolved reference case for a given runtime or other complexity indicators of interest than another aggregation technique is a superior one.

3.3.1. A Priori Indicators

A priori indicators are exclusively focus on input data and compare the original time series to those predicted by the aggregation process. However, they cannot capture the importance of the individual time series for the optimized energy system, which is an outcome of the energy system model. Due to the penny switching effect, a smaller or bigger aggregation-induced error of one time series, which is connected to a specific technology, might moreover lead to the preference of another technology. Therefore, an iterative approach of weighting different time series based on their economic impact on a preliminarily solved aggregated problem does not converge. For this reason, it is generally assumed in literature that all aggregated time series contribute equally to deviations of the aggregated energy system optimization from the fully resolved case. In the following, some a priori indicators are introduced that are frequently used in clustering or time series analysis. Among them, the root-mean-square error (RMSE) between the original time series and the aggregated time series [48, 63] or average inter-cluster-distance [74, 143] and the root-mean-square error of the respective duration curves [26, 42, 61, 63, 97, 98, 100, 147, 178, 185] have gained a great popularity. Further, the Mean Absolute Error (MAE) is traditionally used as an alternative to the root-mean-square error and is therefore considered as well.

3.3.1.1. Root-Mean-Square Error (RMSE)

The root-mean-square error is both, directly addressed by the objective function of many clustering algorithms such as the k-means and k-medoids algorithm and is moreover common for estimating the prediction error of time series. Therefore, it is frequently used in in the context of temporal aggregation for energy system optimization as well.

“In the following, we define the root-mean-square error of an aggregated time series as follows:

$$\mathrm{RMSE} = \sqrt{\frac{1}{|\mathrm{P}| \times |\mathrm{T}|} \sum_{|\mathrm{C}|} \sum_{\mathrm{p} \in \mathrm{C}_\mathrm{k}} \sum_{|\mathrm{T}|} \left(\mathrm{x}_{\mathrm{p,t}} - \tilde{\mathrm{x}}_{\mathrm{k,t}}\right)^2} \tag{3.15}$$

with $|\mathrm{P}|$ the number of periods, $|\mathrm{T}|$ the number of time steps per periods and $|\mathrm{C}|$ the number of representative periods (typical days or typical time steps). $\mathrm{x}_{\mathrm{p,t}}$ is the value of the original time series at

a specific time step, e.g. for typical days, $x_{3,6}$ is the value of a time series on January 3rd at 6 a.m. and $\tilde{x}_{k,t}$ is the value of the kth cluster, which represents the respective value $x_{p,t}$ in the aggregated time series. For multiple time series (attributes) a, we form the root-mean-square error as follows:

$$RMSE_{tot} = \sqrt{\frac{1}{|A| \times |P| \times |T|} \sum_{|A|} \sum_{|C|} \sum_{p \in C_k} \sum_{|T|} \left(x_{a,p,t} - \tilde{x}_{a,k,t}\right)^2} = \sqrt{\frac{1}{|A|} \sum_{|A|} RMSE_a^2} \quad (3.16)$$

Figure 3.22 depicts the calculation of the root-mean-square error for a single attribute. Here, two days of exemplary data consisting of 24 hourly time steps each are represented by a single typical day. The squared difference between each time step and its respective aggregated time step is used for calculating the root-mean-square error." (Hoffmann et al. [2])

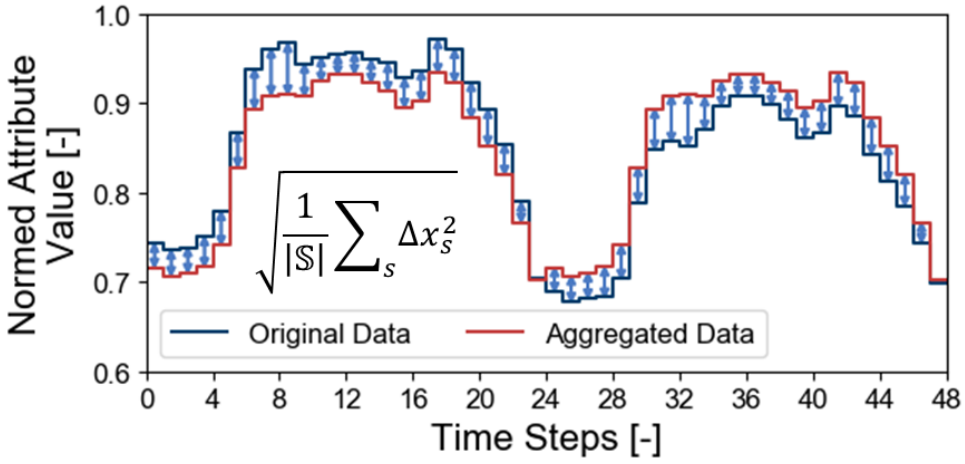

Figure 3.22. Illustration of squared summands used for calculating the root-mean-square error (taken from Hoffmann et al. [2])

3.3.1.2. Root-Mean-Square Error of the Duration Curve ($RMSE_{DC}$)

Duration curves are traditionally used in energy system optimization, e.g. because load duration curves have a big impact on the optimal full load operation time of different supply technologies. Therefore, many publications [26, 42, 61, 63, 97, 98, 100, 147, 178, 185] evaluate the effectiveness of an aggregation procedure by comparing the duration curve of the fully resolved time series against the aggregated one.

"To calculate the root-mean-square error of the aggregated time series' duration curves ($RMSE_{DC}$), the values of the clusters' representatives are repeated according to the respective cluster size

$|C_k|$, i.e. the number of days a typical day represents or the number of time steps a typical time step represents. If the values of the original and predicted time series are sorted, we receive the duration curves $x_{DC,s}$ and $\tilde{x}_{DC,s}$. Accordingly, the root-mean-square error of a duration curve is calculated as follows:

$$RMSE_{DC} = \sqrt{\frac{1}{|S|}\sum_{|S|}\left(x_{DC,s} - \tilde{x}_{DC,s}\right)^2} \tag{3.17}$$

With $|S|$ the number of total time steps. For multiple time series, the root-mean-square error of the duration curves is calculated analogously:

$$RMSE_{DC,tot} = \sqrt{\frac{1}{|A| \times |S|}\sum_{|A|}\sum_{|S|}\left(x_{DC,a,s} - \tilde{x}_{DC,a,s}\right)^2} = \sqrt{\frac{1}{|A|}\sum_{|A|} RMSE_{DC,a}^2} \tag{3.18}$$

Figure 3.23 illustrates the calculation of the root-mean-square error based on the duration curve for a single attribute based on the same exemplary time series as in Figure 3.22. In contrast to the calculation of the root-mean-square error, the root-mean-square error of the duration curve is calculated based on the sorted time series. Accordingly, the root-mean-square error of the duration curve is smaller than the root-mean-square error, which becomes evident by comparing the length of the blue arrows in both figures." (Hoffmann et al. [2])

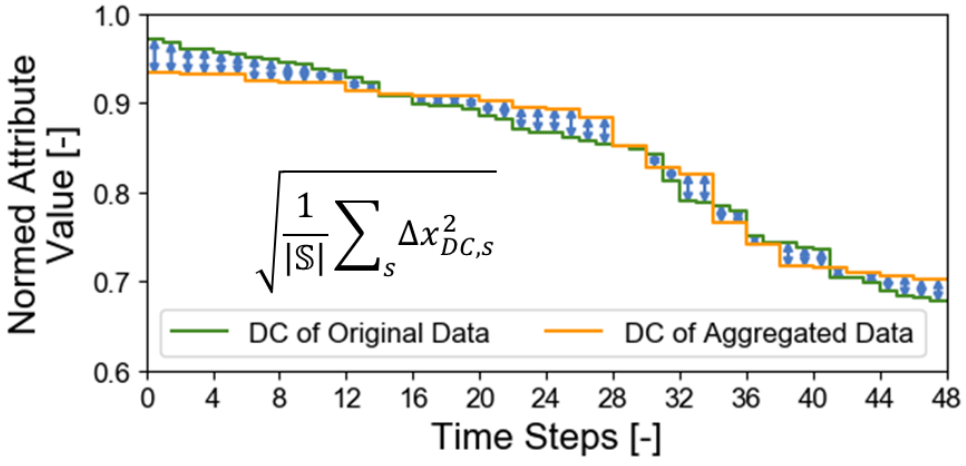

Figure 3.23. Illustration of squared summands between duration curves used for calculating the root-mean-square error of the duration curve (taken from Hoffmann et al. [2])

3.3.1.3. Mean-Absolute Error (MAE)

The MAE is the last error indicator, which uses the average error instead of the squared error, i.e.:

$$\mathrm{MAE} = \frac{1}{|\mathrm{P}| \times |\mathrm{T}|} \sum_{|\mathrm{C}|} \sum_{p \in C_k} \sum_{|\mathrm{T}|} \left| x_{p,t} - \tilde{x}_{k,t} \right| \tag{3.19}$$

And

$$\mathrm{MAE}_{\mathrm{tot}} = \frac{1}{|\mathrm{A}| \times |\mathrm{P}| \times |\mathrm{T}|} \sum_{|\mathrm{A}|} \sum_{|\mathrm{C}|} \sum_{p \in C_k} \sum_{|\mathrm{T}|} \left| x_{a,p,t} - \tilde{x}_{a,k,t} \right| = \frac{1}{|\mathrm{A}|} \mathrm{MAE}_{\mathrm{a}} \tag{3.20}$$

Figure 3.24 depicts the calculation of the MAE for the same exemplary time series. In contrast to the root-mean-square error, the absolute simple differences between the original and aggregated time steps are taken as summands for the calculation of the root-mean-square error.

Note: Because of

$$\begin{aligned} |\mathrm{S}|\mathrm{RMSE}^2 &= \sum_{\mathrm{s}} \left| \Delta x_{\mathrm{s}} \right|^2 = \sum_{\mathrm{s}} \left(\left| \overline{\Delta x_{\mathrm{s}}} \right| + \left| \Delta x_{\mathrm{s}} \right| - \left| \overline{\Delta x_{\mathrm{s}}} \right| \right)^2 \\ &= \sum_{\mathrm{s}} \left| \overline{\Delta x_{\mathrm{s}}} \right| + 2 \left| \overline{\Delta x_{\mathrm{s}}} \right| \sum_{\mathrm{s}} \left(\left| \Delta x_{\mathrm{s}} \right| - \left| \overline{\Delta x_{\mathrm{s}}} \right| \right) + \sum_{\mathrm{s}} \left(\left| \Delta x_{\mathrm{s}} \right| - \left| \overline{\Delta x_{\mathrm{s}}} \right| \right)^2 \\ &= |\mathrm{S}| \left| \overline{\Delta x_{\mathrm{s}}} \right|^2 + \sum_{\mathrm{s}} \left(\left| \Delta x_{\mathrm{s}} \right| - \left| \overline{\Delta x_{\mathrm{s}}} \right| \right)^2 \geq |\mathrm{S}| \left| \overline{\Delta x_{\mathrm{s}}} \right|^2 = |\mathrm{S}| \mathrm{MAE}^2 \end{aligned} \tag{3.21}$$

$\Leftrightarrow \mathrm{RMSE} \geq \mathrm{MAE}$

the MAE is always smaller than the root-mean-square error.

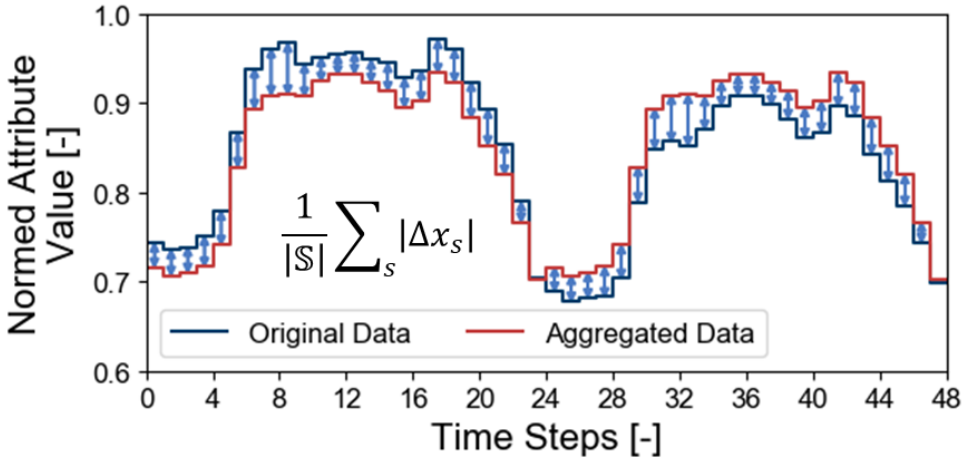

Figure 3.24. Illustration of absolute summands between duration curves used for calculating the MAE

As discussed earlier, temporal aggregation in the narrow sense fully relies on the reduction of the number of time steps considered

by the energy system model. Accordingly, the only meaningful complexity indicator for aggregated time series is the number of total time steps in the aggregated time series in relation to the original time series, i.e.:

$$\mathrm{I}_{\mathrm{complexity,pre}} = \frac{|\mathrm{P}| \times |\mathrm{T}|}{|\mathrm{S}|} \tag{3.22}$$

As all aggregations are performed on one year of hourly data, the total number of time steps always equals $|\mathrm{S}| = 8760$. Accordingly, the number of total time steps in the aggregated time series $|\mathrm{P}| \times |\mathrm{T}|$ can be directly compared between different methods.

3.3.2. A Posteriori Indicators

A posteriori indicators serve to analyze the result of an energy system optimization based on aggregated data compared to the fully resolved reference case. Because an optimal objective is defined by a set of optimized variables, all variables as well as the objective value in the optimal point of the aggregated solution system could be used for estimating the deviation from the reference case. From a political and engineering perspective, the build capacities of the system's components and the total annualized costs are of special interest. However, as it was shown earlier, energy systems are likely to suffer from the so-called penny switching effect, which means that the optimal size of components is highly sensitive to slight deviations in the input data, if the system comprises different component types with comparable functions and prices as shown by Example 6 in Appendix I.2.2.1. From a mathematical point of view, it is therefore not necessarily meaningful to use optimized variables such as built capacities as an indicator for the quality of an aggregation, if many system configurations exist, which are close to cost optimality. Therefore, the total annualized costs remain as dominant option for error quantification for a diversity of models.

Of course, a major purpose of energy system models is to provide information about cost-efficient system configurations and can accordingly not be neglected. Moreover, the energy systems used for validation of the presented methods are also analyzed with respect to built capacities, because a strong variability of system designs despite of a small deviation of the total annualized costs indicate the penny switching effect and that many system designs might be cost-efficient.

With respect to a posteriori complexity indicators, temporal aggregation is capable of reducing the model's complexity in many regards: Due to the reduction of considered time steps, the number of operational variables and constraints are likewise reduced. In the solving process, this affects multiple aspects such as solving time, data storage consumption and ultimately energy consumption as well. In times of large computer clusters with large random access memories, the most restrictive limitation to large energy system models are non-converging or incrementally slow converging optimizations, i.e. commercial solvers such as Gurobi fail to handle the model size properly. Accordingly, the most crucial complexity indicator for solving the model is the runtime because it cannot be addressed by using a computer with larger memory. Yet, if models should be solved on desktop PCs, storage consumption can also become an interesting aspect to be addressed by temporal aggregation.

Table 3.1 summarizes the indicators and indicator types discussed in the previous two sections depending on whether they focus on input data or output data of the optimization model. Further, it distinguished whether they indicate an aggregation-induced error or the complexity of the data or the model itself.

Table 3.1. Overview of the discussed indicators and indicator types

		Model Stage	
		A Priori	**A Posteriori**
Indicator Type	**Error**	• RMSE • $RMSE_{DC}$ • MAE	• Relative Cost Deviation • Relative Capacity Deviation

	Complexity	• Number of Total Time Steps
		  • Typical Periods
		  • Segments
			• Runtime
			• Data Storage Consumption

3.3.3. Quantifying the Quality of A Priori Indicators

In order to assess the validity of using an a priori indicator for assessing the quality of an aggregation for energy system models, mathematical connections between an a priori error and the introduced a posteriori indicator must be determined. The connection between both indicators is obviously not strict as not only the input time series, but also component specific prices drive the optimal

solution of an arbitrary energy system. As an example, we can consider one of the prior minimal examples with two rival technologies (wind and solar). Even though a big deviation between the aggregated and the original solar irradiance time series might occur, which would be indicated by bad a priori indicators, this would not necessarily lead to a big deviation of the optimal objective, e.g. if solar electricity is too expensive and solar panels are thus not part of an optimal solution.

Accordingly, the only meaningful approach for evaluating the quality of an a priori indicator is a statistical one. For this, e.g. its correlation to the a posteriori indicator can be estimated. For this, a large set of model configurations needs to be optimized with differently aggregated input data, e.g. for different numbers of typical days and different numbers of segments. In this way, the a priori and a posteriori indicators can be seen as random variables that are connected by an unknown process (the aggregation itself). One way of measuring the correlation between the a priori and a posteriori error indicators is to use the Pearson correlation coefficient, which can be calculated by:

$$\begin{aligned}\rho\left(I_{pre}, I_{post}\right) &= \frac{\mathrm{cov}\left(I_{pre}, I_{post}\right)}{\sigma_{I_{pre}}\sigma_{I_{post}}} = \frac{E\left(\left(I_{pre}-\mu_{I_{pre}}\right)\left(I_{post}-\mu_{I_{post}}\right)\right)}{\sigma_{I_{pre}}\sigma_{I_{post}}} \\ &= \frac{1}{N_{sample}} \frac{\sum_{i=1}^{N_{sample}}\left(I_{pre,i}-\mu_{I_{pre}}\right)\left(I_{post,i}-\mu_{I_{post}}\right)}{\sigma_{I_{pre}}\sigma_{I_{post}}} \\ &= \frac{1}{N_{sample}} \sum_{i=1}^{N_{sample}} I^{z}_{pre,i} \cdot I^{z}_{post,i}\end{aligned} \tag{3.23}$$

With

$$\begin{aligned} I_{pre} &= f(\#TD, \#Seg) & I_{post} &= f(\#TD, \#Seg) \\ \mu_{I_{pre}} &= \frac{1}{N_{sample}} \sum_{i=1}^{N_{sample}} I_{pre,i} & \mu_{I_{post}} &= \frac{1}{N_{sample}} \sum_{i=1}^{N_{sample}} I_{post,i} \\ \sigma_{I_{pre}} &= \sqrt{\frac{1}{N_{sample}} \sum_{i=1}^{N_{sample}} \left(I_{pre,i}-\mu_{I_{pre}}\right)^2} & \sigma_{I_{post}} &= \sqrt{\frac{1}{N_{sample}} \sum_{i=1}^{N_{sample}} \left(I_{post,i}-\mu_{I_{post}}\right)^2} \\ I^{z}_{pre,i} &= \frac{I_{pre,i}-\mu_{I_{pre}}}{\sigma_{I_{pre}}} & I^{z}_{post,i} &= \frac{I_{post,i}-\mu_{I_{post}}}{\sigma_{I_{post}}} \end{aligned} \tag{3.24}$$

Here, N_{sample} describes the sample size of model configurations used for statistically evaluating a relationship between a priori and

a posteriori indicators. It is e.g. given by the total number of aggregated system configurations based on aggregated time series given by different numbers of typical days and segments, i.e. $N_{sample} = \#TD \cdot \#Seg$. The correlation coefficient offers a compact option to quantify the validity of an a priori indicator forecasting the a posteriori indicator with a value range of $[-1,1]$ with 1 indicating perfect correlation, -1 indicating perfect anti-correlation and 0 indicating a meaninglessness of the chosen a priori indicator.

The Pearson correlation coefficient and the proposed visual analysis only account for linear dependencies between two statistical variables, but it is to this state unknown whether this assumption is justified. A more general approach is to use Spearman's rank correlation, which measures a monotonic correlation between to statistical variables only instead of a linear one. Spearman's correlation coefficient is equivalent to the Pearson correlation coefficient between the rank variables of two statistical measures, i.e.:

$$\rho\left(rg_{I_{pre}}, rg_{I_{post}}\right) = \frac{cov\left(rg_{I_{pre}}, rg_{I_{post}}\right)}{\sigma_{rg_{I_{pre}}} \sigma_{rg_{I_{post}}}} \tag{3.25}$$

Accordingly, Spearman's correlation coefficient does not compare absolute values of two stochastic variables with each other. Instead, it evaluates whether they appear in the same order when being ordered by size. Therefore, every monotonic correlation between two stochastic variables can be efficiently investigated using Spearman's rank correlation.

The proposed methods allow for a visual and a statistical analysis of the quality of a priori indicators for energy system models that are generally applicable, if the reference case is solvable. In this way, it is possible to derive the most meaningful a priori indicators for small systems and to use them for models that are more complex if it is assumed that their techno-economic structure is similar.

3.3.4. Optimal Aggregation Based on A Priori Indicators

As a two-fold clustering to fewer typical days containing fewer time steps each leads to numerous possible aggregation configurations with a comparable number of typical time steps, it is important to find a good trade-off between the number of typical days and the number of segments within each typical day. For that reason, an algorithm was developed within the scope of this thesis, which

searches for a good combination of typical days and inner-daily segments based on an arbitrary error indicator. The algorithm is based on three assumptions:

1. The runtime of the energy system model increases strictly monotonously with the number of total time steps, i.e.:

$$\begin{aligned} &\#\mathrm{TD}_1 \cdot \#\mathrm{Seg}_1 < \#\mathrm{TD}_2 \cdot \#\mathrm{Seg}_2 \\ \Leftrightarrow\ &\mathrm{runtime}(\#\mathrm{TD}_1 \cdot \#\mathrm{Seg}_1) < \mathrm{runtime}(\#\mathrm{TD}_2 \cdot \#\mathrm{Seg}_2) \end{aligned} \tag{3.26}$$

2. The chosen aggregation-induced deviation of the optimized solution from the fully resolved case is a strictly monotonous function of the error indicator, i.e.:

$$\mathrm{I}_{\mathrm{pre},1} < \mathrm{I}_{\mathrm{pre},2} \Leftrightarrow \mathrm{I}_{\mathrm{post},1} < \mathrm{I}_{\mathrm{post},2} \tag{3.27}$$

3. The chosen error indicator decreases monotonously with either both, the number of typical periods and the number of segments per typical period, i.e.:

$$\#\mathrm{TD}_1 \leq \#\mathrm{TD}_2 \wedge \#\mathrm{Seg}_1 \leq \#\mathrm{Seg}_2 \Rightarrow \mathrm{I}_{\mathrm{pre},1} \geq \mathrm{I}_{\mathrm{pre},2} \tag{3.28}$$

Concisely, this means that a larger number of typical periods and segments increases the runtime due to assumption 1, and decreases both, the score of the chosen error indicator due to assumption 3 and therefore the deviation of the optimized solution due to assumption 2. In Section 4.2, these assumptions are quantitatively assessed for three different models using Spearman's correlation coefficient.

However, the total number of time steps can be increased by either increasing the number of typical periods or the number of segments per typical period. We therefore adapt the method of steepest descent studied by Haskell [186] and adapt it to the N^2-space of the number of typical days and segments.

Let $\hat{\mathrm{p}}, \hat{\mathrm{s}}, \hat{\mathrm{t}}$ denote the number of aggregated periods, segments and total time steps. Then, the method of steepest descent of a chosen error indicator $\mathrm{I}_{\mathrm{pre}}$ for an incremental increase of the total number of time steps is given by:

$$\hat{\mathrm{t}}_{\mathrm{n}+1} = \hat{\mathrm{t}}_{\mathrm{n}} - \delta \nabla \mathrm{I}_{\mathrm{pre}}(\hat{\mathrm{t}}_{\mathrm{n}}) \tag{3.29}$$

with $\delta > 0$ as an incremental increase of the total number of time steps and $\nabla := \frac{\partial}{\partial \hat{t}} = \frac{d}{d\hat{t}}$ the partial differential of the total number of time steps. As this equation is one-dimensional, it also equals the total differential $d\hat{t}$. Because of:

$$\hat{t} = \hat{p} \cdot \hat{s} \Leftrightarrow \frac{1}{d\hat{t}} = \frac{\partial \hat{p}}{\partial \hat{t}} \cdot \frac{d}{d\hat{p}} + \frac{\partial \hat{s}}{\partial \hat{t}} \cdot \frac{d}{d\hat{s}} = \frac{1}{\hat{s}} \cdot \frac{\partial}{\partial \hat{p}} + \frac{1}{\hat{p}} \cdot \frac{\partial}{\partial \hat{s}} \tag{3.30}$$

We can rewrite:

$$\hat{t}_{n+1} = \hat{t}_n - \delta \left(\frac{1}{\hat{s}} \cdot \frac{\partial I_{pre}(\hat{t}_n)}{\partial \hat{p}} + \frac{1}{\hat{p}} \cdot \frac{\partial I_{pre}(\hat{t}_n)}{\partial \hat{s}} \right) \tag{3.31}$$

As the number of typical days and the number of segments per day are discrete, the method of steepest descent has only two possible directions to move towards the minimum error indicator, namely $\partial \hat{p} > 0$ and $\partial \hat{s} > 0$ due to the monotony assumption 3. As the *steepest* descent is chosen, the equation changes for the discrete case to:

$$\begin{aligned} \hat{t}_{n+1} &= \hat{t}_n + \delta \cdot \min \left(\frac{I_{pre}(\hat{p}_{n+1}, \hat{s}_n) - I_{pre}(\hat{p}_n, \hat{s}_n)}{\hat{s}_n \cdot (\hat{p}_{n+1} - \hat{p}_n)}, \frac{I_{pre}(\hat{p}_n, \hat{s}_{n+1}) - I_{pre}(\hat{p}_n, \hat{s}_n)}{\hat{p}_n \cdot (\hat{s}_{n+1} - \hat{s}_n)} \right) \\ &= \hat{t}_n + \delta \cdot \min \left(\frac{I_{pre}(\hat{p}_{n+1}, \hat{s}_n) - I_{pre}(\hat{p}_n, \hat{s}_n)}{\hat{t}(\hat{p}_{n+1}, \hat{s}_n) - \hat{t}(\hat{p}_n, \hat{s}_n)}, \frac{I_{pre}(\hat{p}_n, \hat{s}_{n+1}) - I_{pre}(\hat{p}_n, \hat{s}_n)}{\hat{t}(\hat{p}_n, \hat{s}_{n+1}) - \hat{t}(\hat{p}_n, \hat{s}_n)} \right) \\ &= \hat{t}_n + \delta \cdot \min \left(\frac{\Delta I_{pre}}{\Delta \hat{t}}\Big|_{\hat{p},n+1}, \frac{\Delta I_{pre}}{\Delta \hat{t}}\Big|_{\hat{s},n+1} \right) \end{aligned} \tag{3.32}$$

This means that the number of total time steps is always increased into the direction with the most negative gradient of the a priori indicator over the number of total time steps. The directions are either an increase of typical days or an increase of segments per typical day. The increment δ is always taken into the direction with the most negative gradient, i.e. it is either an increase of the number of typical days or an increase of the number of segments. A general problem of gradient-driven minimization algorithms is the optimal step width of δ. As the position of the minimum error indicator is known a priori, i.e. 365 days and 24 segments for the non-aggregated case and the convergence of $I_{pre}(\hat{p}_n, \hat{s}_n)$ resembles a two-dimensional hyperbolic function for the error indicators chosen in this thesis, a step width ratio increasing by a factor of $\sqrt{2}$ in each direction proved effective in our case studies.

Figure 3.25 maps three subsequent steps of the algorithm as described above to find the fastest decrease of an a priori error indicator over an increase of the total number of time steps given by the product of the number of segments and the number of typical days.

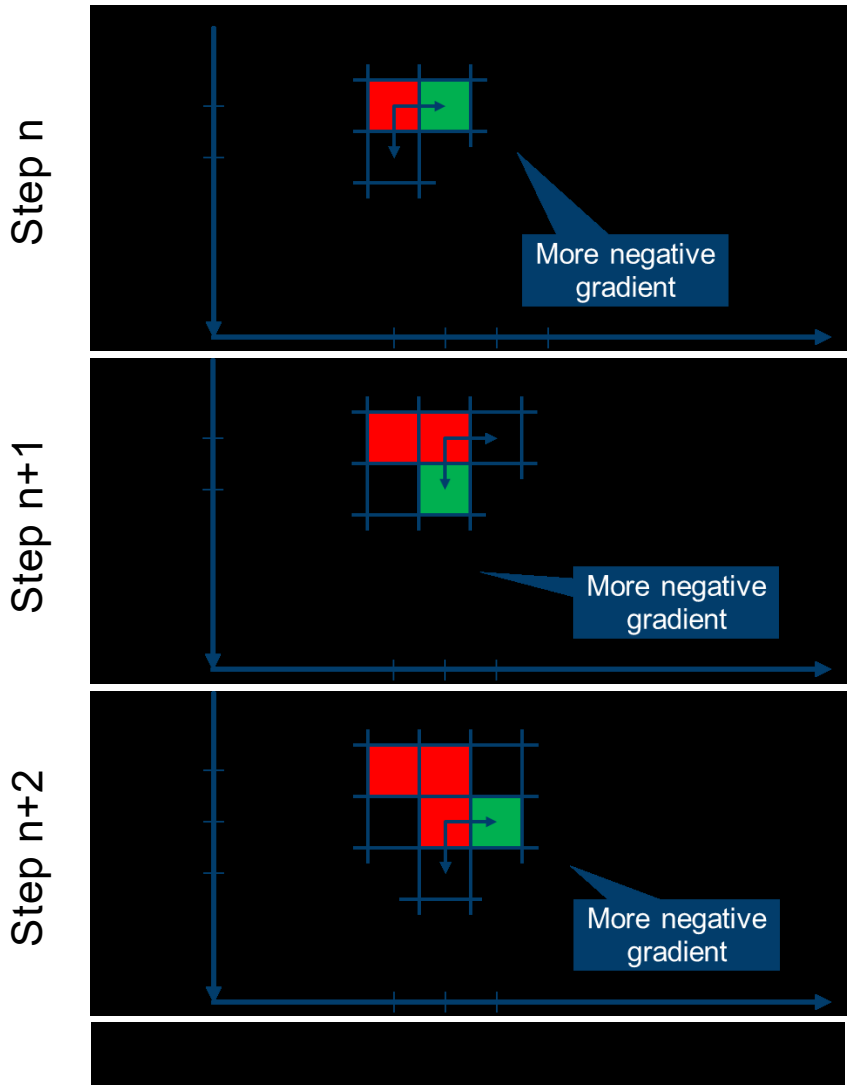

Figure 3.25. Three subsequent steps of the proposed algorithm to find the optimum number of segment and typical days (taken from Hoffmann et al. [3])

As the maximum number of segments or typical days are given by the length and the inner-daily resolution of the original time series, the optimal pathway is bounded in either direction. Therefore, once the maximum number of typical days or segments was reached, the algorithm is limited to increase the temporal resolution into the remaining direction. As soon as the original temporal resolution was reached, the algorithm is terminated. The respective flow chart of the algorithm is depicted in Figure 3.26.

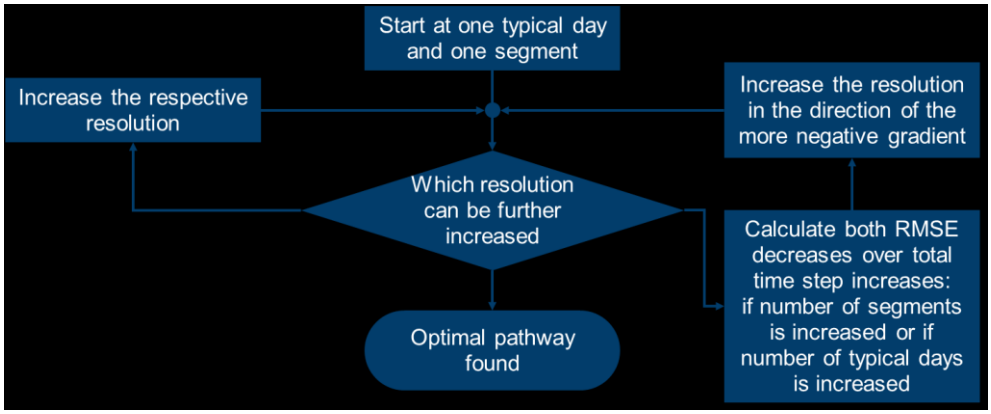

Figure 3.26. The optimal pathway algorithm from minimum to maximum resolution (taken from Hoffmann et al. [3])

It is worth mentioning that the maximum temporal resolution of a model is defined either by the respective model size or according to the modeler's preferences with respect to a reasonable solving time. Therefore, the optimal pathway algorithm can optionally be terminated as soon as it reaches an aggregation configuration whose total number of time steps surpasses a user-defined threshold if higher resolved configurations are not of interest of computationally infeasible.

In order to visualize the proposed procedure, Figure 3.27 shows the algorithm for the root-mean-square error of two single time series, a global horizontal irradiance and a wind speed time series. As clustering method, Ward's hierarchical algorithm was chosen and the found clusters were represented by their centroids. As it can be seen, the step width with which the number of typical days and segments is increased roughly corresponds to the proposed ratio of $\sqrt{2}$. The red path highlights the steps that the algorithm takes in order to decrease the root-mean-square error of the clustered time series as fast as possible. The white numbers within the red fields represent the number of total considered time steps. Accordingly, the algorithm starts at one typical day considering only one segment, i.e. one time step and gradually increases up to 8760 time steps, which means that the time series is not clustered at all. Accordingly, the root-mean-square error is zero for the fully resolved case.

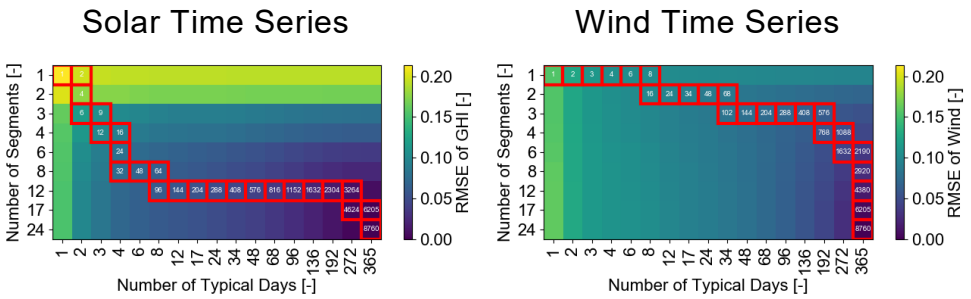

Figure 3.27. The proposed algorithm for the root-mean-square error (RMSE) of an exemplary global horizontal irradiance and a wind speed profile (taken from Hoffmann et al. [3])

As it can be seen, the optimal number of segments and typical days with respect to the chosen error indicator differs significantly for a given number of total time steps: For a solar time series, the algorithm first increases the number of segments in order to reduce the root-mean-square error rapidly and then stagnates at 12 segments per typical days. Then, the number of typical days is increased to reduce the root-mean-square error further. As expected, the algorithm ends at the total minimum of the root-mean-square error, i.e. at the fully resolved configuration. This pathway is chosen by the algorithm because solar profiles have a strong inner-daily variance on the one hand and a strong daily pattern due to the day-night-cycle on the other hand. Accordingly, an increase of the number of inner-daily time steps reduces the aggregation-induced error faster than an increase of typical days. However, this behavior changes at 12 segments per typical day. As solar profiles are approximately zero during nighttime, the two-fold clustering algorithm can choose very few time steps for the nighttime, which refers to about 50% of a day's total number of time steps. Accordingly, increasing the number of typical days in order to reduce the aggregation-induced error further becomes more advantageous.

For the wind time series, the algorithm chooses a fundamentally different pathway to decrease the root-mean-square error as fast as possible. Here, the number of typical periods is first increased while the number of inner-daily segments remains very low with no more than three segments for up to 192 typical days. After that, the number of segments is gradually increased. This can be explained by the comparably smooth but aperiodic wind profile. As wind does not have a daily pattern, local extreme values of the time series can appear at any daytime. Therefore, a high number of typical days is needed in order to approximate the set of possible inter-

daily wind profiles accurately. On the other hand, a relatively small number of inner-daily time steps is sufficient due to the relatively smooth profile. Moreover, the right plot in Figure 3.27 reveals that the number of segments has almost no impact on the aggregation-induced error, if an insufficient number of typical days is chosen. The reason for this is that the inner-daily profiles become even smoother if too many daily wind profiles are assigned to the same typical day cluster. This means, that a large number of typical days needs to be chosen before the number of segments has an impact on the aggregation accuracy.

As mentioned before, all time series of an energy system model are aggregated to the same number of typical days and segments per typical day. Accordingly, the optimal pathway is determined based on the total root-mean-square error that represents the error of all time series. Therefore, the algorithm chooses a trade-off between both extreme cases presented in Figure 3.27 if capacity factor profiles for both, photovoltaic panels and wind turbines are considered simultaneously. However, it is emphasized that different technologies need different temporal resolutions in order to be properly modeled.

3.4. Methods for Systematic Over- and Underestimations

As temporal aggregation techniques are only capable of providing approximations of the original problem, it is usually not possible to quantify the exactness of the applied method if the fully resolved reference model is not solvable due to its size. Therefore, aggregation techniques have emerged in the literature, which can guarantee that the optimal objective of the reference model is either over- or underestimated. The concept of these estimators, which is also referred to as upper and lower bounds, is depicted in Figure 3.28.

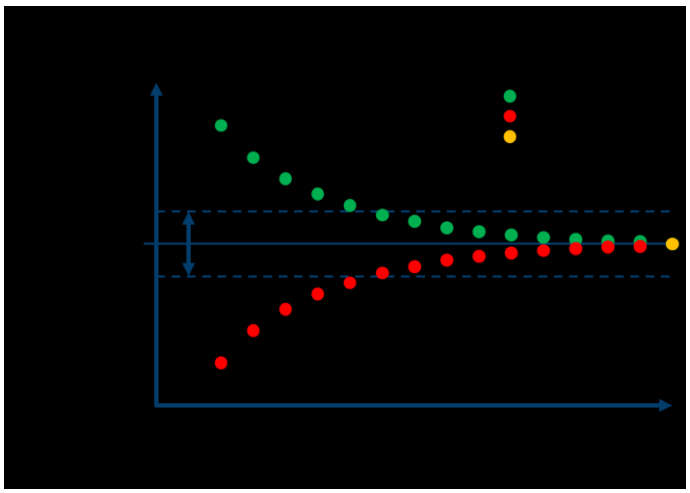

Figure 3.28. The concept of upper and lower bounds to the estimate the maximum deviation from the optimal objective function value of the fully resolved reference case

By solving the energy system twice using aggregation techniques that provide an upper and a lower bound to the original problem, it is guaranteed that the objective function value of the fully resolved system lies in between both bounds. Accordingly, the maximum deviation of it from both bounds is given by the difference between both bounds represented by ε in Figure 3.28. In that way, the maximum error made by temporal aggregation can be quantified despite of the fact that the optimal solution of the fully resolved model is unknown. This so-called optimality gap is generally defined as percentage of either the upper or the lower bound in the literature. Section 4.4 will use the definition given in Equation (3.33) with z^*_{UB} and z^*_{LB} representing the optimal objective function values of the upper and lower bound, respectively.

$$\text{gap} := \frac{z^*_{UB} - z^*_{LB}}{z^*_{LB}} \tag{3.33}$$

As optimality for convex minimization problems implies that there exists no feasible solution with a smaller objective function value, the lower bound always yields a solution, which is infeasible for the original problem. In case of energy system models, this would e.g. mean that unit capacities obtained by a lower bound aggregation are undersized. On the other hand, upper bounds of minimization problems can be feasible, but suboptimal solutions, if large sets of constraints and variables are carefully replaced by fewer but more restrictive ones.

As shown in Appendix H, energy system models created using the **FINE** modelling framework can result in either linear programs, mixed-integer linear programs or quadratic programs. Likewise, the reasons for the complexity may differ. As the energy system models introduced in Section 4.1 comprise linear programs and mixed-integer linear programs, the following Sections 3.4.1 and 3.4.2 focus on determining upper and lower bounds for linear programs (LPs) and mixed-integer linear programs (MILPs) using temporal aggregation. For the sake of brevity, they only summarize theoretical findings that are deduced in Appendix I, which also provides numerous examples and a generally applicable workflow for determining upper and lower bounds for a specific energy system model.

3.4.1. Upper and Lower Bounds for LPs and MILPs

The first option to obtain upper and lower bounds using aggregated data is based on modifying aggregated time series in such a manner that the desired bound is directly obtained by using aggregated time series. Therefore, this method is equally applicable to both, linear programs and mixed-integer linear programs.

In order to obtain upper bounds to the original problem based on aggregated data, the time series used for the respective system can be divided into cost-driving and cost-decreasing time series, which is discussed in detail in Appendix I.2.2. For example, cost and energy demand time series increase the costs of the energy system model if their values are overestimated. In contrast to that, capacity factor time series increase the system costs if they are underestimated because the corresponding net capacities need to

be increased in order to provide the same amount of energy as before. For an individual over- and underestimation of time series in the aggregation process, the maximum and minimum representation introduced in Section 3.2.4 can be used. Table 3.2 lists all time series types that can be used as input for the energy system modelling framework **FINE** and whether they need to be over- or underestimated in order to obtain an upper bound to the original problem.

Table 3.2. Time series to be over- or underestimated in order to receive an upper bound of the fully resolved reference system

Time series	$\min_{t \in C_k}(x)$	$\max_{t \in C_k}(x)$
Capacity factors	✖	
Conversion factors	✖	
Demands		✖
Supplies	✖	
Costs		✖
Revenues	✖	

In order to obtain an upper bound to the fully resolved model using aggregated data, the described over- and underestimations of the individual time series can be inverted as shown in Table 3.3.

Table 3.3. Time series to be over- or underestimated in order to receive a lower bound of the fully resolved reference system

Time series	$\min_{t \in C_k}(x)$	$\max_{t \in C_k}(x)$
Capacity factors		✖
Conversion factors		✖
Demands	✖	
Supplies		✖
Costs	✖	
Revenues		✖

It is noteworthy that a tighter lower bound to the original optimization problem can also be obtained if aggregated time series are represented by centroids. For that, however, the energy system model must not consider time dependent coefficients in the cost vector, but only within the set of constraints. This means, that a representation by centroids only leads to a lower bound of the original problem if the energy system does not consider revenue or cost time series.

A more detailed discussion and subsequent examples are presented in Appendix I.2.3.2. However, an informal explanation for this behavior is the fact that extreme values within time series shape the sizing of the model components in case of capacity expansion models. As observed in 3.2.1, these extreme values are smoothed out in case of centroid-based aggregation techniques and accordingly, sizing of components and the related total annualized costs are underestimated.

Lastly, if linked time steps such as in case of storage technologies are considered, additional restrictions such as the adjacency of clustered time steps must be respected in order to obtain a mathematically correct bound. This aspect is discussed in Appendix I.2.2.2 and I.2.3.3 but is omitted at this point.

3.4.2. Upper and Lower Bounds for MILPs

As shown in Appendix H.2, the solving of mixed-integer linear programs using algorithms like the branch-and-bound algorithm relies on an iterative solving of linear programs that are obtained by either relaxing or fixing binary or integer variables. Therefore, mixed-integer linear programs are more limited in size and obtaining a solution might be limited due to both, the number of integer variables and the size of the corresponding relaxed linear programs. Furthermore, the modelling framework **FINE** only considers binary design variables in order to model cost-curves as affine linear functions. In order to accelerate these mixed-integer linear programs and obtain upper and lower bounds to the original problem in a reasonable amount of time, an extended version of the approach by Kannengießer et al. [4] with multiple steps based on aggregated time series was developed in the scope of this thesis. The procedure is depicted in Figure 3.29.

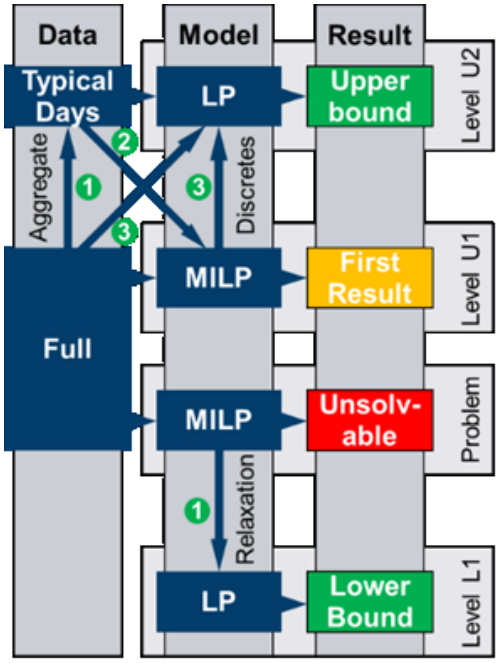

Figure 3.29. A multi-level approach to determine upper and lower bounds of the original mathematically complex mixed-integer linear program (MILP) using aggregated time series, tightening and relaxation

As mentioned in Appendix H.2, the lower bound of the mixed-integer linear program can be determined by relaxing the binary variables and solving a linear program of the form:

$$\begin{aligned} &\min c^T x \\ &\text{s.t. } Ax = b \\ &\quad Cx \leq d \\ &\quad x_i \in Z \quad \forall \quad i \in M_{intvars} \\ &\quad x_i \in R \quad \forall \quad i \notin M_{intvars} \end{aligned} \quad \Rightarrow \quad \begin{aligned} &\min c^T x \\ &\text{s.t. } Ax = b \\ &\quad Cx \leq d \\ &\quad x_i \in R \quad \forall \quad i \end{aligned} \tag{3.34}$$

An upper bound of the original problem can be determined using a two-level procedure as presented by Kannengießer et al. [4]. First, a reduced mixed-integer linear program is solved based on aggregated data. Regardless of the exact aggregation method, the solution of the reduced problem includes solutions for the discrete variables of the original problem. By fixing the discrete variables based on the solution of the aggregated mixed-integer linear program, the solution space of the original mixed-integer linear program is turned into a linear program.

The original mixed-integer linear program is a relaxation of this linear program, or, vice versa, this linear program is a restriction of the original mixed-integer linear program because the discrete variables' solution of the aggregated mixed-integer linear program is a subset of the set of integer numbers, i.e. $x^*_{\widehat{MILP},i} \subseteq Z$.

$$\begin{aligned} &\min c^T x \\ &\text{s.t. } Ax = b \\ &\quad Cx \leq d \\ &\quad x_i \in Z \ \ \forall \ \ i \in M_{intvars} \\ &\quad x_i \in R \ \ \forall \ \ i \notin M_{intvars} \end{aligned} \quad \Rightarrow \quad \begin{aligned} &\min c^T x \\ &\text{s.t. } Ax = b \\ &\quad Cx \leq d \\ &\quad x_i = x^*_{\widetilde{MILP},i} \forall i \in M_{intvars} \\ &\quad x_i \in R \ \ \forall \ \ i \notin M_{intvars} \end{aligned} \tag{3.35}$$

As will be shown in Section 4.4.2, this approach can provide tight upper and lower bounds, if the aggregation technique is deliberately chosen, which will be proven for binary cost variables.

Excursus 1: A Definition of Restriction

A comprehensible definition of a restriction for (general) minimization programs was provided by Geoffrion and Nauss [187]: *"A problem (Q) is said to be a restriction of problem (P) if the feasible region of (Q) is entirely contained within that of (P), and if the objective function value of (Q) is at least as great as that of (P) everywhere on the feasible region of (Q)."*

With respect to the computational tractability, this multi-level approach is superior to the original mixed-integer linear program, because a small gap between upper and lower bound can be obtained by solving two linear programs of the same size as the original mixed-integer linear program and one strongly aggregated mixed-integer linear program. Compared to standardized mixed-integer linear program algorithms, which strive to converge to the real optimum of the original problem, but might not converge at all within a reasonable amount of time, the proposed method is a good alternative.

From a mathematical point of view, this approach is furthermore highly relevant for the purpose of energy system optimization because the upper bound might be suboptimal, but is always a feasible solution to the original problem. This means, that even though the total annualized costs (TAC) might be higher than the real cost minimum, the resulting energy system is operable at any time step. Furthermore, the maximum deviation from the optimal objective of the reference can be quantified with the optimality gap defined in Equation (3.33). Against the background of uncertain input data and the fact that energy systems can only be optimized based on past or expected future data, the accuracy of this method can be sufficient.

4. Validation and Results

In order to validate the theoretical findings of Chapter 3, the impact of the discussed aggregation techniques on the accuracy of a selected set of energy system models is analyzed in the following chapter, whose structure is depicted in Figure 4.1.

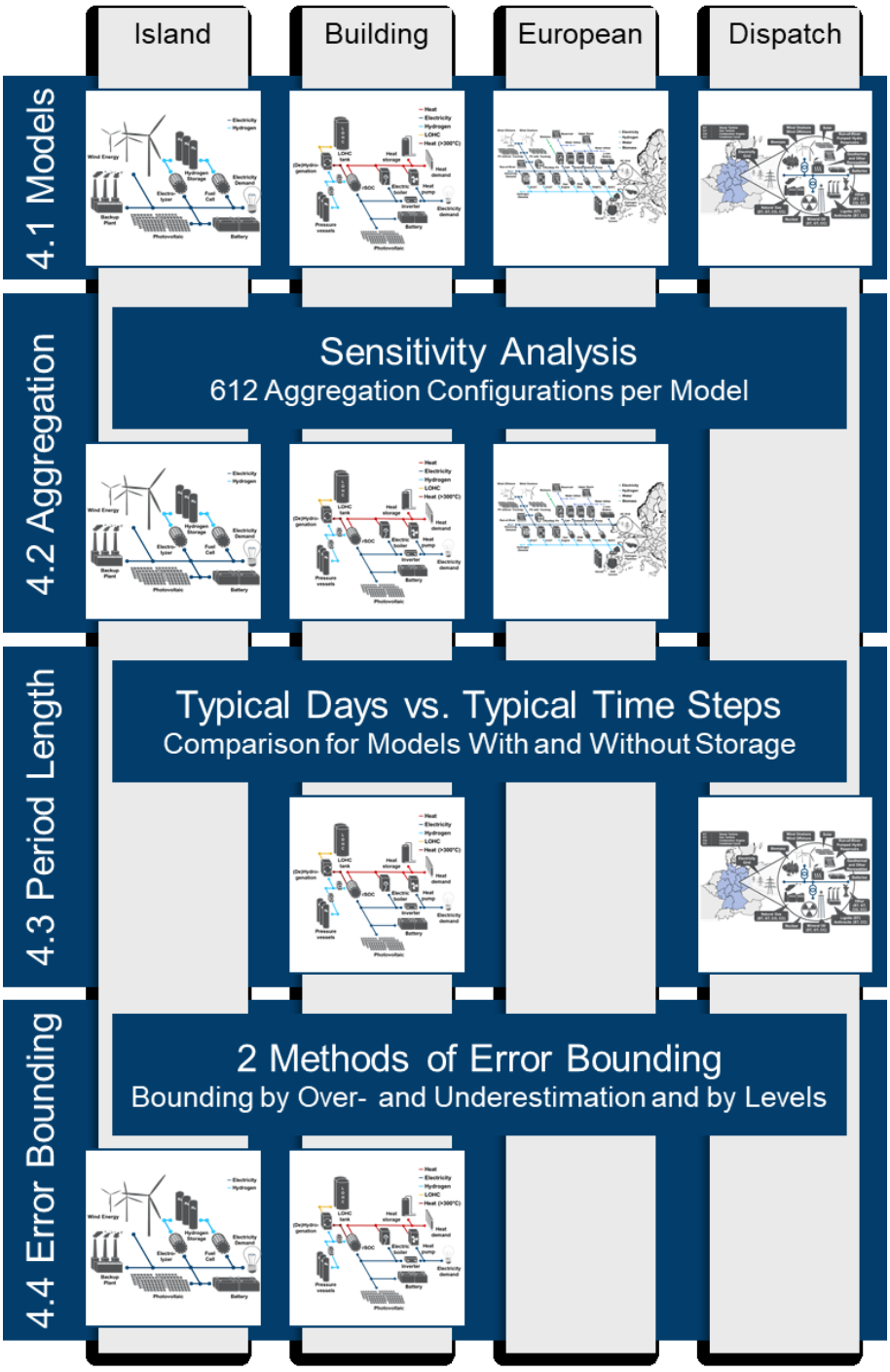

Figure 4.1. Structure of Chapter 4

First, the models that serve as case studies are introduced in Section 4.1 followed by a large-scale sensitivity analysis for capacity expansion models in Section 4.2. For that, each system is solved for 17 different numbers of typical days, 9 different numbers of segments per typical day and at least 4 different representation methods resulting in 612 model runs for each of the three considered models. This analysis delivers a detailed evaluation of the methods developed in Chapter 3, among which the combination of the value distribution preserving representation algorithm developed in Section 3.2.5 and the pathway algorithm for finding balanced combinations of typical days and segments developed in Section 3.3.4 are most effective.

However, as this analysis does not answer the question whether the chosen period length of one day is meaningful itself, the prerequisites for this are discussed in Section 4.3, in which one of the capacity expansion models comprising storage technologies is compared to a storage-less dispatch model. Finally, the options offered by temporal aggregation for obtaining feasible system designs with bounded errors are investigated in Section 4.4 for two models with a small number of time series that roughly resemble those models to which error-bounding methods were applied in the literature.

As the runtime of individual models depends on the chosen hardware, the computational resources used for Chapter 4 are listed in Table 4.1. For Section 4.2 and 4.4, the institute's internal computer cluster Caesar was used, whereas the Jülich Research Center's supercomputer JURECA-DC was used for the calculations in Section 4.3. As shown in Table 4.1, both clusters have a comparable frequency and as each model run was performed on a single thread in order to avoid unpredictable delays due to process allocation and communication, computing speeds of both computer instances are roughly comparable. However, in the following, only those runtimes are compared to each other that were achieved on identical computational resources in order to exclude their impact on the runtime comparisons completely.

Table 4.1. Computational resources used for Chapter 4

	Caesar (4.2 + 4.4)	JURECA-DC (4.3)
CPU Model	Intel(R) Xeon(R) Gold 6144 CPU	Intel(R) Xeon(R) CPU E5-2697 v3
Number of Cores per Computing Node	16	28
Threads per Core	2	2
CPU Max Frequency [MHz]	3.5	3.6
Shared Memory [GB]	1,024	1,024

“Throughout the whole chapter, Ward’s hierarchical clustering algorithm was used because of its good runtime scaling behavior with respect to both, sample number and sample dimensionality. For the considered multi-regional model, it was the only computationally tractable clustering algorithm and for the single-regional models, it was found that the results are less sensitive to the clustering technique than to the representation method. Furthermore, the reproducibility of the results is given due to its deterministic algorithm.” (Hoffmann et al. [3])

A rescaling to fit the time series’ mean values as presented in Section 2.2.2.2.3 was deactivated in order to isolate the impact of different representation methods, i.e. mean values are not preserved in the case of medoids and maxoids.

4.1. Model Overview and Data Resources

“The following section introduces the models used for the validation of the developed temporal aggregation techniques and introduces key features and functionalities of the models. Detailed data resources, which were required to parametrize the models, are provided in Appendix J.

In addition to that, the scientific purpose of each model’s consideration with respect of an accurate temporal representation is discussed.” (Hoffmann et al. [2])

4.1.1. The Island System

The island system is a simplified single-node capacity expansion model with 2030 as target year that was developed to illustrate the interaction of short-term electricity storage and long-term hydrogen storage to satisfy an alternating electricity demand with highly intermittent renewable energy sources. The system was first introduced by Kotzur et al. [20, 48] and later re-used by Kannengießer et al. [4] as case study.

The model contains a wind farm, a photovoltaic plant and a backup plant as potentially rival electricity supply units as well as a single electricity demand to be satisfied at any time step. The backup plant is the only freely dispatchable electricity source of the energy system and considered to rely on fossil fuels. In order to limit the potential CO_2 emissions of the system, its cumulative electricity supply is capped at 10% of the total electricity demand in the considered time span of one year.

In order to satisfy the electricity demand at any point in time, the system additionally contains a battery and hydrogen pressure vessels as energy storage. Here, the hydrogen pressure vessels are connected to the electric subsystem by two conversion units, namely an electrolyzer and a fuel cell. The system layout is depicted in Figure 4.2.

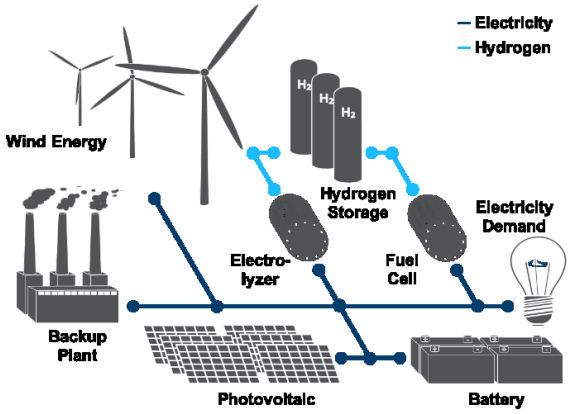

Figure 4.2. Technology portfolio of the island system

4.1.2. The Self-Sufficient Building Model

In contrast to the aforementioned model, the capacity expansion "model of the self-sufficient building is an island system that exclusively relies on a renewable energy source, namely photovoltaic. Moreover, it not only needs to fit an electricity demand, but also a heat demand. This leads to a significantly more complex setup and requires higher storage capacities because the system lacks a freely dispatchable energy source. Therefore, a wider set of potential technologies is considered in this model featuring different electric, thermal, gaseous hydrogen and liquid organic hydrogen carrier (LOHC) subsystems. A simplified scheme of the model based on a layout by Kotzur et al. [188], which was transferred into the energy system modelling framework **FINE,** is depicted in Figure 4.3." (Hoffmann et al. [2])

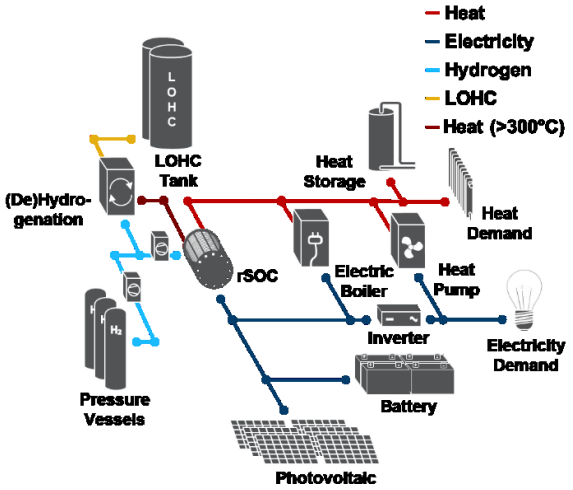

Figure 4.3. A simplified scheme of the self-sufficient building model taken from Hoffmann et al. [2])

Here, it is assumed that the archetype building was built in 1979 but is converted to energetic self-sufficiency in 2030. This means that all cost assumptions for the implemented technologies are extrapolated for the year 2030.

In order to represent the single-family house's capacities for photovoltaic electricity feed-in, three different positions are considered: Two rooftop orientations facing northwest and southeast and an option for ground-mounted photovoltaic systems. The DC subsystem connects the photovoltaic panels to a battery used to balance the daily intermittent electricity supply, a reversible solid oxide fuel cell (rSOC), an electric boiler and an inverter. The inverter is the connection to the AC subsystem that needs to satisfy the domestic electricity demand. Further, a heat pump is connected to the AC subsystem as an alternative to the electric boiler both of which are connected to the domestic hot water cycle.

The hot water subsystem has to satisfy the domestic heat demand. In order to fulfill this task during the night as well, a thermal storage is connected. Moreover, the rSOC is indirectly connected to the hot water cycle to use the excess heat at those times when the rSOC is working as a fuel cell and producing electricity from oxidizing hydrogen to water. Because the excess heat of this process has a temperature of approximately 750°C, two auxiliary heat exchangers are further considered that reduce the temperature in two steps to 300°C and 45°C.

In case the rSOC is run as an electrolyzer to produce hydrogen for storing energy, it is assumed that this endothermal process consumes heat at a temperature level of 300°C. To store the hydrogen, pressure vessels and an LOHC tank are considered as two alternative technologies. As the hydrogen is produced under atmospheric pressure, it needs to be compressed. In a first step, the hydrogen is compressed to 20 bar. At this pressure level, the LOHC (dibenzyltoluene) can be hydrogenated to store hydrogen in an exothermal process releasing heat at a level of assumingly 300°C to store the bound hydrogen in the LOHC tank. In contrast to that, the dehydrogenation is an endothermal process considered to consume heat at a temperature level of 750°C and to release hydrogen at atmospheric pressure. This temperature level is overestimated for the sake of simplicity in order to fit to the operating

temperature of the rSOC at 750°C. The overestimation of both, the endothermal and the exothermal temperature level are considered to balance each other with respect to a realistic energy balance. Although this process usually takes place at lower temperatures, more specifically, about 200°C for the hydrogenation and 350°C for the dehydrogenation, this assumption was made in order to avoid the consideration of too many different heat levels between the rSOC, the (de-)hydrogenation and the space heating cycle. To store the hydrogen in pressure vessels, the hydrogen has to be compressed a second time to a pressure level of 160 bar.

With respect to the auxiliary components, the compressors are connected to the DC subsystem. Further, two expanders are considered to expand the hydrogen to the respective lower pressure levels. The heat at 750°C released by the rSOC during the oxidizing process exceeds the heat demand at 750°C of the dehydrogenation and the heat demand of the electrolysis at 300°C is smaller than the waste heat of the hydrogenation process. However, the heat demand of the electrolysis must also be met in case that the pressure vessels are filled. Therefore, an additional electric heater using DC to provide heat at 750°C is considered to ensure an operation of the electrolyzer when a surplus of electricity is available. Further, the electric heater also offers the opportunity to shift hydrogen between the pressure vessels and the LOHC.

As shown above, “the self-sufficient building model provides numerous options to meet the building’s heat and electricity demand. Furthermore, it is obvious that the energy storage components will most likely work on different time scales depending on the energy form they store.” (Hoffmann et al [2])

Combined with the fact that this model describes a small, but potentially realistic application case for energy modelling, the model is an interesting application for evaluating the impact of different temporal aggregation methods.

4.1.3. The European Model

The European model developed by Çağlayan et al. [189, 190] is the most complex case study considered in the scope of this thesis as it comprises numerous complexity-driving features, among them 96 regions, storage technologies and capacity expansion planning. As the fully resolved case of the model is already on the

edge of computational feasibility, it does not consider binary investment decisions in favor of a non-aggregated solution against whom the proposed aggregation methods can be benchmarked.

Figure 4.4 depicts the technology portfolio that is available in every region of the model, which are interconnected by three transmission technologies, namely a hydrogen grid, an AC and a DC electricity grid. The European model considers capacity expansion until 2050, but is not a greenfield study, i.e. it accounts for both, existing capacities and the option to expand certain technologies. Further, the expansion of each technology is limited by its individual maximum potential in each region, e.g. photovoltaic and wind technologies are limited by a maximum land eligibility in a region that depends on multiple factors such as the distance to built-up area [191].

Apart from capacity expansion, two major differences to the other multi-regional energy system model considered in this thesis, the dispatch model, are the CO_2 neutrality and the consideration of sector coupling [7, 192] within the European model, as it exclusively contains renewable energy sources and needs to meet both, an electricity and a hydrogen demand. Here, 2050 is taken as target year of the analysis and “the hydrogen demand is assumed to originate exclusively from fuel cell electric vehicles with a market penetration of 75% [193]. As described by Çağlayan et al. [189, 190], the electricity demand is obtained from the E-Highway study [194] for a 100% renewable energies scenario. This demand is considered to account for electrified heating in the residential and industrial sector as well as the operation of battery electric and plug-in hybrid vehicles.” (Hoffmann et al. [3])

Although this scenario neglects the multiple applications of hydrogen in industry, i.e. as reactants for chemical processes as well as an energy supply for process heat, the consideration of hydrogen in this model allows for an investigation of hydrogen-based seasonal energy storage.

Electricity can directly be provided to the system via offshore and onshore wind plants, as well as rooftop photovoltaic and open-field PV with and without single-axis tracking. Further, a fix capacity of run-of-river power plants can supply hydroelectricity to the system constrained by spatiotemporally resolved capacity factors.

Apart from that, three more technologies contribute indirectly to the electricity supply: As water is not only directly used for producing electricity, but can also be stored by reservoirs or pumped hydroelectricity storage, these technologies are also taken into account. Similar to the run-of-river power plants, it is assumed that the potential for a further capacity expansion of these technologies is not given in Europe and that only already existing capacities are freely dispatchable. While reservoirs are exclusively fed by inflowing water, which can be withdrawn at a later point in time for electricity production, the upper basins of pumped hydroelectricity plants can be refilled either by inflowing water or actively by pumping water from the lower into the upper basin. In that way, both technologies comprise a storage component and at least one energy conversion component, which is shown in Figure 4.4. The last potential energy source for the system is given by biomass fuel, which can be freely purchased and converted to electricity using biomass-specific combined heat and power (CHP) plants.

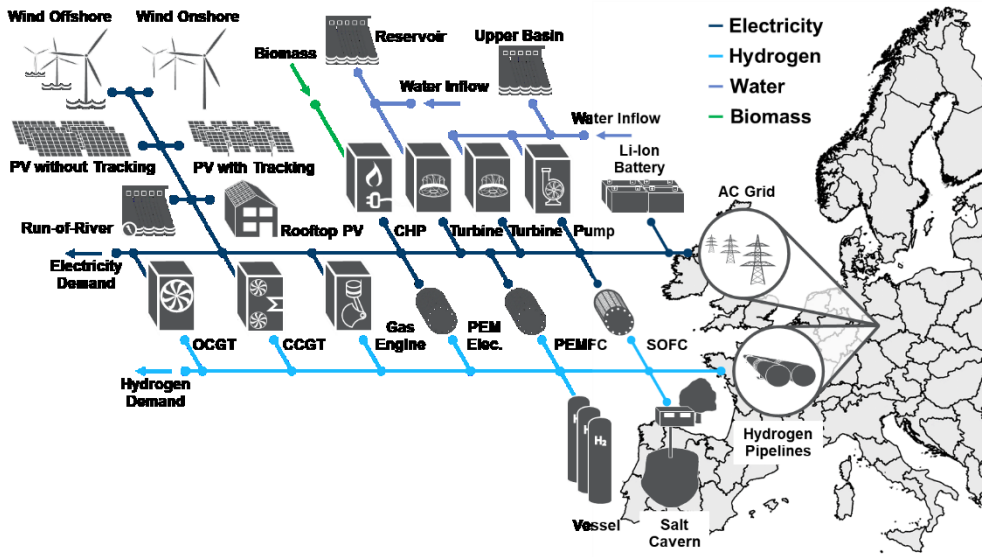

Figure 4.4. The layout of the European model (taken from Hoffmann et al. [3])

Due to the CO_2 neutrality of the scenario, hydrogen can exclusively be produced by Polymer electrolyte membrane electrolyzers and not e.g. by reformation processes. On the other hand, several technologies exist to convert the chemical energy of hydrogen back into electricity. Concisely, the portfolio not only comprises conventional technologies such as open and combined cycle gas turbines

(OCGTs and CCGTs) as well as gas engines, but also the hydrogen-specific technologies of polymer electrolyte membrane fuel cells (PEMFCs) and solid oxide fuel cells (SOFCs).

The close coupling of the electricity and the hydrogen subsystem allows for a dynamic operation of the whole system. Especially with respect to energy storage, this offers new technological options. For that reason, both subsystems consider their own set of storage components: While electricity can directly be stored in lithium-ion batteries, hydrogen can be stored either in pressure vessels of in salt caverns. Together with the water reservoirs and pumped hydroelectricity plants, this leads to both, interesting insights into the potential of future large-scale energy storage systems and a complex case study for temporal aggregation techniques.

A detailed review on the assumed technology-specific parameter assumptions is presented by Çağlayan [190].

4.1.4. The Electricity Dispatch Model

In contrast to the preceding models, “the electricity dispatch model does not consider capacity expansion, i.e. the size of all components is predefined and only their operation is optimized. The multi-regional model is based on the NUTS1 regions of Germany, which corresponds to Germany’s federal states. Accordingly, transmissions are part of the model and power flows between the different regions, as well as neighboring countries, are considered.

The electricity dispatch model is a simplified FINE implementation of the JERICHO dispatch model developed and published by Priesmann et al. [41].” (Hoffmann et al. [2])

An important feature of this energy system model is that it considers the same set of technologies at each of Germany’s 16 NUTS1 regions, but with varying installed capacities.

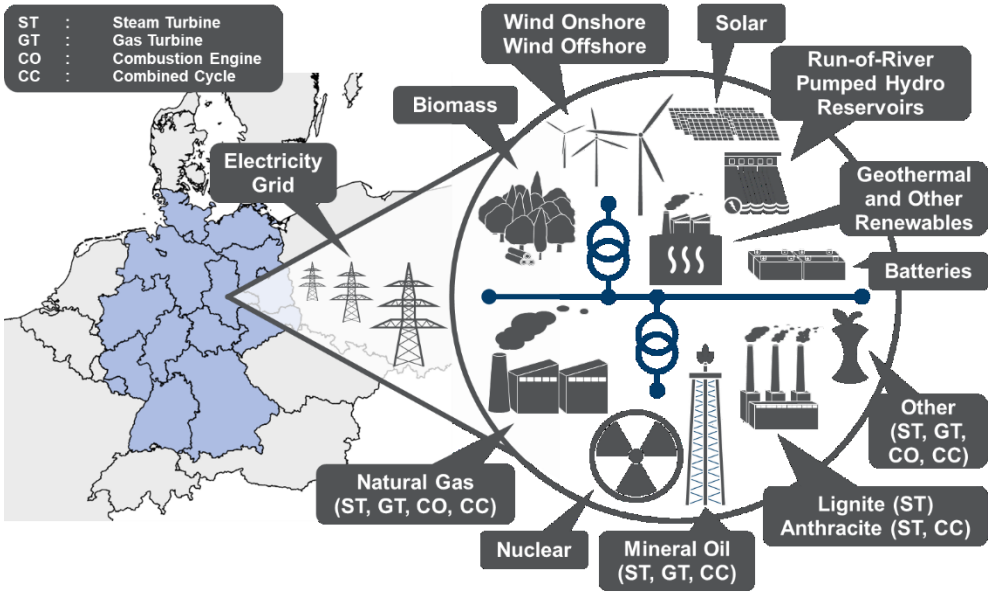

Figure 4.5. The layout of the dispatch model (taken from Hoffmann et al. [2])

In contrast to the preceding models, the dispatch model refers to the current state of the German electricity system. Furthermore, it "incorporates 25 different electricity-generating technologies, of which 15 are based on fossil fuels, eight on renewable energy sources and two are storage technologies. For the analyses conducted in Section 4.3, the storage dispatch was fixed prior to the optimization based on historical values. The technologies relying on fossil fuels, as well as biomass, i.e., the freely dispatchable technologies, were modeled as conversion units that consume a certain amount of lignite, hard coal (anthracite), uranium, methane, or biomass to produce an amount of electricity and CO_2 emissions. The non-dispatchable technologies, comprising wind and solar energy and run-of-the-river hydroelectricity, are modeled as sources of fixed capacity but with constraining capacity factors at an hourly resolution.

The objective of this optimization model is to minimize the costs of covering the inelastic electricity demand at each hour. The costs are the sum of the marginal costs for operating the conversion technologies and based on the time-dependent prices for fuels and EU allowances (EUAs) within the EU Emissions Trading Scheme and the technology-specific operation costs.

The operation of all units is modeled strictly linearly, i.e., unit commitment constraints such as minimum up- and down-time or startup

and shutdown costs that necessitate binary variables are not considered. This leads to the generation of a large, but comparably easily solvable energy system model.

As already noted, the dispatch model considers neither capacity expansion, nor depreciation costs, which is the most significant difference to the prior models. On the other hand, it comprises multiple regions and the largest number of time series. In order to provide an overview of the model's technological structure, Figure 4.6 depicts the share of each electricity supply technology at each of the 16 NUTS1 regions in Germany, as well as the inner German transmission lines and those to neighboring countries, offering the option to export electricity to Germany. Furthermore, the cumulative yearly electricity consumption in each region is highlighted by a corresponding background color." (Hoffmann et al. [2])

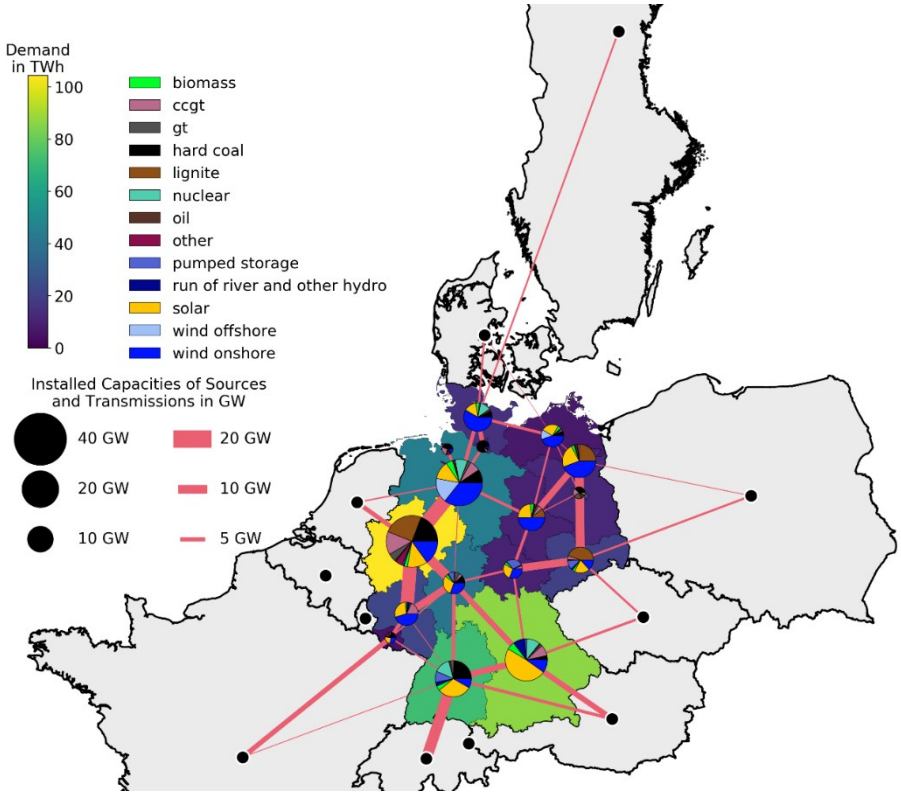

Figure 4.6. Input data of the dispatch model: Aggregated transmission lines, installed capacities, and yearly energy demand (taken from Hoffmann et al. [2])

A more detailed overview of data resources used for the model is provided in Appendix J.3. However, the preceding section reveals that the dispatch model significantly differs from the other models and is therefore suitable to investigate the general applicability and

efficiency of developed temporal aggregation techniques for a variety of different models.

4.1.5. Model Summary

As already mentioned, the model choice focuses on the consideration of preferably diverse model types and features in order to allow for a holistic evaluation of the developed aggregation techniques. With respect to the different common model features considered in the following validation, the configurations can be summed up as depicted in Figure 4.7.

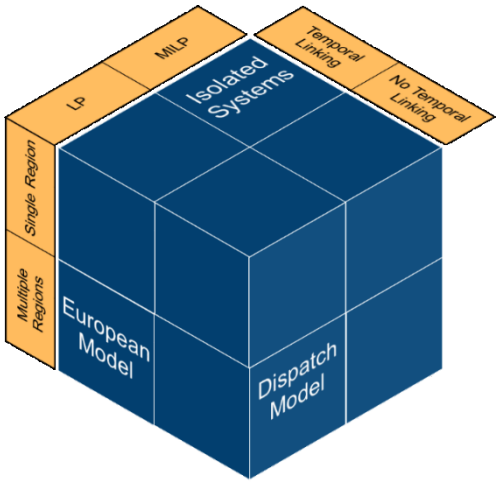

Figure 4.7. Common model features covered by the case studies

The island system model and the self-sufficient building model represent models with a high share of renewable energies, which requires an adequate representation of storage components, and discrete component decisions resulting in mixed-integer linear programming. The mathematically most demanding model, the European model, considers multiple regions as well as temporal linking in order to consider large-scale electricity and hydrogen storage as well as optimal component sizing. However, due to mathematical limitations, the component decisions are not discrete and therefore result in a large-scale linear program as the dispatch model. On the other hand, the electricity dispatch model represents the group of operation optimization models for traditional large-scale multi-regional energy networks and omits storage technologies leading to a temporally decoupled model.

Other features of the considered models, which are not shown in Figure 4.7 due to illustrative limitations, are summarized in Table 4.2. Among these are the type of the optimization problems, which are capacity expansion models in the case of the isolated systems and the European model and a unit commitment model in the case of the dispatch model, as well as the number of considered com-

modities. Due to the fact that sector coupling is an inevitable feature of current and even more so of future energy systems [7, 192], all models at hand consider multiple commodities. Furthermore, the big range of considered time series depending on the number of regions challenges the algorithms developed in the scope of this thesis because they need to be accurate, but computationally efficiently implemented in order to be equally applicable to both, small and large datasets.

Table 4.2. Techno-economic key features of the considered models

	Island System	Self-Sufficient Building	European Model	Dispatch Model
Target Year	2030	2030	2050	2018
Purpose	Capacity Expansion	Capacity Expansion	Capacity Expansion	Dispatch/ Unit Commitment
Number of Regions	1	1	96	16 (+9 Import Regions)
Number of Time Series	3	5	960	6325
Binary Variables	Yes	Yes	No	No
Storage	Yes	Yes	Yes	No
Commodities	Electricity Hydrogen	Electricity Heat Hydrogen LOHC	Biomass Electricity Hydrogen Water	Biomass Electricity Hard Coal Lignite Methane Mineral Oil Uranium

Finally yet importantly, it needs to be highlighted that the considered energy system models are not only relevant for investigating the impact of temporal aggregation on the cost-optimal solutions and layouts of the models, but also form the archetypes of two fundamental developments in energy system modelling. On the one hand, the spatial resolution and diversity of input data stemming from all kinds of renewable energy sources is constantly increasing for large-scale market models and capacity expansion models on a national or international scale, while on the other hand, a growing relevance of decentralized small-scale solutions is inevitable as well. Reliable aggregation techniques need to provide good results for all types of energy system models in order to guarantee a general applicability and to be capable of reducing energy system models appropriately that comprise a high spatial resolution, a big technological diversity and a strong temporal interconnectedness due to a high amount of installed storage capacities.

4.2. The Optimal Aggregation: A Sensitivity Analysis

The following section aims at finding the best possible aggregation method out of the combinations of typical days, segments and representation methods for models considering seasonal and intraday storage, which applies for the island system model, the self-sufficient building model and the European model. The analyses in Sections 4.2.2 and 4.2.3 were also published precedingly in a shortened version by the author of this work [3].

The sensitivity analysis comprises 17 different typical day numbers, 9 different segment numbers and 4 different representation methods resulting in 612 different temporal aggregation configurations per model. Figure 4.8 shows all considered typical day and segment configurations resulting in a number of total time steps represented by the white numbers in the fields. As the number of typical days and segments increases by a factor of approximately $\sqrt{2}$, the number of total time steps approximately increases by a factor of 2 along the diagonal from the upper left to the lower right and is approximately constant along the diagonal from the lower left to the upper right. The fully resolved case is given for 365 typical days and 24 segments resulting in 8760 time steps. Each of the shown configurations is performed for the representation by centroids, medoids, maxoids and using the distribution-preserving algorithm.

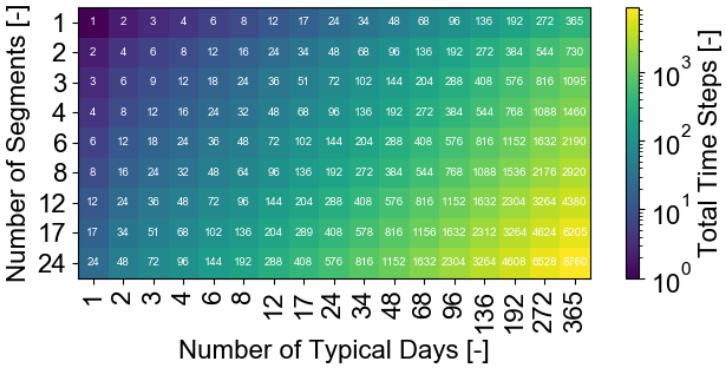

Figure 4.8. Number of total time steps depending on typical day and segment configurations that were considered in the sensitivity analysis for four different representation methods (taken from Hoffmann et al. [3])

First, all possible configurations are optimized and the representation methods are compared to each other with respect to the main a posteriori indicators, the runtime and the objective's deviation from the fully resolved case. In a second step, the best representation method is determined with respect to both, a good tradeoff

between calculation time and aggregation-induced error as well as a predictable and consistent convergence behavior, which means that an increase in temporal resolution monotonously decreases the deviation from the fully resolved reference case. In a third step, the proposed algorithm for finding the optimal ratio between typical days and segments per typical day is evaluated with respect to its capability to further reduce the aggregation-induced error of the energy system models' optimal objective. For this, the statistical methods proposed in Section 3.3 are applied to the database in order to assess the method's reliability. As a side effect, the most reliable a priori error metric is determined and mathematical relationships between aggregation-induced input- and output errors are derived.

4.2.1. Analyses of the Island System Model

First, the large-scale parameter variation is applied to the island system model, as it is the smallest one and yet considers time series for wind and solar capacity factors as well as two different storage technologies. In addition to that, it is likely that the limited amount of imported energy makes it sensitive to peak- and mean value deviations in the aggregated time series. Figure 4.9 depicts the island system as well as the optimal objectives normed by the one of the fully resolved case over runtime for all temporal aggregation configurations.

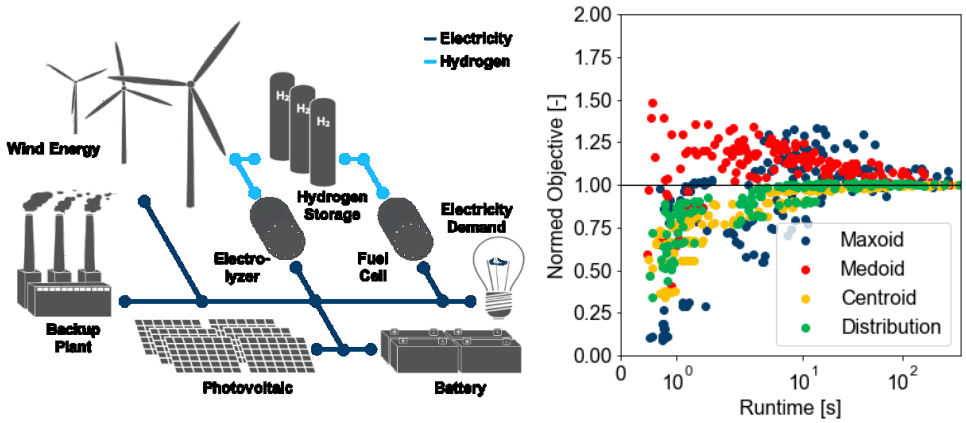

Figure 4.9. The island system and the corresponding normed optimal objectives over computation times for all considered configurations

Evidently, the deviation of the objective function from the fully resolved case decreases with a higher runtime, which corresponds to those model configurations with a higher temporal resolution,

i.e. more typical days and more segments per typical day. With respect to different representation methods, is can be seen that except for the medoid representation, all methods underestimate the system costs in case of strongly aggregated time series.

The representation by medoids leads to a completely arbitrary over- or underestimation of the optimal objective for the fully resolved case at low temporal resolutions and then stabilizes at optimal objectives that are above the one of the reference case.

Likewise, the representation by maxoids leads to an overestimation of the optimal objective for higher temporal resolutions. Interestingly, the representation by maxoids, i.e. the day of each cluster, which is farthest away from the whole dataset's centroid, is not automatically leading to the most conservative, i.e. highest system cost estimation. The reasons for this are manifold. First, the clustering space is high dimensional and therefore many clusters are needed in order to form a convex hull of the data set by the clusters' maxoids. Second, maxoids aim at covering both, minimum and maximum values. Therefore, not only the most critical points for the system (capacity factor minimums and electricity demand maximums), but also the least critical points for the system (capacity factor maximums and electricity demand minimums) are chosen. Only when the total number of typical periods is sufficiently high, the convex hull of the dataset of typical days is sufficiently approximated by the maxoids. In that case, the aggregation by maxoids overestimates the total system costs, which is slowly decreasing again for a higher number of typical days as the clusters become smaller but more numerous until each cluster only contains a single candidate day, i.e. the original temporal resolution is met.

The second group of representation methods comprising the representations by centroids and the distribution-preserving algorithm reveal a much more predictable behavior than medoids and maxoids. In these cases, the great majority of aggregation configurations considering one of these two representation methods lead to an underestimation of the real system cost. While this is always the case for the representation by centroids, some of the configurations of segments and typical days lead to a minimal overestimation in case of the distribution-preserving algorithm.

With respect to a direct comparison between the representation by centroids and by the distribution-preserving algorithm, it can be seen that the distribution-preserving algorithm further shows a slightly faster convergence behavior due to the smaller deviations from the duration curve's extreme values in the latter case. Apart from that, Figure 4.9 highlights that the representation by centroids or by using the distribution-preserving algorithm not only leads to a more consistent aggregation-induced error, but also to a smaller absolute deviation from the optimal objective of the fully resolved model at comparable runtimes. For example, for a runtime of 100 seconds, which refers to a speed-up factor of approximately 60 relative to the fully resolved problem, the spread of maximum deviations lies roughly between 0% and -10% for the centroid- and distribution preserving representation, 0% and +25% for the medoid representation and -25% and +30% for the maxoid representation.

In order to evaluate the impact of the considered numbers of typical days and segments as well as the chosen representation method on the deviation from the optimal objective of the reference case, Figure 4.10 depicts the deviations from the optimal objective of all 612 model runs that were already shown in Figure 4.9 depending on their aggregation configuration.

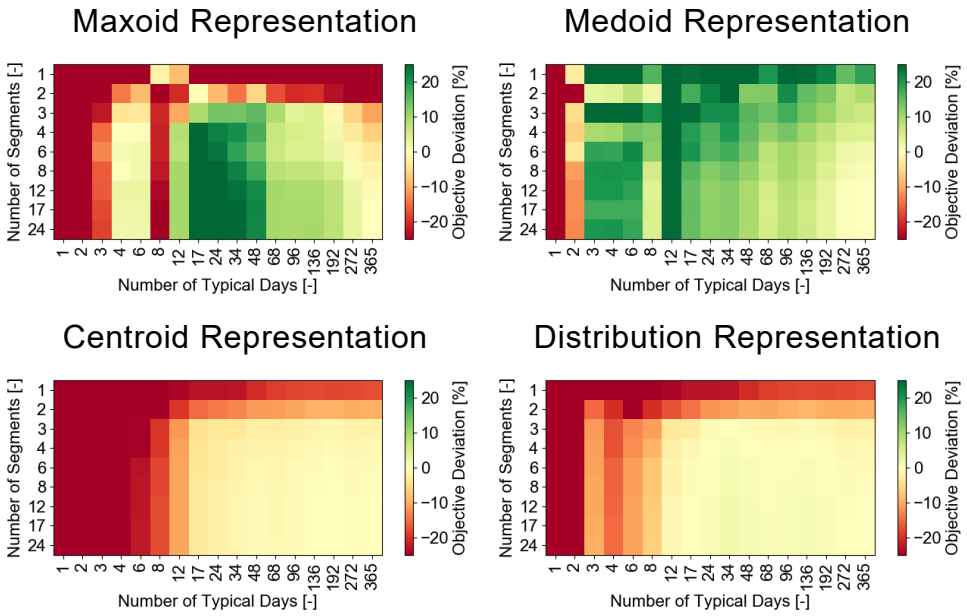

Figure 4.10. The deviation from the optimal objective of the fully resolved case depending on the configuration of the number of typical days and segments as well as the representation method

From Figure 4.10 it becomes evident that aggregation configurations with either a very low number of typical days or a very low number of segments per typical day lead to the strongest deviations. As these model configurations are also those with the shortest runtime, the divergent shape of the data points towards low runtimes in Figure 4.9 can be explained. For the maxoid and medoid representation, it can moreover be observed that both methods tend to over- or underestimate the optimal objective depending on the configuration in an unpredictable manner. Moreover, the absolute error diminishes later than for the representations by centroids or the distribution-preserving algorithm. In case of the representations by centroids or the distribution-preserving algorithm, either a lower number of typical days or a lower number of segments decrease the optimal objective consistently, which makes them more predictable. Furthermore, the aggregation-induced deviation of the optimal objective diminishes earlier than for the representation by medoids or maxoids.

As the lower two graphs in Figure 4.10 show, the deviation from the optimal objective is almost negligible for 17 typical days and 3 segments in case of a representation by centroids and 12 typical days and 3 segments in case of 12 typical days and 3 segments. This means that only 51 and 36 time steps out of 8760 original time steps, i.e. 0.58% and 0.41% of the original number of time steps, are sufficient to approximate the optimal objective of the fully resolved case accurately. Remarkably, the proposed distribution-preserving algorithm shows the best performance out of all considered representation methods.

As mentioned in Section 3.3.4, different types of time series are differently affected by temporal aggregation: While e.g. solar profiles need to be represented at a high inner-daily resolution, wind profiles need a larger number of typical days for a sufficient aggregation. Moreover, because of the penny switching effect, the cost-optimal composition of technologies of a system can react almost arbitrarily sensitive to slight changes in the input data.

However, a good representation method should not only lead to system designs that have a similar objective function value, but should avoid a systematical bias of certain technologies. Therefore, the cost contributions of selected components depending on

the aggregation configuration are likewise worth investigating. In case of the island system, the total annualized cost contributions of the wind plant and the photovoltaic panels normed by those of the fully resolved case are the most reasonable technologies for this investigation because they directly refer to the aforementioned strengths and weaknesses of different aggregation configurations with respect to wind and solar time series.

Figure 4.11 shows the total annualized costs (TAC) for the photovoltaic panels (left column) and the wind turbines (right column) normed by the respective total annualized costs for the fully resolved case for each representation method and combination of considered typical day and segment number. Interestingly, the chosen representation method does not only affect the overall cost of the considered components, but also the effect that different typical day and segment numbers have on the individual components. As the first row of Figure 4.11 shows, a low number of typical days and segments leads to a consistent underestimation of the total annualized costs of both, the photovoltaic panels and the wind turbines. This can be explained by the fact that the representation by maxoids underestimates the objective function of the whole system as well as shown earlier. In contrast to that, it is remarkable that the most common aggregation methods used in literature, the representation by medoids and by centroids, lead to a high sensitivity to the chosen number of typical days and segments. While a low number of typical days leads to an overestimation of photovoltaic capacities and an underestimation of wind capacities in the case of medoids, the opposite can be observed for the representation by centroids.

Moreover, a low number of segments leads to an overestimation of wind capacities in the case of a representation by medoids and an underestimation of wind capacities in the case of a representation by centroids. For centroids, this observation can be explained by prior findings: While a low number of segments has a major impact on the solar profiles, a low number of typical days predominantly affects the wind profiles. Accordingly, a low number of typical days smoothens the wind time series more than the solar time series, which underestimates the wind profile’s intermittency and thus makes it more dispatchable and a more economic energy source. For low numbers of segments, the photovoltaic profile is

stronger smoothened and accordingly becomes a more economical supply option. The fact that the opposite observation holds true for a representation by medoids is much harder to explain. However, possible reasons for this can be the fact that a representation by medoids does generally not meet the average yearly energy supplies and that existing days are chosen as representatives instead of synthesized ones. Accordingly, it is not given that the time series profiles are indeed smoothened by the aggregation.

Yet, it is evident that state-of-the-art representation methods introduce a systematical bias to certain technologies and that the neglect of statistical features such as the time series mean values and variance in the case of a representation by medoids and the variance only in case of the aggregation by centroids might be a reason for it. This is supported by the finding that the distribution-preserving algorithm shown in the last row of Figure 4.11 significantly outperforms the other aggregation methods with respect to both, the deviation of the total annualized costs from those of the reference case at a small temporal resolution, and the absence of a systematical bias that favors one technology over the other. Accordingly, the outperformance of the proposed representation algorithm is evident for both, the overall cost deviation and a fair technology selection.

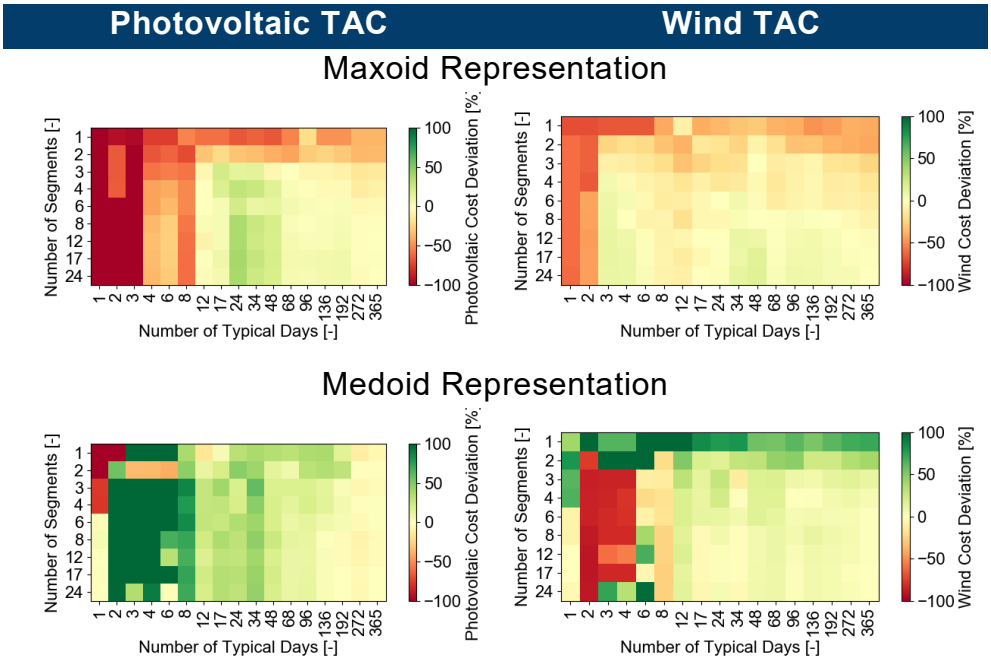

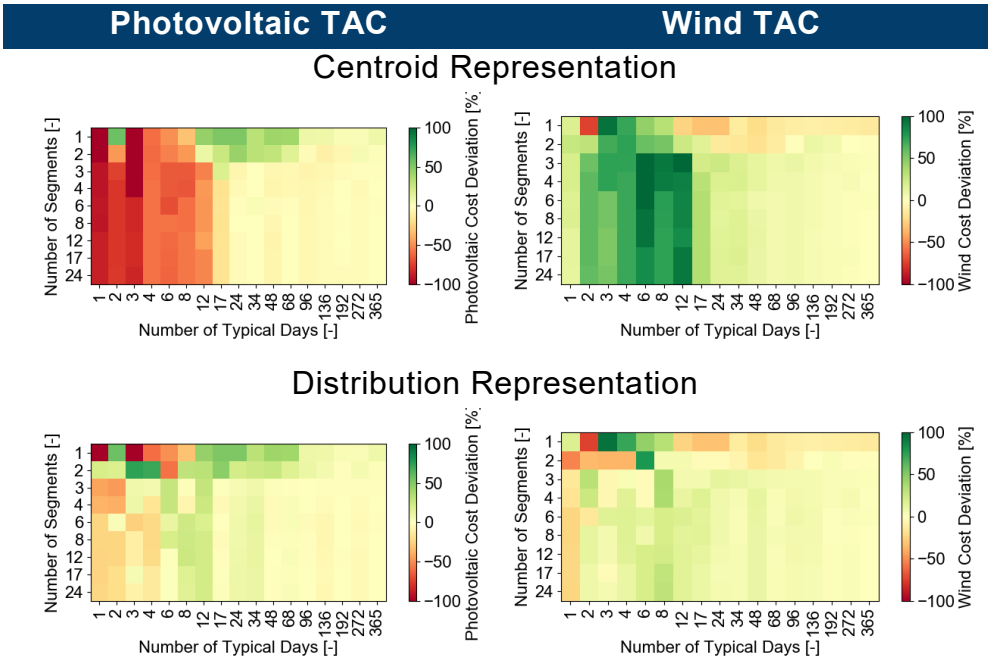

Figure 4.11. The total annualized costs of the photovoltaic panels and the wind turbines normed by their total annualized costs in the fully resolved case

As configurations with a very high number of typical days but with a very low number of intra-daily segments or vice versa might not lead to optimal aggregation results, a method for finding the optimal ratio of typical days and segments for a given number of total time steps was introduced in Section 3.3.4. The proposed method is now applied to the island system model in order to evaluate its effectiveness. The algorithm was based on three mathematical assumptions stated in the equations (3.26), (3.27) and (3.28).

Figure 4.12 shows the correlations between a priori and a posteriori indicators for the representation by centroids in order to evaluate the validity of the three assumptions stated above. The coefficients ρ_p and ρ_s in the upper right legends of the four subfigures represent the values of the respective Pearson and Spearman correlation coefficients. As the three assumptions above presuppose monotony only, ρ_s directly assesses the validity: The closer ρ_s is to +1 or -1, the more the assumption of monotony is fulfilled. Moreover, the Pearson correlation coefficient ρ_p indicates whether the correlation is linear or not. The closer ρ_p is to +1 or -1, the more the assumption of a linear correlation is justified. Although this coefficient cannot be used to assess the validity of the assumptions

stated above directly, it reveals interesting connections between the considered error indicators.

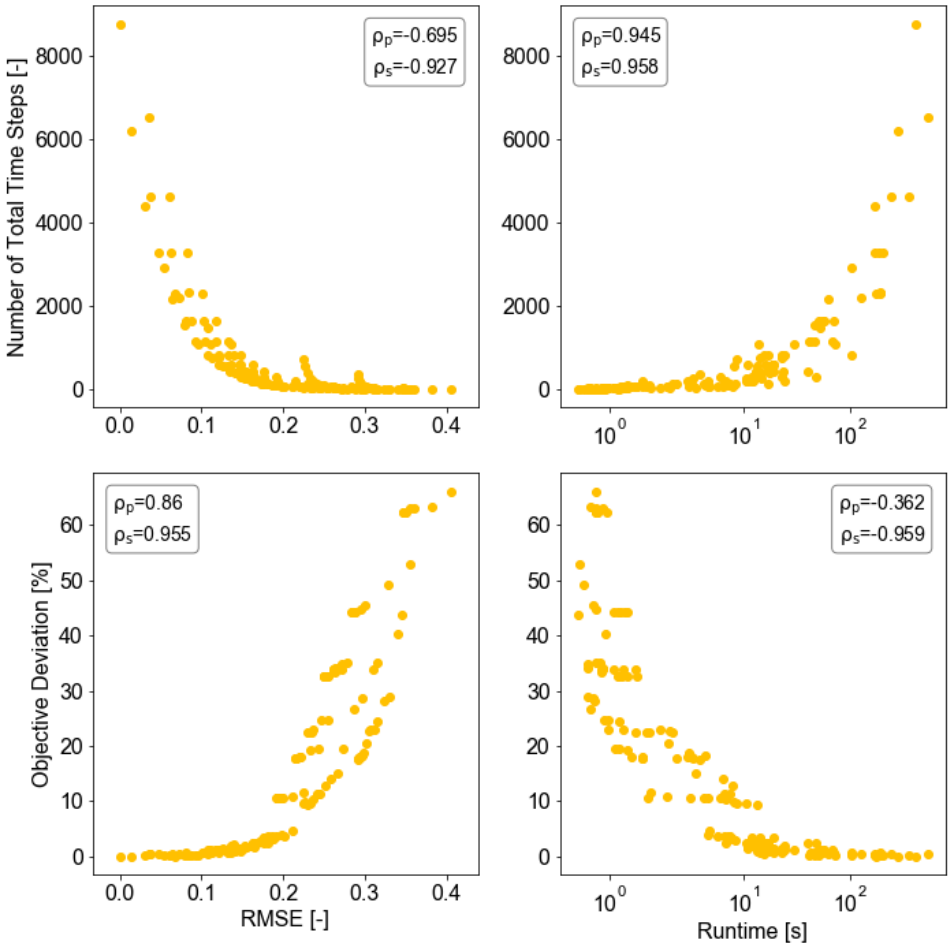

Figure 4.12. The correlation between a priori and a posteriori indicators for the representation by centroids

The validity of assumption 1 that the runtime increases monotonously with the total number of time steps is assessed by the upper right subfigure in Figure 4.8. Here, it can clearly be seen that the runtime increases on average with a higher number of total time steps. With a score of +0.958, the Spearman correlation coefficient is close to +1 which means that the assumption is justified. Moreover, the Pearson correlation coefficient has a score of +0.945, which means that the runtime increases approximately linearly with the total number of time steps. Concisely, this means that apart from a constant time consumption component used for setting up the model and mapping the solution of the solver back into **FINE**,

the runtime of the model can be modeled as a function of the total number of time steps as follows:

$$\text{Runtime} = \text{m} \times \text{n}(\text{time steps}) + \text{b}(\text{other processes}) \tag{4.1}$$

Assumption 2 that the deviation from the optimal objective decreases monotonously with a decreasing root-mean-square error is justified by the lower left graph in Figure 4.12 with a Spearman correlation coefficient ρ_s of +0.955 being close to +1. In contrast, the Pearson correlation coefficient ρ_p with 0.86 is considerably different from +1, i.e. the functional relationship between the root-mean-square error and the objective deviation is nonlinear, which can also be seen in the corresponding subgraph. Interestingly, this implies that all temporal aggregation configurations with an root-mean-square error of 0.15 or lower lead to a satisfying optimization result. A further increase of segments or typical days may therefore decrease the root-mean-square error, but with very little impact on the exactness of the energy system's optimal objective. A comparison with the upper left graph in Figure 4.12 reveals that this further decrease of the root-mean-square error can only be obtained by increasing the number of total time steps disproportionally, which makes this approach mathematically demanding but with only a small improvement of the aggregation-induced error.

The upper left graph in Figure 4.12 also verifies assumption 3, i.e. that an increase of total time steps and therefore an increase of the number of either typical days or segments leads to a decrease of the chosen a priori indicator. Here, the Spearman correlation coefficient ρ_s has an absolute value of 0.927 and is accordingly worse than the correlation coefficients of assumption 1 and 2. However, the correlation coefficient was calculated based on the total number of time steps, which means that it does not directly refer to assumption 3 as it is based on the product of the number of typical days and segments instead of typical days and segments separately as assumption 3 states. Due to the hierarchical structure of Ward's clustering algorithm, the root-mean-square error decreases linearly with a larger number of either typical days or segments. Accordingly, the true Spearman correlation coefficients for any typical day number increase at a fixed segment number or vice versa would be exactly one. This can also be observed in Figure

4.13, in which the root-mean-square error depending on the number of typical days and segments in the case of a representation by centroids is shown. Here, it can be observed that the root-mean-square error decreases monotonously in the direction of both, an increasing number of typical days and an increasing number of segments.

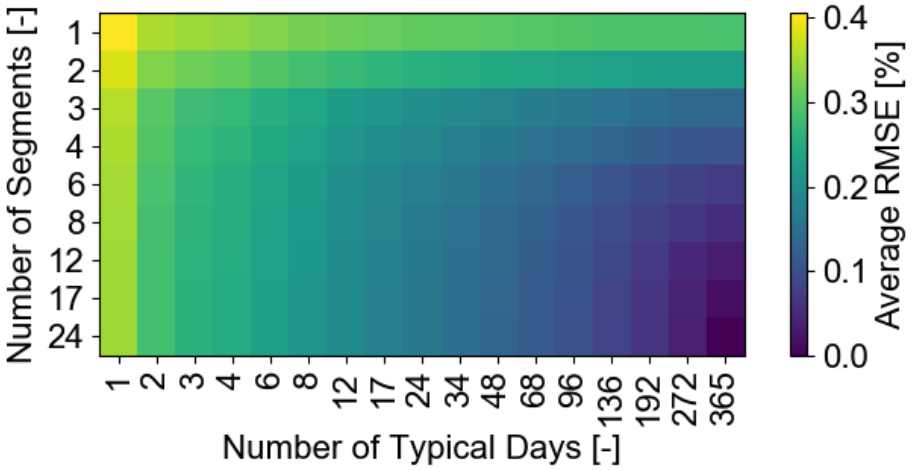

Figure 4.13. The root-mean-square error (RMSE) depending on the number of typical days and segments in the case of a representation by centroids

Further, it needs to be highlighted that the correlation is negative as maintained by assumption 3. Accordingly, the root-mean-square error decreases with an increase of total time steps. Apart from that, the Pearson correlation coefficient ρ_p considerably differs from a linear correlation between the total number of time steps and the root-mean-square error. This is also the reason for the fact that an incremental improvement of the aggregation-induced error can only be realized by a disproportional increase of total time steps below an root-mean-square error of 0.15.

Finally, the lower right graph in Figure 4.12 depicts the correlation of a posteriori indicators, i.e. the absolute deviation from the optimal objective over the model runtime. Here, the negative correlation coefficients indicate that gains in result accuracy are mostly at the price of an increased solving time.

As it was shown before, the representation by medoids or maxoids is less predictable than the representation by centroids or the distribution-preserving algorithm, which might also affect the effectiveness of the proposed algorithm for finding the optimal trade-off between the number of typical days and segments. Accordingly,

the validity of the assumptions must be checked for each representation method individually. For the sake of brevity, the following analysis only considers the representation by medoids instead of all three remaining representation methods, because the results for maxoids have proven to be comparable to those for medoids and the results for the distribution-preserving algorithm were comparable to those obtained for a representation by centroids.

Figure 4.14 depicts the corresponding correlations of Figure 4.12 for the case of a representation by medoids. Obviously, assumption 1 and 3 are also justified as implied by the corresponding Spearman correlation in the upper right and upper left graph of Figure 4.14. In contrast to that, the assumption that the deviation from the optimal objective of the fully resolved case decreases monotonously with the a priori error (in this case the root-mean-square error), is not given for a representation by medoids as the lower left graph of Figure 4.14 shows. This behavior is mirrored by a rather low Spearman correlation coefficient ρ_s of 0.659. Moreover, the missing correlation directly affects the correlation between the model runtime and the objective deviation shown in the lower right graph, which is also relatively arbitrary. Therefore, an algorithm striving at minimizing the root-mean-square error for a minimal increase of total time steps is not universally applicable for the case of medoids. However, as shown before, the representation by medoids or maxoids is outperformed by the representation by centroids and the distribution-preserving algorithm anyways. For that reason, a worse performance of the proposed algorithm for a non-preferable representation method can be tolerated.

Finally yet importantly, the Pearson correlation coefficient ρ_p in the upper right graph of Figure 4.14 with a value of 0.639 indicates a nonlinear correlation between the total number of time steps and the runtime. However, the Pearson correlation coefficient is very sensitive to outliers and because the data samples diverge at high runtimes and total numbers of time steps, it is falsified in this case. The sensitivity to outliers at the upper end of the temporal resolution can be reduced by comparing the logarithms of both, the runtime and the total number of time steps. In that case, the Pearson correlation coefficient for a representation by medoids is $\rho_{p,\log}(\mathrm{Runtime}, \#\mathrm{TD} \cdot \#\mathrm{Seg})$ is 0,932 while it is 0,934 for the repre-

sentation by centroids. Accordingly, an approximately linear correlation between the total number of time steps and the optimization problem's runtime can be presumed.

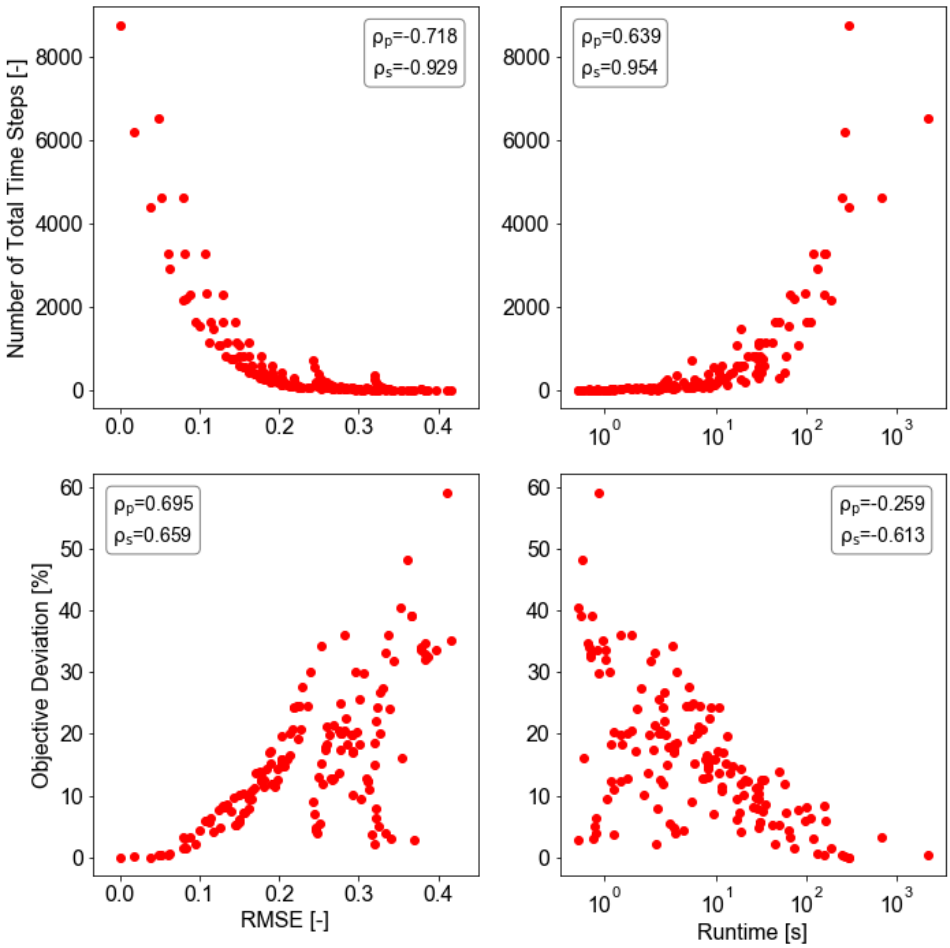

Figure 4.14. The correlation between a priori and a posteriori indicators for the representation by medoids

Finally, the effectiveness of the proposed algorithm is evaluated with respect to its capability to outperform other typical day and segment configurations. For that, the optimal pathway depending on the chosen representation method is first evaluated in Figure 4.15. As it can be seen, the assumption of a decreasing root-mean-square error for a higher number of typical days or a higher number of segments is always approximately justified. Among the different representations, this assumption is violated the most for the representation by maxoids, slightly violated for the distribution preserving representation method for 3 segments and a small number of

typical days and not violated at all for the representation by centroids or medoids. As medoids are those days from the original set of candidate days that are closest to the clusters' centroids, it is understandable that the algorithm identifies an almost identical pathway for medoids and centroids. In contrast to the optimal pathways for a representation by centroids and medoids, the representation by the distribution-preserving algorithm favors an increase of the number of typical days first in order to reduce the root-mean-square error. However, for more than six typical days, the pathway resembles those of the medoid and centroid representation. The optimal pathway of a representation by maxoids differs the most from the other ones, as the root-mean-square error is approximately twice as high as for the other representation methods. Apart from that, a significantly higher number of segments is preferred before the algorithm choses to increase the number of typical days at a number of 12 segments per day. A possible reason for this is that the root-mean-square error is rather indifferent between 4 and 8 typical days in that case. This emphasizes the importance of a monotonic relationship between the number of typical days or segments and the chosen a priori indicator.

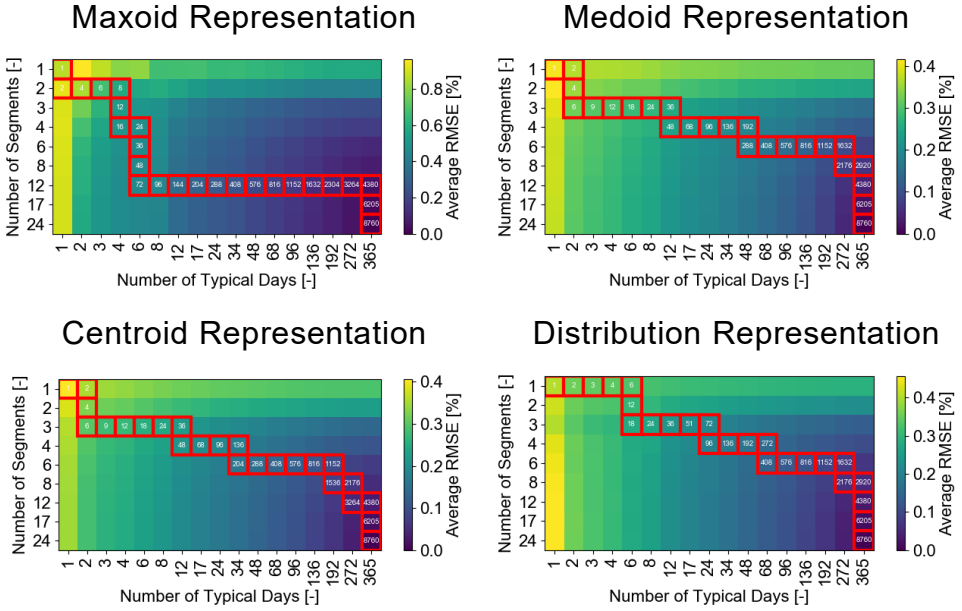

Figure 4.15. The pathway found by the proposed algorithm for an optimal ratio between the number of typical days and segments depending on the representation method

In order to evaluate the effectiveness of the proposed algorithm with respect to its capability to faster converge towards the optimal

objective value of the reference case, i.e. at a smaller runtime, Figure 4.16 compares the convergence behavior of those configurations, which have an optimal ratio of typical days and segments according to the proposed algorithm. Furthermore, this is illustrated for each representation method separately and compared to those aggregation configurations with an hourly intra-daily temporal resolution, which was the status quo in the modeling framework **FINE** before this thesis.

The upper left graph in Figure 4.16 shows that neither those aggregation configurations proposed by the algorithm nor the configurations with an hourly resolution lead to a consistent convergence behavior in the case of maxoids as assumption 2 is violated just as in the case of medoids as observed in Figure 4.14. Accordingly, there is no monotonic relationship between the root-mean-square error and the deviation from the optimal objective.

Analogously, the algorithm neither outperforms other aggregation configurations in the case of medoids due to the violation of assumption 2, which was shown in the upper right graph of Figure 4.14.

However, the fact that the optimal objective is underestimated for low temporal resolutions and overestimated for higher temporal resolutions in the case of medoids is an interesting finding, which illustrates two opposite effects of temporal aggregation, which are also mathematically analyzed in Appendix I.2.1. On the one hand, the temporal aggregation and subsequent representation by means of medoids leads to an underestimation of extreme periods as only those candidate days are chosen which are closest to the respective cluster's centroid. This generally leads to an underestimation of the system cost, if only time series in the constraint matrix and constraint vector are considered (e.g. time series for capacity factors and energy demands, but **not** commodity cost time series) and the system is temporally decoupled. On the other hand, the merging of time steps is based on the assumption that a system operates identically if the outer conditions of the system given by time series are identical. This is generally not the case for temporally coupled systems, which e.g. consider storage technologies, because a system is likely to operate differently if a lot of energy is stored in the system compared to a system with empty storage

components, even if the outer conditions are identical. Accordingly, the assumption of identical operation for time steps, which are aggregated based on their similarity, constrain the system, which leads to an overestimation of the optimal objective. Therefore, a small deviation from the optimal objective does not necessarily equal a good temporal aggregation. Instead, it can also imply that two systematical errors were made that neutralize each other.

With respect to the centroid representation and the representation according to the distribution-preserving algorithm, the proposed method for finding and optimal tradeoff between the number of typical days and the number of segments clearly outperforms all other aggregation configurations as all assumptions for the validity of the proposed algorithm are fulfilled. The algorithm consistently identifies most of the points that are closest to the objective function of the reference case leading to a comparably exact solution that can be found within a small fraction of the original runtime.

It is worth mentioning that the distribution-preserving algorithm moreover significantly outperforms the convergence behavior of the centroid representation for both, typical days at hourly resolution only and those configurations with an optimal trade-off between the number of typical days and segments. Accordingly, the distribution-preserving algorithm with an optimal ratio of typical days and segments according to the optimal pathway algorithm has proved to be the most effective temporal aggregation algorithm with respect to three major criteria: Smallest objective deviation at small runtime, monotonous convergence behavior and low sensitivity with respect to an optimal component capacity choice.

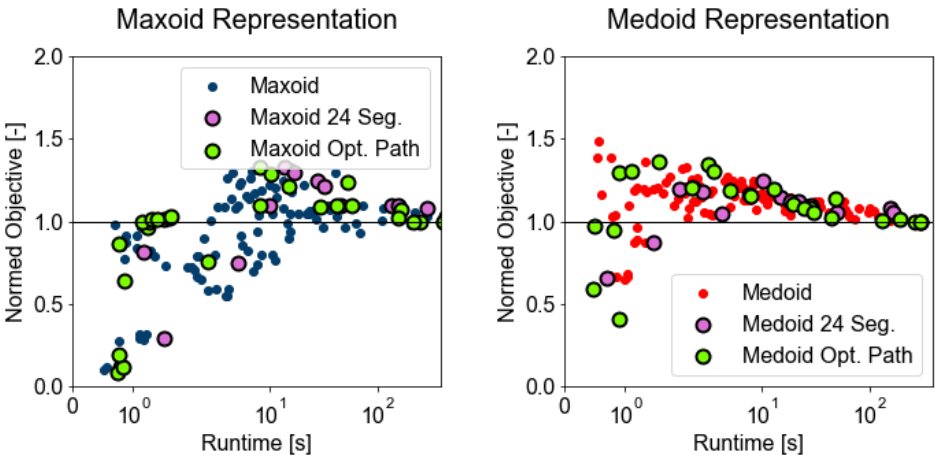

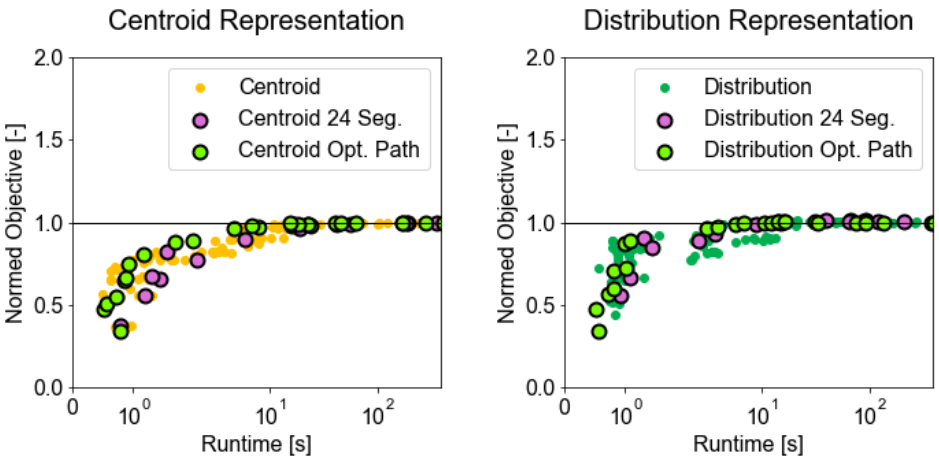

Figure 4.16. Convergence behavior of the different representation methods if an optimal ratio between the number of typical days and the number of segments is chosen based on the root-mean-square error compared to the convergence behavior of different typical day numbers at an hourly resolution

Finally, the findings of this section are used to compare the identified optimal aggregation approach based on the optimal pathway algorithm and the distribution-preserving representation algorithm to the whole set of tested temporal aggregation configurations, which is shown in the left graph of Figure 4.17. Further, the proposed method is also compared to the most common state-of-the-art aggregation approaches, i.e. the cluster representation by medoids and centroids based on typical days with hourly resolution (i.e. without a further segmentation). This is evaluated in the right graph of Figure 4.17. It is evident that the proposed configuration of an optimal ratio between the number of typical days and segments as well as the distribution-preserving representation algorithm is remarkably effective, as it converges very fast to the optimal objective of the reference case. Further, it outperforms the well-known aggregation approaches significantly, which rely on typical days at an hourly resolution with a centroid- or medoid-based cluster representation. The proposed method reveals a runtime speed-up for comparably exact results of almost a magnitude compared to the state of the art methods.

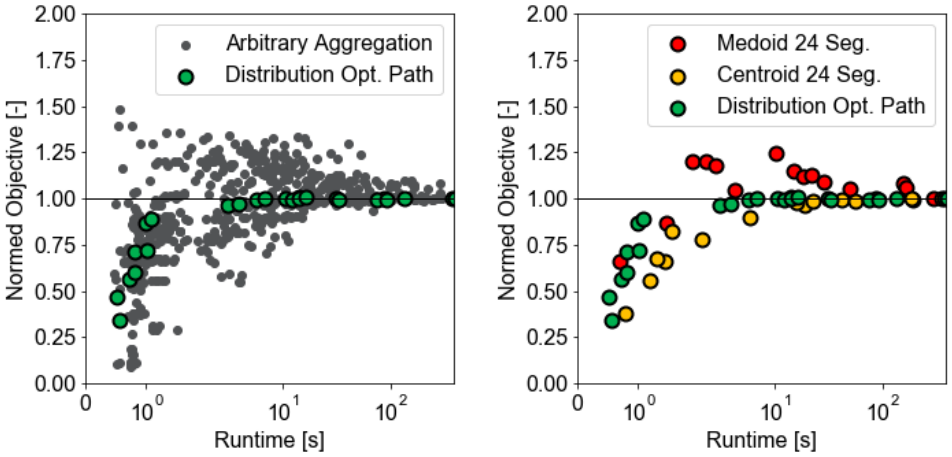

*Figure 4.17. The identified optimal aggregation method among all tested aggregation approaches (left) and a direct comparison to state-of-the-art aggregation methods as used in **FINE** (right)*

4.2.2. Analyses of the Self-Sufficient Building

In the following, the self-sufficient building model is analyzed analogously to the island system. However, as both models are temporally coupled multi-commodity single-node models, the analysis is shortened for the sake of brevity. Yet, the self-sufficient building is an interesting case study as it only considers time series with a strong daily pattern, i.e. photovoltaic profiles, electricity and heat demand. Therefore, this case study can be used in order to evaluate the effectiveness of segmentation even if the time series demand a high intra-daily resolution for an accurate temporal aggregation. Figure 4.18 illustrates the objective function deviations of the aggregated configurations from that of the fully resolved case depending on the runtime of the optimization.

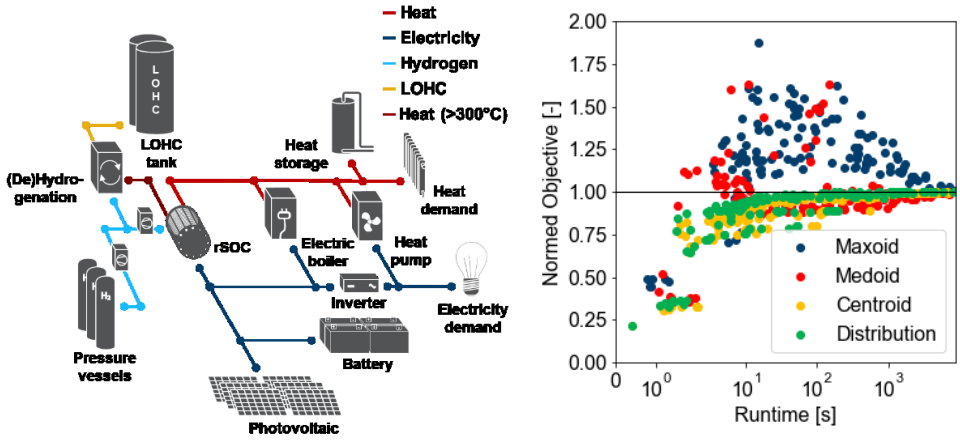

Figure 4.18. The self-sufficient building model and the corresponding normed optimal objectives over computation times for all considered configurations (adapted from Hoffmann et al. [3])

Compared to the corresponding graph for the island system shown in Figure 4.9, it can be stated that most of the major features of all considered clustering configurations are also given in case of the self-sufficient building model. Concisely, higher runtimes indicate more considered time steps resulting from a higher number of typical days and segments per typical day and accordingly, the deviation from the optimal objective is generally decreased. Moreover, the general underestimation of the total system costs with a monotonous convergence behavior in the case of a representation by centroids or the distribution-preserving algorithm for higher temporal resolutions is also analogous to the findings of the prior section. Furthermore, the distribution-preserving algorithm consistently deviates from the optimal objective of the reference case the least, which underlines its benefits in this application case as well.

In contrast to the aforementioned two representation methods, the representations by medoids and maxoids lead again to a more arbitrary deviation from the optimal objective of the fully resolved case. However, two differences can be identified: In this case, the majority of aggregation configurations with a representation by medoids underestimate the optimal objective, while almost all of the maxoid configurations overestimate the optimal objective.

In case of the representation by medoids, the trend of an overestimation for small temporal resolutions and the underestimation for higher temporal resolutions can be explained by the two opposite effects of choosing those candidate days, which are close to the clusters' centroids and accordingly relatively smooth on the one hand and lower operational flexibility on the other hand. In contrast to the island system model, the representation by maxoids fulfills its original purpose to create comparably robust system designs, i.e. designs that are more expensive than those of the fully resolved case. A possible reason for this is the fact that all time series have a strong daily pattern in this case, which means that the data cloud in the hyperdimensional $\mathrm{N_a} \times 24$ space is relatively dense. Therefore, fewer outliers are needed to form a convex hull of the data cloud and to capture all possible extreme cases challenging the energy system model. Accordingly, it can be stated that the representation by maxoids can be a good approach for robust system design under the premise that only few time series with a strong periodic pattern are considered. Otherwise, the number of

potential extreme situations increases drastically with the number of considered time series.

Figure 4.19 quantifies the optimal objective's deviation of all aggregation configurations from the fully resolved reference case depending on the number of typical days, segments and the representation method.

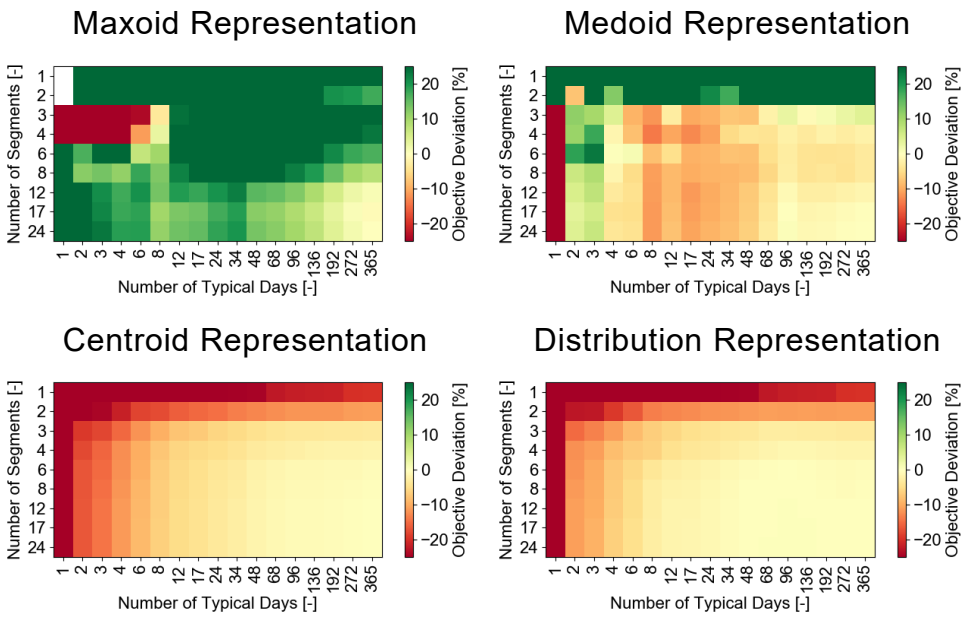

Figure 4.19. The deviation from the optimal objective of the fully resolved case depending on the configuration of the number of typical days and segments as well as the representation method (adapted from Hoffmann et al. [3])

In case of a representation by maxoids and medoids, a varying number of typical days and segments has an unpredictable impact on the objective deviation, which could also be observed for the island system model. In case of a representation by centroids or using the distribution-preserving algorithm, the aggregation-induced error decreases monotonously with an increase of the number of typical days and segments. Again, a small superiority of the distribution-preserving algorithm can be observed for small numbers of typical days and segments.

Analogously to the analyses for the island system in Section 4.2.1, the optimal pathway algorithm for finding a good tradeoff between the number of typical days and segments is investigated for the self-sufficient building model in the following.

Figure 4.20 shows the correlations between the aforementioned four error indicators as well as the corresponding correlation coefficients for the representation by centroids and medoids. Here, Spearman's correlation coefficient ρ_S in the upper right graph of each color assesses the validity of assumption 1 stated in Equation (3.26), the lower left picture the validity of assumption 2 stated in Equation (3.27) and the upper left figure the validity of assumption 3 stated in Equation (3.28).

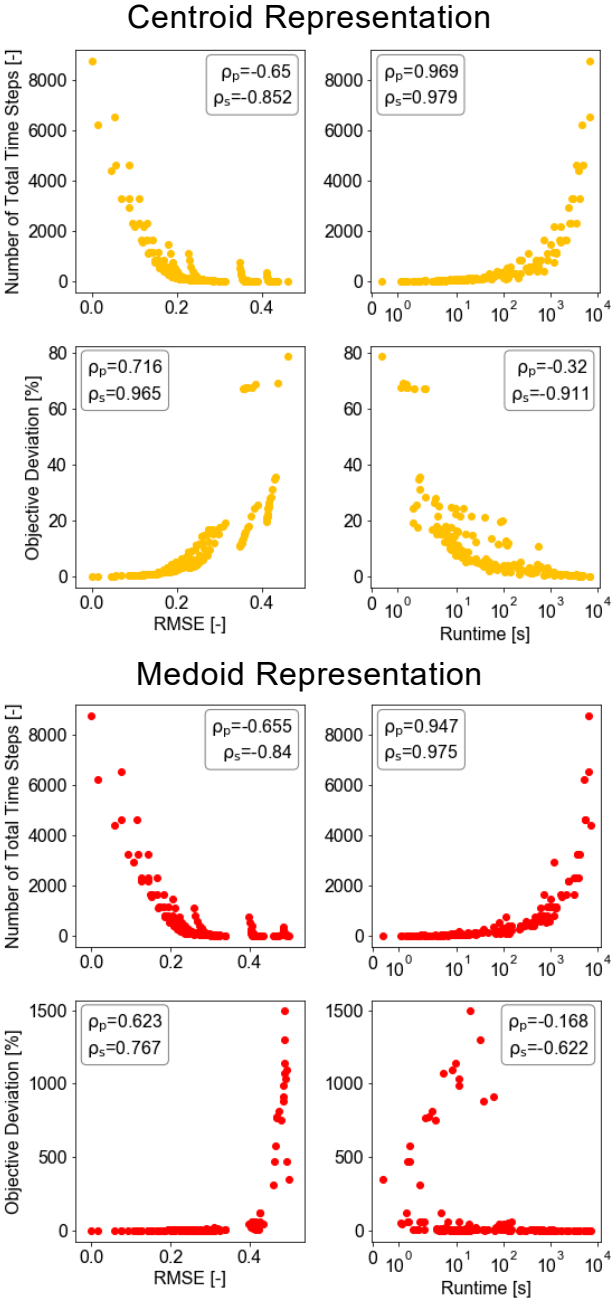

Figure 4.20. The correlation between a priori and a posteriori indicators for the representation by centroids (top) and by medoids (bottom)

As can be seen in Figure 4.20, the assumptions are sufficiently justified by Spearman's correlation coefficients in case of a representation by centroids, as they are close to 1 or -1, respectively. In contrast to that, the assumption of a monotonous correlation between the root-mean-square error and the objective function deviation (assumption 2) is not given in the case of a representation by medoids, as the relatively low correlation coefficient ρ_s of 0.767 in the lower left graph for medoids in Figure 4.20 reveals. Because the correlation results of the distribution-preserving algorithm are quite comparable to those of the representation by centroids, while those for maxoids are comparable to those of the representation by medoids, the validity of the proposed algorithm for finding the optimal number of typical days and segments is given for the representation by centroids and the distribution-preserving algorithm. In contrast to that, it is doubtful for a representation by medoids or maxoids.

Figure 4.21 depicts the pathway of optimal typical day and segment number for an increasing number of total time steps as predicted by the proposed algorithm depending on the representation method.

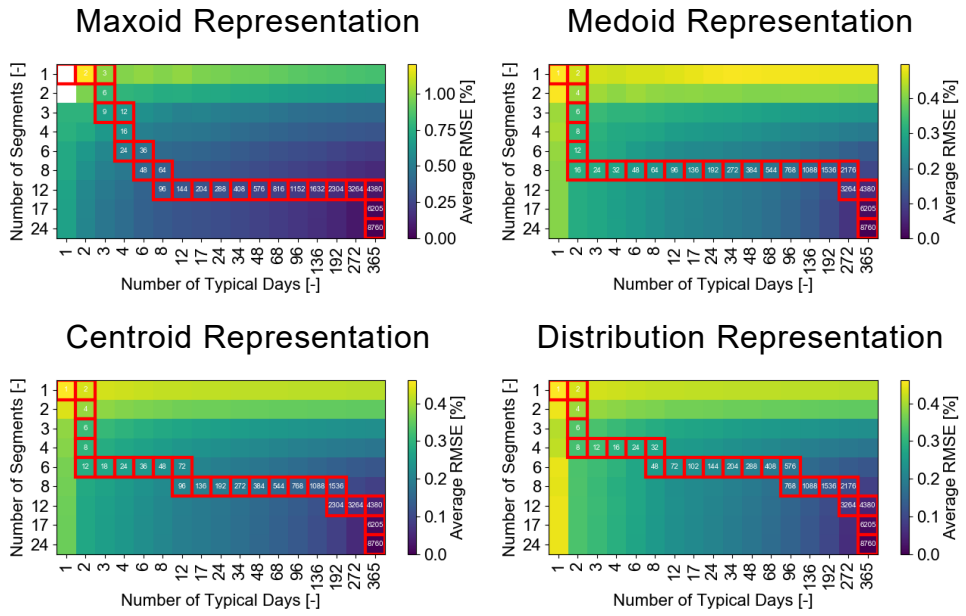

Figure 4.21. The pathway found by the proposed algorithm for an optimal ratio between the number of typical days and segments depending on the representation method (adapted from Hoffmann et al. [3])

Despite of the fact that the found pathway based on the root-mean-square error might not be meaningful due to the low correlation of

the root-mean-square error and the deviation from the optimal objective of the fully resolved model in case of a representation by maxoids and medoids, all pathways bear a certain resemblance to each other. When comparing the pathways for the self-sufficient building model shown in Figure 4.21 to those of the island system model shown in Figure 4.15, however, it becomes clear that the optimal pathways for the self-sufficient building model favor higher numbers of segments and fewer typical days at low temporal resolutions, while the opposite holds true for the island system model. This difference can be explained by the absence of a wind time series in the case of the self-sufficient building, which generally needs to be represented by a large number of typical days in order to capture its aperiodic pattern appropriately. This emphasizes that the optimal pathway algorithm is indeed capable to adapt to different model types.

Figure 4.22 compares the deviations from the optimal objective of the reference case depending on the runtime for each representation method separately. Here, the light green dots mark those configurations that are considered to be optimal with respect to their typical day and segment ratio according to the pathway algorithm, while the purple dots mark those configurations of typical days with an hourly inter-daily resolution.

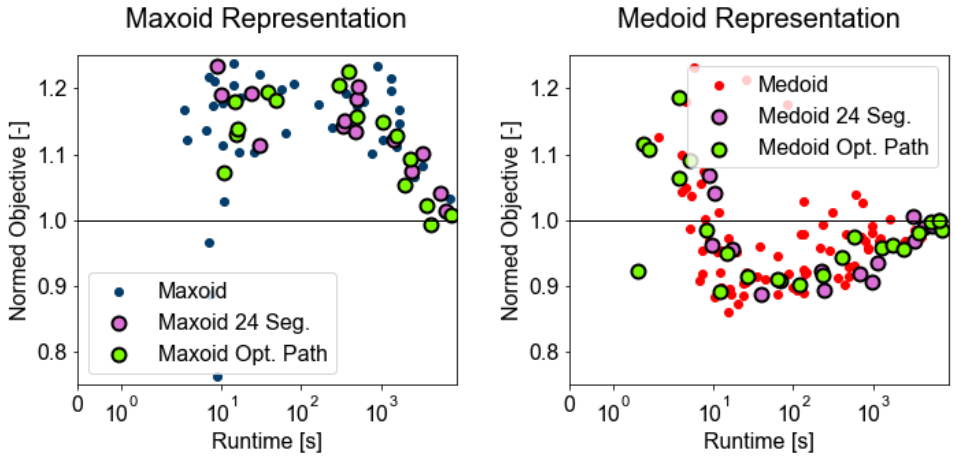

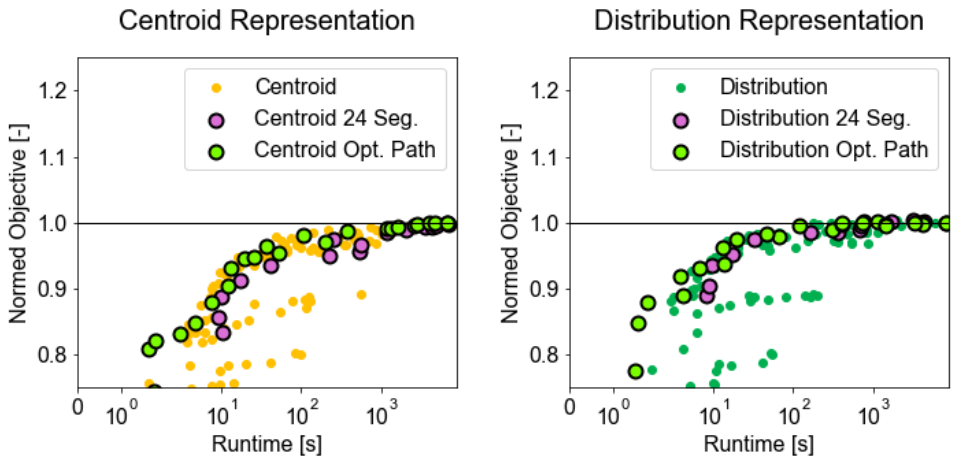

Figure 4.22. Convergence behavior of the different representation methods if an optimal ratio between the number of typical days and the number of segments is chosen based on the root-mean-square error compared to the convergence behavior of different typical day numbers at an hourly resolution (adapted from Hoffmann et al. [3])

As predicted by the statistical investigation in Figure 4.21, the algorithm for finding an optimal trade-off between the number of typical days and the number of segments performs poorly for the representation by maxoids and medoids. This is revealed by the upper two graphs in Figure 4.22. Here, it can be seen that the aggregation configurations proposed by the algorithm do not consistently outperform other aggregation configurations as e.g. those with typical days at an hourly resolution. However, compared to the configurations using representations by centroids or the distribution-preserving algorithm, the aggregations do not show a consistent convergence behavior for an increase of the temporal resolution anyways. In contrast to that, the lower two graphs of Figure 4.22 illustrate that the algorithm for finding an optimal ration between the number of typical days and the number of segments clearly outperforms other aggregation configurations in case of the representation by centroids or the distribution-preserving algorithm. Here, the light green data points are always those points that are closest to the optimal objective of the reference case for a given runtime. Further, these configurations of typical days and segments lead to aggregation configurations, which are, given a certain runtime, significantly closer to the optimal objective than the configurations that do not use the additional segmentation. Accordingly, the advantages of decreasing both, the number of typical days and the number of segments simultaneously, is evident.

Accordingly, the configurations that rely on the distribution-preserving representation and the optimal pathway algorithm are the most efficient ones for the self-sufficient building, which is in line with the findings made for the island system. The left graph in Figure 4.23 highlights those clustering configurations, which are relying on these two algorithms proposed in this thesis. Obviously, they cover those points among all 612 considered clustering configurations, which are optimal with respect to both, the runtime and the deviation from the optimal objective of the fully resolved reference case. Moreover, the left graph in Figure 4.23 illustrates the optimal aggregation configurations based on the two proposed algorithms to the status quo of the temporal aggregation techniques used in **FINE** prior to the contributions of this work, i.e. typical days without a further segmentation represented by medoids or centroids. The combination of the proposed algorithms outperforms the current methods of temporal aggregation by a speed-up factor of one magnitude for a comparable accuracy.

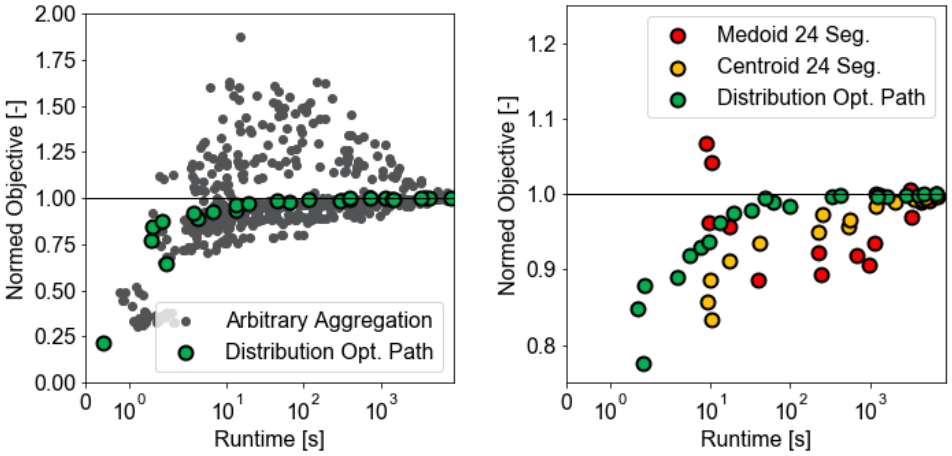

*Figure 4.23. The identified optimal aggregation method among all tested aggregation approaches (left) and a direct comparison to state-of-the-art aggregation methods as used in **FINE** (right) (adapted from Hoffmann et al. [3])*

4.2.3. Analyses of the European Model

The last model that is part of the sensitivity analysis to find an optimal combination of representation method, the number of typical days and the number of segments, is the European model. In contrast to the aforementioned models, the European model is a linear, but multi-regional energy system model with several hundreds of time series comprising low-correlated time series such as wind

profiles, but also time series with a clear daily pattern such as electricity demand and solar profiles.

Analogously to the preceding sections, the right graph of Figure 4.24 depicts the deviations from the optimal objective of the fully resolved reference case depending on the runtime necessary to solve the respective aggregated model configuration. In contrast to the prior models, none of the considered representation methods overestimates the total system cost dramatically. Yet, the representation by the distribution-preserving algorithm leads in general to a higher total system cost than a representation by centroids and the representation by medoids leads to higher system costs than a representation by the distribution-preserving algorithm, which is in line with prior energy system models. Interestingly, the representation by maxoids leads to the strongest underestimation of total system costs. A reason for this might be hypothesis that due to the number of different time series, the dimensionality of the clustering space increases so much that the number of possible extreme situations simply exceeds the number of typical days to be chosen by far. This would result in a representation of the original time series by a few days that might be extreme, but not design relevant. For example, days with maximum capacity factors and minimum electricity demand could be derived, which would not challenge the energy supply system. Accordingly, it can be stated that the representation by maxoids is likely only applicable for energy systems with few time series in which a limited number of candidate days belongs to the outer spheres of the data cloud in the clustering space.

A big contrast to the prior models, however, is the observation that the representation by medoids leads to the smallest deviations from the optimal objective function of the reference case at a given runtime. However, as will be shown in the following, an aggregation by medoids is not necessarily superior with respect to the optimal design capacities and a prognosis, what number of typical days and segments is necessary for a sufficient aggregation.

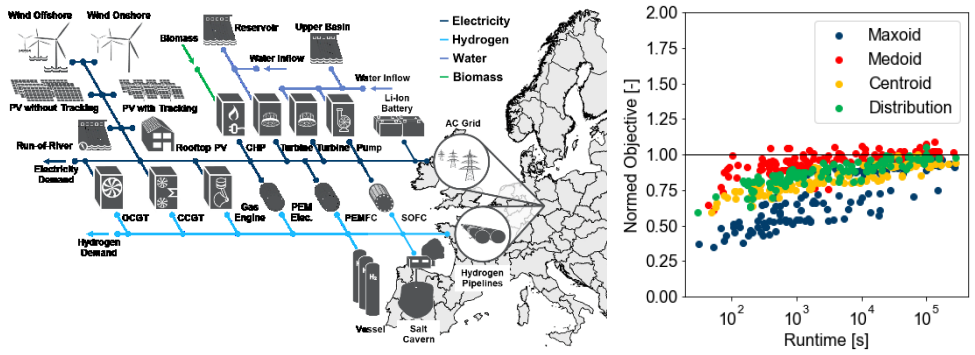

Figure 4.24. The European model and the corresponding normed optimal objectives over computation times for all considered configurations (adapted from Hoffmann et al. [3])

Figure 4.25 depicts the deviations from the optimal objectives of the reference case depending on the chosen representation method and the configuration of the number of typical days and segments used for temporal aggregation. Here, the general tendency of the maxoid representation to underestimate the optimal objective of the reference case severely is illustrated in the upper left graph. Furthermore, the representation by centroids or using the distribution-preserving algorithm lead to aggregation-induced objective deviations, which decrease monotonously with an increasing number of typical days or segments as the lower two graphs in Figure 4.25 reveal. Here, the temporal aggregation using the distribution-preserving representation algorithm, 136 typical days and 6 segments is an outlier due to a suboptimal optimization termination. Moreover, the distribution-preserving algorithm leads to a smaller objective deviation at a given number of typical days and segments than the representation by centroids. Finally, the representation by medoids leads to the smallest deviation from the optimal objective of the fully resolved case for the European model. However, as the upper right graph in Figure 4.25 reveals, the deviation is either an over- or underestimation of the optimal objective and no clear relationship between the typical day- and segment configuration and the deviation of the objective can be observed.

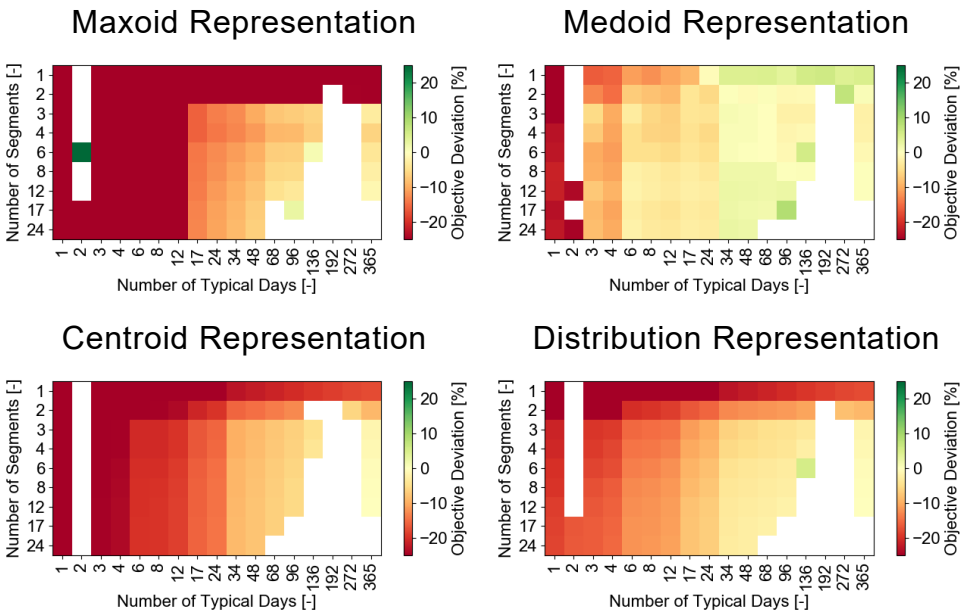

Figure 4.25. The deviation from the optimal objective of the fully resolved case depending on the configuration of the number of typical days and segments as well as the representation method (adapted from Hoffmann et al. [3])

It is worth mentioning that the white fields are clustering configurations that were not solvable within a predefined time (approximately 79 hours). Interestingly, the white fields imply that a higher number of typical days can be considered if less segments are used, e.g. while the maximum number of typical days with an hourly resolution it 48, up to 136 typical days can be considered, if the number of segments is reduced to six. This underlines the additional flexibility options achieved in the context with this work. Moreover, the configurations listed in Table 4.3 were terminated with a suboptimal solution, which makes them numerical outliers:

Table 4.3. Numerical outliers of the European model

Representation	Number of Typical Days	Number of Segments
Maxoid	1	6
Maxoid	96	17
Maxoid	136	6
Medoid	96	17
Medoid	136	6
Medoid	272	2
Distribution	136	6

In order to evaluate, which representation method is robust with respect to a consistent technology selection, the cumulative cost share of the considered photovoltaic technologies (with and without tracking as well as open field) and of the wind technologies (onshore and offshore) are shown in Figure 4.26. This means that the total annualized cost for each technology at each location belonging to either photovoltaics or wind is summed up and its share of the total system costs of the respective aggregation configurations is calculated. Obviously, the general underestimation of the total annualized costs in case of a representation by maxoids is partly caused by the low total annualized costs of the photovoltaic and wind technologies, as the first row of Figure 4.26 reveals. As mentioned earlier, the solar profiles are more strongly affected by a low number of segments, while the wind profiles are more strongly affected by a low number of typical days. Accordingly, the solar profiles are disproportionally more smoothened by a low number of segments, which makes them economically more viable in case of very few segments per day. In contrast to that, the wind technologies profit from a low number of typical days due to a stronger smoothening of their profiles for few typical days.

Interestingly, the representation by medoids leads to relatively small deviations with respect to a certain technology. Yet, the deviations are rather arbitrary and not a direct function of the chosen number of typical days and segments. Furthermore, the accuracy of configurations that capture the features of the reference system with respect to the size of built capacities is not necessarily improved if the number of typical days or segments in increased.

Similar to the representation by maxoids, the representation by centroids and the distribution-preserving algorithm reveal a preference for photovoltaic technologies when a small number of segments is chosen whereas wind technologies are overrepresented for small number of typical days. The reason for this is again the fact that photovoltaic profiles are stronger smoothened by a low number of intra-daily time steps, while wind profiles are disproportionally affected by a small number of typical days due to their aperiodic pattern. Furthermore, the representation using the distribution-preserving algorithm outperforms the representation by centroids for at least 34 typical days as the third and fourth row in

Figure 4.26 reveal. In the case of a representation using the variance-reserving algorithm, almost no deviation from the highly resolved configurations can be observed for photovoltaic technologies for at least three daily segments. For the cost contribution of wind technologies, a configuration of at least 34 typical days and 3 segments seems to be sufficient for the total share of wind costs for higher temporal resolutions. In contrast to that, the representation by centroids continuously overestimates the share of wind technologies at high temporal resolutions such as 96 typical days.

Yet, it can be stated that combined with the fact that the overall system costs deviate very little from reference case, the representation by medoids seems to work best for multi-regional energy system models with a large number of low-correlated time series such as wind profiles throughout Europe. Furthermore, it is remarkable that the number of segments has very little impact on accuracy of the aggregated solutions as three segments per typical day instead of 24 hourly time steps seem to capture the main features of the fully resolved energy system optimization independently of the used representation method.

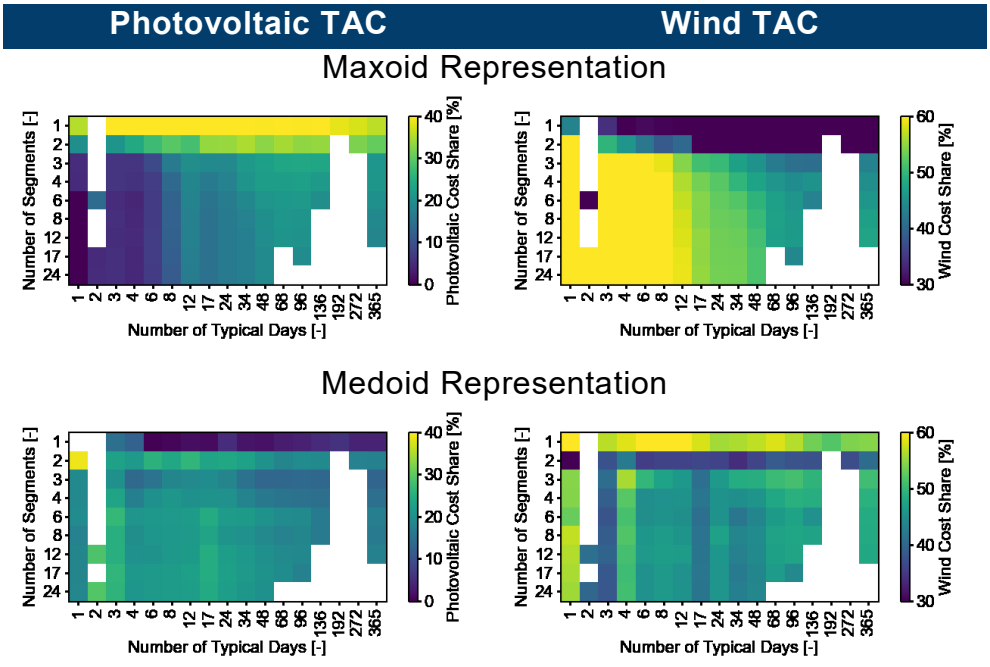

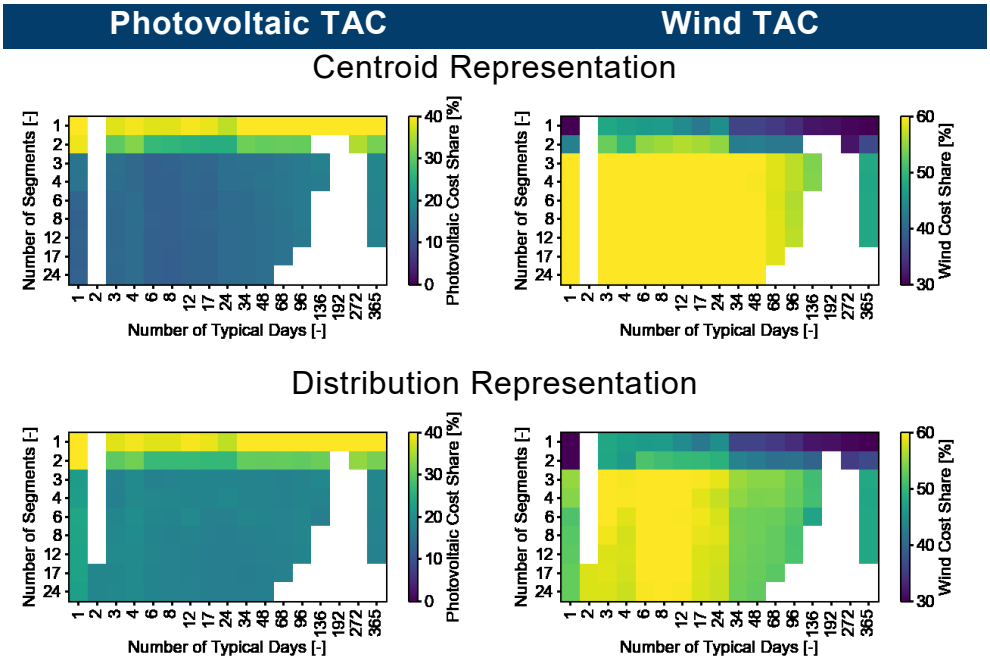

Figure 4.26. The total annualized costs of the photovoltaic technologies and the wind plants normed by their total annualized costs in the fully resolved case

In order to emphasize the impact of varying temporal aggregation configurations on the chosen technologies, Figure 4.27 depicts the energy supply and storage capacities depending on a varying number of typical days and segments using a representation by centroids. Here, a representation by centroids has been chosen because of a comparably predictable impact of the chosen aggregation configuration on individual technologies. Further, 96 typical days with 12 segments shown in the first row of Figure 4.27 have been chosen as an example for an aggregation with a relatively high number of typical days and segments. In order to evaluate the impact of a lower number of typical days or, in contrast to that, a low number of segments, the second and the third line of Figure 4.27 evaluate the impact of 96 typical days and 2 segments and 6 typical days and 12 segments on the technology mix, respectively. As Figure 4.25 and Figure 4.26 illustrate, the representation by centroids is not preferable with respect to its capability to aggregate the European model adequately. Therefore, the comparison in Figure 4.27 only refers to the **relative** impact on the technology mix due to a reduction of the number of typical days or the number of segments.

As the left map in the first row of Figure 4.27 illustrate, the wind and photovoltaic energy supply systems take over a major share in the overall energy supply in case of the model configuration with many typical days and many segments per typical day. However, the technologies are heterogeneously distributed: While large capacities of photovoltaics without tracking are built in the south of Europe, wind plants are preferred in the north of Europe. This is an intuitively plausible result because of the high solar irradiance in the south and the high wind potentials near the North Sea. Further, some of the regions with a coastline also have considerable capacities of offshore wind turbines, e.g. in Northern Germany or Northern Poland. The capacities of Run-of-River hydroelectricity plants are limited to regions near the Alps, e.g. Northern Italy. The right map in the first row shows that considerable amounts of salt caverns are needed in this highly resolved energy system configuration throughout Germany, Poland, Great Britain, the Benelux states and the eastern part of France. Moreover, hydro reservoirs in Scandinavia take over another major part for energy storage. Here, it needs to be highlighted, that the storage capacities of salt caverns are given as TWh of hydrogen and those of the hydro reservoirs as TWh of electricity. Therefore, the capacities are only comparable if usage and electrolyzer and fuel cell efficiencies are considered. Yet, the high temporal resolution leads to a considerable need for seasonal energy storage due to the intermittency of solar and wind energy feed-in. Here, it needs to be highlighted that battery storage does not contribute to the overall storage capacities in a considerable amount, as it is mainly operated on a daily basis. The reason for this are the high capacity-specific costs of batteries compared to those of e.g. salt caverns. Yet, batteries play an important role for compensating short-term residual load fluctuations. Further, despite their small contribution to the overall storage capacities, their cost contribution is not negligible due to their high capacity specific costs.

The second row of graphs in Figure 4.27 illustrate the optimal energy supply and storage capacities, if the European model is aggregated to 96 typical days and 2 segments with a centroid-based representation. In case of this very low inner-daily temporal resolution, the solar capacities are significantly overestimated compared to a resolution of 12 segments per typical day. In contrast to

that, the wind plant capacities are underestimated. The reason for this is that solar profiles are affected stronger by a low inner-daily temporal resolution because of their daily periodicity and their high inner-daily variance. If a typical day is represented by only two segments, that means that the solar profiles are averaged so extremely, that both time steps are spanning over both, day and night time. Accordingly, such an aggregation leads to a mathematical model, in which solar feed-in is also given during nighttime. Further, the profiles are smoothed extremely which moreover leads to an underestimation of the solar profiles' intermittency. As the right subgraph in the second row of Figure 4.27 reveals, the significantly lower number of segments per typical day has only little impact on both, the overall built storage capacities and their spatial distribution. Comparably to the case with 96 typical days and 12 segments, the optimal solution of this aggregation configuration chooses to build major amounts of hydro reservoirs in Scandinavia and salt caverns in central Europe as well as Eastern France and Great Britain. Here, it needs to be highlighted that the lower amount of segments per typical days has a stronger impact on the inner-daily storage systems, but due to their small overall capacities, the impact cannot be identified in this illustration.

The last aggregation configuration with 12 segments but the small number of only six typical days shown in the third row of Figure 4.27 reveals a drastic overestimation of wind capacities, while the solar capacities are underestimated. In this case, wind capacities are not only built close to the North Sea, but also in Southern France, Austria, Czech Republic and Poland. In contrast to that, the distribution of solar capacities varies less than the distribution of the wind turbines. Yet, the solar capacities in each region are consistently small in almost each of the regions compared to an aggregation to 96 typical days. The reason for the much higher amount of wind plant capacities is the circumstance that wind profiles are stronger averaged in case of a low number of typical days due to their aperiodic and daytime independent pattern. Therefore, the intermittency of wind energy is underestimated in case of a low number of typical days, which makes this technology considerably more profitable. In contrast to that, solar profiles are also averaged, but not to the same extent. For that reason, smaller amounts

of solar capacities are needed, because they become less profitable in relation to wind turbines and because smaller amounts are needed due to the averaging effect itself. For the storage technologies, the right map in the last row of Figure 4.27 reveals that although almost the same amount of hydro reservoirs is built in Scandinavia, the overall capacity of salt caverns is drastically reduced for a small number of typical days. The reason for the constant amount of hydro reservoirs compared to the two prior configurations is that they are implemented as fixed and already existing capacities within the setup of the European model because it is assumed that their overall potential in Europe is already fully used. However, in case of the salt caverns, the low number of typical days leads to a drastic underestimation of the storage capacities. As mentioned before, salt caverns mainly serve as seasonal storage of hydrogen due to their low capacity specific costs. In case of only six typical days, the intermittency of wind is drastically underestimated which leads to the erroneous assumptions that electricity can always be supplied by wind turbines. Accordingly, much smaller storage capacities are necessary in order to balance intermittent residual loads. Again, the impact of a small number of typical days on the overall battery capacities does not emerge from the map due to the low overall capacities of this technology. However, it can be stated that seasonal phenomena such as electricity feed-in have generally a big impact on seasonal storage technologies such as salt caverns while the same holds true for daily phenomena such as solar electricity feed-in from photovoltaics and battery capacities. Further, the more the intermittency of the respective renewable energy source is underestimated due to temporal aggregation, the smaller the corresponding storage component becomes.In summary, Figure 4.27 reveals that a strong interdependency between the number of typical days and segments and the optimal technology capacities exists. Although the optimal system layout heavily depends on the chosen representation method as well, Figure 4.27 underlines the observation that a low number of typical days mainly affects wind turbine and salt cavern capacities, i.e. technologies with a seasonal operation pattern, while the number of segments affects technologies with a daily operation pattern such as photovoltaic plants. Against this backdrop, it becomes evident that especially large-scale energy system models, which generally rely on strongly reduced temporal resolutions,

need a careful evaluation, whether the chosen temporal resolution is meaningful or results in an unjustified preference for certain technologies. Even if the energy system is not solvable for an hourly or even higher temporal resolution, a sensitivity analysis in the direct neighborhood of the chosen temporal resolution seems to be mandatory. Moreover, it is advisable to consider always both dimensions of temporal aggregation, the number of typical periods and the inner-daily temporal resolution.

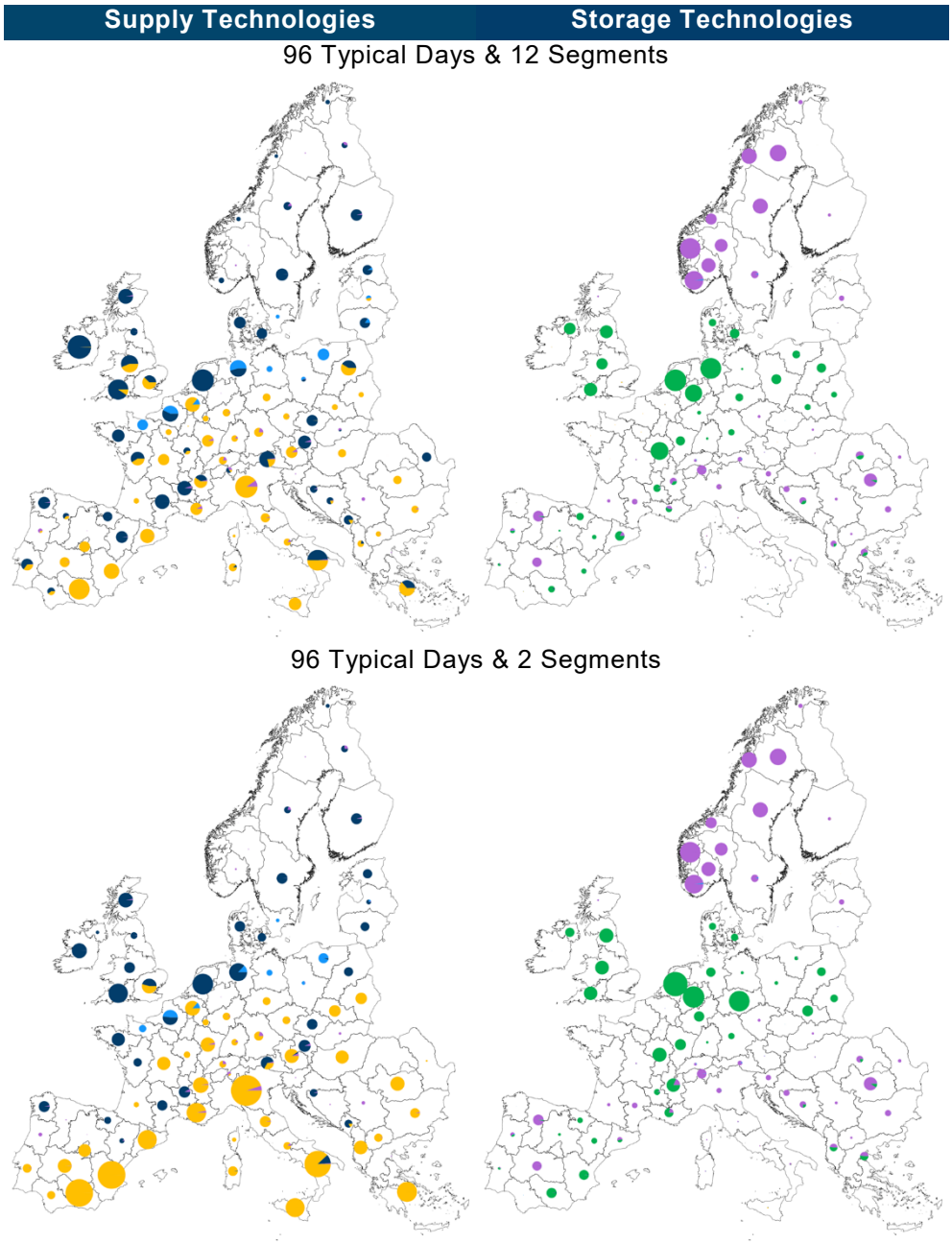

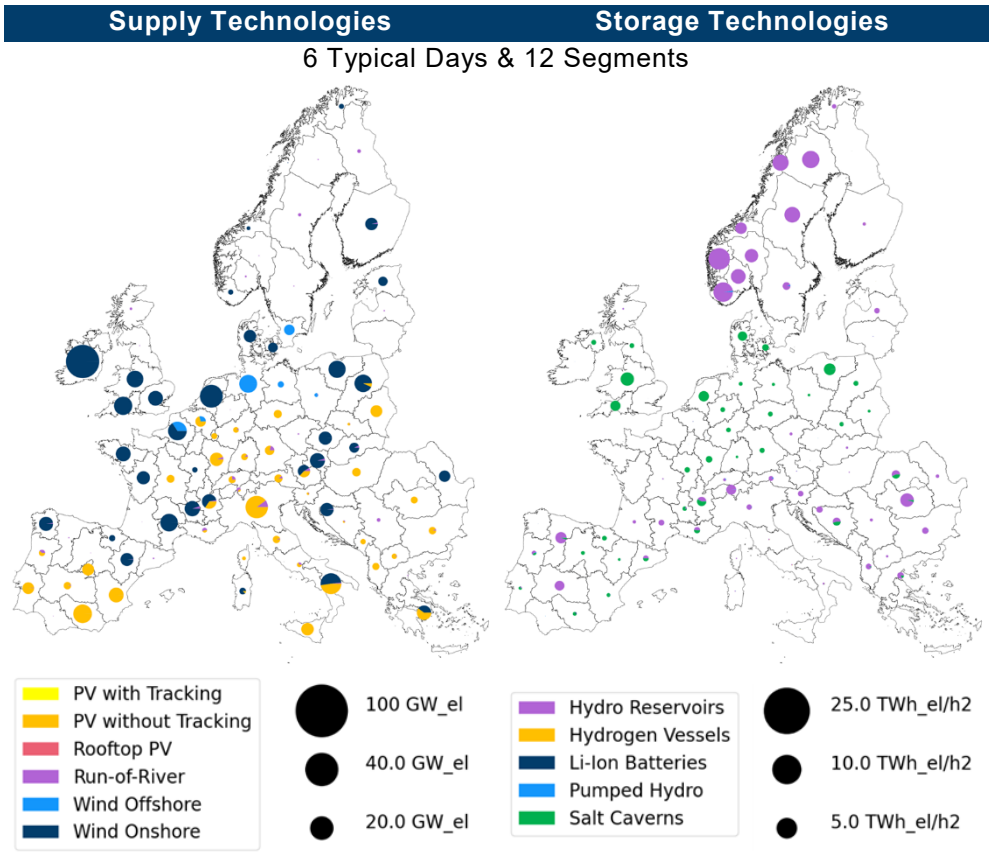

Figure 4.27. Energy supply and storage capacities depending on a varying number of typical days and segments using a representation by centroids (taken from Hoffmann et al. [3])

Analogously to the prior models, it is investigated in the following paragraph whether the algorithm proposed to find an optimal ratio of the number of typical days and the number of segments based on an a priori indicator outperforms the status quo of aggregation techniques, i.e. an aggregation to typical days with an hourly resolution only.

The validity of the three assumptions stated in the equations (3.26), (3.27) and (3.28), on which the optimal pathway algorithm is based, are again evaluated using Spearman's correlation coefficient ρ_s, and Pearson's correlation coefficient ρ_p. Figure 4.28 depicts the different correlations between the a priori indicators root-mean-square error and the total number of time steps and the a posteriori indicators optimization runtime and deviation of the optimal objective of the fully resolved case for the representation by centroids and the representation by medoids. In case of the representation by centroids, the assumptions of a monotonous correla-

tion between the total number of time steps and the runtime, between the a priori indicator root-mean-square error and the aggregation-induced objective function deviation and the a priori indicator and the total number of time steps are sufficiently justified. This is indicated by Spearman's correlation coefficient, which are close to 1 and -1, respectively, in the upper right (for assumption 1), lower left (for assumption 2) and upper left (for assumption 3) graph for centroids. In contrast to that, assumption 2 is violated in the case of a representation by medoids, as the low correlation coefficient ρ_s of 0.682 in the lower left figure for medoids indicates, i.e. the assumption that a lower root-mean-square error of the clustered time series indicates a lower deviation from the optimal objective, is not justified in this case.

Centroid Representation

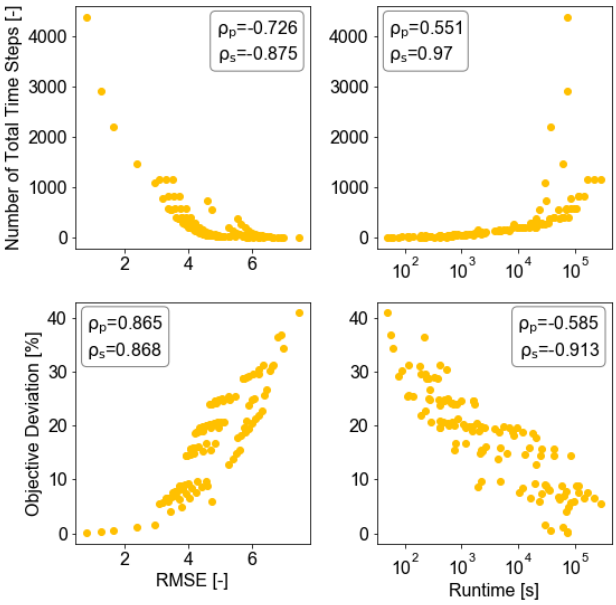

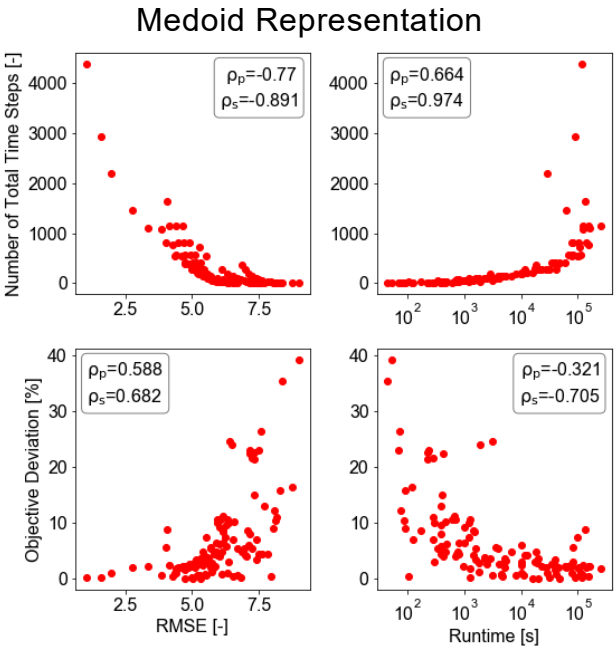

Figure 4.28. The correlation between a priori and a posteriori indicators for the representation by centroids (top) and by medoids (bottom)

Apart from that, it is remarkable that the Pearson correlation coefficient between the number of total time steps and the runtime of the optimization problem is significantly lower than for the island system model and the self-sufficient building model. This means that a reduction of the total number of time steps leads to a disproportional speed-up in case of the European model. However, Figure 4.29 highlights the correlation of the runtime and the total number of time steps in a double logarithmic plot for a representation by centroids and by medoids. As shown, the correlation is approximately linear in this plot, which is also mirrored by the high Pearson correlation coefficient $\rho_{p,log}$ between the logarithms of both variables. This means that the correlation can be described as:

$$\log(\#TS) = m \cdot \log(\text{Runtime}) + \log(b) \Leftrightarrow \text{Runtime} = \left(\frac{1}{b}\#TS\right)^{\frac{1}{m}} \tag{4.2}$$

In this case, the function for both, the representation by centroids and the representation by medoids is approximately given by:

$$\text{Runtime} = 2 \cdot \#TS^{1.5} \tag{4.3}$$

Accordingly, it can be stated that for large energy system models, a reduction of the total number of time steps leads to a stronger speed-up of the optimization runtime compared to small energy

system models, for which the correlation between the number of total time steps and runtime is approximately linear. Taking into account that the deviation from the optimal objective of the reference case have a very small sensitivity to a decrease of the number of segments, reducing the total number of time steps by using both, typical days and segments, reveals big advantages.

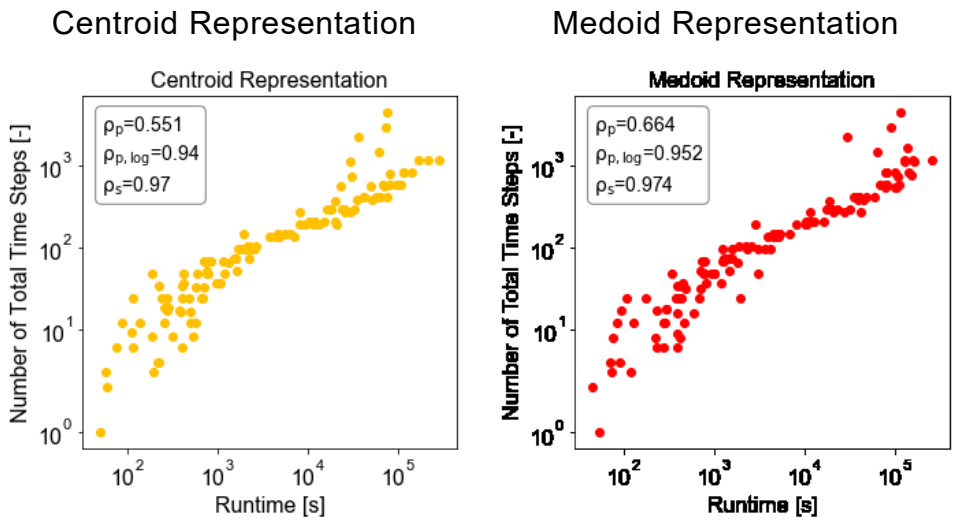

Figure 4.29. The correlation between the logarithm of runtime and the logarithm of the total number of time steps

Figure 4.30 depicts the pathway of optimal typical day and segment numbers for an increasing number of total time steps as proposed by the optimal pathway algorithm depending on the representation method. Evidently, the algorithm never chooses more than eight segments per typical day unless the original number of days, i.e. 365 days, is used. This emphasizes that low auto- and cross-correlation of the wind profiles in each of the considered 96 European regions lead to a set of very heterogeneous candidate days. Accordingly, the idea of clustering typical days based on their mutual similarity always leads to a strong averaging effect of time series in some of the considered regions. Instead, a reduced number of inner-daily time steps and an increased number of typical days seems to be more advantageous. Interestingly, the optimal pathways of the representation by centroids and the representation using the distribution-preserving algorithm differ the most: While the representation by centroids favors eight segments for the most typical day configurations, the distribution-preserving algorithm favors three or four segments per typical day. As shown in Section 3.2.5, the distribution-preserving algorithm increases or decreases

the extreme values slightly in time series that were under- or overestimated due to the averaging effect in order to produce aggregated time series with the same variance as the original ones. In that process, however, the root-mean-square error is slightly increased compared to a representation by centroids. This penalty is obviously decreased by increasing the number of typical days first, as this mitigates the averaging effect due to clustering and therefore also the root-mean-square error increase introduced by the variance-synthesis in case of the distribution-preserving algorithm.

Interestingly, the optimal pathways for an aggregation by maxoids or medoids lie in the middle of the both aforementioned pathways. Together with the fact that the representation by medoids does not lead to an overestimation of the reference case's optimal objective, it may lead to more meaningful results for these representation types than it was the case for the single-regional models.

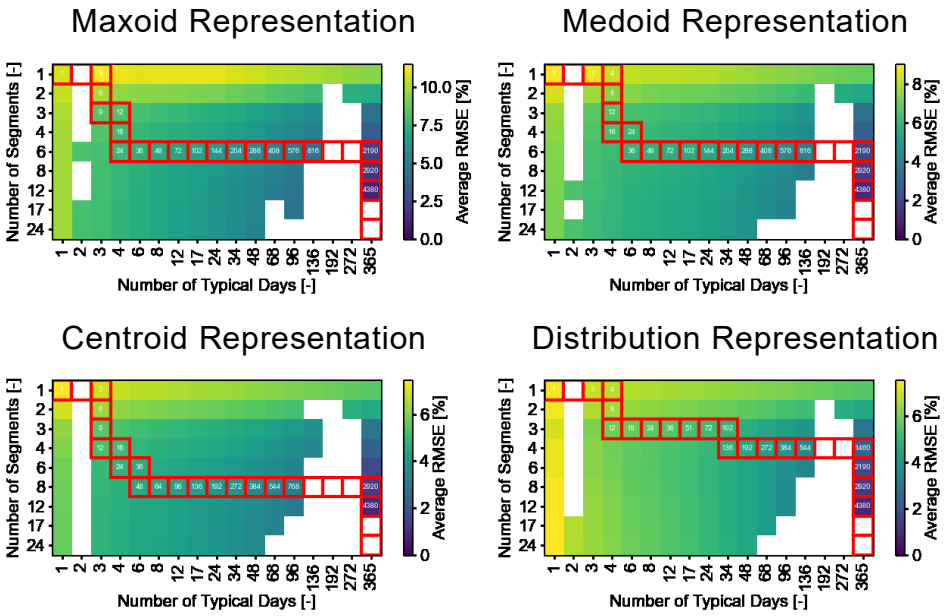

Figure 4.30. The pathway found by the proposed algorithm for an optimal ratio between the number of typical days and segments depending on the representation method (adapted from Hoffmann et al. [3])

In order to evaluate whether the proposed algorithm for finding an optimal tradeoff between the number of typical days and the number of segments succeeds at closer approximating the optimal objective value of the fully resolved reference case at a smaller temporal resolution, Figure 4.31 depicts all temporal aggregation con-

figurations of each representation method separately. Furthermore, those clustering configurations that were proposed by the optimal pathway algorithm are highlighted in light green, whereas those configurations considering typical days at an hourly resolution, i.e. without an additional segmentation, are highlighted in purple. The latter represent the status quo in the **FINE** framework before the option for segmentation was implemented within the scope of this thesis.

Evidently, the algorithm determines clustering configurations of typical days and segments that are consistently closer to the optimal objective of the reference case for a given runtime than those configurations that consider a number of typical days with hourly resolution only. In contrast to the single-regional energy system models, this also holds true for the representation by maxoids and medoids despite of the fact that only a low correlation between the root-mean-square error and the objective function deviation could be observed for these configurations in Figure 4.28. However, as shown in Figure 4.30, the optimal pathways laid in-between those for the representation by centroids and the distribution-preserving clustering algorithm, so that the found clustering configurations seem to be still meaningful. A possible reason for this could be the fact that in contrast to the single-regional energy system models, the representation by means and medoids does not significantly overestimate the total system costs in case of the European model. In case of the single-regional energy system models, this overestimation of the total system costs was caused by the fact that fewer time steps led to fewer operation options in the optimization and therefore stiffened the storage operation. Furthermore, maxoids and medoids do not preserve the original time series' mean values, which likely led to further unpredictable deviations. In contrast to that, these effects are of minor importance to the European model and the major error in this case is the underestimation of extreme values. For that reason, a smaller underestimation of the original time series' extreme values leads to a smaller underestimation of the optimal objective in case of the European model. This hypothesis is supported by the fact that although the clustering configurations proposed by the optimal pathway algorithm consistently lead to higher objective function values compared to the aggrega-

tion to typical days with an hourly solution, they almost never overshoot the optimal objective value of the reference case. Here, it needs to be highlighted that the green data point in the upper right graph of Figure 4.31 belongs to one of the outliers mentioned in Table 4.3, for which the optimization problem did not converge properly. Accordingly, this outlier can be neglected.

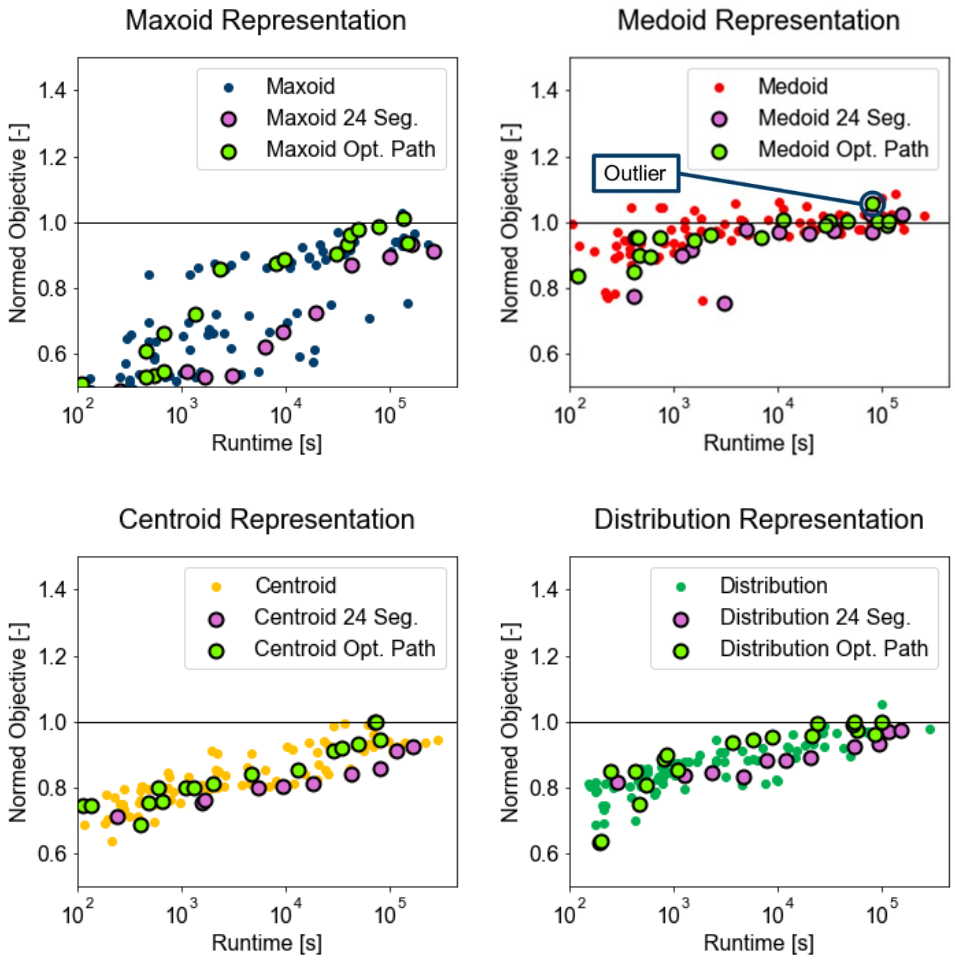

Figure 4.31. Convergence behavior of the different representation methods if an optimal ratio between the number of typical days and the number of segments is chosen based on the root-mean-square error compared to the convergence behavior of different typical day numbers at an hour (adapted from Hoffmann et al. [3])

The optimal aggregation configurations identified for the European model are depicted in the left graph of Figure 4.32, whereas they are compared to the status quo consisting of typical days with hourly resolution found using centroid or medoid representation in the right graph. As it can be seen in the left subfigure, the representation by medoids using typical day and segment numbers as proposed by the optimal pathway algorithm leads to aggregated

model configurations which are consistently among those clustering configurations that are closest to the optimal objective of the fully resolved case. Moreover, the right subfigure emphasizes that especially the aggregation by means of centroids with an hourly resolution shows an extremely slow convergence behavior with an increase of the temporal resolution. Compared to an aggregation to typical days using a medoid representation, the aggregation configurations using medoids as well as an optimal tradeoff between the number of segments and typical days is also consistently closer to the optimal objective, but with a smaller spread between different optimal objectives at a given runtime. Moreover, the optimal objective of the reference case is not overestimated, if a good ratio between the number of typical days and the number of segments is chosen. Here, the outlier due to a suboptimal termination of the optimization algorithm can be neglected.

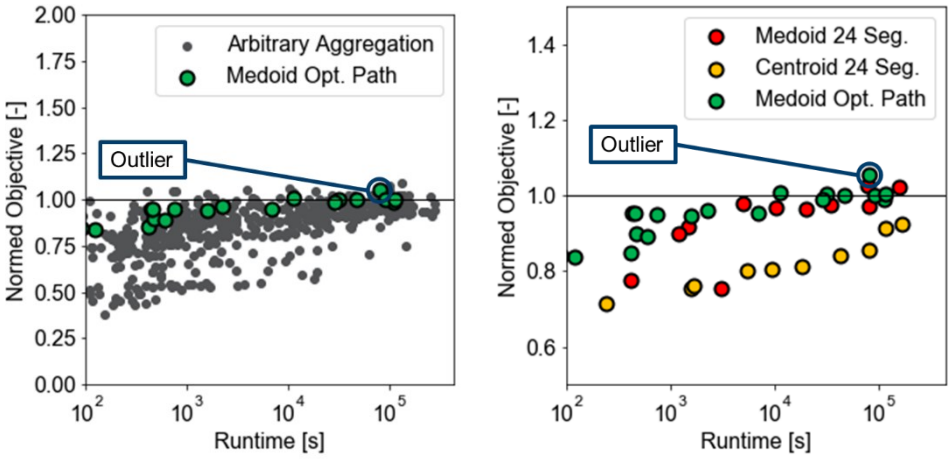

*Figure 4.32. The identified optimal aggregation method among all tested aggregation approaches (left) and a direct comparison to state-of-the-art aggregation methods as used in **FINE** (right)*

Finally yet importantly, the reason, why the representation by medoids slightly outperforms the representation using the distribution-preserving algorithm in case of the European model, whereas it significantly underperforms in case of the single-regional models, remains an open question. As the preceding results imply, especially the onshore and offshore wind turbine capacities are sensitive to a varying number of typical days in case of the distribution-preserving representation method. Furthermore, it was shown in Section 3.3.4 that the root-mean-square error of wind time series mainly decreases with an increase of the number of typical days

as wind time series do not have a daily pattern. As the distribution preserving representation method strives at preserving the value distribution of those days assigned to the same typical day **separately**, the daily mean of the respective typical day equals the mean value of all days that are assigned to the respective cluster of candidate days. Therefore, the preservation of the original time series variance is achieved by an overestimation of the inner-daily variance within typical days of the aggregated time series, which can easily be seen in Figure 3.19. At the same time, the variance across the mean value of different typical days is underestimated, which is supported by Figure 4.33. Here, two sample days where aggregated to one typical day using either centroids (C) or the distribution-preserving algorithm (DP). While the distribution-preserving algorithm captures the total variance of the original time series by overestimating the variance within the typical days, the daily mean of both aggregated time series coincide, as the orange dashed line completely covers the red dashed line. In the original time series, however, also the daily mean value varies over time as represented by the dashed blue line.

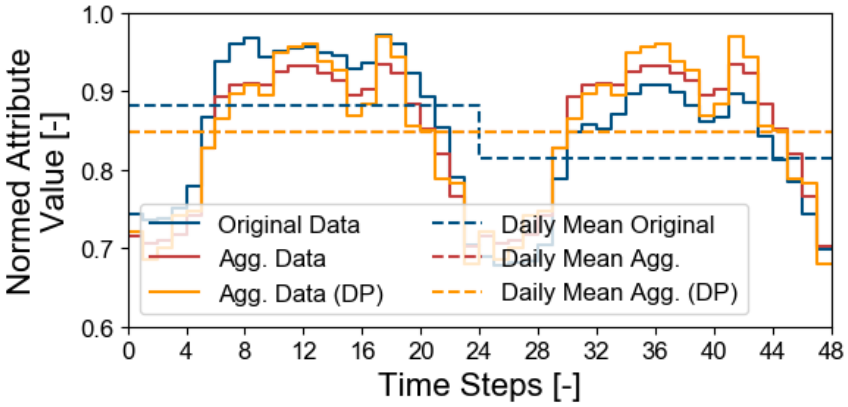

Figure 4.33. Impact of the centroid (C) and distribution-preserving (DP) representation on both, the inner-daily and inter-daily variance

In order to analyze this impact on the European model, one can define the variance of daily mean values of an attribute a, i.e. a technologies time series at a certain location, as follows:

$$\mathrm{Var}_p(\bar{x}_{a,p}) = \sqrt{\frac{1}{|P|}\sum_{|P|}\left(\bar{\bar{x}}_a - \bar{x}_{a,p}\right)^2} = \sqrt{\frac{1}{|P|}\sum_{|P|}\left(\frac{1}{|P|\times|T|}\sum_{|P|}\sum_{|T|} x_{a,p,t} - \frac{1}{|T|}\sum_{|T|} x_{a,p,t}\right)^2} \quad (4.4)$$

Equation (4.4) defines the variance of daily mean values as variance between the total mean of an attribute a containing $|P| \times |T|$

values and the daily mean comprising |T| values each. As shown in Figure 4.26, especially wind capacities were less accurate represented using the variance-preserving algorithm compared to the medoid representation. For that reason, Figure 4.34 compares the variance of daily means of the regionally resolved onshore wind capacity factors of the European model for different numbers of typical days represented by either medoids or using the distribution-preserving algorithm. As the effects described in the following do not significantly differ in case of offshore wind capacities and the data is only defined for the subset of regions with a coastline, the corresponding analysis for offshore wind time series is omitted for the sake of brevity.

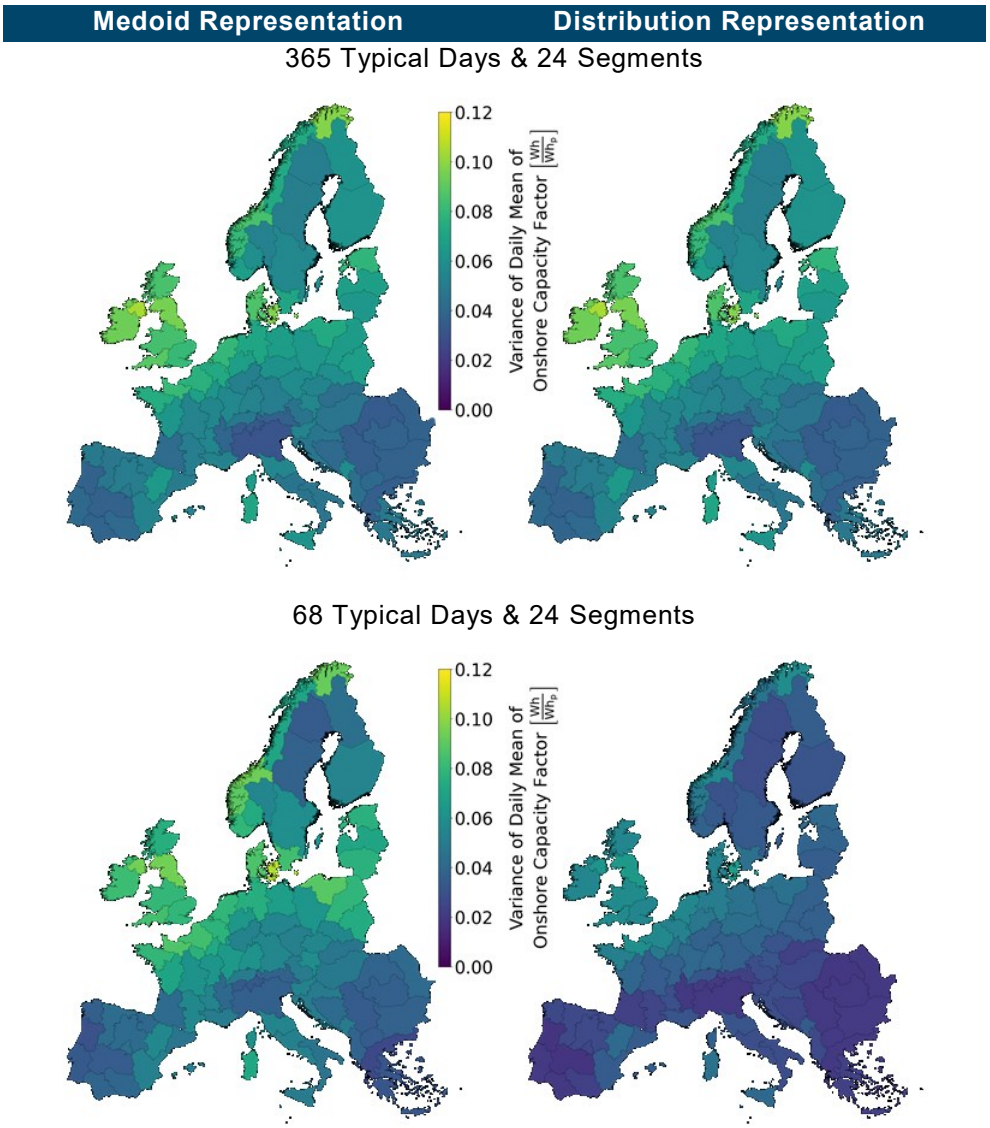

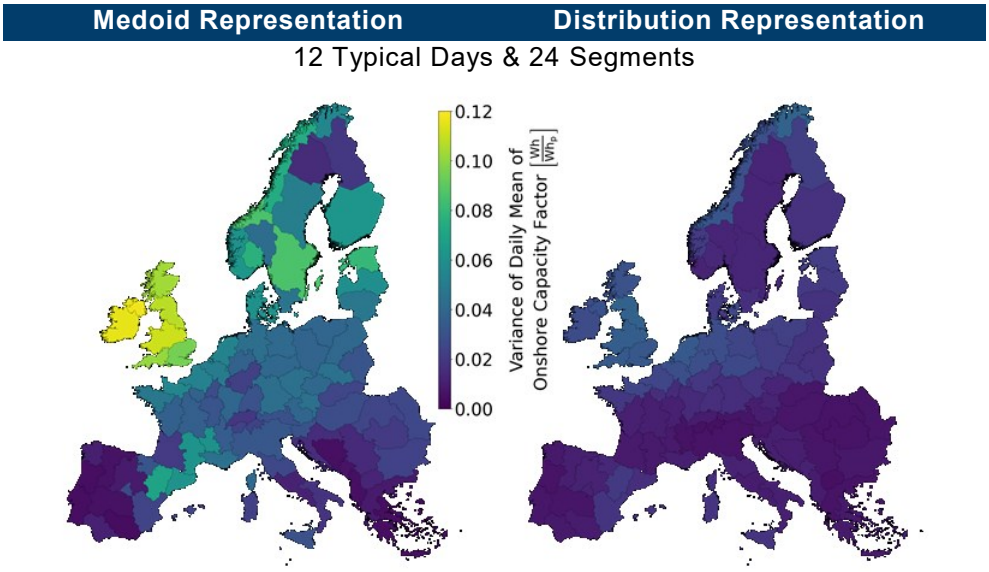

Figure 4.34. Variance of daily means of onshore capacity factors for varying numbers of typical days depending on the representation method

As shown in Figure 4.34, the spatially resolved variance of the daily mean of onshore capacity factors is identical for both representation method in case of 365 typical days, because the aggregated time series equal the original ones. If the number of typical days is decreased, however, the medoid representation chooses a subset of days from the original dataset in order to represent the full time series. Accordingly, the daily means equal those of a subset of real days and are not affected by subsequent calculations. This results in a variance of daily means, which is similar in scale, but not necessarily with respect to spatial distribution. While the spatial distribution in case of 68 typical days represented by medoids is comparable to the reference case, the most variable areas within Europe shift from Norway to Great Britain and Ireland if only twelve typical days are used for representation. In that case, the variance of the daily mean of onshore wind capacity factors is also considerably underestimated on the Iberian Peninsula. This implies that a medoid representation is suitable for models in which the cumulative capacities of a technology throughout all regions is of interest, but the exact spatial distribution of capacities can suffer from a considerable misallocation. In contrast to that, the variance of the daily means decreases monotonously with a smaller number of typical days in case of a representation based on the distribution-preserving algorithm. As shown before in Figure 4.33, the daily

mean of a typical day represented by the variance-preserving algorithm coincides with the daily mean if a centroid representation is used. For that reason, the daily mean suffers from the same averaging effect as centroid representations with respect to the inter-daily variance, whereas the intra-daily variance is overestimated. As shown before, wind time series do not have a daily pattern rather than an irregular pattern, which varies between different days. For that reason, the intermittency of wind capacity factors is predominantly underestimated by this effect. Accordingly, electricity feed-in from wind turbines is economically more viable and consequently, the wind capacities are systematically overestimated if a small number of typical days are represented by the distribution-preserving algorithm. Yet, in contrast to the medoid representation, those regions with the highest and lowest variance of daily means, i.e. northern Norway and northern Italy, remain the same for fewer typical days. Accordingly, the regional allocation of capacities is less affected.

Another aspect that affects the accuracy of temporal aggregation in case of the European model is the large number of low-correlated time series, which form a much less redundant dataset than those of the prior models because the number of potential extreme situations grows exponentially with the number of time series considered in a model as shown in Section 2.3.1.1. To illustrate this effect, Figure 4.35 illustrates the convergence behavior of the three different aggregated energy systems' optimal objective value to the reference value, if centroid-based typical days with an hourly resolution (no segmentation) are used. Here, the number of total time steps divided by 24 equals the number of typical days that were used for this analysis. Further, the centroid-based representation was chosen because it has the most predictable convergence behavior as shown in prior analyses. Accordingly, the maximum number of total time steps refers to the reference case and comprises 8760 time steps or 365 typical days. It is worth mentioning that some typical day configurations in the case of the European model did not converge within a set time-out of three days. Accordingly, the calculations were interrupted and some data points are missing in this case. Yet, it can be clearly seen that the aggregation-induced error converges asymptotically to the optimal objective value of the reference case for both the single-regional

models with a small number of different time series. Moreover, in case of the island system model, a knee point can be observed at well below 1000 total time steps, i.e. approximately 40 typical days. Accordingly, the whole set of days can be accurately represented by only 10% of days that are obtained by averaging all days that are assigned to a common cluster. In case of the self-sufficient building, the knee point is not as distinct as for the island system model; however, it is clearly visible that despite the logarithmic scale of the x-axis, the optimal objective converges. In contrast to that, correlation between the aggregation-induced deviation from the optimal objective and the logarithm of the total number of time steps used in the aggregated energy system model is almost linear in the case of the European model. This can clearly be seen in the right subgraph of Figure 4.35. This finding is supported by the following Pearson correlation coefficient:

$$\rho_{\mathrm{p}}\big(\log(\#\mathrm{TS})\,,\mathrm{Objective}(\#\mathrm{TS})\big)_{\mathrm{European}} = 0.985 \tag{4.5}$$

Accordingly, the relationship between the number of considered time steps and the optimal objective can be approximated by the following function:

$$\mathrm{Objective}(\#\mathrm{TS}) = \mathrm{m} \cdot \log(\#\mathrm{TS}) + \mathrm{b} \tag{4.6}$$

As the logarithm is an unbounded function, however, this would imply that the objective function value would further increase as long as the number of total time steps is increased. In other words, this would imply that the total costs of the energy system model would further logarithmically increase, the more days are considered. This also implies that 365 days as database is insufficient for a reliable design of a multi-regional model with a large number of low-correlated time series. Apart from that, it means that days stemming from a heterogeneous set of multi-regional input data can hardly be aggregated to fewer days, e.g. the error and the clustering-induced averaging effect will always be significant. Against this backdrop, the choice of real days from the original dataset, as it is the case for a representation using medoids, seems to be a more advantageous approach than synthesizing typical days by averaging a set of very heterogeneous days. This can be understood as a good example for the curse of dimensionality. Further, the existence of a knee point as observed for the island system model and the self-sufficient building model using clustered

time series can be used as a tool to investigate whether the ground truth, i.e. the fully resolved time series, is sufficient.

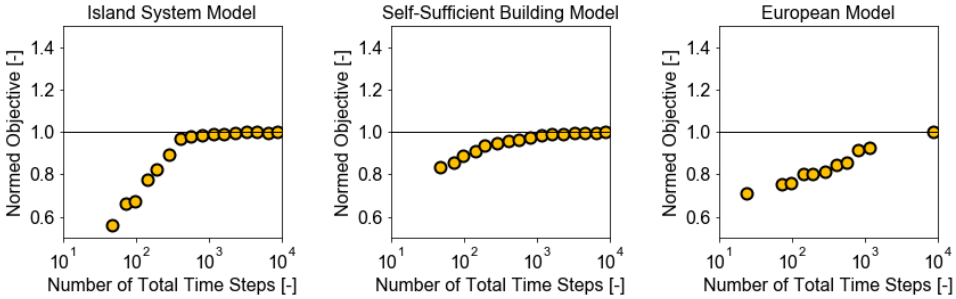

Figure 4.35. The convergence behavior of the three different aggregated energy systems' optimal objective value to the reference value, if centroid-based typical days with an hourly resolution (no segmentation) are used (adapted from Hoffmann et al. [3])

4.2.4. Adaption of the Distribution-Preserving Algorithm

As shown in the prior section, the distribution-preserving representation increases the inner-daily variance while the variance of the daily mean, i.e. the variance on a longer time scale, is decreased, which especially affects the predicted wind turbine capacities. In order to address this issue, the representation algorithm is adapted as shown in Figure 4.36. In contrast to the first approach, the adapted representation method now strives at preserving the value distribution of the whole attribute's time series only rather than to preserve the value distribution of each typical day cluster separately. The corresponding algorithm is defined as follows:

For a given attribute, the centroids of each cluster are calculated (1) and the time steps of all clusters are sorted **together** according to their size (2). Then, the original time series of the attribute is likewise sorted to a duration curve (3) and every $|C_k|$ values of the original duration curve are averaged and assigned to the respective value of the sorted centroid value list starting from the biggest to the smallest value (4). Lastly, the newly calculated values replace the values of the cluster centroids using the inverse bijection function that stored the order of centroid values (5).

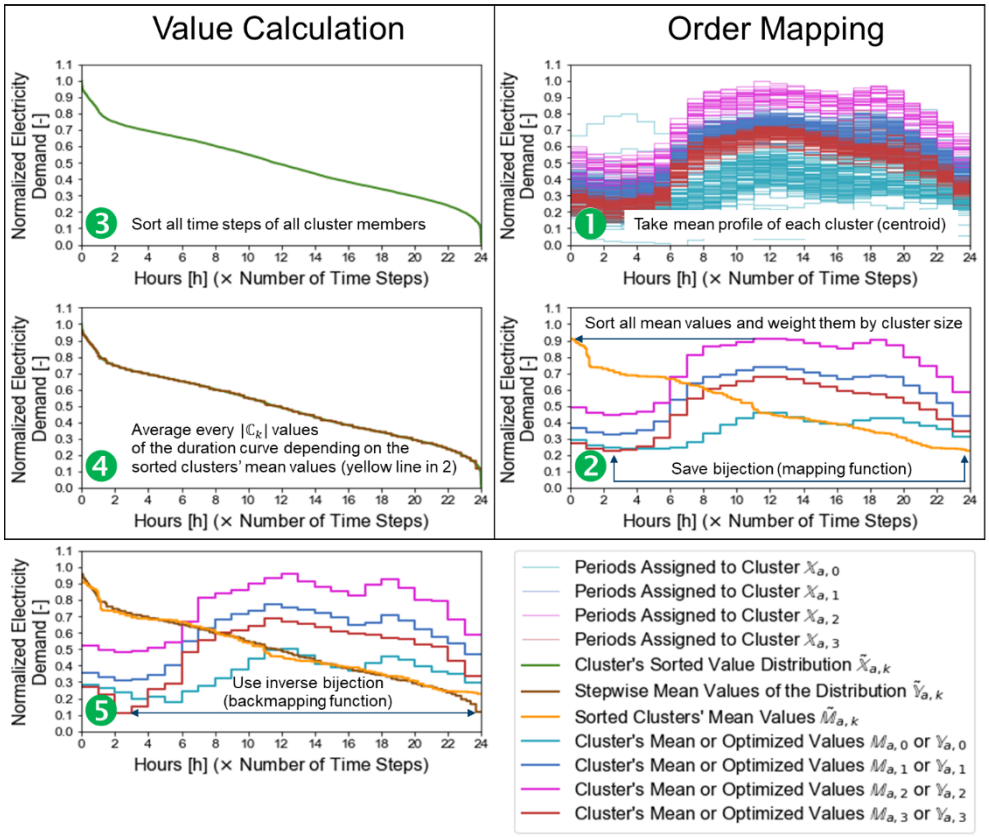

Figure 4.36. The graphical interpretation of the adapted distribution-preserving algorithm

The impact of the modified approach on the variance of the daily mean of onshore capacity factor time series is depicted in Figure 4.37. As the representation by medoids performed best for the European model among the previously introduced representation algorithms, the subsequent evaluations of the adapted distribution-preserving algorithm use the medoid representation as a benchmark.

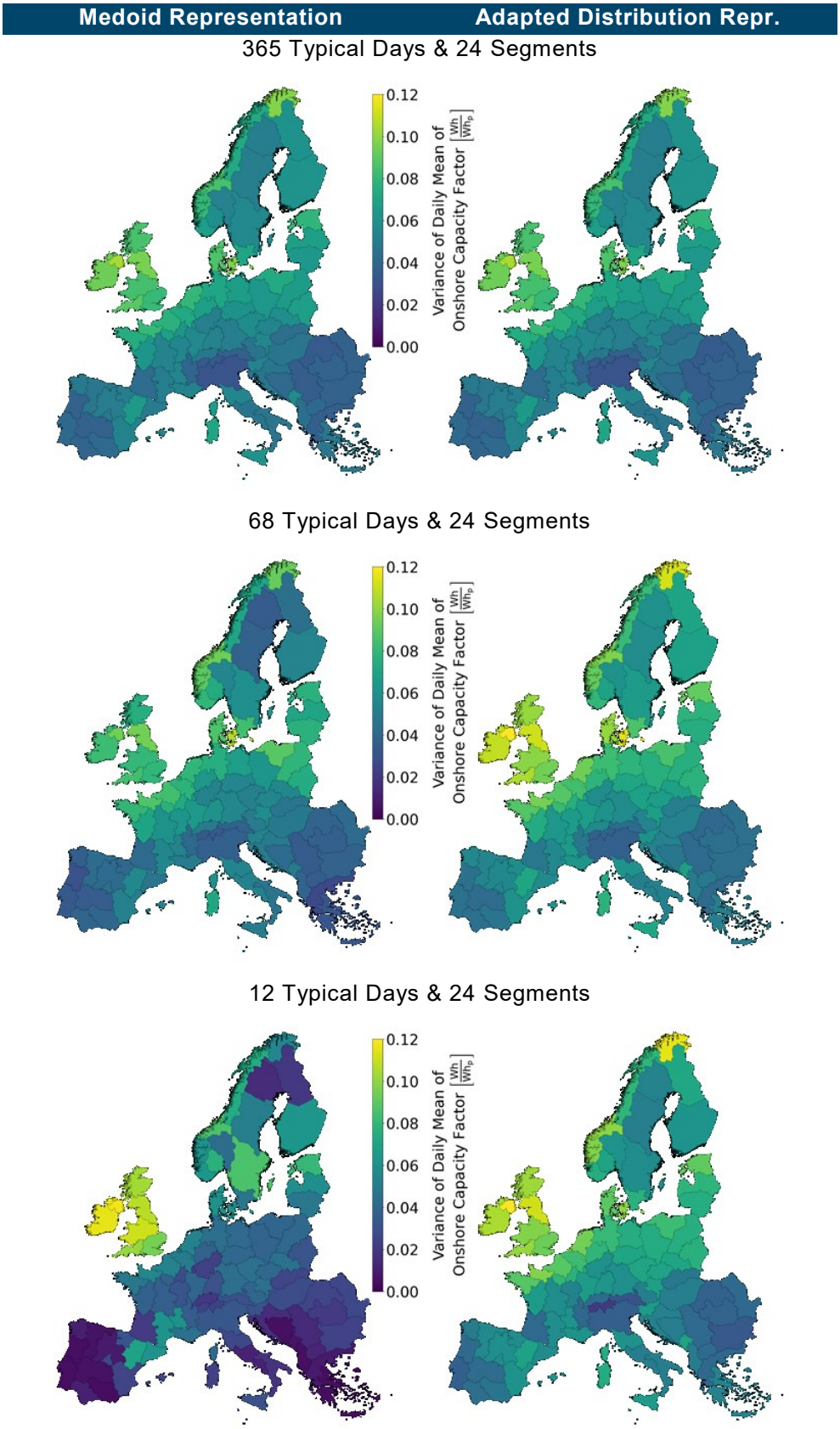

Figure 4.37. Variance of daily means of onshore capacity factors for varying numbers of typical days depending on the representation method

Here, it can be observed that compared to the original version of the distribution-preserving representation, the modified algorithm does not underestimate the variance of daily means of the onshore wind time series for a decreasing number of total time steps in the aggregated time series. In contrast to the representation by medoids, it can also be observed that the spatial distribution of more and less variant areas remain almost constant, i.e. the most variant areas remain in Northern Norway and Northern Ireland, whereas the least variant areas are to be found on the Iberian Peninsula, Northern Italy and the Balkan. In case of a representation by 12 medoid days, however, the variance in Northern Scandinavia and central Italy is underestimated, while it is overestimated on the British Isles.

In order to validate the assumption that the preservation of the variance of daily means plays an important role for the appropriate sizing of those technology that usually do not work on a daily scale rather than on a seasonal one, the European model was optimized for the adapted distribution-preserving algorithm as well. Subsequently, the results are compared to those of the original distribution-preserving algorithm and the medoid representation.

Figure 4.38 depicts the optimal pathway of clustering configurations for a rising number of total time steps as proposed in Section 3.3.4. Here, it can be observed that the optimal pathways for the medoid representation and the adapted distribution-preserving algorithm both favor six segments per typical day for more than 24 typical days.

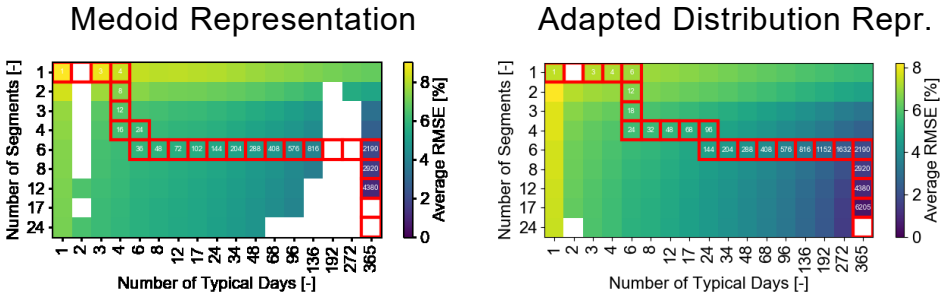

Figure 4.38. The pathway found by the proposed algorithm for an optimal ratio between the number of typical days and segments depending on the representation method (adapted from Hoffmann et al. [3])

Figure 4.39 depicts the normed optimal objective for all considered representation methods over the corresponding runtime (left) and

the normed objectives along the optimal pathway for the distribution-preserving algorithm, the medoid representation and the modified distribution preserving algorithm (right). As it can be seen, the adapted distribution-preserving algorithm clearly outperforms the prior version with respect to its deviation from the optimal objective for comparable running time. Further, it neither leads to significant overestimations of the optimal objective as the representation by medoids. Further, if only clustering configurations along the optimal pathway are considered, the adapted distribution-preserving algorithm is the first one, which stabilizes at a solution close to the original objective function at well below 10^4 seconds. In contrast to that, the other representation methods proceed to oscillate around the optimal objective for up to 10^5 seconds.

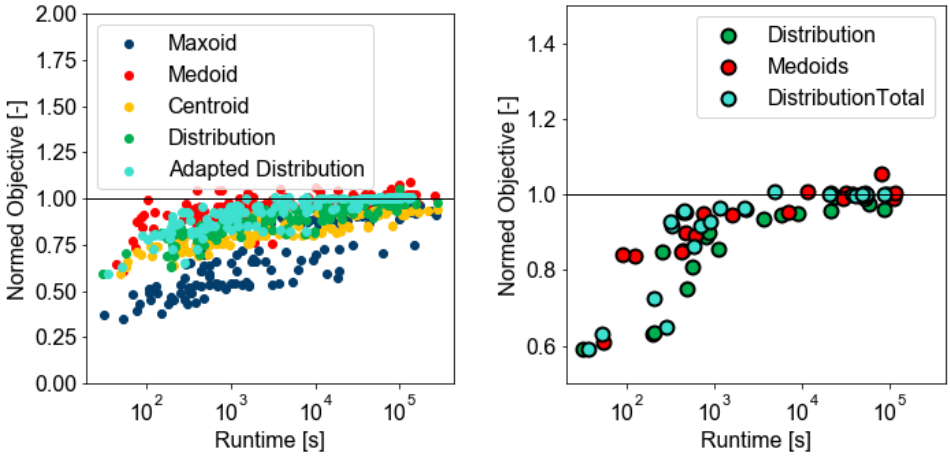

Figure 4.39. The normed optimal objective for all considered representation methods over the corresponding runtime (left) and the normed objectives along the optimal pathway for the distribution preserving algorithm, the medoid representation and the modified distribution preserving algorithm (right) (adapted from Hoffmann et al. [3])

Another aspect of interest is the deviation of the optimal objective value from the one of the fully resolved reference case as well as the cost share of certain technologies on the overall costs depending on the chosen aggregation configuration. For that, the wind turbine and photovoltaic related costs depicted in Figure 4.40 are analyzed in accordance to Section 4.2.3.

In contrast to the representation by medoids, the adapted distribution preserving algorithm leads of a consistently negligible total cost deviation from the reference case if at least 34 typical days and 3 segments are chosen, which equals a reduction from 8760 total time steps to 102, i.e. a reduction factor of 98,84%. The same

phenomenon can be observed for the cost share of wind and solar technologies, which likewise stabilize at the mentioned aggregation configuration. Furthermore, a comparison with Figure 4.26 reveals that the adapted distribution-preserving algorithm especially improves the sizing of wind technologies, but at the cost of a slightly deteriorated sizing of photovoltaic units.

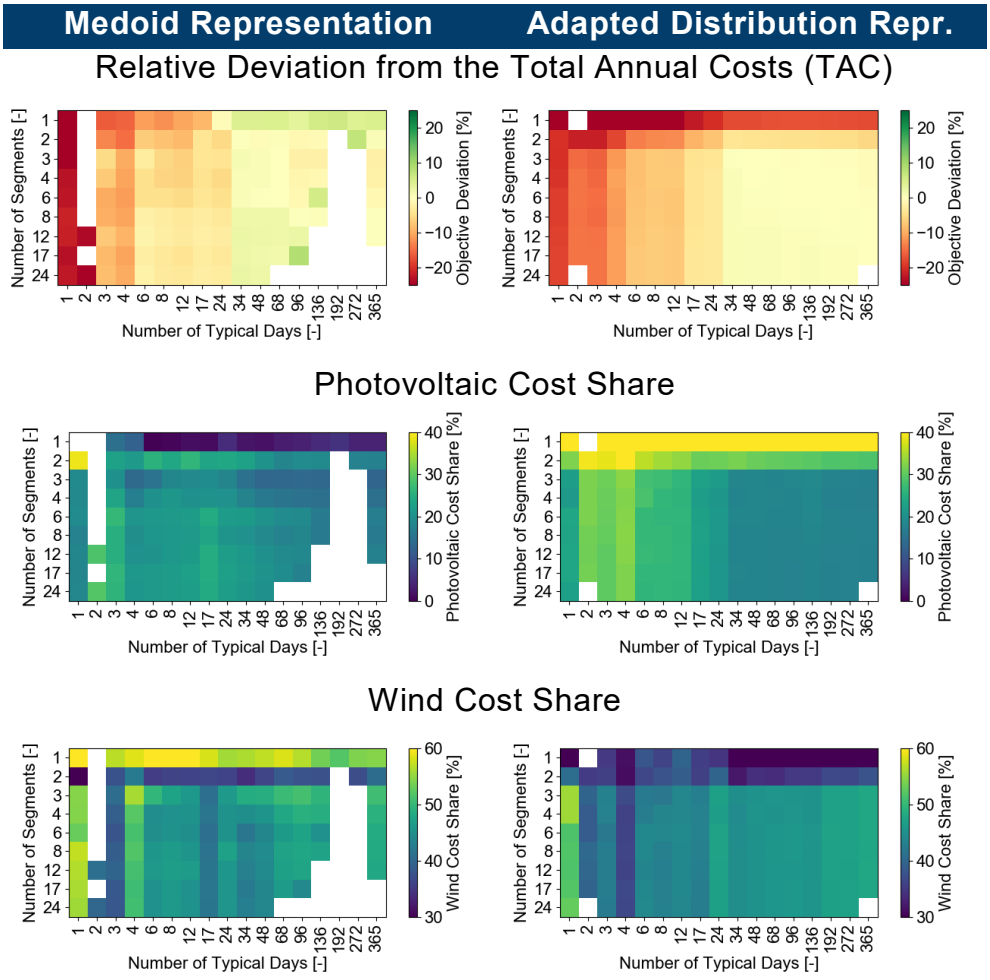

Figure 4.40. The deviation from the optimal objective value of the reference case and the total cost shares of photovoltaic and wind capacities for the medoid and adapted distribution-preserving representation

As temporal aggregation heavily affects the sizing of storage capacities and total costs as well, Figure 4.41 shows the individual cost shares of lithium-ion batteries and salt caverns having the highest cost share among all storage technologies. In general, a too low inner-daily time resolution leads to an underestimation of battery storage, whereas a too low number of typical days leads to an underestimation of salt cavern storage due to the inaccurate

representation of seasonality. Despite the fact that batteries predominantly balance inner-daily energy fluctuations due to their higher capacity-specific costs, 3 segments per typical day deem sufficient to approximate their total cost share closely to the benchmark in case of the adapted distribution-preserving algorithm. In summary, the proposed representation method provides a close estimate of the total cost share for both technologies if at least 34 typical days and 3 segments are chosen. In contrast to that, the cost shares of storage using the medoid representation have not stabilized at this high aggregation level.

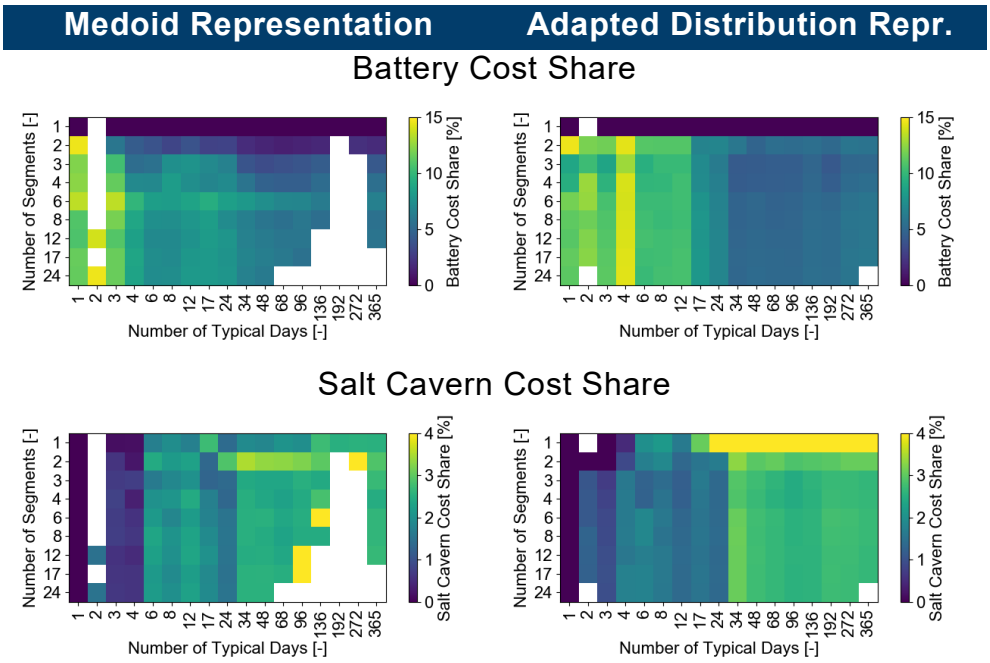

Figure 4.41. The total cost shares of battery and salt cavern capacities for the medoid and adapted distribution-preserving representation

Lastly, we investigate the impact of temporal aggregation on the spatial distribution of source capacities, because not only the cumulative capacity costs, but also their correct allocation are of interest. As the optimal pathway for both, the medoid and the adapted distribution-preserving representation contain the aggregation configurations of 34 and 48 typical days with six segments each, we consider these two configuration in order to investigate whether the allocation of capacities significantly deviates for this gradual increase of temporal resolution. Figure 4.42 depicts the energy supply capacities depending on a varying number of typical days and segments using the medoid and the adapted distribution-preserving representation. Here, it can be seen that the optimal

energy supply capacities as well as the allocation vary between 34 and 48 typical days in case of a representation by medoids. For example, the installed photovoltaic capacities in Northern Italy are considerably smaller in case of 48 typical days, whereas the on-shore wind turbine capacities in Middle and Southeast England as well as Ireland are larger compared to the corresponding optimal solution based on 34 typical days. In contrast to that, the size and allocation of supply technologies varies significantly less in case of the adapted distribution-preserving algorithm which mirrors the observation made in Figure 4.37 that the regional distribution of variance is much stronger affected if medoid days are chosen.

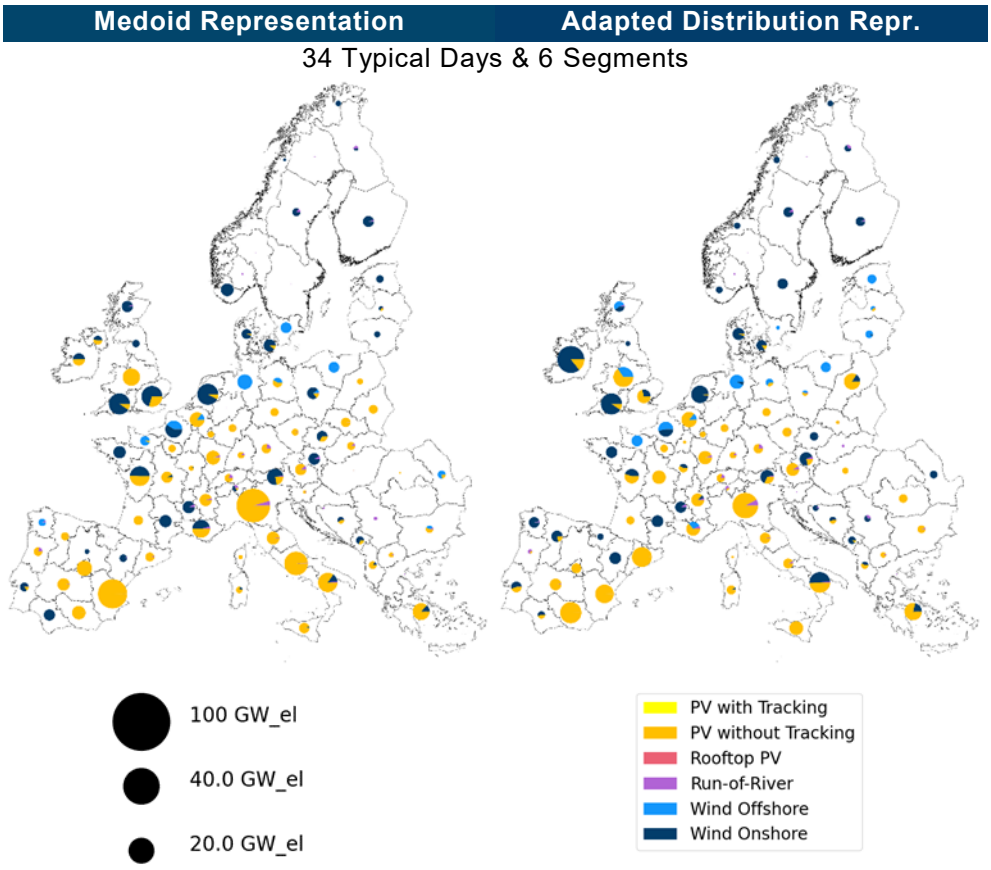

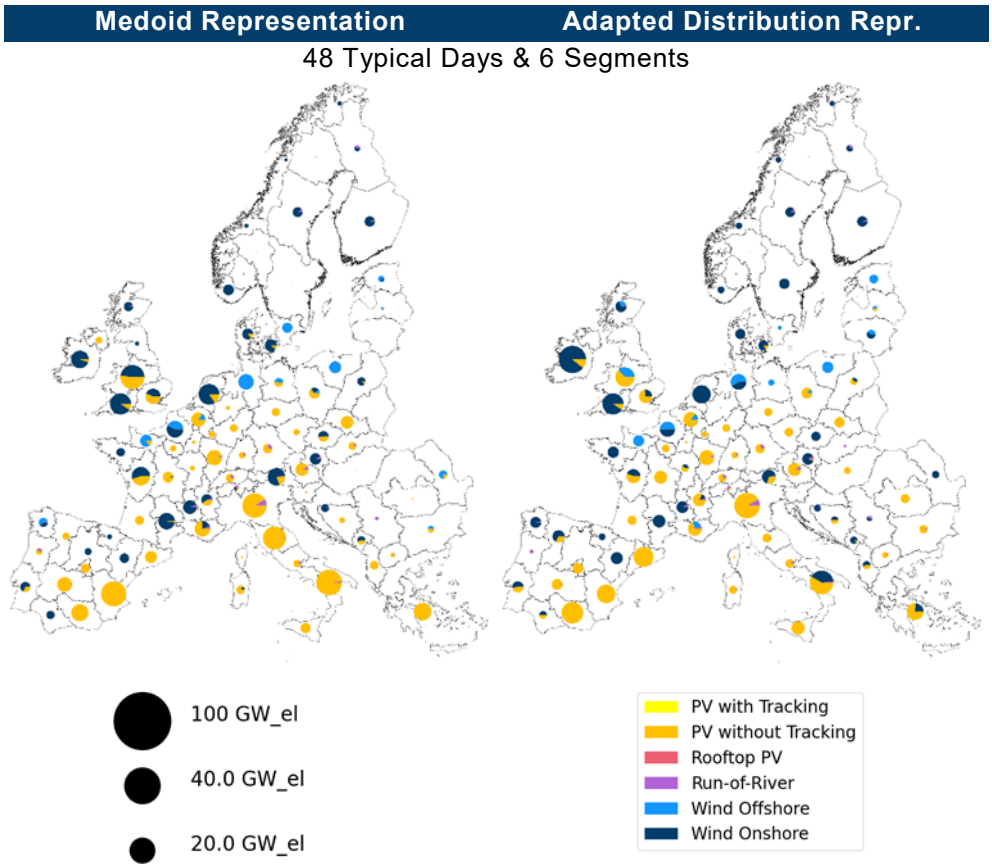

Figure 4.42. Energy supply capacities depending on a varying number of typical days and segments using the medoid and the adapted distribution-preserving representation

In order to evaluate whether the adapted distribution-preserving algorithm is also more accurate with respect to the technology allocation compared to the reference case, Figure 4.43 depicts the technology allocation for 365 typical days and 24 segments per typical day using the distribution-preserving algorithm solving within about 10 days. As this configuration equals the fully resolved case, the time series equal the original ones and the configuration is independent from the chosen representation method. Compared to the capacity allocation using 48 typical days, 6 segments and the proposed algorithm, only small deviations can be observed. Among those are a substitution of offshore wind capacities by onshore ones in Middle England and larger onshore wind capacities in Eastern Poland. However, the deviations from the reference case are larger in case of the representation by medoids, e.g. in case of 48 typical days and 6 segments, the solution obtained using a representation by medoids does not at all consider onshore

wind turbine capacities in Southern Italy or Northwestern Germany.

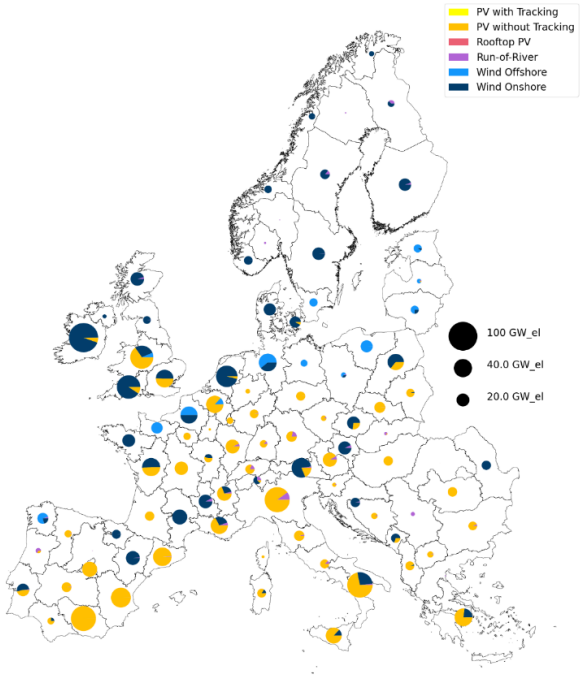

Figure 4.43. The energy supply capacities for 365 typical days, 24 segments and the adapted distribution-preserving representation

In summary, it can be stated that the proposed adapted distribution-preserving algorithm succeeds in outperforming all other representation methods with respect to both, technology sizing and technology allocation. Further, the allocation of technologies seems to be more sensitive with respect to small changes in the input data compared to the absolute technology-specific costs, which implies that there exist many possible layouts of technology allocation, which lead to close-optimal total annual costs for the entire system.

4.2.5. Summary

Section 4.2 has revealed numerous important features of time series that are either neglected or only implicitly considered in traditional aggregation methods.

First, the good performance of variance preserving algorithms implies that the preservation of statistical features of the original time series apart from extreme or mean values is indeed important for an appropriate temporal aggregation.

Second, an appropriate aggregation must not focus on solely decreasing either the number of typical periods or the temporal resolution, because both methods affect different technologies unequally. Instead, a good trade-off using heuristics based on input data analysis such as the optimal pathway algorithms were proven to provide better approximations of the fully resolved reference case if the assumptions of monotonous relationships between a priori and a posteriori accuracy indicators are sufficiently satisfied.

Third, the differences between the original version of the variance preserving-algorithm and the adapted version as well as the relatively good performance of the medoid representation for the European model imply two more findings. First, not only the variance and the value distribution (duration curve) of a time series, but also the variance on different time scales, e.g. across multiple days, is important for systems considering aperiodic time series and seasonal storage in case that the overall number of time series and the error related to clustering are relatively large. Second, the covariance between multiple regions may be important in systems that consider energy transmission. This explains why simply taking sample days (medoids) from the original time series underperforms synthesizing aggregated data focusing on certain statistical features less significantly if the underlying dataset is relatively short (i.e., one weather year), but high-dimensional due to the number of considered time series.

After all, however, the combination of the distribution preserving algorithm in Section 3.2.5 and the optimal pathway algorithm in Section 3.3.4 allow for remarkably smaller aggregation-induced errors for a given number of total time steps and for significantly faster runtimes at a given error tolerance on all three capacity expansion models. In particular, speed-ups by the order of two magnitudes could be achieved with an optimal objective value deviation well below 5%. These findings are condensed in Figure 4.17, Figure 4.23 and Figure 4.39 for each model. Compared to state-of-the-art methods for temporal aggregation, this is at least an additional speed-up by the order of one magnitude given the same error tolerance.

4.3. Typical Days or Typical Time Steps

The core idea of this section, which is based on a prior publication of the author [2], is the cross-comparison of two different period lengths, i.e. the use of typical days and typical time steps, by applying them to two fundamentally different models and benchmarking them to the respective fully resolved cases. As case studies, the self-sufficient building model and the dispatch model are chosen, as they differ from each other with respect to three important model aspects, as shown in Table 4.4.

Table 4.4. Differences of the self-sufficient building model and the dispatch model with a mathematical relevance

Feature	Self-Sufficient Building Model	Dispatch Model
Number of Regions	Single-Node	Multi-Node
Model Type	MILP	LP
Temporal Coupling	Yes (Storage)	No

The framework used to compare typical periods against typical time steps for energy system models is shown in Figure 4.44.

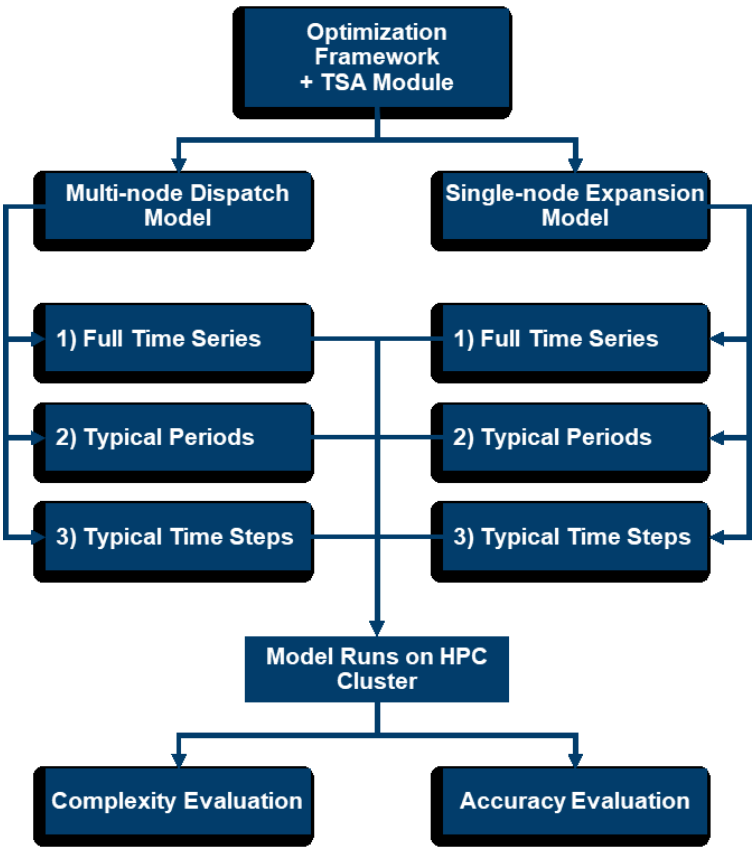

Figure 4.44. Method applied to compare typical periods and typical time steps for different types of energy system models (adapted from Hoffmann et al. [2])

“In order to enable a fair comparison to be made between the tested models and applied aggregation methods, we maintain aggregation intervals and computing power constant for all models and model runs. All model runs were performed using the JURECA HPC Cluster [195] with the technical resources given in Table 4.1 at the beginning of Chapter 4.” (Hoffmann et al. [2])

“For all aggregation procedures, Ward’s hierarchical clustering algorithm was chosen and each cluster of time steps was represented by its centroid. The total number of considered time steps has a major impact on the computational complexity. To facilitate a comparison between typical time steps and typical days, only integer-multiples of 24 time steps were chosen for both typical days and typical time steps, which leads to the configuration of model runs and time steps per run shown in Table 4.5.” (Hoffmann et al. [2])

Table 4.5. The model run configuration with respect to the total number of time steps considered (adapted from Hoffmann et al. [2])

Fully Resolved	Typical Days	Typical time steps
		24 x 1
		48 x 1
		96 x 1
	5 x 24	120 x 1
	10 x 24	240 x 1
	20 x 24	480 x 1
	40 x 24	960 x 1
	80 x 24	1920 x 1
	160 x 24	3840 x 1
8760	365 x 24	8760 x 1

“This means that for typical days, 365 sample points comprising 24 dimensions of consecutive time steps per time series of the respective model were clustered, whereas for the typical time steps, 8760 data points with one dimension for each time series were aggregated.” (Hoffmann et al. [2])

“The following sections first investigate the impact of aggregated configurations with respect to the accuracy of the data aggregation using a set of clustering indicators. Subsequently, the deviation of the aggregated models’ optimal objective to the fully resolved reference cases are compared, with consideration to the individual

computational speedup. Then, the aggregation-induced deviations of both models are analyzed in detail by investigating the cost contributions of the systems' components. Finally, the time consumption of the individual processes, as well as the memory consumption of each model, is evaluated over time." (Hoffmann et al. [2])

4.3.1. Input-Data Driven Analysis

From an input-data point of view, the major difference between typical periods and typical time steps is the fact that typical periods are groups of conjoined time steps while typical time steps are independent time steps. Both can either directly be chosen from the original time series of by synthesizing them, i.e. by representing clusters of time steps or periods by their centroids, in case the typical time steps or typical days are determined using clustering. In that case, also the dimensionality of the space in which the data is clustered, fundamentally differs. While for typical time steps each attribute of the input time series becomes one dimension in the clustering space, each time step of each attribute within the periods becomes an own dimension in the case of period clustering. As stated in Equation (2.4), the multi-dimensional row vectors used for time series aggregation are defined as follows:

$$\mathrm{D_{arr}} = \begin{pmatrix} \mathrm{x}_{1,1,1} & \cdots & \mathrm{x}_{1,1,\mathrm{N_t}} & \mathrm{x}_{1,2,1} & \cdots & \mathrm{x}_{1,\mathrm{N_a},\mathrm{N_t}} \\ \vdots & \ddots & \vdots & \vdots & \ddots & \vdots \\ \mathrm{x}_{\mathrm{N_p},1,1} & \cdots & \mathrm{x}_{\mathrm{N_p},1,\mathrm{N_t}} & \mathrm{x}_{\mathrm{N_p},2,1} & \cdots & \mathrm{x}_{\mathrm{N_p},\mathrm{N_a},\mathrm{N_t}} \end{pmatrix} \quad \text{with} \quad \begin{matrix} \mathrm{a} \in \mathrm{A} = \{1, \dots, \mathrm{N_a}\} \\ \mathrm{p} \in \mathrm{P} = \{1, \dots, \mathrm{N_p}\} \\ \mathrm{t} \in \mathrm{T} = \{1, \dots, \mathrm{N_t}\} \end{matrix} \tag{4.7}$$

With A the set of attributes (time series), P the set of candidate periods, T the set of time steps per period and $|\mathrm{S}| = |\mathrm{P}| \times |\mathrm{T}|$ the number of original time steps. For typical time steps comprising only one time step per period, i.e., $\mathrm{N_p} = |\mathrm{P}| = |\mathrm{S}| = \mathrm{N_s}$, this leads to:

$$\mathrm{D_{TTS}} = \begin{pmatrix} \mathrm{x}_{1,1,1} & \cdots & \mathrm{x}_{1,\mathrm{N_a},1} \\ \vdots & \ddots & \vdots \\ \mathrm{x}_{\mathrm{N_s},1,1} & \cdots & \mathrm{x}_{\mathrm{N_s},\mathrm{N_a},1} \end{pmatrix} = \begin{pmatrix} \mathrm{x}_{\mathrm{cand},1} \\ \vdots \\ \mathrm{x}_{\mathrm{cand},\mathrm{N_s}} \end{pmatrix} \tag{4.8}$$

In contrast to that, for typical periods, the candidates are given by:

$$\mathrm{D_{TD}} = \begin{pmatrix} \mathrm{x}_{1,1,1} & \cdots & \mathrm{x}_{1,1,\mathrm{N_t}} & \mathrm{x}_{1,2,1} & \cdots & \mathrm{x}_{1,\mathrm{N_a},\mathrm{N_t}} \\ \vdots & \ddots & \vdots & \vdots & \ddots & \vdots \\ \mathrm{x}_{\mathrm{N_p},1,1} & \cdots & \mathrm{x}_{\mathrm{N_p},1,\mathrm{N_t}} & \mathrm{x}_{\mathrm{N_p},2,1} & \cdots & \mathrm{x}_{\mathrm{N_p},\mathrm{N_a},\mathrm{N_t}} \end{pmatrix} = \begin{pmatrix} \mathrm{x}_{\mathrm{cand},1} \\ \vdots \\ \mathrm{x}_{\mathrm{cand},\mathrm{N_p}} \end{pmatrix} \tag{4.9}$$

Accordingly, in the case of typical time steps, $\mathrm{N_s}$ candidates with a dimensionality of $\mathrm{N_a}$ are clustered, whereas in the case of typical

periods, $N_p = \frac{N_s}{N_t}$ candidates with a dimensionality of $N_a \times N_t$ are clustered. This means that in the case of typical time steps N_t times more data points are clustered in an N_t times lower dimensional space compared to typical periods.

Apart from that, the total number of considered time steps is a major driver for computational complexity. As typical periods consist of multiple consecutive time steps, more typical time steps than typical periods can be chosen for the same computational cost. This in turn leads to the phenomenon that for an equivalent number of total time steps, the aggregated time series based on typical time steps bear more resemblance to the original time series than the aggregated time series based on typical periods.

“Figure 4.45 shows the a priori accuracy indicators introduced in Section 3.3.1 for the normed time series (with values between 0 and 1) of the self-sufficient building (top) and dispatch model (bottom) for both typical periods and typical time steps.

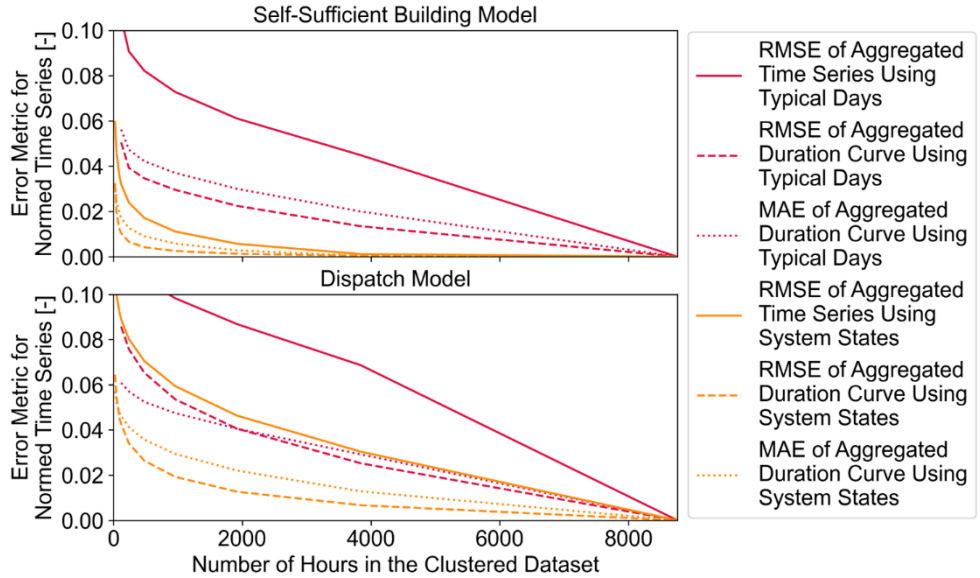

Figure 4.45. Error indicators for the self-sufficient building (top) and the dispatch model (bottom) for both, typical days and typical time steps (adapted from Hoffmann et al. [2])

For the typical periods, 365 sample points consisting of 24 dimensions of consecutive time steps were clustered, while for the typical time steps, 8760 1-dimensional data points were aggregated. The x-axis shows the number of equivalent typical time steps, i.e., the

number of time steps to which the time series has been aggregated. In the case of typical days, this equals the number of typical days multiplied by 24 time steps per day. Here, it can be seen that, from an input data perspective, the aggregation of the time series to single time steps outperforms the aggregation to conjoined periods for any clustering indicator and both models. The reason for this is that in the case of typical time steps, each time step is a single candidate for clustering and can be freely grouped with any other time step, which is similar enough. When typical days are clustered, however, time steps are only compared to other time steps in the same daytime. Furthermore, the clustering of typical days is performed in a 24-times higher dimensional space with 24-times fewer candidates. Therefore, the 'curse of dimensionality' leads to higher aggregation-induced deviations from the original time series.

4.3.2. Output-Data Driven Analysis

The main purpose of the aggregation techniques for energy system models is to reduce computational complexity while keeping the impact on the optimized solution as small as possible. As discussed in Section 3.3, the main determinants for the quality of a good aggregation are the calculation time and a small deviation from the original, optimal objective value, i.e. the total annual costs.

Figure 4.46 shows the absolute deviation from the optimized objective function value from the reference case over the calculation time for the self-sufficient building (top) and dispatch model (bottom).

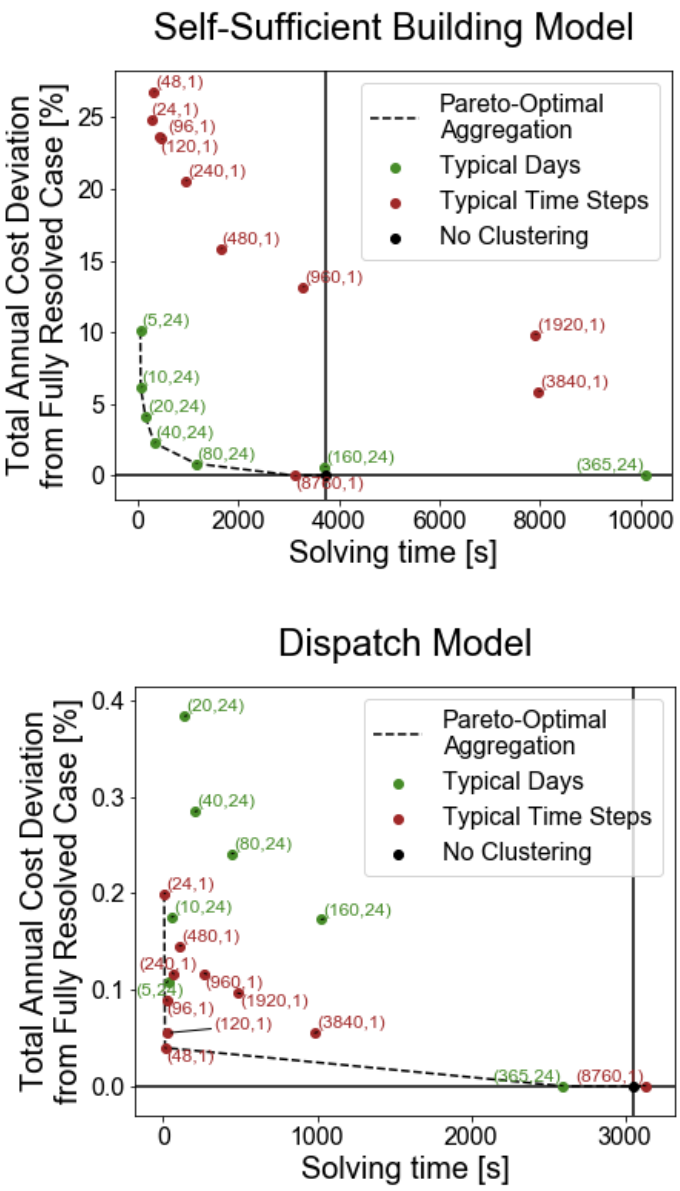

Figure 4.46. Absolute deviation from the optimized objective function value of the fully resolved case over calculation time for the self-sufficient building (top) and the dispatch-model (down) (adapted from Hoffmann et al. [2])

In the case of the self-sufficient building model, the deviation from the optimal objective is consistently much greater than in the case of the dispatch model. Accordingly, it is much more sensitive to temporal aggregation due to the strong temporal coupling of the fully resolved model, as induced by the numerous storage technologies. Although typical time steps consistently outperform the aggregation to typical days with respect to the clustering indicators, and therefore the deviation between the aggregated and original time series, it is evident from Figure 4.46 that the typical time steps

represent the superior aggregation option for the dispatch model, as they lead to smaller deviations with low calculation times. In contrast, they also lead to significantly larger deviations from the optimal objective value of the fully resolved self-sufficient building model. Here, typical days are the better aggregation option, which is also supported by the dashed lines in Figure 4.46 representing the respective Pareto fronts. Furthermore, it can be observed that the optimal objectives converge to the one of the fully resolved case if the number of typical time steps or typical days is increased, which can be expected, but which supports the mathematical validity of the aggregation. Moreover, it can be observed that, especially in the case of the self-sufficient building, the modeling approach for seasonal storage with a reduced number of capacity constraints introduced by Kotzur et al. [20] leads to a computational overhead in the case of aggregation configurations with a large number of typical days or typical time steps. Similar observations were made by Wogrin et al. [88] with respect to temporally-linked typical time steps to model storage components, in spite of the aggregation.

In order to analyze the aggregation-induced errors further, the individual cost contributions for the self-sufficient model (top) and dispatch model (bottom) for all aggregation configurations are depicted in Figure 4.47.

As the Figure 4.47 shows, the centroid-based aggregation to typical time steps or typical days generally leads, in three out of four cases, to a consistent underestimation of the reference optimal objective values. In the case of typical time steps for the self-sufficient building, however, the aggregation leads to a significant overestimation of the optimal objective value. Interestingly, this observation approves the inconsistent results in the literature, e.g., Zatti et al. [145] observed that, depending on the model, the centroid-based aggregation of the k-means algorithm could lead to over- or underestimation. This indicates that the impact of the aggregation method is highly dependent on the model to which it is applied.

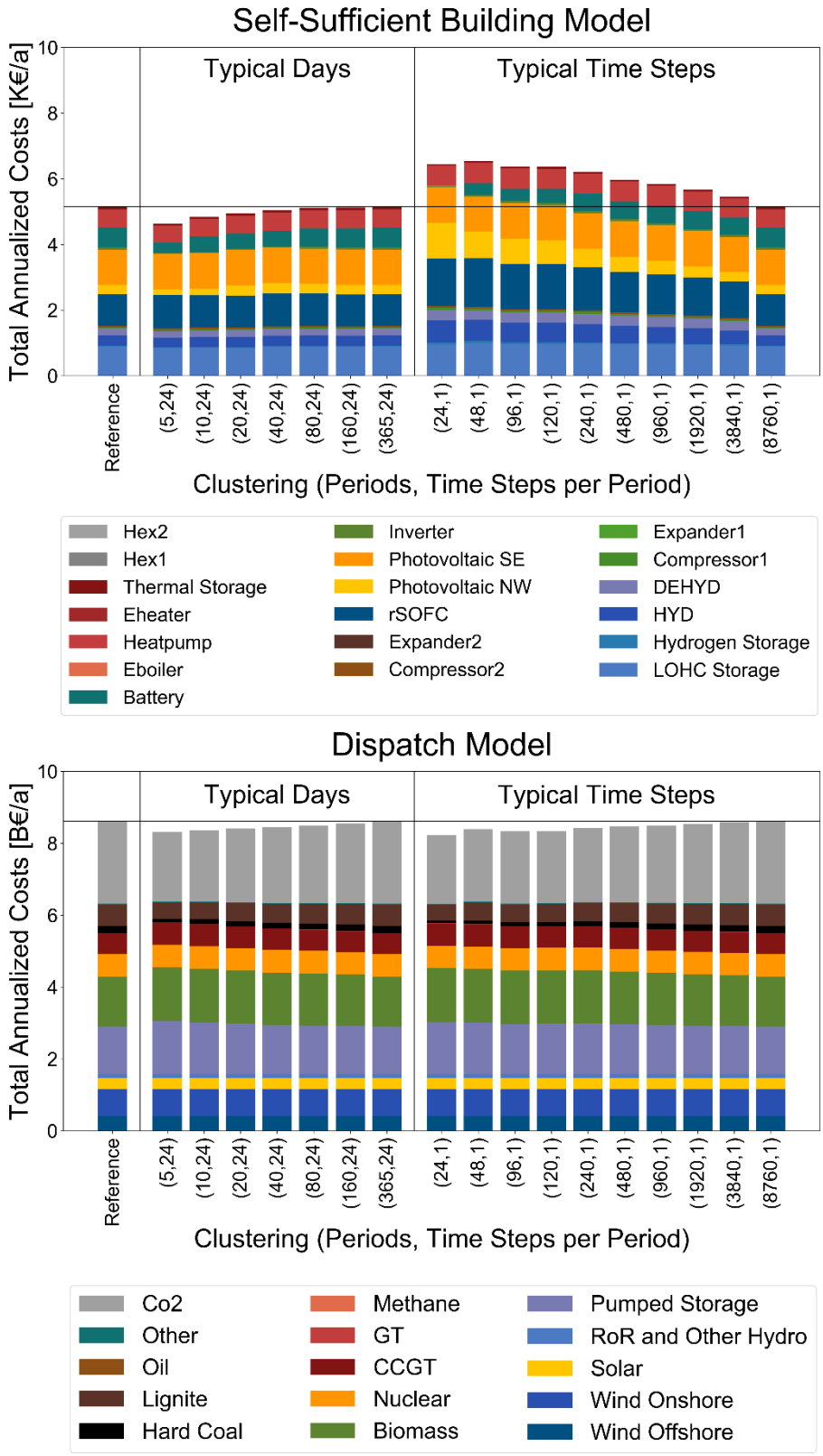

Figure 4.47. The individual cost contributions for the self-sufficient model (top) and the dispatch model (bottom) for all aggregation configurations (adapted from Hoffmann et al. [2])

In general, the underestimation of the majority of the aggregated models can be attributed to the fact that the time series are affected by the averaging effect of the centroid-based cluster representation, i.e., the minimum values of a time series are overestimated by the aggregation, whereas the maximum values are underestimated. As is mathematically shown by Teichgräber et al. [47], the centroid-based representation of the time series that form coefficients in the constraint vector lead to a relaxation of temporally-decoupled models. This applies, for instance, to demand time series. However, in the case of the dispatch model, the cost time series, which yield coefficients in the cost vector of the optimization problem, are clustered as well. As Teichgräber et al. [47] have shown, the aggregation of the cost vector and the reduction in the corresponding variables reduce the optimization model's feasible solution space. However, this counteracting effect is of minor importance for the dispatch model, as the objective function based on typical days or typical time steps is consistently smaller than the one of the reference case. However, the impact of the latter effect can be observed between 48 and 96 typical time steps in the case of the dispatch model shown in Figure 4.47. Here, the total annual costs decrease for a higher temporal resolution, despite the use of hierarchical clustering, which should gradually decrease the aggregation-induced error. This implies the existence of at least two opposing effects on the optimal objective value due to aggregation: One that increases the optimal objective due to fewer variables in the aggregated model and one that decreases it due to fewer constraints.

Storage components, as in the case of the self-sufficient building, lead to a much less predictable impact of centroid-based clustering compared to the dispatch model, as shown in the upper half of Figure 4.47. Compared to typical time steps, the aggregation using typical days has a relatively small impact on the component's cost contributions. Yet, it can be observed that a smaller number of typical days most prominently decreases the optimum battery capacity, as the aggregation-induced smoothing of the aggregated time series profiles intensifies, and therefore smaller battery capacities are needed to balance intra-daily demand and supply fluctuations.

In contrast to that, an increase in the number of typical time steps decreases the capacity-induced cost contribution of the northwestern-oriented PV panels and the reversible solid oxide cell (rSOC). Simultaneously, the size of the battery slowly increases with a higher number of typical time steps.

The battery has relatively large capacity-specific investment costs (€/kWh$_{storage}$) and a relatively high self-discharge rate, whereas the hydrogen storage has higher power-specific investment costs (€/kW$_{(dis)charge}$) due to the expensive rSOC. This predetermines batteries for short daily storage cycles and small capacities, whereas hydrogen storage is preferable for large capacities and long storage cycles at low charge or discharge rates.

In the case of typical time steps, all storage components function identically at time steps that are assigned to the same cluster based on their similarities. The fact that the electricity demand profile and solar profiles resemble themselves during the morning and evening hours, leads to an eventual assignment of these hours to the same cluster. This in turn forces the battery to operate in the same way during morning and evening hours and inhibits a daily operation cycle. Accordingly, in an aggregated model, it is less economically viable based on typical time steps. Instead, the operational feasibility of the model is maintained by oversizing the solar panels and hydrogen subsystem used for storing energy over longer time scales.

In summary, the existence of storage technologies is one of the most determinant factors for an accurate temporal aggregation, even if the time series have a strong daily pattern (which is also the case for the dispatch model).

4.3.3. In-depth Analysis of Computational Resources

Apart from the manifold impacts that temporal aggregation has on a model's optimal solution, the main purpose of temporal aggregation remains computational speedup. Therefore, the contributions of the different processes to the overall runtime, as well as individual memory consumption, are analyzed in the following. Figure 4.48 illustrates the runtime contributions of each process for the self-sufficient building model (top) and dispatch model (bottom) for all aggregation configurations.

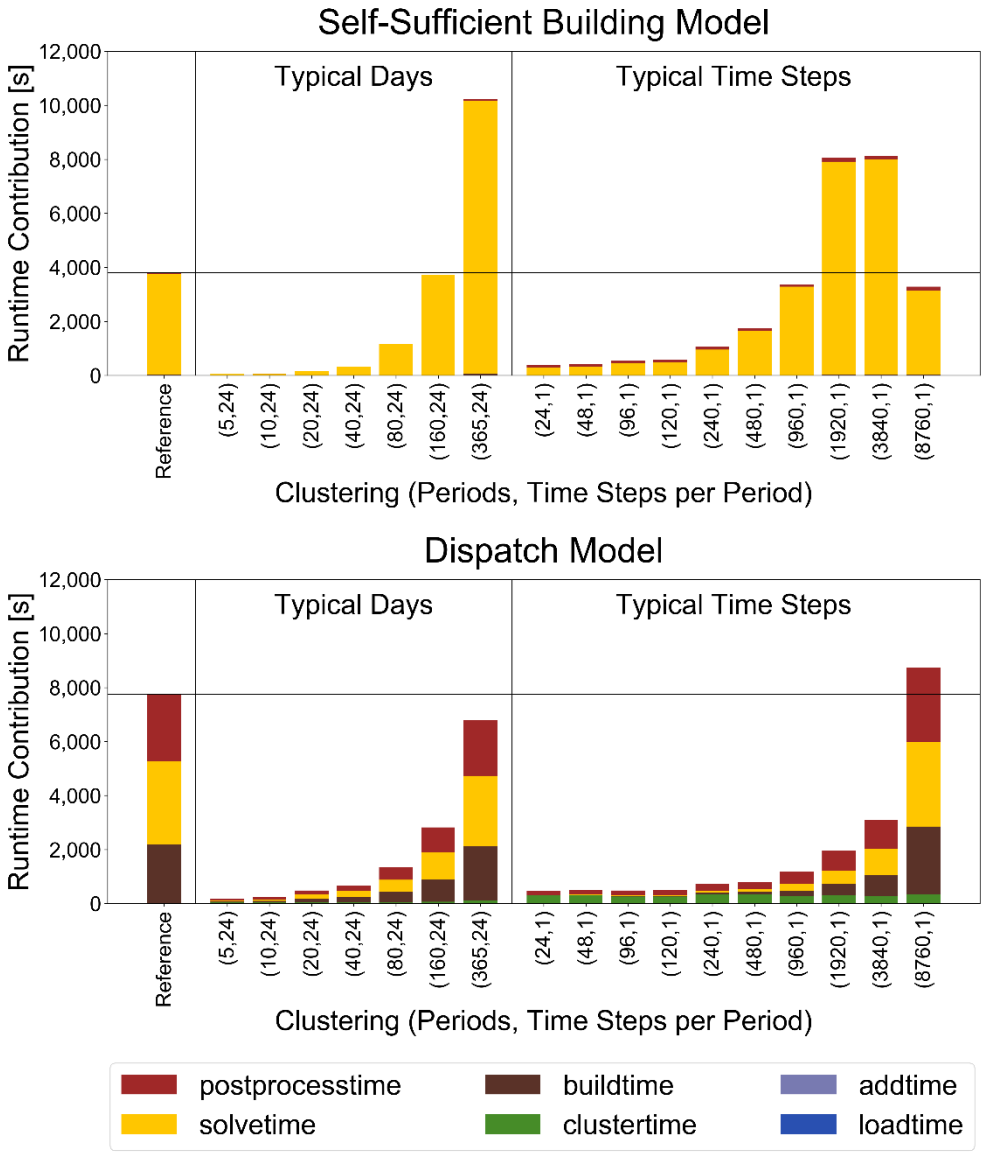

Figure 4.48. Calculation times of the self-sufficient building (top) and the dispatch-model (bottom) depending on the aggregation configuration (adapted from Hoffmann et al. [2])

As it can be seen for the self-sufficient building, almost all of the overall runtime is needed for solving the optimization problem. The time consumption for loading the data, adding components, clustering the input data, setting up the mathematical problem structure using Pyomo and mapping the solution from Gurobi back to the model's individual variables, is negligible. This can be explained by the mathematical connectivity [196] of the variables and constraints caused by a complex component structure and time step linking storage equations while on the other hand only one region and five time series are considered.

In contrast to that, the overall runtime of the dispatch model is mainly determined by three operations: The time for setting up the problem structure, the time for solving the problem and the time for mapping the solution back to the set-up problem structure. The reason for this is the large amount of input data given by 6325 time series as well as the large number of regions (16 national and 9 international), while the problem structure is relatively simple due to the absence of storage components and a flat system structure because all components are connected to a single electricity grid. Moreover, the time for clustering becomes a significant share of the overall calculation time in case of aggregating typical time steps which can be explained by the fact that the computational complexity of ward's hierarchical clustering algorithm scales with $O(n^2)$ and that typical time steps have 24 times more starting candidates than typical days. Moreover, the process itself is much slower than for the self-sufficient building because of the much larger number of time series. Apart from that, the aggregation tends to take longer for stronger aggregated model configuration as more iterations for merging clusters are carried out, which makes the aggregation time an even more significant runtime contribution for strongly aggregated models. On the other hand, this motivates the use of simple clustering approaches instead of new but computationally expensive aggregation techniques that erode the original purpose of temporal aggregation, i.e. the computational speedup.

Figure 4.49 shows the memory consumption of the self-sufficient building (top) and the dispatch model (bottom) depending on the aggregation configuration. The vertically aligned values over the boxplots refer to the median memory consumption during the optimization.

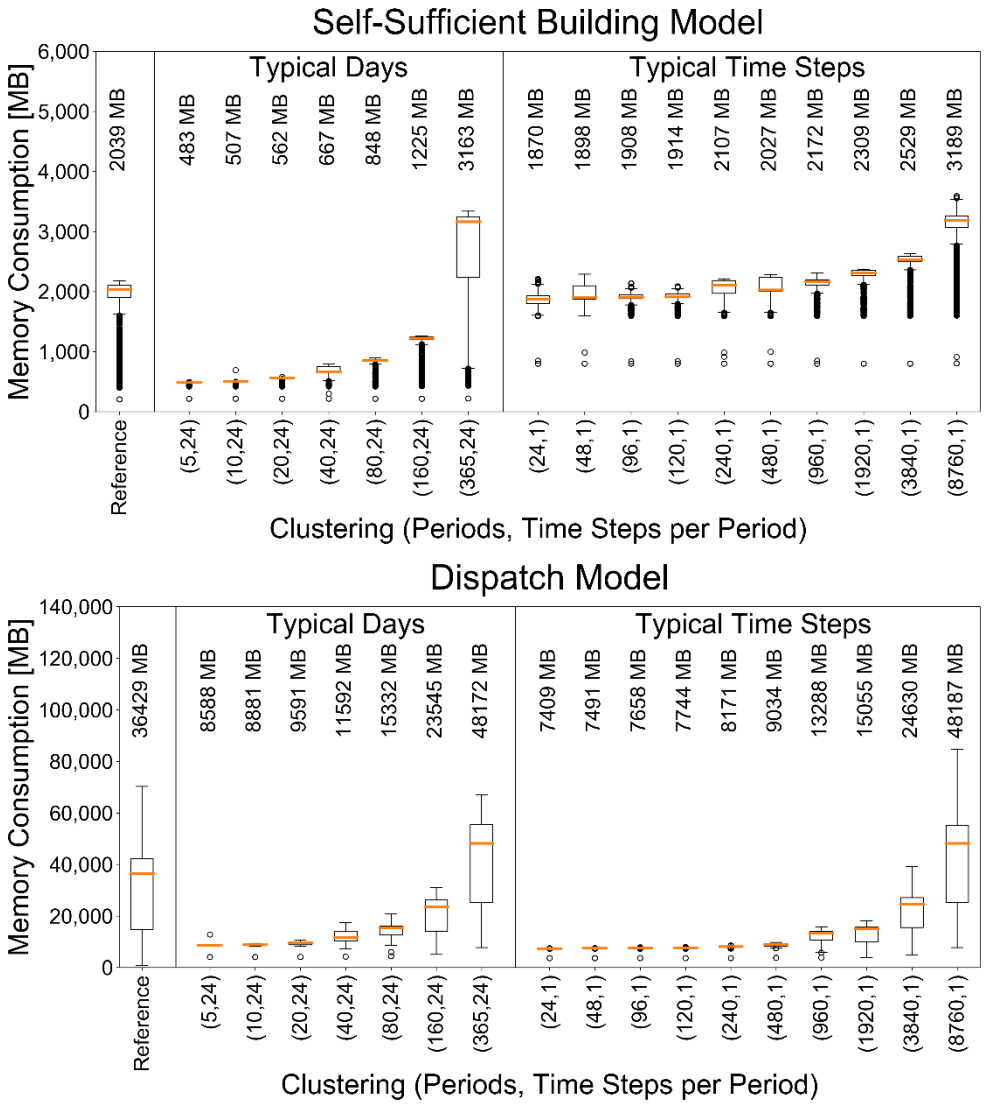

Figure 4.49. Memory consumption of the self-sufficient building (top) and the dispatch-model (bottom) depending on the aggregation configuration (adapted from Hoffmann et al. [2])

Another interesting difference between both models is shown in Figure 4.49: As expected, the memory consumption of both models increases with a higher number of typical days or typical time steps. However, the total amount of memory consumption of the dispatch model is more than an order of magnitude larger than that of the corresponding aggregation configuration of the self-sufficient building. It is notable that the solving time for both models is comparable, as is shown in Figure 4.48. This emphasizes the impact of strong mathematical interconnectedness, as in the self-sufficient building model, on the overall solving time, whereas large-scale but easy-to-decompose energy system models such as the

dispatch model are relatively quickly solvable compared to their overall size, but consume a large amount of memory.

In addition, a comparison between the aggregation using typical days and typical time steps reveals that the memory consumption for a certain number of total time steps is, in the case of the dispatch model, almost identical for both the typical time steps and typical days. For instance, the boxplots for 40 typical days and 960 typical time steps in the lower part of Figure 4.49 are almost identical. This highlights that the assumption that the complexity of the model scales with the total number of time steps is valid if no storage components are taken into account. In the case of the self-sufficient building, however, an overhead due to more complex coupling storage conditions can be observed in the case of typical time steps compared to the application of typical days. Combined with the high deviations induced by an aggregation to typical time steps and a long solving time, this approach appears to be highly inconvenient for models with storage components. Moreover, the storage conditions for coupling aggregated typical time steps lead to a constant offset to the complexity of an energy system model.

In summary, the findings imply that the overall memory consumption of an energy system model during the solving process is composed of three summands. The first one scales with the number of considered time steps, the second one depends on the model's intrinsic number of coupling constraints, e.g., for modeling states of charge of storage components over the entire time horizon and the third one is an additional offset introduced by other processes.

4.3.4. Summary

The results outlined in the preceding section reveal that the clustering of time series to typical time steps consistently leads to better clustering indicators in a priori input data analyses of the clustered time series compared to clustered typical days. However, the analysis of the results reveal that typical time steps are not necessarily the superior aggregation method.

Specifically, this means that an optimal choice of time-series aggregation technique cannot be made a priori based on its capacity to represent the original time series. Although typical time steps outperformed typical days in the a priori input data analysis for both investigated models, they did not lead to more accurate results for

the building model. However, smaller clustering indicators for a predefined model and period length can be used to indicate smaller deviations in the optimization results.

Furthermore, the results indicate that certain aggregation techniques are predetermined for certain types of energy system models and underlying research questions.

With respect to the scope of Section 4.3, aggregation techniques based on typical time steps outperform typical days on the temporally decoupled dispatch model, whereas the application of typical days is the Pareto optimal method for the self-sufficient building model, which takes a variety of different storage systems into account. This is even more remarkable as both typical time steps and typical days are modeled in such a way that storage capacities can be considered [20].

These findings are summarized in Figure 4.50, i.e., the choice of whether to use typical time steps or typical periods depends on the role of storage components or other temporally-coupled constraints and clustering indicators should only be used for comparing different clustering configurations if the model and period lengths are fixed.

In conclusion, the findings of this section place common assumptions regarding temporal aggregation for energy system models into a new context. First, the autocorrelation of time series, e.g., a daily pattern of solar and electricity profiles, is not of major importance for the question to what length time periods should be aggregated for an energy system model. The more important indicator is the existence of storage components and the duration of their cycles. Secondly, it was clearly shown that no relationship exists between clustering indicators and the quality of the aggregated energy system's optimal solution, if it is compared for different period lengths." (Hoffmann et al. [2])

Unfortunately, the storage cycle duration of considered storage components may differ for the individual components and the energy system model is generally unknown in advance, because it is a result of a model's operational optimization. Future research could therefore strive at finding the optimal period lengths based on a model's specific mathematical features.

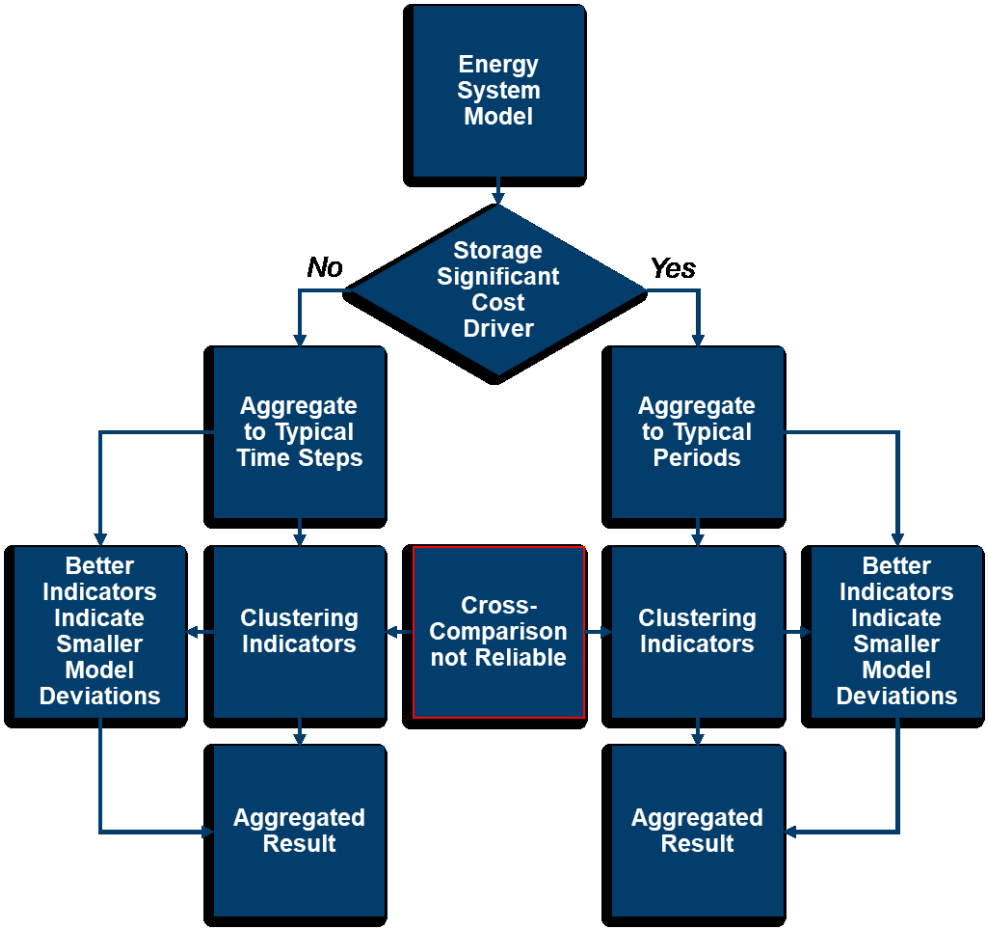

Figure 4.50. Summary of the findings of Section 4.3 (adapted from Hoffmann et al. [2])

4.4. Error Bounding Methods

The last research question that arose from the rising trend of iterative solving approaches based on error bounding using temporal aggregation techniques is whether these methods are useful for the models regarded in this thesis.

4.4.1. Bounds Based on Over- and Underestimation

The first approach refers to the representation methods proposed in Section 3.2.4 and relies on a systematic over- and underestimation of the original time series using temporal aggregation. As discussed in Section 3.4, an energy system optimization can either be relaxed or further restricted if values of the original time series are substituted by their respective maximum or minimum value. In order to obtain an upper or lower bound to the original problem, each time series has to be considered individually to decide whether an overestimation or underestimation leads to the desired bound. For the sake of comprehensibility, the island system and the self-sufficient building model are analyzed in the following due to their small number of different time series.

4.4.1.1. Bounds of the Island System Model

The island system comprises two capacity factor time series for electricity generation from wind and solar energy and one time series for electricity demand. As the total annual costs are driven by the constraint to fulfill the energy demand at any point in time, an increase of the energy demand or a decrease of the capacity factors will both increase the system costs. Accordingly, for an upper bound of the original problem, the aggregated time series need to overestimate the energy demand and underestimate the capacity factors. The exact opposite holds true in order to obtain a lower bound to the original problem, which is summarized in Table 4.6.

Table 4.6. Estimations of time series to obtain upper or lower bounds of the island system model

Time Series	For Upper Bound	For Lower Bound
Electricity Demand	Overestimate	Underestimate
Wind Capacity Factor	Underestimate	Overestimate
Solar Capacity Factor	Underestimate	Overestimate

As the systematic over- and underestimation can be equally applied to the aggregation process to typical days and the aggregation to fewer segments within each day, the same aggregation configurations are used as in Section 4.2, i.e. 153 different upper and lower bounds were calculated depending on the respective clustering configuration. The results of the deviation from the optimal objective of the fully resolved case depending on the chosen number of typical days and segments per typical day are depicted in Figure 4.51.

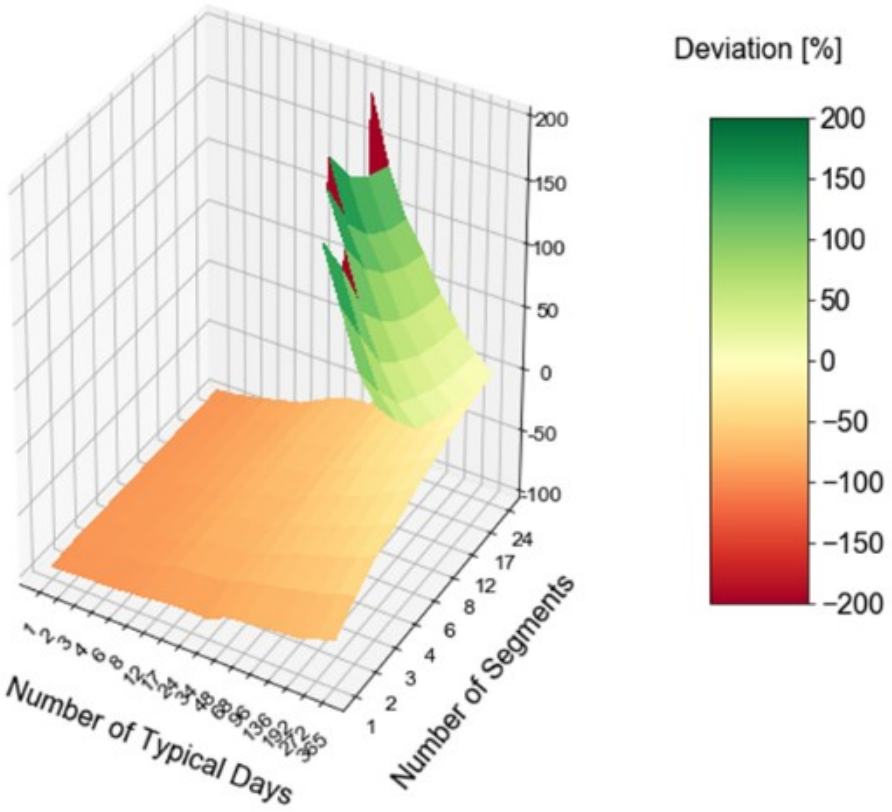

Figure 4.51. Upper and lower bounds of the island system model depending on the aggregation configuration

As it can be seen, the method proposed in literature indeed delivers upper and lower bounds to the original problem, as both bounds form surfaces that approach each other monotonously for a rising number of both, typical days and segments. In case of 365 typical days and 24 segments per typical days, the gap between both bounds becomes zero, as the temporal resolution equals the one of the reference case. With respect to the absolute deviation from the optimal objective of the reference case, however, the found solutions are remarkably worse than the representation

methods discussed before. Consequently, the deviations yielded by the systematic over- and underestimation require relatively highly resolved aggregation configurations in order to be tolerable. The impact of this observation is shown in Figure 4.52 depending on the runtime.

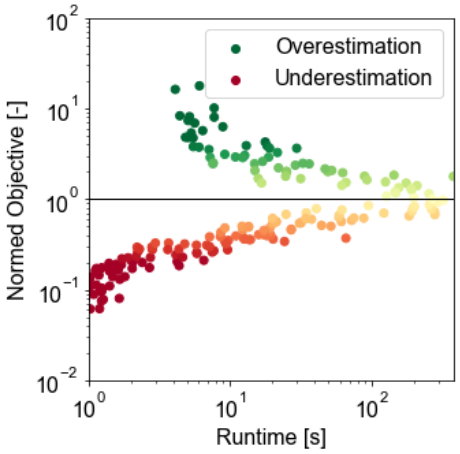

Figure 4.52. Upper and lower bounds of the island system model depending on the runtime

Here, it can be observed that the fastest aggregation configurations provided lead to the biggest deviations from the optimal objective, as they are simultaneously those considering the fewest total time steps. Furthermore, the fastest-solving configurations in case of the upper bounds are taking longer than the fastest solving configurations of the lower bounds, which can be explained by the fact that the system is allowed to obtain up to 10% of the original electricity demand from the grid. In case of heavily underestimated total electricity demand, this amount of energy is enough to cover the demand. In those cases, no additional capacities are build and the optimal solution is trivial. In case of upper bounds, these technologies are needed in any case and accordingly, a minimum number of iterations is needed to solve the optimization problem.

4.4.1.2. Bounds of the Self-Sufficient Building Model

In contrast to the island system model, the self-sufficient building model considers additional heat demand, does not consider wind feed-in and has no option to obtain electricity from the grid. In total, it considers five time series, namely, an electricity and heat demand as well as solar capacity factor time series of PV panels with northeastern (NE) and southwestern (SW) orientation as well as ground-mounted ones (G). Analogously to the island system model, demand time series need to be overestimated and capacity factor time series need to be underestimated in order to obtain an upper bound of the original problem whereas the opposite holds true for lower bounds, which is summarized in Table 4.7.

Table 4.7. Estimations of time series to obtain upper or lower bounds of the self-sufficient building model

Time Series	For Upper Bound	For Lower Bound
Electricity Demand	Overestimate	Underestimate
Heat Demand	Overestimate	Underestimate
Solar Cap.-Factor (NE)	Underestimate	Overestimate
Solar Cap.-Factor (SW)	Underestimate	Overestimate
Solar Cap.-Factor (G)	Underestimate	Overestimate

The obtained upper and lower bounds for the different aggregation configurations are highlighted in Figure 4.53.

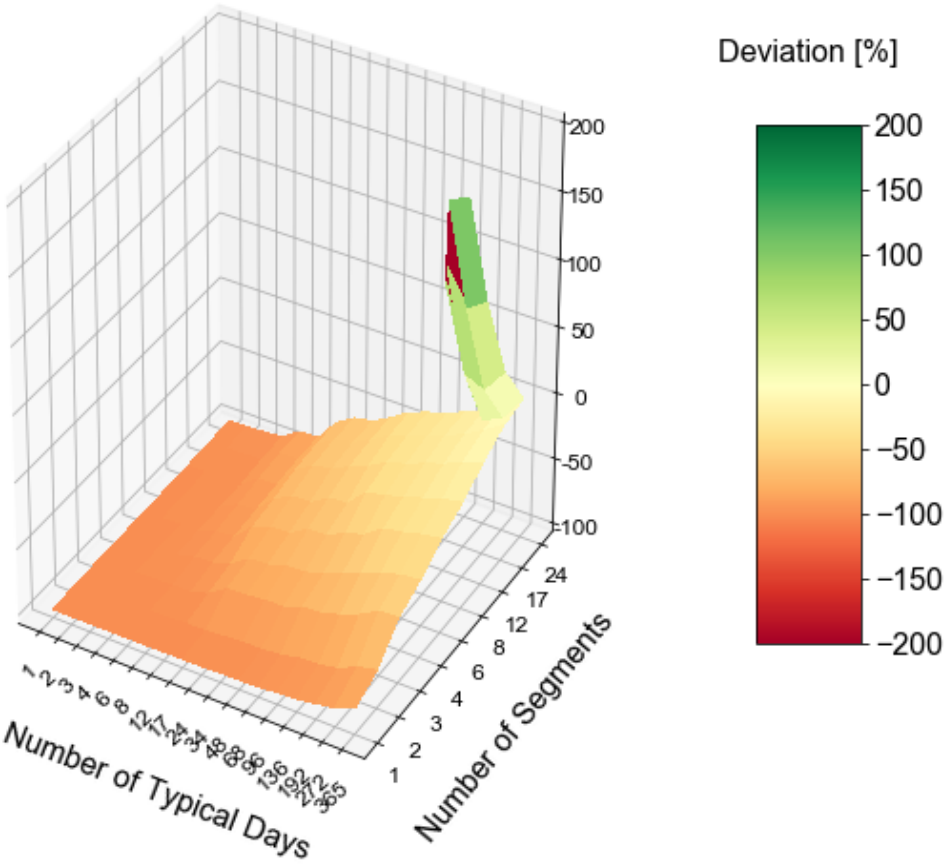

Figure 4.53. Upper and lower bounds of the self-sufficient building model depending on the aggregation configuration:

The observations that can be obtained from Figure 4.53 resemble those for the island system model, i.e., the upper and lower bounds approach each other for a rising number of typical days and segments per typical days and lead to the same optimal objective if the used time series equal those of the reference case.

Figure 4.54 depicts the objective function values depending on the runtime of the respective aggregated model. In contrast to the island system, it can be observed that the smallest runtimes of the upper and lower bound configurations are comparable, because the self-sufficient building does not have the option to obtain energy from the electricity or gas network. Furthermore, the deviations from the optimal objective of the reference case are much worse for strongly aggregated configurations for the same reason: In case of a completely isolated system, the model completely relies on storage technologies for times at which feed-in from the solar panels is not available. As an over- or underestimation of time series based on aggregation also change the cumulative feed-in and demand for the system, storage technologies are disproportionally affected.

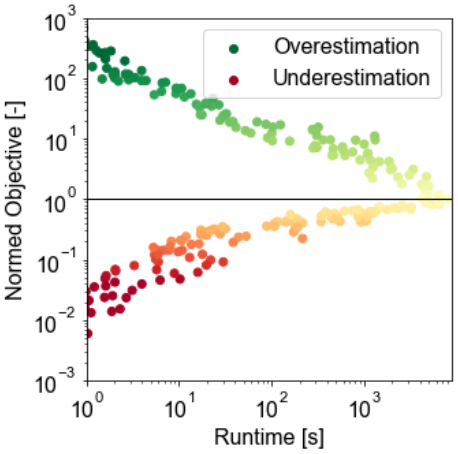

Figure 4.54. Upper and lower bounds of the self-sufficient building model depending on the runtime

4.4.1.3. Tightness of Bounds Based on Over- and Underestimation

In summary, the method of over- and underestimating time series does not provide tight upper and lower bounds in case of the tested models, unless aggregation configurations are chosen with a high number of total time steps and a correspondingly small computational speedup compared to the fully resolved case. Furthermore, the approach suffers from the curse of dimensionality. As an explanation, we can adapt the method of taking shoulder values for representing a group of values by their “shoulder values” introduced in Figure 2.19 and add hypothetical data points as depicted in Figure 4.55:

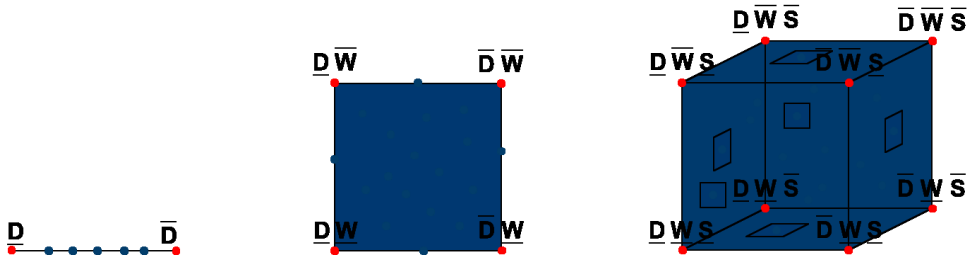

Figure 4.55. Increasing distance from over- or underestimating representative values for a rising dimensionality of the considered data

While the extreme values (the red dots) in Figure 4.55 from a single time series, e.g., a demand time series D, are values that appear in the original data (the blue dots), they become synthetic values if more time series are considered. For instance, if an additional wind time series is considered as shown in the middle of Figure 4.55, the representative (red) extreme values do not match any of the original data sets' (blue) values. This effect becomes more dominant with a growing dimensionality of the input data as shown in the right of Figure 4.55. Simply put, this would result in the assumption that in a multiregional model, a minimum wind capacity factor would appear in all regions simultaneously, which is an unrealistically conservative assumption for obvious reasons. Therefore, the application of this method was limited to single-node co- or trigeneration systems as in [79, 181]. Further, the models to which the presented method was applied in the literature were always connected to an electricity or gas grid and storage was of minor importance to the models. Moreover, no capacity factor time series with a large spread between minimum and maximum values were considered. Accordingly, the method provided much smaller gaps in these models. Further, the models considered a large number of operational binary variables whose number grows proportionally to the number of considered time steps, which prolonged the solving process of the fully resolved model disproportionally. Therefore, iterative procedures where proposed to gradually tighten the bounds. Against the backdrop of relatively loose bounds at relatively highly resolved aggregation configurations, however, these iterative methods are not likely to outperform the fully resolved model and are therefore not further investigated.

4.4.2. Model-Specific Bounds for MILPs without Cost Time Series

As shown in Section 4.4.1, bounds based on over- or underestimating time series are not tight, especially, if multiple time series

enter the model and storage technologies play an important role. However, for mixed-integer linear program models that neither consider cost nor revenue time series, the temporal aggregation using a centroid representation and the multi-level approach proposed in Section 3.4.2 provide alternatives for tighter bounds and computational speed-up. Both conditions are fulfilled by the island system model, i.e. it is a mixed-integer linear program and does not consider cost or revenue time series. Instead, a constant price for the electricity obtained from the backup-plant is assumed. Therefore, binary variables of the island system model can be relaxed or the model can be aggregated using centroids in order to obtain lower bounds to the original problem. For the upper bound, the binary variables can be fixed to values obtained from an aggregated model run followed by a re-run as linear program considering the fully resolved time series. Figure 4.56 depicts the two lower bounds obtained from temporal aggregation using centroid representation (yellow) as well as relaxation of the mixed-integer linear program (red) and the upper bound using a linear program with fixed binary variables based on the optimal solution of a preceding aggregated model run (green) on the left. On the right, the corresponding gap depending on runtime for the respective Pareto-optimal combination of bounds is shown.

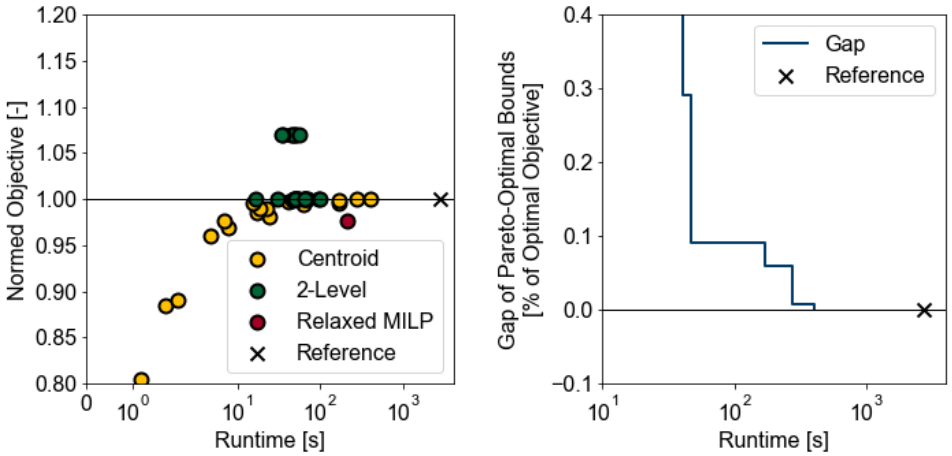

Figure 4.56. Left: Lower bounds obtained from temporal aggregation using centroid representation (yellow) and relaxation of the mixed-integer linear program (red) and an upper bound using a linear program with fixed binary variables based on the optimal solution of a preceding aggregated model run (green). Right: Gap depending on runtime for the respective Pareto-optimal combination of bounds

It is worth mentioning that only those numbers of segments and typical days were chosen for the centroid-based aggregation, which where optimal according to the optimal pathway algorithm, i.e. they are the same clustering configurations as represented by the green dots in the lower left graph of Figure 4.16. For the first stage of the 2-Level algorithm, the distribution-preserving algorithm was chosen because it outperformed all other algorithms with respect to accurate system designs at low temporal resolutions. As the first stage only serves for fixing the set of binary variables, the result after the second stage remains an upper bound irrespectively of the representation method chosen in the first stage. Analogously to the lower bound given by centroids, only those configurations were chosen, which were proposed by the optimal pathway algorithm for the distribution-preserving representation.

Compared to Figure 4.52, the bounds obtained in Figure 4.56 are significantly tighter. Especially the centroid-based representation of aggregated time series provides tighter lower bounds at small runtimes than the systematic under- and overestimation of time series to obtain lower bounds. The main reason for this is the fact that the centroid-based algorithm preserves the mean value and likewise the cumulative value of a time series. For models that heavily rely on storage technologies, not only the values of time series itself, but also the mean or cumulative values of time series play an important role, as for instance, a mean capacity factor can also be interpreted as mean energy availability factor. Even though extreme values are not preserved in the aggregation, the possible mean feed-in into storages remains the same, which is not the case if capacity factors are systematically overestimated.

Moreover, Figure 4.56 reveals that the configurations incorporating the solving of linear programs with both fixed or relaxed binary variables and a comparable size as the reference mixed-integer linear program take a longer minimum amount of time because the overall number of variables remains approximately the same as in the reference mixed-integer linear program. Here, the speed-up is obtained by solving at most one aggregated mixed-integer linear program and one linear program instead of iteratively solving linear programs in a branch-and-bound algorithm as in the reference case. In summary, the centroid-based aggregation and the 2-Level approach using the distribution-preserving algorithm in the first

stage provide the tightest bounds in case of the island system model.

By taking the Pareto-optimal upper and lower bounds with respect to their corresponding runtime, the gap shown in the right graph of Figure 4.56 can be calculated using Equation (3.33). Here, it can be stated that it is indeed possible to achieve a significant speed-up of solving times by more than a factor of ten with a remaining optimality gap of 0.1% in case of the island system, if all model features are exploited and the right aggregation configurations are chosen.

However, it is not known a priori, which aggregation configurations lead to which optimality gaps. Therefore, practical algorithms could either rely on parallel solving of many different aggregation configurations and taking the lowest upper and upmost lower bound after a predefined runtime, or they could focus on iteratively increasing the number of typical days and segments until a desired optimality gap is reached in case that parallel computing is not an option.

4.4.3. Summary

In conclusion, Section 4.4 has shown that aggregation techniques indeed offer an option for obtaining upper and lower bounds to the optimal objective value of the fully resolved reference system and that it is possible to quantify the maximum deviation from it without solving the fully resolved model. Yet, the results also imply that a profound knowledge about the respective model as well as tailor-made aggregation approaches are required in order to obtain tight bounds. Moreover, this implies that methods found in the literature do not necessarily provide good or even meaningful solutions when applied to different models. Against this backdrop, heuristics such as the optimal pathway algorithm or the distribution-preserving representation method, which were developed in the scope of this thesis and proven to outperform status quo methods on various different models, will most likely keep their raison d’être as they require very little knowledge about the individual model and yet provide good solutions.

4.5. Discussion

The following section first debates the major results of this work and subsequently puts them into context with a broader general modeling error in order to provide an outlook on the interaction between temporal aggregation and other model simplifications.

4.5.1. Discussion of the Main Results

Against the background of a steadily growing research field of energy system modeling and the pressing necessity to capture the impact of renewable energy sources on a diversity of energy systems, the methods developed in the scope of this thesis supplement temporal aggregation techniques in multiple ways.

In contrast to existing works in this discipline, the methods developed within the scope of this thesis were challenged by fundamentally different energy system models. Despite the fact that a multitude of temporal aggregation methods existed in order to reduce the complexity of models, these methods were never applied to more than three models as shown in Appendix B. If multiple models were considered, they did not substantially differ from each other as opposed to the models introduced in Section 4.1. Accordingly, the effectiveness of a method could be hardly predicted.

This major drawback of existing methods was systematically addressed in this work, as it categorized both, methods and models. The reduction of methods to the most promising ones with respect to general applicability and the simplification of model structures to a subset of determinants allowed for a large-scale cross-comparison of all promising methods on a set of fundamentally different models. Here, methodological improvements presented in Chapter 3 were rigorously designed for a general applicability for different types of models.

As it could be shown, the effectiveness of a method always depends on certain model requisites, but the latest methods still offer room for improvements that are generally applicable and outperform current state-of-the-art methods.

In order to link the results of Chapter 4 semantically, Figure 4.57 depicts a decision tree to find the optimal aggregation method depending on the model type.

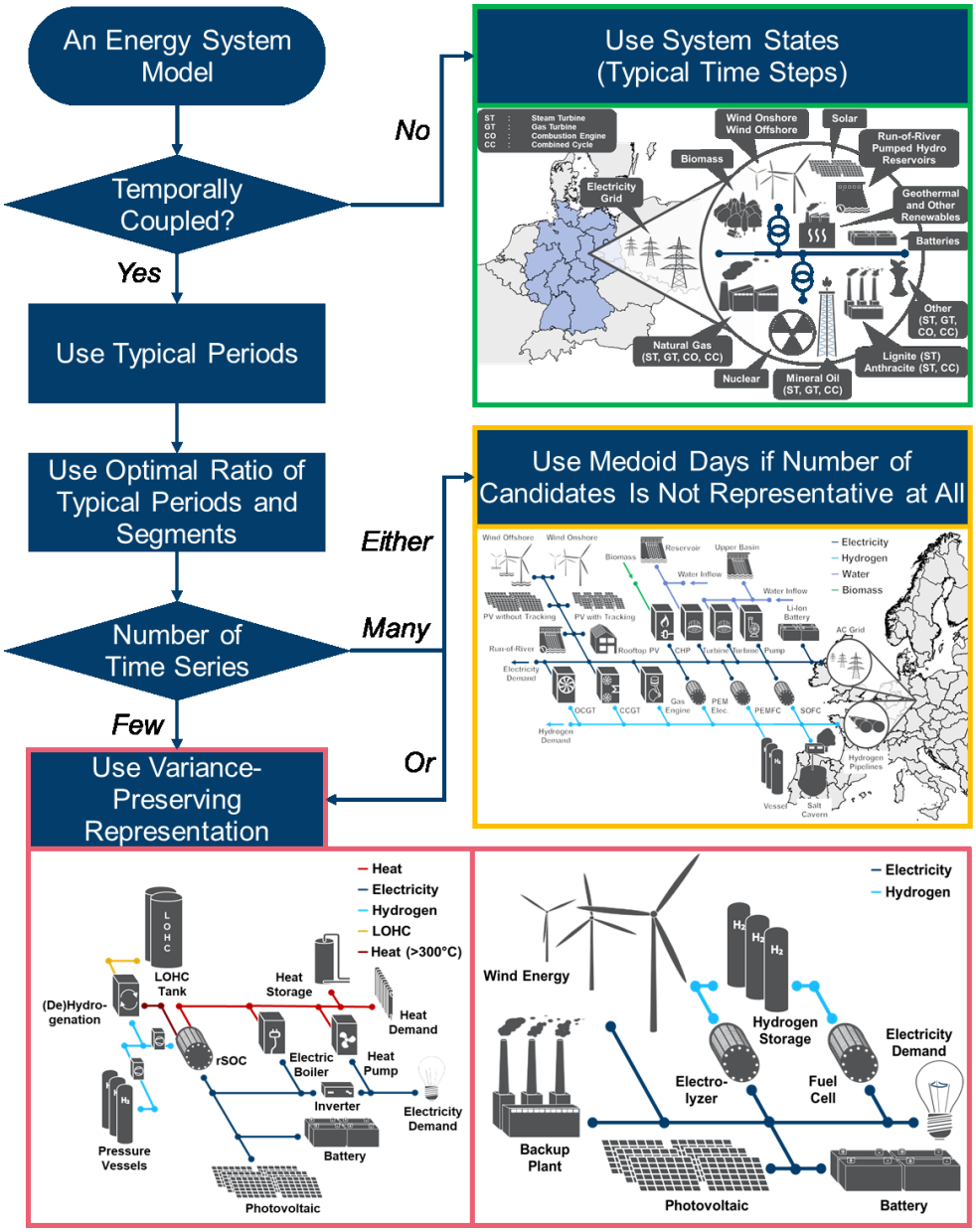

Figure 4.57. Decision tree illustrating how to find an optimal temporal aggregation based on the model type and the findings of Section 4.2 and 4.3

The first decision, i.e. whether an aggregation using typical time steps or typical days is advisable, relates to Section 4.3, in which the self-sufficient building model was compared to the electrical dispatch model. The major finding derived from this section is the dependency on the model structure: While the self-sufficient building model considers multiple storage technologies, the dispatch model is temporally decoupled. Therefore, the model is independent from the chronology of time steps. As many low-dimensional time step candidates are more convenient for clustering than many

high-dimensional typical day candidates, the aggregation to typical time steps outperforms the aggregation by typical days. In contrast to that, the chronology between intra-daily time steps was important to the battery and the thermal storage and the chronology between typical days is crucial for the appropriate modeling of storage technologies in case of the self-sufficient building model. Accordingly, the aggregation to typical days was the significantly better choice in this case. In this context, the finding that the optimal aggregation method does not depend on the periodicity of the input data, but on the model structure itself, is an important contribution of this work.

In case of the energy system models that consider storage technologies working on a daily or seasonal level, i.e. the island system model, the self-sufficient building model and the European model, multiple options for enhancing the quality of temporal aggregation were developed within the scope of this thesis. First, it was shown that an aggregation to typical days with an hourly resolution only is significantly outperformed by combined solutions that reduce both, the number of typical days and the number of time steps (segments) within each typical day. Furthermore, an algorithm was developed that searches for an optimal ratio between the number of typical days and the number of segments for a given number of total time steps without being forced to solve the energy system model itself. Those aggregation configurations that were proposed by the algorithm proved to be closest to the optimal objective function of the fully resolved case under the premise that the representation method itself was meaningful. Further, a novel representation algorithm was proposed that not only aims at preserving the first statistical momentum, the mean, but also at preserving the second one, the variance, as well as the value distribution in the aggregation process. This algorithm outperformed all other representation methods significantly in case of single-regional energy system models and yielded good results for the European model.

Yet, the representation by medoids slightly outperformed the distribution-preserving algorithm in the latter case, because the European model comprises numerous low-correlated and aperiodic wind time series, whose variance on longer time scales (daily means) was underestimated by the distribution-preserving algorithm. Due to the consideration of different storage technologies

working on different time scale lengths, variances on different time scales affect the sizing of components as well. By addressing this observation, an adapted version of the distribution-preserving algorithm was developed that approximately preserved the variance of daily means as well. Consequently, it outperformed the representation by medoids with respect to both, technology sizing and technology allocation.

Moreover, 365 days itself considered by the reference case are likely not sufficient to capture enough possible operation situations of the model. Accordingly, the use of existing days in case of large multi-regional energy system models with low-correlated time series seems appropriate, if the database itself is not sufficiently large and the exact allocation of technologies is not of great interest.

Apart from that, it could be shown that the runtime is nearly proportional to the total number of time steps in case of the small models, whereas the runtime decreases disproportionally with a lower number of total time steps in case of the much larger European model. Accordingly, the benefit of temporal aggregation increases the bigger the model becomes.

With respect to error bounding based on time series aggregation, Section 4.4 revealed both, potentials and limitations. On the one hand, approaches based on a simple over- and underestimation of the aggregated time series do not provide tight bounds if the considered model is isolated and relies on renewable energy sources as well as a high share of storage technologies. On the other hand, it could also be shown that in case of the island system model, tighter bounds could be derived if model-specific features such as the presence of binary design variables or the absence of cost time series were exploited. However, these tighter bounds come at the expense of general applicability.

As major practical advices for future applications of temporal aggregation techniques for energy system modeling, the following aspects are to be stressed:

- Temporal aggregation techniques are heuristics and can bias some time series and the subsequent sizing and operation of the corresponding technologies more than they can

bias others. Therefore, a sensitivity analysis using marginal deviations from the temporal resolution is inevitable in order to detect and avoid these biases.

- The majority of aggregation techniques do not aim at preserving statistical features of the original time series other than their mean. The results of this work imply that the preservation of additional statistical features is crucial for improving existing methods. Future research could also focus on an explicit consideration of cross-correlations of time series and their impact on energy flows.
- The No-Free-Lunch-Theorem for optimization [197] appears to apply to temporal aggregation methods as well: For a large number of sufficiently different energy system models, it is unlikely that an aggregation method can be found that outperforms all the others and on all models. Although it could be shown that some methods significantly dominate others in general, this implies that the more a method is tuned to a given model, the less applicable it is to others.

4.5.2. Temporal Aggregation in the Context of Other Simplifications

As discussed previously, temporal aggregation is based on a mathematically conclusive theory and can be used as a plausible and efficient heuristic to simplify energy system models or to define analytically correct upper or lower bounds of the original problem. Furthermore, the results demonstrated that numerous indicators exist for quantifying the effectiveness of these approaches. However, these indicators always refer to input data or models, which may already be strongly simplified themselves and which may therefore influence the effectiveness of an additional temporal aggregation. This means that temporal aggregation is generally applied to a model that could already be inaccurate with respect to numerous other aspects. This raises the question what impact temporal aggregation has on an overall model error, i.e. whether temporal aggregation can be used without introducing a new major source of inaccuracy.

One approach to address this issue is a large-scale sensitivity analysis in which a model is iteratively solved for numerous different model simplifications and their cross-combinations. These large-scale sensitivity analyses comprise many different simplifi-

cation approaches, which are explicitly considered within the project that granted the funding for this work, and among which temporal aggregation is only one. For one of the models within this project, the FINE-infrastructure model, a multi-regional energy system model considering gas and electricity infrastructure as well as renewable capacity expansion, a large-scale analysis was conducted comprising more than 8000 model configurations with the following parameter variations:

- The number of typical days
- The number of segments per typical day
- The number of regions
- The number of technologies (of a kind) per region
- The cost-curve modeling: linear vs. intercept-slope
- The electricity grid model: loss-free (noLoss) vs. linear-optimal power flow (lopf)
- The storage modeling approach: Daily storage only vs. seasonal storage formulation
- The emission reduction target scenario
- The PV potential scenario

The first two parameters were widely discussed within this work. The number of regions refers to the number of energy hubs between which energy can be exchanged and the number of technologies refers to the number of wind turbine and PV panel types. In case of fewer technologies, different turbine or panel types are aggregated to single ones with averaged operation profiles. The cost-curve modeling addresses the way that annualized investment costs are modeled depending on the installed capacities. While there is a linear relationship between the built capacity and the total annualized investment costs in the linear case, the intercept-slope formulation considers an additional binary cost if the respective component is build. In this way, economies of scale can be approximated because capacity-specific component costs can decrease for larger component sizes. The electricity grid modeling refers to whether phase angles within the AC grid are omitted or approximated by a linearization. In the latter case, their impact on the active power can be considered. Storage components can be modeled in a simplified way either, such that their state of charge at the end of each day equals the one at the beginning of each day, or, with an additional set of variables and constraints, this

state of charge can be superposed with a seasonal state of charge. The emission reduction target refers to the percentage by which the total CO_2 emissions should be reduced compared to the level of 1990. Lastly, the PV potential refers to the total amount of available area for photovoltaic panels and different scenarios were used to account for uncertainties with respect to this aspect.

The first seven aspects can be understood as model-related level of detail, whereas the last two are related to scenario aspects, i.e. they specify the input data to use rather than the modeling approach. In order to allow for comparability, these scenarios were fixed to a 100% emission reduction target and an identical predefined maximum PV potential. As the runtime was limited to 24 h, not all configurations were solved within this time window. Concisely, those configurations that were “comparably complex” with respect to more than four out of the seven varied model features did not stay within the time limit. Therefore, the following analysis further focuses on a subset of model features, namely the number of regions, the number of typical days and segments per typical day and whether the electricity grid is modeled using the linear optimal power flow approach or not.

Figure 4.58 depicts the root-mean-square error of the cost shares and the deviation of the total annualized costs from the fully resolved reference case of all remaining model runs depending on the runtime. The color of the sample points represents the number of total time steps of the respective model run and those with a red edge are Pareto-optimal. The points connected by red and orange arrows are configurations that differ by only one model attribute, and they are separately listed in Table 4.8. Here, the labels refer to the number of regions, time steps, segments and the power flow modeling of the electricity grid.

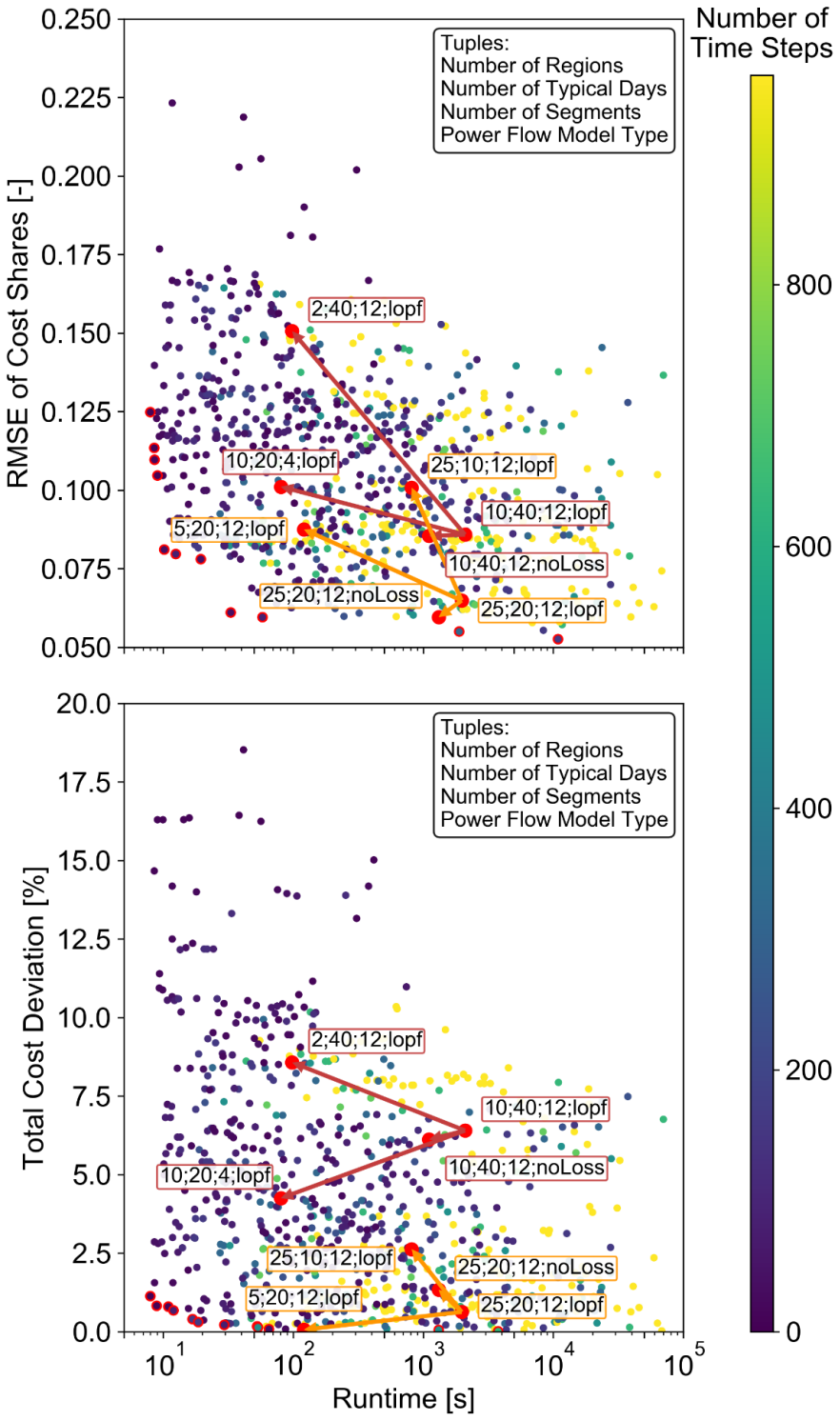

Figure 4.58. Root-mean-square error (RMSE) of the cost shares and deviation of the total annualized costs from the fully resolved reference case depending on the runtime. The color of the sample points represents the number of total time steps of the respective model run and those with a red edge are Pareto-optimal. The points connected by red and orange arrows are configurations that differ by only one model attribute.

Table 4.8. The model runs connected by red and orange arrows: Each configuration differs from the respective base case by only one attribute, which is further simplified

Configuration	Number of Regions	Number of Typical Days	Number of Segments	Linear Optimal Power Flow	Runtime [s]	RMSE of Cost Shares [-]	Total Cost Deviation [%]
Base 1	10	40	12	Yes	2097.99	0.085841	6.4034
Simp. 1.1	2	40	12	Yes	98.21	0.150613	8.5714
Simp. 1.2	10	20	4	Yes	80.21	0.101107	4.2478
Simp. 1.3	10	40	12	No	1107.87	0.085427	6.1195
Base 2	25	20	12	Yes	1973.52	0.064875	0.6282
Simp. 2.1	5	20	12	Yes	120.81	0.087521	0.0653
Simp. 2.2	25	10	12	Yes	814.02	0.100840	2.6295
Simp. 2.3	25	20	12	No	1310.26	0.059544	1.3388

Once again, Figure 4.58 illustrates the significant correlation between the number of total time steps and runtime of the model. However, as multiple model simplification approaches are involved, longer runtimes do not necessarily indicate smaller errors, because some features may still not be sufficiently detailed despite of a high number of typical days and segments.

Furthermore, it is remarkable that for both a posteriori error metrics, i.e., the root-mean-square error of the cost shares and the total cost deviation, the Pareto-optimal model configurations consider a comparably small number of typical days, which indicates that temporal aggregation is capable of significantly reducing the model complexity while maintaining small model deviations. This is explicitly not the case for other model simplifications, which implies that temporal aggregation is among the most effective complexity reduction techniques.

With respect to an exact quantification of the effectiveness of temporal aggregation compared to other simplification techniques, Figure 4.58 demonstrates that this is hardly possible. As the two sets of model configurations connected by arrows imply, the error introduced by temporal aggregation does not only depend on the extent to which the model is already temporally aggregated, but also on the other model simplifications, e.g., the number of regions and

power flow modeling. The base configuration of the red arrow set with 10 regions, 40 typical days, 12 segments per day and linear optimal power flow modeling is already spatially strongly aggregated, whereas it is temporally comparably highly resolved. Here, a further aggregation of regions leads to a stronger error increase than a reduction of typical time steps. In contrast to that, the base case of the orange arrow set with 25 regions, 20 typical days and 12 segments per typical day has a smaller temporal resolution and a higher spatial resolution. In this case, the opposite effect can be observed: While a further reduction of the number of typical days has a larger impact on the respective model error, a reduction of the number of regions is more effective in this case.

For both configurations, it can be observed that the choice of the power flow modeling has comparably small effects on both, errors and runtime. Further, it can be seen that different error indicators may assess an aggregated model's quality differently. This leads to the effect that some further model simplifications may in fact counterbalance the deviations introduced by other simplifications and thereby decrease certain errors. For example, the optimal objective function value of a simplified model may be underestimated. However, a further simplification with respect to the modeling of a certain component may make it less flexible and therefore economically less attractive. Furthermore, the optimal objective function value can be increased again by this simplification suggesting that the chosen simplification would improve the model accuracy again. In fact, however, other accuracy measures such as the root-mean-square error of cost shares can further deteriorate. From a practical point of view, this implies that the choice of an error metric should always fit the aspects the respective model focuses on. However, this also impedes an assessment of simplification methods when being applied to different models with different research foci.

To summarize, the fact that temporal aggregation is much more favorable for a regionally strongly aggregated model than for a regionally higher resolved one with already aggregated time series implies that a clear assignment of shares of a model's overall error to its respective simplifying assumptions is not directly possible.

Still, it is possible to compare the effectiveness of different simplification measures to each other based on a ceteris paribus assumption. This means that the runtime gains and accuracy losses of a simplification approach, which is ceteris paribus applied to a given model instance, can be compared to those of another simplification approach. In case that one simplification approach offers larger gains in runtime while maintaining a smaller loss of accuracy or result deviations, this approach can be preferred to the other one. If this observation also holds true for different models with diverse model foci, it is valid to call this method superior to the other one.

Remarkably, the complex and often enough neither known, nor quantifiable interactions of different simplifications or modeling approaches can be tackled by the same methods as introduced in Section 3.3. Concisely, the Pareto-principle and sensitivity analyses are applicable for different models, accuracy and performance indicators as well as different simplification approaches. Furthermore, the Pareto-principle and sensitivity analyses are also applicable in an even more general way regarding which model features to choose and which to neglect when creating models for new application cases. In this context, it deems advisable to start with a simple model and iteratively test novel model features with a potentially higher level of detail. If the results shift remarkably, these additional features should be kept, as they may be crucial for an accurate solution, whereas those with little impact on the result could be omitted. Furthermore, an increase in the level of detail should always be deliberately distributed across multiple (potential) model features with a likely impact on the model results as the gains in accuracy are often degressive with respect to the level of detail of a single model feature, which could be shown for temporal and spatial resolution in Figure 4.58.

These findings support the approach to apply all temporal aggregation methods with different period lengths, numbers of typical periods, segments per period, and representation methods to a set of heterogeneous models in order to derive relatively generalizable empirical findings on the chosen method as presented in Chapter 4.

5. Summary

The following section outlines the chain of reasoning of this work and points out its scientific contributions by summarizing its key aspects and condensing its main conclusions.

5.1. Scope and Objective

Energy systems are becoming more complex and so are their models. Solving complexity issues in models means mastering complex system-related questions.

Over the last decades, energy systems have become increasingly complex due to the development of new technologies, new ways of energy consumption and a growing connectivity between different energy sectors. Even more significantly, energy systems are progressively challenged by the need for reducing greenhouse gas emissions and a substitution of fossil energy sources by intermittent renewable ones such as solar and wind energy.

To address this rising complexity and support planning or decision-making processes in the operation and transformation of energy systems, optimization-based time-discrete models have emerged as a tool to account for different technologies and measures, time horizons, system locations as well as numerous other aspects of real energy systems.

Yet, the polynomial and in some cases exponential dependency of the models' runtime and their respective number of variables and constraints limits their maximum size, level of detail or inner-structural connectivity. In concert with the increasing complexity of modern energy systems, this issue outweighs algorithmic progress in mathematical optimization or hardware development.

For that reason, different approaches can be found in the literature which aim for a heuristic simplification of these energy system models, among which temporal aggregation focuses on a reduction of the model's number of time steps to a representative smaller one. Due to the time-discreteness of the optimization models, this directly reduces the number of time-dependent variables and constraints and ultimately reduces the model size to guarantee the solvability of large or complex energy system models within a reasonable amount of time. However, the solutions obtained are gen-

erally either suboptimal to or mathematically infeasible for the original fully resolved problem due to the heuristic nature of this approach.

This work focuses on the enhancement of temporal aggregation and development of novel methods in order to decrease the aggregation-induced error for optimization problems and to allow for even stronger aggregations while maintaining the quality of the achieved optimization-based system solution. In this way, even more complex energy system models can be optimized, which can equip decision makers with more reliable information on a cost-efficient design of the future energy system.

5.2. General Approach and State of the Art

As models become increasingly complex, a case-specific handling of complexity issues becomes impracticable. Therefore, a systematic handling of complexity issues and a clear categorization of simplification approaches is an emerging research topic.

In most cases in the literature, temporal aggregation is applied to a model solely to ensure its computational solvability, i.e. the focus lies on the model rather than the employed model simplifications, whereas only a small part of the literature on energy system models deals with aggregation approaches explicitly. Therefore, a large variety of different methods existed prior to this work, which, in many cases, did not refer to each other or did not assess the quality of the respective aggregation approach systematically.

In order to address this lacking transparency and to use the most promising state-of-the-art approaches as a starting point for further improvements on temporal aggregation, more than 130 different publications were reviewed with respect to the employed temporal aggregation technique, the model and its features, to which the aggregation was applied.

The review reveals that the most promising approaches rely on clustering as this technique aggregates only those periods or time steps that are similar to each other and therefore reduces the errors that occur by omitting time steps. However, in most cases, either periods or single time steps were clustered, but both ap-

proaches were generally not combined with each other, i.e. an aggregation of periods with a further aggregation of time steps within these periods was widely neglected.

Furthermore, the approaches to represent the clusters of similar time steps by either the clusters' centroids or medoids proved to be insufficient for many applications as it underestimates extreme values of the original dataset. Therefore, many approaches include a post-processing step in which assumingly relevant additional time steps of the original dataset are added to the aggregated one, which, however, is often solely based on specific knowledge about the model and cannot be generalized.

Apart from that, the vast majority of studies in the literature relied on at most two different models, which belonged predominantly to the same model or application type. Therefore, an important additional prerequisite of this work was to develop a generally applicable method and to ensure the consistent outperformance compared to state-of-the-art methods for different model types.

Based on these findings, this work identified two major research gaps as key elements of current temporal aggregation with potential for improvement:

1. The combination of different temporal aggregation approaches in order to leverage their respective potential with respect to speed-up and accuracy
2. An approach of clustering-based temporal aggregation that automatically accounts for system-relevant features of the original time series

5.3. Methodology

The chronology and the statistical features of time series are crucial determinants for a reliable design and operation of energy systems. Preserving them as much as necessary while reducing the number of time steps as strong as possible is the key to superior temporal aggregation techniques.

Clustering-based methods for reducing the number of total time steps by determining typical periods and by merging adjacent time steps to longer ones bear a certain degree of similarity and can be freely cross-combined. For that reason, the general process of ag-

gregating typical periods and further reducing their temporal resolution is first explained in detail based on the respective latest developments in either approach.

Subsequently, the clustering procedure itself is decomposed into the grouping of time series data and the representation of each group of time steps or periods by a single typical one. In that way, the question how to represent a group of time steps or periods by a single representative in an optimal way with respect to its implications on the operation (and design) of an energy system can be handled in an isolated way.

In this context, prior research has shown that especially certain statistic features of the employed time series determine the cost optimal design and operation of an energy system. Therefore, an algorithm is developed that directly constructs representative periods based on groups of periods in such a way that the original time series' value distribution is approximated as close as possible and thereby circumvents the requirement of manually adding extreme periods or time steps from the original time series to the aggregated ones.

Furthermore, as it is possible to combine the number of aggregated typical periods and the number of inner-period time steps freely, an algorithm is developed which decides on a close-optimal trade-off between both parameters. Thereby, the concept of Pareto-optimality is introduced to distinguish superior aggregation algorithms from inferior ones with respect to their capability to accelerate the energy system optimization while keeping the aggregation-induced deviations low.

Lastly, the potential of aggregating time series to determine tight upper and lower bounds of the fully resolved optimization problem is investigated from an exact mathematical instead of an experimental point of view. These approaches allow for quantifying the worst-case error of using aggregated time series without being able to solve the fully resolved optimization problem itself by comparing the model's upper bound approximation to its lower one.

In order to substantiate the outperformance of the aggregation approach developed within this work compared to state-of-the-art

temporal aggregation techniques, four fundamentally different energy system models are introduced as case studies. These vary with respect to their purpose (dispatch model vs. capacity expansion model), scope (single-nodal vs. multi-regional) and their mathematical structure (linear and temporally decoupled, linear and temporally coupled as well as mixed-integer linear and temporally coupled).

On these models, up to four different temporal aggregation techniques are performed, two of which are the current state-of-the-art approaches, and the respective number of typical periods and inner-period time steps is varied resulting in over 2,400 different model runs.

5.4. Results and Main Conclusions

The optimal temporal aggregation approach works on every energy system model and outperforms any other aggregation approach with respect to model acceleration and accuracy for any extent of aggregation. Although the No-Free-Lunch-Theorem also applies to temporal aggregation, the algorithm developed in this work still outperforms other methods considerably for various models.

With respect to all temporally coupled models, a significant outperformance of the approach developed in this thesis could be observed. Choosing a good trade-off between the number of aggregated time periods and the temporal resolution within each period as well as an explicit preservation of the original time series' value distribution in the corresponding aggregated data set significantly outperforms even the most recent temporal aggregation approaches considerably. Specifically, the methods developed in this work were able to accelerate all temporally coupled models by the order of two magnitudes while keeping the deviation of the optimal objective function value well below 5%. Compared to state-of-the-art temporal aggregation methods, this corresponds to an additional speedup by the order of one magnitude at a constant or even smaller error level.

Yet, the heuristic nature of temporal aggregation approaches and the diversity of energy system models reveal that there are also special model types for which different aggregation approaches can perform slightly better. In particular, it could be shown that the

consideration of time-coupling constraints, e.g., of storage technologies, is a remaining important explanatory variable for choosing an appropriate temporal aggregation method. In case storage technologies and other time-linking constraints are neglected, the chronology of time steps becomes irrelevant for the optimization model and time steps can be aggregated in an arbitrary order. However, given rising shares of intermittent renewable energy sources, storage technologies steadily gain importance and it can therefore be expected that these model types remain an exception.

Concerning approaches for defining upper and lower bounds to the fully resolved energy system model using aggregated time series, a comparable model dependency was found. For linear programs, these approaches are of minor practical use, as they do not provide tight upper bounds in a non-iterative manner. In contrast to that, error bounding using temporal aggregation has revealed a certain potential for mixed-integer linear programs, in which it can assist in finding good incumbent solutions for a subsequent branch-and-bound procedure.

These findings support the hypothesis that the No-Free-Lunch-Theorem, which is well known in mathematical folklore, also applies to temporal aggregation. This means that the more a temporal aggregation technique is adapted to a specific model class or specific model instance in order to tweak its performance, the less likely it becomes to work sufficiently on other model instances. Against this background, it is remarkable that the following general conclusions can still be drawn from this work:

- Temporal aggregation should be based on clustering in order to keep the error induced by merging similar time steps as small as possible.
- If the model is temporally decoupled, single time steps should be clustered; otherwise, periods corresponding to expected storage cycles and their inner temporal resolution should be clustered in a balanced manner.
- Not only extreme values, but in fact the whole value distribution of the original time series should be preserved as closely as possible in the aggregated data set in order to obtain both appropriate system designs and reasonable operation schedules.

- In case mixed-integer linear programs are to be solved, solutions based on aggregated data bear a considerable potential for defining promising incumbent solutions for subsequent branch-and-bound routines.
- Compared to exact mathematical methods, temporal aggregation for energy system models is a generally applicable heuristic, which yields good results independently of the model type and very good results when being slightly adapted to the model type.
- For the most common type of temporally coupled energy system models, an algorithm could be developed that does not require additional knowledge of the modeler and achieves speed-up by a factor of more than 100 with a result deviation well below 5%.

Appendix

A. Glossary Used For Literature Research

Table A.1. Glossary used for literature research (taken from Hoffmann et al. [1])

Keyword Used for Literature Research	Synonym (Term in this Review)	Definition
Clustering	Grouping, (Clustering)	"Given a dataset of n time series data $D = \{F_1, F_2, \dots, F_n\}$, the process of unsupervised partitioning of D into $C = \{C_1, C_2, \dots, C_k\}$ in such a way that homogeneous time series data are grouped together based on a certain similarity measure" [135]
Complexity Reduction	None, (Complexity Reduction)	Different techniques to increase the computational tractability of energy system models [41]
Energy System Optimization Model, Energy System Model	Energy System Optimization Model, (Energy System Model)	A model "the analysis of existing national energy systems, as well as the prediction of potential future scenarios, is usually performed with" [15]
Typical Period	None, (Period)	A group of consecutive time steps describing a regular amount of time (e.g., 24 h)
Representative Day, Representative Week	Typical, (Typical)	A single time step or a period representing a group of time steps or periods determined by clustering
Sampling, Random Sampling, Subsampling	None, (Sample)	A single time step or period taken from the original time series
Snapshot	System State, Time Step, (Time Step, If subset of time series: Typical Time Step)	A term used in the literature for typical time steps
System State	Snapshot, Time Step, (Time Step, If subset of time series: Typical Time Step)	A term misleadingly used in the literature for typical time steps. It actually describes the state of a system under both external conditions (e.g., capacity factors) and internal state variables (e.g., storage levels) at a specific time step

Keyword Used for Literature Research	Synonym (Term in this Review)	Definition
Temporal Resolution	None, (Temporal Resolution)	The resolution of a discretized time series given by the length of its time steps
Time Series Aggregation, Temporal Aggregation	Temporal Aggregation, (Time Series Aggregation)	In the narrow sense: The reduction of time steps in time series In a broader sense: The reduction of the number of time steps or time series
Time Slice	Time Slot, (Time Slice)	Hierarchically merged time steps appearing in a systematic order as used by the TIMES framework
Time Step Typical Time Step	Snapshot System State (Time Step)	The smallest possible time interval of a discrete time series represented by a single value for each attribute
Typical Day Typical Week	Representative (Typical)	Periods or single time steps considered to capture the basic characteristics of the external operating conditions of an energy system are named “typical”

B. Table of Methods

Table B.1. Table of methods (taken from Hoffmann et al. [1])

Year	Author	Energy System Model for Case Study, *(Framework)*	Normalization	Distance Metric	Clustering/ Grouping	Representative	Extreme periods	Linking Periods	Duration Curve
1999	Balachandra et al. [59]	None (just approach)	No	No	Multiple discriminant analysis	mean	No	Yes	No
2002	Yokoyama et al. [71]	Building or district model, no storage technologies, but multiple commodities	No	No	Season-based (summer, mid-season, winter) with 4, 2, or 1h resolution	(probably) mean	No	No	No
2007	Lee et al. [168]	unit commitment problem for 48 unit power system (not further specified)	No	No	No	No	No	Yes	No
2007	Swider et al. [132]	Single-node model for electricity production in Germany with wind and pumped hydro storage	No	No	Every two months, one weekday and one weekend day with 2h resolution	(probably) mean	No	No	No
2008	Marton et al. [103]	None (just approach)	No	Integral of absolute error (L1 norm)	Clustering by comparing each new day to clusters of preceding days	mean	Yes, if outlier surpass a certain threshold of the IAE and the following day is close to the preceding cluster	Yes	No, although curve was called the duration curve
2008	Mavrotas et al. [60]	Building model for a hospital, no storage technologies, but multiple commodities	No	No	Monthly average	mean	No	No	No
2008	Mavrotas et al. [60]	Building model for a hospital, no storage technologies, but multiple commodities	No/ not mentioned	No/not mentioned	Seasonal rescaled average further segmented	Rescaled mean	Peak demand value of each cluster is kept for each attribute	No	No
2009	Alzate et al. [198]	Customer or unit partitioning/ none (just approach)	Z-normalization	No (Hamming distance for out-of-sample extension)	Spectral clustering	None (just grouped)	No	No	No
2009	Casisi et al. [124]	District model, no storage technologies, but multiple commodities	No	No	Season-based (3 seasons for energy demand and	(probably) mean	No	No	No

Year	Author	Energy System Model for Case Study, *(Framework)*	Normalization	Distance Metric	Clustering/ Grouping	Representative	Extreme periods	Linking Periods	Duration Curve
					24 for sold energy to the grid)				
2009	Lozano et al. [121]	Building model for a hospital, no storage technologies, but multiple commodities	No	No	Monthly average with distinction between weekday and weekend	(probably) mean	No	No	No
2010	Lozano et al. [104]	District model, thermal storage units, multiple commodities	No	No	Monthly average	(probably) mean	No	No	No
2010	Nicolosi et al. [109]	Single-node electricity dispatch model for Texas (ERCOT), no storage, technologies mentioned, **(THEA)**	No	No	Full resolution, 4 seasons, Wednesday, Saturday and Sunday with hourly resolution, 16 time slices	means	No	No	No
2011	Domínguez-Muñoz et al. [61]	None (just approach)	Yes, but not mentioned which	Euclidean	k-medoids	medoids	Peak heating and peak cooling day	No	No
2011	Haydt et al. [110]	Island electricity model for Flores (Azores), no explicitly modeled storage technologies (only via availability), **(TIMES, LEAP, EnergyPlan)**	No	No	LEAP: 9 time slices from the duration curve TIMES: 4 seasons, Wednesday, Saturday and Sunday with hourly resolution EnergyPLAN: full hourly resolution	means	No	Yes	LEAP: Yes TIMES: No
2011	Ortiga et al. [164]	Building model, thermal storage units, multiple commodities	No/not mentioned	No/not mentioned	Graphical method	existing days	Peak heating and peak cooling day	No	Yes
2011	Pina et al. [113]	Island electricity model for São Miguel (Azores), no explicitly modeled storage technologies (only via availability), no storage technologies, **(TIMES)**	No	No	4 seasons, weekday, Saturday and Sunday with hourly resolution	(probably) mean	No	Yes	No
2011	Weber et al. [122]	Multi-node district model, daily heat and electricity storages, multiple commodities	No	No	3 seasons further segmented into 6 irregular periods	(probably) mean	No	No	No

Year	Author	Energy System Model for Case Study, *(Framework)*	Normalization	Distance Metric	Clustering/ Grouping	Representative	Extreme periods	Linking Periods	Duration Curve
2012	Buoro et al. [94]	Building model, thermal storage units, multiple commodities	No	No	Monthly average, typical weeks with 168 h	(probably) mean	No	No	No
2012	Devogelaer et al. [114]	Multi-node model for Belgium, multiple storage technologies, multiple commodities, **(JRC-EU-TIMES)**	No	No	26 2-week periods with three daily levels	(probably) mean	Peak demand slice	Yes	No
2012	Mehleri et al. [134]	District model, no storage technologies, multiple commodities	No	No	3 seasons further segmented into 6 irregular periods	(probably) mean	No	No	No
2012	Van der Weijde et al. [165]	Multi-node electricity model for Great Britain, no explicitly modeled storage technologies (only as source/sink)	No	No	N hourly samples	Existing hours	No	No	No
2012	Welsch et al. [111]	Single-node electricity model for a town, battery storages, demand shifting, **(OSeMOSYS)**	No	No	In Proposal: 4 seasons, work days and weekends, 3 daily intervals. In example: Just one day in hourly resolution	(probably) mean	No	Yes	No
2013	De Sisternes et al. [98]	Single-node electricity model, no storage technologies, but minimum up- and down-times	Min-max normalization for NLDC	Euclidean	Exhaustive search or heuristic	existing weeks	Including peak week or peak day	No	Yes
2013	Kannan et al. [115]	Single-node electricity model for Switzerland and pumped hydro storage, **(TIMES)**	No	No	Season-based (four seasons and to diurnal time slices), or weekdays, Saturdays, Sundays in hourly resolution	Average	No	Yes	No
2013	Mehleri et al. [199]	District model, thermal storage units, multiple commodities	No	No	3 seasons with hourly resolution	(probably) mean	No	No	No
2013	Pina et al. [125]	Electricity model for Portugal, storage technologies considered, but modeling	No	None	One weekday, one Saturday and one Sunday, 4 seasons	Not mentioned	No	No	No

Year	Author	Energy System Model for Case Study, *(Framework)*	Normalization	Distance Metric	Clustering/ Grouping	Representative	Extreme periods	Linking Periods	Duration Curve
		not explained, number of regions not mentioned, **(TIMES and EnergyPLAN)**							
2013	Simões et al. [116]	Multi-node model for Europe, multiple storage technologies, multiple commodities, **(TIMES)**	No	No	Season-based (four seasons, day, night and peak time slice)	Average	Average peak demand during each season	Yes	No
2013	Spiecker et al. [126]	Multi-node electricity model for Europe, hydro storage units, cogeneration units on regional scale	No/not mentioned	None	One weekday and one weekend day for every two months with 2h resolution	Not mentioned	Yes, with stochastic approach	Yes	No
2013	Voll et al. [108]	District model, no storage technologies, multiple commodities	No	No	Monthly average	mean	Two more time steps for summer and winter peak loads	No	No
2014	Adhau et al. [200]	Stochastic single-node electricity model, no storage technologies	No/not mentioned	Euclidean	k-means	centroids	No	No	No
2014	Benítez et al. [201]	Customer or unit partitioning/ none (just approach)	No/not mentioned (only one attribute)	Euclidean	Dynamic k-means	centroids	No	Yes (yearly trajectory)	No
2014	Deane et al. [69]	unit commitment of the Irish electricity system, pumped hydro storage, **(PLEXOS)**	No	No	Downsampling (5, 15, 30 and 60 min)	average	No	Yes	No
2014	Fazlollahi et al. [143]	District heating model, no storage technologies	Min-max normalization	Euclidean	k-means	centroids	Attribute peaks	No	No
2014	Fazlollahi et al. [74]	Two single-node district models with fixed capacities, no storage technologies, multiple commodities, unit commitment (minimizing operating costs)	Min-max normalization	Euclidean	k-means and segmentation	centroids	Attribute peaks	No	No
2014	Green et al. [177]	Electric dispatch model for UK, pumped hydro stor-	No (just two attributes of same	Euclidean	k-means	centroids	Dominant ramp integration	No	No

Year	Author	Energy System Model for Case Study, *(Framework)*	Normalization	Distance Metric	Clustering/ Grouping	Representative	Extreme periods	Linking Periods	Duration Curve
		age simulated, number of regions not mentioned	scale clustered)						
2014	Poncelet et al. [42]	Island electricity model for Belgium, no storage technologies or transmissions, re-evaluation with unit commitment model, **(TIMES)**	No	No	Season-based (four seasons, night, day and peak slice)	(probably) mean	By choosing peak slice	No	No
2014	Stadler et al. [123]	Building model, multiple storage technologies, multiple commodities **(DER-CAM)**	No	No	(seven typical days or one typical weekday, one typical weekend day and one peak day)	(probably) mean	Peak demand day in case of typical weekday and typical weekend day	No	No
2014	Wakui et al. [120]	Building model, thermal storage units, multiple commodities	No	No	Season-based	(probably) mean	Peak summer day and peak winter day	No	No
2014	Wogrin et al. [90]	Single-node electricity model, no storage technologies	No (attributes of the same unit)	Euclidean	k-means, hourly, 6 typical time steps (system states)	centroids	No	No	No
2014	Xiao et al. [171]	Island electricity model for, no storage technologies	No	No	No	No	No	Yes	No
2015	Agapoff et al. [68]	Multi-node electricity model for capacity expansion planning, no storage technologies	No/not mentioned	Euclidean	k-means, typical hours (snapshots)	medoids	Included as clustered features (min, max, std., local difference and avg.)	No	No
2015	Brodrick et al. [202]	Single-node model of a coal-plant with alternative natural gas and solar thermal heat sources and carbon capture and storage, CO_2 solvent storage unit, multiple commodities	Normalization by dividing by the average	Euclidean	k-means	centroids	No	No	No
2015	Bungener et al. [75]	unit commitment of a chemical cluster, multiple commodities	Normalized by average values and multiplied by weight	None, but variance indicator and zero flowrate indicator	Evolutionary mechanisms (segmentation)	means	No	Yes (adjacent time steps are merged)	No

Year	Author	Energy System Model for Case Study, *(Framework)*	Normalization	Distance Metric	Clustering/ Grouping	Representative	Extreme periods	Linking Periods	Duration Curve
2015	Deml et al. [76]	Single-node electric dispatch model, pumped hydro storage	No	No	Progressive downsampling	means	No	Yes	No
2015	Fitiwi et al. [146]	IEEE 24-bus Reliability Test System [203], multi-node electricity model, no storage technologies	Normalized by maximum line length and base load	Euclidean	k-means, typical hours (snapshots)	Medoids closest to the clusters' centroids	No	No	No
2015	Harb et al. [106]	Building model and district model, thermal storage units, multiple commodities	No	No	Monthly average, also 15 min. and hourly resolution	mean	No	No	No
2015	Harb et al. [95]	District model, thermal and battery storage units, multiple commodities	No	No	Cluster by sums of weeks (sensitivity analysis also for different day numbers), typical weeks	means	No	No	No
2015	Marquant et al. [152]	District heating model, no storage technologies, multiple commodities	No/not mentioned	Euclidean	k-medoids	medoids	Peak electricity and peak heating days	No	Yes
2015	Merkel et al. [96]	District model, thermal storage units, multiple commodities	No	No	Season based (three weeks from spring/autumn, summer and winter), 15 min. resolution	(probably) existing weeks	No	No	No
2015	Munoz et al. [166]	IEEE Reliability Test System [173], multi-node electricity model, no storage technologies	No/not mentioned	Euclidean	Daily moment-matching, k-means for hours, typical hours (snapshots)	centroids	Top 10 peak load hours included	No	No
2015	Poncelet et al. [185]	None (just approach)	No/not mentioned	L1-Norm	Using so-called "bins"	existing days	No	No	Yes
2015	Samsatli et al. [22]	Multi-node island model, multiple hydrogen storage technologies, multiple commodities	No	No	Season-based (four seasons, weekdays and weekend days)	(probably) mean	No	Yes	No
2015	Schiefelbein et al. [158]	District model, thermal storage units, multiple commodities	No/not mentioned	Euclidean	k-medoids	medoids		No	No

Year	Author	Energy System Model for Case Study, *(Framework)*	Normalization	Distance Metric	Clustering/ Grouping	Representative	Extreme periods	Linking Periods	Duration Curve
2015	Wakui et al. [118]	Building model, thermal and battery storage units, multiple commodities	No	No	Season based	(probably) mean	Peak summer day and peak winter day	No	No
2015	Wouters et al. [127]	District model, heat, cold and battery storage technologies, multiple commodities	No	No	Season-based (spring/autumn, summer and winter)	(probably) mean	Sensitivity analysis by adding variability to PV input data	No	No
2015	Yang et al. [128]	District model, heat and cold storage technologies, multiple commodities	No	No	Season-based (spring/autumn, summer and winter), 2h resolution	(probably) mean	No	No	No
2015	Yokoyama et al. [72]	Building model for a hotel, no storage technologies, but multiple commodities	No	No	Season-based (summer, mid-season, winter) with 8, 4, or 2h resolution and for commercial solver 1h	(probably) mean	No	No	No
2016	Ameri et al. [129]	District model no storage technologies, multiple commodities	No	No	Season-based (summer and winter)	(probably) mean	No	No	No
2016	Beck et al. [70]	Electric building model, battery storage	No	No	Single day downsampled (10, 30, 60, 300, 900, 3600s), analyzed single days	mean	No	Yes	No
2016	Bracco et al. [130]	District model, thermal and battery storage technologies, multiple commodities, **(DESOD)**	No/not mentioned	No	Season-based (summer, winter, mid-season)	(probably) mean	No	No, initial conditions at each day, e.g. SOC(p,t=0)=0	No
2016	De Sisternes et al. [97]	Single-node electricity model, battery storage and minimum up- and downtimes	Min-max normalization for NLDC	Euclidean	Exhaustive search or heuristic (refers to [98], but with additional cycled power error), typical weeks	existing weeks	Including peak week or peak day	No	Yes
2016	Frew et al. [167]	Multi-node electric model of the US, pumped hydro, thermal and battery storage technologies, **(POWER)**	Yes, but not mentioned is which, but averaged across all potential	None	Random days	Existing days, weights calculated with least squares method	Extreme days containing the peak value for each of the eight attributes	No (net storage vuels of each day must be zero or SOC at start of each day equals that at the end)	Yes

Year	Author	Energy System Model for Case Study, *(Framework)*	Normalization	Distance Metric	Clustering/ Grouping	Representative	Extreme periods	Linking Periods	Duration Curve
			developable sites						
2016	Haikarainen et al. [204]	Customer or unit partitioning/ district model, thermal storage units, multiple commodities	No	Euclidean	k-means	means	No	No	No
2016	Kools et al. [107]	District electricity model, battery storage units, heat demand driven CHP units considered	No	No	Averaging of eight consecutive weeks in each season to one typical day	mean	Normal distributions added for 1 min, 15 min and 1h resolution (stochastic impact)	Control policy for the storage (not across days)	No
2016	Lin et al. [179]	Multiple building models, thermal and battery storage units, multiple commodities	No/not mentioned (attributes of the same unit)	Euclidean	k-means	Existing day which is closest to the centroid	No	No (periodic SOC)	No
2016	Lythcke-Jørgensen et al. [93]	CHP-plant model, no storage technologies, multiple commodities	Heat demand normed by maximum value	No/not mentioned	So-called "CHOP" aggregation (graphical method) for five years of hourly data	means	No	No	No
2016	Merrick et al. [46]	Single-node electricity model, no storage technologies	No	None	Monthly median and peak electricity demand day with 4h resolution and only one averaged period	medoids	Peak electricity demand days	No	No
2016	Nahmmacher et al. [63]	Multi-node electricity model LIMES-EU [205] with intraday storage technologies, **(LIMES-EU)**	Demand: region-specific divided by maximum value VRE: divided by maximum value across all regions	Euclidean	hierarchical	medoids	No	No	No
2016	Oluleye et al. [133]	Single-node district model, thermal storage units, multiple commodities	None	None	One weekday and one weekend day for winter, summer and	Not mentioned	No	No	No

Year	Author	Energy System Model for Case Study, *(Framework)*	Normalization	Distance Metric	Clustering/ Grouping	Representative	Extreme periods	Linking Periods	Duration Curve
					transition with 7 (6) time bands (slices)				
2016	Patteeuw et al. [99]	Building heating model of nine buildings, thermal storage units, multiple commodities	No/not mentioned, Demand: region-specific divided by maximum value	L1-Norm	Using so-called “bins”, heuristic, hierarchical clustering according to Nahmmacher et al. [63] for the years of 2013-2016	existing weeks (6)	Coldest week and week with highest e-demand (same week)	No	Yes
2016	Ploussard et al. [92]	IEEE 24-bus Reliability Test System [203], multi-node electricity model, no storage technologies	No/not mentioned	Euclidean	k-means, , typical hours (snapshots)	Existing snapshot closest to the centroids	No	No	No
2016	Poncelet et al. [117]	Island electricity model for Belgium, no storage technologies or transmissions, re-evaluation with unit commitment model, **(TIMES)**	No	None	For each of the four seasons one night, day and peak electricity time slice	mean	Peak electricity time slice	No	No
2016	Poncelet et al. [147]	Single-node electricity model based on [206], no storage technologies, **(LUSYM)**	No/not mentioned, Demand: region-specific divided by maximum value	L1-Norm, Euclidean	Using so-called “bins”, heuristic, hierarchical clustering according to Nahmmacher et al. [63]	existing days, medoids	No, for heuristics days with highest and lowest value for E-demand and highest and lowest average for wind and PV	No	Yes
2016	Samsatli et al. [23]	Multi-node hydrogen-electricity model for Great Britain, multiple hydrogen storage units, multiple commodities	No	No	Season-based (four seasons, work days and weekend days)	(probably) mean	No	Yes	No
2016	Schütz et al. [144]	Building model, thermal and battery storage units, multiple commodities	Min-max normalization	Euclidean	k-means k-medians k-medoids k-centers	centroids medians medoids centers	No	No	No
2016	Stenzel et al. [44]	unit commitment of building electricity	No	None	downsampling	means	No	Yes	No

Year	Author	Energy System Model for Case Study, *(Framework)*	Normalization	Distance Metric	Clustering/ Grouping	Representative	Extreme periods	Linking Periods	Duration Curve
		model with battery storage							
2016	Wakui et al. [119]	Building model, thermal and battery storage units, multiple commodities	No	No	Season based	(probably) mean	Peak summer day and peak winter day	No	No
2016	Wogrin et al. [88]	Single-node electricity model, pumped hydro and battery storage	No/not mentioned	Euclidean	k-means (98 typical time steps (system states))	centroids	No, but the first and last hour of the time horizon were manually added	Yes	No
2017	Bahl et al. [180]	District model from Voll et al. [108], no storage technologies, multiple commodities	No/not mentioned (attributes of same scale clustered)	(probably) Euclidean	k-means, typical hours (snapshots)	centroids	Feasibility time steps (peak values) and operation optimization for full time series	No	No
2017	Brodrick et al. [149]	unit commitment of an integrated solar combined cycle, no storage technologies, multiple commodities	Z-normalization	Euclidean	k-means	centroids	No	No	No
2017	Härtel et al. [91]	Multi-node transmission expansion planning model, no storage technologies	Either normed by highest value per market or highest value across all markets	Euclidean	k-means, k-medoids, hierarchical, systematic sampling, moment-matching, , typical hours (snapshots)	Centroids, medoids, sample points	Heurisitc defining new cluster centers if 95% of a cluster's data points are below or above a 6h moving average, with the lowest or highest chosen as the new cluster center	No	No
2017	Heuberger et al. [176]	Single-node electricity model with carbon capture and storage and grid-level storage	Yes, but not mentioned which	Euclidean	k-means	means	Day with annual electricity peak demand	No	No
2017	Marquant et al. [153]	District heating model, thermal and battery storage units, multiple commodities	No/not mentioned	Euclidean	k-medoids	medoids	Peak electricity and peak heating days	No	Yes
2017	Moradi et al. [131]	Sinlge-node model of an energy hub, thermal and battery	No	No	Season-based (one work day	(probably) mean	No	No	No

Year	Author	Energy System Model for Case Study, *(Framework)*	Normalization	Distance Metric	Clustering/ Grouping	Representative	Extreme periods	Linking Periods	Duration Curve
		storage, multiple commodities			and one weekend day per spring, summer, autumn and winter)				
2017	Pfenninger et al. [43]	Multi-node electricity model for Great Britain, pumped hydro and battery storage units	Normalized by the maximum value across all time steps and model zones	Euclidean	k-means, hierarchical, downsampling, heuristics	centroids, medoids	Min/max solar and wind days, wind and pv weeks and wind-demand weeks	No	No
2017	Renaldi et al. [66]	Single-node district heating system, long- and short-term thermal storage units, multiple commodities	No	None	Multiple time grids for different storage technologies	Downsampled 3h steps for long-term storage	No	Yes	No
2017	Timmerman et al. [112]	Two business park models (one based on the model of Voll et al. [108]), thermal and electrical storage units, multiple commodities, **(Syn-E-Sys)**	No	No	Season and weekday-based (4x2x4 6h intervals)	(probably) mean	No	Yes	No
2017	Schütz et al. [105]	Building model, thermal and battery storage units, multiple commodities	No	No	Monthly average (one typical day per month and weighted)	(probably) mean	No	No	No
2017	Sun et al. [141]	Customer or unit partitioning/ none (just approach)	Time steps wise (in period) average s divided by maximum value of each customer	Likelihood-function	Vine-copula mixture model	None	No	No	No
2017	Teichgräber et al. [150]	Oxyfuel natural gas plant, liquid oxygen storage, multiple commodities	Z-Normalization	Euclidean	k-means	centroids	No	No	No

Year	Author	Energy System Model for Case Study, *(Framework)*	Normalization	Distance Metric	Clustering/ Grouping	Representative	Extreme periods	Linking Periods	Duration Curve
2017	vom Stein et al. [84]	Multi-node electricity dispatch model for Europe, pumped hydro storage	No	L1-Norm	Clustering of consecutive time steps with objective to minimize gradients within clusters	mean	No	Yes (clustering of consecutive time steps)	No
2017	Yang et al. [207]	Customer or unit partitioning/ none (just approach)	Z-normalization	Shape-based distance	k-shape	none	No	No	No
2017	Zhu et al. [208] (refers to [61])	Building model for an airport in China optimizing economics or CO_2 emissions, no storage technologies, but start-up and shut-down costs	Yes, but not mentioned which	Euclidean	k-medoids (only three season-specific typical days)	medoids	No	No	No
2018	Almaimouni et al. [142]	Single-node capacity expansion planning for electricity, validated with rolling horizon unit commitment, no storage technologies	Normalize by $\sqrt{m-1}$ with m as number of days, principal components	Euclidean	k-means	centroids	No	No	Only as error estimator
2018	Bahl et al. [181]	District model from Voll et al. [108] and a single-node pump system, no storage technologies, multiple commodities	No/not mentioned (attributes of same scale clustered)	Euclidean	k-means, typical hours (snapshots)	undersestimators from minimum values of each cluster	Feasibility time steps (peak values) and operation optimization for full time series	No	No
2018	Bahl et al. [79]	District model from Voll et al. [108] with additional heat and cold storage units, multiple commodities	Yes, but not mentioned which	Euclidean	k-medoids (daily clustering and segmentation)	medoids further segmented	Feasibility time steps (peak values) and operation optimization for full time series	No	No
2018	Brodrick et al. [102] refers to [149]	unit commitment of an integrated solar combined cycle, no storage technologies, multiple commodities	Z-normalization	Euclidean	k-means (6 representative days) further reduced to three extreme hours	centroids	Three extreme hours	No	No
2018	Gabrielli et al. [21]	Single-node district model, thermal, battery and hydrogen storage, multiple commodities	No/not mentioned	Not mentioned (probably Euclidean/ default for	k-means	centroids	Maximum and minimum values of the demand profiles	Yes	No

Year	Author	Energy System Model for Case Study, *(Framework)*	Normalization	Distance Metric	Clustering/ Grouping	Representative	Extreme periods	Linking Periods	Duration Curve
				Matlab k-means)					
2018	Kotzur et al. [48]	Three single-node models (CHP system, residential building, island system), thermal, battery and hydrogen storage, multiple commodities	Min-max normalization	Euclidean	k-means, averaging, k-medoids, hierarchical, typical days and typical weeks	centroids medoids	Peak periods heat and electricity demand, minimum PV feed-in	No	No
2018	Kotzur et al. [20]	Three single-node models (CHP system, residential building, island system), thermal, battery and hydrogen storage, multiple commodities	Min-max normalization	Euclidean	Exact k-medoids	medoids	No	Yes	No
2018	Lara et al. [30]	Multi-node electricity model for Texas, multiple storage units (e.g., lithium-ion, lead-acid, and flow batteries)	Mentioned, but not which one	Euclidean	k-means for the years of 2004-2010	centroids	No	No, 50% SOC heuristic	No
2018	Liu et al. [151]	Multi-node electricity model for Texas (greenfield capacity expansion planning), storage units and ramping constraints considered	Z-Normalization	DTW distance, Euclidean as benchmark	(k-means initially), hierarchical, k-means as benchmark	medoids, centroids for k-means-benchmark	No	No	No
2018	Mallapragada et al. [45] (2004-2010)	Electricity capacity expansion planning model for Texas, no storage or transmission units, ramping in production cost simulation considered	Min-max normalization between 0 and 2	Euclidean and L1-Norm (as benchmark)	4 seasons and 4 daily segments vs. k-means	medoids	No	No, refers to [30], 50% SOC heuristic	No
2018	Neniškis et al. [57]	Electricity and district heat model of Lithuania, pumped hydro storage, multiple commodities, **(MESSAGE)**	No	None	Workday and weekend day either for four seasons or for twelve months	means	No (but synthesized wind time series)	No	No
2018	Pineda et al. [77]	Multi-node electricity model of Europe, in-	Mentioned, but	Euclidean	Hierarchical	medoids	No	Yes, by clustering adjacent periods	No

Year	Author	Energy System Model for Case Study, *(Framework)*	Normalization	Distance Metric	Clustering/ Grouping	Representative	Extreme periods	Linking Periods	Duration Curve
		traday, interday storage and ramping constraints considered	not which one						
2018	Schütz et al. [64]	Building model, thermal and battery storage units, multiple commodities	Min-max normalization	Euclidean	k-means k-medians k-medoids k-centers	centroids medians medoids centers	No	No	No
2018	Stadler et al. [209]	Building model, thermal and battery storage units, multiple commodities	No/not mentioned	(probably) Euclidean	k-medoids	medoids	No	No	No
2018	Teichgräber et al. [157]	Two minimal unit commitment problems: An electricity storage model and a gas turbine dispatch model	Element-wise Z-Normalization	Euclidean, Dynamic Time Warping, Shape-based Distance	k-means k-medoids Barycenter Averaging k-shape hierarchical	Centroid, medoids	No	No	No
2018	Tejada-Arango et al. [25]	unit commitment of the Spanish electricity system, battery and pumped hydro storage	Yes, but not mentioned what kind of normalization	(probably) Euclidean	k-medoids for RP, k-means for SS	medoids centroids	No	Yes	No
2018	Tejada-Arango et al. [89]	unit commitment of the IEEE 14 bus electricity model, battery and pumped hydro storage	No/not mentioned (attributes of same scale clustered)	Euclidean	k-means (for typical hours)	centroids	No	No	No
2018	Tupper et al. [210]	unit commitment of the IEEE 30 bus electricity model with wind generation, no storage technologies	No/not mentioned	Euclidean, band distance	k-medoids	medoids	No	No	No
2018	Van der Heijde et al. [100]	Single-node district heating model, thermal storage	No/not mentioned	L1-Norm	Using so-called “bins” and four seasons	existing weeks	No, but each season needs to contain at least one typical week	Yes	Yes
2018	Voulis et al. [148]	Customer or unit partitioning/ none (just approach)	Normalization by maximum e-demand	Euclidean	k-means (spatio-temporal differentiation between workdays, weekends, neighborhoods, districts	Centroids	No	No	No

Year	Author	Energy System Model for Case Study, *(Framework)*	Normalization	Distance Metric	Clustering/ Grouping	Representative	Extreme periods	Linking Periods	Duration Curve
					and municipalities)				
2018	Welder et al. [24]	Multi-node model for power-to- hydrogen in Germany, hydrogen storage technologies, multiple commodities	Min-max normalization	Euclidean	hierarchical	medoids	No	Yes	Yes
2019	Baumgärtner et al. [83]	District model from Voll et al. [108] with additional heat and cold storage units and a single-node pump system, multiple commodities	No/not mentioned	Euclidean	k-medoids	Segmented under- and overestimators	Feasibility time steps (peak values) and operation optimization for full time series	No	No
2019	Baumgärtner et al. [82]	Single-node model for industrial site based on Baumgärtner et al. [211] with heat, cold and battery storage, Multi-node model for Germany with battery and hydrogen storage, multiple commodities	No/not mentioned	Euclidean	k-means	Centroids, segmented under- and overestimators	Feasibility time steps (peak values) and operation optimization for full time series	Yes	No
2019	Gabrielli et al. [160]	Single-node district model, thermal, battery and hydrogen storage, multiple commodities	No/not mentioned	Not mentioned (probably Euclidean/ default for Matlab k-means)	k-means	centroids	Maximum and minimum values of the demand profiles	Yes	No
2019	Hilbers et al. [161]	Single-node electricity model of Great Britain, no storage technologies	Yes, but not mentioned which	Euclidean	Samples (hourly) As benchmark: k-medoids (days)	Existing hours As benchmark: medoids (days)	Yes with the method of sub-sampling and keeping the most expensive days	No	No
2019	Kannengießer et al. [4]	Multi-node district model and single-node island model, thermal, battery and hydrogen storage, multiple commodities	Min-max normalization	Euclidean	hierarchical	medoids	No, but operation optimization for full time series	No	Yes

Year	Author	Energy System Model for Case Study, *(Framework)*	Normalization	Distance Metric	Clustering/ Grouping	Representative	Extreme periods	Linking Periods	Duration Curve
2019	Motlagh et al. [212]	Customer or unit partitioning/ none (just approach)	No/not mentioned	Adjacency metric, in mapping parameter space: Euclidean d	Feature-based clustering or dynamic load-clustering	None	No	No	No
2019	Pavičević et al. [213]	Customer or unit partitioning/ multi-node electricity model of the western Balkan, pumped hydro storage and CHP with thermal storage, **(Dispa-SET)**	No	None	By technology and location	means	No	No	No
2019	Pöstges et al. [172]	Single-node electricity model, no storage technologies, analytically solved as peak-load-pricing model	Yes, cap-specific costs	None	Segments in the duration curve implying use of different technologies (hours)	Sorted existing hours	Yes, by determining the capacity of each component from the merit order	No	Yes
2019	Savvidis et al. [85]	unit commitment of dispatch electricity model for Germany, pumped hydro storage, **(E2M2)**	No	No	No	No	Certain time series qualities define intervals in which can be downsampled	Yes, by clustering adjacent periods	No
2019	Sun et al. [140]	Multi-node electricity model of Great Britain with intraday storage	Min-max normalization, dimensionality reduction applied	Euclidean	hierarchical	medoids	No	No	No
2019	Teichgräber et al. [47]	Two minimalUC problems: An electricity storage model and a gas turbine dispatch model	Element-wise Z-Normalization	Euclidean, Dynamic Time Warping, Shape-based Distance	k-means k-medoids Barycenter Averaging k-shape hierarchical	Centroid, medoids	No	No	No
2019	Van der Heijde et al. [26]	Multi-node district heating model, thermal storage	No/not mentioned	L1-Norm	Using so-called “bins”	existing days	No, but rearranging the typical days to the original sequence using a MIP	Yes	Yes

Year	Author	Energy System Model for Case Study, *(Framework)*	Normalization	Distance Metric	Clustering/ Grouping	Representative	Extreme periods	Linking Periods	Duration Curve
2019	Yokoyama et al. [73]	Building model for two hotels and four office buildings, no storage technologies, but multiple commodities	No	None	downsampling	means	No	No	No
2019	Zatti et al. [145]	District model of Parma university campus and building model, thermal and battery storage, multiple commodities	Min-max normalization	Euclidean	(k-means, k-medoids) k-MILP (modification of k-medoids)	(centroids), medoids	Automatically integrating atypical days	No	No
2019	Zhang et al. [214]	Single-node electricity model consisting of hydro, PV and wind power plants with reservoir storage	No/ not mentioned	Euclidean	k-means	means	No, but used Vine-Copula, ARMA-model and latin hypercube sampling to generate scenarios	No	No

C. Customer and Unit Partitioning

“It is noteworthy that aggregations based on time series do not necessarily mean the aggregation of the temporal dimension. Instead, similar time series can also be clustered in order to generate a smaller number of possible technologies or regions with similar demand behavior or similar technologies. This is referred to as customer [141] and unit [213] partitioning. Given the fact that in some cases new methods were first introduced in this field of time series aggregation, a short overview of methods used in this field could imply possible approaches for the temporal aggregation methods presented above.

One of these examples was published by Alzate et al. [198], who used spectral clustering with an out-of-sample extension to cluster customer profiles for electricity demand. For this, 123 time series were used for training and 122 for validation. The approach significantly outperformed the selection found by k-means clustering. Benítez et al. [201] implemented a modified version of k-means for customer partitioning that was not only capable of clustering groups of customers with their daily profiles, but also with respect to their yearly profiles. This means that each cluster center of a (daily) period followed a trajectory throughout the year resulting in representative yearly profiles. Sun et al. [141] used a C-vine copula-based mixture model to cluster residential electricity demands by maximizing a log-likelihood function, which slightly outperformed k-means clustering but was computationally significantly more demanding. Yang et al. [207] used k-shape clustering for forming typical residential daily profiles before applying it to time series aggregation purposes. This highlights the importance of cross-linking different research fields within energy system analysis. Recently, Motlagh et al. [212] applied two different clustering algorithms on electricity demands for customer partitioning. The first one included a preliminary principal component analysis to decrease the complexity, followed by clustering using the adjacency metric, while the second one was model-based and transferring the profiles into the phase space. Then, a mapping strategy based on neural regression was used and the Euclidean distance between the map parameters was calculated, which outperformed the first, feature-based approach.” (Hoffmann et al. [1])

With respect to unit partitioning, Pavičević et al. [213] introduced three levels of potential clustering scopes. The first was based on similar characteristics if the components were small, at the same location, with the same commodities and comparable temporal characteristics, while the second focused on the same location and the same commodities, and the third only on the same commodities, such as averaged heat and electricity demands of industrial sites and residential buildings. Haikarainen et al. [204] used k-means clustering for grouping different nodes in an energy network that were then represented as a single component with averaged costs and the traits of all of the included technologies (supply, demand, storage). Based on decisions made for a coarse clustering, the number of clusters was stepwise increased, and, in a final run, all binary decision variables were retained and a linear program was solved for the fully resolved energy grid. This means that the clustering was not based on temporal features, but on spatial ones. This means that the units were merged based on their distance to each other, not their traits.

This highlights that temporal, spatial and technological information can theoretically be aggregated based on their own or based on each other. Thus, time series aggregation is traditionally seen as the aggregation of time series derived from temporal information.

D. An Example for Time Series Normalization

“In the following, a hypothetical time series is normalized as per equations (2.1)-(2.3). The time series is given as six-dimensional row vectors including only positive values, representing 4 h intervals of electricity demand in kW for January 1st:

$$x = [1 \quad 2 \quad 3 \quad 3 \quad 2 \quad 1] \tag{D.1}$$

Min-Max-Normalization:

$$\begin{aligned} x_{Min-Max} &= \frac{x - \min(x)}{\max(x) - \min(x)} = \frac{x - 1}{3 - 1} = \frac{[0 \quad 1 \quad 2 \quad 2 \quad 1 \quad 0]}{2} \\ &= [0 \quad 0.5 \quad 1 \quad 1 \quad 0.5 \quad 0] \end{aligned} \tag{D.2}$$

Max-Normalization:

$$x_{Max} = \frac{x}{\max(x)} = \frac{x}{3} = \frac{[1 \quad 2 \quad 3 \quad 3 \quad 2 \quad 1]}{3} = \left[\frac{1}{3} \quad \frac{2}{3} \quad 1 \quad 1 \quad \frac{2}{3} \quad \frac{1}{3}\right] \tag{D.3}$$

Z-Normalization:

$$x_Z = \frac{x - \mu}{\sigma} \tag{D.4}$$

$$\mu = \frac{1}{N}\sum_{i=1}^{N} x_i = \frac{1}{6}(1 + 2 + 3 + 3 + 2 + 1) = 2 \tag{D.5}$$

$$\begin{aligned} \sigma &= \sqrt{\frac{1}{N}\sum_{i=1}^{N}(x_i - \mu)^2} \\ &= \sqrt{\frac{1}{6}((1-2)^2 + (2-2)^2 + (3-2)^2 + (3-2)^2 + (2-2)^2 + (1-2)^2)} \\ &= \frac{2}{\sqrt{6}} \end{aligned} \tag{D.6}$$

This means:

$$x_Z = \frac{x - 2}{\frac{2}{\sqrt{6}}} = \frac{\sqrt{6}}{2}[-1 \quad 0 \quad 1 \quad 1 \quad 0 \quad -1] = \left[-\frac{\sqrt{6}}{2} \quad 0 \quad \frac{\sqrt{6}}{2} \quad \frac{\sqrt{6}}{2} \quad 0 \quad -\frac{\sqrt{6}}{2}\right] \tag{D.7}$$

” (Hoffmann et al. [1])

E. Clustering Algorithms Applied in the Literature

"One of the most common partitional clustering algorithms used in energy system optimization is the **k-means** algorithm, which has been used in a variety of studies [20, 21, 30, 43, 48, 64, 68, 74, 79, 83, 88-92, 102, 142-146, 148-151, 157, 160, 176, 177, 179, 180, 200, 202, 214]. The objective of the k-means algorithm is to minimize the sum of the squared distances between all cluster members of all clusters and the corresponding cluster centers, i.e.:

$$\min \sum_{k=1}^{N_k} \sum_{p \in C_k} \mathrm{dist}\left(x_p, r_k\right)^2 \tag{E.1}$$

The distance metric in this case is the Euclidean distance between the hyperdimensional period vectors with the dimension $\dim\left(\mathrm{vec}(T \times A)\right)$ and their cluster representatives $r_{k,a,t}$, i.e.:

$$\mathrm{dist}\left(x_p, r_k\right) = \sqrt{\sum_{a=1}^{N_a} \sum_{t=1}^{N_t} \left(x_{p,a,t} - r_{k,a,t}\right)^2} \tag{E.2}$$

Here, the cluster centers are defined as the centroid of each cluster, i.e.:

$$r_{k,a,t} = \frac{1}{|C_k|} \sum_{p \in C_k} x_{p,a,t} \tag{E.3}$$

This NP-hard problem is generally solved by an adopted version [81] of Lloyd's algorithm [80], a greedy algorithm that heuristically converges to a local minimum. As multiple runs are performed in order to improve the local optimum, improved versions (such as k-means++) for setting initial cluster centers have also been proposed in the literature [215].

The only difference regarding the **k-medoids** algorithm is that the cluster centers are defined as samples from the dataset that minimize the sum of the intra-cluster distances, i.e., that are closest to the clusters' centroids.

$$r_k = \underset{x_l \in C_k}{\mathrm{argmin}} \frac{1}{N_k} \sum_{p \in C_k} \mathrm{dist}\left(x_p, x_l\right)^2 \tag{E.4}$$

This clustering algorithm was used by numerous authors [20, 25, 47, 48, 61, 64, 79, 83, 91, 144, 145, 152, 153, 157, 158, 161, 208-

210], either by using the Partitioning Around Medoids (PAM) introduced by Kaufman et al. [216] or by using a mixed-integer linear program formulation introduced by Vinod et al. [156] and used in several studies [20, 47, 48, 61, 144, 157, 208]. The mixed-integer linear program can be formulated as follows:

$$\min \sum_{i=1}^{N_p} \sum_{j=1}^{N_p} d(x_i, x_j) \times z_{i,j} \tag{E.5}$$

Subject to:

$$\sum_{j=1}^{N_p} z_{i,j} = 1 \; \forall \, j \in 1, \dots, N_i \tag{E.6}$$

$$z_{i,j} \leq y_i \; \forall \, i, j \in 1, \dots, N_i \tag{E.7}$$

$$\sum_{i=1}^{N_i} y_i = N_k \tag{E.8}$$

In a number of publications [47, 48, 64, 91, 144, 145, 157], k-medoids clustering was directly compared to k-means clustering. The general observation is that k-medoids clustering is more capable of preserving the intra-period variance, while k-means clustering underestimates extreme events more gravely. Nevertheless, the medoids lead to higher root-mean-square errors compared to the original time series. This leads to the phenomenon that k-medoids outperforms k-means in the cases of energy systems sensitive to high variance, as in self-sufficient buildings, e.g., as shown by Kotzur et al. [48] and Schütz et al. [144]. In contrast to that, k-means outperforms k-medoids clustering in the case of smooth demand time series and non-rescaled medoids that do not match the overall annual demand in the case of k-medoids clustering, as shown by Zatti et al. [145] for the energy system of a university campus.

In contrast to partitional clustering algorithms that iteratively determine a set consisting of k clusters in each iteration step, agglomerative clustering algorithms such as Ward's **hierarchical** algorithm [78] stepwise merge clusters aimed at minimizing the increase in intra-cluster variance

$$\mathrm{SSE} = \sum_{p \in C_k} \mathrm{dist}\left(x_p, r_k\right)^2 \tag{E.9}$$

in each merging step until the data is agglomerated to k clusters. The algorithm is thus deterministic and does not require multiple random starting point initializations. Analogously to k-means and k-medoids, the cluster centers can either be represented by their centroids [47, 157] or by their medoids [4, 24, 43, 47, 48, 63, 77, 91, 140, 147, 151, 157]. The general property that centroids underestimate the intra-period variance more severely due to the averaging effect is equivalent to the findings when using k-means instead of k-medoids.

Apart from the frequently used clustering algorithms in the literature, two more clustering algorithms were used in the context of determining typical periods based on unsorted time intervals of consistent lengths.

k-medians clustering is another partitional clustering algorithm that is closely related to the k-means algorithm and has been used in other studies [64, 144]. Taking into account that the Euclidean distance is only the special case for $\gamma = 2$ of the Minkowski distance [217]

$$\mathrm{dist}\left(x_p, r_k\right) = \left(\sum_{a=1}^{N_a} \sum_{t=1}^{N_t} \left| x_{p,a,t} - r_{k,a,t} \right|^{\gamma} \right)^{\frac{1}{\gamma}} \tag{E.10}$$

k-medians generally tries to minimize the sum of the distances of all data points to their cluster center in the Manhattan norm, i.e., for $\gamma = 1$ and the objective function [218, 219]:

$$\min \sum_{k=1}^{N_k} \sum_{p \in C_k} \mathrm{dist}\left(x_p, r_k\right) \quad \text{with} \quad \mathrm{dist}\left(x_p, r_k\right) = \sum_{a=1}^{N_a} \sum_{t=1}^{N_t} \left| x_{p,a,t} - r_{k,a,t} \right| \tag{E.11}$$

For this, the L1 distance is usually used in the assignment step [218] and the median is calculated in each direction to minimize the L1 distance within each cluster [219]. However, Schütz et al. [64, 144] used the Euclidean distance (like for k-means) in the assignment step to isolate the influence of using dimension-wise medians instead of dimension-wise means (i.e., centroids). Thus, all values come from the original dataset, but not necessarily from the same candidates [64].

Moreover, Schütz et al. [64, 144] used **k-centers** clustering, which minimizes the maximum distance of all candidates to its cluster center, i.e., according to Har-Peled [220]

$$\min_{C,|C|=k}\left(\max_{p\in C_k}\left(\mathrm{dist}\left(x_p,r_k\right)\right)\right) \quad \text{with} \quad \mathrm{dist}\left(x_p,r_k\right) = \sqrt{\sum_{a=1}^{N_a}\sum_{t=1}^{N_t}\left(x_{p,a,t}-r_{k,a,t}\right)^2} \tag{E.12}$$

The last group of clustering algorithms applied for time series aggregation in energy system models is time shift-tolerant clustering algorithms. These algorithms not only compare to the values of different time series at single time steps (pointwise), but also compare values along the time axis with those of other time series (pairwise). In the literature [47, 157], **dynamic time warping** (DTW) and the **k-shape** algorithm are used, both of which are based on distance measures that are not sensitive to phase shifts within a typical period, which is the case for the Euclidean distance. The dynamic time-warping distance is defined as:

$$\mathrm{dist}\left(x_p,r_k\right)=\min_{w}\sqrt{\sum_{l=1}^{L}w_l} \tag{E.13}$$

Here, w describes the so-called warping path, which is the path of minimal deviations across the matrix of cross-deviations between any entry of x_p and any entry of r_k [47, 221]. The cluster representative r_k are determined using DTW Barycenter Averaging, which is the centroid of each time series value (within an allowed warping window) assigned to the time step [222]. Moreover, a warping window [47, 157] can be determined that limits the assignment of entries across the time steps. Shape-based clustering uses a similar algorithm and tries to maximize the cross-correlation amongst the periods. Here, the distance measure to be minimized is the cross-correlation and the period vectors are uniformly shifted against each other to maximize it [47, 157, 221, 223]. It must be highlighted that both dynamic time warping and shape-based distance, have only been applied on the clustering of electricity prices, i.e. only one attribute [47, 157]. Moreover, Liu et al. [151] also applied dynamic time warping to demand, solar and wind capacity

factors simultaneously. However, it is unclear how it was guaranteed that different attributes were not compared to each other within the warping window, which remains a field of future research. Furthermore, a band distance, which is also a pairwise rather than a pointwise distance measure, was used in a k-medoids algorithm by Tupper et al. [210], leading to significantly less loss of load when deriving operational decisions for the next day using a stochastic optimization model." (Hoffmann et al. [1])

F. Modified Feature-Based Merging

“Apart from the methods that are based on the direct clustering of the time series’ values or periods, a number of methods exist that group time series in a consecutive manner [59] or by means of other features, such as sorted time series (i.e. duration curves) [4, 24, 26, 97-100, 147, 152, 153, 185]. Other publications use use statistical features such as the average, variance, minimal and maximal values [68] or predefine the clusters based on additional information [93]. These methods will be presented in the following.

With respect to grouping consecutive typical periods, an early publication by Balachandra et al. [59] started by grouping daily residual load profiles by month, then applied multiple discriminant analysis to these groups and reclassified the days at the beginning or end of a group (month) to the preceding or subsequent group if they were more similar to it. This resulted in nine consecutive groups represented by their centroids. However, this aggregation was not applied to an energy system optimization.

Furthermore, a number of publications [26, 99, 100, 147] rely on the principle introduced by Poncelet et al. [185]. For this, the normalized duration curves were placed into bins, i.e., how many hours of the year surpass a certain level between zero and the maximum level of the specific attribute. The same was performed for each candidate day. Then, the sum of absolute differences between the hours at which the reference curve surpassed a bin border and the hours at which the curve derived from a linear combination of a given number of candidates surpassed the same bin borders was minimized in a mixed-integer linear program.

Another approach aimed at reproducing a yearly duration curve was introduced by de Sisternes et al. [97, 98]. Here, the duration curve of power feed-in by wind and solar at a certain penetration level was calculated and approximated by an exhaustive search for a combination from a subset of typical weeks. As it was a combinatorial problem, the computation time rapidly increased for higher numbers of weeks. In a later publication [97], the variability of the selected weeks was used as an additional metric.

Instead of clustering the original time series, the yearly duration curve was approximated in a number of publications [4, 24, 152,

153]. For this, the candidate days were simply sorted prior to being clustered. This decreased the averaging effect of statistical events such as wind, as the largest value and second largest, etc. always lay in the first dimension and second dimension, etc.

With respect to the clustering of other statistical features apart from the distribution curve (duration curve), Agapoff et al. [68] applied k-means clustering to snapshots (i.e., typical time steps) and used different features for the clustering: Either absolute values or average, minimum, maximum and standard deviation of all considered regions for either price differences, non-controllable demand and generation or both. This is an extension with promising results to all thus far used clustering algorithms only applied to normalized absolute values.

Finally, yet significantly, Lythcke-Jørgensen et al. [93] introduced a so-called CHOP-method that was based on splitting the range of each attribute, in this case the power price and relative heat demand on a five-year basis, into different intervals based on important values (e.g., zero-price) and even divisions between them. Then, all values (i.e., hours) were transferred in a 2d space in which the intervals for both attributes formed a grid. From each cell, the centroid was subsequently calculated if it contained any candidate hours. As information about the chronology of these typical time steps was lost, the design of storage technologies resulted in large deviations from the reference case.

These cases highlight that methods based on well-known approaches are constantly customized for specific energy system models and improved where possible, which illustrates that the development of temporal aggregation methods is a dynamic process.” (Hoffmann et al. [1])

G.Proofs and Lemmata for Section 3.2

Lemma 1:

Given a set $X = \{x_i\}_{i=1}^{N}$ of M-dimensional real valued data vectors with $x_i = (x^1, \dots, x^M)^T$, let $\mu = (\mu^1, \dots, \mu^M)^T$ be an M-dimensional real valued data vector and let $\|\cdot\|$ be the Euclidean norm. Then

$$\mu = \frac{1}{N}\sum_{i=1}^{N} x_i \Leftrightarrow \mu^j = \frac{1}{N}\sum_{i=1}^{N} x_i^j \qquad \forall\, j = 1, \dots, M \tag{G.1}$$

is the vector that minimizes the sum of squared distances to all vectors of the set X, i.e.

$$f(\mu) = \frac{1}{N}\sum_{i=1}^{N} \|x_i - \mu\|^2 = \frac{1}{N}\sum_{i=1}^{N}\sum_{j=1}^{M} \left(x_i^j - \mu^j\right)^2 \tag{G.2}$$

Proof:

The necessary condition for a minimum is given by:

$$f_{\mu^j}(\mu) = \frac{\partial f(\mu)}{\partial \mu^j} = 0 \tag{G.3}$$

The sufficient condition for a minimum of a multidimensional function is given by the positive definiteness of the Hessian matrix:

$$H_f(\mu) := \left(\frac{\partial^2 f}{\partial \mu^i\, \partial \mu^j}\right)_{i,j=1,\dots,M} \quad \text{positive definite} \tag{G.4}$$

Inserting yields the critical point for the necessary condition:

$$\begin{aligned} f_{\mu^j}(\mu) &= \frac{\partial}{\partial \mu^j}\left(\frac{1}{N}\sum_{i=1}^{N}\sum_{j=1}^{M}\left(x_i^j - \mu^j\right)^2\right) = -\frac{2}{N}\sum_{i=1}^{N}\left(x_i^j - \mu^j\right) \\ &= -\frac{2}{N}\left(\sum_{i=1}^{N} x_i^j - N\mu^j\right) = 0 \Leftrightarrow \mu^j = \frac{1}{N}\sum_{i=1}^{N} x_i^j \qquad \forall\, j = 1, \dots, M \end{aligned} \tag{G.5}$$

and for the entries of the Hessian matrix, inserting yields:

$$\begin{aligned} f_{\mu^j\mu^j}(\mu) &= \frac{\partial^2}{(\partial \mu^j)^2}\left(\frac{1}{N}\sum_{i=1}^{N}\sum_{j=1}^{M}\left(x_i^j - \mu^j\right)^2\right) = \frac{\partial}{\partial \mu^j}\left(-\frac{2}{N}\sum_{i=1}^{N}\left(x_i^j - \mu^j\right)\right) \\ &= -\frac{2}{N}\sum_{i=1}^{N} -1 = 2 \qquad \forall\, j = 1, \dots, M \end{aligned} \tag{G.6}$$

$$\begin{aligned} f_{\mu^i\mu^j}(\mu) &= \frac{\partial^2}{\partial\mu^i\,\partial\mu^j}\left(\frac{1}{N}\sum_{i=1}^{N}\sum_{j=1}^{M}\left(x_i^j-\mu^j\right)^2\right) \\ &= \frac{\partial}{\partial\mu^i}\left(-\frac{2}{N}\sum_{i=1}^{N}\left(x_i^j-\mu^j\right)\right)=0 \qquad\qquad \forall\, i,j=1,\dots,M\wedge i\neq j \end{aligned} \tag{G.7}$$

Therefore, the $M\times M$ Hessian matrix takes the following form:

$$H_f(\mu) \coloneqq \begin{pmatrix} 2 & 0 & \cdots & 0 & 0\\ 0 & 2 & \cdots & 0 & 0\\ \vdots & \vdots & \ddots & \vdots & \vdots\\ 0 & 0 & \cdots & 2 & 0\\ 0 & 0 & \cdots & 0 & 2 \end{pmatrix} = 2I_M \tag{G.8}$$

with I_M being the $M\times M$ identity matrix.

Lastly, the positive definiteness of the Hessian matrix in the critical point needs to be shown. Positive definiteneness can e.g. be shown using Eigenvalues as sufficient condition, which must be strictly positive for the given matrix. Therefore, it must hold that:

$$\det(H_f(\mu)-\lambda I)=0 \;\wedge\; \lambda>0 \tag{G.9}$$

Insertion of Equation (G.8) yields:

$$\det(2I_M-\lambda I_M)=(2-\lambda)^M=0\Leftrightarrow\lambda=2>0 \tag{G.10}$$

Since the unique Eigenvalue of the Hessian matrix is strictly larger than 0, $f(\mu)$ is minimized for $\mu=\frac{1}{N}\sum_{i=1}^{N}x_i$. ■

Lemma 2:

Note: The following lemma (i.e. the problem definition and the proof) is derived from Sifa et al. [184], who used it to show that a maxoid is the point of a dataset which is furthest away from the dataset's centroid. Analogously, we use this lemma to show that a dataset's medoid is defined as that sample point which is closest to the dataset's centroid.

Given a set $X=\{x_i\}_{i=1}^{N}$ of real valued data vectors, let $\mu=\frac{1}{N}\sum_{i=1}^{N}x_i$ be the sample mean and $\|\cdot\|$ be the Euclidean norm. Further, let x_j and x_k be two sample points of the dataset X, i.e. $x_j, x_k\in X$, then

$$\frac{1}{N}\sum_{i=1}^{N}\|x_j-x_i\|^2\geq\frac{1}{N}\sum_{i=1}^{N}\|x_k-x_i\|^2 \tag{G.11}$$

implies that

$$\left\|x_j - \mu\right\|^2 \geq \|x_k - \mu\|^2 \tag{G.12}$$

This means that x_k is closer to the dataset's centroid than x_j (Equation (G.12)) if the sum of squared Euclidean distances between x_k and all the other sample points in X is smaller than the respective value for x_j (Equation (G.11)).

With respect to maxoids and medoids, this means in particular that the maxoid is the sample point furthest away from a dataset's centroid because it maximizes the sum of squared Euclidean distances whereas the medoid is the sample point is the sample point closest to the centroid as it minimizes the sum of Euclidean distances.

Proof:

The left hand side of the equation above can be expanded and the squared expression can be resolved as follows:

$$\begin{aligned}
\frac{1}{N}\sum_{i=1}^{N}\left\|x_j - x_i\right\|^2 &= \frac{1}{N}\sum_{i=1}^{N}\left\|(x_j - \mu) - (x_i - \mu)\right\|^2 \\
&= \frac{1}{N}\sum_{i=1}^{N}\left(\left\|x_j - \mu\right\|^2 - 2(x_j - \mu)^T(x_i - \mu) + \|x_i - \mu\|^2\right) \\
&= \left\|x_j - \mu\right\|^2 - 2(x_j - \mu)^T\left(\frac{1}{N}\sum_{i=1}^{N}x_i - \frac{1}{N}\sum_{i=1}^{N}\mu\right) + \frac{1}{N}\sum_{i=1}^{N}\|x_i - \mu\|^2 \\
&= \left\|x_j - \mu\right\|^2 - 2(x_j - \mu)^T\left(\mu - \frac{1}{N}N\mu\right) + \frac{1}{N}\sum_{i=1}^{N}\|x_i - \mu\|^2 \\
&= \left\|x_j - \mu\right\|^2 + \frac{1}{N}\sum_{i=1}^{N}\|x_i - \mu\|^2
\end{aligned} \tag{G.13}$$

As this transformation is also valid for the right hand side of the equation above, one yields:

$$\frac{1}{N}\sum_{i=1}^{N}\|x_k - x_i\|^2 = \|x_k - \mu\|^2 + \frac{1}{N}\sum_{i=1}^{N}\|x_i - \mu\|^2 \tag{G.14}$$

and thus:

$$\begin{aligned}
&\left\|x_j - \mu\right\|^2 + \cancel{\frac{1}{N}\sum_{i=1}^{N}\|x_i - \mu\|^2} \geq \|x_k - \mu\|^2 + \cancel{\frac{1}{N}\sum_{i=1}^{N}\|x_i - \mu\|^2} \\
&\Leftrightarrow \left\|x_j - \mu\right\|^2 \geq \|x_k - \mu\|^2 \quad \blacksquare
\end{aligned} \tag{G.15}$$

Lemma 3:

Given two sets $X = \{x_{i,k}\}_{i=1,k=1}^{N\times K}$ and $Y = \{y_i\}_{i=1}^{N}$ of real valued m-dimensional data vectors, let $\mu_j = \frac{1}{N}\sum_{k=1}^{K} x_{j,k}$ be the sample mean, let $z_{i,j}$ be an $N \times N$ matrix and let $\|\cdot\|$ be the Euclidean norm. Then the optimal solution y_i^* of the following two mixed-integer linear programs is identical:

$$\begin{aligned} &\min \sum_{i=1}^{N}\sum_{j=1}^{N}\sum_{k=1}^{K} \|y_i - x_{j,k}\|^2 \times z_{i,j} \\ &\text{s.t.} \sum_{i=1}^{N} z_{i,j} = 1 \;\forall\, j \\ &\quad \sum_{j=1}^{N} z_{i,j} = 1 \;\forall\, i \\ &\quad z_{i,j} \in \{0,1\} \end{aligned} \qquad \begin{aligned} &\min \sum_{i=1}^{N}\sum_{j=1}^{N} \|y_i - \mu_j\|^2 \times z_{i,j} \\ &\text{s.t.} \sum_{i=1}^{N} z_{i,j} = 1 \;\forall\, j \\ &\quad \sum_{j=1}^{N} z_{i,j} = 1 \;\forall\, i \\ &\quad z_{i,j} \in \{0,1\} \end{aligned} \tag{G.16}$$

Proof:

This is a direct consequence of **Lemma 2**. For the optimal solution $y_i^{*,1}$, the following holds for the left minimization problem with F as the feasible solution space:

$$\sum_{i=1}^{N}\sum_{j=1}^{N}\sum_{k=1}^{K} \|y_i^{*,1} - x_{j,k}\|^2 \times z_{i,j} \leq \sum_{i=1}^{N}\sum_{j=1}^{N}\sum_{k=1}^{K} \|y_i - x_{j,k}\|^2 \times z_{i,j} \quad \forall \; y_i \in F \tag{G.17}$$

Analogously, for the optimal solution $y_i^{*,2}$ of the right optimization problem we yield:

$$\sum_{i=1}^{N}\sum_{j=1}^{N} \|y_i^{*,2} - \mu_j\|^2 \times z_{i,j} \leq \sum_{i=1}^{N}\sum_{j=1}^{N} \|y_i - \mu_j\|^2 \times z_{i,j} \quad \forall \; y_i \in F \tag{G.18}$$

From **Lemma 2** we extract the following relationship:

$$\sum_{k=1}^{K} \|y_i - x_{j,k}\|^2 = K\|y_i - \mu_j\|^2 + \sum_{i=1}^{K} \|x_{j,k} - \mu_j\|^2 \tag{G.19}$$

Inserting this into the upper equation, we yield:

$$\begin{aligned} &\sum_{i=1}^{N}\sum_{j=1}^{N}\left(K\|y_i^{*,1} - \mu_j\|^2 + \sum_{i=1}^{K} \|x_{j,k} - \mu_j\|^2\right) \times z_{i,j} \\ &\leq \sum_{i=1}^{N}\sum_{j=1}^{N}\left(K\|y_i - \mu_j\|^2 + \sum_{i=1}^{K} \|x_{j,k} - \mu_j\|^2\right) \times z_{i,j} \quad \forall \; y_i \in F \end{aligned} \tag{G.20}$$

Removing identical parts on both sides of the equation leads to:

$$\sum_{i=1}^{N}\sum_{j=1}^{N}\left\|y_i^{*,1}-\mu_j\right\|^2\times z_{i,j}\leq\sum_{i=1}^{N}\sum_{j=1}^{N}\left\|y_i-\mu_j\right\|^2\times z_{i,j}\quad\forall\quad y_i\in F \tag{G.21}$$

Which is identical to the optimal solution of the right optimization problem. Therefore:

$$y_i^{*,1}=y_i^{*,2}\quad\blacksquare \tag{G.22}$$

Lemma 4:

Given two sets $X=\{x_i\}_{i=1}^{N}$ and $Y=\{y_i\}_{i=1}^{N}$ of real valued m-dimensional data vectors, let $z_{i,j}$ be a $N\times N$ matrix and let $\|\cdot\|$ be the Euclidean norm. Then the linear relaxation of the minimization problem

$$\begin{aligned}&\min\sum_{i=1}^{N}\sum_{j=1}^{N}\left\|y_i-x_j\right\|^2\times z_{i,j}\\&\text{s.t.}\sum_{i=1}^{N}z_{i,j}=1\;\forall\,j\\&\quad\sum_{j=1}^{N}z_{i,j}=1\;\forall\,i\\&\quad\quad z_{i,j}\in\{0,1\}\end{aligned} \tag{G.23}$$

is convex if y_i and x_j are known.

Proof:

The linear relaxation of the above mentioned minimization problem is:

$$\begin{aligned}&\min\sum_{i=1}^{N}\sum_{j=1}^{N}\left\|y_i-x_j\right\|^2\times z_{i,j}\\&\text{s.t.}\sum_{i=1}^{N}z_{i,j}=1\;\forall\,j\\&\quad\sum_{j=1}^{N}z_{i,j}=1\;\forall\,i\\&\quad\quad z_{i,j}\leq 1\\&\quad\quad z_{i,j}\geq 0\end{aligned} \tag{G.24}$$

Substitution by $c_{i,j} \coloneqq \left\|y_i - x_j\right\|^2$ as **parameter** yields:

$$\begin{aligned} &\min(c_{1,1} \quad \dots \quad c_{1,N} \quad c_{2,1} \quad \dots \quad c_{N,N})(z_{1,1} \quad \dots \quad z_{1,N} \quad z_{2,1} \quad \dots \quad z_{N,N})^T \\ &\text{s.t.} \sum_{i=1}^{N} z_{i,j} = 1 \; \forall \, j \\ &\sum_{j=1}^{N} z_{i,j} = 1 \; \forall \, i \\ &\begin{pmatrix} I_{N^2 \times N^2} \\ -I_{N^2 \times N^2} \end{pmatrix} (z_{1,1} \quad \dots \quad z_{1,N} \quad z_{2,1} \quad \dots \quad z_{N,N})^T \leq \begin{pmatrix} 1_{N^2} \\ 0_{N^2} \end{pmatrix} \end{aligned} \tag{G.25}$$

This is obviously of the shape:

$$\begin{aligned} &\min c^T x \\ &\text{s.t.} \, Ax = b \\ &\quad Cx \leq d \end{aligned} \tag{G.26}$$

And hence a linear program. ■

Lemma 5:

Given two sets $X = \{x_i\}_{i=1}^2$ and $Y = \{y_i\}_{i=1}^2$ with two real valued data vectors each, and let $\|\cdot\|$ be the Euclidean norm. Then the optimal solution of the minimization problem

$$\begin{aligned} &\min \sum_{i=1}^{N=2} \sum_{j=1}^{N=2} \left\|y_i - x_j\right\|^2 \times z_{i,j} \\ &\text{s.t.} \sum_{i=1}^{N=2} z_{i,j} = 1 \; \forall \, j \\ &\sum_{j=1}^{N=2} z_{i,j} = 1 \; \forall \, i \\ &\quad z_{i,j} \in \{0; 1\} \end{aligned} \tag{G.27}$$

is given by:

$$\|y_1 - x_1\|^2 + \|y_2 - x_2\|^2 \tag{G.28}$$

Proof:

For $z_{i,j}$, only two allowed solutions exist, i.e. $z_{i,j} = \begin{pmatrix} 1 & 0 \\ 0 & 1 \end{pmatrix}$ and $z_{i,j} = \begin{pmatrix} 0 & 1 \\ 1 & 0 \end{pmatrix}$.

This means, that the optimal solution has to be one of the following:

$$\mathrm{SSE}_1 = \|\mathrm{y}_1 - \mathrm{x}_1\|^2 + \|\mathrm{y}_2 - \mathrm{x}_2\|^2 \tag{G.29}$$

And

$$\mathrm{SSE}_2 = \|\mathrm{y}_2 - \mathrm{x}_1\|^2 + \|\mathrm{y}_1 - \mathrm{x}_2\|^2 \tag{G.30}$$

If we define $\mathrm{x}_2 = \mathrm{x}_1 + \Delta\mathrm{x}$ with $\Delta\mathrm{x} \geq 0$ and $\mathrm{y}_2 = \mathrm{y}_1 + \Delta\mathrm{y}$ with $\Delta\mathrm{y} \geq 0$.

Then, inserting into SSE_1 yields:

$$\begin{aligned}\mathrm{SSE}_1 &= \|\mathrm{y}_1 - \mathrm{x}_1\|^2 + \|\mathrm{y}_1 + \Delta\mathrm{y} - \mathrm{x}_1 - \Delta\mathrm{x}\|^2 \\ &= \mathrm{y}_1^2 - 2\mathrm{y}_1^{\mathrm{T}}\mathrm{x}_1 + \mathrm{x}_1^2 \\ &\quad +\mathrm{y}_1^2 + \mathrm{y}_1^{\mathrm{T}}\Delta\mathrm{y} - \mathrm{y}_1^{\mathrm{T}}\mathrm{x}_1 - \mathrm{y}_1^{\mathrm{T}}\Delta\mathrm{x} + \mathrm{y}_1^{\mathrm{T}}\Delta\mathrm{y} + \Delta\mathrm{y}^2 - \Delta\mathrm{y}^{\mathrm{T}}\mathrm{x}_1 - \Delta\mathrm{y}^{\mathrm{T}}\Delta\mathrm{x} \\ &\quad -\mathrm{y}_1^{\mathrm{T}}\mathrm{x}_1 - \Delta\mathrm{y}^{\mathrm{T}}\mathrm{x}_1 + \mathrm{x}_1^2 + \mathrm{x}_1^{\mathrm{T}}\Delta\mathrm{x} - \mathrm{y}_1^{\mathrm{T}}\Delta\mathrm{x} - \Delta\mathrm{y}^{\mathrm{T}}\Delta\mathrm{x} + \mathrm{x}_1^{\mathrm{T}}\Delta\mathrm{x} + \Delta\mathrm{x}^2 \\ &= 2\mathrm{y}_1^2 + \Delta\mathrm{y}^2 + 2\mathrm{x}^2 + \Delta\mathrm{x}^2 + 2\mathrm{y}_1^{\mathrm{T}}\Delta\mathrm{y} + 2\mathrm{x}_1^{\mathrm{T}}\Delta\mathrm{x} - 2\mathrm{y}_1^{\mathrm{T}}\Delta\mathrm{x} - 2\Delta\mathrm{y}^{\mathrm{T}}\mathrm{x}_1 \\ &\quad -4\mathrm{y}_1^{\mathrm{T}}\mathrm{x}_1 - 2\Delta\mathrm{y}^{\mathrm{T}}\Delta\mathrm{x}\end{aligned} \tag{G.31}$$

For SSE_2, we obtain:

$$\begin{aligned}\mathrm{SSE}_2 &= \|\mathrm{y}_1 + \Delta\mathrm{y} - \mathrm{x}_1\|^2 + \|\mathrm{y}_1 - \mathrm{x}_1 - \Delta\mathrm{x}\|^2 \\ &= \mathrm{y}_1^2 + \mathrm{y}_1^{\mathrm{T}}\Delta\mathrm{y} - \mathrm{y}_1^{\mathrm{T}}\mathrm{x}_1 + \mathrm{y}_1^{\mathrm{T}}\Delta\mathrm{y} + \Delta\mathrm{y}^2 - \Delta\mathrm{y}^{\mathrm{T}}\mathrm{x}_1 - \mathrm{y}_1^{\mathrm{T}}\mathrm{x}_1 - \Delta\mathrm{y}^{\mathrm{T}}\mathrm{x}_1 + \mathrm{x}_1^2 \\ &\quad +\mathrm{y}_1^2 - \mathrm{y}_1^{\mathrm{T}}\mathrm{x}_1 - \mathrm{y}_1^{\mathrm{T}}\Delta\mathrm{x} - \mathrm{y}_1^{\mathrm{T}}\mathrm{x}_1 + \mathrm{x}_1^2 + \mathrm{x}_1^{\mathrm{T}}\Delta\mathrm{x} - \mathrm{y}_1^{\mathrm{T}}\Delta\mathrm{x} + \mathrm{x}_1^{\mathrm{T}}\Delta\mathrm{x} + \Delta\mathrm{x}^2 \\ &= 2\mathrm{y}_1^2 + \Delta\mathrm{y}^2 + 2\mathrm{x}^2 + \Delta\mathrm{x}^2 + 2\mathrm{y}_1^{\mathrm{T}}\Delta\mathrm{y} + 2\mathrm{x}_1^{\mathrm{T}}\Delta\mathrm{x} - 2\mathrm{y}_1^{\mathrm{T}}\Delta\mathrm{x} - 2\Delta\mathrm{y}^{\mathrm{T}}\mathrm{x}_1 \\ &\quad -4\mathrm{y}_1^{\mathrm{T}}\mathrm{x}_1\end{aligned} \tag{G.32}$$

Substitution provides:

$$\mathrm{SSE}_1 = \mathrm{SSE}_2 - 2\Delta\mathrm{y}^{\mathrm{T}}\Delta\mathrm{x} \tag{G.33}$$

And because $\Delta\mathrm{y}, \Delta\mathrm{x} \geq 0$

$$\mathrm{SSE}_1 \leq \mathrm{SSE}_2 \tag{G.34}$$

This means that the minimum solution is achieved when the biggest y is assigned to the bigger x and the smaller y is assigned to the smaller x. ■

H. Classification of Optimization Problems

Depending on the application, optimization-based energy system models contain different formulations of the objective function and a diverse number of side constraints. Those not only differ with respect to the represented component characteristics, but also with respect to the mathematical classification of equations and inequalities.

As shown by Kotzur et al. [224], the most common program types appearing in energy system models based on optimization are linear programs (LPs), mixed-integer linear programs (MILPs) and (convex) quadratic programs (QPs). Generally, only a loose connection between the model application and the optimization program type exists, i.e. different model approaches of a single energy system might exist that lead to different program types. However, the algorithms' complexity of the corresponding program type limits the size of the model.

The following section provides an overview of the program types frequently used in energy system models and highlights the challenges for corresponding solving algorithms. Moreover, for each program type a small example is provided to illustrate the individual challenges of corresponding solving algorithms. Subsequently, the acceleration potential of each program type is evaluated for temporal aggregation techniques.

H.1. Linear Programs (LPs)

Due to the simplicity of linear program solving algorithms, this program type is predominantly used for large scale energy system models. A linear program consists of a linear objective function and exclusively linear side constraints consisting of equalities and inequalities, i.e.:

$$\begin{aligned} &\min c^{T}x \\ &\text{s.t. } Ax = b \\ &\quad Cx \leq d \\ &\quad x_i \in R \quad \forall \quad i \end{aligned} \tag{H.1}$$

Here, the variables are defined as real-valued entries in the vector x. In the case of combined capacity expansion and unit commitment models, this vector contains both, design and operation variables such as unknown capacities and energy outputs at a certain

time step. The cost vector c captures the cost contributions of each value in x. Moreover, the variables are constrained by equations defined by the matrix A and the constraint vector b as well as inequalities defined by the matrix C and the inequality vector d. As will be shown in the following sections, theses matrices have a certain block structure if the constraints and variables of energy system models are sorted by the time step to which they refer. This is essential for an in-depth understanding of temporal aggregation techniques.

As linear programs are always convex, i.e. a minimum is always unique and global, if the optimization program is neither unbounded nor infeasible, solving algorithms such as the simplex algorithm [225] or the interior point algorithm [226] can be directly applied to the problem and rapidly converge. The following extremely simple energy system model may serve as an example for the structure of linear programs.

Example 1

Consider an energy system consisting of two potential energy sources and one energy sink whose energy demand (e.g. electricity) needs to be satisfied at a single time step as shown in Figure H.1. Cost parameters assumed in the following are fictitious.

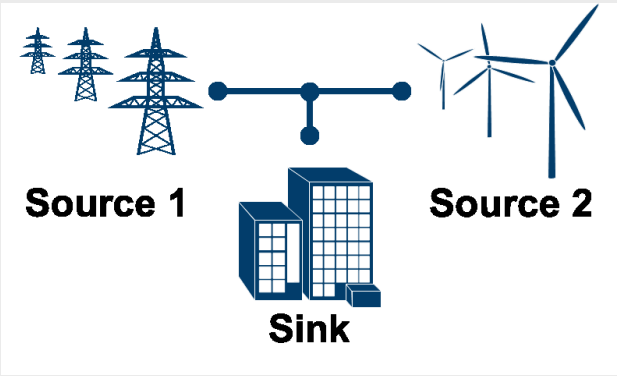

Figure H.1. A hypothetical simple energy system

Option 1 is to buy the electricity from the grid for $300\,\frac{€}{\mathrm{MWh}}$. Option 2 is to produce the electricity from another local component park for $250\,\frac{€}{\mathrm{MWh}}$. The demand to be satisfied in this time step is $1\,\mathrm{MWh}$. Moreover, electricity can only be supplied by the sources and not fed into them. Accordingly, the optimization problem is:

$$\min(\mathrm{TAC}) = \min\left(\mathrm{W}_{\mathrm{grid}} * 300\,\frac{€}{\mathrm{MWh}} + \mathrm{W}_{\mathrm{local}} * 250\,\frac{€}{\mathrm{MWh}}\right) \tag{H.2}$$

$$W_{grid}, W_{local} \geq 0$$

Of course, the solution is trivial, i.e. the electricity is completely produced in the local component park for $250\frac{€}{MWh}$. As $1MWh$ is demanded, the minimum objective is $\min(TAC) = 250€$. Despite of its simplicity, the example is already sufficient to illustrate the convexity of this program type and its most common solving algorithms.

Figure H.2 shows the graphical interpretation of the problem and the most basic solving algorithms, the simplex algorithm and the interior point algorithm.

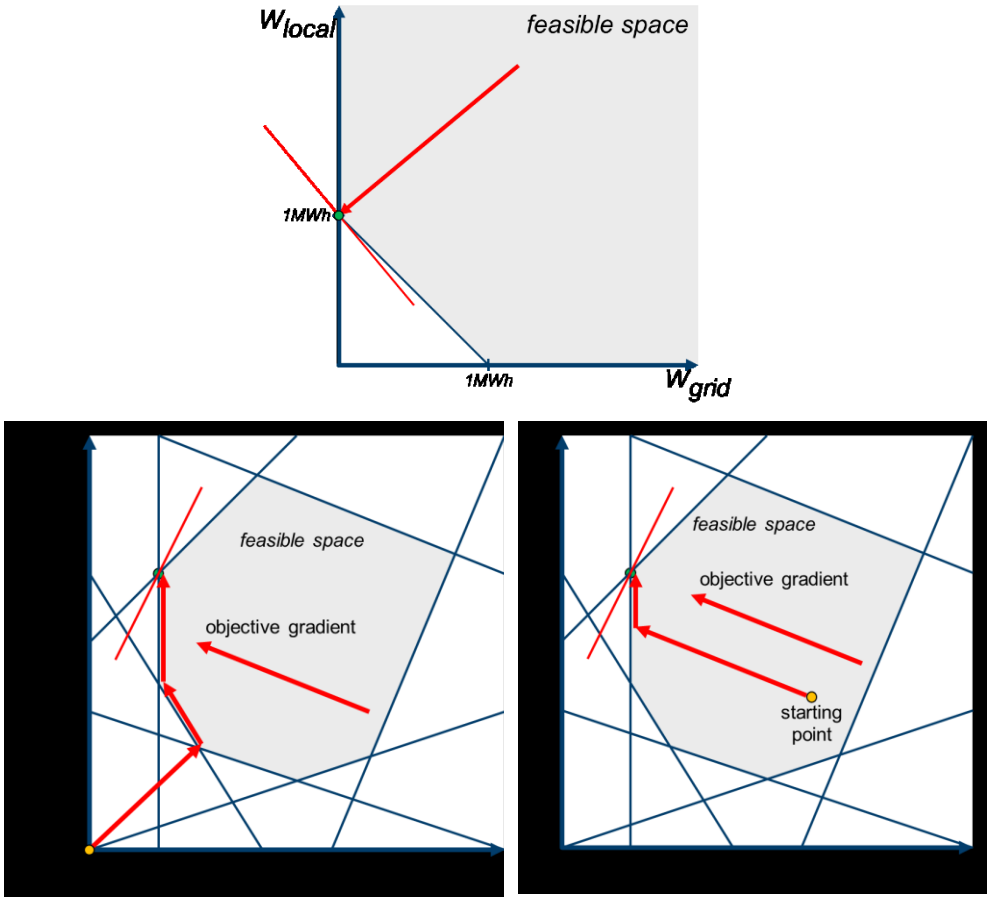

Figure H.2. The picture at the top shows the solution space and the optimal value for the optimization problem above. The picture on the bottom left shows the standard simplex algorithm for a linear program. The picture on the bottom right shows the interior point algorithm for a linear program

Although this work does not focus on a manipulation of solving algorithms for mathematical optimization, a sufficient knowledge about the most basic algorithms is essential to understand the mechanisms that lead to their acceleration using aggregated data.

Generally, the solution space formed by linear equations and inequalities is always defining a convex polyhedron [227, 228]. Since the gradient of maximum ascent or descent of the objective function is constant throughout the solution space, the extreme values lie either on the edge of the polyhedron, if this edge is orthogonal to the objective functions' gradient of maximum descent (ascent), or on a vertex.

One way to reach the minimum of a linear program is to find an arbitrary vertex of the polyhedral solution space, which is a feasible, but suboptimal solution of the linear program and to move from vertex to vertex along the edges of steepest descent (ascent). This step is repeated until the vertex with the minimum (maximum) value is reached, which is the general procedure of the simplex algorithm shown in Figure H.2 b.

Another way to find the minimum (maximum) value of a linear program is to find an arbitrary feasible point and to travel through the inner of the solution space, e.g. by following the gradient of steepest descent (ascent) until a facet, edge or vertex of the polyhedral is reached. From there, the search can be proceeded along the convex hull until the optimal vertex is found. In fact, multiple interior-point algorithms exist, however, for the sake of simplicity, the most important feature of these methods is, that they search the inner of a feasible region for an optimal solution as shown in Figure H.2 c.

Taking these methods into consideration, the reason for an acceleration of the optimization when using aggregation techniques such as temporal or spatial aggregation now becomes evident: By using an aggregated set of variables, the dimensionality of the polyhedral solution space is reduced and accordingly the number of edges and vertices. The impact of this geometric simplification is especially comprehensible for the simplex algorithm because a smaller number of edges is equivalent to a smaller number of iterations until the optimal vertex is found. Furthermore, the complexity of matrix operations decreases as well which holds true for both, the simplex algorithm and interior point algorithms. The following section will focus on the mathematical meanings of aggregation techniques in detail.

H.2. Mixed-Integer Linear Programs (MILPs)

In contrast to linear programs, mixed-integer linear programs also contain discrete variables, i.e. some of the variables are only defined for certain values, although the constraints and the objective function are still linear, i.e.:

$$\begin{aligned} &\min c^T x \\ &\text{s.t. } Ax = b \\ &\quad Cx \leq d \\ &\quad x_i \in Z \quad \forall \quad i \in M_{integervariables} \\ &\quad x_i \in R \quad \forall \quad i \notin M_{integervariables} \end{aligned} \tag{H.3}$$

However, this leads to non-convex mathematical problems and computationally more expensive solving algorithms. Mixed-integer linear programs more realistically capture the nature of energy systems, e.g. when modeling a discrete number of components is of interest. Furthermore, discrete variables are also needed when decisions are to be modeled, e.g. the on/off status of certain components as needed when minimum up- and downtimes should be represented in the model.

Excursus 2: A Definition of Relaxation

A comprehensible definition of relaxation for (general) minimization programs was provided by Geoffrion and Nauss [187]:
"A problem (R) is said to be a relaxation of problem (P), if the feasible region of (R) contains that of (P) and if the objective function of (R) is less than or equal to that of (P) on the feasible region of (P)."
For mixed-integer linear programs however, *relaxation* most frequently refers to the specific process of replacing binary or integer variables by continuous real-valued variables [229].

Basic algorithms to solve mixed-integer linear programs are inter alia the branch-and-bound and branch-and-cut algorithm. Generally, these algorithms are based on relaxing the discrete variables and solving the resulting linear program. In a branching step, the solution space is divided into subspaces across those discrete variables, which are closest to optimum of the relaxed solution. Then, the subspaces are relaxed again and the algorithm repeats this process. Those subspaces, which cannot lead to the optimal solution anymore, e.g. because the optimization of another subspace has already led to a better and feasible solution (including the dis-

crete variables), are discarded in order to reduce the computational load. Branch-and-Cut algorithms additionally strive to remove parts of the relaxed solution space in such a way that as many integer variables as possible lie on the convex hull of the relaxed solution space. In that way the probability is increased that the optimization of relaxed sub spaces directly lead to a feasible solution of the mixed-integer linear program. This supports an early removal of suboptimal branches.

Example 2

As an example for this process, the model of the preceding section is extended. Given the fact that the component park used to produce the demanded electricity consist of discrete components, it is now considered that the component park contains identical units with the capability to provide $0.4\frac{\mathrm{MWh}}{\mathrm{unit}}$ in the regarded time step. This leads to unit-specific costs of $250\frac{€}{\mathrm{MWh}} * 0.4\frac{\mathrm{MWh}}{\mathrm{unit}} = 100\frac{€}{\mathrm{unit}}$. As the number of components has to be an integer, this ultimately leads to the following mixed-integer linear program:

$$\begin{aligned} \min(\mathrm{TAC}) = \min\left(\mathrm{W_{grid}} * 300\frac{€}{\mathrm{MWh}} + \mathrm{N_{unit}} * 100\frac{€}{\mathrm{unit}}\right) \\ \text{s.t.} \quad \mathrm{W_{grid}} + \mathrm{N_{unit}} * 0.4\frac{\mathrm{MWh}}{\mathrm{unit}} \geq 1\mathrm{MWh} \\ \mathrm{W_{grid}}, \mathrm{N_{unit}} \geq 0 \\ \mathrm{N_{unit}} \in \mathrm{N} \end{aligned} \tag{H.4}$$

The corresponding solution space is shown in Figure H.3 a. In contrast to the linear program, the solution space now consists of single horizontal lines, which are further constrained by the minimum demand to be provided and the non-negativity constraints, which is obviously not convex.

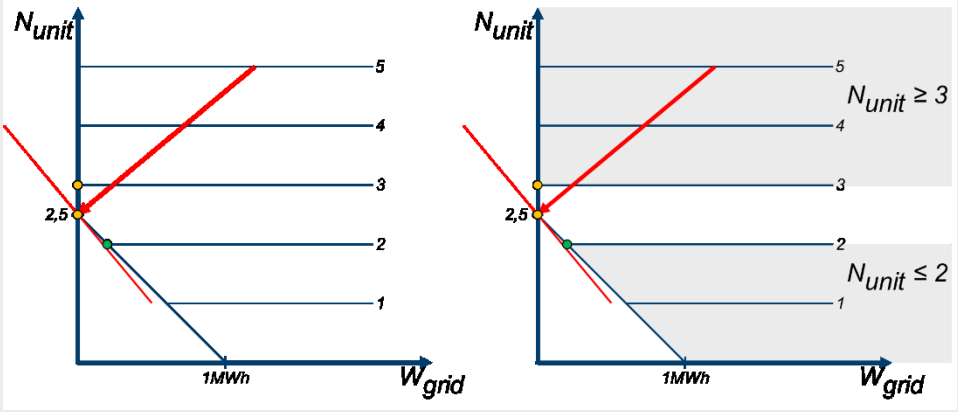

Figure H.3. The solution space of the mixed-integer linear program is depicted on the left and the single Branch-and-Bound step to determine the solution with linear programs is shown on the right

In order to determine a solution for this problem, a single Branch-and-Bound step is performed, which is shown in Figure H.3 b. For this, the problem is first relaxed, i.e. the integer-constraint is removed from the optimization problem. The optimal solution of this linear program is again trivial, because it is most economic to provide the electricity completely with the component park. Since each component can provide $0.4\frac{\text{MWh}}{\text{unit}}$ and 1MWh are demanded, $2.5\ \text{units}$ are required and the minimum cost to provide the electricity is again $2.5\ \text{units} * 100\frac{€}{\text{unit}} = 250€$. The corresponding solution is represented by the orange dot on the arrowhead in Figure H.3 b. Obviously, this solution is not feasible for the original mixed-integer linear program. Therefore, a branching step is performed which means that the solution space is divided into two subspaces, namely at the two integer variables which are closest to the optimal number of units for the relaxed linear program of the first stage, i.e. $2.5\ \text{units}$. The relaxed problems of the two subspaces are thus:

$$\begin{aligned} \min(\text{TAC}) &= \min\left(\text{W}_{\text{grid}} * 300\frac{€}{\text{MWh}} + \text{N}_{\text{unit}} * 100\frac{€}{\text{unit}}\right) \\ \text{s.t.}\quad \text{W}_{\text{grid}} + \text{N}_{\text{unit}} * 0.4\frac{\text{MWh}}{\text{unit}} &\geq 1\text{MWh} \\ \text{W}_{\text{grid}}, \text{N}_{\text{unit}} &\geq 0 \\ \text{N}_{\text{unit}} &\leq 2 \end{aligned} \tag{H.5}$$

And

$$\begin{aligned} \min(\text{TAC}) &= \min\left(\text{W}_{\text{grid}} * 300\frac{€}{\text{MWh}} + \text{N}_{\text{unit}} * 100\frac{€}{\text{unit}}\right) \\ \text{s.t.}\quad \text{W}_{\text{grid}} + \text{N}_{\text{unit}} * 0.4\frac{\text{MWh}}{\text{unit}} &\geq 1\text{MWh} \\ \text{W}_{\text{grid}}, \text{N}_{\text{unit}} &\geq 0 \\ \text{N}_{\text{unit}} &\geq 3 \end{aligned} \tag{H.6}$$

The solution spaces of these two subproblems are represented by the gray areas in Figure H.3 b. Solving both linear programs leads to two feasible solutions of which only one is in fact optimal for the original problem. For the first subproblem, the optimal solution is to use $2\,\text{units}$ to provide $0.8\,\text{MWh}$ of electricity from the component park and buy $0.2\,\text{MWh}$ from the grid. This leads to total costs of $0.2\,\text{MWh} * 300\frac{€}{\text{MWh}} + 2\,\text{units} * 100\frac{€}{\text{unit}} = 260€$. The solution of the second subproblem is to operate $3\,\text{units}$ and not to purchase electricity from the grid. This leads to electricity costs of $3\,\text{units} * 100\frac{€}{\text{unit}} = 300€$, which is obviously more expensive. Therefore, the optimal solution of the original mixed-integer linear program is 260€ at the coordinate $(0.2\,\text{MWh} \mid 2\,\text{units})$ which is marked by the green dot in Figure H.3 b.

As shown, the solution of the mixed-integer linear program required the solution of three linear programs for one discrete variable only. A higher number of discrete variables leads to a disproportionately higher number of linear programs to be solved. Although modern solving algorithms are significantly faster due to the early removal of suboptimal branches, the significantly higher computational cost to solve mixed-integer linear programs is comprehensible. It is worth mentioning that mixed-integer linear programs are accelerated in two ways by using aggregated time series:

1. If the binary variables are operational variables defined for each time steps, their number is directly reduced by the use of aggregated time series and accordingly, less branch and cut steps are needed. Further, also the size of the relaxed linear programs is reduced.
2. If the binary variables are design variables, their number remains the same in the temporally aggregated model. However, the size of the relaxed linear programs is reduced due to the smaller number of time steps. Accordingly, each branch and cut iteration takes less time.

Unlike operational variables, design variables are not defined for each time step and therefore their number is generally smaller by magnitudes. For large-scale energy system models, binary design variables are therefore often the only computationally feasible option, which is also the case for the modeling framework **FINE**.

H.3. Quadratic Programs (QPs)

The last program type that has recently been used for energy system models are the so-called quadratic programs. This optimization class contains quadratic terms in the objective function and exclusively linear equations and inequalities as side constraints, i.e.:

$$\begin{aligned} &\min \frac{1}{2} x^T Q x + c^T x \\ &\text{s.t. } Ax = b \\ &\quad Cx \leq d \\ &\quad x_i \in R \quad \forall \quad i \end{aligned} \tag{H.7}$$

In case the side constraints contain quadratic terms as well, the problems are called quadratically constrained quadratic programs (QCQPs). In contrast to linearly constrained solution spaces that resemble n-dimensional polyhedrons like the polygons in Figure H.2 b and c, quadratically constrained solution spaces can be non-convex. For the reasons of non-convex solution spaces, no application in energy system models to the best of the author's knowledge and substantially different solving algorithms, quadratically constrained quadratic programs are not regarded in the following.

Example 3

As an example for a quadratic program the linear program of the preceding sections is once again modified. Consider the government wants to balance the electricity demand and thus imposes a tax that grows linearly with the amount of consumed electricity with $100 \frac{\%}{\text{MWh}} = 1 \frac{1}{\text{MWh}}$ by source. Although this tax is unrealistically high, it simplifies the following calculations. This leads to the following quadratic program:

$$\begin{aligned} \min(\text{TAC}) = \min \Bigg(& W_{\text{grid}} * 300 \frac{€}{\text{MWh}} * \left(1 + W_{\text{grid}} * \frac{1}{\text{MWh}}\right) + W_{\text{local}} \\ & * 250 \frac{€}{\text{MWh}} * \left(1 + W_{\text{local}} * \frac{1}{\text{MWh}}\right) \Bigg) \\ \text{s.t.} \quad & W_{\text{grid}} + W_{\text{local}} \geq 1\text{MWh} \\ & W_{\text{grid}}, W_{\text{local}} \geq 0 \end{aligned} \tag{H.8}$$

This problem is now obviously quadratic and is graphically represented by the diagram in Figure H.4 a. The elliptical contour plot of the objective function is derived by setting the objective function equal to a constant value, i.e.:

$$C_1 = W_{\text{grid}} * 300 \frac{€}{\text{MWh}} * \left(1 + W_{\text{grid}} * \frac{1}{\text{MWh}}\right) \tag{H.9}$$

$$
\begin{aligned}
&+\mathrm{W_{local}} * 250\frac{€}{\mathrm{MWh}} * \left(1 + \mathrm{W_{local}} * \frac{1}{\mathrm{MWh}}\right)\\
\Leftrightarrow\ \mathrm{C_2} &= 1.2\left(\mathrm{W_{grid}^2}\frac{1}{\mathrm{MWh^2}} + \mathrm{W_{grid}}\frac{1}{\mathrm{MWh}}\right)\\
&+\left(\mathrm{W_{local}^2}\frac{1}{\mathrm{MWh^2}} + \mathrm{W_{local}}\frac{1}{\mathrm{MWh}}\right)\\
\Leftrightarrow\ \mathrm{C_3} &= \frac{\left(\mathrm{W_{grid}} + 0.5\ \mathrm{MWh}\right)^2}{(1\ \mathrm{MWh})^2} + \frac{(\mathrm{W_{local}} + 0.5\ \mathrm{MWh})^2}{(1.0954\ \mathrm{MWh})^2}
\end{aligned}
$$

This means that the contours are ellipses with their center at $(-0.5\ \mathrm{MWh} \mid -0.5\ \mathrm{MWh})$ and a y- to x-semi-axis ratio of $\frac{\mathrm{a_y}}{\mathrm{a_x}} = 1.0954$. As shown in Figure H.4 a, the solution moreover lies on the line of $\mathrm{W_{grid}} + \mathrm{W_{local}} = 1\mathrm{MWh}$. Substitution and setting the first derivative to 0 thus yields:

$$
\begin{aligned}
0 &= \left(\mathrm{W_{grid}} * 300\frac{€}{\mathrm{MWh}} * \left(1 + \mathrm{W_{grid}} * \frac{1}{\mathrm{MWh}}\right)\right)'\\
&+\left((1\ \mathrm{MWh} - \mathrm{W_{grid}}) * 250\frac{€}{\mathrm{MWh}} * \left(1 + (1\ \mathrm{MWh} - \mathrm{W_{grid}}) * \frac{1}{\mathrm{MWh}}\right)\right)'\\
\Leftrightarrow\ 0 &= \left(1.2\left(\mathrm{W_{grid}^2}\frac{1}{\mathrm{MWh^2}} + \mathrm{W_{grid}}\frac{1}{\mathrm{MWh}}\right)\right)'\\
&+\left(\left(1 - \mathrm{W_{grid}}\frac{1}{\mathrm{MWh}}\right)^2 + \left(1 - \mathrm{W_{grid}}\frac{1}{\mathrm{MWh}}\right)\right)'\\
\Leftrightarrow\ 0 &= \left(2.2\ \mathrm{W_{grid}^2}\frac{1}{\mathrm{MWh^2}} - 1.8\ \mathrm{W_{grid}}\frac{1}{\mathrm{MWh}} + 2\right)'\\
\Leftrightarrow\ 0 &= 4.4\ \mathrm{W_{grid}}\frac{1}{\mathrm{MWh}} - 1.8\\
\Leftrightarrow\ \mathrm{W_{grid}} &= \frac{9}{22}\mathrm{MWh} \Rightarrow \mathrm{W_{local}} = \frac{13}{22}\mathrm{MWh}\ \Rightarrow \mathrm{TAC_{min}} \approx 407{,}55€
\end{aligned}
\tag{H.10}
$$

As it can be seen, the quadratic taxation of energy balances the usage of similar technologies. Although this minimal example does not capture the majority of real energy system model features, it yet succeeds to highlight a well-known tendency of them, namely, the so-called penny-switching: Optimization-based energy system models usually choose exclusively the cheapest technology from a set of rival technologies, even if their specific cost difference is negligible. This leads to an unrealistic favoring of single components among almost comparable ones. The dampening of this effect is one of the major motivations for using quadratic programs for energy system models as presented by Lopion et al. [31].

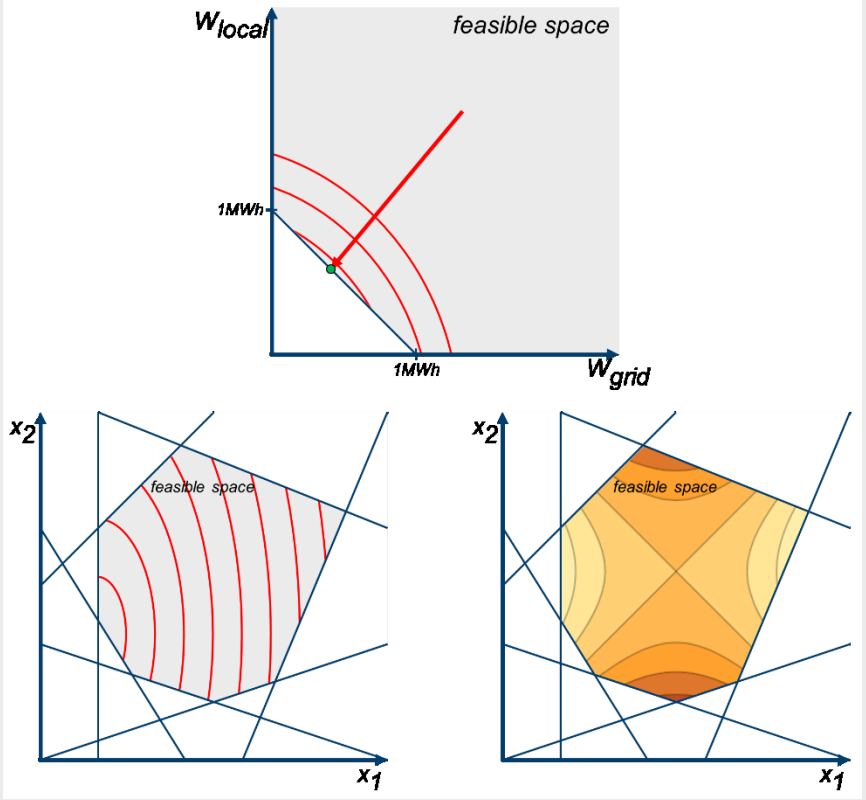

Figure H.4. The graph at the top illustrates the quadratic program at hand, the bottom left and the bottom right picture highlight the impact definiteness on the existence of a single minimum of a quadratic program

At this point, it is noteworthy that a convex solution space due to exclusively linear constraints and inequalities is not a sufficient condition for the convexity of the quadratic program itself. For minimization problems, the objective function must be at least positive semi-definite [230], i.e.:

$$x^T Q x \geq 0 \quad \forall \quad x_i \in R \tag{H.11}$$

Simply put, this condition states that the unconstrained objective has a minimum point. In particular, this means that the function has no saddle points. For maximization problems, the objective needs to be negative semi-definite, respectively, i.e.:

$$x^T Q x \leq 0 \quad \forall \quad x_i \in R \tag{H.12}$$

Figure H.4 b shows the general form of a quadratic program with a positive semi-definite objective function for the two-dimensional case. It is especially obvious that the quadratic program has only one minimum since the curvature radius of the objective's contour lines are always facing towards the minimum point. However, this is not the case for the maximums, which means that a minimization

quadratic program with a positive semi-definite objective function has only one minimum but can have multiple maximums. The opposite holds true for maximization quadratic programs with negative semi-definite objective functions.Figure H.4 c shows the case of an indefinite objective function, i.e. depending on the values of x, $x^T Q x$ can be positive or negative. The objective in this case is:

$$\begin{aligned} f(x_1, x_2) &= -(x_1 - c_1)^2 + (x_2 - c_2)^2 \\ &= -x_1^2 + x_2^2 + 2c_1 x_1 - 2c_2 x_2 - c_1^2 + c_2^2 \\ &= \frac{1}{2} x^T \begin{pmatrix} -2 & 0 \\ 0 & 2 \end{pmatrix} x + (2c_1 \quad -2c_2) x - c_1^2 + c_2^2 \end{aligned} \tag{H.13}$$

As can be seen, the function contains a saddle point at $(c_1 | c_2)$ which lies within the convex solution space and leads to two maximum and two minimum values within the feasible region. Accordingly, the impact of non-definiteness is intuitively comprehensible.

Excursus 3: Implications of Positive Definiteness on energy system models

With respect to cost-minimizing quadratic programs for energy system models, the positive definiteness means in particular that e.g. positive taxations as shown in the example can be considered with a quadratic objective, but cost degression cannot without losing the convexity of the program. For that reason, certain effects, which could be appropriately represented by quadratic functions, cannot be efficiently solved due to the non-convexity of the resulting problem. Although solvers for non-convex quadratic programs exist (c.f. [231]), these problems are np-hard [232] and thus not efficiently solvable in a reasonable amount of time.

In these cases, nonlinearities are frequently modelled using piecewise linear functions in literature. This, in turn, requires additional binary variables, e.g. for special ordered sets [233]. In these cases, the programs become mixed-integer linear programs instead of quadratic programs.

Because of the convexity and thus the globality and uniqueness of minimums in linear programs and positive semi-definite minimization quadratic programs, the interior-point method is applicable to quadratic programs as well. Apart from that, a convex quadratic program can also be solved using a modified simplex-algorithm. The modification of the algorithm is necessary because the simplex algorithm moves from vertex to vertex along the edges of steepest

descent of the polyhedral solution space until the desired minimum is reached. In contrast to linear programs however, the minimum of a convex minimization quadratic program is not necessarily a vertex of the solution space but van also lie on the middle of an edge as shown in the example or even within the solution space, which the modified simplex algorithm has to consider. Yet, the solving algorithms are not significantly slower than those for linear programs and significantly faster than those for non-convex problems.

With respect to temporal aggregation techniques, quadratic programs only marginally differ from linear programs, as the constraints of a quadratic program and its corresponding linear program are identical. The only difference that has to be carefully considered is the question how the weighting factors w_t for aggregated time series contribute to the objective function. The weighting factors express how many original time steps are represented by the respective aggregated time step.

Excursus 4: The Generalization of Weighting Factors for Aggregated Quadratic Objectives

For an objective function including component-wise time-independent ($C_{TI,c}$), time-dependent ($C_{TD,c,t}$) and time-dependent cumulative ($C_{TDc,c,t}$) linear and cumulative costs (index l and q) the aggregated time series are to be transformed as follows:

(H.14)

$$
\begin{aligned}
TAC = &\sum_{c\in Co}\left(C_{TI,l,c}x_{TI,c} + C_{TI,q,c}x_{TI,c}^2\right) \\
&+ \sum_{c\in Co}\sum_{t=0}^{T}\left(C_{TD,l,c,t}x_{TD,c,t} + C_{TD,q,c,t}x_{TD,c,t}^2\right) \\
&+ \sum_{c\in Co}\left(C_{TDc,l,c,t}\sum_{t=0}^{T}x_{TDc,c,t}\right) \\
&+ \sum_{c\in Co}\left(C_{TDc,q,c,t}\left(\sum_{t=0}^{T}x_{TDc,c,t}\right)^2\right)
\end{aligned}
\quad\Rightarrow\quad
\begin{aligned}
\widetilde{TAC} = &\sum_{c\in Co}\left(C_{TI,l,c}\tilde{x}_{TI,c} + C_{TI,q,c}\tilde{x}_{TI,c}^2\right) \\
&+ \sum_{c\in Co}\sum_{t=0}^{T_{Agg}}\left(C_{TD,l,c,t}w_t\tilde{x}_{TD,c,t} + C_{TD,q,c,t}w_t\tilde{x}_{TD,c,t}^2\right) \\
&+ \sum_{c\in Co}\left(C_{TDc,l,c,t}\sum_{t=0}^{T_{Agg}}w_t\tilde{x}_{TDc,c,t}\right) \\
&+ \sum_{c\in Co}\left(C_{TDc,q,c,t}\left(\sum_{t=0}^{T_{Agg}}w_t\tilde{x}_{TDc,c,t}\right)^2\right)
\end{aligned}
$$

This is a generalization of the objective used by Lopion et al. [31]. Accordingly, the question whether the weighting factors contribute not at all, linearly or quadratically to the objective function depends on the corresponding variable.

H.4. Summary

Figure H.5 summarizes the theoretical findings of this section for common cost-minimizing energy system models, which are by far the most common class of energy system models to be found in literature. As can be seen, the majority of nonlinearities captured in energy system models lead to mixed-integer linear programs and only the minority of nonlinearities can be depicted by (convex) quadratic programs.

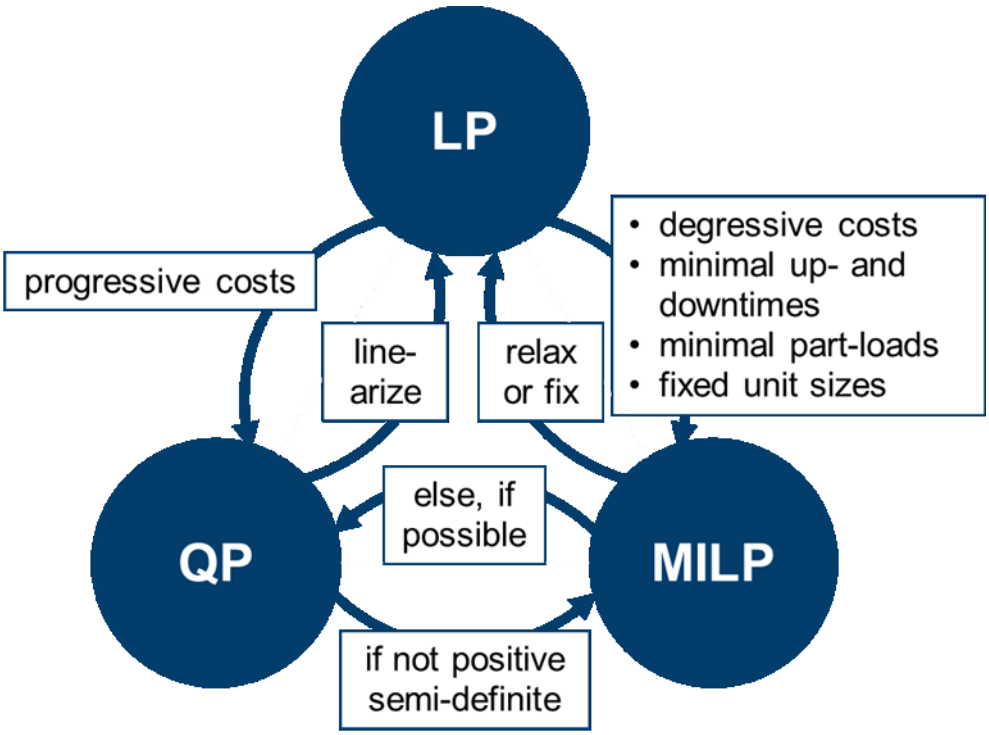

Figure H.5. A summary of general energy system features whose consideration transforms the program type into another one

Moreover, for each of the regarded program types the potential of time series aggregation was evaluated and for mixed-integer linear programs, a multi-level approach was developed to maintain the feasibility of the aggregated solution. As especially the constraining equalities and inequalities of the considered program types do not substantially differ from each other, Appendix I mainly focuses on the mathematical meaning of aggregating linear programs. The impact of time series aggregation on mixed-integer linear programs and quadratic programs can then easily be derived.

I. Matrix Aggregation and Error Bounding

Apart from the aggregation of input data, the energy system model needs to be adapted to the aggregated time series as well. The following chapter is dedicated to describing and analyzing the impact of time series aggregation on the energy system model itself. As will be shown in the following, the process of time series aggregation for energy system models does not only affect the optimal solution of an energy system model due to fewer time steps with modified values for each time series, but also due to the absence of equations that were part of the fully resolved model. Therefore, aggregation **could** have an impact on the energy system model even if the time series could be perfectly represented by fewer time steps (e.g., if storage equations are considered).

Section I.1 focuses on a general categorization of the shape, in which (linear) energy system models typically appear. Section I.2 focuses on the impact that certain aggregation techniques have on the error made by aggregation itself. These findings are used to systematically over- and underestimate the reference system, which enables the modeler to quantify the maximum aggregation-induced error with respect to the fully resolved reference system.

Here, only linear programs will be considered, because some of the applied mathematical principles hold for linear programs only. However, as shown before, e.g. mixed-integer linear programs can be relaxed to linear programs in a preceding step.

I.1. Matrix Aggregation

In order to derive the theoretical findings of the following section, we introduce a simple energy system in Example 4, which captures basic mathematical features of the energy system modelling framework **FINE**. Here, it is important to highlight that FINE has far more equation types. However, the procedures described in the following are applicable to general energy system models with a temporal discretization to time steps.

Example 4: An Example for the Typical Shape of Linear Programs for Energy System Models

We consider a modified version of the energy system model from Appendix H, which is now also equipped with a battery storage as shown in Figure I.1.

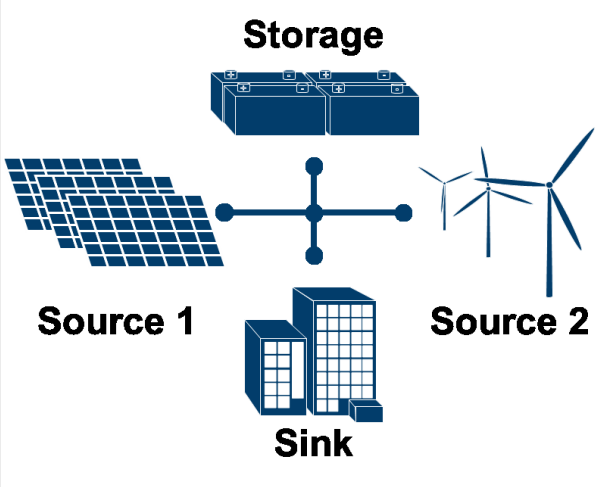

Figure I.1. Modified sample energy system with an additional battery storage

The objective of the energy system model is to minimize the total annual costs, which are the sum of the capacity-specific annualized investment costs and the capacity-specific operation costs at each time step, i.e.:

$$\begin{aligned}&\min(\mathrm{ic}_{S1}\cdot c_{S1}+\mathrm{ic}_{S2}\cdot c_{S2}+\mathrm{ic}_{St}\cdot c_{St})\\&+\min\left(\sum_{t=1}^{T}\mathrm{oc}_{S1}(t)\cdot o_{S1}(t)+\mathrm{oc}_{S2}(t)\cdot o_{S2}(t)+\mathrm{oc}_{St,c}(t)\cdot o_{St,c}(t)+\mathrm{oc}_{St,d}(t)\cdot o_{St,d}(t)\right)\end{aligned} \quad (I.1)$$

With c, o capacities and operations of the components and ic, oc annualized investment costs and operation costs of the components. Here, the storage can either charge ($o_{St,c}(t) \geq 0$) or discharge ($o_{St,d}(t) \geq 0$).

The commodity balance for each time step is given by:

$$o_{S1}(t)+o_{S2}(t)+o_{St,c}(t)-o_{St,d}(t)=o_{Si}(t)\ \ \forall\ \ t\in\{1,\dots,T\} \quad (I.2)$$

Here, the energy sink is a component which is considered to exist already and whose energy demand needs to be fulfilled at any time step. Accordingly, the operation of the sink o_{Si} equals the energy demand, i.e.:

$$o_{Si}(t)=\mathrm{dem}(t) \quad (I.3)$$

For the energy sources, which are assumed renewable, the operation never exceeds the product of the capacity and the capacity factor, i.e.:

$$c_{S1}\cdot \mathrm{cf}_{S1}(t)-o_{S1}(t)\geq 0\ \ \forall\ \ t\in\{1,\dots,T\} \quad (I.4)$$

$$c_{S2}\cdot \mathrm{cf}_{S2}(t)-o_{S2}(t)\geq 0\ \ \forall\ \ t\in\{1,\dots,T\} \quad (I.5)$$

For the battery storage, the state of charge (SOC) should never exceed its capacity c_{St} i.e.:

$$c_{St} \geq SOC(t) \quad \forall \quad t \in \{1, \dots, T\} \tag{I.6}$$

The state of charge is calculated as forward-sum depending on charging and discharging rates over the time steps, i.e.:

$$SOC(t+1) = SOC(t) \cdot \eta_{sd} + \eta_c \cdot o_{St,c}(t) - \frac{1}{\eta_d} \cdot o_{St,d}(t) \quad \forall \quad t \in \{1, \dots, T\} \tag{I.7}$$

With η_{sd} the self-discharge over a time step, η_c the charge efficiency and η_d the discharge efficiency.
As mentioned in Appendix H, linear programs can be represented by the following shape:

$$\begin{aligned} &\min c^T x \\ &\text{s.t. } Ax = b \\ &\quad Cx \leq d \\ &\quad x \in R \end{aligned} \tag{I.8}$$

For the considered energy system model, this leads to the following shape:

(I.9)

$$A = \begin{pmatrix} 0 & 0 & 0 & 1 & 1 & 1 & -1 & 0 & & & & & & & & & & & & \\ 0 & 0 & 0 & & & & & & 1 & 1 & 1 & -1 & 0 & & & & & & & \\ \vdots & & & & & & & & & & & & & \ddots & & & & & & \\ 0 & 0 & 0 & & & & & & & & & & & & 1 & 1 & 1 & -1 & 0 \\ 0 & 0 & 0 & & \eta_C & \frac{-1}{\eta_D} & \eta_{sd} & & & & & -1 & & & & & & & & \\ 0 & 0 & 0 & & & & & & & \eta_C & \frac{-1}{\eta_D} & \eta_{sd} & & \ddots & & & & & & \\ \vdots & & & & & & & & & & & & & & & & & & & \\ 0 & 0 & 0 & & & & & & & & & & & & & & & & -1 \end{pmatrix}$$

$$C = \begin{pmatrix} cf_{s1}(1) & & & -1 & & & & & & & & & & & & & & & & \\ & cf_{s2}(1) & & & -1 & & & & & & & & & & & & & & & \\ & & 1 & & & 0 & 0 & -1 & & & & & & & & & & & & \\ cf_{s1}(2) & & & & & & & & -1 & & & & & & & & & & & \\ & cf_{s2}(2) & & & & & & & & -1 & & & & & & & & & & \\ & & 1 & & & & & & & & 0 & 0 & -1 & & & & & & & \\ \vdots & & & & & & & & & & & & & \ddots & & & & & & \\ cf_{s1}(T) & & & & & & & & & & & & & & -1 & & & & & \\ & cf_{s2}(T) & & & & & & & & & & & & & & -1 & & & & \\ & & 1 & & & & & & & & & & & & & & 0 & 0 & -1 \end{pmatrix}$$

$$c = (ic_{S1} \quad ic_{S2} \quad ic_{St} \quad oc_{S1}(1) \quad oc_{S2}(1) \quad oc_{St,c}(1) \quad oc_{St,d}(1) \quad 1 \quad \dots \quad oc_{S1}(T) \quad oc_{S2}(T) \quad oc_{St,c}(T) \quad oc_{St,d}(T) \quad 1)^T$$

$$x = (c_{S1} \quad c_{S2} \quad c_{St} \quad o_{S1}(1) \quad o_{S2}(1) \quad o_{St,c}(1) \quad o_{St,d}(1) \quad SOC(1) \quad \dots \quad o_{S1}(T) \quad o_{S2}(T) \quad o_{St,c}(T) \quad o_{St,d}(T) \quad SOC(T))^T$$

$$b = (dem(1) \quad \dots \quad dem(T) \quad 0(1) \quad \dots \quad 0(T-1))^T$$

$$dl = 0^{3 \cdot T \times 1}$$

$$du = \emptyset$$

As shown above, the matrices for constraining equalities A and inequalities C are usually very sparse. Furthermore, if the order of variables is sorted by their corresponding time step, the constraining matrices form a structure of blocks as marked by the red rectangles. Commonly, the shape of linear energy system models can thus be generalized as shown in Figure I.2:

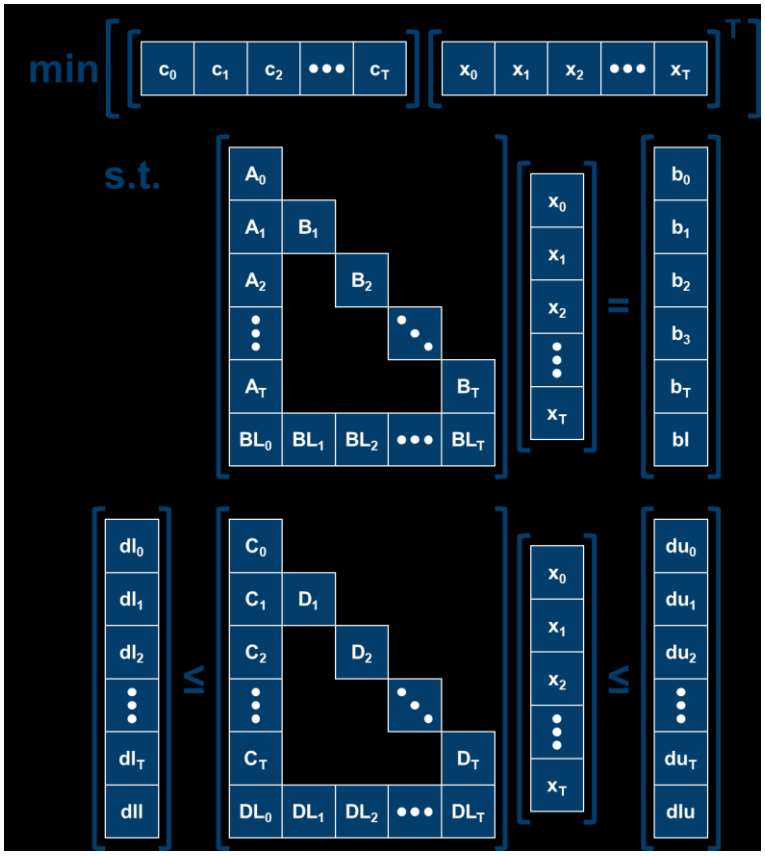

Figure I.2. The general structure of energy system models with variables sorted by time steps

The example illustrates that both, the equality matrix A and the inequality matrix C, can possess parameter blocks B_i and D_i with $i \in \{1, \dots, T\}$ for time-dependent variables, e.g. the components' operational variables. Furthermore, both matrices can possess parameter blocks A_i and C_i with $i \in \{0, \dots, T\}$ for time-invariant variables such as component capacities. Apart from that, energy system optimization problems also comprise the constraining vectors b, dl and du. While the vector b is a parameter vector and contains e.g. energy demands that need to be fulfilled at any time step, dl is, as seen in the example, likely to be a null vector. Furthermore, the upper bound vector du is often not defined at all. The cost vector c contains all cost contributions of capacities and operations. Moreover, many energy system models comprise parameter blocks BL_i and DL_i with $i \in \{0, \dots, T\}$ that couple time steps with each other. As shown in the example, these blocks e.g. result from storage equations in which a state of charge is modeled using the forward Euler method [234, 235]. It is worth mentioning that variables like the state of charge of the battery SOC are so-called state variables,

which means that they depict a differential relationship for discrete time steps [236]. As will be shown in the following, these variable types have a severe impact on the efficiency of aggregation methods. If neither state variables (that is, storage components) are part of the optimization model, nor other complicating constraints such as maximum cumulative energy supplies for certain energy sources, the BL and DL blocks are empty and can be removed from the optimization problem. In this case, the problem can be simplified as illustrated in Figure I.3:

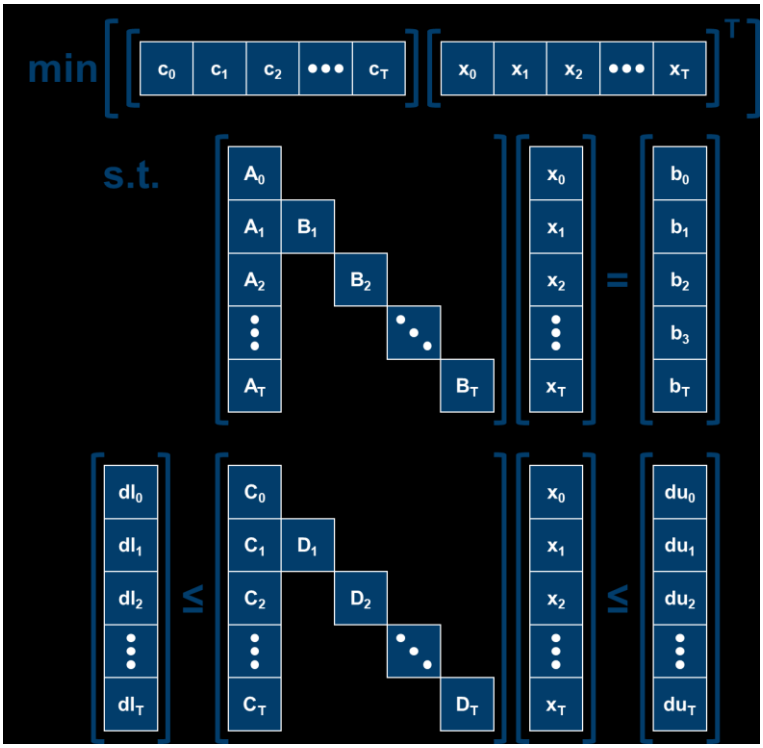

Figure I.3. The general structure of energy system models with variables sorted by time steps without complicating constraints

Although the inner structure of each of the matrix and vector blocks shown above differs from energy system model to energy system model, their outer structure can be generalized by Figure I.2 or Figure I.3 for temporally decoupled energy system models, provided that they are based on time discretization. As shown in the example, time series are parameter sets that could theoretically appear in any block within the optimization problem. However, two basic features they have in common:

- Time series are either coefficients in the matrix or constants in the vectors.

- Each matrix or vector block contains exactly n values per time series if it comprises n time steps.

An optimization problem with aggregated time steps possesses less time steps, which also means that it has less blocks, accordingly less variables, and less constraints. The structure of the aggregated optimization problem with and without temporal coupling constraints is illustrated in Figure I.4 and Figure I.5.

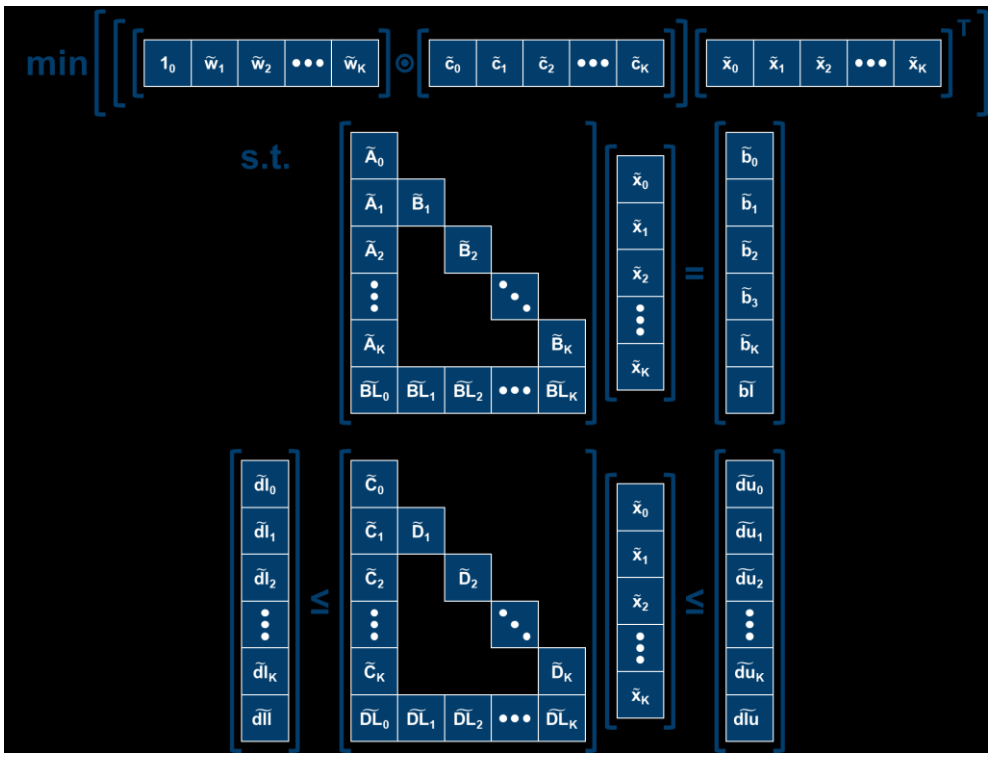

Figure I.4. The general structure of aggregated energy system models with variables sorted by clustered time steps

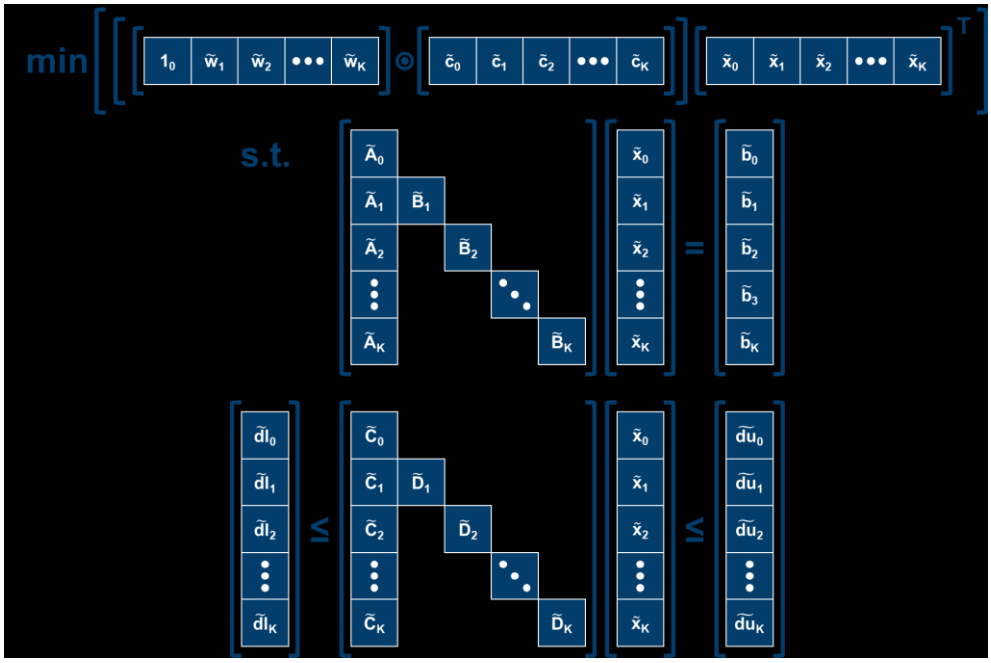

Figure I.5. The general structure of aggregated energy system models with variables sorted by clustered time steps without complicating constraints

As Figure I.4 and Figure I.5 reveal, the aggregated optimization problems bear a significantly similar structure as the original energy system models: In both the temporally coupled case and the temporally decoupled case, the diagonal block structure is preserved. Further, the complicating variables and, for the temporally coupled case, the linking blocks are at the same position as well. However, there are three main differences:

1. The number of blocks is equivalent to the number of clustered time steps or periods K, which is always smaller than or equal to the number of time steps T of the original problem.
2. In general, neither the coefficients and constants of the blocks, nor their inner structure is identical to those of the original blocks. An exception is the case of a temporally decoupled system, in which single time steps are clustered to typical time steps. Here, the inner structure of the blocks remains and only the coefficients and constants within the blocks are changed.
3. The objective function of the aggregated problem possesses an additional weighting vector which weighs the cost contribution of the aggregated time-dependent variables (index k) according to the number of original time steps represented

by the respective cluster. The time-independent variables (e.g. capacities of a component) (index 0) are not affected by aggregation and therefore not weighted (multiplied by 1).

As described in the introduction, the most common approach to temporally aggregate energy system models is the utilization of typical periods or, more specifically, typical days. In this case, not sets of time steps are clustered and represented by a single time step, but sets of periods, i.e. sets of groups of consecutive time steps are represented by a single group of consecutive time steps. In order to illustrate the process of aggregation by means of periods, the most general temporally coupled optimization problem shown in Figure I.2 is restructured to blocks of periods as shown in Figure I.6.

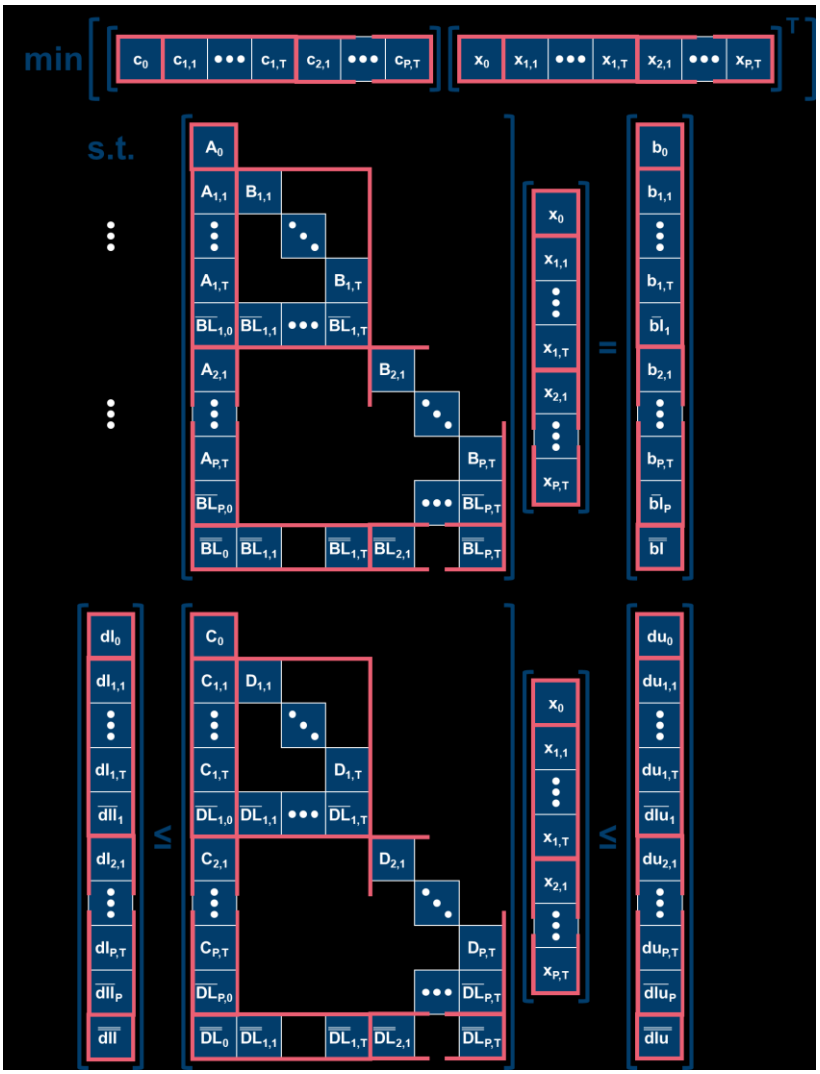

Figure I.6. The general structure of energy system models with variables sorted by periods

In this case, the blocks are restructured to bigger period blocks, which consist of smaller consecutive time step blocks. As highlighted in Figure I.6, those constraints that only link time steps within a period and were part of BL or DL before, can now be restructured to be part of the larger diagonal period blocks. These inner-period linking blocks are now denoted by $\overline{\mathrm{BL}}$ and $\overline{\mathrm{DL}}$, while the blocks that contain the remaining constraints linking periods to each other are denoted by $\overline{\overline{\mathrm{BL}}}$ and $\overline{\overline{\mathrm{DL}}}$. Accordingly, the temporal restructuring of an optimization problem by means of time periods instead of single time steps can lead to a structure with bigger but fewer diagonal blocks, but smaller linking blocks, as $\overline{\overline{\mathrm{BL}}}$ and $\overline{\overline{\mathrm{DL}}}$ contain less equations than BL or DL.

As the outer structure of the period-wise ordered optimization problem in Figure I.6 resembles that of Figure I.2, it can also be summarized as shown in Figure I.7 with P blocks of each kind and comparably small linking blocks $\widehat{\mathrm{BL}}$ and $\widehat{\mathrm{DL}}$ because the majority of time-linking constraints is part of the diagonal blocks $\widehat{\mathrm{B}}$ and $\widehat{\mathrm{D}}$.

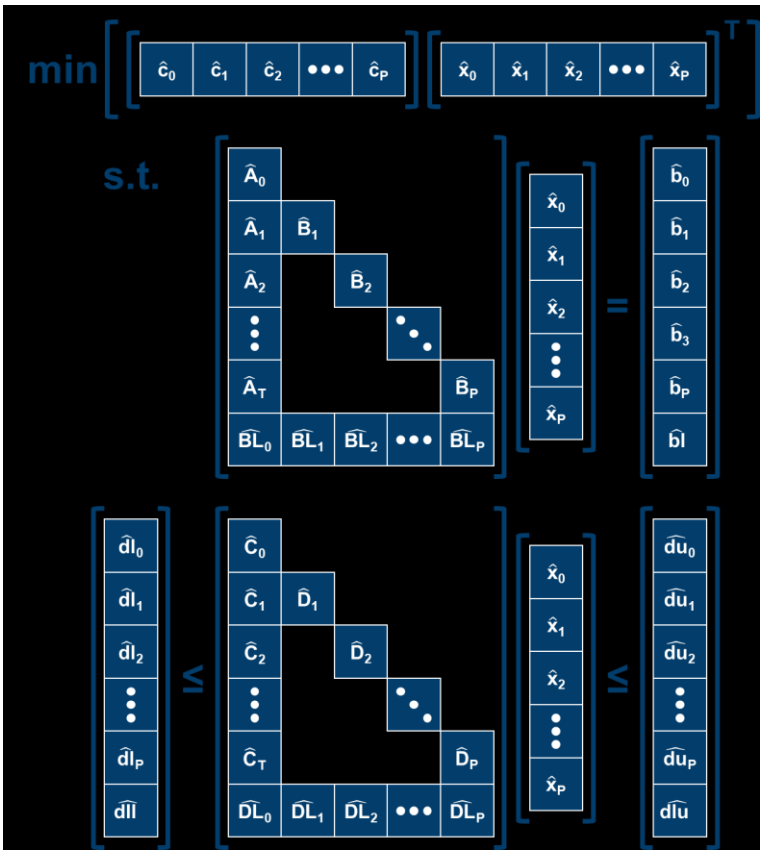

Figure I.7. The general structure of energy system models with variables sorted by periods

A frequent approach to aggregate the block structure shown in Figure I.7 is to neglect the comparably small linking blocks $\widehat{\mathrm{BL}}$ and $\widehat{\mathrm{DL}}$ and to reduce the remaining blocks to an optimization problem as shown in Figure I.5 with K clusters instead P periods with $\mathrm{K} \leq \mathrm{P}$. As the constraints connecting linking periods to each other, which are contained in the $\widehat{\mathrm{BL}}$ and $\widehat{\mathrm{DL}}$ blocks, are neglected in this process, only the linking constraints for time steps within a period are preserved in this approach, because these equations became part of the diagonal period-wise blocks $\widehat{\mathrm{B}}$ and $\widehat{\mathrm{D}}$. For storage components, this means that the modelling of the state of charge within clustered typical days is possible, while it is not possible across multiple typical days. As highlighted in the introduction, this property is common among most approaches that use either typical days or typical weeks for aggregation. It is noteworthy that a more realistic storage behavior is often modelled using a cyclic storage constraint, which forces the storage components to have the same state of charge at the beginning and the end of each typical period. This constraint is then coupling all clustered typical periods K to each other as a linking constraint that forms auxiliary linking blocks $\widetilde{\mathrm{BL}}$ or $\widetilde{\mathrm{DL}}$ as shown in Figure I.4. As a cyclic state of charge constraint at the beginning and the end of each typical day is relatively restrictive, the aggregated energy system model can also contain additional variables, which were not part of the original problem. An example for this are the inter-daily state of charge variables introduced by Kotzur et al. [20], which allow to cumulate energy in the storage components over a sequence of typical days which represents the original time series.

In conclusion, two major factors affect the structure of a linear program for an energy system model with discrete time steps, if it is temporally aggregated:

- The existence of temporally linking constraints, which connect temporally dependent variables of one time step to those of another time step, and how they are represented in the aggregated problem.
- The number of consecutive time steps serving as an aggregation candidate, i.e. single time steps or whole periods (e.g. typical days).

Besides, the in-depth analysis of linear optimization problems (to which also mixed-integer linear programs can be relaxed) and the impact of temporal aggregation on their structure, are a novelty of this work. Furthermore, a profound knowledge about temporal aggregation is needed in the following sections, in which general procedures and specific examples will be introduced that allow for a systematic bounding of aggregation-induced errors in energy system models. As will be shown in the following, the distinction between temporally coupled and temporally decoupled systems as well as aggregation by time steps and aggregation by periods is furthermore reasonable and helpful with respect to the choice of the most suitable over- and underestimation technique.

I.2. Error Bounding

One of the main conclusions of the prior chapters is the fact that time series aggregation can significantly decrease the computational burden and lead to plausible system designs and operations, if the method is wisely chosen, but the precise error induced by the usage of aggregated data is generally not estimated. Accordingly, the development of these error estimates contributes to the reliability of optimization results based on time series aggregation and thus ultimately to the validity of aggregation techniques.

Therefore, the following section focuses on the over- and underestimation of a linear program's optimal solution, if an appropriate aggregation technique is chosen. Simply put, it is discussed, which temporal aggregation methods lead to upper and lower bounds of the fully resolved energy system model. If upper and lower bounds to the original problem are known, three key questions can be answered that still lack in the majority of modern aggregation techniques:

What is the aggregation-induced error with respect to the original optimization problem at worst?
This worst-case error equals the difference between the upper and the lower bound to the original problem.

Under what circumstances is the solution based on aggregated time series a feasible solution to the original problem?
A feasible, but suboptimal solution is generally provided by the upper bound of the original problem.

What is the impact of a too small temporal resolution for energy system models?
This question can be implicitly answered by analyzing the lower bound of the original problem, which often relies on averaged time steps at a smaller temporal resolution, as well as the gap between the upper and the lower bound, which is significantly reduced if the aggregation is performed on an adequate level. Moreover, this analysis might even raise the question whether the temporal resolution of the reference case itself is sufficient at all.

The succeeding section first introduces a general workflow for systematically determining upper and lower bounds of linear energy system models in Section I.2.1, which shortly summarizes the findings of the preceding sections and explains important mathematical concepts (**invariance** and **symmetry**) of optimization problems, which are needed to aggregate them systematically. These concepts are then specifically applied determining upper bounds in Section I.2.2 followed by methods for lower bounds in Section I.2.3. As it will be shown in the following, a distinct case analysis for ESOMs with linked and independent time steps is needed in order to provide as tight bounds as possible without the loss of generality. Therefore, each of the sections is further divided into these two cases.

I.2.1. A General Workflow to Determine Bounds

As shown in the previous section, the actual reason for a speed-up of temporally aggregated energy system models is the removal of both variables and constraints and accordingly the application of solving algorithms in a lower-dimensional hyperspace. In case of linear programs, this also includes lower-dimensional polyhedral feasible spaces with less vertices and edges. Although this concept is easily understandable, the specific mathematical consequences of these approaches remain widely neglected. The drawback of a heuristic usage of temporal aggregation techniques is that:

- neither the deviation from the optimal solution of the fully resolved reference case is known
- nor the operational feasibility for the reference system can be guaranteed.

In a worst-case scenario, a model-based system design might be realized which is more expensive than necessary and does not live up to its tasks and expectations. Concretely, the system might lead to supply shortages or even outages and could ultimately be useless. This is a strong motivation for systematically quantifying an aggregation-induced error and thereby finding feasible solutions for the original yet non-solvable optimization model. Moreover, these theoretical investigations also help to assess modeling assumptions more critical and in more detail.

As mentioned in the introduction, the concept of error bounding in temporal aggregation originates from recent publications of which the most influential publications were those of Bahl et al. [79, 180, 181, 237] and Baumgärtner et al. [82, 83]. Furthermore, the mathematical abstraction of temporal aggregation in order to distinguish between aggregated models, which are a relaxation of the full model and vice versa, could also be observed in a publication by Teichgräber et al. [47]. Apart from that, earlier efforts to model seasonal storage with regularly ordered time slices [22, 111] and to neglect non-critical state of charge constraints have led to the development of a distinction between temporally coupled and temporally decoupled optimization problems within this thesis.

To this end, however, all mathematical proofs were focusing on temporally decoupled systems and some of the methods were empirically, but without a corresponding proof, transferred to temporally coupled systems. Moreover, the more general the proof was, the less useful it was for specific problems and vice versa. Furthermore, only the mathematical concept of relaxation and implicitly its counterpart, the concept of restriction, were considered. The novelties developed within the scope of this thesis are:

- The establishment of a stepwise guide for determining upper feasible and lower infeasible bounds to the original problem based on aggregation.
- The application of invariance and symmetry concepts from optimization theory, which dictate desirable features of future aggregation approaches.
- The extension of theoretical proofs on temporally coupled systems.

- The application of the methods to a number of different time series simultaneously (demand, capacity factors, costs) instead of demand time series (Bahl et al. [79, 180, 181, 237], Baumgärtner et al. [82, 83]) or cost time series (Teichgräber et al. [47]) only.
- The implementation of the features into a general model framework instead of a model, which means that these approaches are valid **for each model** designed with **FINE**.
- Apart from some known, but yet partly unproven over- or underestimating aggregation techniques, this will also lead to the development of some novel aggregation techniques.

It is hence obvious that the implications of errors induced by temporal aggregation in energy system modelling are still a widely unknown research field with many open questions and with a need for an easy-to-use applicability.

With respect to the first above-mentioned bullet point, the general workflow for a systematical temporal aggregation of energy system models comprises two steps in order to obtain a model with a reduced size:

1. It is assumed that coefficients and constants in constraints and the objective function are sufficiently similar for groups of time steps so that these time steps can be identically parametrized.
2. It is assumed that the sets of constraints and variables of identically parametrized time steps can be replaced by a set of constraints and a set of variables for a single *representative* time step. It is further assumed that the set of coefficients for these identically parametrized time steps can be represented by a single set of coefficients multiplied by a weighting factor. Accordingly, this assumption contains three arbitrarily ordered sub-steps:
    - Removal of constraints
    - Removal of variables
    - Multiplication of time-dependent variables by weighting factors in the objective function

Depending on the purpose of a systematical aggregation, it can be more suitable to remove the constraints before the variables or vice versa. For upper and lower bounds, these roughly defined

steps can further be refined to the general workflow for systematic temporal aggregation shown in Figure I.8.

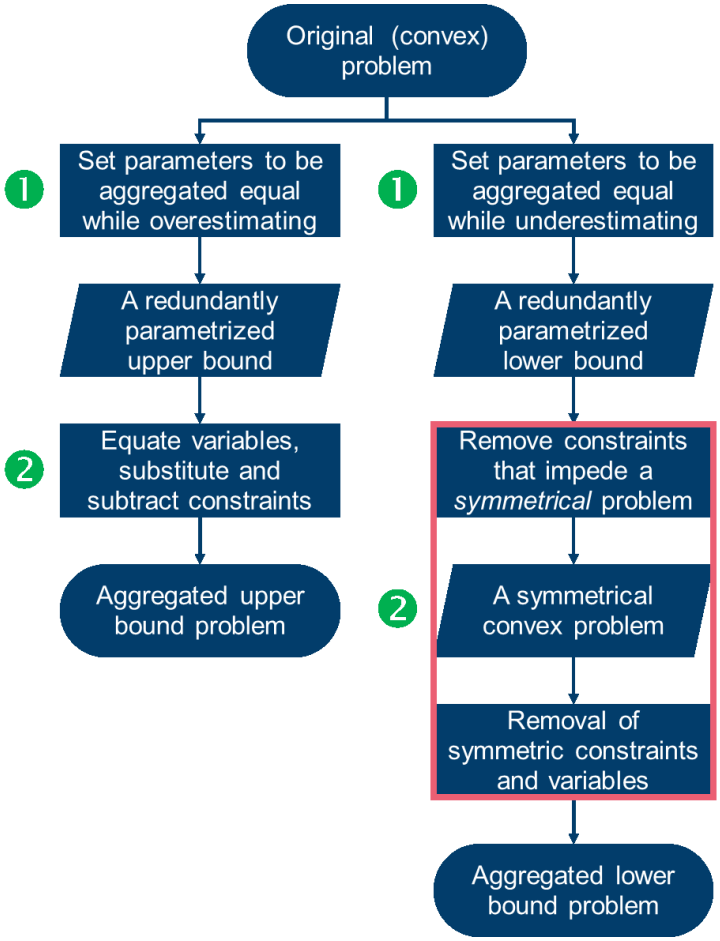

Figure I.8. A generally applicable workflow for determining aggregation-induced upper and lower bounds for energy system models

Figure I.8 illustrates that steps 1 and 2 are also generally applicable for the workflow to define upper and lower bounds systematically of a computationally intractable energy system model by temporally aggregating it.

However, the approaches differ in step 1 with respect to the equalization of coefficients and constants of time steps to be aggregated. While the coefficients and constants of cost-driving variables (capacities, operations, demands) need to be changed in such a way that the variables and the cost-coefficients in the objective function need to be bigger in the end for an upper bound of the problem, the opposite holds true for a lower. As the number of overall equations and variables does not change in neither of these cases, step 1 is a relaxation of the original problem in case of the

lower bound, as the feasible space is relaxed and (positive) cost coefficients are underestimated. Conversely, step 1 is a restriction in case of the upper bound because the feasible space is tightened and (positive) cost coefficients are underestimated. For the sake of clarity, the definition of the terms *relaxation* and *restriction* as provided by by Geoffrion and Nauss [187] is repeated below.

Excursus 5: A Definition of Relaxation and Restriction by Geoffrion and Nauss [187]

"A problem (R) is said to be a relaxation of problem (P) if the feasible region of (R) contains that of (P) and if the objective function of (R) is less than or equal to that of (P) on the feasible region of (P)."

"A problem (Q) is said to be a restriction of problem (P) if the feasible region of (Q) is entirely contained within that of (P), and if the objective function value of (Q) is at least as great as that of (P) everywhere on the feasible region of (Q)."

Step 2 differs depending on whether an under- or overestimation is pursued. The overall goal is identical, i.e. to remove identically parametrized equations and variables without violating the individual goal to overestimate an overestimation or to underestimate an underestimation further.

In case of an overestimation, it is simpler to first equalize the corresponding variables of those time steps in step 2 that are to be represented by a single time step in the aggregated problem. This approach is per definition a restriction of the original problem, which coincides with the goal to overestimate only. Then, variables and constraints can be removed by substitution and subtraction in order to obtain an upper bound of the fully resolved model.

In case of an underestimation, it is more suitable to remove constraints that impede a symmetrical problem, because the removal of side constraints is again a further relaxation of the original problem. The second operation in step 2, the removal of constraints and variables that refer to time steps to be aggregated due to the assumption that they are identical, is the most critical step for an underestimation of the original problem based on temporal aggregation. The reason for this is the circumstance that setting variables equal in order to remove them and the corresponding equations by substitution and subtraction from the optimization model generally works by adding additional equality constraints to the

system. This is per definition a restriction of the original optimization problem because the feasible space of the optimization is reduced. Therefore, it cannot be guaranteed that the aggregated problem is still a lower bound unless the problem is *symmetrical*. Here, the application of the concepts of variable *invariance* and *symmetry* in convex optimization are a novelty of this thesis, which can be used to guarantee that the lower bound provided by the aggregated problem remains a lower bound. A definition can be found below.

As it can be seen, the workflow for determining a lower bound based on an aggregated problem bears one more challenge than the workflow for determining an upper bound. While both approaches face the challenge to systematically over- or underestimate coefficients and constraints in order to over- or underestimate the original problem, a lower bound can moreover only be found by aggregation, if the problem is symmetrical after step 1 or after unsymmetrical equations have been relaxed or removed. Therefore, symmetry is an important concept in the area of temporal aggregation, which was neglected in literature to this end. In the following, it will be shown that symmetries are especially impeded by temporally coupling constraints, for example in storage constraints.

Excursus 6: Invariance in Optimization Problems

A formal but yet understandable definition of invariance and symmetry in optimization problems was provided by Boyd et al. [229]: *"Symmetries and convex optimization. Suppose* $G = \{Q_1, \dots, Q_k\} \subseteq R^{n \times n}$ *is a group, i.e. closed under products and inverse. We say that the function* $f: R^n \to R$ *is* G*-invariant, or symmetric with respect to* G*, if* $f(Q_i x) = f(x)$ *holds for all* x *and* $i = 1, \dots, k$*."*

"We define the fixed subspace of G *as* $F = \{x | Q_i x = x, i = 1, \dots, k\}$*."*

"We say the optimization problem

$$\begin{aligned} &\text{minimize} && f_0(x) \\ &\text{subject to} && f_i(x) \leq 0, \quad i = 1, \dots, m \end{aligned} \tag{I.10}$$

is G*-invariant if the objective* f_0 *is* G*-invariant, and the feasible set is* G*-invariant, which means*

$$f_1(x) \leq 0, \dots, f_m(x) \leq 0 \Rightarrow f_1(Q_i x) \leq 0, \dots, f_m(Q_i x) \leq 0 \tag{I.11}$$

for $i = 1, \dots, k$*.” … “If the problem is convex and* G*-invariant, and there is an optimal point, then there exists an optimal point in* F*. In other words, we can adjoin the equality constraints* $x \in F$ *to the problem, without loss of generality.”*

Excursus 6 states that for convex optimization problems such as linear programs, the optimal values of a set of variables is identical if the optimization problem is symmetric with respect to these variables. With this proposition it is possible to set variables equal, which is defined by the set $F = \{x | Q_i x = x, i = 1, \dots, k\}$ and tightens the feasible space, without removing the optimal solution of the lower bound problem. This further allows the removal of variables by substitution and the removal of constraints by subtraction, shortly, aggregation. In the following, a short example for the proposed workflow is presented in which the validity of step 2 is chosen (as it is a minimum example, step 1 is skipped).

Example 5: Symmetry, Variable Equalizing and Constraint Subtraction for Upper and Lower Bounds

Given the following linear program

$$\begin{aligned} & f_0(x) = \min(x_1 + x_2) \\ \text{s.t.} \quad & f_1(x) = 2 - 2x_1 - x_2 \leq 0 \\ & f_2(x) = 2 - x_1 - 2x_2 \leq 0 \\ & f_3(x) = 3 - 3x_1 - x_2 \leq 0 \end{aligned} \tag{I.12}$$

The solution of the original problem is to be found at the intersection of $f_2(x)$ and $f_3(x)$, i.e. we solve the following linear system of equations

$$\{x_1, x_2 \in R | 2 - x_1 - 2x_2 = 0 \wedge 3 - 3x_1 - x_2 = 0\} \tag{I.13}$$

which leads to

$$x_1^* = 0.8 \quad x_2^* = 0.6 \quad \text{and} \quad f_0(x^*) = \min(x_1^* + x_2^*) = 1.4 \tag{I.14}$$

We now strive to aggregate the problem by removing at least one variable and at least one constraint and thereby determine an upper and lower bound based on aggregated time steps.
As discussed above, the upper bound is relatively simple to be determined. As we want to aggregate at last one variable and one constraint, we simply state $x_1 \overset{!}{=} x_2$. Accordingly, we obtain the following aggregated upper bound problem:

$$\begin{aligned} &\hat{f}_0(x) = \widehat{\min}(2x_1) \\ &\text{s.t.}\ \ f_1(x) = 2 - 3x_1 \leq 0 \Leftrightarrow x_1 \geq \frac{2}{3} \\ &\qquad f_3(x) = 3 - 4x_1 \leq 0 \Leftrightarrow x_2 \geq \frac{3}{4} \end{aligned} \tag{I.15}$$

$f_2(x)$ was removed from the problem as it was identical to $f_1(x)$. The solution of this problem with $f_3(x)$ as the binding constraint is:

$$\hat{x}_1^* = \frac{3}{4} \ \text{ and } \ \hat{f}_0(\hat{x}^*) = \widehat{\min}(x_1^*) = 1{,}5 \tag{I.16}$$

For the determination of a lower bound according to the workflow described above, those equation need to be removed first, which impede a symmetrical problem. In the example, this is $f_3(x)$. Although asymmetry is much more difficult to prove, than symmetry can be shown, we consider the reflection matrix $Q = \begin{pmatrix} 0 & 1 \\ 1 & 0 \end{pmatrix}$ to prove the symmetry of $f_1(x)$ and $f_2(x)$ with respect to $x = \begin{pmatrix} x_1 \\ x_2 \end{pmatrix}$ which can be realized using the equation in Excursus 6:

$$f_1(Qx) = 2 - (2 \quad 1) \cdot \begin{pmatrix} 0 & 1 \\ 1 & 0 \end{pmatrix} \cdot \begin{pmatrix} x_1 \\ x_2 \end{pmatrix} = 2 - (2 \quad 1) \cdot \begin{pmatrix} x_2 \\ x_1 \end{pmatrix} = f_2(x) \leq 0 \tag{I.17}$$

$$f_2(Qx) = 2 - (1 \quad 2) \cdot \begin{pmatrix} 0 & 1 \\ 1 & 0 \end{pmatrix} \cdot \begin{pmatrix} x_1 \\ x_2 \end{pmatrix} = 2 - (1 \quad 2) \cdot \begin{pmatrix} x_2 \\ x_1 \end{pmatrix} = f_1(x) \leq 0 \tag{I.18}$$

Further, the objective $f_0(x)$ is obviously symmetric as well because $f_0(Qx) = f_0(x)$. Accordingly, $f_3(x)$ will be removed from the problem. The symmetrical problem is now:

$$\begin{aligned} &f_0(x) = \min(x_1 + x_2) \\ &\text{s.t.}\ \ f_1(x) = 2 - 2x_1 - x_2 \leq 0 \\ &\qquad f_2(x) = 2 - x_1 - 2x_2 \leq 0 \end{aligned} \tag{I.19}$$

Due to Excursus 6, we can now assume $x_1 \overset{!}{=} x_2$ without removing the optimal solution of the lower bound from the problem. Accordingly, we obtain the following aggregated lower bound problem:

$$\begin{aligned} &\check{f}_0(x) = \widecheck{\min}(2x_1) \\ &\text{s.t.}\ \ f_1(x) = 2 - 3x_1 \leq 0 \Leftrightarrow x_1 \geq \frac{2}{3} \end{aligned} \tag{I.20}$$

$f_2(x)$ was removed from the problem as it was identical to $f_1(x)$. The solution of this problem is

$$\check{x}_1^* = \frac{2}{3} \ \text{ and } \ \check{f}_0(\check{x}^*) = \widecheck{\min}(\check{x}_1^*) = 1{,}\overline{3} \tag{I.21}$$

As $\check{f}_0(\check{x}^*) = 1,\overline{3} \leq f_0(x^*) = 1.4 \leq \hat{f}_0(\hat{x}^*) = 1{,}5$, the general applicability step 2 has been demonstrated. The graphical interpretation of the upper and lower bound as well as the original problem are shown in Figure I.9.

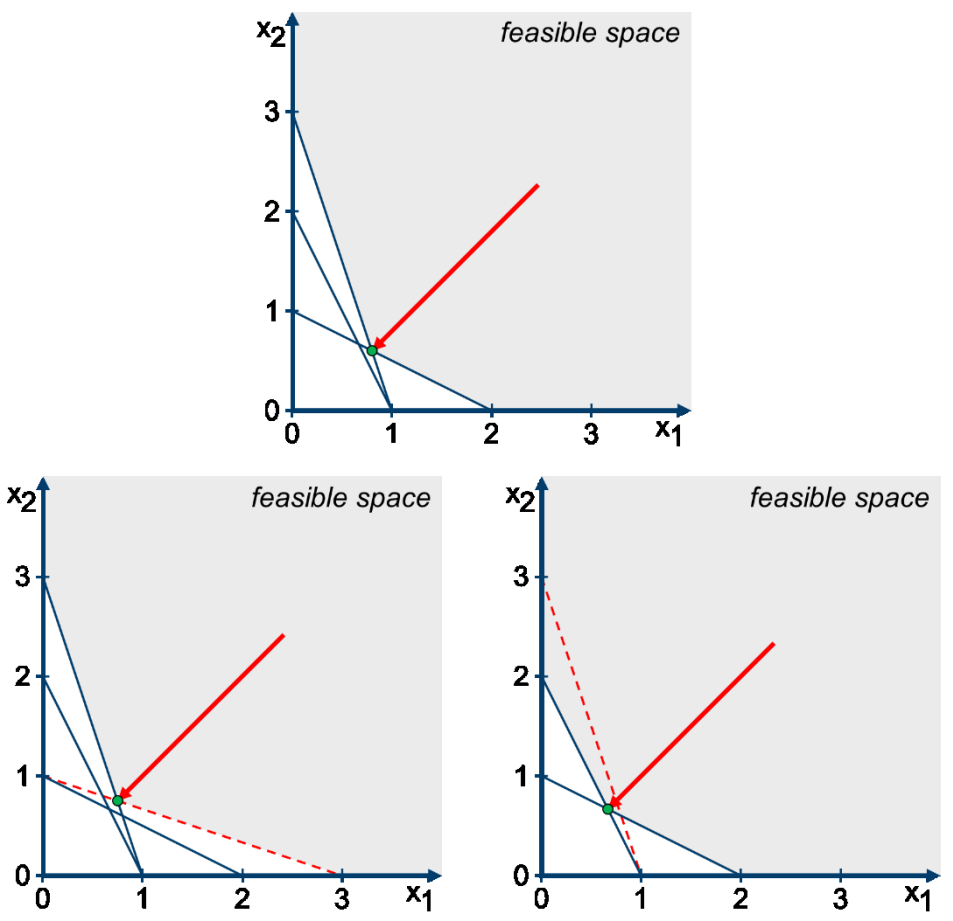

Figure I.9. The original optimization problem (top), the upper bound due to equalizing variables and removing redundant constraints (bottom left), and the lower bound due to removal of the asymmetric constraint and equalizing variables due to symmetry (bottom right)

The picture at the top of Figure I.9 visualizes the original asymmetric problem, in which the solution is obviously neither symmetric. The bottom left picture shows the visual representation of the upper bound problem. Here, the variables x_1 and x_2 were directly equalized. Geometrically, this can be understood as a reflection of constraint $f_3(x)$ on the angle bisector line because $f_3(x) = f_3(Qx)$ holds for $Q = \begin{pmatrix} 0 & 1 \\ 1 & 0 \end{pmatrix}$, if $x_1 = x_2$. The reflection of constraint $f_3(x)$ is represented by a dashed red line and the space, which it removes from the original feasible space, is visualized as white area. Obviously, both, the optimization problem and the optimal solution of the upper bound are now symmetric

again. The bottom right picture depicts the lower bound according to the workflow. The removed asymmetric constraint is highlighted by a dashed red line while the minimization gradient is highlighted as red vector. The remaining optimization problem is clearly symmetric to the angle bisector line and convex, which means that for the optimal solution of the lower problem $\check{x}_1^* = \check{x}_2^*$ holds.

To conclude, symmetry is an important principle that is essential to estimate the aggregation-induced deviation from the optimal objective if the optimization problems are convex and invariant with respect to certain variables. However, for this, the optimization problem needs to contain groups of blocks of variables that are identically parametrized, which is highlighted by the preceding step 1 in Figure I.8. Accordingly, the following two sections focus on the question how to change the parameters of energy system models by using data based on aggregated time series data systematically in order to obtain an upper or lower bound. As will be seen in the following, this can be realized by representing clusters of time series data by certain values they contain. Namely, for a systematical over- or underestimation of the original problem, the minimum or maximum representation or in seldom cases, in which the optimization problem has a special structure, also a centroid-based representation can provide a tight bound.

Note: mixed-integer linear programs need to be either restricted or relaxed to a linear program first because Excursus 6 does not hold for non-convex problems. A small example is given in Excursus 7.

Excursus 7: Symmetric non-convex problems with non-symmetrical solution

Given the following mixed-integer linear program

$$\begin{aligned} & f_0(x) = \min(x_1 + x_2) \\ & \text{s.t. } f_1(x) = 1 - x_1 - x_2 \leq 0 \\ & \quad x_1, x_2 \in Z^+ \end{aligned} \tag{I.22}$$

The problem is obviously symmetric as $f_0(x) = f_0(Qx)$ and $f_1(x) = f_1(Qx)$ with $Q = \begin{pmatrix} 0 & 1 \\ 1 & 0 \end{pmatrix}$. However, the optimal solutions are either $(x_1^*|x_2^*) = (1|0)$ or $(x_1^*|x_2^*) = (0|1)$. This proves the a-symmetry of optimal solutions for non-convex symmetric programs.

I.2.2. Upper bounds

As highlighted in the introduction, upper bounds of the original problem are not only needed to determine the maximum error based on data aggregation by calculating the gap to the lower bound, but they also provide a solution which is also feasible for the fully resolved case. Further, once the parameters for time steps to be aggregated are equalized based on an appropriate overestimation according to step 1 of the aggregation workflow, the removal of variables and constraints based on equalizing variables is straightforward. First, the approach will be explained for temporally decoupled systems. In a second step, the approach will then be applied to temporally coupled systems. However, this is comparably simple for upper bounds since equalizing variables never leads to an underestimation of the optimal objective value.

I.2.2.1. An Upper Bound for ESOMs with Unlinked Time Steps

From the previous section, we know that temporally decoupled models can be written as:

$$\begin{aligned}
&\min(c_0^T x_0 + c_t^T x_t)\\
&\text{s.t.} \quad A_t x_0 + B_t x_t = b_{RHS,t}\\
&dl_t \le C_t x_0 + D_t x_t \le du_t\\
&x_0 \in R_+^{J_0}, x_t \in R_+^{J_T}\\
&c_0 \in R^{J_0}, c_t \in R^{J_T}\\
&A_t \in R^{I_{Eq} \times J_0}, B_t \in R^{I_{Eq} \times J_T} \quad \forall \ t \in T\\
&C_t \in R^{I_{Neq} \times J_0}, D_t \in R^{I_{Neq} \times J_T} \quad \forall \ t \in T\\
&b_{RHS,t} \in R^{I_{Eq}}, dl_t, du_t \in R^{I_{Neq}} \quad \forall \ t \in T
\end{aligned} \tag{I.23}$$

As any equality $A_t x_0 + B_t x_t = b_{RHS}$ can be expressed as $b_{RHS}^- \le A_t x_0 + B_t x_t \le b_{RHS}^+$ with $b_{RHS}^- = b_{RHS}^+$, it is sufficient to focus on inequalities only in the following, i.e. $dl \le C_t x_0 + D_t x_t \le du$. Further, we assume all cost contributions to be positive for the sake of brevity and in order not to shorten the case distinction, i.e. $c_0 \in R_+^{J_0}, c_t \in R_+^{J_T}$. This assumption is reasonable for the majority of energy system models implemented in **FINE** because apart from revenues of exported energy amounts, all costs are usually positive, e.g. capacity and operation costs as well as import costs. This assumption helps us to understand the optimization problem stated above better as the target is to minimize each variable in x_0 and x_t without violating any of the side constraints. In index notation, we yield from $dl \le C_t x_0 + D_t x_t \le du$ the following set of constraints:

$$dl_{i_{neq},t} \leq \sum_{j_0} c_{i_{neq},j_0,t} x_{j_0,0} + \sum_{j_t} d_{i_{neq},j_t,t} x_{j_t,t} \leq du_{i_{neq},t} \quad \forall \quad i_{neq} \in I_{neq}, t \in T \qquad (I.24)$$

We can now resolve this equation to one specific time independent variable $x_{j_0=\lambda,0}$ (the transformation for time-dependent variables works analogously) depending on whether the coefficient $c_{i_{neq},j_0=\lambda,t}$ is positive or negative. For $c_{i_{neq},j_0=\lambda,t} > 0$, we yield:

$$x_{j_0=\lambda,0} \geq \frac{1}{c_{i_{neq},j_0=\lambda,t}} \left(dl_{i_{neq},t} - \sum_{j_0 \neq \lambda} c_{i_{neq},j_0,t} x_{j_0,0} - \sum_{j_t} d_{i_{neq},j_t,t} x_{j_t,t} \right) \quad \forall \quad i_{neq} \in I_{neq}, t \in T \qquad (I.25)$$

$$x_{j_0=\lambda,0} \leq \frac{1}{c_{i_{neq},j_0=\lambda,t}} \left(du_{i_{neq},t} - \sum_{j_0 \neq \lambda} c_{i_{neq},j_0,t} x_{j_0,0} - \sum_{j_t} d_{i_{neq},j_t,t} x_{j_t,t} \right) \quad \forall \quad i_{neq} \in I_{neq}, t \in T \qquad (I.26)$$

And for $c_{i_{neq},j_0=\lambda,t} < 0$ the formula reads:

$$x_{j_0=\lambda,0} \leq \frac{1}{c_{i_{neq},j_0=\lambda,t}} \left(dl_{i_{neq},t} - \sum_{j_0 \neq \lambda} c_{i_{neq},j_0,t} x_{j_0,0} - \sum_{j_t} d_{i_{neq},j_t,t} x_{j_t,t} \right) \quad \forall \quad i_{neq} \in I_{neq}, t \in T \qquad (I.27)$$

$$x_{j_0=\lambda,0} \geq \frac{1}{c_{i_{neq},j_0=\lambda,t}} \left(du_{i_{neq},t} - \sum_{j_0 \neq \lambda} c_{i_{neq},j_0,t} x_{j_0,0} - \sum_{j_t} d_{i_{neq},j_t,t} x_{j_t,t} \right) \quad \forall \quad i_{neq} \in I_{neq}, t \in T \qquad (I.28)$$

Here, it was assumed that a coefficient has the same sign for all time steps, as coefficients in energy systems are generally either constant throughout time (compare the example of the previous section) or are based on time series that do not cross zero (e.g. efficiencies, capacity factors, energy supply and energy demand). Alternatively, they can be represented by two independent variables, e.g. a price time series with negative prices can be divided into a non-negative cost time series and a non-positive revenue time series.

According to the non-negativity of the cost vectors defined above, each variable reduces the costs if it is reduced itself. Accordingly, the second and third equation are non-binding with respect to $x_{j_0=\lambda,0}$ and can thus be neglected.

The first inequality becomes more restrictive if the right hand side is overestimated because $x_{j_0=\lambda,0}$ is tried to be minimized. Accordingly, a conservative estimate is:

$$\hat{x}_{j_0=\lambda,0} \geq \frac{1}{\min\limits_{t\in C_k}\left(c_{i_{neq},j_0=\lambda,t}\right)}\left(\max_{t\in C_k}\left(dl_{i_{neq},t}\right) - \sum_{j_0\neq\lambda}^{J_0}\min_{t\in C_k}\left(c_{i_{neq},j_0,t}\right)x_{j_0,0} + \sum_{j_t}^{J_T}\min_{t\in C_k}\left(d_{i_{neq},j_t,t}\right)x_{j_t,t}\right) \quad \text{(I.29)}$$
$$\forall\ i_{neq} \in I_{neq}, t \in T$$

The fourth inequality is only a binding constraint if both factors on the right hand side are negative. Otherwise, the expression is negative and $\hat{x}_{j_0=\lambda,0} \geq 0$ is the binding constraint. This means that the expression grows if the denominator is negative but gets closer to zero and the numerator is negative but moves away from zero, i.e.:

$$\hat{x}_{j_0=\lambda,0} \geq \frac{1}{\max\limits_{t\in C_k}\left(c_{i_{neq},j_0=\lambda,t}\right)}\left(\min_{t\in C_k}\left(du_{i_{neq},t}\right) - \sum_{j_0\neq\lambda}^{J_0}\max_{t\in C_k}\left(c_{i_{neq},j_0,t}\right)x_{j_0,0} + \sum_{j_t}^{J_T}\max_{t\in C_k}\left(d_{i_{neq},j_t,t}\right)x_{j_t,t}\right) \quad \text{(I.30)}$$
$$\forall\ i_{neq} \in I_{neq}, t \in T$$

The example of the previous section has shown that $dl_{i_{neq},t}$ is often undefined, which means that this inequality can be omitted in certain cases.

With respect to the objective function, an overestimation of the original costs is achieved by:

$$\min\left(c_{j_0,0}^T x_{j_0,0} + c_{j_t,t}^T x_{j_t,t}\right) \leq \min\left(c_{j_0,0}^T x_{j_0,0} + \max_{t\in C_k}\left(c_{j_t,t}^T x_{j_t,t}\right)\right) \quad \text{(I.31)}$$

For negatively defined revenue time series, this equation also holds since the maximization leads to a minimization of their absolute values.

Although the proposed method for overestimating the original problem seems to be highly dependent on the mathematical structure of the problem, the direction in which a time series of coefficients needs to be overestimated is usually intuitively understandable, e.g. for a conservative estimation the following holds for cost-minimizing systems implemented in **FINE**:

Table I.1. Time series to be over- or underestimated in order to receive an upper bound of the fully resolved reference system

Time series	$\min\limits_{t\in C_k}(x)$	$\max\limits_{t\in C_k}(x)$
Capacity factors	✖	
Conversion factors	✖	
Demands		✖
Supplies	✖	
Costs		✖
Revenues	✖	

Moreover, as the number of clustered time steps K increases, less time steps are assigned to the same cluster $t \in C_k$, i.e. less coefficients are in the groups of which $\min_{t \in C_k}(x)$ and $\max_{t \in C_k}(x)$ choose the most conservative one. This means that the error due to this estimation decreases with the number of clusters. However, the computational complexity rises likewise. Finally yet importantly, it needs to be highlighted that all blocks that are assigned to the same cluster $\widetilde{A}_{t \in C_k}, \widetilde{B}_{t \in C_k}, \widetilde{C}_{t \in C_k}, \widetilde{D}_{t \in C_k}$ as well as the corresponding vector sections $\tilde{b}_{RHS,t \in C_k}, \widetilde{dl}_{t \in C_k}, \widetilde{du}_{t \in C_k}$ then share identical coefficients, i.e. a temporally decoupled system is then symmetric with respect to the time steps assigned to the same cluster. This means in turn that all symmetric variables and constraints can directly be removed, if the symmetric variables are multiplied by the cardinality of the corresponding cluster group, which is in this case also a symmetry group.

In order to illustrate the validity of the proposed method for unlinked time steps, we adapt the extremely simple energy system of the previous section to an energy system that comprises a capacity-driven objective function, and a time-dependent energy balance and component constraints.

Example 6: Upper bounds for a simple temporally decoupled problem

As depicted in Figure I.10, the energy system now "consists of two renewable energy sources with unknown capacities and hourly depreciation costs of $120 \frac{€}{MW_{inst}h}$ for source 1 and $100 \frac{€}{MW_{inst}h}$ for source 2. Again, these assumptions are fictitious, however, the scale of component costs are roughly comparable to the costs of solar cells with $120 \frac{€}{MW_{inst}d} * 365 \frac{d}{a} * 30\,a \approx 1.31\,Mio.€$ and wind turbines with $100 \frac{€}{MW_{inst}d} * 365 \frac{d}{a} * 20\,a \approx 0.73\,Mio.€$.

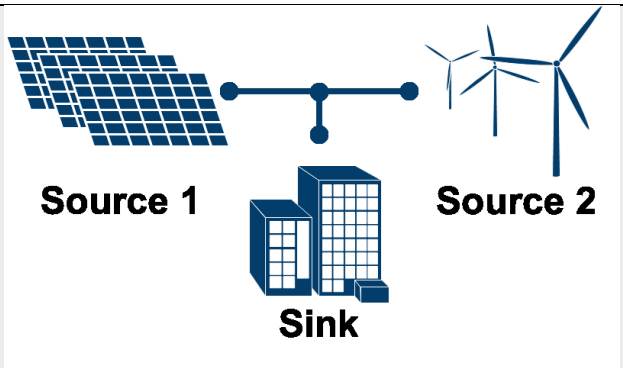

Figure I.10. The adapted energy system comprising two different renewable energy sources

Together with the side constraint, that the operation should never exceed the installed capacity multiplied by the time-dependent capacity factor of each component, this leads to the following linear program:

$$\begin{aligned}
&\min(\mathrm{TAC}) = \min\left(\mathrm{Cap}_{\mathrm{comp1}} * 120\frac{€}{\mathrm{MW_{inst}d}} + \mathrm{Cap}_{\mathrm{comp2}} * 100\frac{€}{\mathrm{MW_{inst}d}}\right) * 365\frac{\mathrm{d}}{\mathrm{a}} \\
&\text{s.t.} \quad \mathrm{Op}_{\mathrm{comp1}} + \mathrm{Op}_{\mathrm{comp2}} \geq \mathrm{Dem} \qquad \forall\ \mathrm{t} \in \mathrm{T} \\
&\qquad \mathrm{Op}_{\mathrm{comp1}}, \mathrm{Op}_{\mathrm{comp2}} \geq 0 \qquad \forall\ \mathrm{t} \in \mathrm{T} \\
&\mathrm{CapFac}_{\mathrm{comp1}} * \mathrm{Cap}_{\mathrm{comp1}} \geq \mathrm{Op}_{\mathrm{comp1}} \quad \forall\ \mathrm{t} \in \mathrm{T} \\
&\mathrm{CapFac}_{\mathrm{comp2}} * \mathrm{Cap}_{\mathrm{comp2}} \geq \mathrm{Op}_{\mathrm{comp2}} \quad \forall\ \mathrm{t} \in \mathrm{T}
\end{aligned} \tag{I.32}$$

Substitution of the operation variables $\mathrm{Op}_{\mathrm{comp1}}$ and $\mathrm{Op}_{\mathrm{comp2}}$ by the capacity factors and the capacities yield:

$$\begin{aligned}
&\min(\mathrm{TAC}) = \min\left(\mathrm{Cap}_{\mathrm{comp1}} * 120\frac{€}{\mathrm{MW_{inst}d}} + \mathrm{Cap}_{\mathrm{comp2}} * 100\frac{€}{\mathrm{MW_{inst}d}}\right) * 365\frac{\mathrm{d}}{\mathrm{a}} \\
&\text{s.t.} \quad \mathrm{CapFac}_{\mathrm{comp1}} * \mathrm{Cap}_{\mathrm{comp1}} + \mathrm{CapFac}_{\mathrm{comp2}} * \mathrm{Cap}_{\mathrm{comp2}} \geq \mathrm{Dem} \qquad \forall\ \mathrm{t} \in \mathrm{T}
\end{aligned} \tag{I.33}$$

As the demand needs to be satisfied at any point in time, the inequality above has to be satisfied for each time step. To illustrate the impact of the proposed approach for tightening the feasible space of the original linear program using aggregated time steps, we now consider four hourly time steps with varying capacity factors and electricity demand, e.g. during a spring day.

$$\begin{aligned}
&\min(\mathrm{TAC}) = \min\left(\mathrm{Cap}_{\mathrm{comp1}} * 120\frac{€}{\mathrm{MW_{inst}d}} + \mathrm{Cap}_{\mathrm{comp2}} * 100\frac{€}{\mathrm{MW_{inst}d}}\right) * 365\frac{\mathrm{d}}{\mathrm{a}} \\
&\text{s.t.} \quad 0.25\frac{\mathrm{MWh}}{\mathrm{MW_{inst}}} * \mathrm{Cap}_{\mathrm{comp1}} + 0.2\frac{\mathrm{MWh}}{\mathrm{MW_{inst}}} * \mathrm{Cap}_{\mathrm{comp2}} \geq 1\ \mathrm{MWh} \\
&\qquad 0.2\frac{\mathrm{MWh}}{\mathrm{MW_{inst}}} * \mathrm{Cap}_{\mathrm{comp1}} + 0.25\frac{\mathrm{MWh}}{\mathrm{MW_{inst}}} * \mathrm{Cap}_{\mathrm{comp2}} \geq 1\ \mathrm{MWh} \\
&\qquad 0.2\frac{\mathrm{MWh}}{\mathrm{MW_{inst}}} * \mathrm{Cap}_{\mathrm{comp1}} + 0.2\frac{\mathrm{MWh}}{\mathrm{MW_{inst}}} * \mathrm{Cap}_{\mathrm{comp2}} \geq 0.8\ \mathrm{MWh} \\
&\qquad 0.25\frac{\mathrm{MWh}}{\mathrm{MW_{inst}}} * \mathrm{Cap}_{\mathrm{comp1}} + 0.25\frac{\mathrm{MWh}}{\mathrm{MW_{inst}}} * \mathrm{Cap}_{\mathrm{comp2}} \geq 1\ \mathrm{MWh}
\end{aligned} \tag{I.34}$$

These are linear equations, which can be transformed to the following intercept-slope forms:

$$\begin{aligned} \mathrm{Cap}_{\mathrm{comp2}} &\geq 5\ \mathrm{MW}_{\mathrm{inst}} - 1.25\ \mathrm{Cap}_{\mathrm{comp1}} \\ \mathrm{Cap}_{\mathrm{comp2}} &\geq 4\ \mathrm{MW}_{\mathrm{inst}} - 0.8\ \mathrm{Cap}_{\mathrm{comp1}} \\ \mathrm{Cap}_{\mathrm{comp2}} &\geq 4\ \mathrm{MW}_{\mathrm{inst}} - 1\ \mathrm{Cap}_{\mathrm{comp1}} \\ \mathrm{Cap}_{\mathrm{comp2}} &\geq 4\ \mathrm{MW}_{\mathrm{inst}} - 1\ \mathrm{Cap}_{\mathrm{comp1}} \end{aligned} \tag{I.35}$$

The feasible space and the constraining linear equations are depicted in the upper graph of Figure I.11.

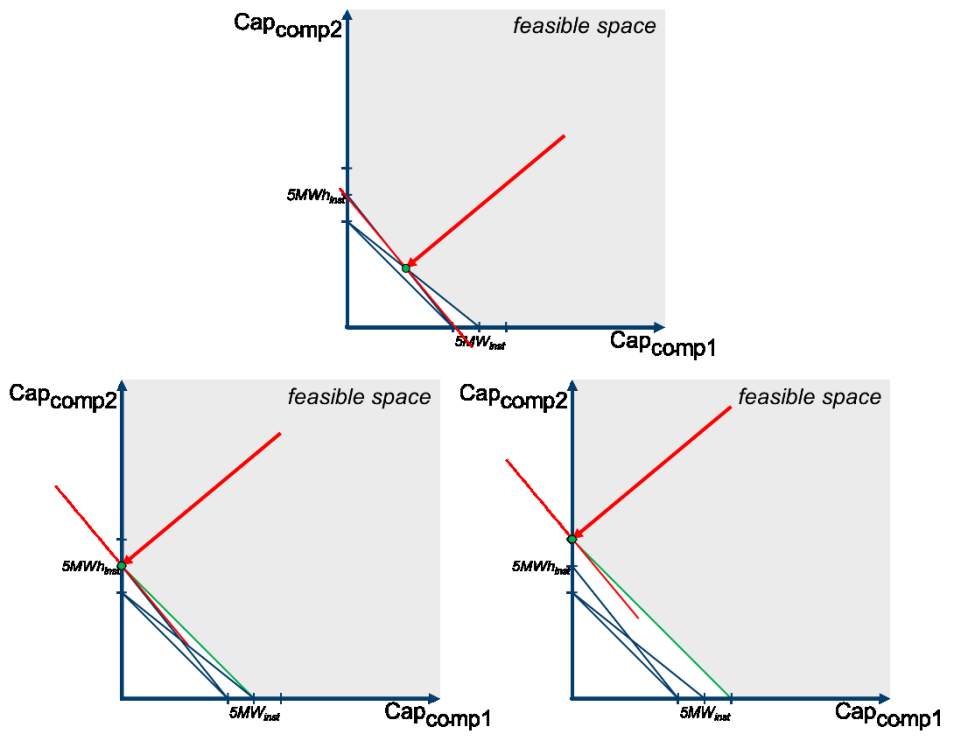

Figure I.11. The optimal solution for three time steps (top) and the optimal solution for the aggregated overestimation (bottom left) as well as the optimal solution for the aggregated overestimation with a manipulated fourth equation (bottom right)

As it can be seen, the optimal solution based on the three time steps lies on the intercept of the first and the second linear equation, which leads to optimal capacities of $\left(\mathrm{Cap}^{*}_{\mathrm{comp1}} \middle| \mathrm{Cap}^{*}_{\mathrm{comp2}}\right) = (2, \overline{2}\ \mathrm{MW}_{\mathrm{inst}} | 2, \overline{2}\ \mathrm{MW}_{\mathrm{inst}})$ and an optimal solution of $\min(\mathrm{TAC}) = 488, \overline{8}\,\frac{€}{\mathrm{d}} * 365\,\frac{\mathrm{d}}{\mathrm{a}}$." (Hoffmann et al [2])

Now, it is assumed that the three considered time steps are assigned to the same cluster. According to the proposed method for overestimating the linear program's optimal solution with an aggregated linear program, the capacity factor time series are now represented by their minimum value and the demand time series is represented by its maximum, i.e.:

$$\widetilde{\mathrm{Cap}}_{\mathrm{comp1}} = 0.2\,\frac{\mathrm{MWh}}{\mathrm{MW_{inst}}}$$
$$\widetilde{\mathrm{Cap}}_{\mathrm{comp2}} = 0.2\,\frac{\mathrm{MWh}}{\mathrm{MW_{inst}}} \tag{I.36}$$
$$\widehat{\mathrm{Dem}} = 1\ \mathrm{MWh}$$

The conservative estimation of the three time steps' constraints is thus the following constraint, which is represented by the green line in the bottom left graph of Figure I.11:

$$0.2\,\frac{\mathrm{MWh}}{\mathrm{MW_{inst}}} * \mathrm{Cap}_{\mathrm{comp1}} + 0.2\,\frac{\mathrm{MWh}}{\mathrm{MW_{inst}}} * \mathrm{Cap}_{\mathrm{comp2}} \geq 1\ \mathrm{MWh} \tag{I.37}$$

According to the lower left graph of Figure I.11, the optimal solution according to the overestimated aggregated optimization problem is now given by $\left(\mathrm{Cap}^*_{\mathrm{comp1}} \middle| \mathrm{Cap}^*_{\mathrm{comp2}}\right) = (0\ \mathrm{MW_{inst}} | 5\ \mathrm{MW_{inst}})$, which leads to an objective value of $\widehat{\min}(\mathrm{TAC}) = 500\,\frac{€}{\mathrm{d}} * 365\,\frac{\mathrm{d}}{\mathrm{a}}$. As it can be seen, the optimal objective value is now indeed slightly higher than for the original problem. However, significantly different component capacities are chosen. The reason for this strong deviation with respect to the chosen capacities is the aforementioned penny switching effect.
It is noteworthy that the proposed representation method is sensitive to the value range of each attribute assigned to the same cluster. As an example, the third and the fourth constraint are linearly dependent equations, i.e. their feasible region is the same. However, if we consider the fourth equation to be

$$0.3\,\frac{\mathrm{MWh}}{\mathrm{MW_{inst}}} * \mathrm{Cap}_{\mathrm{comp1}} + 0.3\,\frac{\mathrm{MWh}}{\mathrm{MW_{inst}}} * \mathrm{Cap}_{\mathrm{comp2}} \geq 1.2\ \mathrm{MWh} \tag{I.38}$$

Which is still a linearly dependent multiple of the third equation, the proposed method leads to an overestimating constraint of:

$$0.2\,\frac{\mathrm{MWh}}{\mathrm{MW_{inst}}} * \mathrm{Cap}_{\mathrm{comp1}} + 0.2\,\frac{\mathrm{MWh}}{\mathrm{MW_{inst}}} * \mathrm{Cap}_{\mathrm{comp2}} \geq 1.2\ \mathrm{MWh} \tag{I.39}$$

This bound is illustrated in the bottom right picture of Figure I.11. As it can be seen, the bound is now more restrictive despite of the fact that the feasible regions of the fully resolved optimization problem and the fully resolved problem with a manipulated fourth equation are congruent. Here, the optimal solution according to the newly calculated upper bound of the problem would be $\left(\mathrm{Cap}^*_{\mathrm{comp1}} \middle| \mathrm{Cap}^*_{\mathrm{comp2}}\right) = (0\ \mathrm{MW_{inst}} | 6\ \mathrm{MW_{inst}})$, which leads to an objective value of $\widehat{\min}(\mathrm{TAC}) = 600\,\frac{€}{\mathrm{d}} * 365\,\frac{\mathrm{d}}{\mathrm{a}}$. This emphasizes that

the clustering errors must be as small as possible in order to prevent a too conservative overestimation of the original energy system optimization. An alternative method to provide tighter upper bounds would be the normalization of all equations that belong to the same cluster and choosing the most conservative configurations from that normalized set of equations. However, this approach needs detailed information about the attributes belonging to a set of equivalent equations and is thus not directly applicable in an aggregation procedure. Therefore, it exceeds the scope of this thesis.

This small example illustrates the theoretically shown validity of the approach for ESOMs with independent time steps, but also highlights that there is no guarantee for a good approximation of the individual capacities of a large set of similar technologies (similar costs, production of similar commodities, similar time series). This, in turn, supports the earlier mentioned finding that only the derivation of the TAC is a meaningful measure for the quality of an aggregation, if feasibility of the design and operation are given.

I.2.2.2. An Upper Bound for ESOMs with Linked Time Steps

If the energy system model comprises linking constraints between time steps, the energy system model is generally not symmetric after step 1 of the aggregation workflow. Accordingly, the equalizing of variables and their subsequent substitution as described in step 2 is required in order to reduce the complexity of the energy system model.

As mentioned earlier, the equalizing of variables is always a restriction of the optimization problem and therefore in line with the overall target described in this section to overestimate the optimization problem. Concretely, those variables are equalized that describe corresponding system features in different time steps if these time steps are assigned to the same cluster. As an example, the operation of a component is defined for three time steps, i.e. $\mathrm{op}_{\mathrm{comp,t}}\ \forall\, \mathrm{t} \in \{1,2,3\}$. Then, if the time horizon is clustered and time step 1 and 3 are assigned to the same cluster, it is assumed that $\mathrm{op}_{\mathrm{comp},1} = \mathrm{op}_{\mathrm{comp},3}$. The last partial step within step 2 is the removal of those constraints, which have become identical due to the

equalizing of variables. More concretely, those constraints are redundant, which refer to time steps of the same clusters and do not couple time steps with each other. This means simultaneously that e.g. storage constraints should not be removed in the aggregation process and remain part of the aggregated problem. If this rule is followed, i.e. if time-coupling constraints are not removed from the aggregated optimization problem, it can be guaranteed that the aggregated program with systematically over- and underestimated coefficients according to Table I.1 remains an upper bound o the reference program.

I.2.3. Lower Bounds

In order to define the maximum aggregation-induced error, a lower bound is needed as well. In accordance with the previous section, the following one will first focus on temporally decoupled systems and will then specify how a lower bound for temporally decoupled systems can be achieved using symmetry and by symmetrizing generally asymmetrical linking constraints.

I.2.3.1. A Lower Bound for ESOMs with Unlinked Time Steps

For temporally decoupled systems, the approach to determine lower bounds is analogous to the procedure for determining upper bounds. The only exception is that the $\min(x)$-operator is swapped with the $\max(x)$-operator. This means that for the given optimization problem

$$\begin{aligned}
&\min(c_0^T x_0 + c_t^T x_t)\\
&\text{s.t.} \quad A_t x_0 + B_t x_t = b_{RHS,t}\\
&dl_t \le C_t x_0 + D_t x_t \le du_t\\
&x_0 \in R_+^{J_0}, x_t \in R_+^{J_T}\\
&c_0 \in R^{J_0}, c_t \in R^{J_T}\\
&A_t \in R^{I_{Eq} \times J_0}, B_t \in R^{I_{Eq} \times J_T} \quad \forall \ t \in T\\
&C_t \in R^{I_{Neq} \times J_0}, D_t \in R^{I_{Neq} \times J_T} \quad \forall \ t \in T\\
&b_{RHS,t} \in R^{I_{Eq}}, dl_t, du_t \in R^{I_{Neq}} \quad \forall \ t \in T
\end{aligned} \tag{I.40}$$

it is again sufficient to focus on the term $dl_t \le C_t x_0 + D_t x_t \le du_t$ only. Using the index notation of this equation

$$dl_{i_{neq},t} \le \sum_{j_0}^{J_0} c_{i_{neq},j_0,t} x_{j_0,0} + \sum_{j_t}^{J_T} d_{i_{neq},j_t,t} x_{j_t,t} \le du_{i_{neq},t} \quad \forall \ i_{neq} \in I_{neq}, t \in T \tag{I.41}$$

We can again specify the two constraints for an arbitrary design variable in case $c_{i_{neq},j_0=\lambda,t}$ is positive:

$$x_{j_0=\lambda,0} \geq \frac{1}{c_{i_{neq},j_0=\lambda,t}} \left(dl_{i_{neq},t} - \sum_{j_0 \neq \lambda}^{J_0} c_{i_{neq},j_0,t} x_{j_0,0} - \sum_{j_t}^{J_T} d_{i_{neq},j_t,t} x_{j_t,t} \right) \quad \forall \; i_{neq} \in I_{neq}, t \in T \qquad (I.42)$$

$$x_{j_0=\lambda,0} \leq \frac{1}{c_{i_{neq},j_0=\lambda,t}} \left(du_{i_{neq},t} - \sum_{j_0 \neq \lambda}^{J_0} c_{i_{neq},j_0,t} x_{j_0,0} - \sum_{j_t}^{J_T} d_{i_{neq},j_t,t} x_{j_t,t} \right) \quad \forall \; i_{neq} \in I_{neq}, t \in T \qquad (I.43)$$

And two constraints in case $c_{i_{neq},j_0=\lambda,t}$ is negative:

$$x_{j_0=\lambda,0} \leq \frac{1}{c_{i_{neq},j_0=\lambda,t}} \left(dl_{i_{neq},t} - \sum_{j_0 \neq \lambda}^{J_0} c_{i_{neq},j_0,t} x_{j_0,0} - \sum_{j_t}^{J_T} d_{i_{neq},j_t,t} x_{j_t,t} \right) \quad \forall \; i_{neq} \in I_{neq}, t \in T \qquad (I.44)$$

$$x_{j_0=\lambda,0} \geq \frac{1}{c_{i_{neq},j_0=\lambda,t}} \left(du_{i_{neq},t} - \sum_{j_0 \neq \lambda}^{J_0} c_{i_{neq},j_0,t} x_{j_0,0} - \sum_{j_t}^{J_T} d_{i_{neq},j_t,t} x_{j_t,t} \right) \quad \forall \; i_{neq} \in I_{neq}, t \in T \qquad (I.45)$$

Again, only the first one and the fourth one are binding if it is assumed that all cost coefficients are positive. Furthermore, the proof is analogous for time-dependent variables.

Here, the first inequality becomes less restrictive if the right hand side is underestimated because $x_{j_0=\lambda,0}$ is tried to be minimized for a positive corresponding cost coefficient. Accordingly, an underestimation is:

$$\hat{x}_{j_0=\lambda,0} \geq \frac{1}{\max\limits_{t \in C_k} \left(c_{i_{neq},j_0=\lambda,t} \right)} \left(\min_{t \in C_k} \left(dl_{i_{neq},t} \right) - \sum_{j_0 \neq \lambda}^{J_0} \max_{t \in C_k} \left(c_{i_{neq},j_0,t} \right) x_{j_0,0} - \sum_{j_t}^{J_T} \max_{t \in C_k} \left(d_{i_{neq},j_t,t} \right) x_{j_t,t} \right) \qquad (I.46)$$
$$\forall \; i_{neq} \in I_{neq}, t \in T$$

As explained above, the fourth inequality is only a binding constraint if both factors on the right hand side are negative. Otherwise, the expression is negative and $\hat{x}_{j_0=k,0} \geq 0$ is the binding constraint. This means that the expression decreases if the denominator is negative but moves away from zero and the numerator is negative but gets closer to zero, i.e.:

$$\hat{x}_{j_0=\lambda,0} \geq \frac{1}{\min\limits_{t \in C_k} \left(c_{i_{neq},j_0=\lambda,t} \right)} \left(\max_{t \in C_k} \left(du_{i_{neq},t} \right) - \sum_{j_0 \neq \lambda}^{J_0} \min_{t \in C_k} \left(c_{i_{neq},j_0,t} \right) x_{j_0,0} - \sum_{j_t}^{J_T} \min_{t \in C_k} \left(d_{i_{neq},j_t,t} \right) x_{j_t,t} \right) \qquad (I.47)$$
$$\forall \; i_{neq} \in I_{neq}, t \in T$$

For objective function, an underestimation of the original costs is achieved by:

$$\min\left(c_{j_0,0}^T x_{j_0,0} + c_{j_t,t}^T x_{j_t,t} \right) \geq \min \left(c_{j_0,0}^T x_{j_0,0} + \min_{t \in C_k} \left(c_{j_t,t}^T x_{j_t,t} \right) \right) \qquad (I.48)$$

The following table summarizes the required over- and underestimation of **FINE**-specific time series in order to achieve a systematic underestimation of the reference system based on aggregated data:

Table I.2. Time series to be over- or underestimated in order to receive a lower bound of the fully resolved reference system

Time series	$\min_{t \in C_k}(x)$	$\max_{t \in C_k}(x)$
Capacity factors		✖
Conversion factors		✖
Demands	✖	
Supplies		✖
Costs	✖	
Revenues		✖

I.2.3.2. A Centroid-Based Alternative Lower Bound

In case that time-dependent variables of a temporally decoupled optimization model do not have a time-dependent cost contribution, it can also be shown that a centroid-based representation of the energy system's aggregated time series lead to a tighter lower bound of the energy system model. This effect was frequently observed for capacity expansion models combined with k-means clustering, in which the time-independent capacity costs have the biggest impact on the overall costs. Theoretically, this was shown by Teichgräber et al. [47] in case of time series in the upper bound vector du. In the following, we further generalize this approach to time series contained in either the matrices A_t, B_t, C_t, D_t or the constraining vectors $b_{RHS}, \mathrm{dl}, \mathrm{du}$. For this, it is again sufficient to focus on the inequality $\mathrm{dl}_t \leq C_t x_0 + D_t x_t \leq \mathrm{du}_t$ only. In index notation, we yield:

$$\mathrm{dl}_{i_{neq},t} \leq \sum_{j_0}^{J_0} c_{i_{neq},j_0,t} x_{j_0,0} + \sum_{j_t}^{J_T} d_{i_{neq},j_t,t} x_{j_t,t} \leq \mathrm{du}_{i_{neq},t} \quad \forall \; i_{neq} \in I_{neq}, t \in T \tag{I.49}$$

The representation of clustered time steps by centroids leads to the following inequality:

$$\frac{1}{|C_k|} \sum_{t \in C_k} \mathrm{dl}_{i_{neq},t} \leq \frac{1}{|C_k|} \sum_{t \in C_k} \sum_{j_0}^{J_0} c_{i_{neq},j_0,t} x_{j_0,0} + \frac{1}{|C_k|} \sum_{t \in C_k} \sum_{j_t}^{J_T} d_{i_{neq},j_t,t} x_{j_t,t} \leq \frac{1}{|C_k|} \sum_{t \in C_k} \mathrm{du}_{i_{neq},t} \tag{I.50}$$
$$\forall \; i_{neq} \in I_{neq}, k \in K$$

As this constraint is a linear combination of the preceding equation with respect to those time steps that are assigned to the same

cluster, the constraint is not further restricting the original problem if it is applied time step and variable wise ($i_{neq} \in I_{neq}, t \in T$). Therefore, it can be added to the original set of constraints without increasing the optimal solution. If the original equations are then removed, the original problem is relaxed because the removal of constraints is always a relaxation of the original problem unless the removed constraints are not linear dependent.

Due to the fact that the energy system model is assumed to be temporally decoupled and the cost contributions of all time-depending variables are considered constant, i.e. $c_{j_t,t_1} = c_{j_t,t_2}\ \forall\, t_1, t_2 \in \{1, \dots, T\}$ and accordingly also $c_{j_t,t_1} = c_{j_t,t_2}\ \forall\, t_1, t_2 \in C_k$, the optimization problem is then symmetric with respect to those time steps that are assigned to the same cluster. As the optimization problem is convex in case of a linear program, the optimal solution of the corresponding operating variables is also symmetric, i.e. $x^*_{j_t,t_1} = x^*_{j_t,t_2} := \bar{x}^*_{j_t,k}\ \forall\, t_1, t_2 \in C_k$. For time-independent variables, this holds anyways.

This proof generalized theorem 2 provided by Teichgräber et al. [47] for time-dependent coefficients in equality or inequality constraints. In case of **FINE**, these are e.g. time series for capacity factors and therefore an important generalization for renewable energy system models. Apart from the proof based on linear combinations, the error due to averaged time series can more formally be quantified for time-independent variables as presented in Excursus 8.

Excursus 8: Error of Temporally Averaged Constraints and Time-Independent Variables

If we resolve the equation above for a time-independent variable $x_{j_0=\lambda,0}$, we obtain $\forall\, i_{neq} \in I_{neq}, t \in T \wedge \sum_{t \in C_k} c_{i_{neq},j_0=\lambda,t} > 0$:

$$x_{j_0=\lambda,0} \geq \frac{1}{\sum_{t \in C_k} c_{i_{neq},j_0=\lambda,t}} \sum_{t \in C_k} \left(dl_{i_{neq},t} - \sum_{j_0 \neq \lambda}^{J_0} c_{i_{neq},j_0,t} x_{j_0,0} - \sum_{j_t}^{J_T} d_{i_{neq},j_t,t} x_{j_t,t} \right) \quad \text{(I.51)}$$

$$x_{j_0=\lambda,0} \leq \frac{1}{\sum_{t \in C_k} c_{i_{neq},j_0=\lambda,t}} \sum_{t \in C_k} \left(du_{i_{neq},t} - \sum_{j_0 \neq \lambda}^{J_0} c_{i_{neq},j_0,t} x_{j_0,0} - \sum_{j_t}^{J_T} d_{i_{neq},j_t,t} x_{j_t,t} \right) \quad \text{(I.52)}$$

And $\forall\, i_{neq} \in I_{neq}, t \in T \wedge \sum_{t \in C_k} c_{i_{neq}, j_0=\lambda, t} < 0$:

$$x_{j_0=\lambda,0} \leq \frac{1}{\sum_{t \in C_k} c_{i_{neq}, j_0=\lambda, t}} \sum_{t \in C_k} \left(dl_{i_{neq},t} - \sum_{j_0 \neq \lambda}^{J_0} c_{i_{neq},j_0,t} x_{j_0,0} - \sum_{j_t}^{J_T} d_{i_{neq},j_t,t} x_{j_t,t} \right) \quad \text{(I.53)}$$

$$x_{j_0=\lambda,0} \geq \frac{1}{\sum_{t \in C_k} c_{i_{neq}, j_0=\lambda, t}} \sum_{t \in C_k} \left(du_{i_{neq},t} - \sum_{j_0 \neq \lambda}^{J_0} c_{i_{neq},j_0,t} x_{j_0,0} - \sum_{j_t}^{J_T} d_{i_{neq},j_t,t} x_{j_t,t} \right) \quad \text{(I.54)}$$

For the fully resolved case, we obtain, analogously to the previous sections, the constraints $\forall\, i_{neq} \in I_{neq}, t \in T \wedge c_{i_{neq}, j_0=\lambda, t} > 0$:

$$\begin{aligned} x_{j_0=\lambda,0} &\geq \frac{1}{c_{i_{neq}, j_0=\lambda, t}} \left(dl_{i_{neq},t} - \sum_{j_0 \neq \lambda}^{J_0} c_{i_{neq},j_0,t} x_{j_0,0} - \sum_{j_t}^{J_T} d_{i_{neq},j_t,t} x_{j_t,t} \right) \\ &= \max_{t \in C_k} \left(\frac{1}{c_{i_{neq}, j_0=\lambda, t}} \left(dl_{i_{neq},t} - \sum_{j_0 \neq \lambda}^{J_0} c_{i_{neq},j_0,t} x_{j_0,0} - \sum_{j_t}^{J_T} d_{i_{neq},j_t,t} x_{j_t,t} \right) \right) \end{aligned} \quad \text{(I.55)}$$

$$\begin{aligned} x_{j_0=\lambda,0} &\leq \frac{1}{c_{i_{neq}, j_0=\lambda, t}} \left(du_{i_{neq},t} - \sum_{j_0 \neq \lambda}^{J_0} c_{i_{neq},j_0,t} x_{j_0,0} - \sum_{j_t}^{J_T} d_{i_{neq},j_t,t} x_{j_t,t} \right) \\ &= \min_{t \in C_k} \left(\frac{1}{c_{i_{neq}, j_0=\lambda, t}} \left(du_{i_{neq},t} - \sum_{j_0 \neq \lambda}^{J_0} c_{i_{neq},j_0,t} x_{j_0,0} - \sum_{j_t}^{J_T} d_{i_{neq},j_t,t} x_{j_t,t} \right) \right) \end{aligned} \quad \text{(I.56)}$$

And $\forall\, i_{neq} \in I_{neq}, t \in T \wedge c_{i_{neq}, j_0=\lambda, t} < 0$:

$$\begin{aligned} x_{j_0=\lambda,0} &\leq \frac{1}{c_{i_{neq}, j_0=\lambda, t}} \left(dl_{i_{neq},t} - \sum_{j_0 \neq \lambda}^{J_0} c_{i_{neq},j_0,t} x_{j_0,0} - \sum_{j_t}^{J_T} d_{i_{neq},j_t,t} x_{j_t,t} \right) \\ &= \min_{t \in C_k} \left(\frac{1}{c_{i_{neq}, j_0=\lambda, t}} \left(dl_{i_{neq},t} - \sum_{j_0 \neq \lambda}^{J_0} c_{i_{neq},j_0,t} x_{j_0,0} - \sum_{j_t}^{J_T} d_{i_{neq},j_t,t} x_{j_t,t} \right) \right) \end{aligned} \quad \text{(I.57)}$$

$$\begin{aligned} x_{j_0=\lambda,0} &\geq \frac{1}{c_{i_{neq}, j_0=\lambda, t}} \left(du_{i_{neq},t} - \sum_{j_0 \neq \lambda}^{J_0} c_{i_{neq},j_0,t} x_{j_0,0} - \sum_{j_t}^{J_T} d_{i_{neq},j_t,t} x_{j_t,t} \right) \\ &= \max_{t \in C_k} \left(\frac{1}{c_{i_{neq}, j_0=\lambda, t}} \left(du_{i_{neq},t} - \sum_{j_0 \neq \lambda}^{J_0} c_{i_{neq},j_0,t} x_{j_0,0} - \sum_{j_t}^{J_T} d_{i_{neq},j_t,t} x_{j_t,t} \right) \right) \end{aligned} \quad \text{(I.58)}$$

Here, the second line of each equation emphasizes that the upper and lower bounds of a variable are always defined by the most restrictive constraints. Therefore, taking only the most restrictive constraints of all time steps assigned to the same cluster

$t \in C_k$ does not change the feasible range of each time-independent variable $x_{j_0=\lambda,0}$. In case of an upper bound, the most restrictive constraint of a constraint class i_{neq} is the minimum one of that cluster, and in case of a lower bound, it is the maximum one.

From Excursus 9, we receive the following inequalities $\forall\, i_{neq} \in I_{neq}, t \in T \wedge\ c_{i_{neq},j_0=\lambda,t} > 0$:

$$\begin{aligned} x_{j_0=\lambda,0} &\geq \max_{t\in C_k}\left(\frac{1}{c_{i_{neq},j_0=\lambda,t}}\left(dl_{i_{neq},t} - \sum_{j_0\neq\lambda}^{J_0} c_{i_{neq},j_0,t}x_{j_0,0} - \sum_{j_t}^{J_T} d_{i_{neq},j_t,t}x_{j_t,t}\right)\right) \\ &\geq \frac{1}{\sum_{t\in C_k} c_{i_{neq},j_0=\lambda,t}} \sum_{t\in C_k}\left(dl_{i_{neq},t} - \sum_{j_0\neq\lambda}^{J_0} c_{i_{neq},j_0,t}x_{j_0,0} - \sum_{j_t}^{J_T} d_{i_{neq},j_t,t}x_{j_t,t}\right) \end{aligned} \tag{I.59}$$

$$\begin{aligned} x_{j_0=\lambda,0} &\leq \min_{t\in C_k}\left(\frac{1}{c_{i_{neq},j_0=\lambda,t}}\left(du_{i_{neq},t} - \sum_{j_0\neq\lambda}^{J_0} c_{i_{neq},j_0,t}x_{j_0,0} - \sum_{j_t}^{J_T} d_{i_{neq},j_t,t}x_{j_t,t}\right)\right) \\ &\leq \frac{1}{\sum_{t\in C_k} c_{i_{neq},j_0=\lambda,t}} \sum_{t\in C_k}\left(du_{i_{neq},t} - \sum_{j_0\neq\lambda}^{J_0} c_{i_{neq},j_0,t}x_{j_0,0} - \sum_{j_t}^{J_T} d_{i_{neq},j_t,t}x_{j_t,t}\right) \end{aligned} \tag{I.60}$$

And $\forall\, i_{neq} \in I_{neq}, t \in T \wedge\ c_{i_{neq},j_0=\lambda,t} < 0$:

$$\begin{aligned} x_{j_0=\lambda,0} &\leq \min_{t\in C_k}\left(\frac{1}{c_{i_{neq},j_0=\lambda,t}}\left(dl_{i_{neq},t} - \sum_{j_0\neq\lambda}^{J_0} c_{i_{neq},j_0,t}x_{j_0,0} - \sum_{j_t}^{J_T} d_{i_{neq},j_t,t}x_{j_t,t}\right)\right) \\ &\leq \frac{1}{\sum_{t\in C_k} c_{i_{neq},j_0=\lambda,t}} \sum_{t\in C_k}\left(dl_{i_{neq},t} - \sum_{j_0\neq\lambda}^{J_0} c_{i_{neq},j_0,t}x_{j_0,0} - \sum_{j_t}^{J_T} d_{i_{neq},j_t,t}x_{j_t,t}\right) \end{aligned} \tag{I.61}$$

$$\begin{aligned} x_{j_0=\lambda,0} &\geq \max_{t\in C_k}\left(\frac{1}{c_{i_{neq},j_0=\lambda,t}}\left(du_{i_{neq},t} - \sum_{j_0\neq\lambda}^{J_0} c_{i_{neq},j_0,t}x_{j_0,0} - \sum_{j_t}^{J_T} d_{i_{neq},j_t,t}x_{j_t,t}\right)\right) \\ &\geq \frac{1}{\sum_{t\in C_k} c_{i_{neq},j_0=\lambda,t}} \sum_{t\in C_k}\left(du_{i_{neq},t} - \sum_{j_0\neq\lambda}^{J_0} c_{i_{neq},j_0,t}x_{j_0,0} - \sum_{j_t}^{J_T} d_{i_{neq},j_t,t}x_{j_t,t}\right) \end{aligned} \tag{I.62}$$

As the upper bounds based on averaged coefficients are bigger than the original bounds and the lower bounds based on averaged coefficients are smaller than the original bounds, the constraints as defined by averaged coefficients obviously define looser bounds for time-independent variables.

Graphically, the impact of averaging the coefficients in the constraint matrix on the feasible space of time independent variables can be illustrated by the following example:

Consider a feasible space F given by:

$$\mathrm{F} = \left\{ \mathrm{x} = \begin{pmatrix} \mathrm{x}_1 \\ \mathrm{x}_2 \end{pmatrix} \in \mathrm{R}_+^2 \middle| \, \mathrm{dl}_{\mathrm{neq}_1} \leq \mathrm{C}_{\mathrm{neq}_1}\mathrm{x} \wedge \mathrm{dl}_{\mathrm{neq}_2} \leq \mathrm{C}_{\mathrm{neq}_2}\mathrm{x} \wedge \mathrm{dl}_{\mathrm{neq}_3} \leq \mathrm{C}_{\mathrm{neq}_3}\mathrm{x} \wedge \mathrm{dl}_{\mathrm{neq}_4} \leq \mathrm{C}_{\mathrm{neq}_4}\mathrm{x} \right\} \tag{I.63}$$

With

$$\mathrm{C}_{\mathrm{neq}_1} = \begin{pmatrix} -0.5 & 1 \\ -1 & 1 \end{pmatrix}, \mathrm{dl}_{\mathrm{neq}_1} = \begin{pmatrix} -1 \\ -2 \end{pmatrix} \tag{I.64}$$

$$\mathrm{C}_{\mathrm{neq}_2} = \begin{pmatrix} 2 & 1 \\ 1 & 1 \end{pmatrix}, \mathrm{dl}_{\mathrm{neq}_2} = \begin{pmatrix} 4 \\ 4 \end{pmatrix} \tag{I.65}$$

$$\mathrm{C}_{\mathrm{neq}_3} = \begin{pmatrix} 0.5 & -1 \\ 1 & -1 \end{pmatrix}, \mathrm{dl}_{\mathrm{neq}_3} = \begin{pmatrix} -4 \\ -2 \end{pmatrix} \tag{I.66}$$

$$\mathrm{C}_{\mathrm{neq}_4} = \begin{pmatrix} -2 & -1 \\ -1 & -1 \end{pmatrix}, \mathrm{dl}_{\mathrm{neq}_4} = \begin{pmatrix} -14 \\ -8 \end{pmatrix} \tag{I.67}$$

It is now assumed that the first and second equation of each matrix describe constraints for two different time steps. If these time steps are now aggregated by averaging the coefficients in all matrices and constraint vectors, we yield:

$$\tilde{\mathrm{C}}_{\mathrm{neq}_1} = (-0.75 \quad 1), \tilde{\mathrm{dl}}_{\mathrm{neq}_1} = (-1.5) \tag{I.68}$$

$$\tilde{\mathrm{C}}_{\mathrm{neq}_2} = (1.5 \quad 1), \tilde{\mathrm{dl}}_{\mathrm{neq}_2} = (4) \tag{I.69}$$

$$\tilde{\mathrm{C}}_{\mathrm{neq}_3} = (0.75 \quad -1), \tilde{\mathrm{dl}}_{\mathrm{neq}_3} = (-3) \tag{I.70}$$

$$\tilde{\mathrm{C}}_{\mathrm{neq}_4} = (-1.5 \quad -1), \tilde{\mathrm{dl}}_{\mathrm{neq}_4} = (-11) \tag{I.71}$$

The feasible spaced based on aggregated data with averaged constraints for the time-independent variables is then given by:

$$\tilde{\mathrm{F}} = \left\{ \mathrm{x} = \begin{pmatrix} \mathrm{x}_1 \\ \mathrm{x}_2 \end{pmatrix} \in \mathrm{R}_+^2 \middle| \, \tilde{\mathrm{dl}}_{\mathrm{neq}_1} \leq \tilde{\mathrm{C}}_{\mathrm{neq}_1}\mathrm{x} \wedge \tilde{\mathrm{dl}}_{\mathrm{neq}_2} \leq \tilde{\mathrm{C}}_{\mathrm{neq}_2}\mathrm{x} \wedge \tilde{\mathrm{dl}}_{\mathrm{neq}_3} \leq \tilde{\mathrm{C}}_{\mathrm{neq}_3}\mathrm{x} \wedge \tilde{\mathrm{dl}}_{\mathrm{neq}_4} \leq \tilde{\mathrm{C}}_{\mathrm{neq}_4}\mathrm{x} \right\} \tag{I.72}$$

Figure I.12 illustrates the impact of averaging the constraints that define the feasible space F. As it can be seen, the feasible space based on the original set of constraints is smaller than the one based on aggregated data $\tilde{\mathrm{F}}$. If the objective function is not affected by the aggregation, i.e. if the direction of the objective function's gradient remains the same, which is the case for time-independent cost contributions of time dependent variables, this is obviously a relaxation of the original problem.

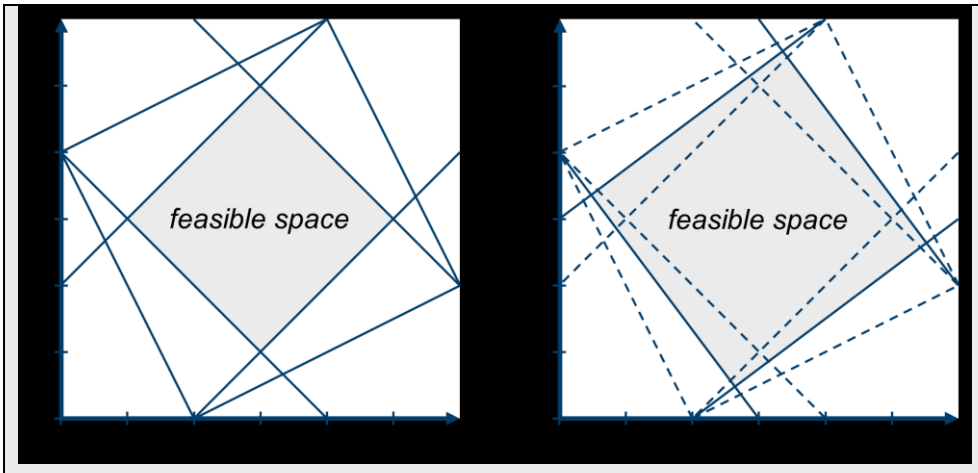

Figure I.12. The feasible space F and the feasible space based on averaged constraints $\tilde{F}$

Excursus 9: Proof for Extreme Values of Sets of Ratios

Given two sets of values $a_i, b_i \in R$ with $i = 1, \dots, n$. Then, the following inequalities hold:

$$\max_i\left(\frac{a_i}{b_i}\right) \geq \frac{\sum_i a_i}{\sum_i b_i} \quad \forall \quad \sum_i b_i > 0 \quad \wedge \quad \max_i\left(\frac{a_i}{b_i}\right) \leq \frac{\sum_i a_i}{\sum_i b_i} \quad \forall \quad \sum_i b_i < 0 \tag{I.73}$$

$$\min_i\left(\frac{a_i}{b_i}\right) \leq \frac{\sum_i a_i}{\sum_i b_i} \quad \forall \quad \sum_i b_i > 0 \quad \wedge \quad \min_i\left(\frac{a_i}{b_i}\right) \geq \frac{\sum_i a_i}{\sum_i b_i} \quad \forall \quad \sum_i b_i < 0 \tag{I.74}$$

Proof:

$$\begin{aligned} & a_j = b_j \frac{a_j}{b_j} \leq b_j \max_i\left(\frac{a_i}{b_i}\right) \quad \forall \quad j \in \{1, \dots, n\} \\ & \Rightarrow \sum_i a_i \leq \sum_i b_i \max_i\left(\frac{a_i}{b_i}\right) \\ & \Leftrightarrow \max_i\left(\frac{a_i}{b_i}\right) \geq \frac{\sum_i a_i}{\sum_i b_i} \quad \forall \quad \sum_i b_i > 0 \quad \wedge \quad \max_i\left(\frac{a_i}{b_i}\right) \leq \frac{\sum_i a_i}{\sum_i b_i} \quad \forall \quad \sum_i b_i < 0 \end{aligned} \tag{I.75}$$

And

$$\begin{aligned} & a_j = b_j \frac{a_j}{b_j} \geq b_j \min_i\left(\frac{a_i}{b_i}\right) \quad \forall \quad j \in \{1, \dots, n\} \\ & \Rightarrow \sum_i a_i \geq \sum_i b_i \min_i\left(\frac{a_i}{b_i}\right) \\ & \Leftrightarrow \min_i\left(\frac{a_i}{b_i}\right) \leq \frac{\sum_i a_i}{\sum_i b_i} \quad \forall \quad \sum_i b_i > 0 \quad \wedge \quad \min_i\left(\frac{a_i}{b_i}\right) \geq \frac{\sum_i a_i}{\sum_i b_i} \quad \forall \quad \sum_i b_i < 0 \end{aligned} \tag{I.76}$$

Excursus 8 shows exemplary that averaging of constraint coefficients leads to a relaxation in case that the cost contributions of time-dependent variables (e.g. operation variables) are time-independent (e.g. the cost of operating a component is constant for each

time step) and in case that the energy system is temporally decoupled. This is also the reason that aggregation algorithms such as k-means that use centroids as representation often lead to an underestimation of system costs and necessary capacities, which is frequently described in literature. This can also be the case if the time dependent operation costs of components in general and the capacity-costs of time-coupling storage components are small compared to the capacity-specific costs of the other components. However, in these cases it cannot mathematically be guaranteed anymore that averaging is providing a lower bound. Therefore, the next section will also specify under what conditions the aggregation of time-coupling constraints is not a restriction to the desired lower bound.

At this point, it is worth mentioning that averaging is generally providing a tighter lower bound then the proposed method of over- and underestimating the time series listed in Table I.2. This is shown in Excursus 10.

Excursus 10: Proof That a Lower Bound Based on Averaging is a Tighter Bound Than Based on Over- and Underestimation

As

$$\sum_{t\in C_k} c_{i_{neq},j_0=\lambda,t} \geq |C_k| \min_{t\in C_k}\left(c_{i_{neq},j_0=\lambda,t}\right) = \sum_{t\in C_k} \min_{t\in C_k}\left(c_{i_{neq},j_0=\lambda,t}\right) \tag{I.77}$$

$$\sum_{t\in C_k} c_{i_{neq},j_0=\lambda,t} \leq \sum_{t\in C_k} \max_{t\in C_k}\left(c_{i_{neq},j_0=\lambda,t}\right) = |C_k| \max_{t\in C_k}\left(c_{i_{neq},j_0=\lambda,t}\right) \tag{I.78}$$

And

$$\begin{aligned}
&\sum_{t\in C_k}\left(dl_{i_{neq},t} - \sum_{j_0\neq\lambda}^{J_0} c_{i_{neq},j_0,t}x_{j_0,0} - \sum_{j_t}^{J_T} d_{i_{neq},j_t,t}x_{j_t,t}\right)\\
&\geq \sum_{t\in C_k}\left(\min_{t\in C_k}\left(dl_{i_{neq},t}\right) - \sum_{j_0\neq\lambda}^{J_0}\max_{t\in C_k}\left(c_{i_{neq},j_0,t}x_{j_0,0}\right) - \sum_{j_t}^{J_T}\max_{t\in C_k}\left(d_{i_{neq},j_t,t}x_{j_t,t}\right)\right)\\
&= |C_k|\left(\max_{t\in C_k}\left(dl_{i_{neq},t}\right) - \sum_{j_0\neq\lambda}^{J_0}\min_{t\in C_k}\left(c_{i_{neq},j_0,t}x_{j_0,0}\right) - \sum_{j_t}^{J_T}\min_{t\in C_k}\left(d_{i_{neq},j_t,t}x_{j_t,t}\right)\right)
\end{aligned} \tag{I.79}$$

$$\begin{aligned}
&\sum_{t\in C_k}\left(dl_{i_{neq},t}-\sum_{j_0\neq\lambda}^{J_0}c_{i_{neq},j_0,t}x_{j_0,0}-\sum_{j_t}^{J_T}d_{i_{neq},j_t,t}x_{j_t,t}\right)\\
&\leq\sum_{t\in C_k}\left(\max_{t\in C_k}\left(dl_{i_{neq},t}\right)-\sum_{j_0\neq\lambda}^{J_0}\min_{t\in C_k}\left(c_{i_{neq},j_0,t}x_{j_0,0}\right)-\sum_{j_t}^{J_T}\min_{t\in C_k}\left(d_{i_{neq},j_t,t}x_{j_t,t}\right)\right)\\
&=|C_k|\left(\max_{t\in C_k}\left(dl_{i_{neq},t}\right)-\sum_{j_0\neq\lambda}^{J_0}\min_{t\in C_k}\left(c_{i_{neq},j_0,t}x_{j_0,0}\right)-\sum_{j_t}^{J_T}\min_{t\in C_k}\left(d_{i_{neq},j_t,t}x_{j_t,t}\right)\right)
\end{aligned}\tag{I.80}$$

The following holds $\forall\, i_{neq}\in I_{neq}, t\in T\wedge\ c_{i_{neq},j_0=\lambda,t}>0$:

$$\begin{aligned}
x_{j_0=\lambda,0}&\geq\frac{1}{\sum_{t\in C_k}c_{i_{neq},j_0=\lambda,t}}\sum_{t\in C_k}\left(dl_{i_{neq},t}-\sum_{j_0\neq\lambda}^{J_0}c_{i_{neq},j_0,t}x_{j_0,0}-\sum_{j_t}^{J_T}d_{i_{neq},j_t,t}x_{j_t,t}\right)\\
&\geq\frac{1}{\max_{t\in C_k}\left(c_{i_{neq},j_0=\lambda,t}\right)}\left(\min_{t\in C_k}\left(dl_{i_{neq},t}\right)-\sum_{j_0\neq\lambda}^{J_0}\max_{t\in C_k}\left(c_{i_{neq},j_0,t}\right)x_{j_0,0}-\sum_{j_t}^{J_T}\max_{t\in C_k}\left(d_{i_{neq},j_t,t}\right)x_{j_t,t}\right)
\end{aligned}\tag{I.81}$$

$$\begin{aligned}
x_{j_0=\lambda,0}&\leq\frac{1}{\sum_{t\in C_k}c_{i_{neq},j_0=\lambda,t}}\sum_{t\in C_k}\left(du_{i_{neq},t}-\sum_{j_0\neq\lambda}^{J_0}c_{i_{neq},j_0,t}x_{j_0,0}-\sum_{j_t}^{J_T}d_{i_{neq},j_t,t}x_{j_t,t}\right)\\
&\leq\frac{1}{\min_{t\in C_k}\left(c_{i_{neq},j_0=\lambda,t}\right)}\left(\max_{t\in C_k}\left(du_{i_{neq},t}\right)-\sum_{j_0\neq\lambda}^{J_0}\min_{t\in C_k}\left(c_{i_{neq},j_0,t}\right)x_{j_0,0}-\sum_{j_t}^{J_T}\min_{t\in C_k}\left(d_{i_{neq},j_t,t}\right)x_{j_t,t}\right)
\end{aligned}\tag{I.82}$$

And $\forall\, i_{neq}\in I_{neq}, t\in T\wedge\ c_{i_{neq},j_0=\lambda,t}<0$:

$$\begin{aligned}
x_{j_0=\lambda,0}&\leq\frac{1}{\sum_{t\in C_k}c_{i_{neq},j_0=\lambda,t}}\sum_{t\in C_k}\left(dl_{i_{neq},t}-\sum_{j_0\neq\lambda}^{J_0}c_{i_{neq},j_0,t}x_{j_0,0}-\sum_{j_t}^{J_T}d_{i_{neq},j_t,t}x_{j_t,t}\right)\\
&\leq\frac{1}{\max_{t\in C_k}\left(c_{i_{neq},j_0=\lambda,t}\right)}\left(\min_{t\in C_k}\left(dl_{i_{neq},t}\right)-\sum_{j_0\neq\lambda}^{J_0}\max_{t\in C_k}\left(c_{i_{neq},j_0,t}\right)x_{j_0,0}-\sum_{j_t}^{J_T}\max_{t\in C_k}\left(d_{i_{neq},j_t,t}\right)x_{j_t,t}\right)
\end{aligned}\tag{I.83}$$

$$\begin{aligned}
x_{j_0=\lambda,0}&\geq\frac{1}{\sum_{t\in C_k}c_{i_{neq},j_0=\lambda,t}}\sum_{t\in C_k}\left(du_{i_{neq},t}-\sum_{j_0\neq\lambda}^{J_0}c_{i_{neq},j_0,t}x_{j_0,0}-\sum_{j_t}^{J_T}d_{i_{neq},j_t,t}x_{j_t,t}\right)\\
&\geq\frac{1}{\min_{t\in C_k}\left(c_{i_{neq},j_0=\lambda,t}\right)}\left(\max_{t\in C_k}\left(du_{i_{neq},t}\right)-\sum_{j_0\neq\lambda}^{J_0}\min_{t\in C_k}\left(c_{i_{neq},j_0,t}\right)x_{j_0,0}-\sum_{j_t}^{J_T}\min_{t\in C_k}\left(d_{i_{neq},j_t,t}\right)x_{j_t,t}\right)
\end{aligned}\tag{I.84}$$

Here, the first right hand side of the equations shown above is the upper or lower bound as obtained by averaging constraint coefficients and the second right hand side as obtained by systematic maximization of minimization of coefficients for a systematic underestimation of the objective. As the upper bounds of variables based on averaged coefficients are further overestimated by the systematic minimization and maximization of coefficients and as the lower bounds are further underestimated respectively,

the averaging of coefficients based on centroids used as representation method after clustering is a tighter bound than the systematic over- and underestimation of coefficients. Here, the proof for time-dependent variables is completely analogous.

The validity of the previously shown approaches is now illustrated with the example, which was already used for the upper bounds. This example for lower bounds was also published in a prior publication by the author of this work [2].

Example 7: Two kinds of lower bounds for a simple temporally decoupled problem

The cost minimization problem from Section I.2.2.1 reads

$$\begin{aligned} \min(\mathrm{TAC}) = \min\left(\mathrm{Cap}_{\mathrm{comp1}} * 120\,\frac{€}{\mathrm{MW_{inst}d}} + \mathrm{Cap}_{\mathrm{comp2}} * 100\,\frac{€}{\mathrm{MW_{inst}d}}\right) * 365\,\frac{\mathrm{d}}{\mathrm{a}} \\ \text{s.t.} \quad 0.25\,\frac{\mathrm{MWh}}{\mathrm{MW_{inst}}} * \mathrm{Cap}_{\mathrm{comp1}} + 0.2\,\frac{\mathrm{MWh}}{\mathrm{MW_{inst}}} * \mathrm{Cap}_{\mathrm{comp2}} \geq 1\ \mathrm{MWh} \\ 0.2\,\frac{\mathrm{MWh}}{\mathrm{MW_{inst}}} * \mathrm{Cap}_{\mathrm{comp1}} + 0.25\,\frac{\mathrm{MWh}}{\mathrm{MW_{inst}}} * \mathrm{Cap}_{\mathrm{comp2}} \geq 1\ \mathrm{MWh} \\ 0.2\,\frac{\mathrm{MWh}}{\mathrm{MW_{inst}}} * \mathrm{Cap}_{\mathrm{comp1}} + 0.2\,\frac{\mathrm{MWh}}{\mathrm{MW_{inst}}} * \mathrm{Cap}_{\mathrm{comp2}} \geq 0.8\ \mathrm{MWh} \\ 0.25\,\frac{\mathrm{MWh}}{\mathrm{MW_{inst}}} * \mathrm{Cap}_{\mathrm{comp1}} + 0.25\,\frac{\mathrm{MWh}}{\mathrm{MW_{inst}}} * \mathrm{Cap}_{\mathrm{comp2}} \geq 1\ \mathrm{MWh} \end{aligned} \tag{I.85}$$

and is once more shown in the upper diagram of Figure I.13 for the sake of clarity.

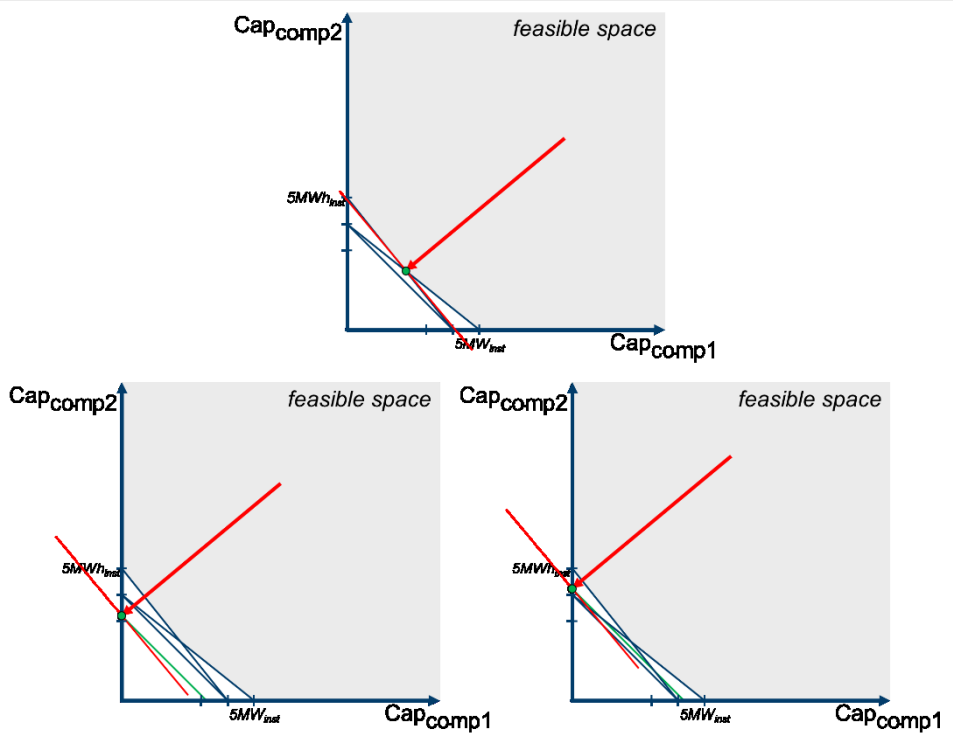

Figure I.13. The problem introduced before with lower bounds based on the proposed minimization approach and based on averaging

The first proposed approach is analogous to the method for upper bounds and is based on the representation of a cluster's attributes according to Table I.2. For the simplified model, in which all four constraints are assigned to the same cluster, this leads to the following values:

$$\begin{aligned} \widehat{\mathrm{Cap}}_{\mathrm{comp1}} &= 0.25\,\frac{\mathrm{MWh}}{\mathrm{MW}_{\mathrm{inst}}} \\ \widehat{\mathrm{Cap}}_{\mathrm{comp2}} &= 0.25\,\frac{\mathrm{MWh}}{\mathrm{MW}_{\mathrm{inst}}} \\ \widetilde{\mathrm{Dem}} &= 0.8\ \mathrm{MWh} \end{aligned} \tag{I.86}$$

The underestimating aggregated constraint according to the first proposed method is thus:

$$0.25\,\frac{\mathrm{MWh}}{\mathrm{MW}_{\mathrm{inst}}} * \mathrm{Cap}_{\mathrm{comp1}} + 0.25\,\frac{\mathrm{MWh}}{\mathrm{MW}_{\mathrm{inst}}} * \mathrm{Cap}_{\mathrm{comp2}} \geq 0.8\ \mathrm{MWh} \tag{I.87}$$

This constraint is represented by the green line in the lower left picture of Figure I.13. The cost-optimal component sizes according to this approach are $\left(\mathrm{Cap}^*_{\mathrm{comp1}} \middle| \mathrm{Cap}^*_{\mathrm{comp2}}\right) = (0\ \mathrm{MW}_{\mathrm{inst}} | 3.2\ \mathrm{MW}_{\mathrm{inst}})$, which leads to total annual costs of $\widetilde{\mathrm{min}}(\mathrm{TAC}) = 320\,\frac{€}{\mathrm{d}} * 365\,\frac{\mathrm{d}}{\mathrm{a}}$ and is accordingly smaller than the reference case of $488,\overline{8}\,\frac{€}{\mathrm{d}} * 365\,\frac{\mathrm{d}}{\mathrm{a}}$. Because this method is the corresponding underestimation method to the overestimation method proposed in Section I.2.2.1, it suffers from the same sensitivity to equations of different scales and is, in general, not a very tight lower bound. Therefore, we also investigate the impact of the underestimation method based on averaging.

For this, each cluster is represented by their centroid. As only one cluster is considered in this example, all time series are represented by their averages. This leads to the following capacity factors and electricity demand:

$$\begin{aligned} \overline{\mathrm{Cap}}_{\mathrm{comp1}} &= 0.225\,\frac{\mathrm{MWh}}{\mathrm{MW}_{\mathrm{inst}}} \\ \overline{\mathrm{Cap}}_{\mathrm{comp2}} &= 0.25\,\frac{\mathrm{MWh}}{\mathrm{MW}_{\mathrm{inst}}} \\ \overline{\mathrm{Dem}} &= 0.95\ \mathrm{MWh} \end{aligned} \tag{I.88}$$

This further leads to the following constraining linear equation, which is represented by the green line in the lower right graph of Figure I.13:

$$0.225\,\frac{\mathrm{MWh}}{\mathrm{MW}_{\mathrm{inst}}} * \mathrm{Cap}_{\mathrm{comp1}} + 0.225\,\frac{\mathrm{MWh}}{\mathrm{MW}_{\mathrm{inst}}} * \mathrm{Cap}_{\mathrm{comp2}} \geq 0.95\ \mathrm{MWh} \tag{I.89}$$

The optimal layout of the energy system is now $\left(\mathrm{Cap}^{*}_{\mathrm{comp1}} \middle| \mathrm{Cap}^{*}_{\mathrm{comp2}}\right) = (0\ \mathrm{MW_{inst}} | 4.\overline{2}\ \mathrm{MW_{inst}})$ with total annual costs of $\overline{\mathrm{min}}(\mathrm{TAC}) = 422.\overline{2}\,\frac{€}{\mathrm{d}} * 365\,\frac{\mathrm{d}}{\mathrm{a}}$.

This illustrates that the centroid-based representation provides a tighter lower bound than the previously proposed underestimation method. However, it needs to be evaluated whether the proposed methods remain lower bounds if temporally linking constraints are considered.

I.2.3.3. A Lower Bound for ESOMs with Linked Time Steps

As already mentioned for the upper bounds, energy system models with linked time steps are generally not symmetric after step 1, i.e., even if the equations of those time steps, which are assigned to the same cluster, are identically parametrized. However, the straightforward equalizing of those time step specific variables, whose time steps are assigned to the same cluster, cannot be applied if a lower bound of the original should be found because this would be a restriction and would therefore overestimate the lower bound determined in step 1. The only way to avoid an overestimation in step 2 is thus to ensure that time steps assigned to the same cluster are symmetric despite of their temporal coupling. As will be shown in the following, this can only be achieved if the clustered time steps (or periods) are adjacent.

As shown earlier, the state of charge of storage components is given by:

$$\mathrm{SOC}(t+1) = \mathrm{SOC}(t) \cdot \eta_{\mathrm{sd}} + \eta_{\mathrm{c}} \cdot o_{\mathrm{St,c}}(t) - \frac{1}{\eta_{\mathrm{d}}} \cdot o_{\mathrm{St,d}}(t) \ \forall \ \ t \in \{1, \dots, T\} \tag{I.90}$$

This equation can also be expressed as an explicit equation:

$$\mathrm{SOC}(t) = \mathrm{SOC}_0 \cdot \eta_{\mathrm{sd}}^{t} + \eta_{\mathrm{c}} \cdot \sum_{i}^{t} \eta_{\mathrm{sd}}^{i} \cdot o_{\mathrm{St,c}}(i) - \frac{1}{\eta_{\mathrm{d}}} \cdot \sum_{i}^{t} \eta_{\mathrm{sd}}^{i} \cdot o_{\mathrm{St,d}}(i) \tag{I.91}$$

According to step 2 of the workflow, the first step is to remove constraints that impede a symmetry with respect to the time steps to be aggregated. It is not directly obvious for what cases the constraint at hand is symmetric. However, the self-discharge rate η_{sd} leads to an exponential expression that impedes symmetry for values $\eta_{\mathrm{sd}} \neq 1$. If $\eta_{\mathrm{sd}} = 1$ is assumed, the state of charge can be calculated as follows:

$$\mathrm{SOC}(t) = \mathrm{SOC}_0 + \sum_{i}^{t} \left(\eta_c \cdot o_{St,c}(i) - \frac{1}{\eta_d} \cdot o_{St,d}(i) \right) \tag{I.92}$$

This equation is neither symmetrical, but significantly simpler to interpret. If we now consider that only adjacent time steps are clustered, e.g. the specific time steps t_1 and $t_1 + 1$, the constraints above yield for a storage component in these two time steps:

$$\mathrm{SOC}(t_1 + 1) = \mathrm{SOC}(t_1) + \eta_c \cdot o_{St,c}(t_1) - \frac{1}{\eta_d} \cdot o_{St,d}(t_1) \tag{I.93}$$

$$\mathrm{SOC}(t_1 + 2) = \mathrm{SOC}(t_1 + 1) + \eta_c \cdot o_{St,c}(t_1 + 1) - \frac{1}{\eta_d} \cdot o_{St,d}(t_1 + 1) \tag{I.94}$$

Substitution into the second equation yields for the second equation:

$$\begin{aligned} &\mathrm{SOC}(t_1 + 2) = \mathrm{SOC}(t_1) + \eta_c \cdot \left(o_{St,c}(t_1) + o_{St,c}(t_1 + 1) \right) \\ &- \frac{1}{\eta_d} \cdot \left(o_{St,d}(t_1) + o_{St,d}(t_1 + 1) \right) \end{aligned} \tag{I.95}$$

For a symmetry with respect to the time steps t_1 and $t_1 + 1$, the constraint for $\mathrm{SOC}(t_1 + 1)$ needs to be omitted. As mentioned above, the removal of constraints is a relaxation and thus only leads to a further underestimation the of the original optimization problem. The last remaining constraint for time-linking storage components, for which symmetry needs to be shown, is thus derived from the constraint for $\mathrm{SOC}(t_1 + 2)$:

$$\begin{aligned} &f_0(x) = \mathrm{SOC}(t_1) + \eta_c \cdot \left(o_{St,c}(t_1) + o_{St,c}(t_1 + 1) \right) \\ &- \frac{1}{\eta_d} \cdot \left(o_{St,d}(t_1) + o_{St,d}(t_1 + 1) \right) - \mathrm{SOC}(t_1 + 2) = 0 \end{aligned} \tag{I.96}$$

As shown in Excursus 6, a set of constraints is symmetrical if the optimization problem is convex (given for all linear programs) and can be transferred into each other with a transformation matrix. For the constraint function $f_0(x)$ above, this can be shown as follows:

$$
\begin{aligned}
f_0(Qx) &= SOC(t_1) + \begin{pmatrix} \eta_c & & & \\ & \eta_c & & \\ & & -\frac{1}{\eta_d} & \\ & & & -\frac{1}{\eta_d} \end{pmatrix} \begin{pmatrix} 0 & 1 & & \\ 1 & 0 & & \\ & & 0 & 1 \\ & & 1 & 0 \end{pmatrix} \begin{pmatrix} o_{St,c}(t_1) \\ o_{St,c}(t_1+1) \\ o_{St,d}(t_1) \\ o_{St,d}(t_1+1) \end{pmatrix} - SOC(t_1+2) \\
&= SOC(t_1) + \eta_c \cdot \left(o_{St,c}(t_1) + o_{St,c}(t_1+1)\right) - \frac{1}{\eta_d} \cdot \left(o_{St,d}(t_1) + o_{St,d}(t_1+1)\right) - SOC(t_1+2) \\
&= SOC(t_1) + \eta_c \cdot \left(o_{St,c}(t_1+1) + o_{St,c}(t_1)\right) - \frac{1}{\eta_d} \cdot \left(o_{St,d}(t_1+1) + o_{St,d}(t_1)\right) - SOC(t_1+2) \\
&= SOC(t_1) + \begin{pmatrix} \eta_c & & & \\ & \eta_c & & \\ & & -\frac{1}{\eta_d} & \\ & & & -\frac{1}{\eta_d} \end{pmatrix} \begin{pmatrix} o_{St,c}(t_1) \\ o_{St,c}(t_1+1) \\ o_{St,d}(t_1) \\ o_{St,d}(t_1+1) \end{pmatrix} - SOC(t_1+2) \\
&= f_0(x)
\end{aligned}
\tag{I.97}
$$

This means that now also the time-dependent charge and discharge rates of an arbitrary storage component are symmetric to its adjacent time step and that the time steps are symmetric to each other despite of their linking if all the other (temporally unlinked) variables and constraints are identically parametrized, which is guaranteed by step 1.

As shown in the previous section, also complete periods of time steps can be interpreted as candidate blocks for temporal aggregation. While an underestimation within these periods can already be achieved with the proposed minimization and maximization technique of time series according to step 1 of the workflow, a lower bound to an energy system model that considers seasonal storage can only be found if the clustered periods are adjacent.

To sum up, finding lower bounds to the original optimization problem based on temporal aggregation is a much more challenging task than finding upper bounds as it requires a profound knowledge on time step related asymmetries in the original optimization problem. With respect to models, in which the state of charge equation for storage components is the only asymmetric equation, which is the case in the models that were considered in the scope of this thesis, one can state that two conditions have to be fulfilled in order to find a true lower bound:

1. The self-discharge has to be zero or underestimated to be zero
2. Periods to be clustered have to be adjacent. This is an exceptional side constraint for the clustering process. Further segmentation to an even smaller number of time steps is

possible, as segmentation always considers adjacent time steps only.

Finally yet importantly, it needs to be highlighted that the validity of the introduced workflow has been shown and that it can be dynamically adapted to the problem structure at hand. This systematic procedure as well as the extension of proofs for over- and underestimating temporal aggregation techniques to temporally coupled systems are the major contributions of this chapter and a novelty of this work, although similar concepts existed before that were proven for narrowly defined and temporally decoupled problem structures only.

J. Techno-Economic Model Assumptions

In the following, the techno-economic data for the island system, the self-sufficient building and the electricity dispatch model are listed. The data for the latter two models was also published in a preceding publication by the author of this work [2].

J.1.Model Assumptions for the Island System Model

The component parameters of the island system model are derived from Kotzur et al. [20] and described in Appendix J.1. Despite the fact that the parameters are fictitious and are not discussed in detail because the model is not meant to mirror a real energy system, their scale is roughly oriented at real cost, efficiency and lifetime values. Further, an interest rate of 4% was assumed.

Table J.1. Unit parameters of the island system derived from Kotzur et al. [20]

	$CAPEX_{Cap}$ [€/kW$_p$]	$CAPEX_{Fix}$ [€]	$OPEX_{Cap}$ [€/kWp]	$OPEX_{Fix}$ [€]	$OPEX_{Var}$ [€/kWh]	Efficiency [%]	Charge Efficiency [%]	Discharge Efficiency [%]	Self-Discharge [%/h]	Lifetime [a]
Photovoltaic	800	1,000	8	100	0					20
Wind Energy	1,000	100,000	20	2,000	0					20
Backup Plant	1,000	0	30	0	0.2					25
Electrolyzer	500	100,000	15	3,000	0	70				15
Fuel Cell	1,100	100,000	33	3,000	0	50				15
Battery	300	0	3	0	0		96	96	0.05	15
Hydrogen Storage	15	0	0	0	0		90	1	0	25

As shown in Table J.1, the wind farm, the photovoltaic plant, the electrolyzer and the fuel cell are modelled with capacity-independent fixed expenditures ($CAPEX_{Fix}$ and $OPEX_{Fix}$) if the components are chosen to be built as well as capacity-specific capacity- and operation costs ($CAPEX_{Cap}$ and $OPEX_{Cap}$). In contrast to that,

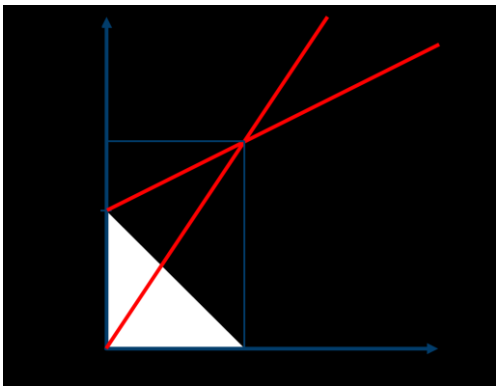

Figure J.1.Trade-Off between fixed and capacity-specific expenditures

the storage components, i.e. the battery and the hydrogen pressure vessels are modelled by linear capacity-specific costs only. However, as the hydrogen pressure vessels can only be linked to the electric subsystem via the electrolyzer and the fuel cell, the hydrogen subsystem for storing energy has fixed expenditures itself if it is chosen to be built. This setup favors the hydrogen subsystem for storing large amount of energy for a long time period, while the battery is economically more convenient for short term storing cycles, which is schematically shown in Figure J.1. Here, the fixed expenditures of the relevant components - in case of their construction - are modelled with binary variables, which turns the optimization program into a mixed-integer linear program. The backup plant meanwhile is considered to exist already. For that reason, it is assumed that energy specific costs of $20\,\frac{\mathrm{ct}}{\mathrm{kWh}}$ are its only cost contribution.

The island system considers three different input time series, namely the capacity factors of the wind farm and the photovoltaic plant in $\frac{\mathrm{kW_{el}}}{\mathrm{kW_{installed}}}$ and the electricity demand in $\mathrm{kW_{el}}$.

For the electricity demand, the ENTSO-e profile for Germany in 2013 was used and normalized to 1 MW peak demand in order to achieve a more realistic sizing of an island system. However, it needs to be highlighted that the profile is not representative for demand profiles of that range because they normally do not contain industrial base loads in contrast to the cumulative electricity demand profile of Germany. Both, the electricity demand and the capacity factor time series for the wind feed-in are drawn from Robinius et al. [238], while the capacity factors for the photovoltaic plant are determined with PV-Lib [239].

In summary, the island system is not suitable to derive findings for a real application. However, the fact that it considers binary variables and three substantially different time series as well as two different storage technologies enables it to answer research questions on the accuracy of the temporal aggregation with respect to the components' dynamic behavior.

J.2. Model Assumptions for the Self-Sufficient Building Model

A detailed discussion of the cost parameters is presented in the thesis of Röben [240] and is not repeated at this point for the sake of brevity.

Table J.2 provides an overview of the components' cost contributions and the data is qualitatively discussed with respect to its meaning for the model from a mathematical point of view.

Table J.2. Cost parameters of the self-sufficient building (taken from Hoffmann et al. [2])

	Capex				Opex		Life-time		Source
Components	**Fixed**		**Variable**		**Fixed + Variable**				
Photovoltaic GR	—	—	4000	€/kW$_p$	1	% Inv./a	20	a	
Photovoltaic RT	—	—	769	€/kW$_p$	1	% Inv./a	20	a	[241]
Inverter	—	—	75	€/kW$_p$	—	—	20	a	[242]
Battery	—	—	301	€/kWh$_p$	—	—	15	a	[241]
rSOC	5,000	€	2,400	€/kW$_{H2}$	1	% Inv./a	15	a	[240]
Heatpump	4,230	€	504.9	€/kW$_{th}$	1.5	% Inv./a	20	a	[243]
Thermal Storage	—	—	90	€/kWh$_{th}$	0.01	% Inv./a	25	a	[244]
E-Heater & E-Boiler	—	—	60	€/kW$_{th}$	2	% Inv./a	30	a	[244]
Tank	—	—	0.79	€/kWh$_{H2}$	—	—	25	a	[245]
Dibenzyltoluene	—	—	1.25	€/kWh$_{H2}$	—	—	25	a	[246, 247]
Hydrogen Vessels	—	—	15	€/kWh$_{H2}$	—	—	25	a	[248]
HYD	2,123.3	€	761.1	€/kW$_{H2}$	1	% Inv./a	20	a	[246]
DEHYD	1,140	€	408.6	€/kW$_{H2}$	1	% Inv./a	20	a	[246]
LP-Compressor	—	—	1716.71	€/kW$_p$	1	% Inv./a	25	a	[249]
HP-Compressor	560	€	1329.8	€/kW$_p$	1	% Inv./a	25	a	[249]
Heat-Exchangers 1 and 2	—	—	1	€/kW$_{th}$	1	% Inv./a	—	a	—
Expanders 1 and 2	—	—	1	€/kW$_{th}$	1	% Inv./a	25	a	—

If cost curves of the respective components were available, they were approximated by an inhomogeneous linear function with a binary fix cost, if the component is chosen to be built, and a continuous capacity specific cost contribution. As Table J.2 reveals, this applies for the rSOC, the heat pump, the (de-) hydrogenation units and the high-pressure compressor. Analogously to the preceding island system, this feature turns the optimization model into a mixed-integer linear program. Besides, the cost for the organic hydrogen carrier (dibenzyl-toluene) is implicitly added to the capacity specific costs of the LOHC storage.

Apart from that, the non-referenced data needs to be explained in detail. The disproportionally high costs of the ground-mounted photovoltaic panels can be interpreted as an arbitrarily high penalty factor. This guarantees that the rooftop panels are favored in any case because ground-mounted photovoltaic panels are socially not accepted in the residential sector. Yet, the option is still considered in order to ensure that the system is always feasible (even if the building's energy demand would be unrealistically high). In contrast to that, the heat exchangers and the expanders do not contribute significantly to the overall costs of domestic renewable energy systems. However, in order to avoid an indifferent solution with arbitrarily sized heat exchangers and expanders, marginal costs of these components are implemented.

Finally yet importantly, "the time series data of the building model comprises five different time series with hourly resolution: Three solar profiles for the three differently oriented PV modules as well as the electricity and the heat demand time series. The profiles were generated using the open source software tsib [250, 251], which was used to transform weather information such as global horizontal irradiance and ambient temperature into demand profiles for archetype buildings and capacity factors for renewable energy sources used in the domestic sector. The raw weather data used for generating the input time series is based on the COSMO dataset [252-254] at the location of Berlin for the year 2013." (Hoffmann et al. [2])

J.3.Model Assumptions for the Electricity Dispatch Model

"The list of plant technologies for the electricity dispatch model, their rated power, and position are drawn from the Federal Network Agency (Bundesnetzagentur) for 2019 [255] as well as the Internation Energy Agency (IEA) and Nuclear Energy Agency (NEA) [256]. The data for the length and capacity of the inner- and trans-German transmission lines are derived from the preceding project SciGRID [257]. The geoinformation data used for the illustrations was obtained from Eurostat [258]. The electricity demand time series are taken from the ENTSO-E Transparency Platform [259] and regionalized using data from the Country Working Group on Energy Balances (Länderarbeitskreis Energiebilanzen) [260] and the Federal and State Statistical Offices (Statistische Ämter des Bundes und der Länder) [261]. Finally, the import costs per country

and the capacity factors for renewable energy sources were all derived from the ENTSO-E database for the year 2019 [259]. The techno-economic assumptions of the generation units are depicted in Table J.3." (Hoffmann et al. [2])

Table J.3. Cost parameters of the dispatch model (taken from Hoffmann et al. [2])

Components	Efficiency		Operational Cost		Emission Factor		Number of units
Biomass	38-45	%	22.2-23.0	€/MWh	0.016	t_{CO2}/MWh	16,157
Gas (combined)	41-63	%	5.0-8.7	€/MWh	0.204	t_{CO2}/MWh	90
Gas (simple)	29-42	%	4.2-7.0	€/MWh	0.204	t_{CO2}/MWh	184
Hard coal	23-50	%	10.6-16.8	€/MWh	0.342	t_{CO2}/MWh	77
Lignite	20-43	%	11.1-19.3	€/MWh	0.4	t_{CO2}/MWh	60
Nuclear	33	%	7.5	€/MWh	0	t_{CO2}/MWh	7
Mineral Oil	30-40	%	4.8-8.4	€/MWh	0.266	t_{CO2}/MWh	47
Hydro (pumped storage)	75	%	10.0	€/MWh	—	—	74
Hydro (run of river)	—	—	10.0	€/MWh	—	—	7,254
Photovoltaic (ground)	—	—	7.5	€/MWh	—	—	8,795
Photovoltaic (rooftop)	—	—	7.5	€/MWh	—	—	1,991,267
Wind (onshore)	—	—	7.5	€/MWh	—	—	28,777
Wind (offshore)	—	—	17.0	€/MWh	—	—	1,497
Other (generation)	15-45	%	6.1-7.0	€/MWh	0.016 – 0.3	t_{CO2}/MWh	463
Other (storage)	90	%	5.0-10.0	€/MWh	—	—	112,154

Bibliography

1. Hoffmann, M., L. Kotzur, D. Stolten, and M. Robinius, *A Review on Time Series Aggregation Methods for Energy System Models.* Energies, 2020. **13**(3), DOI: https://doi.org/10.3390/en13030641.
2. Hoffmann, M., J. Priesmann, L. Nolting, A. Praktiknjo, L. Kotzur, and D. Stolten, *Typical periods or typical time steps? A multi-model analysis to determine the optimal temporal aggregation for energy system models.* Applied Energy, 2021. **304**: p. 117825, DOI: https://doi.org/10.1016/j.apenergy.2021.117825.
3. Hoffmann, M., L. Kotzur, and D. Stolten, *The Pareto-optimal temporal aggregation of energy system models.* Applied Energy, 2022. **315**: p. 119029, DOI: https://doi.org/10.1016/j.apenergy.2022.119029.
4. Kannengießer, T., M. Hoffmann, L. Kotzur, P. Stenzel, F. Schuetz, K. Peters, S. Nykamp, D. Stolten, and M. Robinius, *Reducing Computational Load for Mixed Integer Linear Programming: An Example for a District and an Island Energy System.* Energies, 2019. **12**(14): p. 2825, DOI: https://doi.org/10.3390/en12142825.
5. Kotzur, L., L. Nolting, M. Hoffmann, T. Groß, A. Smolenko, J. Priesmann, H. Büsing, R. Beer, F. Kullmann, B. Singh, A. Praktiknjo, D. Stolten, and M. Robinius, *A modeler's guide to handle complexity in energy systems optimization.* Advances in Applied Energy, 2021. **4**: p. 100063, DOI: https://doi.org/10.1016/j.adapen.2021.100063.
6. Singh, B., O. Rehberg, T. Groß, M. Hoffmann, L. Kotzur, and D. Stolten, *Budget-Cut: Introduction to a budget based cutting-plane algorithm for capacity expansion models.* Optimization Letters, 2021, DOI: https://doi.org/10.1007/s11590-021-01826-w.
7. Robinius, M., A. Otto, P. Heuser, L. Welder, K. Syranidis, D.S. Ryberg, T. Grube, P. Markewitz, R. Peters, and D. Stolten, *Linking the Power and Transport Sectors—Part 1: The Principle of Sector Coupling.* Energies, 2017. **10**(7): p. 956, DOI: https://doi.org/10.3390/en10070956.
8. Barnett, H.J., *Energy uses and supplies, 1939, 1947, 1965*. 1950, Bureau of Mines, Washington, DC (USA).
9. Boiteux, M., *La Tarification des Demandes en Pointe.* Revue Generale de l'Electricite, 1949. **58**: pp. 157-179.
10. Boiteux, M., *Peak-Load Pricing.* The Journal of Business, 1960. **33**(2): pp. 157-179.
11. Steiner, P.O., *Peak loads and efficient pricing.* The Quarterly Journal of Economics, 1957. **71**(4): pp. 585-610.
12. Sherali, H.D., A.L. Soyster, F.H. Murphy, and S. Sen, *Linear programming based analysis of marginal cost pricing in electric utility capacity expansion.* European Journal of Operational Research, 1982. **11**(4): pp. 349-360, DOI: https://doi.org/10.1016/0377-2217(82)90200-4.
13. Helm, D., *Energy policy: security of supply, sustainability and competition.* Energy Policy, 2002. **30**(3): pp. 173-184, DOI: https://doi.org/10.1016/S0301-4215(01)00141-0.

14. Hoffman, K.C. and D.O. Wood, *Energy System Modeling and Forecasting.* Annual Review of Energy, 1976. **1**(1): pp. 423-453, DOI: https://doi.org/10.1146/annurev.eg.01.110176.002231.
15. Lopion, P., P. Markewitz, M. Robinius, and D. Stolten, *A review of current challenges and trends in energy systems modeling.* Renewable and Sustainable Energy Reviews, 2018. **96**: pp. 156-166, DOI: https://doi.org/10.1016/j.rser.2018.07.045.
16. Caramanis, M.C., R.D. Tabors, K.S. Nochur, and F.C. Schweppe, *The Introduction of Non-Dispatchable Technologies as Decision Variables in Long-Term Generation Expansion Models.* IEEE Power Engineering Review, 1982. **PER-2**(8): pp. 40-41, DOI: https://doi.org/10.1109/MPER.1982.5519756.
17. Bhattacharyya, S.C. and G.R. Timilsina, *A review of energy system models.* International Journal of Energy Sector Management, 2010. **4**(4): pp. 494-518, DOI: https://doi.org/10.1108/17506221011092742.
18. Pfenninger, S., A. Hawkes, and J. Keirstead, *Energy systems modeling for twenty-first century energy challenges.* Renewable and Sustainable Energy Reviews, 2014. **33**: pp. 74-86, DOI: https://doi.org/10.1016/j.rser.2014.02.003.
19. Ringkjøb, H.-K., P.M. Haugan, and I.M. Solbrekke, *A review of modelling tools for energy and electricity systems with large shares of variable renewables.* Renewable and Sustainable Energy Reviews, 2018. **96**: pp. 440-459, DOI: https://doi.org/10.1016/j.rser.2018.08.002.
20. Kotzur, L., P. Markewitz, M. Robinius, and D. Stolten, *Time series aggregation for energy system design: Modeling seasonal storage.* Applied Energy, 2018. **213**: pp. 123-135, DOI: https://doi.org/10.1016/j.apenergy.2018.01.023.
21. Gabrielli, P., M. Gazzani, E. Martelli, and M. Mazzotti, *Optimal design of multi-energy systems with seasonal storage.* Applied Energy, 2018. **219**: pp. 408-424, DOI: https://doi.org/10.1016/j.apenergy.2017.07.142.
22. Samsatli, S. and N.J. Samsatli, *A general spatio-temporal model of energy systems with a detailed account of transport and storage.* Computers & Chemical Engineering, 2015. **80**: pp. 155-176, DOI: https://doi.org/10.1016/j.compchemeng.2015.05.019.
23. Samsatli, S., I. Staffell, and N.J. Samsatli, *Optimal design and operation of integrated wind-hydrogen-electricity networks for decarbonising the domestic transport sector in Great Britain.* International Journal of Hydrogen Energy, 2016. **41**(1): pp. 447-475, DOI: https://doi.org/10.1016/j.ijhydene.2015.10.032.
24. Welder, L., D. Ryberg, L. Kotzur, T. Grube, M. Robinius, and D. Stolten, *Spatio-Temporal Optimization of a Future Energy System for Power-to-Hydrogen Applications in Germany*. 2018, DOI: https://doi.org/10.1016/j.energy.2018.05.059.
25. Tejada-Arango, D.A., M. Domeshek, S. Wogrin, and E. Centeno, *Enhanced Representative Days and System States Modeling for Energy Storage Investment Analysis.* IEEE Transactions on Power Systems, 2018. **33**(6): pp. 6534-6544, DOI: https://doi.org/10.1109/TPWRS.2018.2819578.

26. van der Heijde, B., A. Vandermeulen, R. Salenbien, and L. Helsen, *Representative days selection for district energy system optimisation: a solar district heating system with seasonal storage*. Vol. 248. 2019. 79-94, DOI: https://doi.org/10.1016/j.apenergy.2019.04.030.
27. Ören, T.I. *Computer-Aided Systems technology: Its role in advanced computerization*. in *Computer Aided Systems Theory — EUROCAST '93*. 1994. Berlin, Heidelberg: Springer Berlin Heidelberg, DOI: https://doi.org/10.1007/3-540-57601-0_37.
28. Sass, S. and A. Mitsos, *Optimal Operation of Dynamic (Energy) Systems: When are Quasi-Steady Models Adequate?* Computers & Chemical Engineering, 2019, DOI: https://doi.org/10.1016/j.compchemeng.2019.02.011.
29. Morales-España, G. and D. Tejada-Arango, *Modelling the Hidden Flexibility of Clustered Unit Commitment*. 2018, DOI: https://doi.org/10.1109/TPWRS.2019.2908051.
30. Lara, C.L., D.S. Mallapragada, D.J. Papageorgiou, A. Venkatesh, and I.E. Grossmann, *Deterministic electric power infrastructure planning: Mixed-integer programming model and nested decomposition algorithm.* European Journal of Operational Research, 2018. **271**(3): pp. 1037-1054, DOI: https://doi.org/10.1016/j.ejor.2018.05.039.
31. Lopion, P., P. Markewitz, D. Stolten, and M. Robinius, *Cost Uncertainties in Energy System Optimisation Models: A Quadratic Programming Approach for Avoiding Penny Switching Effects.* 2019. **12**(20): p. 4006, DOI: https://doi.org/10.3390/en12204006.
32. Klinge Jacobsen, H., *Integrating the bottom-up and top-down approach to energy–economy modelling: the case of Denmark.* Energy Economics, 1998. **20**(4): pp. 443-461, DOI: https://doi.org/10.1016/S0140-9883(98)00002-4.
33. Subramanian, A., T. Gundersen, and T. Adams, *Modeling and simulation of energy systems: A review.* Processes, 2018. **6**(12): p. 238, DOI: https://doi.org/10.3390/pr6120238.
34. Böhringer, C. and T.F. Rutherford, *Integrating bottom-up into top-down: a mixed complementarity approach.* ZEW-Centre for European Economic Research Discussion Paper, 2005. **Discussion Paper No. 05-028**, DOI: https://doi.org/10.2139/ssrn.770725.
35. Herbst, M., F. Toro, F. Reitze, and J. Eberhard, *Bridging Macroeconomic and Bottom up Energy Models-the Case of Efficiency in Industry*, in *ECEEE Summer Study on Energy Efficiency in Industry 2012*. 2012, ECEEE: Arnhem, The Netherlands. p. 409-417.
36. Helgesen, P.I., *Top-down and Bottom-up: Combining energy system models and macroeconomic general equilibrium models.* CenSES: Trondheim, Norway, 2013. **30**.
37. Schaller, R.R., *Moore's law: past, present and future.* IEEE Spectrum, 1997. **34**(6): pp. 52-59, DOI: https://doi.org/10.1109/6.591665.

38. Robison, R.A., *Moore's Law: Predictor and Driver of the Silicon Era.* World Neurosurgery, 2012. **78**(5): pp. 399-403, DOI: https://doi.org/10.1016/j.wneu.2012.08.019.
39. Koch, T., A. Martin, and M.E. Pfetsch, *Progress in Academic Computational Integer Programming*, in *Facets of Combinatorial Optimization: Festschrift for Martin Grötschel*, M. Jünger and G. Reinelt, Editors. 2013, Springer Berlin Heidelberg: Berlin, Heidelberg. p. 483-506, DOI: https://doi.org/10.1007/978-3-642-38189-8_19.
40. Theis, T.N. and H.P. Wong, *The End of Moore's Law: A New Beginning for Information Technology.* Computing in Science & Engineering, 2017. **19**(2): pp. 41-50, DOI: https://doi.org/10.1109/MCSE.2017.29.
41. Priesmann, J., L. Nolting, and A. Praktiknjo, *Are complex energy system models more accurate? An intra-model comparison of power system optimization models.* Applied Energy, 2019. **255**: p. 113783, DOI: https://doi.org/10.1016/j.apenergy.2019.113783.
42. Poncelet, K., E. Delarue, J. Duerinck, D. Six, and W. D'haeseleer, *The Importance of Integrating the Variability of Renewables in Long-term Energy Planning Models*, in *TME Working Paper - Energy and Environment*. 2014, KU Leuven: Leuven.
43. Pfenninger, S., *Dealing with multiple decades of hourly wind and PV time series in energy models: A comparison of methods to reduce time resolution and the planning implications of inter-annual variability.* Applied Energy, 2017. **197**: pp. 1-13, DOI: https://doi.org/10.1016/j.apenergy.2017.03.051.
44. Stenzel, P., J. Linssen, J. Fleer, and F. Busch. *Impact of temporal resolution of supply and demand profiles on the design of photovoltaic battery systems for increased self-consumption*. in *2016 IEEE International Energy Conference (ENERGYCON)*. 2016. DOI: https://doi.org/10.1109/ENERGYCON.2016.7514010.
45. Mallapragada, D.S., D.J. Papageorgiou, A. Venkatesh, C.L. Lara, and I.E. Grossmann, *Impact of model resolution on scenario outcomes for electricity sector system expansion.* Energy, 2018. **163**: pp. 1231-1244, DOI: https://doi.org/10.1016/j.energy.2018.08.015.
46. Merrick, J.H., *On representation of temporal variability in electricity capacity planning models.* Energy Economics, 2016. **59**: pp. 261-274, DOI: https://doi.org/10.1016/j.eneco.2016.08.001.
47. Teichgraeber, H. and A.R. Brandt, *Clustering methods to find representative periods for the optimization of energy systems: an initial framework and comparison.* Applied Energy, 2019. **239**: pp. 1283-1293, DOI: https://doi.org/10.1016/j.apenergy.2019.02.012.
48. Kotzur, L., P. Markewitz, M. Robinius, and D. Stolten, *Impact of different time series aggregation methods on optimal energy system design.* Renewable Energy, 2018. **117**: pp. 474-487, DOI: https://doi.org/10.1016/j.renene.2017.10.017.
49. Hall, L.M.H. and A.R. Buckley, *A review of energy systems models in the UK: Prevalent usage and categorisation.* Applied

Energy, 2016. **169**: pp. 607-628, DOI: https://doi.org/10.1016/j.apenergy.2016.02.044.
50. Van der Voort, E., *The EFOM 12C energy supply model within the EC modelling system.* Omega, 1982. **10**(5): pp. 507-523, DOI: https://doi.org/10.1016/0305-0483(82)90007-X.
51. Kydes, A.S., *The Brookhaven Energy System Optimization Model: Its Variants and Uses*, in *Energy Policy Modeling: United States and Canadian Experiences: Volume II Integrative Energy Policy Models*, W.T. Ziemba and S.L. Schwartz, Editors. 1980, Springer Netherlands: Dordrecht. p. 110-136, DOI: https://doi.org/10.1007/978-94-009-8751-7_7.
52. Loulou, R., A. Kanudia, and G. Goldstein, *Documentation for the TIMES Model PART II*. 2016.
53. Loulou, R., G. Goldstein, A. Kanudia, A. Lettila, and U. Remne, *Documentation for the TIMES Model PART I*. 2016.
54. Loulou, R., U. Remne, A. Kanudia, A. Lehtila, and G. Goldstein, *Documentation for the TIMES Model PART I*. 2005.
55. Loulou, R., A. Lehtilä, A. Kanudia, U. Remne, and G. Goldstein, *Documentation for the TIMES Model PART II*. 2005.
56. Kannan, R., *The development and application of a temporal MARKAL energy system model using flexible time slicing.* Applied Energy, 2011. **88**(6): pp. 2261-2272, DOI: https://doi.org/10.1016/j.apenergy.2010.12.066.
57. Neniškis, E. and A. Galinis, *Representation of wind power generation in economic models for long-term energy planning.* Energetika, 2018. **64**(1), DOI: https://doi.org/10.6001/energetika.v64i1.3726
58. Rosen, J., *The future role of renewable energy sources in European electricity supply : A model-based analysis for the EU-15*. 2008, Karlsruher Institut für Technologie: Karlsruhe, DOI: https://doi.org/10.5445/KSP/1000007531.
59. Balachandra, P. and V. Chandru, *Modelling electricity demand with representative load curves.* Energy, 1999. **24**(3): pp. 219-230, DOI: https://doi.org/10.1016/S0360-5442(98)00096-6.
60. Mavrotas, G., D. Diakoulaki, K. Florios, and P. Georgiou, *A mathematical programming framework for energy planning in services' sector buildings under uncertainty in load demand: The case of a hospital in Athens.* Energy Policy, 2008. **36**(7): pp. 2415-2429, DOI: https://doi.org/10.1016/j.enpol.2008.01.011.
61. Domínguez-Muñoz, F., J.M. Cejudo-López, A. Carrillo-Andrés, and M. Gallardo-Salazar, *Selection of typical demand days for CHP optimization.* Energy and Buildings, 2011. **43**(11): pp. 3036-3043, DOI: https://doi.org/10.1016/j.enbuild.2011.07.024.
62. Chen, C., F. Ibekwe-SanJuan, and J. Hou, *The structure and dynamics of cocitation clusters: A multiple-perspective cocitation analysis.* Journal of the American Society for information Science and Technology, 2010. **61**(7): pp. 1386-1409, DOI: https://doi.org/10.1002/asi.21309.
63. Nahmmacher, P., E. Schmid, L. Hirth, and B. Knopf, *Carpe diem: A novel approach to select representative days for long-term power system modeling.* Energy, 2016. **112**: pp. 430-442, DOI: https://doi.org/10.1016/j.energy.2016.06.081.

64. Schütz, T., M. Schraven, M. Fuchs, P. Remmen, and D. Mueller, *Comparison of clustering algorithms for the selection of typical demand days for energy system synthesis*. Vol. 129. 2018, DOI: https://doi.org/10.1016/j.renene.2018.06.028.
65. Andrews, R.W., J.S. Stein, C. Hansen, and D. Riley. *Introduction to the open source PV LIB for python Photovoltaic system modelling package*. in *2014 IEEE 40th Photovoltaic Specialist Conference (PVSC)*. 2014. DOI: https://doi.org/10.1109/PVSC.2014.6925501.
66. Renaldi, R. and D. Friedrich, *Multiple time grids in operational optimisation of energy systems with short- and long-term thermal energy storage.* Energy, 2017. **133**: pp. 784-795, DOI: https://doi.org/10.1016/j.energy.2017.05.120.
67. Nanopoulos, A., R. Alcock, and Y. Manolopoulos, *Feature-based classification of time-series data.* International Journal of Computer Research, 2001. **10**(3): pp. 49-61.
68. Agapoff, S., C. Pache, P. Panciatici, L. Warland, and S. Lumbreras. *Snapshot selection based on statistical clustering for Transmission Expansion Planning*. in *2015 IEEE Eindhoven PowerTech*. 2015. DOI: https://doi.org/10.1109/PTC.2015.7232393.
69. P. Deane, J., G. Drayton, and B. O Gallachoir, *The impact of sub-hourly modelling in power systems with significant levels of renewable generation*. Vol. 113. 2014. 152-158, DOI: https://doi.org/10.1016/j.apenergy.2013.07.027.
70. Beck, T., H. Kondziella, G. Huard, and T. Bruckner, *Assessing the influence of the temporal resolution of electrical load and PV generation profiles on self-consumption and sizing of PV-battery systems.* Applied Energy, 2016. **173**: pp. 331-342, DOI: https://doi.org/10.1016/j.apenergy.2016.04.050.
71. Yokoyama, R., Y. Hasegawa, and K. Ito, *A MILP decomposition approach to large scale optimization in structural design of energy supply systems.* Energy Conversion and Management, 2002. **43**(6): pp. 771-790, DOI: https://doi.org/10.1016/S0196-8904(01)00075-9.
72. Yokoyama, R., Y. Shinano, S. Taniguchi, M. Ohkura, and T. Wakui, *Optimization of energy supply systems by MILP branch and bound method in consideration of hierarchical relationship between design and operation.* Energy Conversion and Management, 2015. **92**: pp. 92-104, DOI: https://doi.org/10.1016/j.enconman.2014.12.020.
73. Yokoyama, R., Y. Shinano, Y. Wakayama, and T. Wakui, *Model reduction by time aggregation for optimal design of energy supply systems by an MILP hierarchical branch and bound method.* Energy, 2019. **181**: pp. 782-792, DOI: https://doi.org/10.1016/j.energy.2019.04.066.
74. Fazlollahi, S., S.L. Bungener, P. Mandel, G. Becker, and F. Maréchal, *Multi-objectives, multi-period optimization of district energy systems: I. Selection of typical operating periods.* Computers & Chemical Engineering, 2014. **65**: pp. 54-66, DOI: https://doi.org/10.1016/j.compchemeng.2014.03.005.

75. Bungener, S., R. Hackl, G. Van Eetvelde, S. Harvey, and F. Marechal, *Multi-period analysis of heat integration measures in industrial clusters.* Energy, 2015. **93**: pp. 220-234, DOI: https://doi.org/10.1016/j.energy.2015.09.023.
76. Deml, S., A. Ulbig, T. Borsche, and G. Andersson. *The role of aggregation in power system simulation*. in *2015 IEEE Eindhoven PowerTech*. 2015. DOI: https://doi.org/10.1109/PTC.2015.7232755.
77. Pineda, S. and J.M. Morales, *Chronological Time-Period Clustering for Optimal Capacity Expansion Planning With Storage.* IEEE Transactions on Power Systems, 2018. **33**(6): pp. 7162-7170, DOI: https://doi.org/10.1109/TPWRS.2018.2842093.
78. Ward, J.H., *Hierarchical Grouping to Optimize an Objective Function AU - Ward, Joe H.* Journal of the American Statistical Association, 1963. **58**(301): pp. 236-244, DOI: https://doi.org/10.1080/01621459.1963.10500845.
79. Bahl, B., T. Söhler, M. Hennen, and A. Bardow, *Typical Periods for Two-Stage Synthesis by Time-Series Aggregation with Bounded Error in Objective Function.* Frontiers in Energy Research, 2018. **5**(35), DOI: https://doi.org/10.3389/fenrg.2017.00035.
80. Lloyd, S., *Least squares quantization in PCM.* IEEE Transactions on Information Theory, 1982. **28**(2): pp. 129-137, DOI: https://doi.org/10.1109/TIT.1982.1056489.
81. MacQueen, J. *Some methods for classification and analysis of multivariate observations*. in *Proceedings of the Fifth Berkeley Symposium on Mathematical Statistics and Probability, Volume 1: Statistics*. 1967. Berkeley, Calif.: University of California Press.
82. Baumgärtner, N., F. Temme, B. Bahl, M. Hennen, D. Hollermann, and A. Bardow. *RiSES4 Rigorous Synthesis of Energy Supply Systems with Seasonal Storage by relaxation and time- series aggregation to typical periods*. in *Ecos 2019 - The 32nd International Conference on Efficiency, Cost, Optimization, Simulation and Environmental Impact of Energy Systems*. 2019. Wroclaw, Poland.
83. Baumgärtner, N., B. Bahl, M. Hennen, and A. Bardow, *RiSES3: Rigorous Synthesis of Energy Supply and Storage Systems via time-series relaxation and aggregation.* Computers & Chemical Engineering, 2019. **127**: pp. 127-139, DOI: https://doi.org/10.1016/j.compchemeng.2019.02.006.
84. Stein, D.v., N.v. Bracht, A. Maaz, and A. Moser. *Development of adaptive time patterns for multi-dimensional power system simulations*. in *2017 14th International Conference on the European Energy Market (EEM)*. 2017. DOI: https://doi.org/10.1109/EEM.2017.7981868.
85. Georgios Savvidis, K.H., *How well do we understand our power system models?*, in *42nd International Association for Energy Economics (IAEE) Annual Conference* 2019: Montréal, Canada.
86. Bauer, D., R. Marx, J. Nußbicker-Lux, F. Ochs, W. Heidemann, and H. Müller-Steinhagen, *German central solar heating plants with seasonal heat storage.* Solar Energy, 2010. **84**(4): pp. 612-623, DOI: https://doi.org/10.1016/j.solener.2009.05.013.

87. Sorknæs, P., *Simulation method for a pit seasonal thermal energy storage system with a heat pump in a district heating system.* Energy, 2018. **152**: pp. 533-538, DOI: https://doi.org/10.1016/j.energy.2018.03.152.
88. Wogrin, S., D. Galbally, and J. Reneses, *Optimizing Storage Operations in Medium- and Long-Term Power System Models.* IEEE Transactions on Power Systems, 2016. **31**(4): pp. 3129-3138, DOI: https://doi.org/10.1109/TPWRS.2015.2471099.
89. Tejada-Arango, D.A., S. Wogrin, and E. Centeno, *Representation of Storage Operations in Network-Constrained Optimization Models for Medium- and Long-Term Operation.* IEEE Transactions on Power Systems, 2018. **33**(1): pp. 386-396, DOI: https://doi.org/10.1109/TPWRS.2017.2691359.
90. Wogrin, S., P. Dueñas, A. Delgadillo, and J. Reneses, *A New Approach to Model Load Levels in Electric Power Systems With High Renewable Penetration.* IEEE Transactions on Power Systems, 2014. **29**(5): pp. 2210-2218, DOI: https://doi.org/10.1109/TPWRS.2014.2300697.
91. Härtel, P., M. Kristiansen, and M. Korpås, *Assessing the impact of sampling and clustering techniques on offshore grid expansion planning.* Energy Procedia, 2017. **137**: pp. 152-161, DOI: https://doi.org/10.1016/j.egypro.2017.10.342.
92. Ploussard, Q., L. Olmos, and A. Ramos, *An operational state aggregation technique for transmission expansion planning based on line benefits.* IEEE Transactions on Power Systems, 2016. **32**(4): pp. 2744-2755, DOI: https://doi.org/10.1109/TPWRS.2016.2614368.
93. Lythcke-Jørgensen, C.E., M. Münster, A.V. Ensinas, and F. Haglind, *A method for aggregating external operating conditions in multi-generation system optimization models.* Applied Energy, 2016. **166**: pp. 59-75, DOI: https://doi.org/10.1016/j.apenergy.2015.12.050.
94. Buoro, D., M. Casisi, P. Pinamonti, and M. Reini, *Optimal synthesis and operation of advanced energy supply systems for standard and domotic home.* Energy Conversion and Management, 2012. **60**: pp. 96-105, DOI: https://doi.org/10.1016/j.enconman.2012.02.008.
95. Harb, H., C. Schwager, R. Streblow, and D. Mueller. *Optimal design of energy systems in residential districts with interconnected local heating and electrical networks*. in *Building Simulation Conference 2015*. 2015. Hyderabad, India, DOI: https://doi.org/10.13140/RG.2.1.2144.6488.
96. Merkel, E., R. McKenna, and W. Fichtner, *Optimisation of the capacity and the dispatch of decentralised micro-CHP systems: A case study for the UK.* Applied Energy, 2015. **140**: pp. 120-134, DOI: https://doi.org/10.1016/j.apenergy.2014.11.036.
97. de Sisternes, F.J., J.D. Jenkins, and A. Botterud, *The value of energy storage in decarbonizing the electricity sector.* Applied Energy, 2016. **175**: pp. 368-379, DOI: https://doi.org/10.1016/j.apenergy.2016.05.014.
98. De Sisternes Jimenez, F. and M.D. Webster, *Optimal selection of sample weeks for approximating the net load in generation*

planning problems, in *ESD Working Papers*. 2013, DOI: https://doi.org/1721.1/102959.

99. Patteeuw, D. and L. Helsen, *Combined design and control optimization of residential heating systems in a smart-grid context.* Energy and Buildings, 2016. **133**: pp. 640-657, DOI: https://doi.org/10.1016/j.enbuild.2016.09.030.
100. van der Heijde, B., L. Scapino, A. Vandermeulen, D. Patteeuw, L. Helsen, and R. Salenbien. *Using representative time slices for optimization of thermal energy storage systems in low-temperature district heating systems*. in *31st International Conference on Efficiency, Cost, Optimization, SImulation and Environmental Impact of Energy Systems*. 2018. Guimarães, Portugal: University of Minhos; Guimarães.
101. K. Jain, A., M. Murty, and P. J. Flynn, *Data clustering: a review. ACM Comput Surv*. Vol. 31. 1999. 264-323, DOI: https://doi.org/10.1145/331499.331504.
102. Brodrick, P.G., A.R. Brandt, and L.J. Durlofsky, *Optimal design and operation of integrated solar combined cycles under emissions intensity constraints.* Applied Energy, 2018. **226**: pp. 979-990, DOI: https://doi.org/10.1016/j.apenergy.2018.06.052.
103. Marton, C.H., A. Elkamel, and T.A. Duever, *An order-specific clustering algorithm for the determination of representative demand curves.* Computers & Chemical Engineering, 2008. **32**(6): pp. 1365-1372, DOI: https://doi.org/10.1016/j.compchemeng.2007.06.010.
104. Lozano, M.A., J.C. Ramos, and L.M. Serra, *Cost optimization of the design of CHCP (combined heat, cooling and power) systems under legal constraints.* Energy, 2010. **35**(2): pp. 794-805, DOI: https://doi.org/10.1016/j.energy.2009.08.022.
105. Schütz, T., L. Schiffer, H. Harb, M. Fuchs, and D. Müller, *Optimal design of energy conversion units and envelopes for residential building retrofits using a comprehensive MILP model.* Applied Energy, 2017. **185**: pp. 1-15, DOI: https://doi.org/10.1016/j.apenergy.2016.10.049.
106. Harb, H., J. Reinhardt, R. Streblow, and D. Mueller, *MIP approach for designing heating systems in residential buildings and neighbourhood.* Journal of Building Performance Simulation, 2015, DOI: https://doi.org/10.1080/19401493.2015.1051113.
107. Kools, L. and F. Phillipson, *Data granularity and the optimal planning of distributed generation.* Energy, 2016. **112**: pp. 342-352, DOI: https://doi.org/10.1016/j.energy.2016.06.089.
108. Voll, P., C. Klaffke, M. Hennen, and A. Bardow, *Automated superstructure-based synthesis and optimization of distributed energy supply systems.* Energy, 2013. **50**: pp. 374-388, DOI: https://doi.org/10.1016/j.energy.2012.10.045.
109. Nicolosi, M., *The importance of high temporal resolution in modeling renewable energy penetration scenarios.* 2010.
110. Haydt, G., V. Leal, A. Pina, and C.A. Silva, *The relevance of the energy resource dynamics in the mid/long-term energy planning models.* Renewable Energy, 2011. **36**(11): pp. 3068-3074, DOI: https://doi.org/10.1016/j.renene.2011.03.028.

111. Welsch, M., M. Howells, M. Bazilian, J.F. DeCarolis, S. Hermann, and H.H. Rogner, *Modelling elements of Smart Grids – Enhancing the OSeMOSYS (Open Source Energy Modelling System) code.* Energy, 2012. **46**(1): pp. 337-350, DOI: https://doi.org/10.1016/j.energy.2012.08.017.
112. Timmerman, J., M. Hennen, A. Bardow, P. Lodewijks, L. Vandevelde, and G. Van Eetvelde, *Towards low carbon business park energy systems: A holistic techno-economic optimisation model.* Energy, 2017. **125**: pp. 747-770, DOI: https://doi.org/10.1016/j.energy.2017.02.081.
113. Pina, A., C. Silva, and P. Ferrão, *Modeling hourly electricity dynamics for policy making in long-term scenarios.* Energy Policy, 2011. **39**(9): pp. 4692-4702, DOI: https://doi.org/10.1016/j.enpol.2011.06.062.
114. Devogelaer, D., *Towards 100% renewable energy in Belgium by 2050*. 2012, Brussels, Belgium: Federal Planning Bureau.
115. Kannan, R. and H. Turton, *A Long-Term Electricity Dispatch Model with the TIMES Framework.* Environmental Modeling & Assessment, 2013. **18**(3): pp. 325-343, DOI: https://doi.org/10.1007/s10666-012-9346-y.
116. Simões, S., W. Nijs, P. Ruiz, A. Sgobbi, d. radu, P. Yilmaz Bolat, c. thiel, and e. peteves, *The JRC-EU-TIMES model - Assessing the long-term role of the SET Plan Energy technologies*. 2013, DOI: https://doi.org/10.2790/97596.
117. Poncelet, K., E. Delarue, D. Six, J. Duerinck, and W. D'haeseleer, *Impact of the level of temporal and operational detail in energy-system planning models.* Applied Energy, 2016. **162**: pp. 631-643, DOI: https://doi.org/10.1016/j.apenergy.2015.10.100.
118. Wakui, T. and R. Yokoyama, *Optimal structural design of residential cogeneration systems with battery based on improved solution method for mixed-integer linear programming.* Energy, 2015. **84**: pp. 106-120, DOI: https://doi.org/10.1016/j.energy.2015.02.056.
119. Wakui, T., H. Kawayoshi, and R. Yokoyama, *Optimal structural design of residential power and heat supply devices in consideration of operational and capital recovery constraints.* Applied Energy, 2016. **163**: pp. 118-133, DOI: https://doi.org/10.1016/j.apenergy.2015.10.154.
120. Wakui, T. and R. Yokoyama, *Optimal structural design of residential cogeneration systems in consideration of their operating restrictions.* Energy, 2014. **64**: pp. 719-733, DOI: https://doi.org/10.1016/j.energy.2013.10.002.
121. Lozano, M.A., J.C. Ramos, M. Carvalho, and L.M. Serra, *Structure optimization of energy supply systems in tertiary sector buildings.* Energy and Buildings, 2009. **41**(10): pp. 1063-1075, DOI: https://doi.org/10.1016/j.enbuild.2009.05.008.
122. Weber, C. and N. Shah, *Optimisation based design of a district energy system for an eco-town in the United Kingdom.* Energy, 2011. **36**(2): pp. 1292-1308, DOI: https://doi.org/10.1016/j.energy.2010.11.014.
123. Stadler, M., M. Groissböck, G. Cardoso, and C. Marnay, *Optimizing Distributed Energy Resources and building retrofits*

with the strategic DER-CAModel. Applied Energy, 2014. **132**: pp. 557-567, DOI: https://doi.org/10.1016/j.apenergy.2014.07.041.

124. Casisi, M., P. Pinamonti, and M. Reini, *Optimal lay-out and operation of combined heat & power (CHP) distributed generation systems.* Energy, 2009. **34**(12): pp. 2175-2183, DOI: https://doi.org/10.1016/j.energy.2008.10.019.
125. Pina, A., C.A. Silva, and P. Ferrão, *High-resolution modeling framework for planning electricity systems with high penetration of renewables.* Applied Energy, 2013. **112**: pp. 215-223, DOI: https://doi.org/10.1016/j.apenergy.2013.05.074.
126. Spiecker, S., P. Vogel, and C. Weber, *Evaluating interconnector investments in the north European electricity system considering fluctuating wind power penetration.* Energy Economics, 2013. **37**: pp. 114-127, DOI: https://doi.org/10.1016/j.eneco.2013.01.012.
127. Wouters, C., E.S. Fraga, and A.M. James, *An energy integrated, multi-microgrid, MILP (mixed-integer linear programming) approach for residential distributed energy system planning – A South Australian case-study.* Energy, 2015. **85**: pp. 30-44, DOI: https://doi.org/10.1016/j.energy.2015.03.051.
128. Yang, Y., S. Zhang, and Y. Xiao, *Optimal design of distributed energy resource systems coupled with energy distribution networks.* Energy, 2015. **85**: pp. 433-448, DOI: https://doi.org/10.1016/j.energy.2015.03.101.
129. Ameri, M. and Z. Besharati, *Optimal design and operation of district heating and cooling networks with CCHP systems in a residential complex.* Energy and Buildings, 2016. **110**: pp. 135-148, DOI: https://doi.org/10.1016/j.enbuild.2015.10.050.
130. Bracco, S., G. Dentici, and S. Siri, *DESOD: a mathematical programming tool to optimally design a distributed energy system.* Energy, 2016. **100**: pp. 298-309, DOI: https://doi.org/10.1016/j.energy.2016.01.050.
131. Moradi, S., R. Ghaffarpour, A.M. Ranjbar, and B. Mozaffari, *Optimal integrated sizing and planning of hubs with midsize/large CHP units considering reliability of supply.* Energy Conversion and Management, 2017. **148**: pp. 974-992, DOI: https://doi.org/10.1016/j.enconman.2017.06.008.
132. Swider, D.J. and C. Weber, *The costs of wind's intermittency in Germany: application of a stochastic electricity market model.* European Transactions on Electrical Power, 2007. **17**(2): pp. 151-172, DOI: https://doi.org/10.1002/etep.125.
133. Oluleye, G., L. Vasquez, R. Smith, and M. Jobson, *A multi-period Mixed Integer Linear Program for design of residential distributed energy centres with thermal demand data discretisation.* Sustainable Production and Consumption, 2016. **5**: pp. 16-28, DOI: https://doi.org/10.1016/j.spc.2015.11.003.
134. Mehleri, E.D., H. Sarimveis, N.C. Markatos, and L.G. Papageorgiou, *A mathematical programming approach for optimal design of distributed energy systems at the neighbourhood level.* Energy, 2012. **44**(1): pp. 96-104, DOI: https://doi.org/10.1016/j.energy.2012.02.009.

135. Aghabozorgi, S., A. Seyed Shirkhorshidi, and T. Ying Wah, *Time-series clustering – A decade review.* Information Systems, 2015. **53**: pp. 16-38, DOI: https://doi.org/10.1016/j.is.2015.04.007.
136. Beyer, K., J. Goldstein, R. Ramakrishnan, and U. Shaft. *When Is "Nearest Neighbor" Meaningful?* in *Database Theory — ICDT'99*. 1999. Berlin, Heidelberg: Springer Berlin Heidelberg, DOI: https://doi.org/10.1007/3-540-49257-7_15.
137. Keogh, E. and A. Mueen, *Curse of Dimensionality*, in *Encyclopedia of Machine Learning*, C. Sammut and G.I. Webb, Editors. 2010, Springer US: Boston, MA. p. 257-258, DOI: https://doi.org/10.1007/978-0-387-30164-8_192.
138. Aggarwal, C.C., A. Hinneburg, and D.A. Keim. *On the Surprising Behavior of Distance Metrics in High Dimensional Space*. in *Database Theory — ICDT 2001*. 2001. Berlin, Heidelberg: Springer Berlin Heidelberg, DOI: https://doi.org/10.1007/3-540-44503-X_27.
139. Guo, X., L. Gao, X. Liu, and J. Yin. *Improved Deep Embedded Clustering with Local Structure Preservation*. in *26th International Joint Conference on Artificial Intelligence*. 2017. Melbourne, Australia: AAAI Press.
140. Sun, M., F. Teng, X. Zhang, G. Strbac, and D. Pudjianto, *Data-Driven Representative Day Selection for Investment Decisions: A Cost-Oriented Approach.* IEEE Transactions on Power Systems, 2019: pp. 1-1, DOI: https://doi.org/10.1109/TPWRS.2019.2892619.
141. Sun, M., I. Konstantelos, and G. Strbac, *C-Vine Copula Mixture Model for Clustering of Residential Electrical Load Pattern Data.* IEEE Transactions on Power Systems, 2017. **32**(3): pp. 2382-2393, DOI: https://doi.org/10.1109/TPWRS.2016.2614366.
142. Almaimouni, A., A. Ademola-Idowu, J. Nathan Kutz, A. Negash, and D.s. Kirschen. *Selecting and Evaluating Representative Days for Generation Expansion Planning*. in *2018 Power Systems Computation Conference (PSCC)*. 2018. Dublin, Ireland IEEE, DOI: https://doi.org/10.23919/PSCC.2018.8442580.
143. Fazlollahi, S., L. Girardin, and F. Maréchal, *Clustering Urban Areas for Optimizing the Design and the Operation of District Energy Systems*, in *Computer Aided Chemical Engineering*, J.J. Klemeš, P.S. Varbanov, and P.Y. Liew, Editors. 2014, Elsevier. p. 1291-1296, DOI: https://doi.org/10.1016/B978-0-444-63455-9.50050-7.
144. Schütz, T., M. Schraven, H. Harb, M. Fuchs, and D. Mueller. *Clustering algorithms for the selection of typical demand days for the optimal design of building energy systems*. in *29th International Conference on Efficiency, Cost, Optimisation, Simulation and Environmental Impact of Energy Systems*. 2016. Portorož, Slovenia: University of Ljubljana / Faculty of Mechanical Engineering.
145. Zatti, M., M. Gabba, M. Freschini, M. Rossi, A. Gambarotta, M. Morini, and E. Martelli, *k-MILP: A novel clustering approach to select typical and extreme days for multi-energy systems design optimization.* Energy, 2019. **181**: pp. 1051-1063, DOI: https://doi.org/10.1016/j.energy.2019.05.044.

146. Fitiwi, D.Z., F. de Cuadra, L. Olmos, and M. Rivier, *A new approach of clustering operational states for power network expansion planning problems dealing with RES (renewable energy source) generation operational variability and uncertainty.* Energy, 2015. **90**: pp. 1360-1376, DOI: https://doi.org/10.1016/j.energy.2015.06.078.
147. Poncelet, K., H. Höschle, E. Delarue, A. Virag, and W. D'haeseleer, *Selecting Representative Days for Capturing the Implications of Integrating Intermittent Renewables in Generation Expansion Planning Problems.* IEEE Transactions on Power Systems, 2016. **32**(3): pp. 1936-1948, DOI: https://doi.org/10.1109/TPWRS.2016.2596803.
148. Voulis, N., M. Warnier, and F.M.T. Brazier, *Understanding spatio-temporal electricity demand at different urban scales: A data-driven approach.* Applied Energy, 2018. **230**: pp. 1157-1171, DOI: https://doi.org/10.1016/j.apenergy.2018.08.121.
149. Brodrick, P.G., A.R. Brandt, and L.J. Durlofsky, *Operational optimization of an integrated solar combined cycle under practical time-dependent constraints.* Energy, 2017. **141**: pp. 1569-1584, DOI: https://doi.org/10.1016/j.energy.2017.11.059.
150. Teichgraeber, H., P.G. Brodrick, and A.R. Brandt, *Optimal design and operations of a flexible oxyfuel natural gas plant.* Energy, 2017. **141**: pp. 506-518, DOI: https://doi.org/10.1016/j.energy.2017.09.087.
151. Liu, Y., R. Sioshansi, and A.J. Conejo, *Hierarchical Clustering to Find Representative Operating Periods for Capacity-Expansion Modeling.* IEEE Transactions on Power Systems, 2018. **33**(3): pp. 3029-3039, DOI: https://doi.org/10.1109/TPWRS.2017.2746379.
152. Marquant, J.F.O., Akomeno; Orehounig, Kristina; Evins, Ralph; Carmeliet, Jan, *Application of Spatial-Temporal Clustering to Facilitate Energy System Modelling*, in *14th International Confrence of IBPSA Building Simulation 2015*, V.R. Khare, Chaudhary, Gaurav, Editor. 2015, IIIT Hyderabad: Hyderabad, India. p. 551 - 558.
153. Marquant, J.F., G. Mavromatidis, R. Evins, and J. Carmeliet, *Comparing different temporal dimension representations in distributed energy system design models.* Energy Procedia, 2017. **122**: pp. 907-912, DOI: https://doi.org/10.1016/j.egypro.2017.07.403.
154. Jain, A.K., *Data clustering: 50 years beyond K-means.* Pattern Recognition Letters, 2010. **31**(8): pp. 651-666, DOI: https://doi.org/10.1016/j.patrec.2009.09.011.
155. Saxena, A., M. Prasad, A. Gupta, N. Bharill, O.P. Patel, A. Tiwari, M.J. Er, W. Ding, and C.-T. Lin, *A review of clustering techniques and developments.* Neurocomputing, 2017. **267**: pp. 664-681, DOI: https://doi.org/10.1016/j.neucom.2017.06.053.
156. Vinod, H., *Integer Programming and the Theory of Grouping*. Vol. 64. 1969, DOI: https://doi.org/10.1080/01621459.1969.10500990.
157. Teichgraeber, H. and A.R. Brandt, *Systematic Comparison of Aggregation Methods for Input Data Time Series Aggregation of Energy Systems Optimization Problems*, in *Computer Aided*

Chemical Engineering, M.R. Eden, M.G. Ierapetritou, and G.P. Towler, Editors. 2018, Elsevier. p. 955-960, DOI: https://doi.org/10.1016/B978-0-444-64241-7.50154-3.

158. Schiefelbein, J., J. Tesfaegzi, R. Streblow, and D. Müller, *Design of an optimization algorithm for the distribution of thermal energy systems and local heating networks within a city district.* Proceedings of ECOS, 2015, DOI: https://doi.org/10.13140/RG.2.1.1546.3521.
159. Tveit, T.-M., T. Savola, A. Gebremedhin, and C.-J. Fogelholm, *Multi-period MINLP model for optimising operation and structural changes to CHP plants in district heating networks with long-term thermal storage.* Energy Conversion and Management, 2009. **50**(3): pp. 639-647, DOI: https://doi.org/10.1016/j.enconman.2008.10.010.
160. Gabrielli, P., F. Fürer, G. Mavromatidis, and M. Mazzotti, *Robust and optimal design of multi-energy systems with seasonal storage through uncertainty analysis.* Applied Energy, 2019. **238**: pp. 1192-1210, DOI: https://doi.org/10.1016/j.apenergy.2019.01.064.
161. Hilbers, A.P., D.J. Brayshaw, and A. Gandy, *Importance subsampling: improving power system planning under climate-based uncertainty.* Applied Energy, 2019. **251**: p. 113114, DOI: https://doi.org/10.1016/j.apenergy.2019.04.110.
162. Ghahramani, Z., *Unsupervised Learning*, in *Advanced Lectures on Machine Learning: ML Summer Schools 2003, Canberra, Australia, February 2 - 14, 2003, Tübingen, Germany, August 4 - 16, 2003, Revised Lectures*, O. Bousquet, U. von Luxburg, and G. Rätsch, Editors. 2004, Springer Berlin Heidelberg: Berlin, Heidelberg. p. 72-112, DOI: 10.1007/978-3-540-28650-9_5.
163. Mohri, M., A. Rostamizadeh, and A. Talwalkar, *Foundations of machine learning.[SI]*. 2012, The MIT Press.
164. Ortiga, J., J.C. Bruno, and A. Coronas, *Selection of typical days for the characterisation of energy demand in cogeneration and trigeneration optimisation models for buildings.* Energy Conversion and Management, 2011. **52**(4): pp. 1934-1942, DOI: https://doi.org/10.1016/j.enconman.2010.11.022.
165. van der Weijde, A.H. and B.F. Hobbs, *The economics of planning electricity transmission to accommodate renewables: Using two-stage optimisation to evaluate flexibility and the cost of disregarding uncertainty.* Energy Economics, 2012. **34**(6): pp. 2089-2101, DOI: https://doi.org/10.1016/j.eneco.2012.02.015.
166. Munoz, F.D. and A.D. Mills, *Endogenous Assessment of the Capacity Value of Solar PV in Generation Investment Planning Studies.* IEEE Transactions on Sustainable Energy, 2015. **6**(4): pp. 1574-1585, DOI: https://doi.org/10.1109/TSTE.2015.2456019.
167. Frew, B.A. and M.Z. Jacobson, *Temporal and spatial tradeoffs in power system modeling with assumptions about storage: An application of the POWER model.* Energy, 2016. **117**: pp. 198-213, DOI: https://doi.org/10.1016/j.energy.2016.10.074.
168. Lee, T.-Y. and C.-L. Chen, *Unit commitment with probabilistic reserve: An IPSO approach.* Energy Conversion and

Management, 2007. **48**(2): pp. 486-493, DOI: https://doi.org/10.1016/j.enconman.2006.06.015.

169. Phan, Q.A., T. Scully, M. Breen, and M.D. Murphy, *Determination of optimal battery utilization to minimize operating costs for a grid-connected building with renewable energy sources.* Energy Conversion and Management, 2018. **174**: pp. 157-174, DOI: https://doi.org/10.1016/j.enconman.2018.07.081.
170. Saravanan, B., S. Das, S. Sikri, and D.P. Kothari, *A solution to the unit commitment problem—a review.* Frontiers in Energy, 2013. **7**(2): pp. 223-236, DOI: https://doi.org/10.1007/s11708-013-0240-3.
171. Xiao, J., L. Bai, F. Li, H. Liang, and C. Wang, *Sizing of Energy Storage and Diesel Generators in an Isolated Microgrid Using Discrete Fourier Transform (DFT).* IEEE Transactions on Sustainable Energy, 2014. **5**(3): pp. 907-916, DOI: https://doi.org/10.1109/TSTE.2014.2312328.
172. Pöstges, A. and C. Weber, *Time series aggregation – A new methodological approach using the "peak-load-pricing" model.* Utilities Policy, 2019. **59**: p. 100917, DOI: https://doi.org/10.1016/j.jup.2019.05.003.
173. Billington, R. and R.N. Allan, *Reliability evaluation of power systems.* 1984, DOI: https://doi.org/10.1002/qre.4680010220.
174. Short, W., P. Sullivan, T. Mai, M. Mowers, C. Uriarte, N. Blair, D. Heimiller, and A. Martinez, *Regional energy deployment system (ReEDS)*. 2011, National Renewable Energy Lab.(NREL), Golden, CO (United States), DOI: https://doi.org/10.2172/1031955.
175. Frew, B.A., S. Becker, M.J. Dvorak, G.B. Andresen, and M.Z. Jacobson, *Flexibility mechanisms and pathways to a highly renewable US electricity future.* Energy, 2016. **101**: pp. 65-78, DOI: https://doi.org/10.1016/j.energy.2016.01.079.
176. Heuberger, C.F., I. Staffell, N. Shah, and N.M. Dowell, *A systems approach to quantifying the value of power generation and energy storage technologies in future electricity networks.* Computers & Chemical Engineering, 2017. **107**: pp. 247-256, DOI: https://doi.org/10.1016/j.compchemeng.2017.05.012.
177. Green, R., I. Staffell, and N. Vasilakos, *Divide and Conquer? k-Means Clustering of Demand Data Allows Rapid and Accurate Simulations of the British Electricity System.* IEEE Transactions on Engineering Management, 2014. **61**(2): pp. 251-260, DOI: https://doi.org/10.1109/TEM.2013.2284386.
178. Scott, I.J., P.M.S. Carvalho, A. Botterud, and C.A. Silva, *Clustering representative days for power systems generation expansion planning: Capturing the effects of variable renewables and energy storage.* Applied Energy, 2019. **253**: p. 113603, DOI: https://doi.org/10.1016/j.apenergy.2019.113603.
179. Lin, F., S. Leyffer, and T. Munson, *A two-level approach to large mixed-integer programs with application to cogeneration in energy-efficient buildings.* Computational Optimization and Applications, 2016. **65**(1): pp. 1-46, DOI: https://doi.org/10.1007/s10589-016-9842-0.

180. Bahl, B., A. Kümpel, H. Seele, M. Lampe, and A. Bardow, *Time-series aggregation for synthesis problems by bounding error in the objective function.* Energy, 2017. **135**: pp. 900-912, DOI: https://doi.org/10.1016/j.energy.2017.06.082.
181. Bahl, B., J. Lützow, D. Shu, D.E. Hollermann, M. Lampe, M. Hennen, and A. Bardow, *Rigorous synthesis of energy systems by decomposition via time-series aggregation.* Computers & Chemical Engineering, 2018. **112**: pp. 70-81, DOI: https://doi.org/10.1016/j.compchemeng.2018.01.023.
182. Conejo, A.J., E. Castillo, R. Minguez, and R. Garcia-Bertrand, *Decomposition techniques in mathematical programming: engineering and science applications*. 2006, Berlin, Germany: Springer Science & Business Media, DOI: https://doi.org/10.1007/3-540-27686-6.
183. Schwele, A., J. Kazempour, and P. Pinson, *Do unit commitment constraints affect generation expansion planning? A scalable stochastic model.* Energy Systems, 2019, DOI: https://doi.org/10.1007/s12667-018-00321-z.
184. Sifa, R. and C. Bauckhage. *Online k-Maxoids Clustering*. in *2017 IEEE International Conference on Data Science and Advanced Analytics (DSAA)*. 2017. DOI: 10.1109/DSAA.2017.76.
185. Poncelet, K., H. Höschle, E. Delarue, and W. D'haeseleer, *Selecting representative days for investment planning models*, in *TME Working Paper - Energy and Environment*. 2015, KU Leuven: Leuven, DOI: https://doi.org/10.1109/TPWRS.2016.2596803.
186. Curry, H.B., *The method of steepest descent for non-linear minimization problems.* Quarterly of Applied Mathematics, 1944. **2**(3): pp. 258-261.
187. Geoffrion, A.M. and R. Nauss, *Exceptional paper—parametric and postoptimality analysis in integer linear programming.* Management science, 1977. **23**(5): pp. 453-466.
188. Kotzur, L., P. Markewitz, M. Robinius, and D. Stolten. *Kostenoptimale Versorgungssysteme für ein vollautarkes Einfamilienhaus*. in *Internationale Energiewirtschaftstagung*. 2017. Graz, Austria.
189. Caglayan, D.G., *Robust Design of a Future 100% Renewable European Energy System with Hydrogen Infrastructure*, in *Faculty of Mechanical Engineering*. 2020, RWTH Aachen UNiversity: Aachen, Germany.
190. Caglayan, D.G., *A Robust Design of a Renewable European Energy System Encompassing a Hydrogen Infrastructure*, in *Schriften des Forschungszentrums Jülich. Reihe Energie & Umwelt / Energy & Environment*. 2020, RWTH Aachen University: Jülich. p. xxii, 312 S.
191. Ryberg, D.S., M. Robinius, and D. Stolten, *Evaluating Land Eligibility Constraints of Renewable Energy Sources in Europe.* 2018. **11**(5): p. 1246.
192. Robinius, M., A. Otto, K. Syranidis, D.S. Ryberg, P. Heuser, L. Welder, T. Grube, P. Markewitz, V. Tietze, and D. Stolten, *Linking the Power and Transport Sectors—Part 2: Modelling a Sector*

Coupling Scenario for Germany. Energies, 2017. **10**(7): p. 957, DOI: https://doi.org/10.3390/en10070957.

193. Robinius, M., G. Erdmann, and D. Stolten, *Strom-und Gasmarktdesign zur Versorgung des deutschen Straßenverkehrs mit Wasserstoff*. 2015, Lehrstuhl für Brennstoffzellen (FZ Jülich).
194. Bruninx, K., D. Orlic, D. Couckuyt, N. Grisey, B. Betraoui, T. Anderski, Y. Surmann, N. Franck, G. Keane, and B. Hickman, *Modular development plan of the Pan-European transmission system 2050: Data sets of scenarios for 2050*, in *Technical Report*. 2015, The e-HIGHWAY 2050 Project.
195. Krause, D. and P. Thörnig, *JURECA: Modular supercomputer at Jülich Supercomputing Centre.* Journal of large-scale research facilities JLSRF, 2018. **4**, DOI: https://doi.org/10.17815/jlsrf-4-121-1.
196. Kotzur, L., L. Nolting, M. Hoffmann, T. Groß, A. Smolenko, J. Priesmann, H. Büsing, R. Beer, F. Kullmann, and B. Singh, *A modeler's guide to handle complexity in energy system optimization.* arXiv preprint arXiv:2009.07216, 2020.
197. Wolpert, D.H. and W.G. Macready, *No free lunch theorems for optimization.* IEEE Transactions on Evolutionary Computation, 1997. **1**(1): pp. 67-82, DOI: 10.1109/4235.585893.
198. Alzate, C., M. Espinoza, B. De Moor, and J.A.K. Suykens. *Identifying Customer Profiles in Power Load Time Series Using Spectral Clustering*. in *Artificial Neural Networks – ICANN 2009*. 2009. Berlin, Heidelberg: Springer Berlin Heidelberg, DOI: https://doi.org/10.1007/978-3-642-04277-5_32.
199. Mehleri, E.D., H. Sarimveis, N.C. Markatos, and L.G. Papageorgiou, *Optimal design and operation of distributed energy systems: Application to Greek residential sector.* Renewable Energy, 2013. **51**: pp. 331-342, DOI: https://doi.org/10.1016/j.renene.2012.09.009.
200. Adhau, S.P., R.M. Moharil, and P.G. Adhau, *K-Means clustering technique applied to availability of micro hydro power.* Sustainable Energy Technologies and Assessments, 2014. **8**: pp. 191-201, DOI: https://doi.org/10.1016/j.seta.2014.09.001.
201. Benítez, I., A. Quijano, J.-L. Díez, and I. Delgado, *Dynamic clustering segmentation applied to load profiles of energy consumption from Spanish customers.* International Journal of Electrical Power & Energy Systems, 2014. **55**: pp. 437-448, DOI: https://doi.org/10.1016/j.ijepes.2013.09.022.
202. Brodrick, P.G., C.A. Kang, A.R. Brandt, and L.J. Durlofsky, *Optimization of carbon-capture-enabled coal-gas-solar power generation.* Energy, 2015. **79**: pp. 149-162, DOI: https://doi.org/10.1016/j.energy.2014.11.003.
203. Grigg, C., P. Wong, P. Albrecht, R. Allan, M. Bhavaraju, R. Billinton, Q. Chen, C. Fong, S. Haddad, and S. Kuruganty, *The IEEE reliability test system-1996. A report prepared by the reliability test system task force of the application of probability methods subcommittee.* IEEE Transactions on power systems, 1999. **14**(3): pp. 1010-1020, DOI: https://doi.org/10.1109/59.780914.

204. Haikarainen, C., F. Pettersson, and H. Saxén, *A decomposition procedure for solving two-dimensional distributed energy system design problems.* Applied Thermal Engineering, 2016. **100**: pp. 30-38, DOI: https://doi.org/10.1016/j.applthermaleng.2016.02.012.
205. Haller, M., S. Ludig, and N. Bauer, *Decarbonization scenarios for the EU and MENA power system: Considering spatial distribution and short term dynamics of renewable generation.* Energy Policy, 2012. **47**: pp. 282-290, DOI: https://doi.org/10.1016/j.enpol.2012.04.069.
206. Stiphout, A.v., K.D. Vos, and G. Deconinck, *The Impact of Operating Reserves on Investment Planning of Renewable Power Systems.* IEEE Transactions on Power Systems, 2017. **32**(1): pp. 378-388, DOI: https://doi.org/10.1109/TPWRS.2016.2565058.
207. Yang, J., C. Ning, C. Deb, F. Zhang, D. Cheong, S.E. Lee, C. Sekhar, and K.W. Tham, *k-Shape clustering algorithm for building energy usage patterns analysis and forecasting model accuracy improvement.* Energy and Buildings, 2017. **146**: pp. 27-37, DOI: https://doi.org/10.1016/j.enbuild.2017.03.071.
208. Zhu, Q., X. Luo, B. Zhang, and Y. Chen, *Mathematical modelling and optimization of a large-scale combined cooling, heat, and power system that incorporates unit changeover and time-of-use electricity price.* Energy Conversion and Management, 2017. **133**: pp. 385-398, DOI: https://doi.org/10.1016/j.enconman.2016.10.056.
209. Stadler, P., L. Girardin, A. Ashouri, and F. Maréchal, *Contribution of Model Predictive Control in the Integration of Renewable Energy Sources within the Built Environment.* Frontiers in Energy Research, 2018. **6**(22), DOI: https://doi.org/10.3389/fenrg.2018.00022.
210. Tupper, L.L., D.S. Matteson, C.L. Anderson, and L. Zephyr, *Band Depth Clustering for Nonstationary Time Series and Wind Speed Behavior.* Technometrics, 2018. **60**(2): pp. 245-254, DOI: https://doi.org/10.1080/00401706.2017.1345700.
211. Baumgärtner, N., R. Delorme, M. Hennen, and A. Bardow, *Design of low-carbon utility systems: Exploiting time-dependent grid emissions for climate-friendly demand-side management.* Applied Energy, 2019. **247**: pp. 755-765, DOI: https://doi.org/10.1016/j.apenergy.2019.04.029.
212. Motlagh, O., A. Berry, and L. O'Neil, *Clustering of residential electricity customers using load time series.* Applied Energy, 2019. **237**: pp. 11-24, DOI: https://doi.org/10.1016/j.apenergy.2018.12.063.
213. Pavičević, M., K. Kavvadias, T. Pukšec, and S. Quoilin, *Comparison of different model formulations for modelling future power systems with high shares of renewables – The Dispa-SET Balkans model.* Applied Energy, 2019. **252**: p. 113425, DOI: https://doi.org/10.1016/j.apenergy.2019.113425.
214. Zhang, H., Z. Lu, W. Hu, Y. Wang, L. Dong, and J. Zhang, *Coordinated optimal operation of hydro–wind–solar integrated*

systems. Applied Energy, 2019. **242**: pp. 883-896, DOI: https://doi.org/10.1016/j.apenergy.2019.03.064.
215. Arthur, D. and S. Vassilvitskii. *k-means++: The advantages of careful seeding*. in *Proceedings of the eighteenth annual ACM-SIAM symposium on Discrete algorithms*. 2007. New Orleans, Louisiana: Society for Industrial and Applied Mathematics.
216. Kaufman, L. and P.J. Rousseeuw, *Clustering by means of medoids*, in *Statistical Data Analysis Based on the L1-Norm and Related Methods*, Y. Dodge, Editor. 1987, Elsevier: Amsterdam, North-Holland. p. 405-416.
217. Singh, A., A. Yadav, and A. Rana, *K-means with Three different Distance Metrics.* International Journal of Computer Applications, 2013. **67**(10), DOI: https://doi.org/10.5120/11430-6785.
218. Bradley, P.S., O.L. Mangasarian, and W.N. Street. *Clustering via concave minimization*. in *Advances in neural information processing systems*. 1997. Denver, Colorado, USA: MIT Press.
219. Whelan, C., G. Harrell, and J. Wang. *Understanding the K-Medians Problem*. in *Proceedings of the International Conference on Scientific Computing (CSC)*. 2015. Las Vegas, Nevada, USA: The Steering Committee of The World Congress in Computer Science, Computer Engineering, & Applied Computing
220. Har-Peled, S., *Geometric Approximation Algorithms*. Mathematical Surveys and Monographs. Vol. 173. 2011, Boston, Massachusetts, USA: American Mathematical Society.
221. Paparrizos, J. and L. Gravano, *k-Shape: Efficient and Accurate Clustering of Time Series.* SIGMOD Rec., 2016. **45**(1): pp. 69-76, DOI: https://doi.org/10.1145/2949741.2949758.
222. Petitjean, F., A. Ketterlin, and P. Gançarski, *A global averaging method for dynamic time warping, with applications to clustering.* Pattern Recognition, 2011. **44**(3): pp. 678-693, DOI: https://doi.org/10.1016/j.patcog.2010.09.013.
223. Niennattrakul, V., D. Srisai, and C. Ratanamahatana, *Shape-based template matching for time series data*. Vol. 26. 2012, DOI: https://doi.org/10.1016/j.knosys.2011.04.015.
224. Kotzur, L., *A modelers' guide to handle complexity in energy systems optimization.* 2020.
225. Nelder, J.A. and R. Mead, *A simplex method for function minimization.* The computer journal, 1965. **7**(4): pp. 308-313.
226. Karmarkar, N. *A new polynomial-time algorithm for linear programming*. in *Proceedings of the sixteenth annual ACM symposium on Theory of computing*. 1984.
227. Kalai, G.J.M.P., *Linear programming, the simplex algorithm and simple polytopes.* 1997. **79**(1-3): pp. 217-233.
228. Maňas, M. and J. Nedoma, *Finding all vertices of a convex polyhedron.* Numerische Mathematik, 1968. **12**(3): pp. 226-229, DOI: 10.1007/BF02162916.
229. Boyd, S., S.P. Boyd, and L. Vandenberghe, *Convex optimization*. 2004: Cambridge university press.
230. Nocedal, J. and S. Wright, *Numerical optimization*. 2006: Springer Science & Business Media.

231. Chen, J. and S. Burer, *Globally solving nonconvex quadratic programming problems via completely positive programming.* Mathematical Programming Computation, 2012. **4**(1): pp. 33-52.
232. Sahni, S.J.S.J.o.c., *Computationally related problems.* 1974. **3**(4): pp. 262-279.
233. Milan, C., M. Stadler, G. Cardoso, and S. Mashayekh, *Modeling of non-linear CHP efficiency curves in distributed energy systems.* Applied Energy, 2015. **148**: pp. 334-347, DOI: 10.1016/j.apenergy.2015.03.053.
234. Hermann, M., *Numerische Verfahren für gewöhnliche Differentialgleichungen*, in *Grid-Computing: Eine Basistechnologie für Computational Science*, D. Fey, Editor. 2010, Springer Berlin Heidelberg: Berlin, Heidelberg. p. 149-205, DOI: 10.1007/978-3-540-79747-0_8.
235. Brio, M., G.M. Webb, and A.R. Zakharian, *Chapter 5 - Problems with Multiple Temporal and Spatial Scales*, in *Mathematics in Science and Engineering*, M. Brio, A. Zakharian, and G.M. Webb, Editors. 2010, Elsevier. p. 175-249, DOI: https://doi.org/10.1016/S0076-5392(10)21310-3.
236. Brogan, W.L., *Modern control theory*. 1991: Pearson education india.
237. Bahl, B., *Optimization-Based Synthesis of Large-Scale Energy Systems by Time-Series Aggregation Strukturoptimierung von Energiesystemen durch Zeitreihenaggregation*. 2018: Aachen.
238. Robinius, M., F.t. Stein, A. Schwane, and D. Stolten, *A Top-Down Spatially Resolved Electrical Load Model.* Energies, 2017. **10**(3): p. 361, DOI: 10.3390/en10030361.
239. Andrews, R.W., J.S. Stein, C. Hansen, and D. Riley. *Introduction to the open source PV LIB for python Photovoltaic system modelling package*. in *IEEE 40th Photovoltaic Specialist Conference (PVSC)*. 2014. DOI: 10.1109/PVSC.2014.6925501.
240. Röben, F., *Techno-economical potential of reversible Solid Oxide Cells for autarkic Buildings and Districts*. 2017, RWTH Aachen University.
241. Krampe, L., M. Wünsch, and M. Koepp, *Eigenversorgung aus Solaranlagen.: Das Potenzial für Photovoltaik-Speicher-Systeme in Ein-und Zweifamilienhäusern Landwirtschaft sowie im Lebensmittelhandel.* 2016.
242. Mayer, J.N., P. Simon, N.S.H. Philipps, T. Schlegl, and C. Senkpiel, *Current and future cost of photovoltaics. Long-term Scenarios for Market Development, System Prices LCOE of Utility-Scale PV Systems.* 2015.
243. Wolf. *Preisliste Heizsysteme*. 2016 [cited 2021 June 11]; Available from: https://www.ck-heiztechnik.de/media/kataloge/wolf/Wolf-Preisliste-Heizsysteme-03-2016.pdf.
244. Lindberg, K.B., D. Fischer, G. Doorman, M. Korpås, and I. Sartori, *Cost-optimal energy system design in Zero Energy Buildings with resulting grid impact: A case study of a German multi-family house.* Energy and Buildings, 2016. **127**: pp. 830-845, DOI: https://doi.org/10.1016/j.enbuild.2016.05.063.

245. Energy, S. *Schütz Heizöl-Lagerbehälter und Tank-Ersatzteil Preisliste*. 2017 [cited 2021 June 11]; Available from: https://www.schuetz-energy.net/downloads/heizoel-lagerbehaeltersysteme/tank-in-tank/heizoel-lagerbehaelter-preisliste-und-tank-ersatzteil-preisliste/schuetz-es-heizoel-lagerbehaelter-preisliste-und-tank-ersatzteil-preisliste-de.pdf?cid=6l7.
246. Eypasch, M., M. Schimpe, A. Kanwar, T. Hartmann, S. Herzog, T. Frank, and T. Hamacher, *Model-based techno-economic evaluation of an electricity storage system based on Liquid Organic Hydrogen Carriers.* Applied Energy, 2017. **185**: pp. 320-330, DOI: https://doi.org/10.1016/j.apenergy.2016.10.068.
247. Teichmann, D., *Konzeption und Bewertung einer nachhaltigen Energieversorgung auf Basis flüssiger Wasserstoffträger*. 2015, Friedrich Alexander Universität Erlangen-Nürnberg.
248. US Department of Energy, *The Fuel Cell Technologies Office Multi-Year Research, Development, and Demonstration Plan*. 2016, Technical report: US Department of Energy.
249. Yang, C. and J. Ogden, *Determining the lowest-cost hydrogen delivery mode.* International Journal of Hydrogen Energy, 2007. **32**(2): pp. 268-286, DOI: https://doi.org/10.1016/j.ijhydene.2006.05.009.
250. Kotzur, L., K. Knosala, P. Markewitz, P. Stenzel, M. Robinius, and D. Stolten, *tsib - Time Series Initialization for Buildings*. 2019.
251. Kotzur, L., P. Markewitz, M. Robinius, G. Cardoso, P. Stenzel, M. Heleno, and D. Stolten, *Bottom-up energy supply optimization of a national building stock.* Energy and Buildings, 2020. **209**: p. 109667, DOI: https://doi.org/10.1016/j.enbuild.2019.109667.
252. Bollmeyer, C., J. Keller, C. Ohlwein, S. Wahl, S. Crewell, P. Friederichs, A. Hense, J. Keune, S. Kneifel, and I.J.Q.J.o.t.R.M.S. Pscheidt, *Towards a high-resolution regional reanalysis for the European CORDEX domain.* 2015. **141**(686): pp. 1-15, DOI: https://doi.org/10.1002/qj.2486.
253. Frank, C.W., S. Wahl, J.D. Keller, B. Pospichal, A. Hense, and S. Crewell, *Bias correction of a novel European reanalysis data set for solar energy applications.* Solar Energy, 2018. **164**: pp. 12-24, DOI: https://doi.org/10.1016/j.solener.2018.02.012.
254. Wahl, S., C. Bollmeyer, S. Crewell, C. Figura, P. Friederichs, A. Hense, J.D. Keller, and C. Ohlwein, *A novel convective-scale regional reanalysis COSMO-REA2: Improving the representation of precipitation.* 2017, DOI: https://doi.org/10.1127/metz/2017/0824.
255. Bundesnetzagentur. *Marktstammdatenregister der Bundesnetzagentur (Market Core Data Register of the Federal Network Agency)*. 2019 [cited 2020 May 15]; Available from: https://www.marktstammdatenregister.de/MaStR.
256. International Energy Agency (IEA) and Nuclear Energy Agency (NEA). *Projected Costs of Generating Electricity – 2020 Edition*. 2020 [cited 2020 May 12]; Available from: https://www.oecd-nea.org/jcms/pl_51110/projected-costs-of-generating-electricity-2020-edition.

257. Matke, C., W. Medjroubi, and D. Kleinhans. *SciGRID – An Open Source Reference Model for the European Transmission Network (v0.2)*. 2016 [cited 2020 June 8]; Available from: http://www.scigrid.de.
258. Eurostat. *GISCO: Geographical Information and maps*. 2020 [cited 2020 June 8]; Available from: https://ec.europa.eu/eurostat/web/gisco/geodata/reference-data/administrative-units-statistical-units/nuts.
259. ENTSO-E. *ENTSO-E transparency platform*. 2020 [cited 2020 October 9]; Available from: transparency.entsoe.eu.
260. Länderarbeitskreis Energiebilanzen. *Endenergieverbrauch nach Energieträgern (Final Energy Consumption by Energy Source)*. 2015 [cited 2020 June 8]; Available from: http://www.lakenergiebilanzen.de/endenergieverbrauch-nach-energietraegern-aktuell/.
261. Statistische Ämter des Bundes und der Länder. *Volkswirtschaftliche Gesamtrechnungen der Länder (National Accounts of the Federal States)*. 2016 [cited 2020 June 8]; Available from: https://www.statistik-bw.de/VGRdL/tbls/?rev=RV2014&lang=de-DE#RV2014KR.